FROM POLYMERS TO PORPHYRINS: SUPRAMOLECULAR CONTROL ASSERTED BY CYCLODEXTRIN OLIGOMERS

Hamish Liam McTernan

Thesis submitted for the degree of

Doctor of Philosophy

in

the University of Adelaide

School of Chemistry and Physics

January, 2016

CONTENTS

ABSTRACT

Cyclodextrin oligomers are non-toxic and biodegradable hosts for a wide array of potential guest molecules. Consequently, they are currently being used in a range of applications for small molecule and polymer-based drug delivery systems. As it stands, the majority of these oligomer systems are derived from α- and β-cyclodextrin. However, cyclodextrin oligomers derived from γ-cyclodextrin are relatively unknown. Oligomer systems derived from γ-cyclodextrins may have the capability to form stable host-guest complexes with larger drug targets such as porphyrins. In order to develop applications for these new γ-cyclodextrin oligomer systems fundamental studies on their host-guest complexes must be performed. A literature review on cyclodextrins as supramolecular hosts as well as some key guest molecules and applications are outlined in Chapter 1.

Chapter 2 investigates the complexation of a known photosensitiser, 5,10,15,20-tetra(*p*-sulfonatophenyl)porphyrinate, H_2TSPP^{4-}, with γ-CD and five of its modified oligomers in aqueous solutions. Two previously reported succinimide-linked γ-CD dimers (33γ-CD_2suc and 66γ-CD_2suc) were prepared as well as two new oxalate-linked γ-CD dimers (33γ-CD_2ox and 66γ-CD_2ox) and a novel benzene linked γ-CD trimer (666γ-CD_3bz). The host-guest complexation of H_2TSPP^{4-} by the cyclodextrin hosts was investigated by 2D ^{1}H NOESY NMR, variable temperature UV-Vis spectroscopy and molecular modelling. The experiments are designed to investigate the effects of the cyclodextrin oligomer subunit orientation (3,3-, 6,6- or 6,6,6-) as well as the variation in length of the covalent bridge. Additionally, the study is intended to give insight into the various host-guest complexes and complex conformers in the H_2TSPP^{4-}. γ-CD oligomer equilibria.

Chapter 3 investigates the host-guest complexation of a less water-soluble porphyrin, 5,10,15,20-tetra(*p*-carboxyphenyl)porphyrinate, H_2TCPP with γ-CD and its oligomers. The

complexation of H_2TCPP in its multiply ionised states H_3TCPP^{3-}/H_2TCPP^{4-} by native γ-CD, 33γ-CD_2suc, 66γ-CD_2suc, 33γ-CD_2ox, 66γ-CD_2ox and 666γ-CD_3bz was investigated by 2D ^{1}H NOESY NMR spectroscopy, UV-Vis spectroscopy and molecular modelling. The experiments are designed to investigate the effects the ionic porphyrin substituents, porphyrin aggregation and the cyclodextrin oligomer subunit orientation (3,3-, 6,6- or 6,6,6-) as well as the variation in length of the covalent bridge on the host-guest complexation of H_3TCPP^{3-} /H_2TCPP^{4-} by the cyclodextrin hosts.

In Chapter 4, a 3% randomly substituted sodium 5-(*p*-β-alanylaminophenyl)-10,15,20-tris(*p*-sulfonatophenyl)-porphyrin poly(acrylate) (PAATSPPala) was prepared. The complexation of the polymer substituents of PAATSPPala (TSPPala) by native γ-CD, 33γ-CD_2suc, 66γ-CD_2suc, 33γ-CD_2ox, 66γ-CD_2ox and 666γ-CD_3bz was investigated by 2D ^{1}H NOESY NMR spectroscopy, variable temperature UV-Vis spectroscopy and rheology. The experiments were designed to give insight into the effects of the different cyclodextrin hosts on the relative strengths of host-guest complexation and the formation of inter-strand poly(acrylate) cross-links in forming photoactive hydrogels.

In Chapter 5, PAA was 3 % randomly substituted with 1- or 2- modified naphthalene to give isomeric poly(acrylate)s PAA1NSen, PAA1NShn, PAA2NSen and PAA2NShn, respectively. The complexation of the polymer substituents by native β-CD or γ-CD and four succinamide-linked cyclodextrin dimers (33β-CD_2suc, 66β-CD_2suc, 33γ-CD_2suc and 66γ-CD_2suc) was investigated by 2D ^{1}H NOESY NMR spectroscopy, fluorescence spectroscopy and rheology. The experiments are designed to give insight into the effects of naphthyl substitution position, the length of the tether attaching the naphthalene substituent to the poly(acrylate) back-bone and the size and geometry of the cyclodextrin hosts. These factors are expected to determine the relative strengths of host-guest complexation and the formation of inter-strand poly(acrylate) cross-links to form hydrogels.

Chapter 6 describes the experimental methodology employed in these studies. The information in this thesis hopes to provide greater insight into the formation of γ-CD oligomer host-guest complexes and may lead to the better design of drug delivery systems, host-guest polymer networks and intrinsically therapeutic hydrogels.

DECLARATION

This is to declare that the work presented within this thesis is original and was carried out at the University of Adelaide during the period of 2010-2015. This work contains no material which has been accepted for the award of any other degree or diploma in any university or other tertiary institution and, to the best of my knowledge and belief, contains no material previously published or written by another person, except where due reference is given.

I give consent to this copy of my thesis, when deposited in the University of Adelaide Library, being made available for loan and photocopying, subject to the provisions of Copyright Act 1968.

I also give permission for the digital version of my thesis to be made available on the web, via the University's digital research repository, the Library catalogue, the Australasian Digital Theses program (ADT) and also through web search engines, unless permission has been granted by the University to restrict access for a period of time.

Hamish Liam McTernan

/ / 2016

ACKNOWLEDGMENTS

This thesis would not have been written without the help of many people that supported me throughout my candidature. First and foremost I would like to thank Prof. Stephen Lincoln for allowing me to undertake a Ph.D. under his tutelage. I will be forever grateful for your insightful advice (in and out of the laboratory), Cold War history lessons, guidance, eye for detail and most of all patience. Thank you for always being a dedicated supervisor from the start of my honours year to the end of this project. Moreover, I would like to thank my second supervisor, Assoc. Prof. Tak Kee, for his collaboration, advice, support and passionate conversations about physical chemistry.

To Dr. Duc Truc Pham you are a true friend and someone I will always look up to. Without your help and mentoring I would have never been able to finish this project. Noby, thank you for friendship, numerous rounds of proof reading, hours of conversation, travel and food advice and your wonderful singing voice (every time I hear *Save the Best for Last* I will think of you). To my weekend lab friend Liang, thank you for always asking if I have had lunch, letting me into the building when I have forgotten my card, helping me with maths and patiently translating numerous Chinese restaurant menus. I would also like to thank Mitch and Tien with their help, friendship and collaboration at the early stages of this project. Furthermore, I would like to thank all of Lincoln and Kee group members I have worked with throughout the years and in particular Hilary (H-bomb), Jianjia, Mandy, Scott, Taka and Trang for their help, support and friendship.

I would like to thank Prof. Xuhong Guo, Dr. Jie Wang and Yiming Wang of East China University of Science and Technology for their collaboration and rheological measurements.

Furthermore, I would like to thank the research groups of Prof. Christopher Easton of the Australian National University and Prof. Robert Prud'homme of Princeton University for their collaboration.

I would like to thank the entire Chemistry Department of The University of Adelaide for their friendship and support. I would like to thank Phil Clements for all of his hard work on all things NMR related in this work. Thank you for all of the reprints, shimming advice and your good taste in music. Gino, thank you for always looking out for me in and out of the teaching laboratory and providing me with employment in the hardest of financial times. Your stories on "the good old days at Adelaide Uni" and advice on high risk superannuation will never be forgotten.

I would like to thank my Mother, Decima, and Father, David, for the love and support they have provided my entire life. Mum, thank you always knowing what I need, even when I don't know myself sometimes. Dad, thank you for teaching me the tenacity needed to continue through the toughest times in life, for always answering the phone (sometimes whilst flying) and for always trying to solve my problems even when you can't. I would like to thank my surrogate mother Iwona, thank you for everything you do (pickups, drop offs, cakes, holidays) and for treating me like one of your own. I would like to thank my all of my friends, and in particular, Fozz, Michael, Tom, and Lachie. Thank you for providing weekend distractions (Michael for the Fortress of Solitude), tales from Naracoorte High and putting life into perspective from time to time. I would like to thank my sister Kristie for being an amazing roommate, sibling and friend. Thank you for lending me the car, picking up my socks, buying the toilet paper and looking after me from the day I was born (except for that time you dropped me on my head).

Finally, I would like to thank my dearest Karolina, we did it. This thesis is as much yours as it is mine as I would have never finished it without meeting you. Thank you for being the love of my life, my best friend, my partner and my Chimlick. I cannot put into words the gratitude I feel towards how much you have changed my life or how much I love you so I'll end it here.

ABBREVIATIONS

1. General

Å	angstrom (10^{-10} m)
Ar	aryl
d	Density (g cm^{-3})
δ	chemical shift (ppm)
Δ*G*	Gibbs free energy change
Δ*H*	enthalpy change
Δ*S*	entropy change
ε	molar absorptivity (mol^{-1} dm^{-3} cm^{-1})
E	heat of formation (kJ mol^{-1})
FL	fluorescence spectroscopy
et al.	et alia
GC-MS	gas chromatography- mass spectrometry
Hz	Hertz
HPLC	high-performance liquid chromatography
I	ionic strength (mol dm^{-3})
I_F	fluorescence intensity
J	coupling constant (Hz)
K	stability constant (dm^{-3} mol^{-1})
K_a	acid dissociation constant
K_{11}	stability constant for 1:1 host-guest complexes (dm^{-3} mol^{-1})
K_{21}	stability constant for 2:1 host-guest complexes (dm^{-3} mol^{-1})
K_D	dimerisation constant
m/z	mass/charge ratio

MS	mass spectrometry
MALDI TOF	matrix-assisted laser desorption-ionisation time-of-flight
NMR	nuclear magnetic resonance
NOE	nuclear Overhauser enhancement
NOESY	nuclear Overhauser enhancement spectroscopy
PDT	photodynamic therapy
pH	$-\log[H^+]$
p*K*a	$-\log[K_a]$
ppm	parts per million
PS	photosensitiser
R_f	retention factor
R_c	relative retention factor to native cyclodextrins (in TLC)
T	temperature (K)
TLC	thin-layer chromatography
UV-Vis	ultraviolet-visible
wt	weight

2. Chemicals

α-, β-, γ-CD	α-, β-, γ-cyclodextrin
33β-CD_2suc	*N*,*N*′-Bis((2^{A}S,3^{A}S)-3^A-deoxy-β-cyclodextrin-3^A-yl) succinamide
66β-CD_2suc	*N*,*N*′-bis(6^A-deoxy-β-cyclodextrin-6^A-yl) succinamide
C18	octadecyl
DCC	*N*,*N*'-dicyclohexylcarbodiimide
DCM	dichloromethane

DMAP	4-(dimethylamino)pyridine
DMF	*N*,*N*-dimethylformamide
DMSO	dimethylsulfoxide
EDC	1-ethyl-3-(3-dimethylaminopropyl)carbodiimide
en	1,2-diaminoethane
33γ-CD_2ox	*N*,*N*′-Bis((2^{A}S,3^{A}S)-3^A-deoxy-γ-cyclodextrin-3^A-yl) oxalamide
66γ-CD_2ox	*N*,*N*′-Bis(6^A-deoxy-γ-cyclodextrin-6^A-yl) oxalamide
33γ-CD_2suc	*N*,*N*′-Bis((2^{A}S,3^{A}S)-3^A-deoxy-γ-cyclodextrin-3^A-yl) succinamide
66γ-CD_2suc	*N*,*N*′-Bis(6^A-deoxy-γ-cyclodextrin-6^A-yl) succinamide
666γ-CD_3bz	1,3,5-*N*,*N*,*N*-tris(6^A-deoxy-6^A-γ-cyclodextrin)-benzene
hn	1,6-diaminohexane
HP	hydroxypropyl
TCPP	5,10,15,20-tetra(*p*-carboxyphenyl)porphyrin
TSPP	5,10,15,20-tetra(*p*-sulfonatophenyl)porphyrin
NMP	*N*-methylpyrrolidin-2-one
1NSen	*N*-(2-aminoethyl)-1-naphthyl-sulfonamide
1NShn	*N*-(6-aminohexyl)-1-naphthyl-sulfonamide
2NSen	*N*-(2-aminoethyl)-2-naphthyl-sulfonamide
2NShn	*N*-(6-aminohexyl)-2-naphthyl-sulfonamide
PAA	poly(acrylate)
PAA1NSen	3% randomly 1NSen substituted PAA
PAA1NShn	3% randomly 1NShn substituted PAA
PAA2NSen	3% randomly 2NSen substituted PAA
PAA2NShn	3% randomly 2NShn substituted PAA
PAATSPPala	3% randomly TSPPala substituted PAA

PAM	poly(acrylamide)
TSPPala	5-(*p*-β-alanylaminophenyl)-10,15,20-tris(*p*-sulfonatophenyl)-porphyrin
TFA	trifluoroacetic acid
THF	tetrahydrofuran

This page is intentionally left blank

Chapter 1

Introduction

1.1. HOST-GUEST CHEMISTRY

1.1.1. Outline and Overview of Host-Guest Chemistry

Host-guest chemistry describes interactions between two or more molecules occurring through forces other than covalent bonding.[1,2] The guest molecule fits closely inside a section or multiple sections of the host molecule, much like a lock and key. The strength in which these two molecules associate is determined by various non-covalent forces such as hydrogen bonds, metal-ligand complexation, ionic bonds, van der Waals forces, and hydrophobic interactions.[1,2] Host molecules are mostly large organic or organometallic structures including: cyclodextrins (CDs),[3-5] porphyrins,[6-9] dendrimers,[10-13] zeolites,[14-16] calixarenes,[17-20] crown ethers (or coronands),[21-25] metallocrowns,[26-29] pillararenes,[30-32] cucurbiturils,[33-36] cyclotriveratrylenes,[37-39] cryptophanes[40-43] and carcerands.[44-46] The structures of a crown ether, or coronand, and a porphyrin are shown in Figure 1:1. Hosts may have one or multiple complexation sites that can accommodate guest molecules. The complexation sites usually include an abundance of electron donating atoms, hydrophobic areas or charged entities.[1,2]

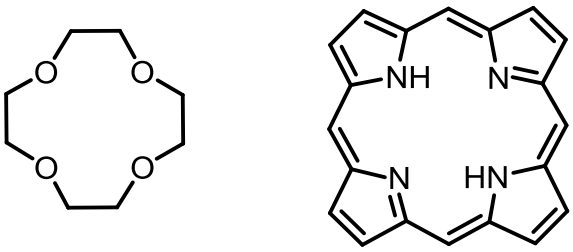

Figure 1.1: The crown ether or coronand (left) and the porphyrin (right) are examples of relatively simple host molecules.

A wide variety of guests can complex within the cavity of a host molecule and this is largely dependent on the size and structure of the host. Research into guests exemplified by biologically active molecules,[47-51] flavour compounds,[52, 53] pollutants[54-58] and metal ions[40,41,59]

have been of particular interest in recent years. Host-guest chemistry has led to advances in the food,[60-62] materials[63] and pharmaceutical industries.[64,65] Furthermore, host-guest chemistry has led to new tools in the search renewable energy[66-70] as well as novel technologies for restoring the environment.[54,56,71]

The host, guest and host-guest complex exist in an equilibrium (Figure 1.2) defined by the host-guest complexation constant, K_{11}. The complexation constant of the interaction between one host molecule and one guest molecule is defined as follows (Equation 1.1).[36]

$$K_{11} = \frac{[HG]}{[H][G]} \qquad 1.1$$

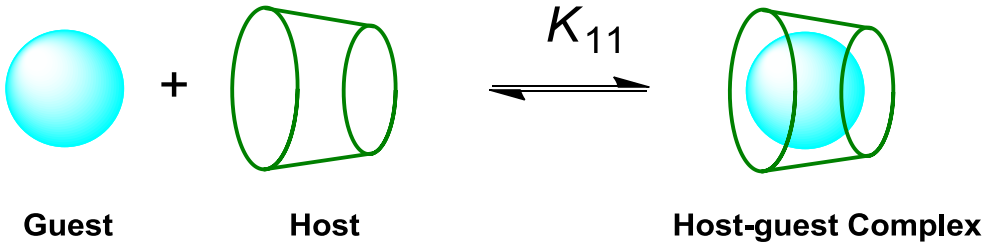

Figure 1.2: Definition of K_{11} in relation to 1:1 host-guest complexes (top), schematic of host-guest complexation (bottom).

Multiple complexation sites on the host or the guest can lead to higher order host-guest complexation stoichiometries (1:2, 2:1, 2:2 etc.) and the corresponding complexation constants can be derived for these equilibria.[72] Host-guest complexation can also be cooperative in nature, where the initial host-guest interaction can increase the likelihood of additional interactions between the host and an additional guest or vice versa.[72]

1.1.2. Host-Guest Chemistry in Drug Delivery

A recent area of host-guest chemistry that has garnered particular interest is that of host-guest drug delivery systems.[12,73,74] Whilst traditional pharmaceutical compounds are often effective in their mode of action, they also have a number of potential drawbacks. Many of these compounds are effective at treating their targeted disease but lack specificity leading to potentially harmful side effects.[75-77] Host-guest complexes, such as drug-loaded polymer networks, allow for site-specific attack against cancer and other life threatening diseases.[78] Another drawback of some traditional medicinal compounds is their short half-lives *in vivo*.[79-82] Complexation of a drug within a host can dramatically increase the half-life of that drug, thereby decreasing the effective dosage and dosage frequency as well as reducing potential side effects.[79-82] Many potentially biologically active compounds also lack aqueous solubility, hindering their application as viable pharmaceuticals.[79-82] Encapsulating hydrophobic guests within a host compound can dramatically increase their solubility, leading to the formation of a new generation of supramolecular drugs.[47,83] Such encapsulation is exemplified for curcumin in Figure 1.3.[86]

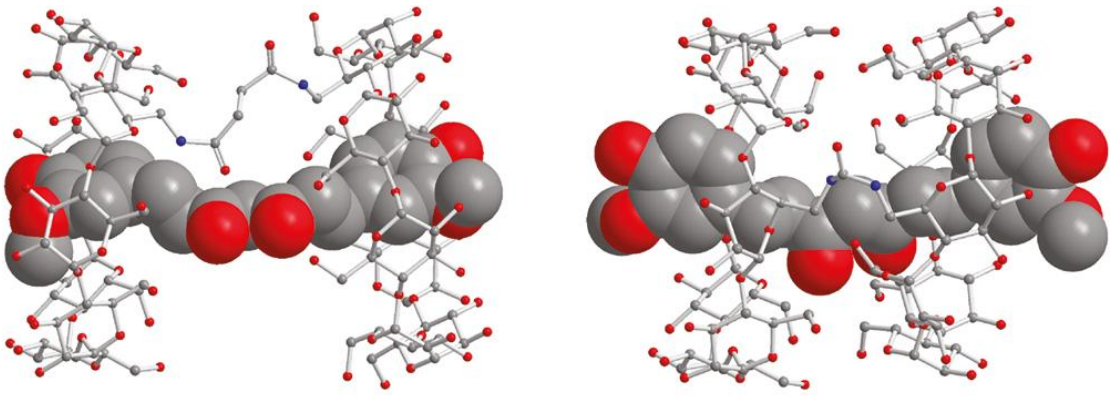

Figure 1.3: Host-guest complex of the medicinal pigment curcumin (space filling) within succinate- (left) or urea-linked (right) γ-CD dimers (ball and stick).[84]

1.2. CYCLODEXTRINS

1.2.1. An Overview of Cyclodextrin Chemistry

Cyclodextrins are large cyclic sugars first discovered in 1891 and further characterised between 1903-11.[73] They are derived through the breakdown of starch by the enzyme cyclodextrin glycosyl transferase, isolated from the bacteria *Bacillus macerans*.[73] They are composed of α-1,4 linked D-glucopyranose subunits forming a macrocyclic oligosaccharide.[85] Their central annulus allows CDs to undergo host-guest interactions with molecules of a suitable size to fit inside the CD annulus.[86] Their low toxicity, excellent biocompatibility and ability to encapsulate a variety of hydrophobic molecules have made CDs the most widely employed host units for biomedical applications.[87]

1.2.2. Structure and Properties of Cyclodextrins

The most common cyclodextrins (CD) are α-, β- and γ-CD (6, 7 and 8 glucopyranose subunits, respectively, Figure 1.4) with a depth of 7.9-8.0 Å and varying narrow and wide annular face widths of 4.7 and 5.3 Å, 6.0 and 6.5 Å and 7.5 and 8.3 Å, respectively, measured for the H atoms bonded to C(5) and the H atoms bonded to C(3), respectively (Figure 1.4).[88] Larger CDs comprised of 9 - 50 subunits have been isolated, however, they are generally too unstable to produce in commercially available quantities.[89] The glucopyranose subunits adopt a $^4C_1$ chair conformation, which leads to a truncated conical structure. The hydroxyl groups attached to carbons in the 2 and 3 positions of each glucopyranose ring (Figure 1.4, blue) compose a ring of hydroxyl groups defining the wider secondary face and hydroxyl groups attached to the carbons in the six position (Figure 1.4, green) compose a ring of hydroxyl groups defining the narrower primary face of the cone. Each of these rings is hydrophilic due to the abundance of hydroxyl groups, whereas the central annulus is hydrophobic (comprised

mostly of glycosidic oxygen bridges and hydrogen atoms), creating a hydrophobic pocket. Each D-glucopyranose subunit contains five chiral carbons making α-, β- and γ-CD homochiral.[90] This property can be exploited in the separation of enantiomeric compounds.[91-93] The glucopyranose subunits are labelled A to H clockwise around the ring (Figure 1.4). Therefore, when identifying a specific carbon in a CD macrocycle, it is identified by its position in the glucopyranose ring as well as the subunit in which it resides e.g. $C3^{A}$.

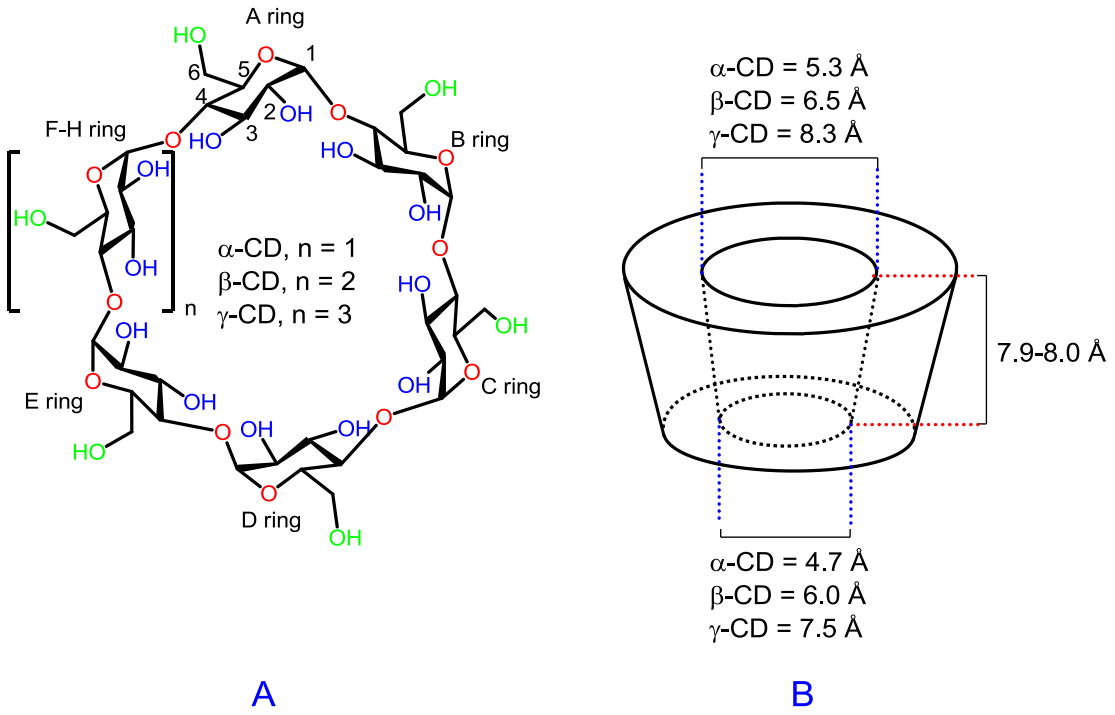

Figure 1.4: A) structure of α-, β-, and γ-CD showing the 6-hydroxyl groups on the primary face (green), 2- and 3-hydroxyl groups on the secondary face (blue). B) Schematic of the conical structure of CDs.

1.2.3. Cyclodextrin Host-Guest Complexes

The ability to form host-guest complexes with a diverse range of molecules has garnered CDs much interest in supramolecular research. In aqueous solutions, the central annulus of a CD is

occupied by water molecules, which can be readily displaced by hydrophobic guests (Figure 1.5).[94,95] In most cases, this process is enthalpy driven, and in general, hydrophobic guests form stronger host-guest complexes with CDs than do hydrophilic guests.[95]

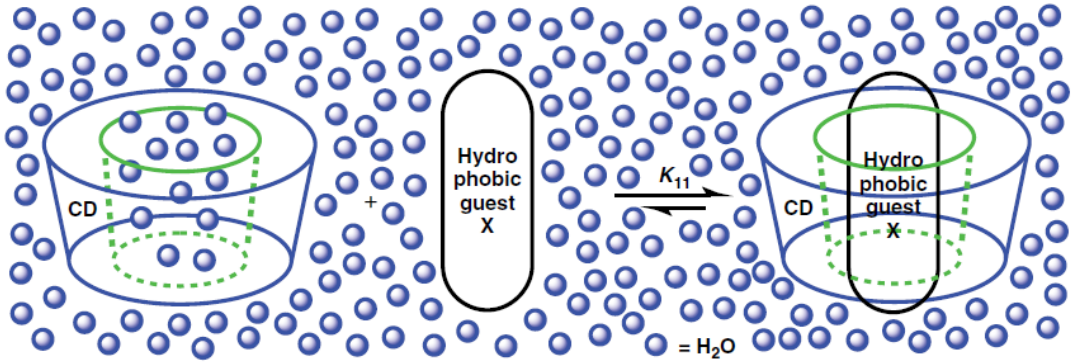

Figure 1.5: Schematic of CD host-guest complexation in aqueous solutions.[94]

1.2.4. Cyclodextrin Complexation Stability and Thermodynamics

A number of factors can drive the complexation of guest molecules by CDs in solution. These can include the displacement of water by the guest, hydrophobic interactions, a decrease in the conformational strain energy of the CD, van der Waals interactions, London dispersion forces, electrostatic interactions (mainly dipole-dipole) and hydrogen bonding.[94] The thermodynamic parameters of complexation may be calculated using the van't Hoff equation.[96] A compensatory effect between the complexation entropy change and enthalpy change has often been observed empirically for CD host-guest complexation (Equation 1.2).[96]

$$T\Delta S = \alpha\Delta H + T\Delta S_0 \qquad 1.2$$

where T is the temperature, ΔS is the entropy change, ΔH is the enthalpy change, ΔS_0 is the entropy change when ΔH is zero, and α is the slope of a linear plot of $T\Delta S$ against ΔH.[96] Thus, α indicates the extent to which the enthalpic gain (ΔH). induced by any alterations in host, guest, and/or solvent, is cancelled by the accompanying entropic loss (ΔS).[96]

Conversely, the intercept ($T\Delta S_0$) represents the stability of the complex when $\Delta H = 0$. Therefore, if $T\Delta S_0$ is positive, the complex is stabilised even in the absence of enthalpic stabilisation.[96]

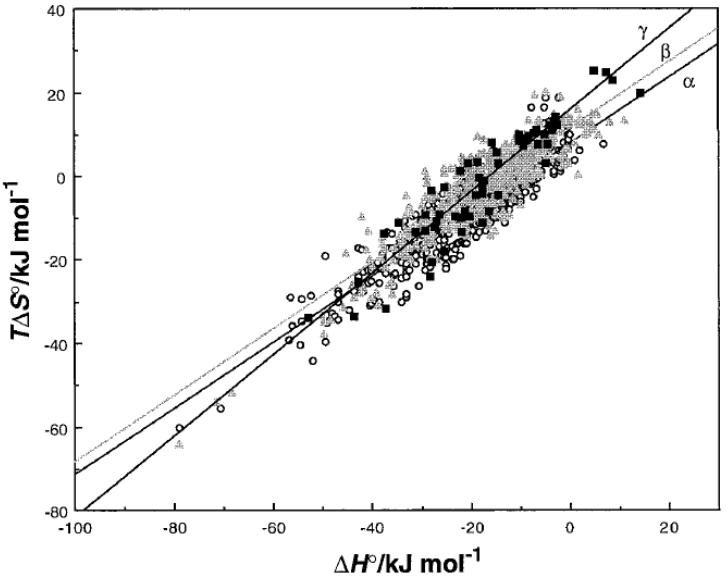

Figure 1.6: Enthalpy-entropy compensation plots for various host-guest complexes of native α- (○), β-(▲) and γ-CD (■).[96]

A previous study of the specific data for native α-, β-, and γ-CD revealed interesting features concerning the conformational changes and desolvation induced by complexation with various guests (Figure 1.6).[96] For α-, β-, and γ-CD, the slope, α, increases gradually from 0.79 to 0.80 to 0.97, respectively. Furthermore, $T\Delta S_0$ increases from 8 kJ mol^{-1} to 11 kJ mol^{-1} to 15 kJ mol^{-1} with an increase in CD ring size. These observations are consistent with greater ring flexibility and a larger number of associated water molecules in the cavities of the larger CDs.[96]

1.2.5. Modified Cyclodextrins

The hydroxyl groups on the primary or secondary face of CDs allow for easy substitution via nucleophilic attack.[97] Various groups such as amines, halides, azides, aldehydes and alkenes can be incorporated for increased functionality.[97,98] The primary hydroxyl groups attached to the carbons in the 6 positions are the most reactive due to a lack of steric hindrance and highest basicity.[98] The hydroxyl groups attached to carbons in the 2 position are the most acidic and have the second highest reactivity followed by the hydroxyl groups attached to carbons in the 3 position, which are the most sterically hindered.[97] A common first step of CD modification is substitution by an arene sulfonyl chloride (such as tosyl chloride), which is readily achieved at the carbons in the 2 or 6 positions of the D-glucopyranose subunits of α-, β- and γ-CD.[97,98] The steric bulk of the arene sulfonyl group favours monosubstitution on the CD.[97,98] The larger annulus of γ-CD can lead to multiple substitutions on the carbons in the 6 position but this can be minimised by altering the reaction conditions or using larger arene sulfonyl groups.[99,100] To achieve substitution on the carbon in the 3 position, a 2,3 manno-epoxide can be formed via the carbon in the 2 position which can be further substituted by nucleophilic attack to afford CDs substituted on carbon 3.[99,101]

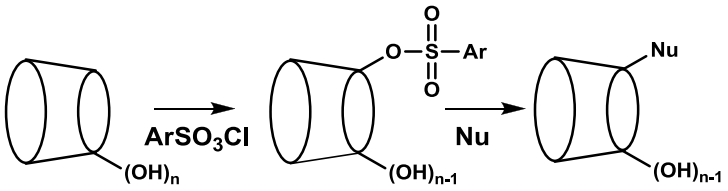

Figure 1.7: Nucleophilic modification of the primary face of CDs using an arene sulfonyl CD intermediate.

1.2.6. Cyclodextrin Oligomers

By linking two or more CDs, their host-guest complexing capabilities can be greatly improved compared with those of monomeric CDs. Cyclodextrin oligomers such as dimers,[77,101,102] trimers,[103-106] tetramers[107,108] and octamers[109,110] can all be prepared by modifying native CDs. The oligomers can be linked in the 2^A, 3^A or 6^A positions (Figure 1.8) allowing for adjustment of the combined volume of the oligomer complexing sites.

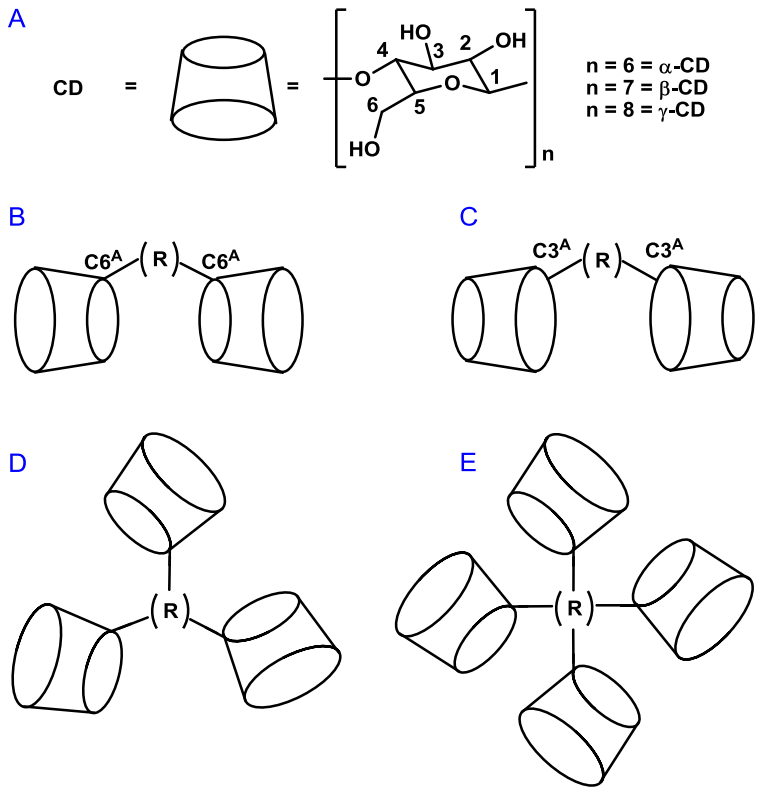

Figure 1.8: Schematic of CD oligomers. A) Structure of native CD monomers. B) Structure of a 6^A-6^A linked CD dimer. C) Structure of a 3^A-3^A linked CD dimer. D) Structure of a CD trimer (linkages can be via 6^A or 3^A carbons). E) Structure of a CD tetramer (linkages can be via 6^A or 3^A carbons).

The covalent linkers can also be varied in size, flexibility and steric bulk, further increasing the functionality of CD oligomers. Linkers such as, porphyrins, aromatics, azo compounds and heterocycles have all been incorporated into CD oligomers.[111-113] This allows for oligomers that can coordinate metals, are photoactive or incorporate molecular switches.[111] The multiple annuli of CD oligomers may allow cooperative complexation, thus forming more stable host-guest complexes than their native CD counterparts.[111]

1.3. POLY(ACRYLATE)S

1.3.1. Poly(acrylate) structure and modification

Poly(acrylic acid) (PAA) (Figure 1.9) is a synthetic polymer consisting of linked repeating units of acrylic acid.[114] The abundance of carboxylic acid groups on the PAA backbone allows addition of various functional groups through substitution reactions.[115,116] The dissociation of the carboxylic acid groups can also make the polymer anionic and highly soluble in aqueous solutions. Poly(acrylic acid) strands can be quite long in length with molecular weights up to 250,000 g mol^{-1} being common.

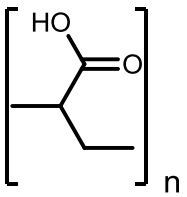

Figure 1.9: Structure of poly(acrylic acid) repeating unit.

Various substituents such as aromatics,[117] alkanes,[118] cycloalkanes[116] and supramolecules[116] have been attached to PAA. This allows previously hydrophobic functional groups to be

solubilised in water, creating new materials with combined the properties of the polymer and substituent. Their low toxicity, high biocompatibility and biodegradability also make PAAs suitable for biological applications.

1.3.2. Poly(acrylate)s in the Formation of Hydrogels

Modified PAAs can form extensive polymer networks capable of absorbing up to 98 % water.[119-121] These networks are often referred to as hydrogels and are a consequence of cross-linking between polymer strands.[119-121] The cross-links can be chemical (covalent) or physical (non-covalent) in nature and are largely dependent on side chains incorporated into the PAA backbone.[119-121]

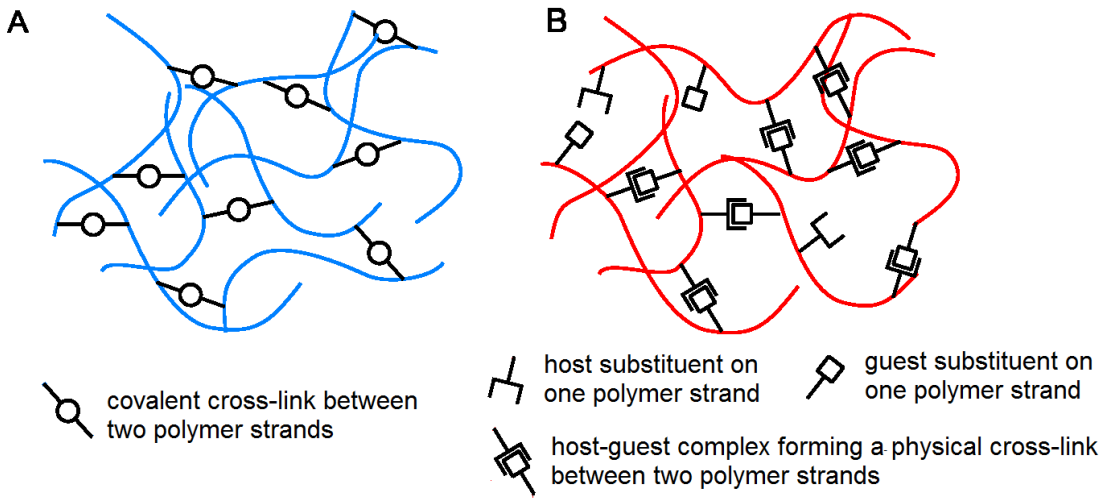

Figure 1.10: Chemically cross-linked polymer network (A) compared with a physically cross-linked polymer network (B).

Covalent hydrogels are formed when permanent and irreversible chemical crosslinks are incorporated into the polymer network (Figure 1.10, A).[121] Such cross-links can be formed by many chemical processes such as Schiff base formation, Michael addition, free radical chain growth photo-polymerisation, photo-polymerisation of thiol and terminal alkenes and

enzyme-catalysed reactions.[119] The manner in which these hydrogels are formed can make them rather brittle, poorly transparent and unable to self-heal once the polymer cross-linking network is broken.[119] The formation of these hydrogel networks is often reliant on catalysts, photo-initiators or ultraviolet light, thus limiting their potential applications.[122] Additionally, poorly-defined structures associated with network defects and large equilibrium volume swelling of the bulk material has hampered their applications *in vivo*.[123]

Physical hydrogels are formed by non-covalent and often reversible interactions that exist in a dynamic equilibrium (Figure 1.10, B).[124-126] These non-covalent forces can include host-guest (Figure 1.10, B), metal-ligand, ionic and biomimetic interactions.[119] Such physical hydrogel formation can be induced in aqueous solutions by molecular self-assembly. Consequently, they do not requiring additional cross-linking reagents and their transition from solution to hydrogel occurs without a significant change in volume.[123] However, physical cross-linking often leads to weaker gel networks that are more susceptible to shearing by mechanical forces. Nevertheless, their dynamic nature is advantageous as it is the basis for both shear-thinning (viscous flow under shear stress) and self-healing (time dependent recovery upon relaxation) properties.[122] These two properties are considered very desirable characteristics for a variety of important applications.[127]

1.3.3. Host-guest Chemistry of Poly(acrylate)s and Cyclodextrins

A number of studies have focussed on the effect of CDs on the formation of PAA hydrogels.[128-130] Native CDs have been shown to significantly reduce (> 5000 fold) the viscosity of PAAs substituted with C18 alkyl chains.[131] This was attributed to the CDs interfering with hydrophobic interactions between the C18 substituents, thus breaking the

hydrogel network.[131] Conversely, other studies have shown that the addition of CD species can drastically increase the viscosity of hydrogels. Both CD dimers and CD trimers were shown to increase the viscosity of admantyl substituted PAAs by up to 350 fold compared to the admantyl-modified PAAs alone.[104,130] This increase in viscosity was attributed to additional cross-links formed by CD-admantyl host-guest complexation. Cyclodextrins have also been randomly covalently substituted onto PAA thereby facilitating the host-guest complexation of a wide array of guests.[115,129,132]

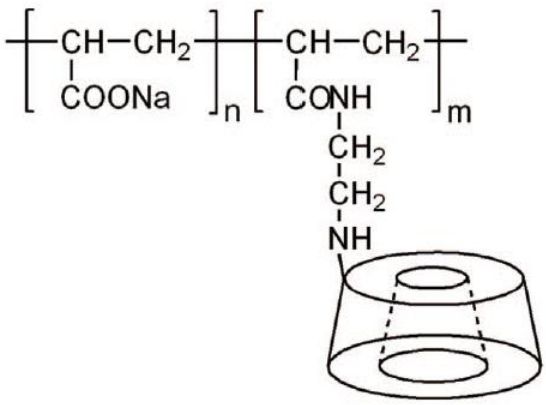

Figure 1.11: Schematic of CD modified PAA, where n = number of unmodified PAA subunits and m = number of subunits modified with CD.[115]

1.4. PORPHYRINS

1.4.1. Structure and Properties of Porphyrins

Porphyrins are large heterocyclic macrocycles composed of four modified pyrrole subunits interconnected at their α carbon atoms via methine bridges (Figure 1.12).[133,134] They are often naturally occurring and are found in high concentrations in plant and animal material.[134] They obey Hückels rule for aromaticity (4n + 2π electrons) leading to electron delocalisation around the large planar molecule.

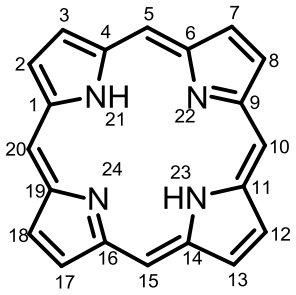

Figure 1.12: Porphine, the simplest example of a porphyrin.

The large number of conjugated double bonds in porphyrins leads to strong absorbance in the UV-visible region such that they are usually purple or deep red in colour.[135] The presence of large aromatic regions make most porphyrins extremely hydrophobic, hence their solubility in aqueous solutions is poor.[136-138]

1.4.2. Synthetic Porphyrins

A common synthetic route to porphyrins is the reaction of pyrrole with substituted aldehydes (Figure 1.13).[139] Functional groups such as halogens, acids, alcohols and heteroatoms can all be incorporated into the porphyrin structure.[140] This is particularly useful in achieving water-soluble porphyrins for biological applications.[136-138] The incorporation of different functional groups also allows for the synthesis of multiply charged cationic[141-143] or anionic porphyrins.[144-146]

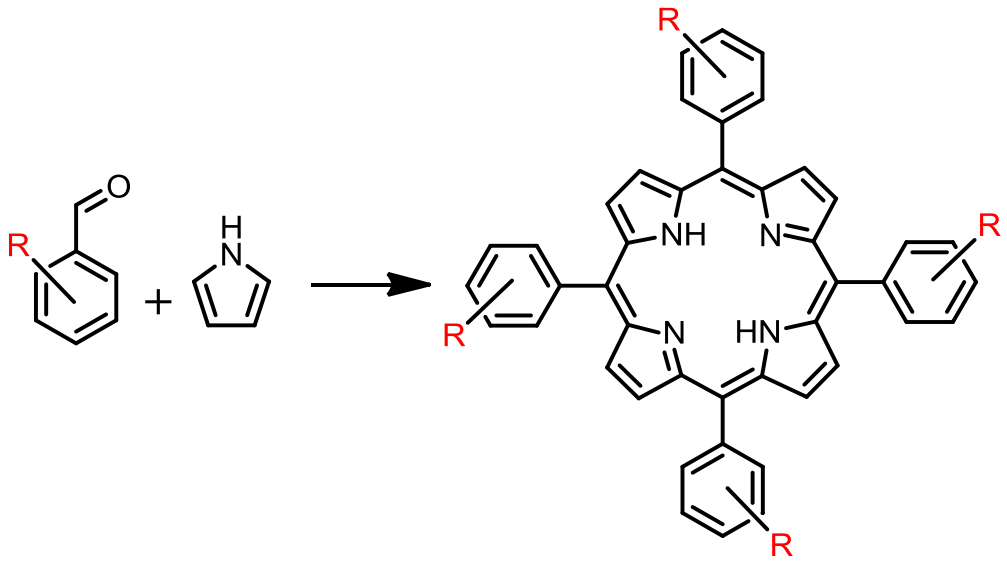

Figure 1.13: Porphyrin synthesis and functional group (R) incorporation.

Two of the most common water-soluble synthetic porphyrins are 5,10,15,20-tetra(*p*-sulfonatophenyl)porphyrin (H_2TSPP, Figure 1.13 R = SO_3H in the *para* position) and 5,10,15,20-tetra(*p*-carboxyphenyl)porphyrin (H_2TCPP, Figure 1.13 R = CO_2H in the *para* position). They can be synthesised from relatively simple starting materials, with reasonable yields and a high purity.[147-150] These porphyrins are often used as their tetrasodium salts to increase their solubility in aqueous solutions giving the tetraanionic forms of each porphyrin; H_2TSPP^{4-} and H_2TCPP^{4-}.

1.4.3. Metalloporphyrins

Metalloporphyrins play a central role in many biological processes. Haem B (Figure 1.14) is essential for oxygen transport in myoglobin and is the active site for cytochrome P450 enzymes.[151-153] The tetrapyrrole arrangement of porphyrin moieties allow them to complex with a wide range of transition metals. Metals such as Fe,[154] Cu,[155] Mn,[156] Co,[157] Zn,[158] Au,[149] Ag,[159] Pd[160] and Pt[161] are all commonly incorporated into porphyrin compounds to increase

their functionality. Furthermore, the incorporation of metals into porphyrins can also broaden their spectral range, making them more suitable for photochemical processes. Metallated porphyrins are employed in catalysis,[162-164] solar cells,[165-168] nanowires,[169] metal organic frameworks,[170] and pharmaceuticals.[171-173]

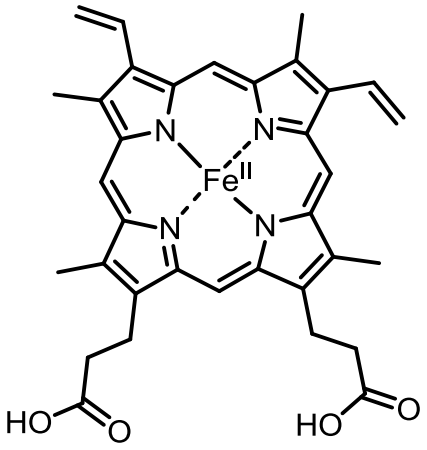

Figure 1.14: Structure of haem B; a metallated porphyrin essential for many biological processes.

1.4.4. Porphyrins in Medicinal Chemistry

Porphyrins have been exploited for their medicinal properties since the early 20th century.[174, 175] Hematoporphyrin (Figure 1.15) was used in early treatments of psychosis associated with many psychiatric disorders. However, the treatment was abandoned due to photosensitivity in patients.[175] Although hematoporphyrin was discarded as an antipsychotic, its photosensitive action led to a new field of research in photodynamic therapy (PDT).[176] Photodynamic therapy is a treatment in which a photosensitiser (PS) is excited using specific wavelengths of light. This process produces singlet oxygen, which causes irreversible damage to the surrounding tissue.[177,178] It is particularly useful in combatting surface cancers as light can be focussed on specific regions of tumour cells in targeted cancer treatments.[177,178] Photodynamic therapy is currently used in the treatment of many cancers including skin,

oesophageal, brain, lung, stomach and ocular.[177-179] Porphyrins are often used in PDT due to their broad spectral absorbance, relative ease of modification and low dark toxicity.[177-179]

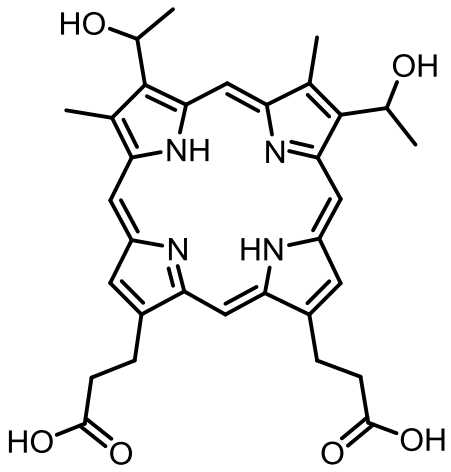

Figure 1.15: Hematoporphyrin, an early porphyrin-type PS.

1.4.5. Porphyrin-Cyclodextrin Host-guest Complexes

Cyclodextrins have been previously shown to be good hosts for porphyrin guests.[180-186] Both β-CD and γ-CD have been shown to complex porphyrins with complexation constant values, K_{11}, in the range of 1 - 10^3 dm^3 mol^{-1}.[180,185,186] However, much higher K_{11} have been reported with modified CDs such as hydroxypropyl (HP) CDs (Table 1.1).[186,187]

Table 1.1: Complexation constants, K_{11}, of common porphyrins by CDs in aqueous solutions at 298.2 K (UV = UV-Visible absorption spectroscopy, FL = fluorescence spectroscopy)

Host	Guest	K_{11} value (dm^3 mol^{-1})	Method	pH
β-CD[186]	H_2TSPP^{4-}	5.6×10^3	UV	7.0
γ-CD[180]	H_2TSPP^{4-}	1.6×10^3	FL	10.1
HP-β-CD[187]	H_2TSPP^{4-}	2.9×10^7	FL	7.0
β-CD[186]	H_2TCPP^{4-}	9.3×10^3	UV	7.0
γ-CD[185]	H_2TCPP^{4-}	5.6×10^3	FL	10.1
HP-γ-CD[186]	H_2TCPP^{4-}	1.6×10^5	UV	7.0

The various CDs were found to greatly increase the solubility of the porphyrins in water, reduce porphyrin aggregation and increase their bioavailability.[179] By complexing porphyrins with linked CD dimers, cooperative host-guest complexes can be formed with significantly greater stabilities than those of their monomer counterparts.[181,188,189]

1.4.6. Cyclodextrin Dimers as Hosts for Porphyrin Guests

Some reports have introduced covalently linked CDs as potential drug delivery systems for porphyrins.[188-190] Nolte et al. showed that CD dimers complex cooperatively with H_2TSPP^{4-} or H_2TCPP^{4-} and that complexation can occur in a *syn* or *anti* conformation (Figure 1.16).[181,189] This concept has since been extended to CD dimer-metalloporphyrin complexes with complex functions such as cyanide treatments[191,192] and oxygen transporters.[193-195] The CD dimer-metalloporphyrin complexes were found to bind both O_2 and CN^- *in vivo* via strong coordination bonds. So far, these studies have focused on α- and β-CD dimers; and porphyrin complexation studies concerning γ-CD dimers are yet to be reported.

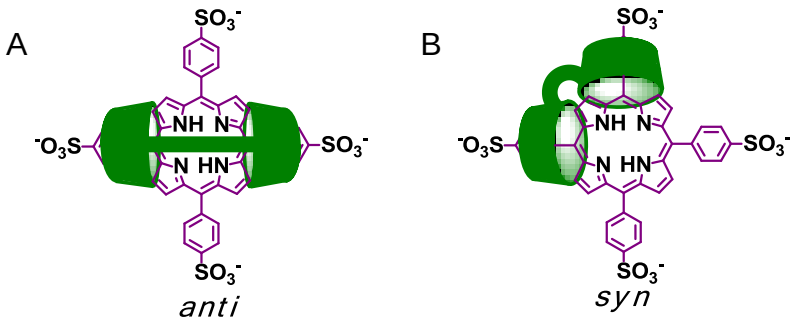

Figure 1.16: Schematic of CD dimer complexing a porphyrin in the *anti* (A) or *syn* (B) conformations.

1.4.7. Porphyrin modified polymers

The incorporation of porphyrins into polymers has been a recently developed topic of research. By incorporating porphyrin subunits into polymers, the desirable properties of each material can be combined. Porphyrin-modified polymers have many potential applications including photovoltaic devices,[196] molecular wires,[197] medical imaging agents[198,199] and models for biological systems.[200-202] Amongst these systems, porphyrins attached to the backbone of PAAs and poly(acrylamide)s (PAMs) are of particular interest for their biocompatibility and hydrogel forming capabilities.

Kano. et al. reported a metalloporphyrin structure complexed with pyridine bridged per-O-methylated β-CD dimers and covalently linked to PAAs as a potential artificial substitute for haemoglobin (Figure 1.17 A).[201] The porphyrin modified PAA was found to complex molecular oxygen and had a longer circulation time *in vivo* than free porphyrins. Harada et al. used metalloporphyrins attached to PAM to investigate metal ligand interactions between haem groups and L-histidine (Figure 1.17 B).[200] It was found that the metal-ligand interactions allowed self-assembly in the formation of hydrogels and this process could be displayed on the macroscopic scale.

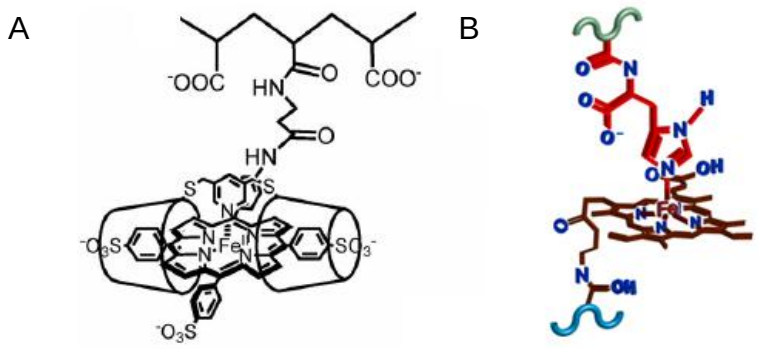

Figure 1.17: A) Porphyrin modified PAA complexed by per-O-methylated β-CD dimers as a haemoglobin substitute.[201] B) Metal-ligand interactions between metalloporphyrin and amino acid modified PAMs.[200]

1.5. AIMS OF THIS PROJECT

The aim of this project is to broaden the understanding of how CD oligomers can assert control over various host-guest systems in aqueous solutions. The study investigates the effects of oligomer tether length, CD annular size, complexing site number and geometry as well as guest composition, size and structure. A number of synthetic pathways as well as various analytical techniques will be employed to seek insight into the nature of the host-guest systems. The knowledge acquired in this project may be of great use to the pharmaceutical and materials chemistry industries. The content of the following chapters are now briefly outlined.

Chapter 2 describes the complexation of H_2TSPP^{4-}, with γ-CD and five of its modified oligomers in aqueous solutions. Two previously reported succinimide-linked γ-CD dimers (33γ-CD_2suc and 66γ-CD_2suc) were prepared as well as two new oxalate-linked γ-CD dimers (33γ-CD_2ox and 66γ-CD_2ox) and a novel benzene linked γ-CD trimer (666γ-CD_3bz). The complexation of H_2TSPP^{4-} by the CD oligomer hosts was investigated by 2D ^{1}H NOESY NMR spectroscopy, variable temperature UV-vis spectroscopy and molecular modelling. The experiments are designed to investigate the effects of the cyclodextrin oligomer subunit orientation (3,3-, 6,6- or 6,6,6-) as well as the length and flexibility of the oligomer linker. Additionally, the study is intended to give information on the various host-guest complexes and complex conformers in the H_2TSPP^{4-}-CD oligomer equilibria.

Chapter 3 investigates the host-guest complexation of a less water-soluble porphyrin, H_2TCPP with native γ-CD and γ-CD dimers. The complexation of a mixture of multiply ionised states of H_2TCPP, H_3TCPP^{3-}/H_2TCPP^{4-} by native γ-CD, 33γ-CD_2suc, 66γ-CD_2suc,

33γ-CD_2ox and 66γ-CD_2ox was investigated by 2D ^{1}H NOESY NMR spectroscopy, UV-vis spectroscopy and molecular modelling. The experiments are designed to investigate the effects of increased porphyrin aggregation and the shape of the ionic porphyrin substituents on host-guest complexation by the CD hosts.

In Chapter 4, PAA was 3 % randomly substituted with H_2TSPP^{4-} to give a porphyrin modified PAA (PAATSPPala). The complexation of the polymer substituents by the CD host molecules described in Chapter 2 was investigated by 2D ^{1}H NOESY NMR spectroscopy, variable temperature UV-vis spectroscopy and rheology. The experiments are designed to give insight into the effects of the polymer backbone on the relative strengths of host-guest complexation compared with that of native H_2TSPP^{4-}. The effect of the oligomer hosts on the formation of inter-strand cross-links between the porphyrin substituents on the PAA backbone is also investigated.

In Chapter 5, PAA was 3 % randomly substituted with 1- or 2- modified naphthalene to give isomeric poly(acrylate)s PAA1NSen, PAA1NShn, PAA2NSen and PAA2NShn, respectively. The complexation of the polymer substituents by native β-CD or γ-CD and four succinamide-linked CD dimers (33β-CD_2suc, 66β-CD_2suc, 33γ-CD_2suc and 66γ-CD_2suc) was investigated by 2D ^{1}H NOESY NMR spectroscopy, fluorescence spectroscopy and rheology. The experiments are designed to give insight into the effects of naphthyl substitution position, the length of the tether attaching the naphthalene substituent to the PAA back-bone and the size and geometry of the cyclodextrin hosts. These factors are expected to determine the relative strengths of host-guest complexation and the formation of inter-strand PAA cross-links to form hydrogels.

Chapter 6 describes the experimental methodology employed in these studies. The information in this thesis hopes to provide greater insight into the formation of γ-CD oligomer host-guest complexes and may lead to the better design of drug delivery systems, host-guest polymer networks and intrinsically therapeutic hydrogels.

1.6. REFERENCES

1. D. J. Cram, *Science*, 1988, **240**, 760-767.
2. J. F. Stoddart, *Annu. Rep. Prog. Chem., Sect. B*, 1989, **85**, 353-386.
3. A. Harada, F. Ito, I. Tomatsu, K. Shimoda, A. Hashidzume, Y. Takashima, H. Yamaguchi and S. Kamitori, *J. Photochem. Photobiol., A*, 2006, **179**, 13-19.
4. T. Harada, D. T. Pham, M. H. Leung, H. T. Ngo, S. F. Lincoln, C. J. Easton and T. W. Kee, *J. Phys. Chem. B*, 2011, **115**, 1268-1274.
5. S. Zhao and J. H. T. Luong, *J. Chem. Soc., Chem. Commun.*, 1994, 2307-2308.
6. H. L. Anderson, C. A. Hunter, M. N. Meah and J. K. M. Sanders, *J. Am. Chem. Soc.*, 1990, **112**, 5780-5789.
7. N. Berova, G. Pescitelli, A. G. Petrovic and G. Proni, *Chem. Commun.*, 2009, 5958-5980.
8. A. Hosseini, S. Taylor, G. Accorsi, N. Armaroli, C. A. Reed and P. D. W. Boyd, *J. Am. Chem. Soc.*, 2006, **128**, 15903-15913.
9. M. Wienkers, J. Ramos, H. Jemal, C. Cardenas, P. Wiget, A. Nelson, S. Free, J. Wu, R. Roach, M. Vulcan, K. Waynant, K. Fort, A. Vladimirova, J. Sun, S. E. Hunt, D. M. Rudkevich and S. D. Starnes, *Org. Lett.*, 2012, **14**, 1370-1373.
10. X. Feng, Y. Cheng, K. Yang, J. Zhang, Q. Wu and T. Xu, *J. Phys. Chem. B*, 2010, **114**, 11017-11026.
11. J. Hu, Y. Cheng, Y. Ma, Q. Wu and T. Xu, *J. Phys. Chem. B*, 2009, **113**, 64-74.
12. K. Yang, L. Weng, Y. Cheng, H. Zhang, J. Zhang, Q. Wu and T. Xu, *J. Phys. Chem. B*, 2011, **115**, 2185-2195.
13. L. Zhao, Y. Cheng, J. Hu, Q. Wu and T. Xu, *J. Phys. Chem. B*, 2009, **113**, 14172-14179.

14. E. N. Coker, W. A. Steen, J. T. Miller, A. J. Kropf and J. E. Miller, *J. Mater. Chem.*, 2007, **17**, 3330-3340.

15. J. Eckert, F. R. Trouw, B. Mojet, P. Forster and R. Lobo, *J. Nanosci. Nanotechnol.*, 2010, **10**, 49-59.

16. X. Solans-Monfort, M. Sodupe and J. Eckert, *J. Phys. Chem. C*, 2010, **114**, 13926-13934.

17. J. Alvarez and M. Gomez-Kaifer, *Chem. Commun.*, 1998, 1455-1456.

18. T. Ishi-i, M. Crego-Calama, P. Timmerman, D. N. Reinhoudt and S. Shinkai, *J. Am. Chem. Soc.*, 2002, **124**, 14631-14641.

19. S. Kunsagi-Mate, G. Nagy and L. Kollar, *Sens. Actuators, B*, 2001, **76**, 545-550.

20. J. W. Steed, R. K. Juneja, R. S. Burkhalter and J. L. Atwood, *J. Chem. Soc., Chem. Commun.*, 1994, 2205-2206.

21. A. N. Basuray, d. R. H.-P. Jacquot, K. J. Hartlieb, T. Kikuchi, N. L. Strutt, C. J. Bruns, M. W. Ambrogio, A.-J. Avestro, S. T. Schneebeli, A. C. Fahrenbach and J. F. Stoddart, *Angew. Chem., Int. Ed.*, 2012, **51**, 11872-11877.

22. D. J. Cram and D. Y. Sogah, *J. Am. Chem. Soc.*, 1985, **107**, 8301-8302.

23. S. S. Peacock, D. M. Walba, F. C. A. Gaeta, R. C. Helgeson and D. J. Cram, *J. Am. Chem. Soc.*, 1980, **102**, 2043-2052.

24. O. E. Sielcken, T. M. M. Van, M. F. M. Roks, R. Hendriks, W. Drenth and R. J. M. Nolte, *J. Am. Chem. Soc.*, 1987, **109**, 4261-4265.

25. P. Tundo and J. H. Fendler, *J. Am. Chem. Soc.*, 1980, **102**, 1760-1762.

26. C. Dendrinou-Samara, G. Psomas, L. Iordanidis, V. Tangoulis and D. P. Kessissoglou, *Chem. Eur. J.*, 2001, **7**, 5041-5051.

27. J. Jankolovits, C.-S. Lim, G. Mezei, J. W. Kampf and V. L. Pecoraro, *Inorg. Chem.*, 2012, **51**, 4527-4538.

28. C.-S. Lim, J. Jankolovits, P. Zhao, J. W. Kampf and V. L. Pecoraro, *Inorg. Chem.*, 2011, **50**, 4832-4841.

29. M. Tegoni and M. Remelli, *Coord. Chem. Rev.*, 2012, **256**, 289-315.

30. Y. Ma, X. Ji, F. Xiang, X. Chi, C. Han, J. He, Z. Abliz, W. Chen and F. Huang, *Chem. Commun.*, 2011, **47**, 12340-12342.

31. S. R. Peerannawar and S. P. Gejji, *Phys. Chem. Chem. Phys.*, 2012, **14**, 8711-8722.

32. N. L. Strutt, R. S. Forgan, J. M. Spruell, Y. Y. Botros and J. F. Stoddart, *J. Am. Chem. Soc.*, 2011, **133**, 5668-5671.

33. F. Biedermann, E. Elmalem, I. Ghosh, W. M. Nau and O. A. Scherman, *Angew. Chem., Int. Ed.*, 2012, **51**, 7739-7743, S7739/7731-S7739/7721.

34. K. Kim, N. Selvapalam, Y. H. Ko, K. M. Park, D. Kim and J. Kim, *Chem. Soc. Rev.*, 2007, **36**, 267-279.

35. T.-C. Lee, E. Kalenius, A. I. Lazar, K. I. Assaf, N. Kuhnert, C. H. Gruen, J. Jaenis, O. A. Scherman and W. M. Nau, *Nat. Chem.*, 2013, **5**, 376-382.

36. M. V. Rekharsky, H. Yamamura, C. Inoue, M. Kawai, I. Osaka, R. Arakawa, K. Shiba, A. Sato, Y. H. Ko, N. Selvapalam, K. Kim and Y. Inoue, *J. Am. Chem. Soc.*, 2006, **128**, 14871-14880.

37. R. J. Blanch, M. Williams, G. D. Fallon, M. G. Gardiner, R. Kaddour and C. L. Raston, *Angew. Chem., Int. Ed.*, 1997, **36**, 504-506.

38. K. T. Holman, M. M. Halihan, S. S. Jurisson, J. L. Atwood, R. S. Burkhalter, A. R. Mitchell and J. W. Steed, *J. Am. Chem. Soc.*, 1996, **118**, 9567-9576.

39. H. K. Travis, O. G. William, J. L. Atwood and J. W. Steed, *Chem. Commun.*, 1998, 2109-2110.

40. T. Brotin and J.-P. Dutasta, *Chem. Rev.*, 2009, **109**, 88-130.

41. P. A. Hill, Q. Wei, T. Troxler and I. J. Dmochowski, *J. Am. Chem. Soc.*, 2009, **131**, 3069-3077.

42. G. Huber, T. Brotin, L. Dubois, H. Desvaux, J.-P. Dutasta and P. Berthault, *J. Am. Chem. Soc.*, 2006, **128**, 6239-6246.

43. E. J. Ruiz, D. N. Sears, A. Pines and C. J. Jameson, *J. Am. Chem. Soc.*, 2006, **128**, 16980-16988.

44. J. A. Bryant, M. T. Blanda, M. Vincenti and D. J. Cram, *J. Am. Chem. Soc.*, 1991, **113**, 2167-2172.

45. L. R. MacGillivray and J. L. Atwood, *Angew. Chem., Int. Ed.*, 1999, **38**, 1018-1033.

46. L. M. Nuwaysir, J. A. Castoro, C. L. C. Yang and C. L. Wilkins, *J. Am. Chem. Soc.*, 1992, **114**, 5748-5751.

47. M. Bayrakci, S. Ertul and M. Yilmaz, *J. Chem. Eng. Data*, 2012, **57**, 233-239.

48. M. Fang, J. Zhang, Q. Wu, T. Xu and Y. Cheng, *J. Phys. Chem. B*, 2012, **116**, 3075-3082.

49. N. A. Peppas, P. Bures, W. Leobandung and H. Ichikawa, *Eur. J. Pharm. Biopharm.*, 2000, **50**, 27-46.

50. A. Suvitha, N. S. Venkataramanan, H. Mizuseki, Y. Kawazoe and N. Ohuchi, *J. Inclusion Phenom. Macrocyclic Chem.*, 2010, **66**, 213-218.

51. P. Gupta, K. Vermani and S. Garg, *Drug Discov.Today*, 2002, **7**, 569-579.

52. A. Arora and S. Damodaran, *J. Am. Oil Chem. Soc.*, 2010, **87**, 673-679.

53. G. Astray, C. Gonzalez-Barreiro, J. C. Mejuto, R. Rial-Otero and J. Simal-Gandara, *Food Hydrocolloids*, 2009, **23**, 1631-1640.

54. B. Sancey, G. Trunfio, J. Charles, P. M. Badot and G. Crini, *J. Inclusion Phenom. Macrocyclic Chem.*, 2011, **70**, 315-320.

55. S. Fourmentin, M. Outirite, P. Blach, D. Landy, A. Ponchel, E. Monflier and G. Surpateanu, *J. Hazard. Mater.*, 2007, **141**, 92-97.

56. W. C. E. Schofield, C. D. Bain and J. P. S. Badyal, *Chem. Mater.*, 2012, **24**, 1645-1653.

57. Y. Yu, X. Chen, Y. Wei, J.-H. Liu and X.-J. Huang, *Anal. Chem.*, 2012, **84**, 9818-9824.

58. G. Zhu, L. Wu, X. Zhang, W. Liu, X. Zhang and J. Chen, *Chem. Eur. J.*, 2013, **19**, 6368-6373.

59. R. M. Fairchild, A. I. Joseph, K. T. Holman, H. A. Fogarty, T. Brotin, J.-P. Dutasta, C. Boutin, G. Huber and P. Berthault, *J. Am. Chem. Soc.*, 2010, **132**, 15505-15507.

60. G. Cravotto, A. Binello, E. Baranelli, P. Carraro and F. Trotta, *Curr. Nutr. Food Sci.*, 2006, **2**, 343-350.

61. T. Korpela, P. Mattsson, J. Hellman, S. Paavilainen and M. Makela, *Food Biotechnol.*, 1989, **2**, 199-210.

62. K. Lindner, L. Szente and J. Szejtli, *Acta Aliment.*, 1981, **10**, 175-186.

63. G. D. Airey and M. H. Mohammed, *Rheologica Acta*, 2008, **47**, 751-763.

64. W. Musial, *Chem. Pharm. Bull.*, 2007, **55**, 1141-1147.

65. N. Pallua and T. P. Wolter, *Plast. Reconstr. Surg.*, 2010, **125**, 1797-1804.

66. M. Freitag and E. Galoppini, *Energy Environ. Sci.*, 2011, **4**, 2482-2494.

67. C. Botta, P. Betti and M. Pasini, *J. Mater. Chem. A*, 2013, **1**, 510-514.

68. G. Calzaferri, *Top. Catal.*, 2010, **53**, 130-140.

69. G. Calzaferri, M. Pauchard, H. Maas, S. Huber, A. Khatyr and T. Schaafsma, *J. Mater. Chem.*, 2002, **12**, 1-13.

70. X. Li, M. Wang, D. Zheng, K. Han, J. Dong and L. Sun, *Energy Environ. Sci.*, 2012, **5**, 8220-8224.

71. P. Montes-Navajas, L. A. Baumes, A. Corma and H. Garcia, *Tetrahedron Lett.*, 2009, **50**, 2301-2304.

72. P. Thordarson, *Chem. Soc. Rev.*, 2011, **40**, 1305-1323.

73. T. Loftsson, S. B. Vogensen, M. E. Brewster and F. Konraosdottir, *J. Pharm. Sci.*, 2007, **96**, 2532-2546.

74. H. E. Junginger and J. C. Verhoef, *Pharm. Sci. Technol. Today*, 1998, **1**, 370-376.

75. Z. Kejik, R. Kaplanek, T. Briza, J. Kralova, P. Martasek and V. Kral, *Supramol. Chem.*, 2012, **24**, 106-116.

76. P. K. Dhal, D. A. Gianolio and R. J. Miller, *J. Macromol. Sci., Part A: Pure Appl. Chem.*, 2011, **48**, 994-1003.

77. Z. Kejik, T. Briza, P. Pouckova, J. Kralova, V. Kral and P. Martasek, *J. Controlled Release*, 2008, **132**, e27-e28.

78. C. Y. Ang, S. Y. Tan, X. Wang, Q. Zhang, M. Khan, L. Bai, S. Tamil Selvan, X. Ma, L. Zhu, K. T. Nguyen, N. S. Tan and Y. Zhao, *J. Mater. Chem. B*, 2014, **2**, 1879-1890.

79. T. Harada, H. L. McTernan, D.-T. Pham, S. F. Lincoln and T. W. Kee, *J. Phys. Chem. B*, 2015, **119**, 2425-2433.

80. T. Harada, D.-T. Pham, S. F. Lincoln and T. W. Kee, *J. Phys. Chem. B*, 2014, **118**, 9515-9523.

81. T. Harada, L. Giorgio, T. J. Harris, D.-T. Pham, H. T. Ngo, E. F. Need, B. J. Coventry, S. F. Lincoln, C. J. Easton, G. Buchanan and T. W. Kee, *Mol. Pharmaceutics*, 2013, **10**, 4481-4490.

82. M. H. M. Leung, T. Harada and T. W. Kee, *Curr. Pharm. Des.*, 2013, **19**, 2070-2083.

83. Y. Huang, S.-F. Xue, Z. Tao, Q.-J. Zhu, H. Zhang, J.-X. Lin and D.-H. Yu, *J. Inclusion Phenom. Macrocyclic Chem.*, 2008, **61**, 171-177.

84. T. Harada, D.-T. Pham, M. H. M. Leung, H. T. Ngo, S. F. Lincoln, C. J. Easton and T. W. Kee, *J. Phys. Chem. B*, 2011, **115**, 1268-1274.

85. A. Braibanti, E. Fisicaro, A. Ghiozzi, C. Compari and G. Bovis, *React. Funct. Polym.*, 1998, **36**, 251-255.

86. H. T. Ngo, P. Clements, C. J. Easton, D.-T. Pham and S. F. Lincoln, *Aust. J. Chem.*, 2010, **63**, 687-692.

87. J. Zhang and P. X. Ma, *Nano Today*, 2010, **5**, 337-350.

88. W. Saenger, J. Jacob, K. Gessler, T. Steiner, D. Hoffmann, H. Sanbe, K. Koizumi, S. M. Smith and T. Takaha, *Chem. Rev.*, 1998, **98**, 1787-1802.

89. T. Endo, *Trends Glycosci. Glycotechnol.*, 2011, **23**, 79-92.

90. C. J. Easton and S. F. Lincoln, *Chem. Soc. Rev.*, 1996, **25**, 163-170.

91. K. Kano, M. Tatsumi and S. Hashimoto, *J. Org. Chem.*, 1991, **56**, 6579-6585.

92. K. Kano, H. Matsumoto, S. Hashimoto, M. Sisido and Y. Imanishi, *J. Am. Chem. Soc.*, 1985, **107**, 6117-6118.

93. N. Kobayashi, R. Saito, Y. Hino, A. Ueno and T. Osa, *J. Chem. Soc., Chem. Commun.*, 1982, 706-707.

94. S. F. Lincoln and D.-T. Pham, *Cyclodextrins: From Nature to Nanotechnology, Chapter 10 in Supramolecular Chemistry: From Molecules to Nanomaterials*, 2012. P. A. Gale and J. W. Steed (eds), John Wiley & Sons Ltd., Chichester, UK, pp. 955-982.

95. S. F. Lincoln and C. J. Easton, *Inclusion Complexes of the Cyclodextrins, Chapter 14 in Polysaccharides*, 1998. S. Dimitriu (ed), Dekker, New York, NY, pp. 473-521.

96. M. V. Rekharsky and Y. Inoue, *Chem. Rev.*, 1998, **98**, 1875-1917.

97. A. R. Khan, P. Forgo, K. J. Stine and V. T. D'Souza, *Chem. Rev.*, 1998, **98**, 1977-1996.

98. A. P. Croft and R. A. Bartsch, *Tetrahedron*, 1983, **39**, 1417-1474.

99. D.-T. Pham, H. T. Ngo, S. F. Lincoln, B. L. May and C. J. Easton, *Tetrahedron*, 2010, **66**, 2895-2898.

100. R. Palin, S. J. A. Grove, A. B. Prosser and M.-Q. Zhang, *Tetrahedron Lett.*, 2001, **42**, 8897-8899.

101. C. J. Easton, S. J. van Eyk, S. F. Lincoln, B. L. May, J. Papageorgiou and M. L. Williams, *Aust. J. Chem.*, 1997, **50**, 9-12.

102. A. Mulder, J. Huskens and D. N. Reinhoudt, *Eur. J. Org. Chem.*, 2005, 838-846.

103. M.-M. Luo, W.-H. Chen, D.-Q. Yuan and R.-G. Xie, *Synth. Commun.*, 1998, **28**, 3845-3848.

104. H.-T. Nguyen, D.-T. Pham, S. F. Lincoln, J. Wang, X. Guo, C. J. Easton and R. K. Prud'homme, *Polym. Chem.*, 2013, **4**, 820-829.

105. H.-T. Nguyen, D.-T. Pham, C. J. Easton and S. F. Lincoln, *Aust. J. Chem.*, 2013, **66**, 1057-1064.

106. M. Sun, H. Zhang, X. Hu, B. Liu and Y. Liu, *Chin. J. Chem.*, 2014, **32**, 771-776.

107. T. Jiang, M. Li and D. S. Lawrence, *J. Org. Chem.*, 1995, **60**, 7293-7297.

108. Y. Liu, C.-F. Ke, H.-Y. Zhang, J. Cui and F. Ding, *J. Am. Chem. Soc.*, 2008, **130**, 600-605.

109. Z.-Q. Li, Y.-M. Zhang, H.-Z. Chen, J. Zhao and Y. Liu, *J. Org. Chem.*, 2013, **78**, 5110-5114.

110. Z.-Q. Li, Y.-M. Zhang, D.-S. Guo, H.-Z. Chen and Y. Liu, *Chem. Eur. J.*, 2013, **19**, 96-100.

111. Y. Liu and Y. Chen, *Acc. Chem. Res.*, 2006, **39**, 681-691.

112. R. R. French, J. Wirz and W.-D. Woggon, *Helv. Chim. Acta*, 1998, **81**, 1521-1527.

113. R. R. French, P. Holzer, M. G. Leuenberger and W.-D. Woggon, *Angew. Chem., Int. Ed.*, 2000, **39**, 1267-1269.

114. K. J. Buchanan, B. Hird and T. M. Letcher, *Polym. Bull.*, 1986, **15**, 325-332.

115. L. Li, X. Guo, J. Wang, P. Liu, R. K. Prud'homme, B. L. May and S. F. Lincoln, *Macromolecules*, 2008, **41**, 8677-8681.

116. X. Guo, J. Wang, L. Li, D. T. Pham, P. Clements, S. F. Lincoln, B. L. May, Q. Chen, L. Zheng and R. K. Prud'homme, *Macromol. Rapid Commun.*, 2010, **31**, 300-304.

117. K. Schillen, D. F. Anghel, M. da Graca Miguel and B. Lindman, *Langmuir*, 2000, **16**, 10528-10539.

118. I. Tomatsu, A. Hashidzume and A. Harada, *Macromol. Rapid Commun.*, 2005, **26**, 825-829.

119. E. A. Appel, J. del Barrio, X. J. Loh and O. A. Scherman, *Chem. Soc. Rev.*, 2012, **41**, 6195-6214.

120. Y. Li, J. Rodrigues and H. Tomas, *Chem. Soc. Rev.*, 2012, **41**, 2193-2221.

121. A. Doering, W. Birnbaum and D. Kuckling, *Chem. Soc. Rev.*, 2013, **42**, 7391-7420.

122. D. M. Ryan and B. L. Nilsson, *Polym. Chem.*, 2012, **3**, 18-33.

123. N. A. Peppas, J. Z. Hilt, A. Khademhosseini and R. Langer, *Adv. Mater.*, 2006, **18**, 1345-1360.

124. A. Harada, Y. Takashima and M. Nakahata, *Acc. Chem. Res.*, 2014, **47**, 2128-2140.

125. J. Li, *Adv. Polym. Sci.*, 2009, **222**, 79-113.

126. K. L. Liu, Z. Zhang and J. Li, *Soft Matter*, 2011, **7**, 11290-11297.

127. K. Y. Lee and D. J. Mooney, *Chem. Rev.*, 2001, **101**, 1869-1879.

128. J. Wang, D.-T. Pham, T. W. Kee, S. N. Clafton, X. Guo, P. Clements, S. F. Lincoln, R. K. Prud'homme and C. J. Easton, *Macromolecules*, 2011, **44**, 9782-9791.

129. J. Wang, D.-T. Pham, X. Guo, L. Li, S. F. Lincoln, Z. Luo, H. Ke, L. Zheng and R. K. Prud'homme, *Ind. Eng. Chem. Res.*, 2010, **49**, 609-612.

130. X. Guo, J. Wang, L. Li, Q. Chen, L. Zheng, D.-T. Pham, S. F. Lincoln, B. L. May, R. K. Prud'homme and C. J. Easton, *AIChE J.*, 2010, **56**, 3021-3024.

131. J. Wang, L. Li, X. Guo, L. Zheng, D.-T. Pham, S. F. Lincoln, H. T. Ngo, P. Clements, B. L. May, R. K. Prud'homme and C. J. Easton, *Ind. Eng. Chem. Res.*, 2011, **50**, 7566-7571.

132. A. Bertrand, M. Stenzel, E. Fleury and J. Bernard, *Polym. Chem.*, 2012, **3**, 377-383.

133. J. L. Hoard, *Science*, 1971, **174**, 1295-1302.

134. E. B. Fleischer, *Acc. Chem. Res.*, 1970, **3**, 105-112.

135. P. S. Song, *Annu. Rep. Prog. Chem., Sect. B*, 1978, **74**, 18-40.

136. R. F. Pasternack, P. R. Huber, P. Boyd, G. Engasser, L. Francesconi, E. Gibbs, P. Fasella, G. Cerio Venturo and L. d. Hinds, *J. Amer. Chem. Soc.*, 1972, **94**, 4511-4517.

137. R. F. Pasternack, *Ann. N. Y. Acad. Sci.*, 1973, **206**, 614-630.

138. R. F. Pasternack, L. Francesconi, D. Raff and E. Spiro, *Inorg. Chem.*, 1973, **12**, 2606-2611.

139. A. D. Adler, F. R. Longo, J. D. Finarelli, J. Goldmacher, J. Assour and L. Korsakoff, *J. Org. Chem.*, 1967, **32**, 476.

140. D. Ostfeld and M. Tsutsui, *Acc. Chem. Res.*, 1974, **7**, 52-58.

141. K. Kano, T. Miyake, K. Uomoto, T. Sato, T. Ogawa and S. Hashimoto, *Chem. Lett.*, 1983, 1867-1870.

142. K. Kano, T. Nakajima, M. Takei and S. Hashimoto, *Bull. Chem. Soc. Jpn.*, 1987, **60**, 1281-1287.

143. K. Kano, T. Nakajima and S. Hashimoto, *J. Phys. Chem.*, 1987, **91**, 6614-6619.

144. K. Kano, T. Sato, S. Yamada and T. Ogawa, *J. Phys. Chem.*, 1983, **87**, 566-569.

145. T. Sato, T. Ogawa and K. Kano, *J. Phys. Chem.*, 1984, **88**, 3678-3682.

146. K. Kano, N. Tanaka, H. Minamizono and Y. Kawakita, *Chem. Lett.*, 1996, 925-926.

147. G. Garcia, V. Sol, F. Lamarche, R. Granet, M. Guilloton, Y. Champavier and P. Krausz, *Bioorg. Med. Chem. Lett.*, 2006, **16**, 3188-3192.

148. L. J. Twyman, A. Ellis and P. J. Gittins, *Macromolecules*, 2011, **44**, 6365-6369.

149. L. Sun, H. Chen, Z. Zhang, Q. Yang, H. Tong, A. Xu and C. Wang, *J. Inorg. Biochem.*, 2012, **108**, 47-52.

150. J. M. Dabrowski, M. M. Pereira, L. G. Arnaut, C. J. P. Monteiro, A. F. Peixoto, A. Karocki, K. Urbanska and G. Stochel, *Photochem. Photobiol.*, 2007, **83**, 897-903.

151. W. Nam, *Acc. Chem. Res.*, 2007, **40**, 522-531.

152. D. Ostovic and T. C. Bruice, *Acc. Chem. Res.*, 1992, **25**, 314-320.

153. R. Zhang and M. Newcomb, *Acc. Chem. Res.*, 2008, **41**, 468-477.

154. E. B. Fleischer, J. M. Palmer, T. S. Srivastava and A. Chatterjee, *J. Amer. Chem. Soc.*, 1971, **93**, 3162-3167.

155. K. M. Smith, G. M. F. Bisset, J. J. Case and H. D. Tabba, *Tetrahedron Lett.*, 1980, **21**, 3747-3750.

156. B. Mestre, A. Jakobs, G. Pratviel and B. Meunier, *Biochemistry*, 1996, **35**, 9140-9149.

157. T. Nakazono, A. R. Parent and K. Sakai, *Chem. Commun.*, 2013, **49**, 6325-6327.

158. A. Uetomo, M. Kozaki, S. Suzuki, K.-i. Yamanaka, O. Ito and K. Okada, *J. Am. Chem. Soc.*, 2011, **133**, 13276-13279.

159. G. Harrach, Z. Valicsek and O. Horvath, *Inorg. Chem. Commun.*, 2011, **14**, 1756-1761.

160. A. Cnossen, L. Hou, M. M. Pollard, P. V. Wesenhagen, W. R. Browne and B. L. Feringa, *J. Am. Chem. Soc.*, 2012, **134**, 17613-17619.

161. J. A. Mercer-Smith and D. G. Whitten, *J. Am. Chem. Soc.*, 1978, **100**, 2620-2625.

162. J. Bonin, M. Chaussemier, M. Robert and M. Routier, *ChemCatChem*, 2014, **6**, 3200-3207.

163. C. Costentin, G. Passard, M. Robert and J.-M. Saveant, *J. Am. Chem. Soc.*, 2014, **136**, 11821-11829.

164. K. Kano, M. Takeuchi, S. Hashimoto and Z. Yoshida, *J. Chem. Soc., Chem. Commun.*, 1991, 1728-1729.

165. J. Luo, M. Xu, R. Li, K.-W. Huang, C. Jiang, Q. Qi, W. Zeng, J. Zhang, C. Chi, P. Wang and J. Wu, *J. Am. Chem. Soc.*, 2014, **136**, 265-272.

166. C. Stangel, A. Bagaki, P. A. Angaridis, G. Charalambidis, G. D. Sharma and A. G. Coutsolelos, *Inorg. Chem.*, 2014, **53**, 11871-11881.

167. C. Vijay Kumar, L. Cabau, E. N. Koukaras, E. J. Palomares and G. D. Sharma, *Nanoscale*, 2015, **7**, 179-189.

168. S. H. Kang, M. S. Kang, I. T. Choi, J. Y. Hong, M. J. Ju and H. K. Kim, *ChemElectroChem*, 2014, **1**, 637-644, 638 pp.

169. M. Fathalla, A. Neuberger, S.-C. Li, R. Schmehl, U. Diebold and J. Jayawickramarajah, *J. Am. Chem. Soc.*, 2010, **132**, 9966-9967.

170. C. Zou and C.-D. Wu, *Dalton Trans.*, 2012, **41**, 3879-3888.

171. O. Oviedo, T. Zoltan, F. Vargas, M. Inojosa and J. C. Vivas, *J. Coord. Chem.*, 2014, **67**, 1715-1730.

172. X. Liang, X. Li, L. Jing, X. Yue and Z. Dai, *Biomaterials*, 2014, **35**, 6379-6388.

173. S. Swavey, *Global J. Inorg. Chem.*, 2012, **3**, 9/1-9/14.

174. A. Juzeniene, Q. Peng and J. Moan, *Photochem. Photobiol. Sci.*, 2007, **6**, 1234-1245.

175. E. A. Strecker, H. P. Palmer and F. G. Braceland, *Sem. Med.*, 1935, **I**, 1534-1541.

176. J. Lai and M. Cooney, *Int. Ophthalmol. Clin.*, 1999, **39**, 163-174.

177. R. Bonnett, *Chem. Soc. Rev.*, 1995, **24**, 19-33.

178. M. Ethirajan, Y. Chen, P. Joshi and R. K. Pandey, *Chem. Soc. Rev.*, 2011, **40**, 340-362.

179. A. Mazzaglia, *Photodynamic Tumour Therapy with Cyclodextrin Nanoassemblies, Chapter 18 in Cyclodextrins in Pharmaceutics, Cosmetics, and Biomedicine*, 2011. E. Bilensoy (ed). John Wiley & Sons, Inc. Hoboken, NJ, pp. 343-361.

180. S. Hamai and T. Koshiyama, *J. Photochem. Photobiol., A*, 1999, **127**, 135-141.

181. F. Venema, A. E. Rowan and R. J. M. Nolte, *J. Am. Chem. Soc.*, 1996, **118**, 257-258.

182. J. Mosinger, M. Deumie, K. Lang, P. Kubat and D. M. Wagnerova, *J. Photochem. Photobiol., A*, 2000, **130**, 13-20.

183. J. Mosinger, L. Slavetinska, K. Lang, P. Coufal and P. Kubat, *Org. Biomol. Chem.*, 2009, **7**, 3797-3804.

184. Y. Liu, J.-H. Pan, Y.-L. Wei and Y. Zhang, *Talanta*, 2004, **63**, 581-584.

185. S. Hamai and T. Ohshida, *J. Inclusion Phenom. Macrocyclic Chem.*, 2004, **50**, 209-217.

186. J. Mosinger, V. Kliment, Jr., J. Sejbal, P. Kubat and K. Lang, *J. Porphyrins Phthalocyanines*, 2002, **6**, 514-526.

187. X.-P. Wang, J.-H. Pan, S.-M. Shuang and Y. Zhang, *Supramol. Chem.*, 2002, **14**, 419-426.

188. Y. Wang, B. Cohen, A. Aykac, A. Vargas-Berenguel and A. Douhal, *Photochem. Photobiol. Sci.*, 2013, **12**, 2119-2129.

189. F. Venema, H. F. M. Nelissen, P. Berthault, N. Birlirakis, A. E. Rowan, M. C. Feiters and R. J. M. Nolte, *Chem. Eur. J.*, 1998, **4**, 2237-2250.

190. K. Kano, H. Kitagishi, M. Kodera and S. Hirota, *Angew. Chem., Int. Ed.*, 2005, **44**, 435-438.

191. K. Watanabe, H. Kitagishi and K. Kano, *ACS Med. Chem. Lett.*, 2011, **2**, 943-947.

192. K. Watanabe, H. Kitagishi and K. Kano, *Angew. Chem., Int. Ed.*, 2013, **52**, 6894-6897.

193. K. Kano, Y. Itoh, H. Kitagishi, T. Hayashi and S. Hirota, *J. Am. Chem. Soc.*, 2008, **130**, 8006-8015.

194. K. Kano, H. Kitagishi, T. Mabuchi, M. Kodera and S. Hirota, *Chem. Asian J.*, 2006, **1**, 358-366.

195. K. Kano, H. Kitagishi, C. Dagallier, M. Kodera, T. Matsuo, T. Hayashi, Y. Hisaeda and S. Hirota, *Inorg. Chem.*, 2006, **45**, 4448-4460.

196. Y.-h. Chao, J.-F. Jheng, J.-S. Wu, K.-Y. Wu, H.-H. Peng, M.-C. Tsai, C.-L. Wang, Y.-N. Hsiao, C.-L. Wang, C.-Y. Lin and C.-S. Hsu, *Adv. Mater.*, 2014, **26**, 5205-5210.

197. G. Sedghi, V. M. Garcia-Suarez, L. J. Esdaile, H. L. Anderson, C. J. Lambert, S. Martin, D. Bethell, S. J. Higgins, M. Elliott, N. Bennett, J. E. MacDonald and R. J. Nichols, *Nat. Nanotechnol.*, 2011, **6**, 517-523.

198. L. Wang, H. Li, G. Fang, J. Zhou and D. Cao, *Sens. Actuators, B*, 2014, **196**, 653-662.

199. M. Sun, H.-Y. Zhang, B.-W. Liu and Y. Liu, *Macromolecules*, 2013, **46**, 4268-4275.

200. Y. Kobayashi, Y. Takashima, A. Hashidzume, H. Yamaguchi and A. Harada, *Sci. Rep.*, 2013, **3**, 1243-1244.

201. K. Kano, T. Ochi, S. Okunaka, Y. Ota, K. Karasugi, T. Ueda and H. Kitagishi, *Chem. Asian J.*, 2011, **6**, 2946-2955.

202. T. Ueda, H. Kitagishi and K. Kano, *Org. Biomol. Chem.*, 2012, **10**, 4337-4347.

This page is intentionally left blank

Chapter 2

Complexation of 5,10,15,20-Tetra(*p*-sulfonatophenyl)porphyrin by γ-Cyclodextrin, Linked γ-Cyclodextrin Dimers and a Linked γ-Cyclodextrin Trimer

2.1. INTRODUCTION

2.1.1. General

Cyclodextrins (CDs) have proven to be good transporters for a wide array of biologically active molecules. Their relatively low cost, low toxicity and ease of modification have made them the centrepiece of a number of pharmacological studies.[1-3] Complexation of pharmaceutical compounds within a CD species can increase their specificity in some biological systems. Furthermore, they allow controlled drug release, prevent biological degradation, decrease side effects, mask tastes and odours and increase bioavailability.[4,5]

Covalently linked CD dimers, trimers and oligomers have shown enhanced complexation of biologically active molecules by comparison with complexation by native CDs.[6,7] Multiple linked CDs can create a cooperative complexing effect that forms particularly stable host-guest complexes.[8] Extensive research has been conducted into the host-guest complexation by β-CD and its oligomers,[9-13] yet such complexation by γ-CD and its oligomers is relatively little studied.[3,14,15] The larger annuli of γ-CD species allow for larger molecules to be encapsulated in host-guest complexes. This property may be utilized in the complexation of many important compounds such as polycyclic aromatic hydrocarbons,[16,17] large hydrophobic drugs,[18,19] steroids[20,21] and porphyrins.[22,23]

Porphyrins are large aromatic heterocyclic macrocycles pivotal in many plant and animal biological processes. They are sought after because of their high functionality and possess a number of interesting properties such as a broad UV-vis absorbance spectrum, strong fluorescence emissions, singlet oxygen production[24] and metal ion coordination capabilities.[25] As a consequence of these properties, porphyrins have been employed in a number of applications including DNA binding,[26] oxygen transport,[27-29] light harvesting[30-34] and photodynamic therapy.[24,35-38]

Photodynamic therapy has emerged as a useful tool in the reduction of localized cancers including: ocular, oral, oesophageal, breast, stomach, intestine, prostate, brain, and dermal cancers.[37] This therapy relies on photosensitisers which are activated by specific wavelengths of light and result in photochemical processes that cause irreversible damage in cancer tissue.[39] A large portion of photosensitisers are based on porphyrins due to their highly conjugated structure allowing a broad spectral range for light absorption.[24] Although photodynamic therapy is a promising treatment which is currently employed in the treatment of cancer, it does have some limitations *in vivo* as is next discussed

The majority of photosensitisers are large and hydrophobic, leading to poor aqueous solubility and self-aggregation, thus diminishing their photodynamic potential.[40] They also are cleared by the body relatively quickly, therefore large and frequent dosages are required, which can lead to photosensitivity in patients.[40] Some of these potential limitations may be addressed by complexing the photosensitisers within supramolecular drug transporters exemplified by CDs. This complexation hinders photosensitiser self-aggregation as well as increasing their aqueous solubility.[23] The increased molecular weight of a cyclodextrin-photosensitiser complex allows improved retention of the photosensitiser in the bloodstream, as well as sustained drug release.[40] The complexation ability of native CDs is not usually strong enough for drug transport as the complexation constants are usually in the range 10^2–10^3 mol dm^{-3}. This problem can be addressed by substitution of a single CD or by the use of more extensive modification as exemplified by linked CD dimers.[41-43]

While some studies of linked β-CD dimer-porphyrin complexes have appeared in the literature[41-47] there have been no detailed studies of similar γ-CD complexes through which the effect of CD annular size variation on complexation processes may be assessed. The larger annuli of γ-CD and its oligomers may be more suitable for the complexation of porphyrin photosensitisers, or allow different complexation geometries which differ from

those reported for the linked β-CD dimers. It is known that both *syn* and *anti* conformations of cooperative complexation can occur with various linked β-CD dimers (Figure 2.1).[7,43] The *syn* conformation may be more prevalent in linked γ-CD species as the larger annuli should allow a greater flexibility of fit. Whilst complexation constants for CD-porphyrin host-guest complexes have been determined, few complexation thermodynamic parameters have been reported.[48-50] There are some reports of thermodynamic parameters for the complexation of porphyrins by linked CD dimers; however, these studies focussed on β-CD dimers with bulky, rigid or charged covalent bridges that favour complexation in the *anti* conformation.[45-47] To the best of our knowledge, complexation constants and thermodynamic parameters for complexation of porphyrins by γ-CD oligomers are yet to be reported. Such studies of the fundamental processes behind porphyrin complexation by CDs could lead to more effective photodynamic therapy treatments.

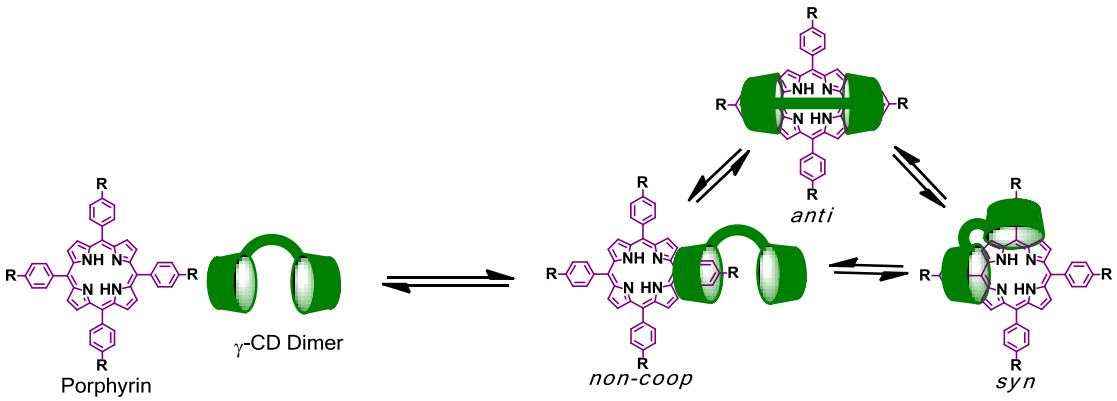

Figure 2.1: Potential cooperative and non-cooperative complexes between porphyrins and linked γ-CD dimers.

2.1.2. Aims of this study

In this study the complexation of the tetra-anionic photosensitiser 5,10,15,20-tetra(*p*-sulfonatophenyl)porphyrinate, H_2TSPP^{4-}, by γ-CD and five of its modified forms are investigated (Figure 2.2). (It has become conventional to indicate the presence of the two NH hydrogens and the 4- charge in the abbreviated formula, H_2TSPP^{4-}.) Two previously reported

succinimide-linked γ-CD dimers, *N*,*N*′-bis(3^{A}-deoxy-γ-cyclodextrin-3^{A}-yl) succinamide (33γ-CD_2suc) and *N*,*N*′-bis(6^{A}-deoxy-γ-cyclodextrin-6^{A}-yl) succinamide (66γ-CD_2suc),[51] two new oxalate-linked γ-CD dimers, *N*,*N*′-bis((2^{A}S,3^{A}S)-3^{A}-deoxy-γ-cyclodextrin-3^{A}-yl) oxalamide (33γ-CD_2ox) and *N*,*N*′-bis(6^{A}-deoxy-γ-cyclodextrin-6^{A}-yl) oxalamide (66γ-CD_2ox), and a new benzene linked γ-CD trimer, 1,3,5-*N*,*N*,*N*-tris(6^{A}-deoxy-6^{A}-γ-cyclodextrin)-benzene (666γ-CD_3bz) are deployed.

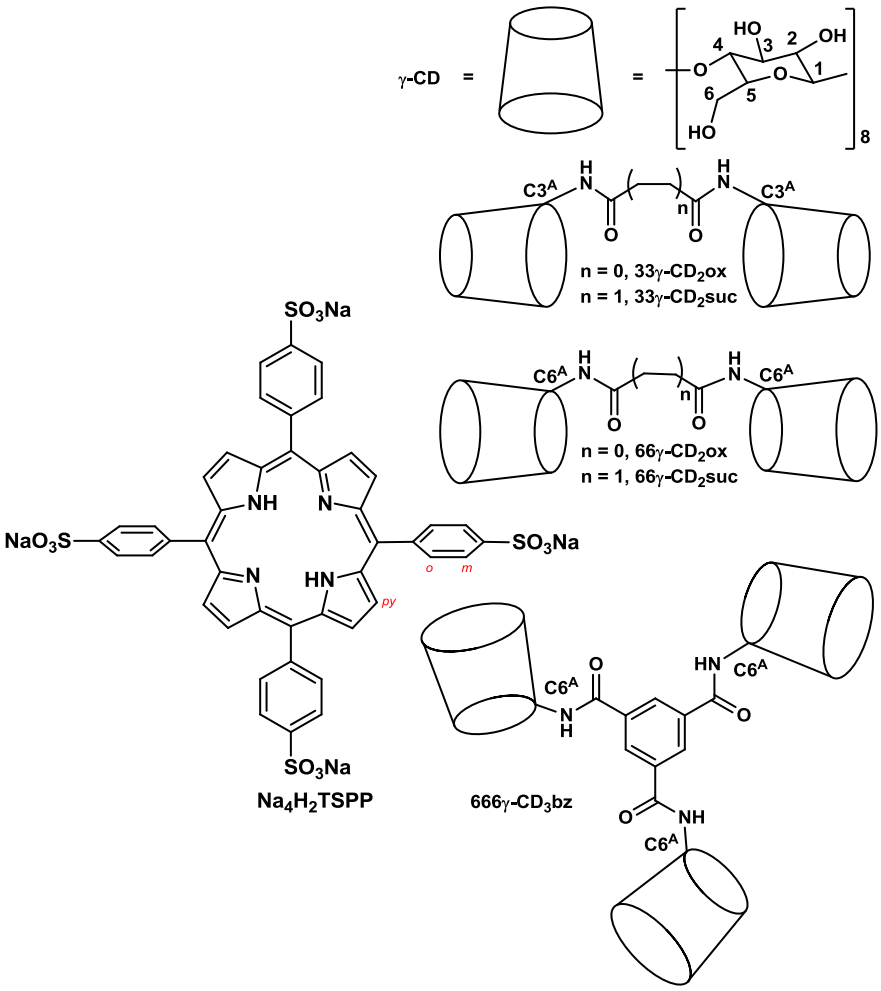

Figure 2.2: γ-Cyclodextrin, γ-CD, and its linked oligomers 33γ-CD_2ox, 33γ-CD_2suc, 66γ-CD_2ox, 66γ-CD_2suc and 666γ-CD_3bz, and the sodium salt of 5,10,15,20-tetra(*p*-sulfonatophenyl)porphyrinate, Na_4H_2TSPP.

The host-guest complexation of the tetraanionic guest H_2TSPP^{4-} by the host γ-CD and its linked oligomers, 33γ-CD_2ox, 66γ-CD_2ox, 33γ-CD_2suc, 66γ-CD_2suc and 666γ-CD_3bz is investigated by 2D ^{1}H NOESY NMR, variable temperature UV-vis spectroscopy and

molecular modelling. These studies are designed to provide insight into the effect of the γ-CD annular orientation (3,3, 6,6 and 6,6,6) as well as the variation in length of the covalent linker between the γ-CD annuli on the nature of the host-guest complexes formed in the γ-CD oligomer/H_2TSPP^{4-} equilibria.

2.2. SYNTHESIS

2.2.1. Sodium 5,10,15,20-Tetra(*p*-sulfonatophenyl)porphyrin, Na_4H_2TSPP

Sodium 5,10,15,20-tetra(*p*-sulfonatophenyl)porphyrin, Na_4H_2TSPP, was prepared from 5,10,15,20-tetraphenyl-porphyrin by a method similar to that reported in the literature.[52]

2.2.2. Succinate and oxalate linked γ-CD dimers

The succinate linked dimers, 33γ-CD_2suc and 66γ-CD_2suc (Figure 2.3), were prepared in 75 % and 92 % yield, respectively, by literature methods.[51] The oxalate linked dimers, 33γ-CD_2ox

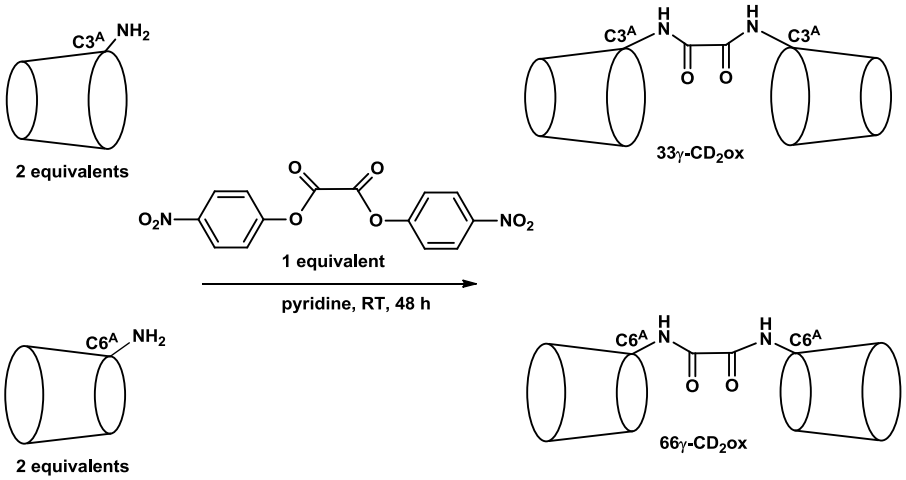

Figure 2.3: Preparation of 33γ-CD_2ox and 66γ-CD_2ox.

and 66γ-CD_2ox, were prepared in 72 % and 60 % yield by modifying the preparation of their succinate analogues[51] by replacing bis(4-nitrophenyl) succinate by bis(4-nitrophenyl) oxalate and retaining all other steps as previously described. Lower yields for the oxalate-linked

dimer preparations than those obtained in the succinate linked dimer preparations were expected for as steric hindrance is increased by the shorter oxalate linker. Experimental and characterisation details appear in Chapter 6.

2.2.3. Benzene linked γ-CD trimer

The benzene linked trimer was prepared by modifying a literature method (Figure 2.4).[12] γ-Cyclodextrin was substituted for β-CD in the literature procedure and all other steps were

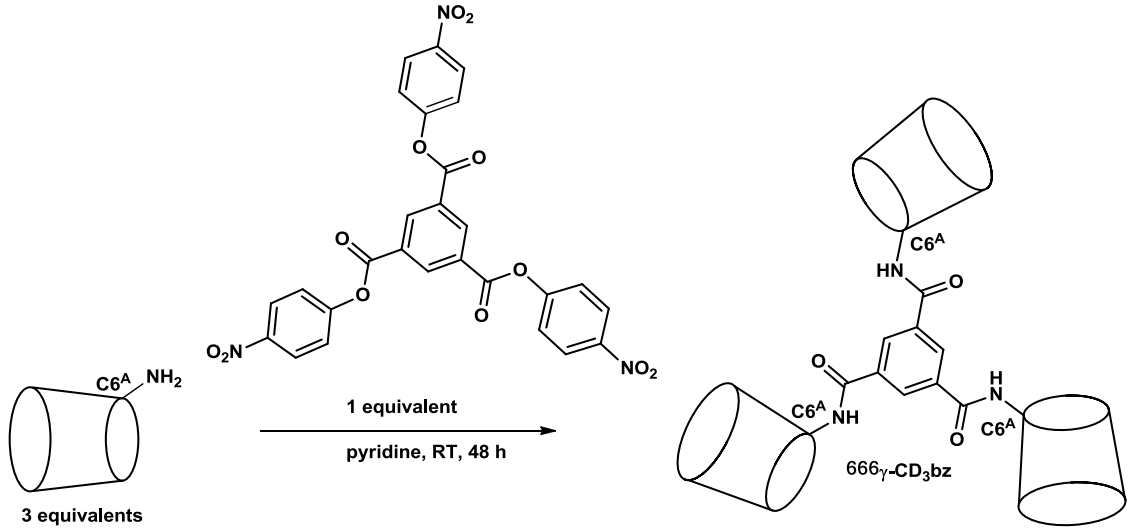

Figure 2.4: Preparation of 666γ-CD_3bz.

as previously described. The reaction afforded 666γ-CD_3bz with a yield of 72 %, slightly higher than that reported for 666β-CD_3bz (68 %).[12] This suggests that the linker is of a sufficient size to accommodate three γ-CD substituents with minimal steric hindrance. Experimental and characterisation details appear in Chapter 6. The dimers and the trimer were characterised by TLC, ^{1}H NMR, ^{13}C NMR, MS and elemental analysis (Chapter 6).

2.3. 2D ^{1}H NOESY NMR STUDIES

While the host-guest complexation equilibria existing between the host γ-CD and its oxalate and succinamide-linked dimers and benzene linked trimer, 33γ-CD_2ox, 33γ-CD_2suc, 66γ-

CD_2ox, 66γ-CD_2suc and 666γ-CD_3bz, and H_2TSPP^{4-} are characterised thermodynamically by UV-vis absorption spectroscopy in section 2.4 of this study, these equilibria are first subjected to investigation by 1D ^{1}H and 2D ^{1}H NOESY NMR spectroscopy to confirm some scattered literature reports of the 1D ^{1}H NMR spectroscopy H_2TSPP^{4-} alone and 1D and 2D ^{1}H NMR of H_2TSPP^{4-} complexed by γ-CD,[23,53-55] and to gain additional insight into the complexation of H_2TSPP^{4-} by γ-CD, 33γ-CD_2ox, 33γ-CD_2suc, 66γ-CD_2ox, 66γ-CD_2suc and 666γ-CD_3bz.

In aqueous solution at neutral pH H_2TSPP^{4-} exists as a tetraanion resulting from deprotonation of the dianion H_4TSPP^{2-} for which pK_{a1} = 4.85 and pK_{a2} = 4.91 in aqueous 0.1 mol dm^{-3} $NaClO_4$ at 298.2 K.[56] The H_2TSPP^{4-} monomer exists in dynamic equilibrium with its dimer in aqueous solution and is characterised by a reported dimerisation constant, K_D = (3.48 ± 0.26) × 10^4 dm^3 mol^{-1} in aqueous phosphate saline buffer at 298 K with ΔH = -19.56 ± 0.06 kJ mol^{-1} and ΔS = 19.27 ± 0.07 J mol^{-1} K^{-1}.[57] (It should be noted that K_D = 2.71 × 10^4 dm^{-3} mol^{-1} at 298.2 K when calculated from these ΔH and ΔS, and it appears that the reported K_D is that determined experimentally at 298 K.) Another study characterised the same equilibrium with (1.54 ± 1.3) × 10^4 dm^3 mol^{-1} in aqueous phosphate buffer at 298.2 K.[53] Thus, it is anticipated that in the present ^{1}H NMR studies where the total H_2TSPP^{4-} concentration is 3.0 × 10^{-3} mol dm^{-3} in D_2O solution a substantial amount of H_2TSPP^{4-} exists in its dimeric form (~90% assuming K_D = (1.54 ± 0.13) × 10^4 dm^3 mol^{-1}). The ^{1}H NMR spectrum of this solution appears in Figure 2.5 from which it is seen that twin doublets arise from AB coupling between the *meta* and *ortho* *p*-sulfonatophenyl protons, H_m (8.23 ppm, J = 7 Hz) and H_o (7.63 ppm, J = 7 Hz), and two broadened pyrrolic proton resonances, H_{py} (7.19 and 8.77 ppm) of equal area arise. This broadening is consistent with a slow to intermediate (NMR timescale) tautomerism of the H_2TSPP^{4-} imine protons.[23,53-55] It is probable that the Na^+ and K^+ of the phosphate buffer partially screen the *p*-sulfonatophenyl group negative

charges and enable the hydrophobic planar porphyrin cores of two H_2TSPP^{4-} to associate as a dimer (sometimes referred to as an 'H face to face dimer') with one H_2TSPP^{4-} plane rotated 45° with respect to the other to minimise sulfonate charge repulsion.

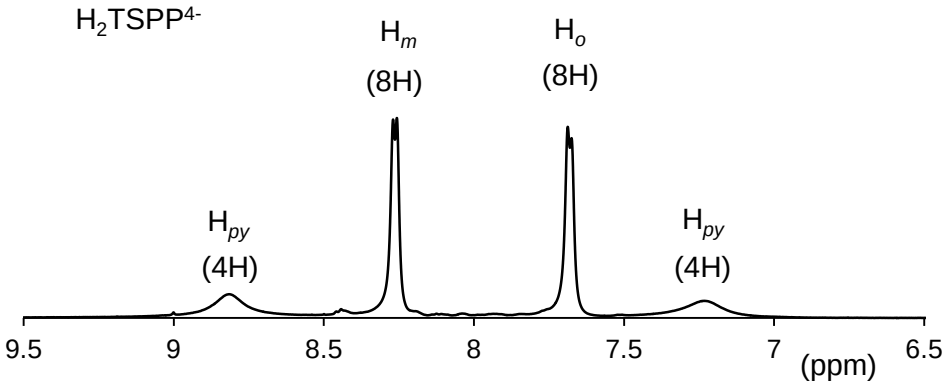

Figure 2.5: ^{1}H NMR (600 MHz) spectrum of a H_2TSPP^{4-} 3.0×10^{-3} mol dm^{-3} solution in D_2O (pD 7.0 phosphate buffer, I = 0.10 mol dm^{-3}) at 298.2 K.

The host–guest complexation of H_2TSPP^{4-} by γ-CD is first examined and the ^{1}H 1D NMR spectrum of a 3.0×10^{-3} mol dm^{-3} γ-CD D_2O solution and of a 3.0×10^{-3} mol dm^{-3} γ-CD and 3.0×10^{-3} mol dm^{-3} H_2TSPP^{4-} D_2O solution appear in Figure 2.6. (Seventy percent of H_2TSPP^{4-} is complexed by γ-CD in this solution, as calculated from the host-guest complexation constants K_{11} and K_{21} for the complexes γ-CD.H_2TSPP^{4-} and γ-CD_2.H_2TSPP^{4-} discussed in Section 2.4, and some of the free H_2TSPP^{4-} is likely to exist as a dimer as discussed above.) Upon complexation with H_2TSPP^{4-}, an upfield shift is observed in the $H_{2\text{-}6}$ resonances of the γ-CD as a consequence of the *p*-sulfonatophenyl groups of H_2TSPP^{4-} complexing within the γ-CD annulus. The resonances for γ-CD H_{6A} and H_{6B} separate and show both greater changes in chemical shift and broadening by comparison with the $H_{2,3,4}$ γ-CD resonances. The multiplets of the $H_{2,4}$ resonances are clearly discerned in the presence of H_2TSPP^{4-} however, their combined area is consistent with their superimposition on a broadened H_5 resonance. The greater chemical shift changes of the $H_{5,6A,6B}$ resonances is consistent with γ-CD complexing H_2TSPP^{4-} though the narrow face of the annulus defined by the primary hydroxyl groups such that $H_{5,6A,6B}$ are closer in to the H_2TSPP^{4-} core and

experience a greater change in magnetic environment and chemical shift than do the $H_{2,3,4}$ protons as shown in Figure 2.7. (The H_1 proton shows minimal interaction with γ-CD and is not further discussed.)

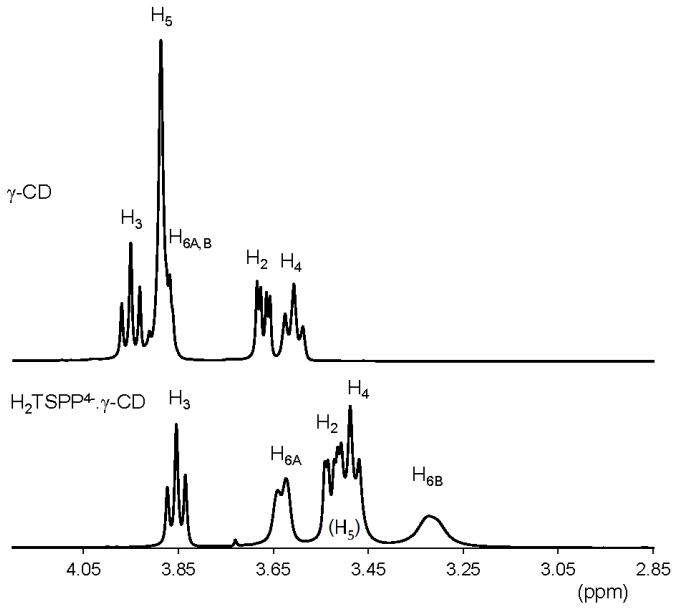

Figure 2.6: Top**,** the $H_{2\text{-}6}$ region of a ^1H NMR (600 MHz) spectrum of a γ-CD (3.0×10^{-3} mol dm^{-3}) solution in D_2O (pD 7.0 phosphate buffer, I = 0.10 mol dm^{-3}) at 298.2 K. Bottom, equimolar solution of H_2TSPP^{4-} and γ-CD under the same experimental conditions.

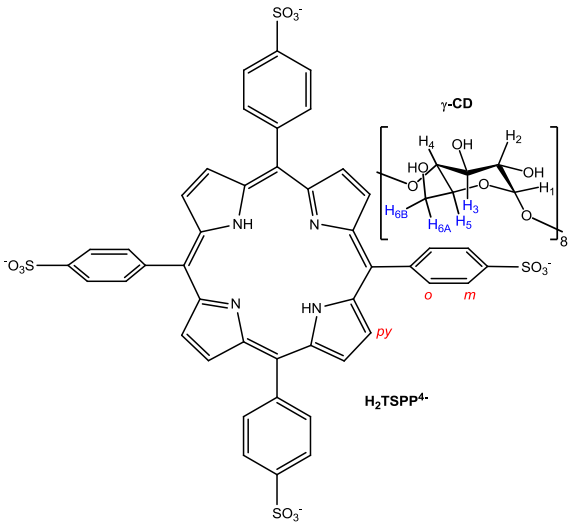

Figure 2.7: The deduced orientation of a single γ-CD complexing H_2TSPP^{4-} and the labelling of the annular γ-CD annular (H_3, H_5, H_{6A}, H_{6B}, blue) and external protons (H_1, H_2, H_4 black) and the H_2TSPP^{4-} pyrrolic and phenyl protons (H_{py}, H_o and H_m, red).

Given the well-defined $H_{2,3,4}$ multiplets observed in the presence of H_2TSPP^{4-} it appears that exchange between the free γ-CD and the complexed γ-CD.H_2TSPP^{4-} and (γ-CD)$_2$.H_2TSPP^{4-} is fast on the NMR timescale for these protons as a consequence of the small chemical shift changes induced by complexation: H_3 δ 3.96 → 3.86 ppm; H_2 δ 3.68 → 3.53 ppm; H_4 δ 3.62 → 3.48 ppm. In contrast, the broadening of the $H_{5,6A,6B}$ resonances indicate that these protons are experiencing exchange between the free γ-CD and the complexed γ-CD.H_2TSPP^{4-} and (γ-CD)$_2$.H_2TSPP^{4-} at an intermediate rate on the NMR timescale which is consistent with their greater changes in magnetic environment and therefore chemical shift: H_5 δ 3.90 → ~ 3.5 ppm;. H_{6A} δ 3.88 → 3.64 ppm; H_{6B} δ 3.88 → 3.34 ppm;

The 2D ^{1}H NOESY NMR spectrum of the 3.0×10^{-3} mol dm^{-3} γ-CD and 3.0×10^{-3} mol dm^{-3} H_2TSPP^{4-} D_2O solution is shown in Figure 2.8 (and Figure A1 in the Appendix), and serves as a comparison for similar spectra of the γ-CD oligomer/H_2TSPP^{4-} solutions. All of the γ-CD $H_{2\text{-}6}$ resonances are separately identified as are the H_2TSPP^{4-} *p*-sulfonatophenyl *meta* and *ortho* hydrogen, H_m and H_o, and pyrrolic hydrogen, H_{py}, resonances. By comparison with the spectrum of H_2TSPP^{4-} alone (Figure 2.5) it is seen that several changes occur: i) only the broad resonance assigned to the downfield H_{py} in the H_2TSPP^{4-} is observed while that of the upfield H_{py} has evidently broadened into the baseline, and ii) the resonance assigned to H_o is now broadened while that assigned to H_m remains a sharp doublet. The origin of the selective broadening of the γ-CD $H_{5,6A,6B}$ resonances has been discussed above in terms of chemical exchange between free γ-CD and the complexed γ-CD.H_2TSPP^{4-} and (γ-CD)$_2$.H_2TSPP^{4-}. This necessarily involves and H_2TSPP^{4-}, its dimer and complexed forms also. Complexation of H_2TSPP^{4-} by γ-CD might increase the rate of tautomerism of the H_2TSPP^{4-} imine protons and broaden the H_{py} resonances, while complexation through the narrow face of γ-CD is likely to cause a greater magnetic environmental change for H_o than for H_m and thereby causes H_o to experience a larger change in chemical shift (δ 7.63 → 8.00 ppm) than

does H_m (δ 8.23 → 8.27 ppm) and a consequently greater likelihood of entering the intermediate exchange regime of the NMR timescale.

Four particularly strong cross-peaks arising from NOE interactions between the H_3, H_5, H_{6A} and H_{6B} annular protons of γ-CD and the H_m *p*-sulfonatophenyl protons of H_2TSPP^{4-} appear in the 2D ^{1}H NOESY NMR spectrum (Figure 2.8 and A1 of the Appendix) as a consequence of their close proximities in the γ-CD.H_2TSPP^{4-} and (γ-CD)$_2$.H_2TSPP^{4-} complexes and the narrowness of the H_m resonance by comparison with those of H_{py} and H_o. Additional cross-peaks arise in order of decreasing intensity for the H_{6A}, H_5, H_{6B} and H_3 protons NOE interactions with the H_o proton.

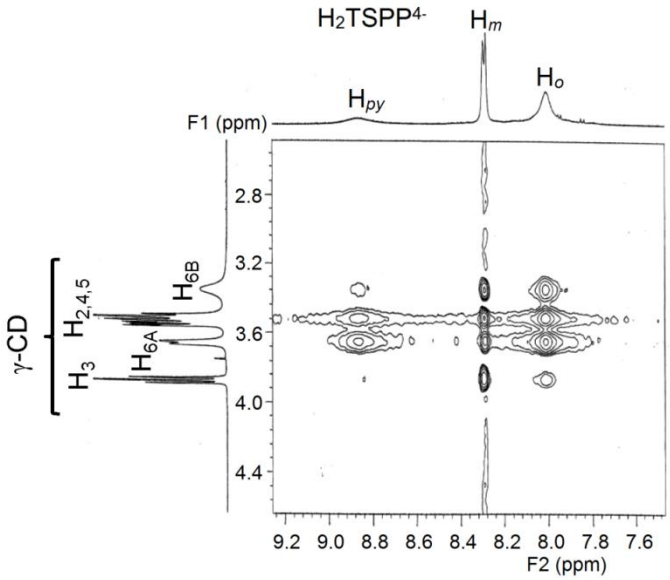

Figure 2.8: 2D ^{1}H NOESY NMR (600 MHz) spectrum of H_2TSPP^{4-} 3.0×10^{-3} mol dm^{-3} and equimolar γ-CD in D_2O (pD 7.0 phosphate buffer, I = 0.10 mol dm^{-3}) at 298.2 K with a mixing time of 300 ms. Cross–peaks arise from NOE interactions between the annular γ-CD protons (H_3, H_5, H_{6A} and H_{6B}) and the pyrrolic and phenyl protons, H_{py}, H_o and H_m of H_2TSPP^{4-}. The amount of H_2TSPP^{4-} in the free state is ~ 30% of the total.

Cross-peaks also arise in the same intensity order with the H_{py} proton but of overall lower intensity. These observations are consistent with the γ-CD H_3 proton being most distant from H_2TSPP^{4-} protons and for complexation occurring through the narrow primary hydroxyl face

of the annulus consistent with earlier deductions.[23] (No cross-peaks arising from the γ-CD H_1 proton are observed for this system or for the γ-CD oligomer systems.)

The host–guest complexation of H_2TSPP^{4-} by the oxalate and succinamide-linked dimers and benzene linked trimer, 33γ-CD_2ox, 33γ-CD_2suc, 66γ-CD_2ox, 66γ-CD_2suc and 666γ-CD_3bz are also studied by 2D ^{1}H NOESY NMR spectroscopy. In all five systems cross-peaks arising from nuclear Overhauser effects (NOE) between the *p*-sulfonatophenyl H_m and H_o protons and the pyrrolic H_{py} protons of H_2TSPP^{4-} and the γ-CD annular H_3, H_5, H_{6A} and H_{6B} protons are observed consistent with complexation of the *p*-sulfonatophenyl groups as guests close in to the porphyrin core by the γ-CD annular host. A previous NMR study of α-CD, β-CD and γ-CD interactions with H_2TSPP^{4-} detected no complexation by α-CD, *p*-sulfonatophenyl group complexation by β-CD through the wider annular face delineated by the C2 and C3 secondary hydroxyl groups and *p*-sulfonatophenyl group complexation by γ-CD through the narrow annular face delineated by the C6 primary hydroxyl groups.[23] The β-CD annulus has narrow and wide face diameters of 600 and 650 pm and a depth of 790 pm, and the corresponding dimensions for γ-CD are 750, 830 and 790 pm.[58] These compare with a phenyl ring width of ~470 pm, and indicate that the tightness of fit of the *p*-sulfonatophenyl groups of H_2TSPP^{4-} in the β-CD and γ-CD annuli is likely to be a major factor in determining host-guest complex stereochemistry and stability.

When H_2TSPP^{4-} is complexed by the γ-CD oligomers the pattern of cross-peaks change significantly as illustrated by Figure 2.9 (and Figures 2.10 and A2-A6 of the Appendix). The mono-substitution of the γ-CD in the oligomers causes their glucopyranose subunits to become chemically and magnetically inequivalent. Accordingly, the γ-CD $H_{2\text{-}6}$ proton resonances of the oligomers increase in number and are significantly broadened in most cases such that it is difficult to assign the individual resonances. The H_2TSPP^{4-} H_{py}, H_o and H_m are also substantially broadened in the five oligomer systems studied and the chemical shift

between the H_o and H_m resonances are substantially decreased. Nevertheless, any cross-peaks observed may be assigned dominantly to interactions between the H_3, H_5, H_{6A} and H_{6B} annular γ-CD protons of the γ-CD oligomers and the H_2TSPP^{4-} H_{py}, H_o and H_m protons.

These changes in the oligomer 2D ^{1}H NOESY NMR spectra are typified in Figure 2.9 by the 66γ-CD_2suc/H_2TSPP^{4-} system where strong cross-peaks are formed by the H_m protons because of the lesser broadening of the H_m resonance (a characteristic of the spectra of all five γ-CD oligomer systems). Cross-peaks of intermediate and weak intensities are formed by the H_{py} and H_o protons, respectively, which is the reverse of these relative intensities for the γ-CD/H_2TSPP^{4-} system discussed earlier. This may be understood on the basis that 66γ-CD_2suc complexes two H_2TSPP^{4-} *p*-sulfonatophenyl groups simultaneously (or ditopically) through the narrow face of each of its two γ-CD substituents in the *anti* configuration shown in Figure 2.1. The cooperative effect of such ditopic complexation is likely to cause a tight complexation which holds the H_{6A} and H_{6B} protons closer to the H_{py} protons than the H_o protons (which is the opposite to the situation for the γ-CD/H_2TSPP^{4-} system) such that the cross-peaks arising from the former are stronger than those arising from the later. (The cross-peaks arising from the H_m are the strongest for the same reasons as for those of the γ-CD/H_2TSPP^{4-} system.) Similar variations are seen in the spectrum of the 66γ-CD_2ox/H_2TSPP^{4-} system in which the H_m and H_o resonances have similar chemical shifts (Figure A4)

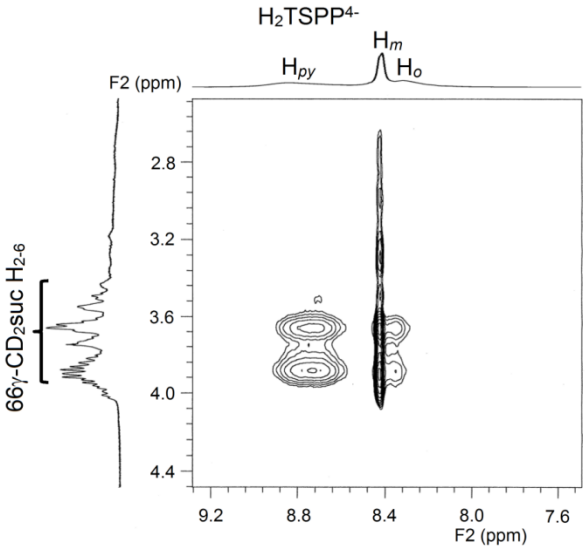

Figure 2.9: 2D ^{1}H NOESY NMR (600 MHz) spectrum of H_2TSPP^{4-} 3.0×10^{-3} mol dm^{-3} and equimolar 66γ-CD_2suc in D_2O (pD 7.0 phosphate buffer, I = 0.10 mol dm^{-3}) at 298.2 K with a mixing time of 300 ms. The amount of H_2TSPP^{4-} in the free state is ~ 1% of the total.

Ditopic complexation of H_2TSPP^{4-} by either 33γ-CD_2ox or 33γ-CD_2suc in the *syn* configuration (Figure 2.1) requires entry of two adjacent *p*-sulfonatophenyl groups H_2TSPP^{4-} through the wide secondary hydroxyl faces of two γ-CD annuli to form a host-guest complex which should produce differences in the resulting 2D ^{1}H NOESY NMR spectra by comparison with those characterising the analogous 66γ-CD_2ox or 66γ-CD_2suc systems.

The spectrum of the 33γ-CD_2ox/H_2TSPP^{4-} system is shown in Figures 2.10 and A2 of the Appendix. The cooperative effect of the ditopic complexation is likely to cause a tight complexation which holds the H_3 protons closer to the H_{py} protons and the $H_{5,}$ H_{6A} and H_{6B} protons closer to H_o and H_m such that the cross-peaks arising from the former are stronger than those arising from the latter. Once again the cross-peak arising from the H_m proton is the strongest because of the sharper resonance arising from it.

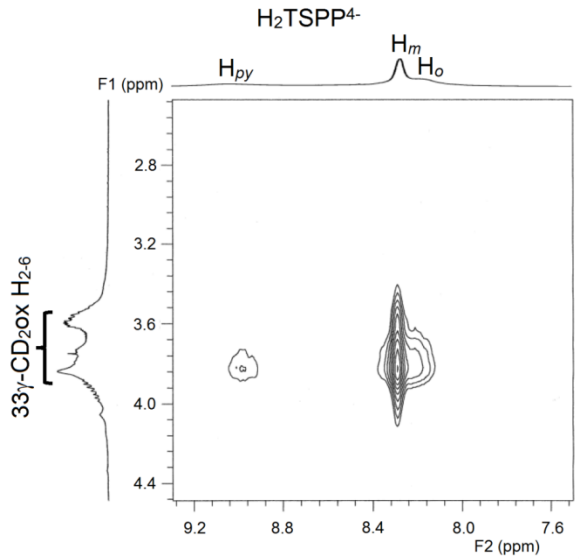

Figure 2.10: 2D ^{1}H NOESY NMR (600 MHz) spectrum of H_2TSPP^{4-} 3.0×10^{-3} mol dm^{-3} and equimolar 33γ-CD_2ox in D_2O (pD 7.0 phosphate buffer, I = 0.10 mol dm^{-3}) at 298.2 K with a mixing time of 300 ms. The amount of H_2TSPP^{4-} in the free state is ~ 10% of the total.

The cross-peak arising from H_o is substantially stronger than that arising from H_{py} due to the greater broadening of the H_{py} resonance. Beyond these observations there is little more that can be deduced concerning host-guest complex structure for either the 33γ-CD_2ox/H_2TSPP^{4-} system or that of the 33γ-CD_2suc/H_2TSPP^{4-} system (Figure A3).

The 2D ^{1}H NOESY NMR spectrum of the 666γ-CD_3bz/H_2TSPP^{4-} system (Figure A6) also shows significant cross-peaks arising from the H_2TSPP^{4-} H_{py}, H_m and H_o proton resonances consistent with host-guest complexation which is expected to be tritopic in nature although this cannot be directly deduced from the spectrum.

Although the 2D ^{1}H NOESY NMR data are consistent with host-guest complexation occurring between γ-CD and the γ-CD oligomers and H_2TSPP^{4-} they do not identify their stoichiometry. The broadening of the H_2TSPP^{4-} resonances is likely to render a more detailed study in which the concentrations of the host and guest are systematically varied difficult to interpret quantitatively. Accordingly, UV-vis spectroscopic studies are undertaken to determine the stoichiometry of host-guest complexation.

2.4. UV-VIS SPECTROSCOPIC STUDIES

2.4.1. H_2TSPP^{4-} Dimerisation

In aqueous solution at pH 7.0 and at I = 0.10 mol dm^{-3} ($NaClO_4$) and 298.2 K the UV-vis absorbance of H_2TSPP^{4-} has been reported to obey Beer's law over the concentration range 10^{-9} – 10^{-4} mol dm^{-3} consistent with H_2TSPP^{4-} existing dominantly as a monomer.[50] However, other studies have determined the dimerisation of H_2TSPP^{4-} to be characterised by a dimerisation constant of K_D = 3.48 ± 0.26 × 10^4 dm^3 mol^{-1} at 298 K in aqueous phosphate buffer at 298 K[54] (or K_D = 2.71 × 10^4 dm^3 mol^{-1} at 298.2 K when calculated from the ΔH and ΔS data in the reference) or (1.54 ± 1.3) × 10^4 dm^3 mol^{-1} in aqueous phosphate buffer at 298.2 K.[55] These reported dimerisation constants suggest that dimerisation would be significant at H_2TSPP^{4-} concentrations of 10^{-4} mol dm^{-3}. As the H_2TSPP^{4-} concentration in the UV-vis studies herein is 1.05 × 10^{-6} mol dm^{-3} the amount of H_2TSPP^{4-} dimer in solution should be < 3% of the total H_2TSPP^{4-} monomer concentration assuming a K_D = 2.71 × 10^4 dm^3 mol^{-1} at 298.2 K such that the dimer should not play a significant role in these complexation studies. At the lowest temperature studied, 278.2 K, a K_D = 4.78 × 10^4 dm^3 mol^{-1} is calculated and H_2TSPP^{4-} dimer in solution should be < 4% of the total H_2TSPP^{4-} monomer concentration.

An indication of the temperature effect on the H_2TSPP^{4-} monomer/dimer equilibrium in the temperature range 308.2 K to 278.2 K was sought by determining the absorption spectrum of a 1.05 × 10^{-6} mol dm^{-3} solution at four temperatures as shown in Figure 2.11. It is seen that there is a decrease in molar absorbance at 413 nm from 4.15 × 10^5 to 4.02 × 10^5 mol^{-1} dm^{-3} cm^{-1} between the temperature extremes and a corresponding change in absorbance maximum, λ_{max}, of 414 nm to 413 nm. This is consistent with a temperature dependence of the H_2TSPP^{4-} monomer/dimer equilibrium. However, little more can be deduced from these data which are unlikely to significantly impinge on the determination of the thermodynamic data for the host-guest complexation of H_2TSPP^{4-} by γ-CD and its oligomers.

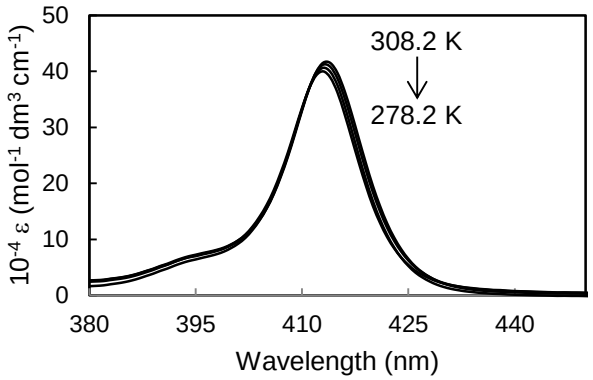

Figure 2.11: Temperature dependence of molar absorbance change of H_2TSPP^{4-} (1.05×10^{-6} mol dm^{-3}) in phosphate buffer, pH 7.0, I = 0.10 mol dm^{-3}.

2.4.2. H_2TSPP^{4-} Host-Guest Complexation

The study of the host-guest equilibria by UV-vis spectroscopy and the protocol for fitting the algorithms describing the equilibria to the changes in absorbance follows methods similar to those previously reported.[13] The model used to determine the host-guest complexation constants assumes that labile equilibria exist such that the concentrations of free H_2TSPP^{4-} and that complexed by either γ-CD or its linked oligomers 33γ-CD_2ox, 33γ-CD_2suc, 66γ-CD_2ox, 66γ-CD_2suc and 666γ-CD_3bz in the formation of 1:1, and possibly 2:1, host-guest complexes very rapidly adjust as the UV-vis titrations proceed. Thus, the 1:1 and 2:1 host-guest γ-CD complexes with H_2TSPP^{4-} form according to Equations 2.1 and 2.2:

$$\gamma\text{-CD} + H_2TSPP^{4-} \overset{K_{11}}{\rightleftharpoons} \gamma\text{-CD}.H_2TSPP^{4-} \quad (\mathbf{2.1})$$

$$\gamma\text{-CD} + \gamma\text{-CD}.H_2TSPP^{4-} \overset{K_{21}}{\rightleftharpoons} (\gamma\text{-CD})_2.H_2TSPP^{4-} \quad (\mathbf{2.2})$$

The complexation constants K_{11} and K_{21}, at equilibrium are given by

$$K_{11} = [\gamma\text{-CD}.H_2TSPP^{4-}]/[\gamma\text{-CD}][H_2TSPP^{4-}] \quad (\mathbf{2.3})$$

$$K_{21} = [(\gamma\text{-CD})_2.H_2TSPP^{4-}]/([\gamma\text{-CD}.H_2TSPP^{4-}][\gamma\text{-CD}]) \quad (\mathbf{2.4})$$

Given that $[H_2TSPP^{4-}]_{total}$ and $[\gamma\text{-CD}]_{total}$ are the initial concentrations of the two complexation partners:

$$[H_2TSPP^{4-}]_{total} = [H_2TSPP^{4-}] + [\gamma\text{-CD}.H_2TSPP^{4-}] + [(\gamma\text{-CD})_2.H_2TSPP^{4-}] \quad (\mathbf{2.5})$$

it follows that:

$$[\gamma\text{-CD}]_{total} = [\gamma\text{-CD}] + [\ \gamma\text{-CD}.H_2TSPP^{4-}] + [(\gamma\text{-CD})_2.H_2TSPP^{4-}] \quad (\mathbf{2.6})$$

The absorbance at a particular wavelength is given by Equation 2.7 when only a 1:1 complex forms, and by Equation 2.8 when both 1:1 and 2:1 complexes form. In Equations 2.7 and 2.8 $A(\lambda)$, ε_1, ε_{11} and ε_{21} represent the observed absorbance and apparent molar absorbances of H_2TSPP^{4-}, γ-CD.H_2TSPP^{4-} and $(\gamma\text{-CD})_2.H_2TSPP^{4-}$ respectively. The values of K_{11} and K_{21} are determined by best-fitting the algorithm for either Equation 2.7 or 2.8 to the H_2TSPP^{4-} absorbance data in the range 400-430 nm at 0.25 nm intervals as the γ-CD concentration is increased using the HypSpec protocol.[59] The same protocol is used for the other five systems.

$$A(\lambda) = \varepsilon_1[H_2TSPP^{4-}] + \varepsilon_{11}[\gamma\text{-CD}.\ H_2TSPP^{4-}] \quad (\mathbf{2.7})$$

$$A(\lambda) = \varepsilon_1[H_2TSPP^{4-}] + \varepsilon_{11}[\gamma\text{-CD}.H_2TSPP^{4-}] + \varepsilon_{21}[(\gamma\text{-CD})_2.H_2TSPP^{4-}] \quad (\mathbf{2.8})$$

2.4.3. UV-vis Titration studies

The experimental details of the UV-vis spectroscopic characterisation of the equilibria in which γ-CD and its oligomers complex H_2TSPP^{4-} are now described. The UV-vis spectra of solutions were determined against reference solutions in matched 1 cm quartz cells and were recorded at 0.25 nm intervals using a Cary 5000 UV-vis spectrophotometer over the wavelength range 250-650 nm. The solutions were freshly prepared in aqueous phosphate buffer at pH 7.0 and I = 0.10 mol dm^{-3}. Samples were 2.0 cm^3 in volume and were thermostated at 278.2, 288.2, 298.2 and 308.2 K for 30 minutes before starting the titration. The H_2TSPP^{4-} solution concentrations were 1.05×10^{-6} mol dm^{-3} and were titrated with sequential injections (10 mm^3 each into both sample and reference cells unless otherwise stated) of either γ-CD (1.18×10^{-2} mol dm^{-3}), 33γ-CD_2ox (9.72×10^{-4} mol dm^{-3}), 33γ-CD_2suc (3.86×10^{-4} mol dm^{-3}), 66γ-CD_2ox (1.89×10^{-4} mol dm^{-3}), 66γ-CD_2suc (5.11×10^{-4} mol dm^{-3}) and 666γ-CD_3bz (3.16×10^{-5} mol dm^{-3}) also in aqueous phosphate buffer at pH 7.0 and I = 0.10 mol dm^{-3}.

The molar absorbance changes of H_2TSPP^{4-} solutions with increasing concentrations of 33γ-CD_2ox, 66γ-CD_2ox and 666γ-CD_3bz and the best fits of algorithms describing the complexation processes at 298.2 K are shown in Figure 2.12. All of the variable temperature UV-vis titrations, derived spectra and speciation plots for the γ-CD and γ-CD oligomer host-guest systems are shown in Figures A7 – A24 of the Appendix.

A decrease in absorption at the λ_{max} of 413 nm of H_2TSPP^{4-} is observed for all six systems with the progressive increase of host-guest complex concentration with increase of the total host concentration. Simultaneously, the red-shifted spectra of the H_2TSPP^{4-} complexes of γ-CD, the four γ-CD dimers and the 666γ-CD_3bz trimer increase and their λ_{max} change from 413 characterising free H_2TSPP^{4-} to 415, 418 and 421 nm upon complexation in γ-CD, its four dimers and its trimer, respectively. These red shifts are consistent with H_2TSPP^{4-} experiencing a change in polarity of the local environment as it enters the hydrophobic γ-CD annulus upon formation of host-guest complexes.[50] The increase in the magnitude of this red-shift in the 33γ-CD_2ox/H_2TSPP^{4-}, 66γ-CD_2ox/H_2TSPP^{4-}, 33γ-CD_2suc/H_2TSPP^{4-} and 66γ-CD_2suc/H_2TSPP^{4-} systems by comparison with that of the γ-CD/H_2TSPP^{4-} system is consistent with a cooperative complexation effect where two γ-CD annuli complex H_2TSPP^{4-} simultaneously. This trend is also exemplified by a further increase in the red shift for the 666γ-CD_3bz/H_2TSPP^{4-} system, which is consistent with cooperative complexation of H_2TSPP^{4-} in three γ-CD annuli.

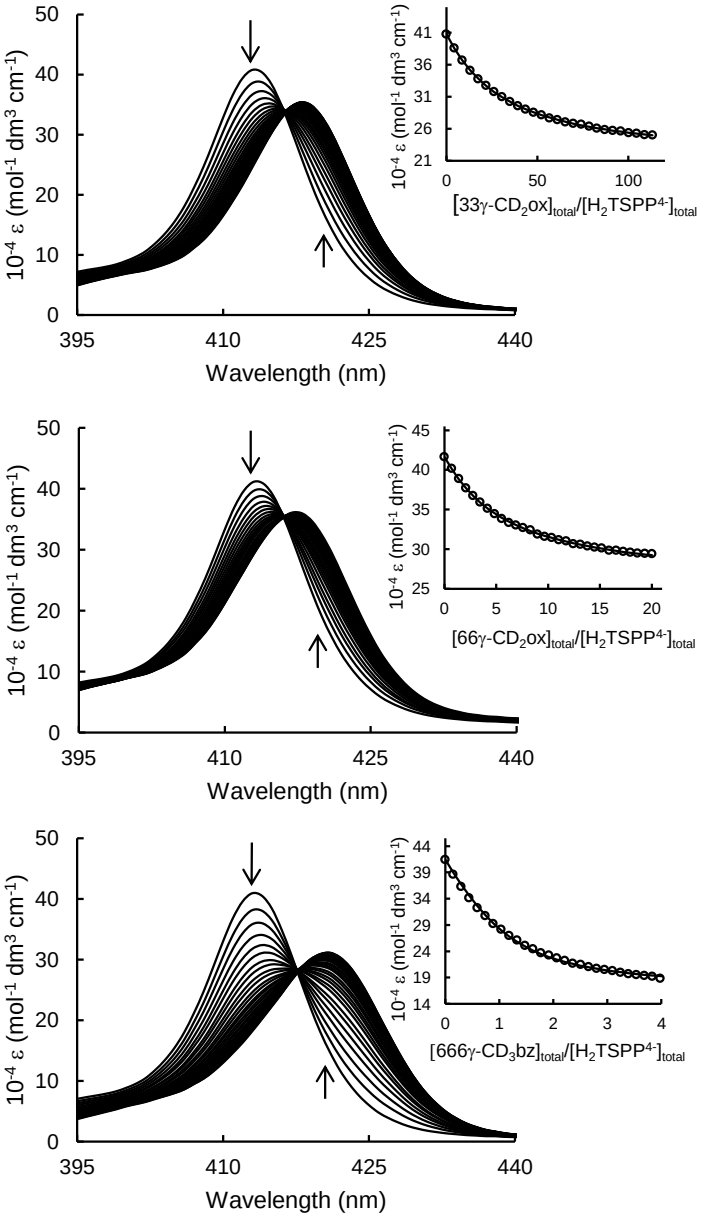

Figure 2.12: Molar absorbance change of H_2TSPP^{4-} (1.05×10^{-6} mol dm^{-3}) in phosphate buffer, pH 7.0, I = 0.10 mol dm^{-3} at 298.2 K with sequential injections (10 mm^3 each) of 33γ-CD_2ox (top, 9.72×10^{-4} mol dm^{-3}), 66γ-CD_2ox (middle, 1.89×10^{-4} mol dm^{-3}) 666γ-CD_3bz (bottom, 3.16×10^{-5} mol dm^{-3}) into both sample and reference cells. The arrows indicate the direction of molar absorbance change as the molar ratio of $[host]_{total}/[H_2TSPP^{4-}]_{total}$ increases. Inset: Molar absorbance variation at 413 nm and the line of best fit of an algorithm for 1:1 and 2:1 host-guest complexation for the 33γ-CD_2ox/H_2TSPP^{4-} system and for 1:1 host-guest complexation for the 66γ-CD_2ox/H_2TSPP^{4-} and 666γ-CD_3bz/H_2TSPP^{4-} systems to the absorbance change over the wavelength range 400-430 nm.

The K_{11} complexation constants for all six systems appear in Table 2.1 and are plotted in Figure 2.13 from which it is seen that those characterising the γ-CD oligomer systems are between 13 - 1800-fold larger than that of the native γ-CD system at 278.2 K. This is consistent with a strong cooperative effect existing for complexation in the oligomer systems. The complexation constants, K_{11}, increase in the order γ-CD < 33γ-CD_2ox ≤ 33γ-CD_2suc < 66γ-CD_2ox < 66γ-CD_2suc < 666γ-CD_3bz at 298.2 K, which indicates that an increase in linker length and the consequent increase in flexibility in the 33γ-CD_2ox/33γ-CD_2suc and 66γ-CD_2ox /66γ-CD_2suc dimer pairs increases K_{11} to a greater extent in the latter pair.

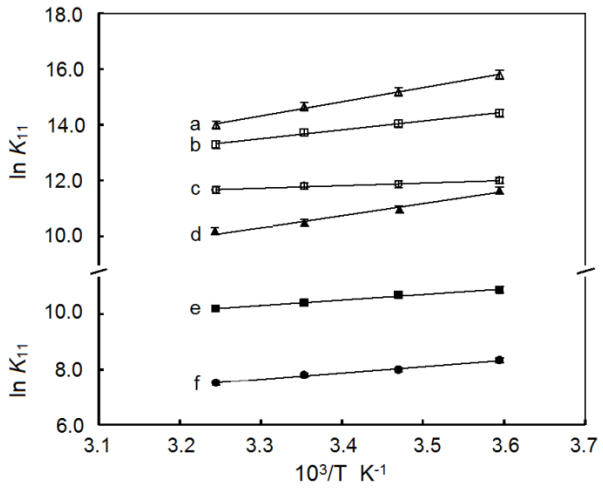

Figure 2.13: Plot of lnK_{11} determined by UV-Vis absorption spectroscopy at various temperatures against 10^3/T for 666γ-CD_3bz.H_2TSPP^{4-} (**a**, R^2 = 0.9966), 66γ-CD_2suc.H_2TSPP^{4-} (**b**, R^2 = 0.9934), 66γ-CD_2ox.H_2TSPP^{4-} (**c**, R^2 = 0.9881), 33γ-CD_2suc.H_2TSPP^{4-} (**d**, R^2 = 0.9911), 33γ-CD_2ox.H_2TSPP^{4-} (**e**, R^2 = 0.9913) and γ-CD.H_2TSPP^{4-} (**f**, R^2 = 0.9882). Solid lines represent the best fit of the van't Hoff equation to the K_{11} data. The R^2 values refer to the fit of Equation 2.11 to the K_{11} data. Experimental error in individual K_{11} is < ± 5 %.

Table 2.1: Complexation constants K_{11} and thermodynamic parameters for the complexation of H_2TSPP^{4-} by γ-CD, 33γ-CD_2ox, 33γ-CD_2suc, 66γ-CD_2ox, 66γ-CD_2suc and 666γ-CD_3bz at different temperatures by UV-Vis titrations in aqueous phosphate buffer at pH 7.0 and I = 0.10 mol dm^{-3}. [a]

Host	T (K)	K_{11} (10^{-3} × dm^3 mol^{-1})	ΔH_{11} (kJ mol^{-1})	ΔG_{11} (kJ mol^{-1})	$T\Delta S_{11}$ (kJ mol^{-1})
γ-CD	308.2	1.939 ± 0.02	-16.37 ± 0.82	-19.46 ± 0.97	3.09 ± 0.15
	298.2	2.496 ± 0.03	-16.37 ± 0.82	-19.36 ± 0.97	2.99 ± 0.15
	288.2	3.216 ± 0.04	-16.37 ± 0.82	-19.26 ± 0.96	2.89 ± 0.14
	278.2	3.840 ± 0.04	-16.37 ± 0.82	-19.16 ± 0.96	2.79 ± 0.14
33γ-CD_2ox	308.2	26.49 ± 0.26	-16.57 ± 0.83	-26.11 ± 1.31	9.54 ± 0.48
	298.2	32.64 ± 0.33	-16.57 ± 0.83	-25.80 ± 1.29	9.23 ± 0.46
	288.2	43.46 ± 0.43	-16.57 ± 0.83	-25.49 ± 1.27	8.92 ± 0.45
	278.2	52.31 ± 0.52	-16.57 ± 0.83	-25.18 ± 1.26	8.61 ± 0.43
33γ-CD_2suc	308.2	24.55 ± 0.25	-36.10 ± 1.81	-25.79 ± 1.29	-10.31 ± 0.52
	298.2	36.67 ± 0.37	-36.10 ± 1.81	-26.12 ± 1.31	-9.98 ± 0.50
	288.2	57.88 ± 0.58	-36.10 ± 1.81	-26.46 ± 1.32	-9.64 ± 0.48
	278.2	113.5 ± 1.13	-36.10 ± 1.81	-26.79 ± 1.34	-9.31 ± 0.47
66γ-CD_2ox	308.2	116.2 ± 1.16	-7.65 ± 0.38	-29.91 ± 1.50	22.27 ± 1.11
	298.2	132.6 ± 1.33	-7.65 ± 0.38	-29.19 ± 1.46	21.54 ± 1.08
	288.2	142.9 ± 1.43	-7.65 ± 0.38	-28.47 ± 1.42	20.82 ± 1.04
	278.2	162.1 ± 1.62	-7.65 ± 0.38	-27.74 ± 1.39	20.10 ± 1.00
66γ-CD_2suc	308.2	591.7 ± 5.92	-26.31 ± 1.32	-34.15 ± 1.71	7.84 ± 0.39
	298.2	941.5 ± 9.41	-26.31 ± 1.32	-33.90 ± 1.69	7.59 ± 0.38
	288.2	1245 ± 12.5	-26.31 ± 1.32	-33.64 ± 1.68	7.34 ± 0.37
	278.2	1830 ± 18.3	-26.31 ± 1.32	-33.39 ± 1.67	7.08 ± 0.35
666γ-CD_3bz	308.2	1148 ± 11.5	-42.09 ± 2.10	-35.86 ± 1.79	-6.23 ± 0.31
	298.2	2210 ± 22.1	-42.09 ± 2.10	-36.07 ± 1.80	-6.03 ± 0.30
	288.2	3740 ± 37.4	-42.09 ± 2.10	-36.27 ± 1.81	-5.82 ± 0.29
	278.2	6911 ± 69.1	-42.09 ± 2.10	-36.47 ± 1.82	-5.62 ± 0.28

[a]The errors quoted for K_{11} are those derived from the best fits of either Equation 2.7 or 2.8 to the absorbance data. The errors quoted for ΔH_{11}, ΔG_{11} and $T\Delta S_{11}$ are those derived from the fit of Equation 2.11 to the K_{11} data. Experimental error in in all four parameters is estimated at < ± 5 %.

This reflects the competing influences of the orientations of the γ-CD annuli whereby a combination of the tighter fit of the H_2TSPP^{4-} *p*-sulfonatophenyl groups entering through the narrow primary hydroxyl faces of 66γ-CD_2suc combined with the increased flexibility of the succinamide linker over the oxalate linker maximises K_{11}. In contrast, the less constrained

fitting of the H_2TSPP^{4-} *p*-sulfonatophenyl groups entering through the wider secondary hydroxyl faces of 33γ-CD_2suc renders the effect of the increased flexibility of the succinamide linker less effective in increasing K_{11}. This is explored in more detail below.

The narrow primary-hydroxyl face is favoured for entrance of H_2TSPP^{4-} into the γ-CD annulus during host-guest complexation, as indicated by the larger K_{11} complexation constants for the 6,6- dimers and the 6,6,6- trimer by comparison with those of the 3,3-dimers. This is consistent with the H_2TSPP^{4-} phenyl rings being dominant factors in forming host-guest complexes. The phenyl rings have widths of ~470 pm which compare with primary- and secondary-hydroxyl γ-CD face widths of 750 and 830 pm (and depth of 790 pm), respectively,[58] and as consequence the smaller primary hydroxyl face more closely fits the phenyl rings to form more stable host-guest complexes. This is in accord with the appearance of cross-peaks between the phenyl protons and the γ-CD annular protons in the 2D ^{1}H NOESY NMR spectra (Figures 2.8 – 2.10 and Figures A2 – A6 of the Appendix).

For the 33γ-CD_2suc and 66γ-CD_2suc dimers, the longer succinamide linker coincides with larger K_{11} than is observed for the 33γ-CD_2ox and 66γ-CD_2ox dimers, respectively, with the shorter oxalate linker as evident from the larger K_{11} associated with the first pair of dimers. This is consistent with the greater length and flexibility of the succinamide linker allowing easier formation of host-guest complexes than is the case for less flexible oxalate linker. Whilst the length and flexibility of the benzene linker of the 666γ-CD_3bz trimer may also aid host-guest complexation, it is difficult to quantify its contribution as the tritopic complexation by three γ-CD annuli is also likely to contribute to the observed higher K_{11} complexation constants.

Although UV-Vis spectroscopy is a useful tool in determining the strength and cooperative nature of host-guest complexation and the number of species in the equilibria, it does not distinguish between the *syn* and *anti* modes of complexation of H_2TSPP^{4-} in the 1:1

host-guest complexes formed by the four γ-CD dimers (or through complexation by two γ-CD) shown in Figure 2.14. If both complexing modes operate they are likely to be in a labile equilibrium as has been reported for the complexation of porphyrins by β-CD dimers.[43]

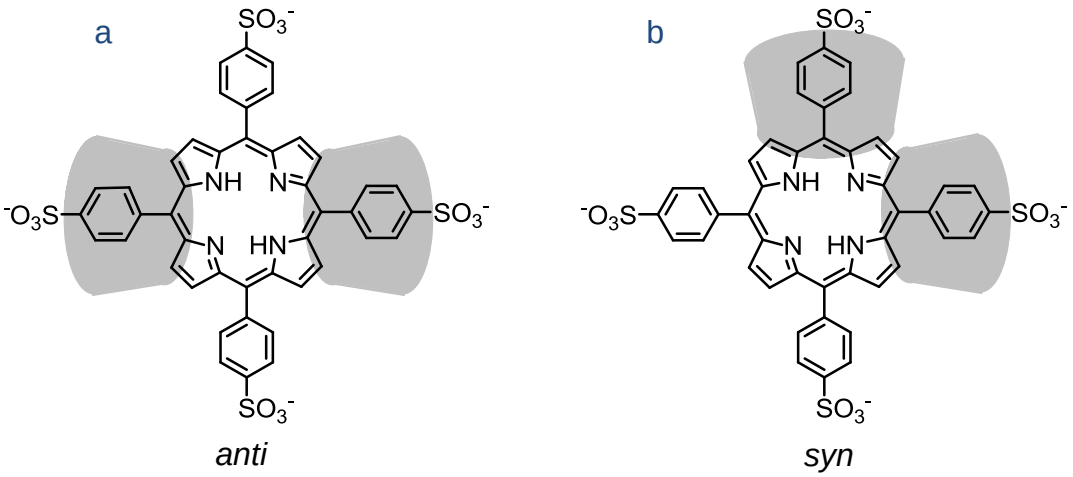

Figure 2.14: The *anti* (a) and *syn* (b) conformations of host-guest complexes in which H_2TSPP^{4-} is complexed by two γ-CD through the narrow annular faces.

For the γ-CD, 33γ-CD_2ox and 33γ-CD_2suc systems, an algorithm for formation of a 1:1 complex corresponding to Equation 2.1 can be fitted to the UV-vis absorbance data. (Figures A20 - A23 of the Appendix). However, a slight broadening of an apparent isosbestic point increases with decreasing temperature consistent with the formation of a second complex; the 2:1 complex. The spectrum of free H_2TSPP^{4-} shows a small decrease in molar absorbance and a small blue shift in λ_{max} with decreasing temperature probably due to a change of position in the monomer/dimer equilibrium as discussed earlier and shown in Figure 2.11. While the fitting of an algorithm for 1:1 complexation gives reasonable fits to the data, the spectrum derived for the 1:1 complex shows a systematic change in molar absorbance with change in temperature (Figures A18 – A23) which is not expected for the γ-CD.H_2TSPP^{4-}, 33γ-CD_2ox.H_2TSPP^{4-} and 33γ-CD_2suc.H_2TSPP^{4-} complexes in which H_2TSPP^{4-} is expected to exist in monomeric form. An algorithm corresponding to the formation of both a 1:1 and a 2:1 complex according to Equations 2.1 and 2.2 is readily fitted to the absorbance data and

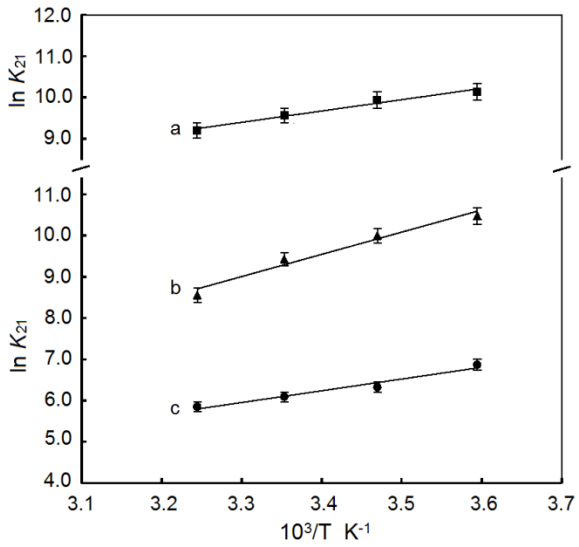

Figure 2.15: Plot of lnK_{21}, determined by UV-vis absorption spectroscopy at various temperatures, against 10^3/T for the complexation of (33γ-CD_2suc)$_2$.H_2TSPP^{4-} (a, R^2 = 0.9612), (33γ-CD_2ox)$_2$.H_2TSPP^{4-} (b, R^2 = 0.9691) and (γ-CD)$_2$.H_2TSPP^{4-} (c, R^2 = 0.9650). Solid lines represent the best fit of the van't Hoff equation to the K_{21} data The R^2 values refer to the fit of Equation 2.11 to the K_{21} data. Experimental error is in individual K_{21} is ≤ ± 5 %.

Table 2.2: Experimental complexation constants K_{21} and the associated ΔH_{21} and $T\Delta S_{21}$ for the complexation of H_2TSPP^{4-} by γ-CD, 33γ-CD_2ox and 33γ-CD_2suc determined from UV-vis titrations in aqueous phosphate buffer at pH 7.0 and I = 0.10 mol dm^{-3}.

Host	T (K)	K_{21} (10^{-3} × dm^3 mol^{-1})	ΔH_{21} (kJ mol^{-1})	ΔG_{21} (kJ mol^{-1})	$T\Delta S_{21}$ (kJ mol^{-1})
γ-CD	308.2	0.35 ± 0.02	-32.77 ± 1.64	-14.22 ± 0.71	-18.55 ± 0.93
	298.2	0.44 ± 0.03	-32.77 ± 1.64	-14.82 ± 0.74	-17.95 ± 0.90
	288.2	0.56 ± 0.03	-32.77 ± 1.64	-15.42 ± 0.77	-17.35 ± 0.87
	278.2	0.96 ± 0.05	-32.77 ± 1.64	-16.02 ± 0.80	-16.75 ± 0.84
33γ-CD_2ox	308.2	9.54 ± 0.46	-22.73 ± 1.14	-23.58 ± 1.18	0.85 ± 0.04
	298.2	13.41 ± 0.69	-22.73 ± 1.14	-23.55 ± 1.18	0.82 ± 0.04
	288.2	20.21 ± 0.92	-22.73 ± 1.14	-23.52 ± 1.18	0.79 ± 0.04
	278.2	24.19 ± 1.26	-22.73 ± 1.14	-23.50 ± 1.17	0.76 ± 0.04
33γ-CD_2suc	308.2	4.98 ± 0.23	-44.85 ± 2.24	-22.20 ± 1.11	-22.66 ± 1.13
	298.2	12.21 ± 0.68	-44.85 ± 2.24	-22.93 ± 1.15	-21.92 ± 1.10
	288.2	21.66 ± 1.19	-44.85 ± 2.24	-23.67 ± 1.18	-21.19 ± 1.06
	278.2	33.87 ± 1.77	-44.85 ± 2.24	-24.40 ± 1.22	-20.45 ± 1.02

[a]The errors quoted for K_{21} are those derived from the best fits of either Equation 2.7 or 2.8 to the absorbance data. The errors quoted for ΔH_{21}, ΔG_{21} and $T\Delta S_{21}$ are those derived from the fit of Equation 2.11 to the K_{21} data. Experimental error in in all four parameters is estimated at < ± 5 %.

the derived 1:1 and 2:1 complex spectra show no significant variation with temperature as may be seen from Figures A7 – A12, and it is concluded that this explains the apparent isosbestic point broadening and is a more reliable representation of the complexation equilibria. The derived K_{11} and K_{21} appear in Tables 2.1 and 2.2, respectively. The K_{21} data for the (γ-CD)$_2$.H$_2$TSPP^{4-}, (33γ-CD$_2$ox)$_2$.H$_2$TSPP^{4-} and (33γ-CD$_2$suc)$_2$.H$_2$TSPP^{4-} complexes are plotted in Figure 2.15.

Two very different gas phased modelled complexing modes for (33γ-CD$_2$ox)$_2$.H$_2$TSPP^{4-} are shown in Figure 2.16 to give an initial idea of the conformational variations possible for the 2:1 host-guest complexes present in solution. In Figure 2.16a steric hindrance is minimised through monotopic *anti* complexation of H$_2$TSPP^{4-}.

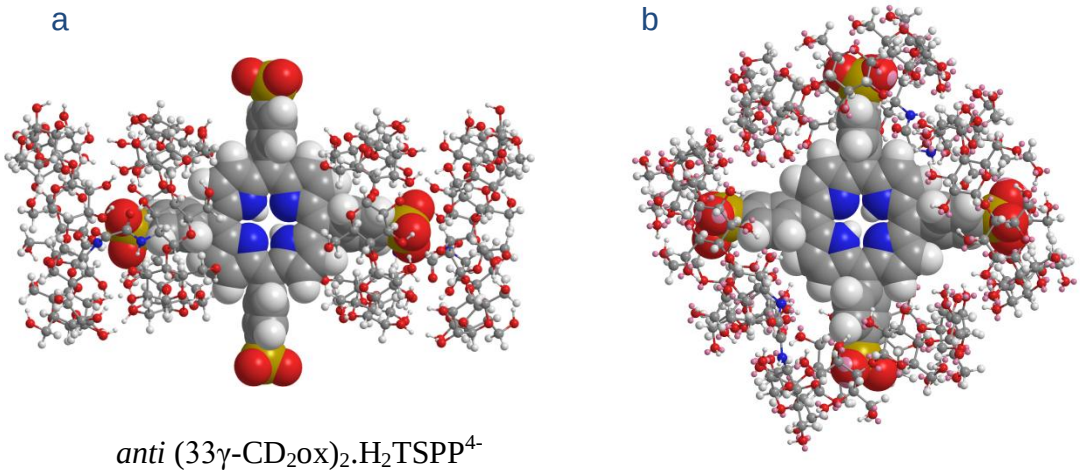

anti (33γ-CD$_2$ox)$_2$.H$_2$TSPP^{4-}
(non-cooperative)

syn (33γ-CD$_2$ox)$_2$.H$_2$TSPP^{4-}
(cooperative)

Figure 2.16: (a) Gas phase energy minimised molecular models for potential 2:1 non-cooperative *anti* (33γ-CD$_2$ox)$_2$.H$_2$TSPP^{4-} (heat of formation E = -32170.01 kJ mol^{-1}) and (b) cooperative *syn* (33γ-CD$_2$ox)$_2$.H$_2$TSPP^{4-} (E = -32342.01 kJ mol^{-1}) host-guest complexes show the latter to be more stable. (The steric crowding in cooperative *anti* (33γ-CD$_2$ox)$_2$.H$_2$TSPP^{4-} is too great for it to form.) Note: 33γ-CD$_2$ox is shown in ball and stick format, and H$_2$TSPP^{4-} in space filling format. Carbon = grey, hydrogen = white, oxygen = red, nitrogen = blue and sulphur = gold.

However, the data in Tables 2.1 and 2.2 show that the K_{21} for (33γ-CD$_2$ox)$_2$.H$_2$TSPP^{4-} and (33γ-CD$_2$suc)$_2$.H$_2$TSPP^{4-} are 5-18 and 28-38 fold greater than K_{11} and K_{21} for the

γ-CD.H_2TSPP^{4-} and (γ-CD)$_2$.H_2TSPP^{4-} complexes which is consistent with ditopic complexation in both (33γ-CD_2ox)$_2$.H_2TSPP^{4-} and (33γ-CD_2suc)$_2$.H_2TSPP^{4-} and *syn* conformations similar to those shown in Figure 2.16b.

The experimental observation of 2:1 complexes for 33γ-CD_2ox and 33γ-CD_2suc, but not for the 66γ-CD_2ox and 66γ-CD_2suc is consistent with the greater width of the secondary hydroxyl γ-CD faces of 33γ-CD_2ox and 33γ-CD_2suc affording more flexibility to minimise steric hindrance in the formation of a 2:1 complex than is the case for the narrower primary hydroxyl faces of 66γ-CD_2ox and 66γ-CD_2suc. Further gas phase modelling is discussed below in Section 2.5.

2.4.4. Determination of Thermodynamic Parameters

The relationship between the Gibbs free energy, Δ*G*, enthalpy, Δ*H*, and entropy, Δ*S*, of host-guest complexation is given by the Equations 2.9 and 2.10:

$$\Delta G = -RT\ln K \qquad (\mathbf{2.9})$$

$$\Delta G = \Delta H - T\Delta S \qquad (\mathbf{2.10})$$

where *R* is the ideal gas constant and *T* is the absolute temperature. It follows that:

$$\ln K = -\Delta H/RT + \Delta S/R \qquad (\mathbf{2.11})$$

from which it follows that a plot of ln*K* versus 1/*T* should be linear (assuming Δ*H* to be constant over the small temperature range considered as is usually the case) with the slope and intercept corresponding to -Δ*H*/*R* and Δ*S*°/*R*, respectively. Such van't Hoff plots (Figure 2.11) of K_{11} for the 1:1 host-guest complexation of H_2TSPP^{4-} by γ-CD, 33γ-CD_2ox, 33γ-CD_2suc, 66γ-CD_2ox, 66γ-CD_2suc and 666γ-CD_3bz are used to determine ΔH_{11} and $T\Delta S_{11}$ for each system. The experimental complexation constants K_{11} at 278.2, 288.2, 298.2 and 308.2 K and thermodynamic parameters ΔG_{11}, ΔH_{11} and $T\Delta S_{11}$ are collected in Table 2.1.

Analogous van't Hoff plots (Figure 2.15) are constructed for the K_{21} characterising the 2:1 complexes: $(\gamma\text{-CD})_2.H_2TSPP^{4-}$, $(33\gamma\text{-CD}_2ox)_2.H_2TSPP^{4-}$ and $(33\gamma\text{-CD}_2suc)_2.H_2TSPP^{4-}$. The experimental complexation constants K_{21} at 278.2, 288.2, 298.2 and 308.2 K and ΔG_{21}, ΔH_{21} and $T\Delta S_{21}$ are collected in Table 2.2. The errors shown for K_{11} and K_{21} are those for fitting Equation 2.7 to the absorbance data when only a 1:1 complex formed and to Equation 2.8 when both a 1:1 and 2:1 complex formed. The maximum experimental errors for K_{11} and K_{21} are estimated to be < ± 5%. The errors shown for the derived ΔG_{11}, ΔH_{11} and $T\Delta S_{11}$ and ΔG_{21}, ΔH_{21} and $T\Delta S_{21}$ are those arising from fitting Equation 2.11 to the K_{11} and K_{21} data, respectively.

It is seen from the K_{11} data presented in Table 2.1 for all six 1:1 complexes that those characterising the γ-CD oligomer systems are between 13 – 1800-fold larger than K_{11} of the γ-CD system at 278.2 K. This is consistent with a strong cooperative effect existing for H_2TSPP^{4-} complexation in the γ-CD oligomer systems. The complexation constants, K_{11}, increased in the order γ-CD < $33\gamma\text{-CD}_2ox \leq 33\gamma\text{-CD}_2suc < 66\gamma\text{-CD}_2ox < 66\gamma\text{-CD}_2suc < 666\gamma\text{-CD}_3bz$ at 298.2 K which indicates that the linker length together with the γ-CD annular orientation substantially influences the strength of host-guest complexation.

The smaller primary-hydroxyl face appears to be favoured for H_2TSPP^{4-} entry into the dimer γ-CD annuli as evidenced by the significantly larger K_{11} characterising the $66\gamma\text{-CD}_2ox.H_2TSPP^{4-}$ and $66\gamma\text{-CD}_2suc.H_2TSPP^{4-}$ complexes by comparison with the $33\gamma\text{-CD}_2ox.H_2TSPP^{4-}$ and $33\gamma\text{-CD}_2suc.H_2TSPP^{4-}$ complexes. The much larger K_{11} characterising the $666\gamma\text{-CD}_3bz.H_2TSPP^{4-}$ complexes are also consistent with H_2TSPP^{4-} complexation through the primary hydroxyl face of the γ-CD annuli being favoured and tritopic complexation by all three γ-CD annuli of the trimer. In accord with the earlier discussed 2D ^{1}H NOESY NMR data, these observations also indicate that the *p*-sulfonatophenyl groups of H_2TSPP^{4-} are a major factor in forming host-guest complexes

and that the smaller primary hydroxyl γ-CD face provides a tighter fit for the *p*-sulfonatophenyl groups and stabilises the host-guest complexes.

The smaller K_{11} for the γ-CD.H_2TSPP^{4-} complex is a consequence of a ΔH_{11} in the mid-range of those in Table 2.1 and a small positive $T\Delta S_{11}$ attributable to the entropy decrease arising from γ-CD and H_2TSPP^{4-} forming a single complex entity being offset by the entropy increase arising from the displacement of water molecules from the γ-CD annulus by H_2TSPP^{4-} on formation of the γ-CD.H_2TSPP^{4-} complex. Analogous relationships hold for the $T\Delta S_{11}$ characterising the 33γ-CD_2ox.H_2TSPP^{4-}, 66γ-CD_2ox.H_2TSPP^{4-}, 66γ-CD_2ox.H_2TSPP^{4-} and 666γ-CD_3bz.H_2TSPP^{4-} complexes. However, the 33γ-CD_2suc.H_2TSPP^{4-} complex $T\Delta S_{11}$ is negative which infers that the entropy decrease on forming 33γ-CD_2suc.H_2TSPP^{4-} from 33γ-CD_2suc and H_2TSPP^{4-} offsets the increase in entropy arising from expulsion of water from the γ-CD annuli while this is not the case for 33γ-CD_2ox.H_2TSPP^{4-}. To some extent this trend in $T\Delta S_{11}$ variation carries through to 66γ-CD_2suc.H_2TSPP^{4-} and 66γ-CD_2ox.H_2TSPP^{4-} where the first complex has the smaller positive $T\Delta S_{11}$. Thus, for both 3,3- and 6,6-linked dimers, the longer succinamide linker favours a greater enthalpic and entropic stabilisation of host-guest complexation by comparison with the shorter oxalate linker as evidenced by larger ΔH_{11} and negative and smaller positive $T\Delta S_{11}$ for the formation of the 33γ-CD_2suc.H_2TSPP^{4-} and 66γ-CD_2suc.H_2TSPP^{4-} complexes, respectively, by comparison with the 33γ-CD_2ox.$H_2TSPP^{4-}$and 66γ-CD_2ox.H_2TSPP^{4-} complexes. (While the ΔH_{11} for the 66γ-CD_2ox.H_2TSPP^{4-} complex is smaller than that for the γ-CD.H_2TSPP^{4-} complex, the much larger positive $T\Delta S_{11}$ for 66γ-CD_2ox.H_2TSPP^{4-} gives it a substantially greater K_{11}.)

The 666γ-CD_3bz.H_2TSPP^{4-} complex is characterised by the largest ΔH_{11} and a negative $T\Delta S_{11}$ which combine to give the largest K_{11} magnitudes over the studied temperature range. This is attributable to the three γ-CD annuli of 666γ-CD_3bz tritopically complexing three

H_2TSPP^{4-} *p*-sulfonatophenyl groups which has the effect of restraining the motion of the three γ-CD annuli of 666γ-CD_3bz by comparison with the uncomplexed state to make a negative $T\Delta S_{11}$ contribution which partially offsets the positive $T\Delta S_{11}$ contribution arising from expulsion of water from the three γ-CD annuli upon complexation.

The thirty-fold greater K_{21} at 298.2 K for the step-wise complexation of a second ditopic 33γ-CD_2ox and 33γ-CD_2suc with H_2TSPP^{4-} by comparison with K_{21} for the complexation with a second γ-CD indicates a cooperative effect applying for the ditopic 33γ-CD_2ox and 33γ-CD_2suc dimers. This infers that in the $(33\gamma\text{-}CD_2ox)_2.H_2TSPP^{4-}$ and $(33\gamma\text{-}CD_2suc)_2.H_2TSPP^{4-}$ each of the four *p*-sulfonatophenyl groups of H_2TSPP^{4-} are complexed by either two 33γ-CD_2ox or two 33γ-CD_2suc probably in a *syn* conformation. While ΔH_{21} for the stepwise formation of $(\gamma\text{-CD})_2.H_2TSPP^{4-}$ is larger than ΔH_{21} for the formation of $(33\gamma\text{-}CD_2ox)_2.H_2TSPP^{4-}$, $T\Delta S_{21}$ for the formation of $(\gamma\text{-CD})_2.H_2TSPP^{4-}$ is substantially negative whereas $T\Delta S_{21}$ for $(33\gamma\text{-}CD_2ox)_2.H_2TSPP^{4-}$ is slightly positive, such that $(33\gamma\text{-}CD_2ox)_2.H_2TSPP^{4-}$ has the more negative ΔG_{21} and a substantially greater K_{21}. In contrast, the ΔH_{21} characterising the formation of $(33\gamma\text{-}CD_2suc)_2.H_2TSPP^{4-}$ is substantially more negative than those characterising $(\gamma\text{-CD})_2.H_2TSPP^{4-}$ and $(33\gamma\text{-}CD_2ox)_2.H_2TSPP^{4-}$ but its $T\Delta S_{21}$ is the most negative such that it is characterised by a K_{21} at 298.2 K much greater than that of $(\gamma\text{-CD})_2.H_2TSPP^{4-}$ and similar to that of $(33\gamma\text{-}CD_2ox)_2.H_2TSPP^{4-}$.

These considerations raise the question as to why the $(66\gamma\text{-}CD_2ox)_2.H_2TSPP^{4-}$ and $(66\gamma\text{-}CD_2suc)_2.H_2TSPP^{4-}$ complexes are not present to a detectable extent. An obvious difference is that the γ-CD annuli of $66\gamma\text{-}CD_2ox.H_2TSPP^{4-}$ and $66\gamma\text{-}CD_2suc.H_2TSPP^{4-}$ complex the H_2TSPP^{4-} *p*-sulfonatophenyl groups through the narrower primary hydroxyl faces of the γ-CD annuli which engenders a tighter complexation than does complexing through the wider secondary hydroxyl faces. This is consistent with the substantially greater K_{11} characterising $66\gamma\text{-}CD_2ox.H_2TSPP^{4-}$ and $66\gamma\text{-}CD_2suc.H_2TSPP^{4-}$ by comparison with K_{11}

for 33γ-CD_2ox.H_2TSPP^{4-} and 33γ-CD_2suc.H_2TSPP^{4-}, respectively. It appears from this that although 66γ-CD_2ox.H_2TSPP^{4-} and 66γ-CD_2suc.H_2TSPP^{4-} are the more stable complexes, their "tighter" stereochemistries allow less flexibility for the complexing of a second 66γ-CD_2ox or 66γ-CD_2suc.

A few earlier studies have characterised the complexation of H_2TSPP^{4-} by cyclodextrins. Thus, in aqueous solution at 298.2 K β-CD.H_2TSPP^{4-} is characterised by $K_{11} = 1.7 \times 10^4$ dm^3 mol^{-1}, ΔH_{11} = 10 kJ mol^{-1} and ΔS_{11} = 119 J mol^{-1} K^{-1} and (β-CD)$_2$.H_2TSPP^{4-} is characterised by $K_{21} = 2.3 \times 10^3$ dm^3 mol^{-1}, ΔH_{11} = -5 kJ mol^{-1} and ΔS_{11} = 48 J mol^{-1} K^{-1}.[49] When all of the β-CD hydroxyl groups are methylated to give heptakis(2,3,6-tri-*O*-methyl)-β-cyclodextrin, TMβ-CD, the complexation constants for H_2TSPP^{4-} complexation in aqueous solution were too high to be determined spectrophotometrically consistent with the greater hydrophobicity of TMβ-CD greatly increasing complex stability. However, in a 3:1 mixture of ethylene glycol and water β-CD.H_2TSPP^{4-} is characterised by $K_{11} = 2.0 \times 10^4$ dm^3 mol^{-1}, ΔH_{11} = -61 kJ mol^{-1} and ΔS_{11} = -121 J mol^{-1} K^{-1} and (TMβ-CD)$_2$.H_2TSPP^{4-} is characterised by $K_{11} = 5.8 \times 10^4$ dm^3 mol^{-1}, ΔH_{11} = -46 kJ mol^{-1} and ΔS_{11} = -62 J mol^{-1} K^{-1}.[49] When four of the 3-hydroxyl groups of β-CD are substituted with 2-hydroxy-3-*N*,*N*,*N*,-trimethylamino propyl groups to give QAβ-CD, the corresponding QAβ-CD.H_2TSPP^{4-} and (QAβ-CD)$_2$.H_2TSPP^{4-} complexes are characterised by $K_{11} = 1.9 \times 10^5$ dm^3 mol^{-1} and $K_{21} = 7 \times 10^3$ dm^3 mol^{-1} respectively, in aqueous solution at 293 K.[50]

There are reports of complexation of H_2TSPP^{4-} by linked cyclodextrin dimers.[43-47] One study reports the complexation of H_2TSPP^{4-} by a 3,3-succinamide-linked β-CD dimer characterised by $K_{11} = 8.0 \times 10^5$ dm^3 mol^{-1} in pH 7.0 phosphate buffer at 298.2 K.[43] This compares with the complexation of H_2TSPP^{4-} by 66γ-CD_2suc in this study, which is characterised by $K_{11} = 9.4 \times 10^5$ dm^3 mol^{-1} under the same conditions. This might be expected, as the dimers in each study have an identical succinate linker and the annular

widths of their complexing sites, the wider face of β-CD (650 pm)[58] and the narrow face of γ-CD (750 pm),[59] are both be of a suitable size to accommodate the *p*-sulfonatophenyl groups of H_2TSPP^{4-}. It may also be noted that 2:1 host-guest complexes between the 3,3-succinamide-linked β-CD dimer and H_2TSPP^{4-} are not observed.[43] This suggests that the extra space associated with complexation of H_2TSPP^{4-} via the wider secondary face of the γ-CD annuli (830 pm)[58] of the 3,3-linked γ-CD dimers is pivotal in the formation of 2:1 host-guest complexes. In another study, H_2TSPP^{4-} was complexed by two β-CDs linked through substitution of one 2-hydroxyl group of each β-CD by 1,6-hexa-2,4–diyne linker in bis(2'-O-cyclomaltoheptasyl)-1,6-hexa-2,4-diyne, diyneβ-CD_2.[44] In aqueous solution at 293 K, K_{11} = 1.9×10^8 dm^3 mol^{-1} for the diyneβ-CD_2.H_2TSPP^{4-} complex which is substantially greater than those determined in the present study possibly as a consequence of the much greater hydrophobicity of the linker in diyneβ-CD_2.[44]

Reinhoudt and coworkers determined the K_{11} values and thermodynamic parameters for the complexation of H_2TSPP^{4-} by photoswitchable dithienyl ethene-linked[45] and bis(phenylthienyl) ethene-linked[46] β-CD dimers as well as EDTA-linked or metal chelated EDTA-linked[47] β-CD dimers in aqueous solution at 298 K (the dimers are linked by substitution of one 3-hydroxyl group of each β-CD subunit). When H_2TSPP^{4-} is complexed by the dithienyl ethene-linked[45] and bis(phenylthienyl) ethene-linked[46] β-CD dimers, the K_{11} values at derived at 298 K (9.7×10^4 −3.3×10^6 dm^3 mol^{-1}) and are comparable with those observed for the oligomers in this study (3.3×10^4 −3.7×10^6 dm^3 mol^{-1}) at 298.2 K. In most cases, the derived ΔH_{11} and ΔS_{11} values for H_2TSPP^{4-}.CD dimer complexes in the Reinhoudt studies[45,46] are more negative than that observed in the present study. This may be a consequence of the increased hydrophobicity of the dithienyl ethene and bis(phenylthienyl) ethene linkers (compared with the oxalate and succinate linkers in this study) allowing additional interactions with H_2TSPP^{4-} and increased complex stability. Although the

thermodynamic parameters differ from that of the present study, greater enthalpic and entropic stabilisation of host-guest complexation with an increase in linker length and flexibility is also observed in the Reinhoudt studies.[45,46] Reinhoudt observed much larger K_{11} values ($2.7 \times 10^5 - 3.4 \times 10^7$ dm^3 mol^{-1}) and more negative ΔH_{11} and ΔS_{11} values for the complexation of H_2TSPP^{4-} by EDTA-linked or metal chelated EDTA-linked β-CD dimers.[47] These studies show that electrostatic interactions between the dimer linker and H_2TSPP^{4-} could greatly affect the stability of host-guest complexes and that an increase in linker length leads to greater enthalpic and entropic stabilisation.

To the best of our knowledge there are no examples in the literature of the complexation of H_2TSPP^{4-} by γ-CD dimers or trimers with which comparison may be made.

2.4.5. Complexation Entropy-Enthalpy Compensation

It has been observed in a wide range of cyclodextrin studies that a linear relationship exists between $T\Delta S_{11}$ and ΔH_{11} for the complexation by α-CD, β-CD and γ-CD hosts of a large variety of guest species in host-guest 1:1 complexes.[60] This relationship is represented by Equation 2.12 in which $T\Delta S_{11}$ and ΔH_{11} are experimental data, α is the slope of a plot of $T\Delta S_{11}$ against ΔH_{11} and $T\Delta S_{11,0}$ is observed when $\Delta H_{11} = 0$ ($\Delta H_{11,0}$) at the zero intercept.

$$T\Delta S_{11} = \alpha\Delta H_{11} + T\Delta S_{11,0} \qquad (\mathbf{2.12})$$

A plot of $T\Delta S_{11}$ and ΔH_{11} data from the literature[60] for a the formation of a wide range of 1:1 γ-CD.guest host-guest complexes is shown in Figure 2.15 and is characterised by $\alpha = 0.97$ and $T\Delta S_{11,0} = 15$ kJ mol^{-1}. Thus, α indicates the extent to which changes in complex stability (proportional to ΔG_{11}) occurring as a consequence of enthalpic stabilisation, $\Delta\Delta H$, induced by variation of the identity of the host is cancelled by entropic loss, $\Delta\Delta S$, through Equation 2.13:

$$\Delta G_{11} = (1 - \alpha)\Delta\Delta H_{11} \quad \textbf{(2.13)}$$

such that only (1 - α) of the enthalpic increase can add to the host-guest complex stabilisation. Thus, $T\Delta S_{11,0}$ is the inherent host-guest complex stability, $\Delta G_{11,0}$, when $\Delta H_{11} = 0$ ($\Delta H_{11,0}$). (It should be noted that Equation 2.12 does not represent a necessary relationship, but is one observed for a variety equilibria not involving cyclodextrins.)

It is seen from Figure 2.17, that the data point representing γ-CD.H_2TSPP^{4-} falls within the envelope of the literature γ-CD data consistent with the complexation characteristics of γ-CD having a major influence on the formation of γ-CD.H_2TSPP^{4-}. The $T\Delta S$ data for 33γ-CD_2ox.H_2TSPP^{4-}, 33γ-CD_2suc.H_2TSPP^{4-}, 66γ-CD_2ox.H_2TSPP^{4-} and 66γ-CD_2suc.H_2TSPP^{4-} fall at the upper edge of the γ-CD literature data envelope due to their slightly higher $T\Delta S$ values by comparison with their γ-CD counterparts exhibiting similar ΔH

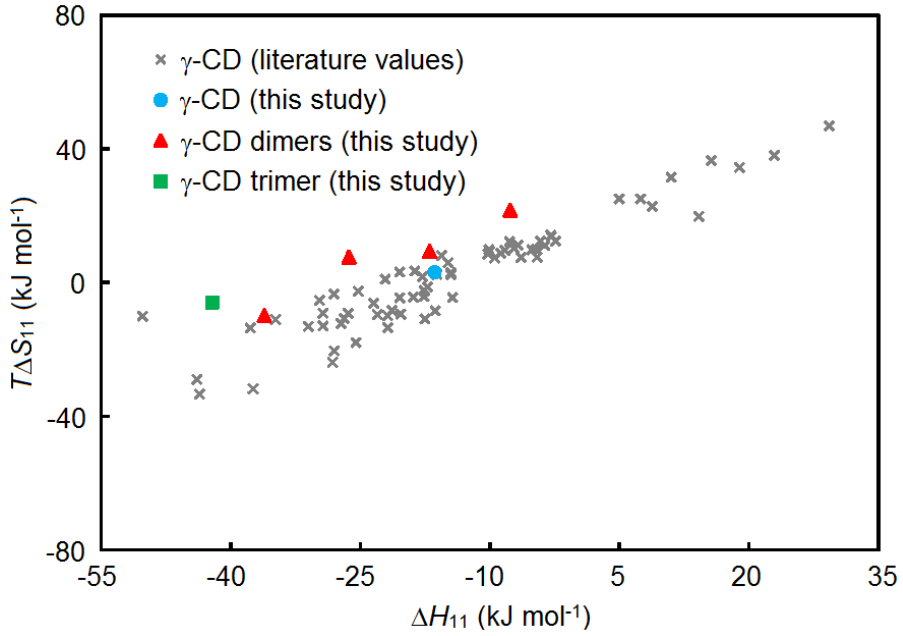

Figure 2.17: Plot of $T\Delta S_{11}$ against ΔH_{11} at 298.2 K for the 1:1 complexes formed by the hosts γ-CD, 33γ-CD_2ox, 33γ-CD_2suc, 66γ-CD_2ox, 66γ-CD_2suc and 666γ-CD_3bz with the guest H_2TSPP^{4-} in this study as well as analogous data from the literature for γ-CD with various guests.[60]

values. This may be attributable to an increase in $T\Delta S_{11}$ associated with the two γ-CD annuli of the dimers contributing twice the amount of water released upon complexation as is the case for γ-CD alone. This trend is further exemplified by the data point for 666γ-CD_3bz.H_2TSPP^{4-} which is also offset from the literature γ-CD data. There is no data in the literature for other γ-CD dimer and trimer 1:1 complexes with which comparison may be made.

2.5. MOLECULAR MODELLING STUDIES

Molecular modelling studies are undertaken to gain greater insight into the possible different stereochemical modes of complexation in the host-guest systems of H_2TSPP^{4-} with γ-CD and its linked γ-CD oligomers which neither the 2D H^1 NOESY NMR or UV-vis studies reveal. Molecular models of the possible 1:1 and 2:1 host-guest complexes are constructed and their geometries optimised through the PM7 semi-empirical method using MOPAC2012.[61] For each 1:1 complex, a cooperative *syn* and cooperative *anti* complex as well as a non-cooperative complex are constructed. Cooperative and non-cooperative 2:1 host-guest complexes are also constructed. In this way the relative stabilities of the different complexation modes may be assessed in the gas phase.

These models are exemplified by non-cooperative *anti* (33γ-CD_2ox)$_2$.H_2TSPP^{4-} and cooperative *syn* (33γ-CD_2ox)$_2$.H_2TSPP^{4-} shown in Figure 2.16, and by the three possible 33γ-CD_2suc.H_2TSPP^{4-} host-guest complexes and the two possible (33γ-CD_2suc)$_2$.H_2TSPP^{4-} host-guest complexes shown in Figure 2.18. (The other twenty four host-guest complexes modelled appear in Figures A25 – A29 in the Appendix). The gas phase heats of formation, *E*, for each complex are collected in Table 2.3.

Although the role of water is likely to be significant in determining the stereochemistries and stoichiometries of the host-guest complexes formed through γ-CD and its oligomers

complexing H_2TSPP^{4-}, the relative energies of these complexes in the gas phase provide insight into the observed aqueous phase stereochemistries and stoichiometries.

Complexation of H_2TSPP^{4-} by a single γ-CD may occur by either the wide or narrow annular face. The *E* values for complexation by the narrow face are slightly lower than that of the wide face (2.73 kJ mol^{-1}, Table 2.3 and Figure A25 of the Appendix). This indicates that the *p*-sulfonatophenyl groups are the major contributing factor of H_2TSPP^{4-} to the energetics of host-guest complexation as partial complexation of the bulky pyrrolic core of H_2TSPP^{4-} would probably favour complexation through the wide face of γ-CD.

When H_2TSPP^{4-} is complexed by two γ-CD in a 2:1 host-guest complex, several different conformations may arise. The γ-CD annuli may complex through either the wide or narrow face in a *syn* or *anti* conformations in six possible 2:1 host-guest complexes: *anti* (two narrow faces), *syn* (two narrow faces), *syn* (two wide faces), *anti* (two wide faces), *anti* (one narrow and one wide face) and *syn* (one narrow and one wide face) as shown in Figure A25 of the Appendix. The *E* data for the complexes suggest that the *anti*-conformation is favoured over the *syn* conformation in all six systems, and is attributable to a lesser steric crowding in the *anti* complexes by comparison with that in the *syn* complexes. The *E* data also indicates that when 2:1 host-guest complexes are formed, the wide face is preferred over the narrow face for entrance into the γ-CD annulus. This may be a consequence of the wide face allowing freedom of movement around H_2TSPP^{4-} such that steric hindrance is minimised in the 2:1 host-guest complexes.

The semi empirical calculations for the γ-CD dimer/H_2TSPP^{4-} systems give insight into the stability of the non-cooperative and cooperative *syn*- and *anti*-conformers of the host-guest complexes. In all cases the cooperative complexation modes showed larger *E*, and therefore a greater stability, than their non-cooperative counterparts. The *anti*-conformers are more stable than the *syn*-conformers in all of the systems.

Table 2.3: Heats of formation, *E*, for the complexation of H_2TSPP^{4-} by γ-CD, 33γ-CD_2ox, 33γ-CD_2suc, 66γ-CD_2ox, 66γ-CD_2suc and 666γ-CD_3bz calculated through MOPAC2012.[61]

Host-Guest Complex	Heat of formation (*E*) kJ mol^{-1}
γ-CD.H_2TSPP^{4-} (wide face)	-8818.52
γ-CD.H_2TSPP^{4-} (narrow face)	-8821.25
anti (γ-CD)$_2$.H_2TSPP^{4-} (two narrow faces)	-16715.58
syn (γ-CD)$_2$.H_2TSPP^{4-} (two narrow faces)	-16604.36
anti (γ-CD)$_2$.H_2TSPP^{4-} (two wide faces)	-16894.85
syn (γ-CD)$_2$.H_2TSPP^{4-} (two wide faces)	-16855.17
anti (γ-CD)$_2$.H_2TSPP^{4-} (1 narrow and 1 wide face)	-16631.34
syn (γ-CD)$_2$.H_2TSPP^{4-} (1 narrow and 1 wide face)	-16597.43
33γ-CD_2ox.H_2TSPP^{4-} (non-coop) (one narrow face)	-16585.37
anti 33γ-CD_2ox.H_2TSPP^{4-} (coop) (two wide faces)	-16909.09
syn 33γ-CD_2ox.H_2TSPP^{4-}(coop) (two wide faces)	-16901.92
33γ-CD_2suc.H_2TSPP^{4-} (non-coop) (one narrow face)	-16604.36
anti 33γ-CD_2suc.H_2TSPP^{4-} (coop) (two wide faces)	-16981.07
syn 33γ-CD_2suc.H_2TSPP^{4-} (coop) (two wide faces)	-16818.70
66γ-CD_2ox.H_2TSPP^{4-} (non-coop) (one wide face)	-16271.94
anti 66γ-CD_2ox.H_2TSPP^{4-}(coop) (two narrow faces)	-17061.17
syn 66γ-CD_2ox.H_2TSPP^{4-} (coop) (two narrow faces)	-16585.46
66γ-CD_2suc.H_2TSPP^{4-} (non-coop) (one wide face)	-16501.35
anti 66γ-CD_2suc.H_2TSPP^{4-} (coop) (two narrow faces)	-16964.35
syn 66γ-CD_2suc.H_2TSPP^{4-} (coop) (two narrow faces)	-16714.31
666γ-CD_3bz.H_2TSPP^{4-} (1 narrow face annulus complexed)	-24070.58
666γ-CD_3bz.H_2TSPP^{4-} (2 narrow face annuli complexed)	-24133.56
666γ-CD_3bz.H_2TSPP^{4-} (3 narrow face annuli complexed)	-24382.68
(33γ-CD_2ox)$_2$.H_2TSPP^{4-} (non-coop) (two narrow faces)	-32170.01
syn (33γ-CD_2ox)$_2$.H_2TSPP^{4-} (coop) (four wide faces)	-32342.01
(33γ-CD_2suc)$_2$.H_2TSPP^{4-} (non.coop) (two narrow faces)	-32241.10
syn (33γ-CD_2suc)$_2$.H_2TSPP^{4-} (coop) (four wide faces)	-32510.07
(66γ-CD_2ox)$_2$.H_2TSPP^{4-} (non-coop) (two wide faces)	-32250.18
(66γ-CD_2suc)$_2$.H_2TSPP^{4-} (non-coop) (two wide faces)	-32339.32

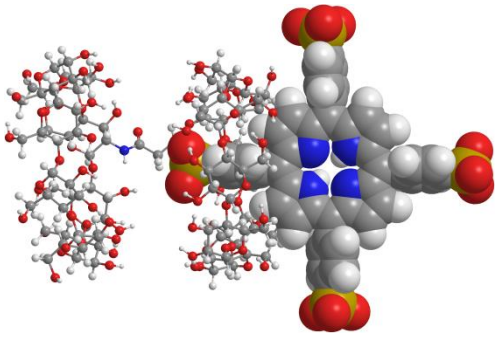

33γ-CD_2suc.H_2TSPP^{4-}
(non-cooperative) one narrow face

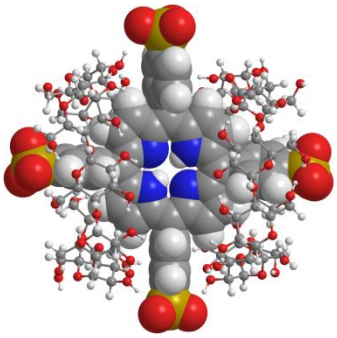

anti 33γ-CD_2suc.H_2TSPP^{4-}
(cooperative) two wide faces

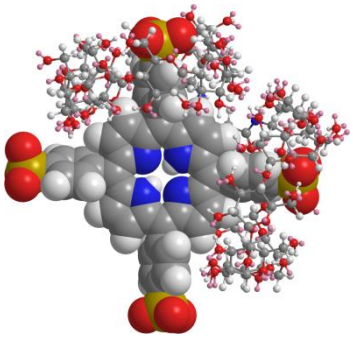

syn 33γ-CD_2suc.H_2TSPP^{4-}
(cooperative) two wide faces

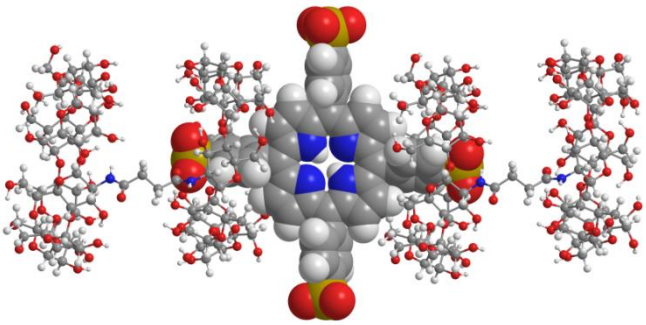

(33γ-CD_2suc)$_2$.H_2TSPP^{4-}
(non-cooperative) two narrow faces

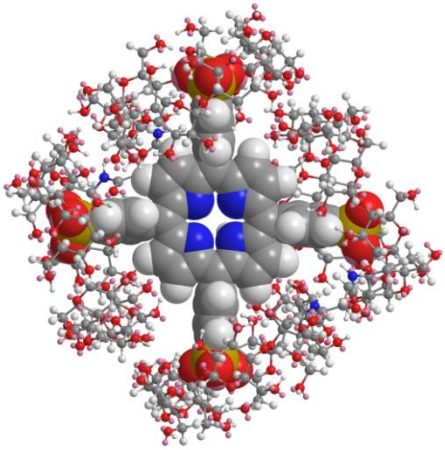

(33γ-CD_2suc)$_2$.H_2TSPP^{4-}
(cooperative) four wide faces

Figure 2.18: Energy minimised molecular models of the possible species involved in the 33γ-CD_2suc/H_2TSPP^{4-} equilibria derived using the PM7 method. For the potential 1:1 non-cooperative 33γ-CD_2suc.H_2TSPP^{4-} the heat of formation, E = -16585.37 kJ mol^{-1}, for *anti* 33γ-CD_2suc.H_2TSPP^{4-} E = -16909.09 kJ mol^{-1}, for *syn* 33γ-CD_2suc.H_2TSPP^{4-} E = -16901.92 kJ mol^{-1}, for 2:1 non-cooperative (33γ-CD_2suc)$_2$.H_2TSPP^{4-} E = -32241.10 kJ mol^{-1} and for cooperative *syn* (33γ-CD_2suc)$_2$.H_2TSPP^{4-} E = -32510.07 kJ mol^{-1}. Note: 33γ-CD_2suc = ball and stick, H_2TSPP^{4-} = space filling. Carbon = grey, hydrogen = white, oxygen = red, nitrogen = blue and sulphur = gold.

For the 66γ-CD_2ox.H_2TSPP^{4-} complex (Figure A27 of the Appendix), the *anti* conformer was the most stable with an *E* 475.71 kJ mol^{-1} greater than that of the *syn* conformer. This may be attributed to the low flexibility of short oxalate linker hindering complexation on adjacent *p*-sulfonatophenyl groups of H_2TSPP^{4-} in the *syn* conformation. This is in accord with the difference in *E* for the *anti* and *syn* 66γ-CD_2suc.H_2TSPP^{4-} decreasing to 250.04 kJ mol^{-1}, (Figure A28 of the Appendix) which is attributable to the increased length and flexibility of the succinamide linker.

For 33γ-CD_2ox.H_2TSPP^{4-} (Figure A26 of the Appendix) and 33γ-CD_2suc.H_2TSPP^{4-} (Figure 2.18), the difference in *E* between the *syn* and *anti* conformers (7.17 and 162.37 kJ mol^{-1}, respectively) is less than in the analogous 6,6- dimer systems but the order of the differences in *E* is reversed. It appears that complexation through the wider γ-CD face may allow adjacent *p*-sulfonatophenyl group complexation with less strain in 33γ-CD_2ox.H_2TSPP^{4-} and 33γ-CD_2suc.H_2TSPP^{4-}. However, the reversal in the *E* differences referred to above indicates both the face through which H_2TSPP^{4-} the dimer γ-CD annuli and the linker contribute to the overall strain involved in the complexes.

Models for the 666γ-CD_3bz.H_2TSPP^{4-} complex, complexing *p*-sulfonatophenyl groups through one, two or three narrow annular faces (Figure A29) show a progressive increase in *E* from -24070.58, to -24133.56 to -24382.68 kJ mol^{-1} with the respective step-wise differences being 62.92 and 249.12 kJ mol^{-1} consistent with increasing stability as the complex progresses from mono- to di- to tritopic. Evidently there is little hindrance to tritopic complexation which may be attributable to the substantially longer linkers between each pair of γ-CD annuli in 666γ-CD_3bz than in the four γ-CD dimers. This is in accord with 666γ-CD_3bz.H_2TSPP^{4-} exhibiting the largest K_{11}, ΔH_{11} and a negative ΔS_{11} (Table 2.1) in the aqueous complexation studies discussed earlier. It is also in accord with

666γ-CD_3bz.H_2TSPP^{4-} exhibiting the largest UV-vis absorption red shift in aqueous solution (Figure 2.12).

The heats of formation, *E*, and the models for the non-cooperative and cooperative *syn* (33γ-CD_2ox)$_2$.H_2TSPP^{4-} and (33γ-CD_2suc)$_2$.H_2TSPP^{4-} 2:1 complexes appear in Table 2.3 and Figure 2.16 and Figure A27 in the Appendix. (The corresponding cooperative *anti* 2:1 complexes could not be energy minimised as a consequence of steric hindrance.) It is seen that *E* for the cooperative complexes are substantial more negative than for the non-cooperative complexes with the differences being 172.00 kJ mol^{-1} (33γ-CD_2ox)$_2$.H_2TSPP^{4-} and 268.97 kJ mol^{-1} (33γ-CD_2suc)$_2$.H_2TSPP^{4-} consistent with ditopic complexation by 33γ-CD_2ox and 33γ-CD_2suc producing greater stability than monotopic complexation, and with the greater length and flexibility of the succinimide linker lessening steric hindrance and structural strain than does the oxalate linker. An overall scheme is shown in Figure 2.19 for the equilibria which are potentially possible for complexation of H_2TSPP^{4-} by 33γ-CD_2ox and 33γ-CD_2suc in the gas phase which may be compared with the complexes which energy minimised (Table 2.3 and Figures 2.16 and 2.18 and Figure A26 in the Appendix).

The *E* values for the non-cooperative complexes of (66γ-CD_2ox)$_2$.H_2TSPP^{4-} and (66γ-CD_2suc)$_2$.H_2TSPP^{4-} (Table 2.3 and Figures A27 and A28 in the Appendix, respectively) are more negative than that for (33γ-CD_2ox)$_2$.H_2TSPP^{4-} and (33γ-CD_2suc)$_2$.H_2TSPP^{4-} (a difference of 80.17 and 98.25 kJ mol^{-1}, respectively). This data is in accord with the trend observed with (γ-CD_2)$_2$.H_2TSPP^{4-}, where the wide face is preferred over the narrow face for the entrance of H_2TSPP^{4-} into the γ-CD annulus. The *E* values for the non-cooperative complexes of (66γ-CD_2ox)$_2$.H_2TSPP^{4-} and (66γ-CD_2suc)$_2$.H_2TSPP^{4-} are less negative than those of the cooperative complexes for (33γ-CD_2ox)$_2$.H_2TSPP^{4-} and (33γ-CD_2suc)$_2$.H_2TSPP^{4-} (a difference of 91.83 and 170.75 kJ mol^{-1}, respectively). This is indicative of the cooperative

complexing effect leading to increase of the inherent stability of the 2:1 host-guest complexes. Neither the cooperative *anti* nor the cooperative *syn* 2:1 $(66\gamma\text{-}CD_2ox)_2.H_2TSPP^{4-}$ and $(66\gamma\text{-}CD_2suc)_2.H_2TSPP^{4-}$ complexes could be energy minimised because of steric hindrance.

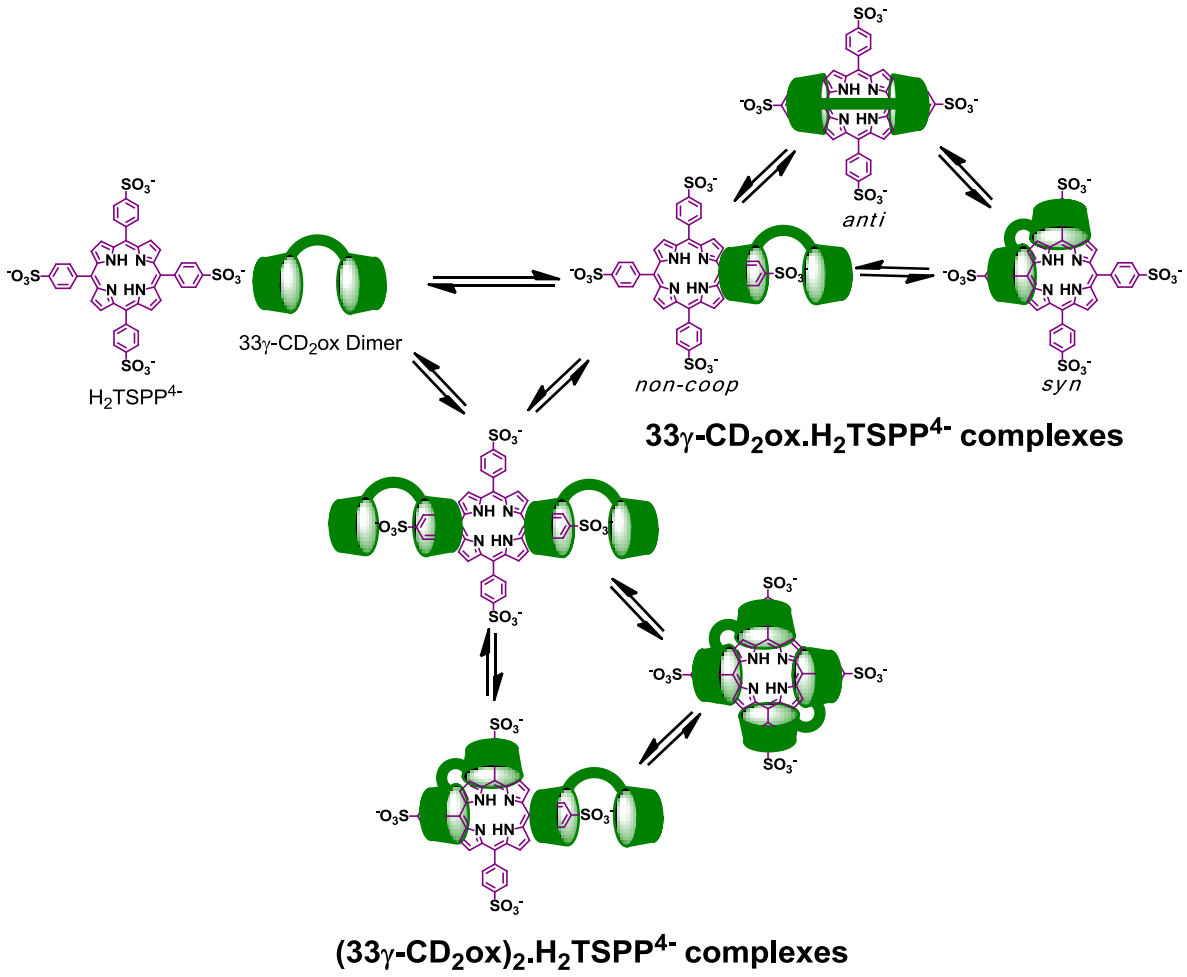

Figure 2.19: Scheme for the potential host-guest equilibria existing between the 33γ-CD_2ox dimer and H_2TSPP^{4-}. A similar scheme applies for the 33γ-CD_2suc dimer and H_2TSPP^{4-}.

2.6. SUMMARY AND CONCLUSIONS

The host-guest complexation of H_2TSPP^{4-} by γ-CD, 33γ-CD_2ox, 33γ-CD_2suc, 66γ-CD_2ox, 66γ-CD_2suc and 666γ-CD_3bz has been characterised in aqueous solution by 2D ^{1}H NOSEY NMR and UV-vis spectroscopy and by computationally in the gas phase by PM7 semi-empirical calculations. The 2D ^{1}H NOESY NMR spectra show that γ-CD and its oligomers

complex H_2TSPP^{4-} as is evident from the cross-peaks arising from NOE interactions between the pyrrolic and *p*-sulfonatophenyl protons of H_2TSPP^{4-} and the annular protons of γ-CD and its oligomers. The UV-vis studies show that 1:1 host-guest complexes are predominant in the 66γ-CD_2ox, 66γ-CD_2suc and 666γ-CD_3bz systems, whilst γ-CD, 33γ-CD_2ox and 33γ-CD_2suc also form 2:1 host-guest complexes. The K_{11} values derived for 1:1 host-guest complexation are 13 – 1800-fold larger for the γ-CD oligomers than for γ-CD at 278.2 K. This observation is consistent with a strong cooperative effect when the γ-CD oligomers complex H_2TSPP^{4-}. The K_{21} values derived for $(33\gamma\text{-}CD_2ox)_2.H_2TSPP^{4-}$ and $(33\gamma\text{-}CD_2suc)_2.H_2TSPP^{4-}$ are high by comparison with K_{21} $(\gamma\text{-}CD)_2.H_2TSPP^{4-}$ consistent with both 33γ-CD_2ox and 33γ-CD_2suc complexing H_2TSPP^{4-} ditopically in their 2:1 complexes.

The ΔH and $T\Delta S$ data characterising γ-CD.H_2TSPP^{4-}, 33γ-CD_2ox.H_2TSPP^{4-}, 66γ-CD_2ox.H_2TSPP^{4-} and 66γ-CD_2suc.H_2TSPP^{4-} shows their formation to be exothermic and entropy-driven where the entropy increase probably dominantly arises through expulsion of water from their γ-CD annuli upon complexation of the *p*-sulfonatophenyl groups of H_2TSPP^{4-}. The formation of the 33γ-CD_2suc.H_2TSPP^{4-} and 666γ-CD_3bz.H_2TSPP^{4-} complexes is exothermic and enthalpically stabilised apparently as a consequence of the entropic increase arising from expulsion of water from their γ-CD annuli being offset by the decrease in entropy resulting from the independent host and guest forming a single host-guest complex. The ΔH for the 2:1 $(\gamma\text{-}CD)_2.H_2TSPP^{4-}$, $(33\gamma\text{-}CD_2ox)_2.H_2TSPP^{4-}$ and $(33\gamma\text{-}CD_2suc)_2.H_2TSPP^{4-}$ complexes are substantially more negative than those for their 1:1 analogues The corresponding $T\Delta S$ changes from positive to negative for $(\gamma\text{-}CD)_2.H_2TSPP^{4-}$, becomes less positive for $(33\gamma\text{-}CD_2ox)_2.H_2TSPP^{4-}$ and becomes more negative for $(33\gamma\text{-}CD_2suc)_2.H_2TSPP^{4-}$. Thus, the first complexation to form a 1:1 complex appears to facilitate a second complexation to form a 2:1 complex possibly because the hydration shell of free H_2TSPP^{4-} is disrupted by the first complexation which facilitates the second complexation step.

Gas phase molecular modelling shows that when two γ-CD annuli complex two adjacent *p*-sulfonatophenyl groups of H_2TSPP^{4-} in the *syn* conformation the heat of formation, *E*, is less negative than when two distant *p*-sulfonatophenyl groups are complexed in the *anti* configuration which is the most stable configuration. The difference in *E* between the *syn* and *anti* 33γ-CD_2ox.H_2TSPP^{4-} and 33γ-CD_2suc.H_2TSPP^{4-} complexes is smaller than for the *syn* and *anti* 66γ-CD_2ox.H_2TSPP^{4-} and 66γ-CD_2suc.H_2TSPP^{4-} complexes. This is attributed to the wide annular γ-CD faces of 33γ-CD_2ox and 33γ-CD_2suc allowing more flexibility in complexing H_2TSPP^{4-} than the narrow annular γ-CD faces of 66γ-CD_2ox and 66γ-CD_2suc. These gas phase models largely reflect the relative stabilities found for the complexes characterised in solution and indicate the importance of steric interactions in determining the relative magnitudes of these stabilities.

This study provides important information on the factors affecting the host-guest equilibria of the photosensitiser, H_2TSPP^{4-} with γ-CD and γ-CD oligomers in aqueous solution and may lead to better design of photodynamic therapy treatments for cancer. Further studies with metallated porphyrins could provide more insight into the host-guest complexation of photosensitisers by γ-CD oligomers.

2.7. REFERENCES

1. J. Rivers-Auty and J. C. Ashton, *Curr. Neurovasc. Res.*, 2013, **10**, 356-360.
2. R. Anand, M. Malanga, I. Manet, F. Manoli, K. Tuza, A. Aykac, C. Ladaviere, E. Fenyvesi, A. Vargas-Berenguel, R. Gref and S. Monti, *Photochem. Photobiol. Sci.*, 2013, **12**, 1841-1854.
3. J. Kralova, Z. Kejik, T. Briza, P. Pouckova, A. Kral, P. Martasek and V. Kral, *J. Med. Chem.*, 2010, **53**, 128-138.
4. K. Kano, *Colloid Polym. Sci.*, 2008, **286**, 79-84.
5. N. Zafar, H. Fessi and A. Elaissari, *Int. J. Pharm.*, 2014, **461**, 351-366.
6. T. Jiang, M. Li and D. S. Lawrence, *J. Org. Chem.*, 1995, **60**, 7293-7297.
7. F. Venema, A. E. Rowan and R. J. M. Nolte, *J. Am. Chem. Soc.*, 1996, **118**, 257-258.
8. Y. Liu and Y. Chen, *Acc. Chem. Res.*, 2006, **39**, 681-691.
9. C. J. Easton, S. J. van Eyk, S. F. Lincoln, B. L. May, J. Papageorgiou and M. L. Williams, *Aust. J. Chem.*, 1997, **50**, 9-12.
10. H. T. Ngo, P. Clements, C. J. Easton, D.-T. Pham and S. F. Lincoln, *Aust. J. Chem.*, 2010, **63**, 687-692.
11. J. Wang, L. Li, X. Guo, L. Zheng, D.-T. Pham, S. F. Lincoln, H. T. Ngo, P. Clements, B. L. May, R. K. Prud'homme and C. J. Easton, *Ind. Eng. Chem. Res.*, 2011, **50**, 7566-7571.
12. H.-T. Nguyen, D.-T. Pham, S. F. Lincoln, J. Wang, X. Guo, C. J. Easton and R. K. Prud'homme, *Polym. Chem.*, 2013, **4**, 820-829.
13. H.-T. Nguyen, D.-T. Pham, C. J. Easton and S. F. Lincoln, *Aust. J. Chem.*, 2013, **66**, 1057-1064.
14. T. Harada, D. T. Pham, M. H. Leung, H. T. Ngo, S. F. Lincoln, C. J. Easton and T. W. Kee, *J. Phys. Chem. B*, 2011, **115**, 1268-1274.

15. T. Harada, H. L. McTernan, D.-T. Pham, S. F. Lincoln and T. W. Kee, *J. Phys. Chem. B*, 2015, **119**, 2425-2433.

16. E. Morillo, M. A. Sanchez-Trujillo, J. R. Moyano, J. Villaverde, M. E. Gomez-Pantoja and J. I. Perez-Martinez, *PLoS One*, 2012, **7**, e44137.

17. H. M. Wang and G. Wenz, *Chem. Asian J.*, 2011, **6**, 2390-2399.

18. D. Xu, L. Wang, D. Gourevich, E. Kabha, F. Arditti, M. Athamna, S. Cochran, A. Melzer and J. M. Gnaim, *Chem Pharm Bull*, 2014, **62**, 627-635.

19. Z. Kejik, T. Briza, P. Pouckova, J. Kralova, V. Kral and P. Martasek, *J. Controlled Release*, 2008, **132**, e27-e28.

20. J. Pitha, E. J. Anaissie and K. Uekama, *J. Pharm. Sci.*, 1987, **76**, 788-790.

21. T. Cserhati and E. Forgacs, *Eur. J. Pharm. Biopharm.*, 1998, **46**, 153-159.

22. S. Hamai and T. Ohshida, *J. Inclusion Phenom. Macrocyclic Chem.*, 2004, **50**, 209-217.

23. J. M. Ribo, J.-A. Farrera, M. L. Valero and A. Virgili, *Tetrahedron*, 1995, **51**, 3705-3712.

24. A. Juzeniene, Q. Peng and J. Moan, *Photochem. Photobiol. Sci.*, 2007, **6**, 1234-1245.

25. C. M. Lemon, P. J. Brothers and B. Boitrel, *Dalton Trans.*, 2011, **40**, 6591-6609.

26. L. Wang, H. Li, G. Fang, J. Zhou and D. Cao, *Sens. Actuators, B*, 2014, **196**, 653-662.

27. K. Kano, H. Kitagishi, S. Tamura and A. Yamada, *J. Am. Chem. Soc.*, 2004, **126**, 15202-15210.

28. T. Ueda, H. Kitagishi and K. Kano, *Inorg. Chem.*, 2014, **53**, 543-551.

29. K. Kano, H. Kitagishi, T. Mabuchi, M. Kodera and S. Hirota, *Chem. Asian J.*, 2006, **1**, 358-366.

30. J. H. Kim, M. Lee, J. S. Lee and C. B. Park, *Angew. Chem., Int. Ed.*, 2012, **51**, 517-520, S517/511-S517/511.

31. H.-J. Son, S. Jin, S. Patwardhan, S. J. Wezenberg, N. C. Jeong, M. So, C. E. Wilmer, A. A. Sarjeant, G. C. Schatz, R. Q. Snurr, O. K. Farha, G. P. Wiederrecht and J. T. Hupp, *J. Am. Chem. Soc.*, 2013, **135**, 862-869.

32. J. G. Woller, J. K. Hannestad and B. Albinsson, *J. Am. Chem. Soc.*, 2013, **135**, 2759-2768.

33. Y.-H. Jeong, M. Son, H. Yoon, P. Kim, D.-H. Lee, D. Kim and W.-D. Jang, *Angew. Chem., Int. Ed.*, 2014, **53**, 6925-6928.

34. J. Luo, M. Xu, R. Li, K.-W. Huang, C. Jiang, Q. Qi, W. Zeng, J. Zhang, C. Chi, P. Wang and J. Wu, *J. Am. Chem. Soc.*, 2014, **136**, 265-272.

35. V. V. Serra, A. Zamarron, M. A. F. Faustino, M. C. Iglesias-de la Cruz, A. Blazquez, J. M. M. Rodrigues, M. G. P. M. S. Neves, J. A. S. Cavaleiro, A. Juarranz and F. Sanz-Rodriguez, *Bioorg. Med. Chem.*, 2010, **18**, 6170-6178.

36. X. Zhu, W. Lu, Y. Zhang, A. Reed, B. Newton, Z. Fan, H. Yu, P. C. Ray and R. Gao, *Chem. Commun.*, 2011, **47**, 10311-10313.

37. Z. Kejik, R. Kaplanek, T. Briza, J. Kralova, P. Martasek and V. Kral, *Supramol. Chem.*, 2012, **24**, 106-116.

38. A. P. Thomas, P. S. Saneesh Babu, S. Asha Nair, S. Ramakrishnan, D. Ramaiah, T. K. Chandrashekar, A. Srinivasan and M. Radhakrishna-Pillai, *J. Med. Chem.*, 2012, **55**, 5110-5120.

39. J. Mosinger, M. Deumie, K. Lang, P. Kubat and D. M. Wagnerova, *J. Photochem. Photobiol., A*, 2000, **130**, 13-20.

40. A. Mazzaglia, in *Cyclodextrins in Pharmaceutics, Cosmetics, and Biomedicine*, John Wiley & Sons, Inc., 2011, pp. 343-361.

41. K. Kano, H. Kitagishi, M. Kodera and S. Hirota, *Angew. Chem., Int. Ed.*, 2005, **44**, 435-438.

42. R. R. French, P. Holzer, M. G. Leuenberger and W.-D. Woggon, *Angew. Chem., Int. Ed.*, 2000, **39**, 1267-1269.

43. F. Venema, H. F. M. Nelissen, P. Berthault, N. Birlirakis, A. E. Rowan, M. C. Feiters and R. J. M. Nolte, *Chem. Eur. J.*, 1998, **4**, 2237-2250.

44. Y. Wang, B. Cohen, A. Aykac, A. Vargas-Berenguel and A. Douhal, *Photochem. Photobiol. Sci.*, 2013, **12**, 2119-2129.

45. A. Mulder, A. Jukovic, F. W. B. Van Leeuwen, H. Kooijman, A. L. Spek, J. Huskens and D. N. Reinhoudt, *Chem. Eur. J.*, 2004, **10**, 1114-1123.

46. A. Mulder, A. Jukovic, J. Huskens and D. N. Reinhoudt, *Org. Biomol. Chem.*, 2004, **2**, 1748-1755.

47. A. Mulder, J. Huskens and D. N. Reinhoudt, *Eur. J. Org. Chem.*, 2005, 838-846.

48. K. Kano, R. Nishiyabu and R. Doi, *J. Org. Chem.*, 2005, **70**, 3667-3673.

49. K. Kano, R. Nishiyabu, T. Asada and Y. Kuroda, *J. Am. Chem. Soc.*, 2002, **124**, 9937-9944.

50. Y. Wang, B. Cohen, L. Jicsinszky and A. Douhal, *Langmuir*, 2012, **28**, 4363-4372.

51. D.-T. Pham, H. T. Ngo, S. F. Lincoln, B. L. May and C. J. Easton, *Tetrahedron*, 2010, **66**, 2895-2898.

52. Z. Dong and P. J. Scammells, *J. Org. Chem.*, 2007, **72**, 9881-9885.

53. A. Corsini and O. Herrmann, *Talanta*, 1986, **33**, 335-339.

54. S. C. M. Gandini, V. E. Yushmanov, I. E. Borissevitch and M. Tabak, *Langmuir*, 1999, **15**, 6233-6243.

55. K. M. Kadish, G. B. Maiya, C. Araullo and R. Guilard, *Inorg. Chem.*, 1989, **28**, 2725-2731.

56. A. Farajtabar, F. Gharib, P. Jamaat and N. Safari, *J. Chem. Eng. Data*, 2008, **53**, 350-354.

57. A. Iosif and U. W. Grummt, *J. Prakt. Chem./Chem.- Ztg.*, 1997, **339**, 420-425.

58. W. Saenger, J. Jacob, K. Gessler, T. Steiner, D. Hoffmann, H. Sanbe, K. Koizumi, S. M. Smith and T. Takaha, *Chem. Rev.*, 1998, **98**, 1787-1802.

59. HypSpec, Protonic Software, 2 Templegate Avenue, Leeds LS15 0HD, UK.

60. M. V. Rekharsky and Y. Inoue, *Chem. Rev.*, 1998, **98**, 1875-1917.

61. J. P. Stewart, Stewart Computational Chemistry, Colorado Springs, CO, 14.139W edn., 2012.

2.8. APPENDIX

2D ^{1}H NOESY NMR Spectra

a)

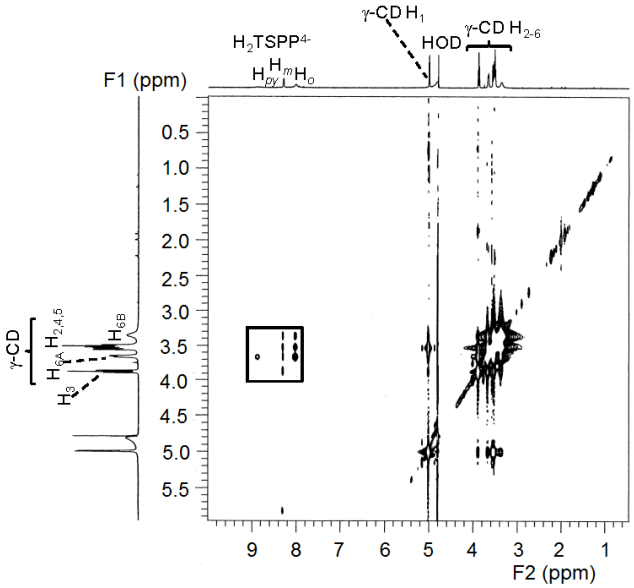

b)

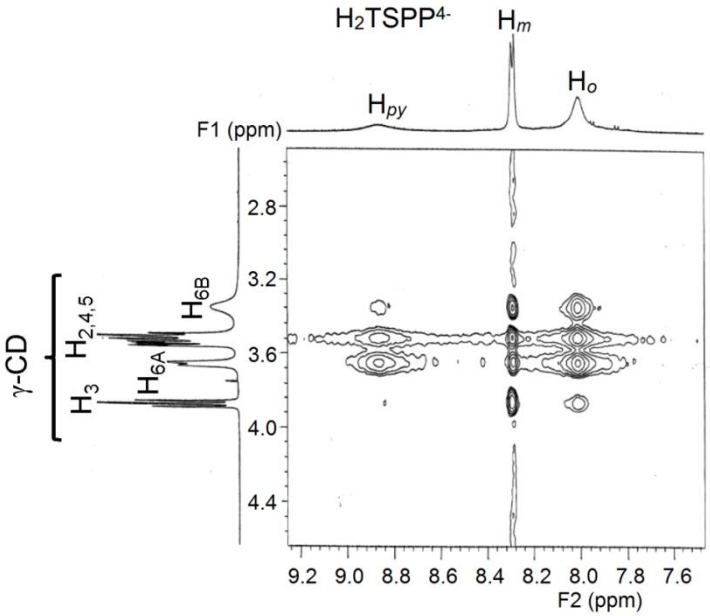

Figure A1: a) 2D ^{1}H NOESY NMR (600 MHz) spectrum of H_2TSPP^{4-} (3.0×10^{-3} mol dm^{-3}) and equimolar γ-CD in D_2O (pD 7.0 phosphate buffer, I = 0.10 mol dm^{-3}) at 298.2 K with a mixing time of 300 ms. b) Expanded aromatic resonance region. The amount of H_2TSPP^{4-} in the free state is ~ 30% of the total.

a)

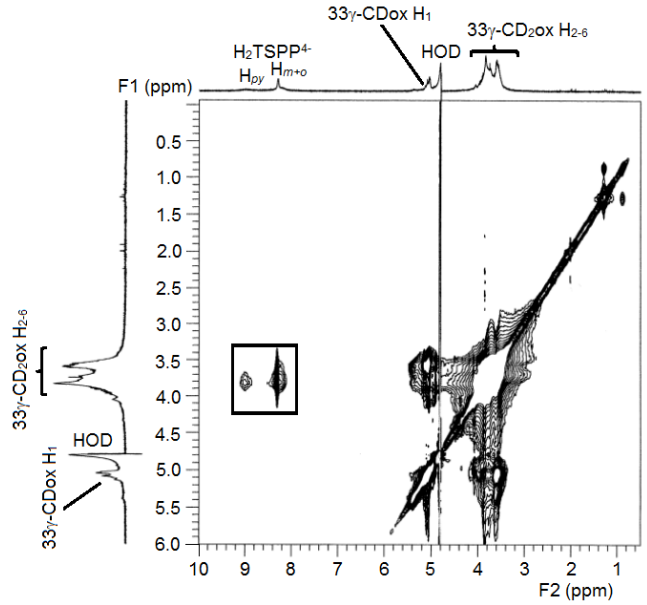

b)

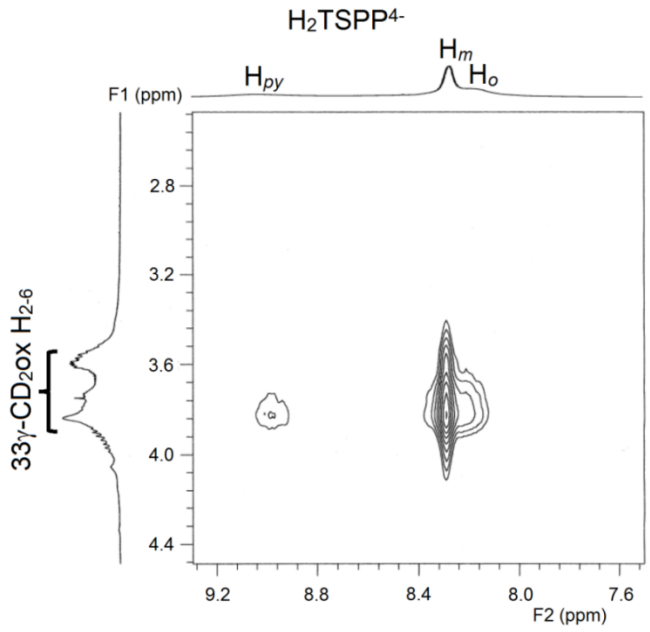

Figure A2: a) 2D ^{1}H NOESY NMR (600 MHz) spectrum of H_2TSPP^{4-} (3.0×10^{-3} mol dm^{-3}) and equimolar 33γ-CD_2ox in D_2O (pD 7.0 phosphate buffer, I = 0.10 mol dm^{-3}) at 298.2 K with a mixing time of 300 ms. Cross–peaks enclosed in the rectangle arise from interaction between the annular γ-CD protons $H_{3,5,6}$ of the CD annulus and the pyrrolic and phenyl protons of H_2TSPP^{4-}. b) Expanded aromatic resonance region. The amount of H_2TSPP^{4-} in the free state is ~ 10% of the total.

a)

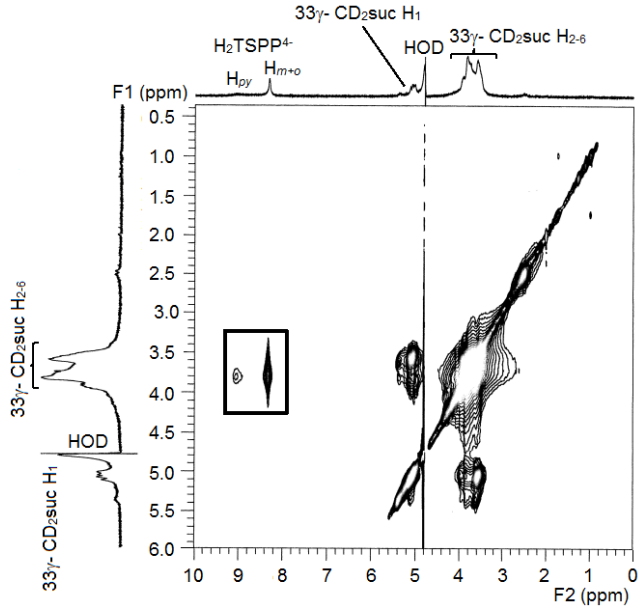

b)

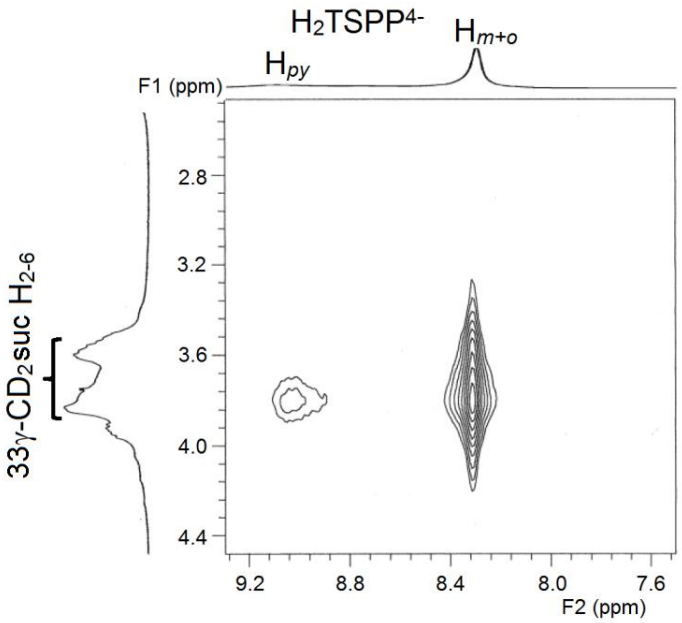

Figure A3: a) 2D ^{1}H NOESY NMR (600 MHz) spectrum of H_2TSPP^{4-} (3.0×10^{-3} mol dm^{-3}) and equimolar 33γ-CD_2suc in D_2O (pD 7.0 phosphate buffer, I = 0.10 mol dm^{-3}) at 298.2 K with a mixing time of 300 ms. Cross–peaks enclosed in the rectangle arise from interaction between the annular γ-CD protons $H_{3,5,6}$ of the CD annulus and the pyrrolic and phenyl protons of H_2TSPP^{4-}. b) Expanded aromatic resonance region. The amount of H_2TSPP^{4-} in the free state is ~ 9% of the total.

a)

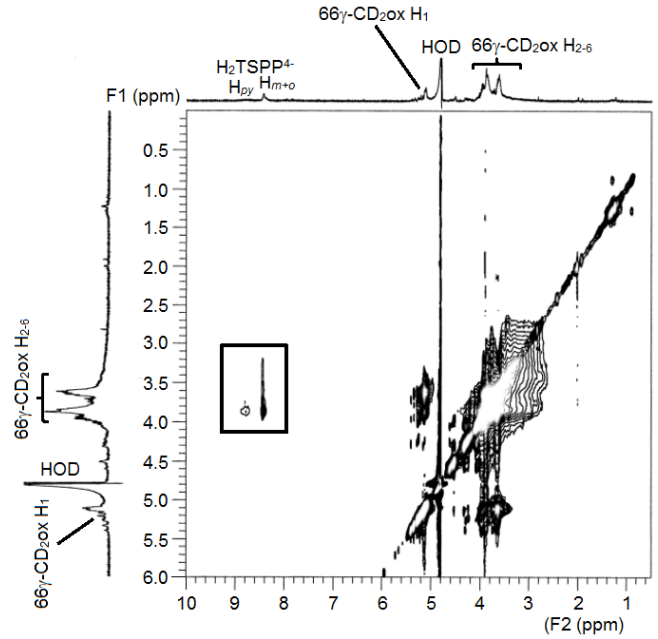

b)

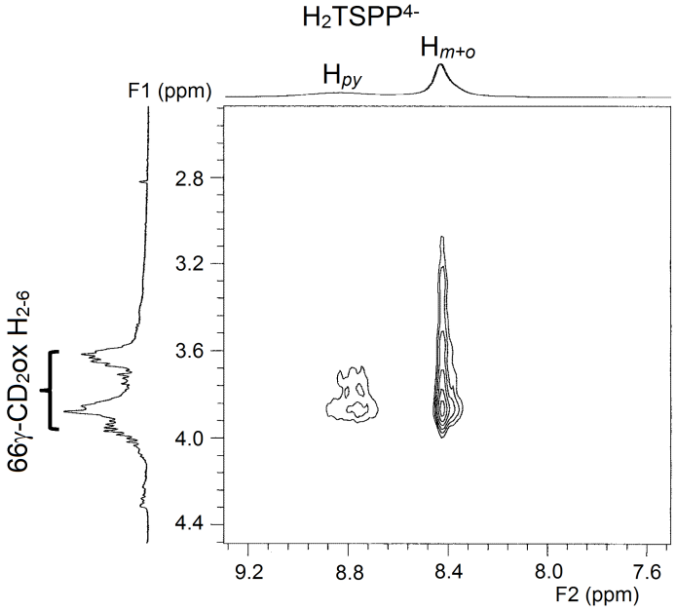

Figure A4: a) 2D ^{1}H NOESY NMR (600 MHz) spectrum of H_2TSPP^{4-} (3.0×10^{-3} mol dm^{-3}) and equimolar 66γ-CD_2ox in D_2O (pD 7.0 phosphate buffer, I = 0.10 mol dm^{-3}) at 298.2 K with a mixing time of 300 ms. Cross–peaks enclosed in the rectangle arise from interaction between the annular γ-CD protons $H_{3,5,6}$ of the CD annulus and the pyrrolic and phenyl protons of H_2TSPP^{4-}. b) Expanded aromatic resonance region. The amount of H_2TSPP^{4-} in the free state is ~ 5% of the total.

a)

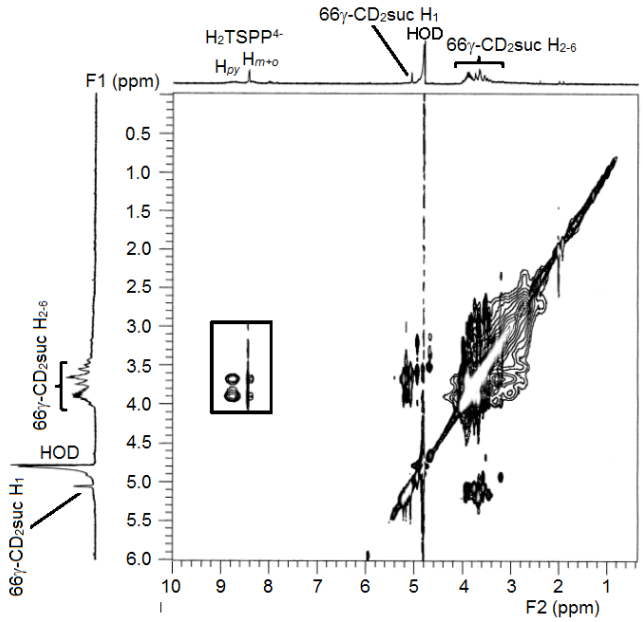

b)

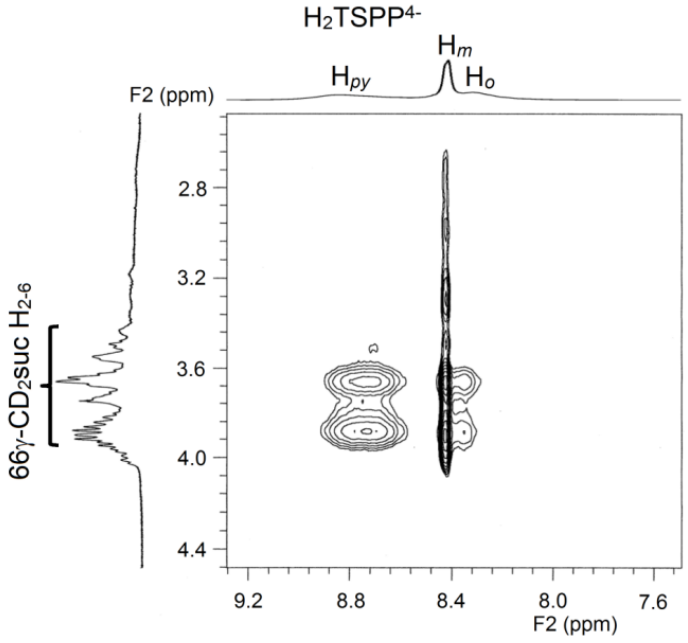

Figure A5: a) 2D ^{1}H NOESY NMR (600 MHz) spectrum of H_2TSPP^{4-} (3.0×10^{-3} mol dm^{-3}) and equimolar 66γ-CD_2suc in D_2O (pD 7.0 phosphate buffer, I = 0.10 mol dm^{-3}) at 298.2 K with a mixing time of 300 ms. Cross–peaks enclosed in the rectangle arise from interaction between the annular γ-CD protons $H_{3,5,6}$ of the CD annulus and the pyrrolic and phenyl protons of H_2TSPP^{4-}. b) Expanded aromatic resonance region. The amount of H_2TSPP^{4-} in the free state is ~ 1% of the total

a)

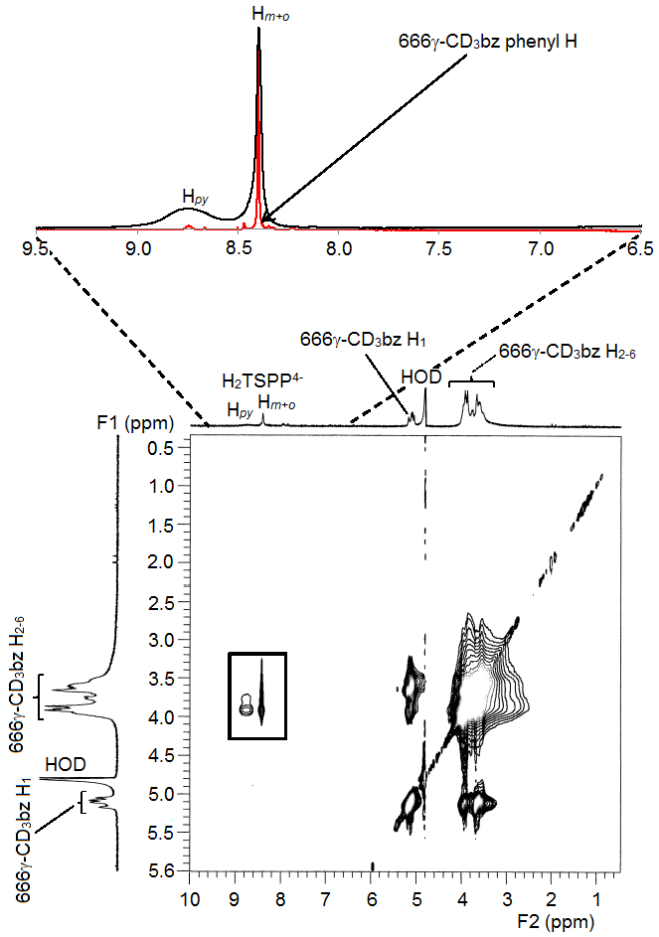

Figure A6: a) 2D ^{1}H NOESY NMR (600 MHz) spectrum of H_2TSPP^{4-} (3.0×10^{-3} mol dm^{-3}) and equimolar 666γ-CD_3bz in D_2O (pD 7.0 phosphate buffer, I = 0.10 mol dm^{-3}) at 298.2 K with a mixing time of 300 ms. Cross–peaks enclosed in the rectangle arise from interaction between the annular γ-CD protons $H_{3,5,6}$ of the γ-CD annulus and the pyrrolic and phenyl protons of H_2TSPP^{4-}. The amount of H_2TSPP^{4-} in the free state is ~ 1%.

b)

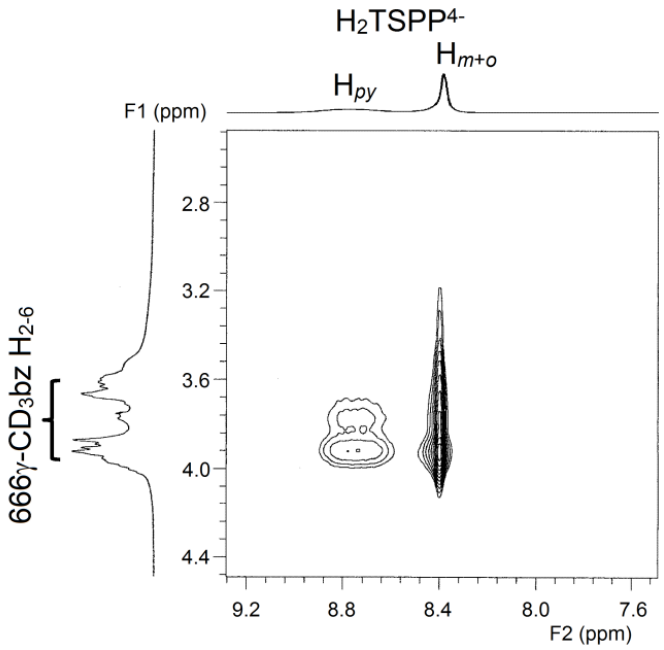

Figure A6: b) Expanded aromatic resonance region of the 2D ^{1}H NOESY NMR (600 MHz) spectrum of H_2TSPP^{4-} (3.0×10^{-3} mol dm^{-3}) and equimolar 666γ-CD_3bz in D_2O (pD 7.0 phosphate buffer, I = 0.10 mol dm^{-3}) at 298.2 K with a mixing time of 300 ms. The amount of H_2TSPP^{4-} in the free state is ~ 1% of the total.

Variable temperature UV-vis spectroscopy

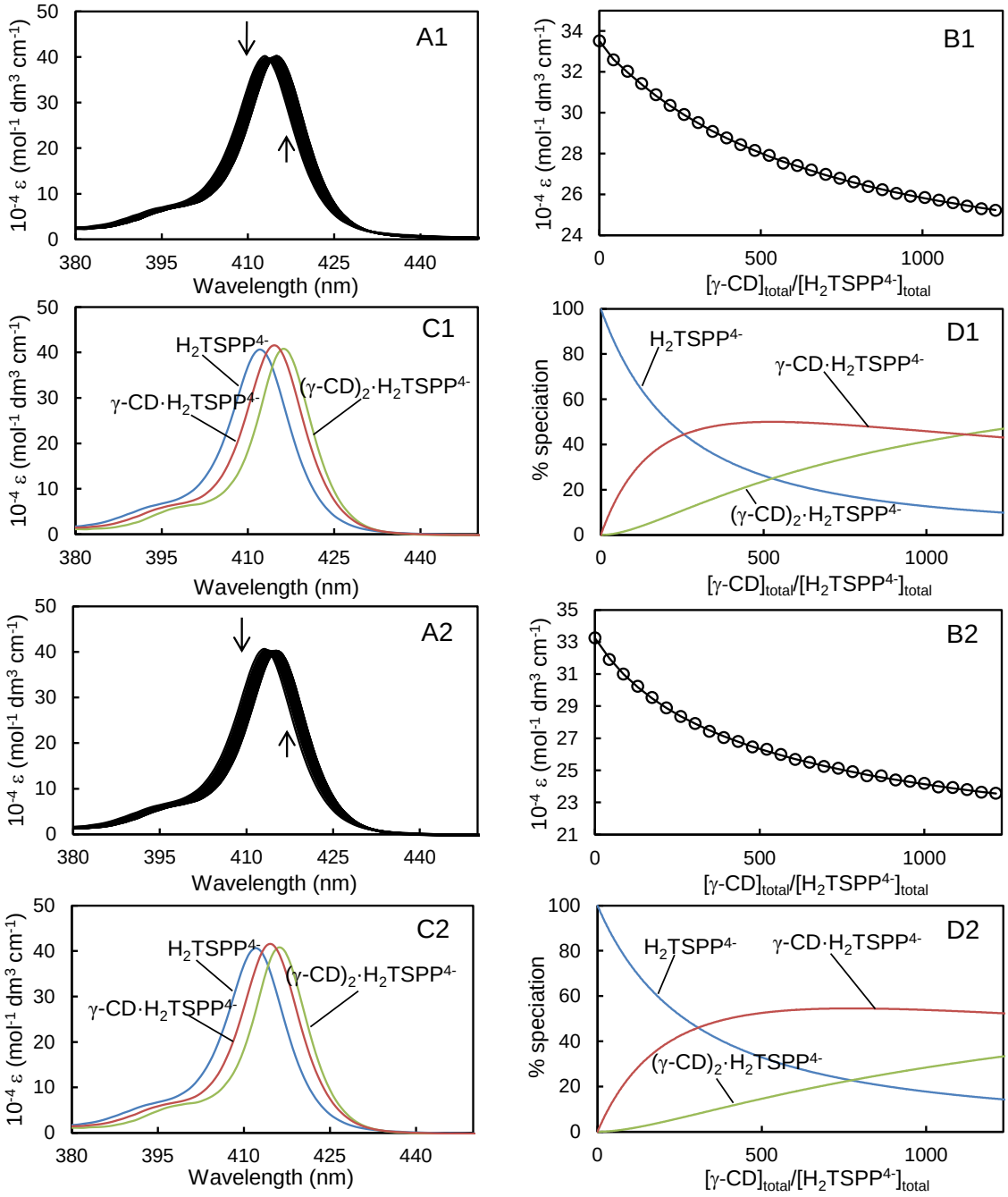

Figure A7: (A1, A2) Molar absorbance change of H_2TSPP^{4-} (1.05×10^{-6} mol dm^{-3}) in phosphate buffer, pH 7.0, I = 0.10 mol dm^{-3} with sequential injections (10 mm^3 each) of γ-CD (9.14×10^{-3} mol dm^{-3}) into both sample and reference cells. The arrows indicate the direction of molar absorbance change as the molar ratio of [γ-CD]/[H_2TSPP^{4-}] increases. (B1, B2) Molar absorbance variation at 410 nm and the line of best fit of an algorithm for 1:1 and 2:1 host-guest complexation over the wavelength range 400-430 nm. (C1, C2) Calculated molar absorbance of free and complexed H_2TSPP^{4-}. (D1, D2) Speciation with $[H_2TSPP^{4-}]_{total}$ = 100%. Note: A1-D1: data at 278.2 K. A2-D2: data at 288.2 K.

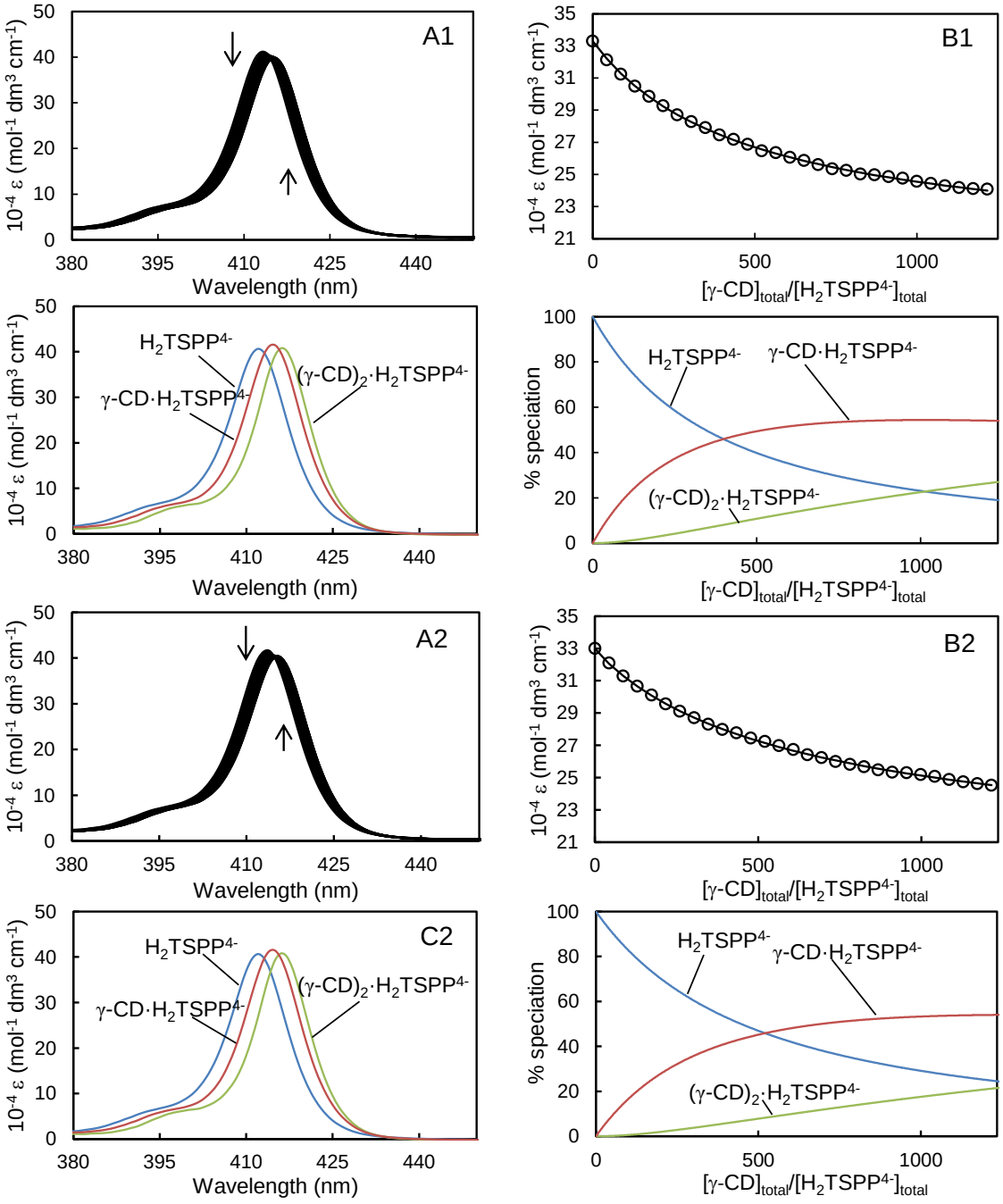

Figure A8: (A1, A2) Molar absorbance change of H_2TSPP^{4-} (1.05×10^{-6} mol dm^{-3}) in phosphate buffer, pH 7.0, I = 0.10 mol dm^{-3} with sequential injections (10 mm^3 each) of γ-CD (9.14×10^{-3} mol dm^{-3}) into both sample and reference cells. The arrows indicate the direction of molar absorbance change as the molar ratio of [γ-CD]/[H_2TSPP^{4-}] increases. (B1, B2) Molar absorbance variation at 410 nm and the line of best fit of an algorithm for 1:1 and 2:1 host-guest complexation over the wavelength range 400-430 nm. (C1, C2) Calculated molar absorbance of free and complexed H_2TSPP^{4-}. (D1, D2) Speciation with [H_2TSPP^{4-}]$_{total}$ = 100%. Note: A1-D1: data at 298.2 K. A2-D2: data at 308.2 K.

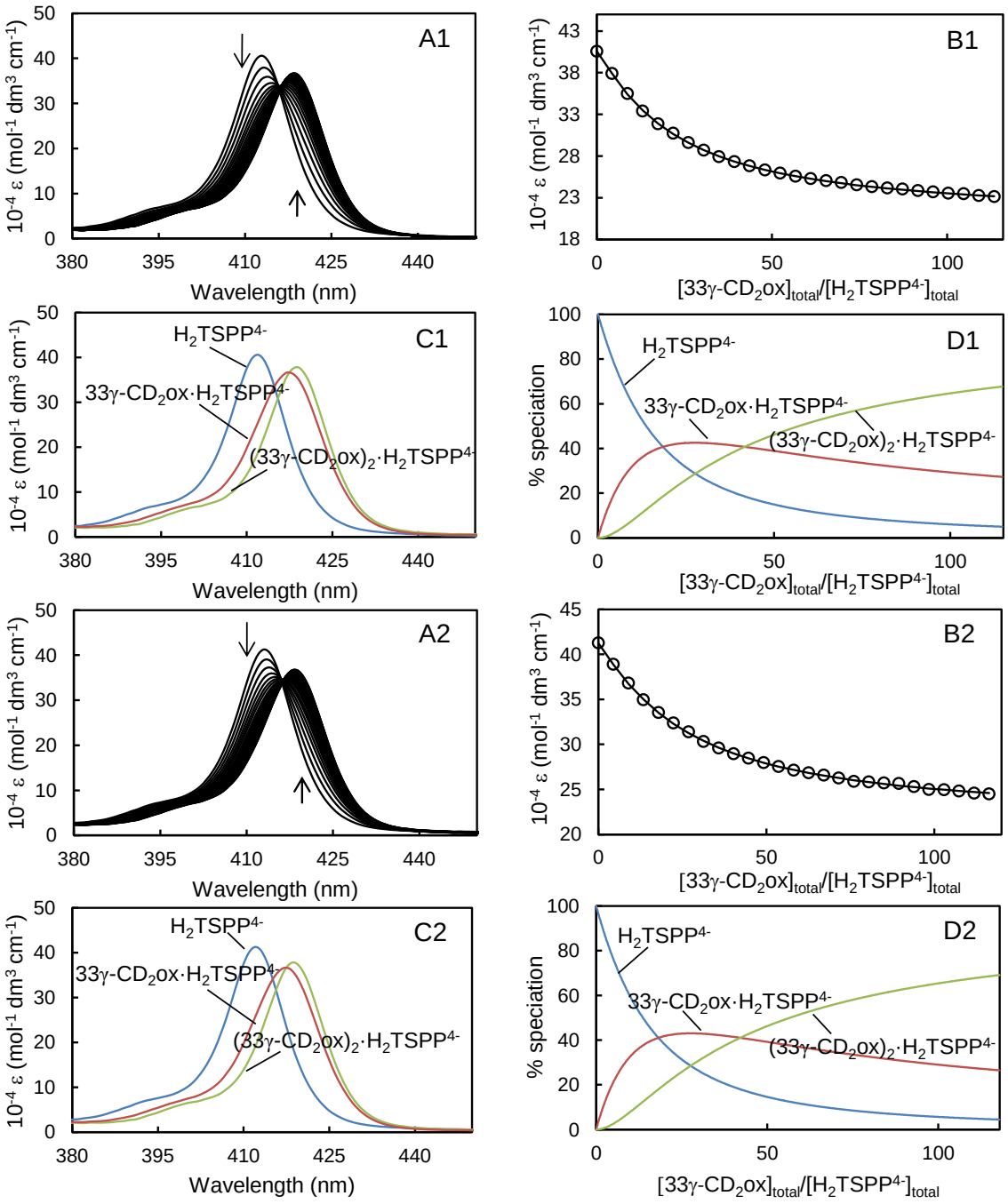

Figure A9: (A1, A2) Molar absorbance change of H_2TSPP^{4-} (1.05×10^{-6} mol dm^{-3}) in phosphate buffer, pH 7.0, I = 0.10 mol dm^{-3} with sequential injections (10 mm^3 each) of 33γ-CD_2ox (9.72×10^{-4} mol dm^{-3}) into both sample and reference cells. The arrows indicate the direction of molar absorbance change as the molar ratio of [33γ-CD_2ox]/[H_2TSPP^{4-}] increases. (B1, B2) Molar absorbance variation at 413 nm and the line of best fit of an algorithm for 1:1 and 2:1 host-guest complexation over the wavelength range 400-430 nm. (C1, C2) Calculated molar absorbance of free and complexed H_2TSPP^{4-}. (D1, D2) Speciation with $[H_2TSPP^{4-}]_{total}$ = 100%. Note: A1-D1: data at 278.2 K. A2-D2: data at 288.2 K.

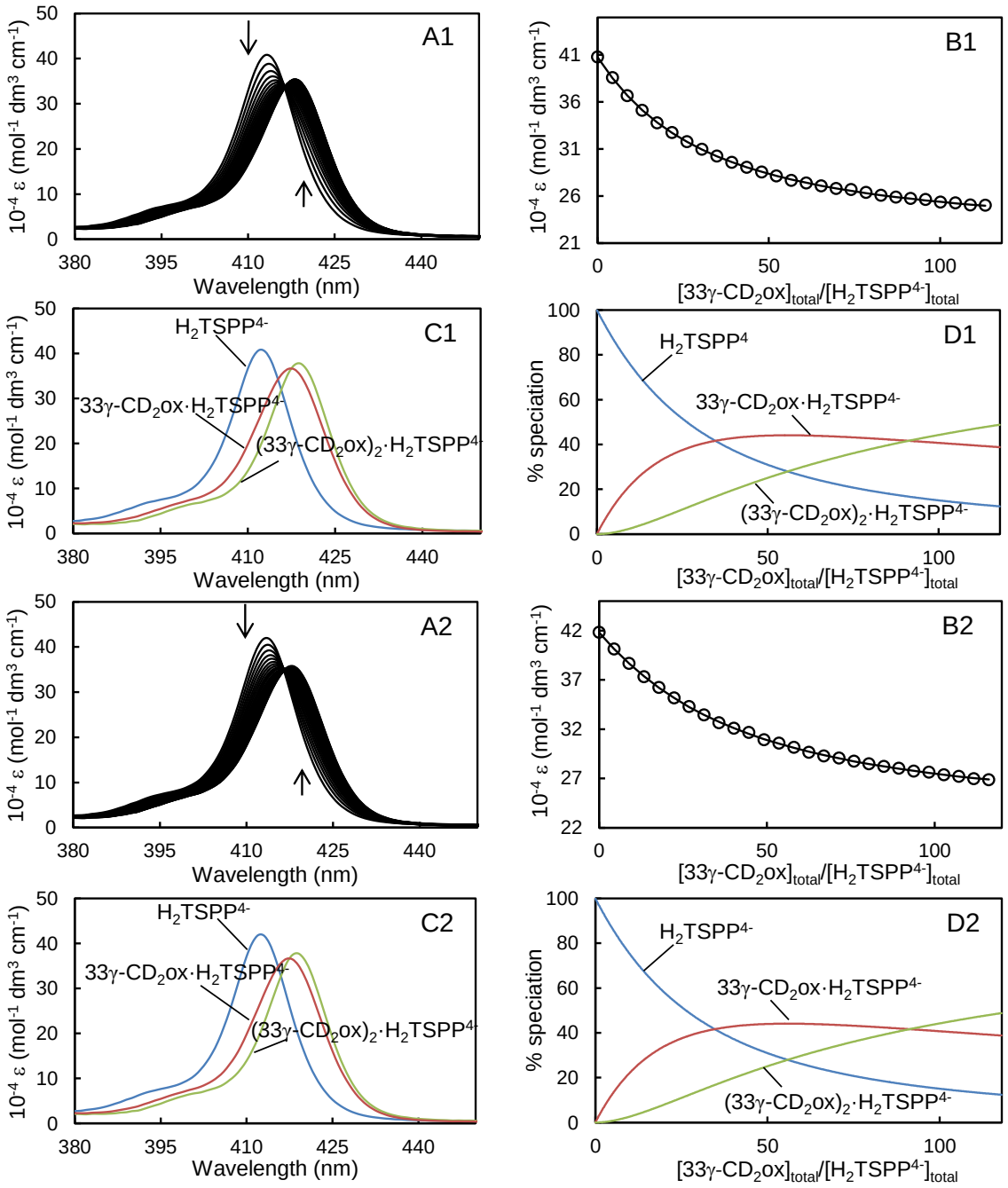

Figure A10: (A1, A2) Molar absorbance change of H_2TSPP^{4-} (1.05×10^{-6} mol dm^{-3}) in phosphate buffer, pH 7.0, I = 0.10 mol dm^{-3} with sequential injections (10 mm^3 each) of 33γ-CD_2ox (9.72×10^{-4} mol dm^{-3}) into both sample and reference cells. The arrows indicate the direction of molar absorbance change as the molar ratio of [33γ-CD_2ox]/[H_2TSPP^{4-}] increases. (B1, B2) Molar absorbance variation at 413 nm and the line of best fit of an algorithm for 1:1 and 2:1 host-guest complexation over the wavelength range 400-430 nm. (C1, C2) Calculated molar absorbance of free and complexed H_2TSPP^{4-}. (D1, D2) Speciation with [H_2TSPP^{4-}]$_{total}$ = 100%. Note: A1-D1: data at 298.2 K. A2-D2: data at 308.2 K.

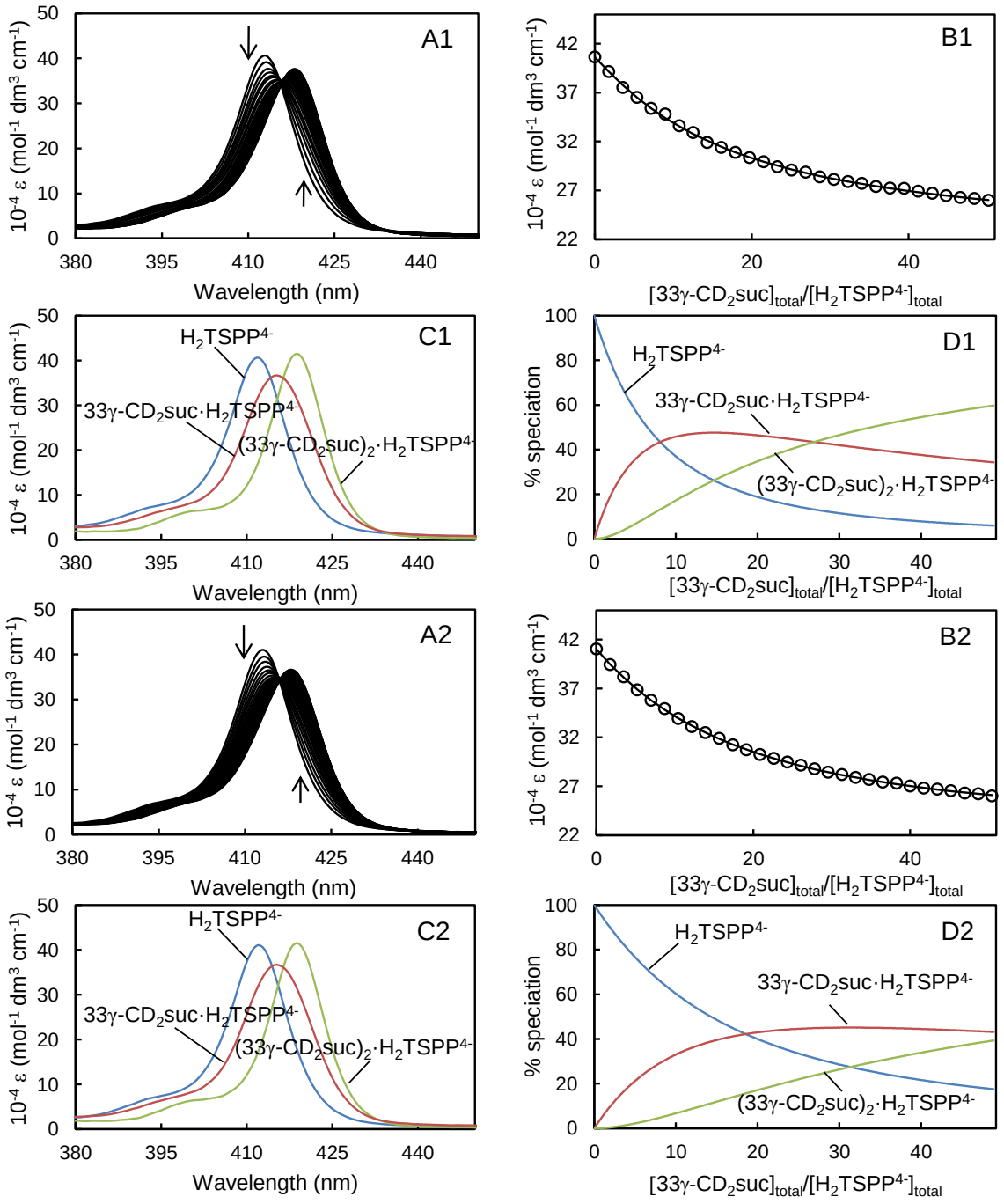

Figure A11: (A1, A2) Molar absorbance change of H_2TSPP^{4-} (1.05×10^{-6} mol dm^{-3}) in phosphate buffer, pH 7.0, I = 0.10 mol dm^{-3} with sequential injections (10 mm^3 each) of 33γ-CD_2suc (3.86×10^{-4} mol dm^{-3}) into both sample and reference cells. The arrows indicate the direction of molar absorbance change as the molar ratio of [33γ-CD_2suc]/[H_2TSPP^{4-}] increases. (B1, B2) Molar absorbance variation at 413 nm and the line of best fit of an algorithm for 1:1 and 2:1 host-guest complexation over the wavelength range 400-430 nm. (C1, C2) Calculated molar absorbance of free and complexed H_2TSPP^{4-}. (D1, D2) Speciation with $[H_2TSPP^{4-}]_{total}$ = 100%. Note: A1-A1: data at 278.2 K. B2-B2: data at 288.2 K.

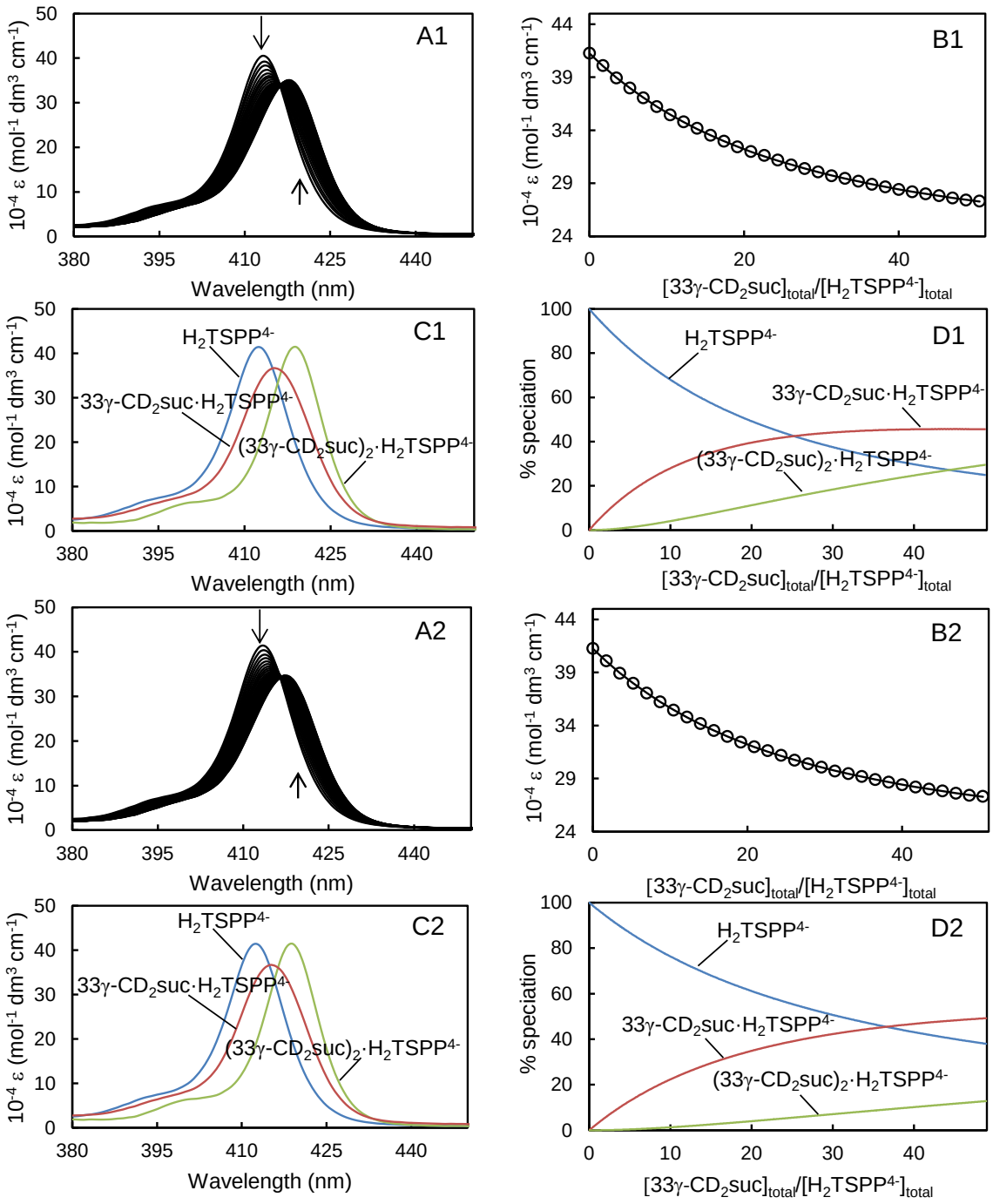

Figure A12: (A1, A2) Molar absorbance change of H_2TSPP^{4-} (1.05×10^{-6} mol dm^{-3}) in phosphate buffer, pH 7.0, I = 0.10 mol dm^{-3} with sequential injections (10 mm^3 each) of 33γ-CD_2suc (3.86×10^{-4} mol dm^{-3}) into both sample and reference cells. The arrows indicate the direction of molar absorbance change as the molar ratio of [33γ-CD_2suc]/[H_2TSPP^{4-}] increases. (B1, B2) Molar absorbance variation at 413 nm and the line of best fit of an algorithm for 1:1 and 2:1 host-guest complexation over the wavelength range 400-430 nm. (C1, C2) Calculated molar absorbance of free and complexed H_2TSPP^{4-}. (D1, D2) Speciation with [H_2TSPP^{4-}]$_{total}$ = 100%. Note: A1-D1: data at 298.2 K. A2-D2: data at 308.2 K.

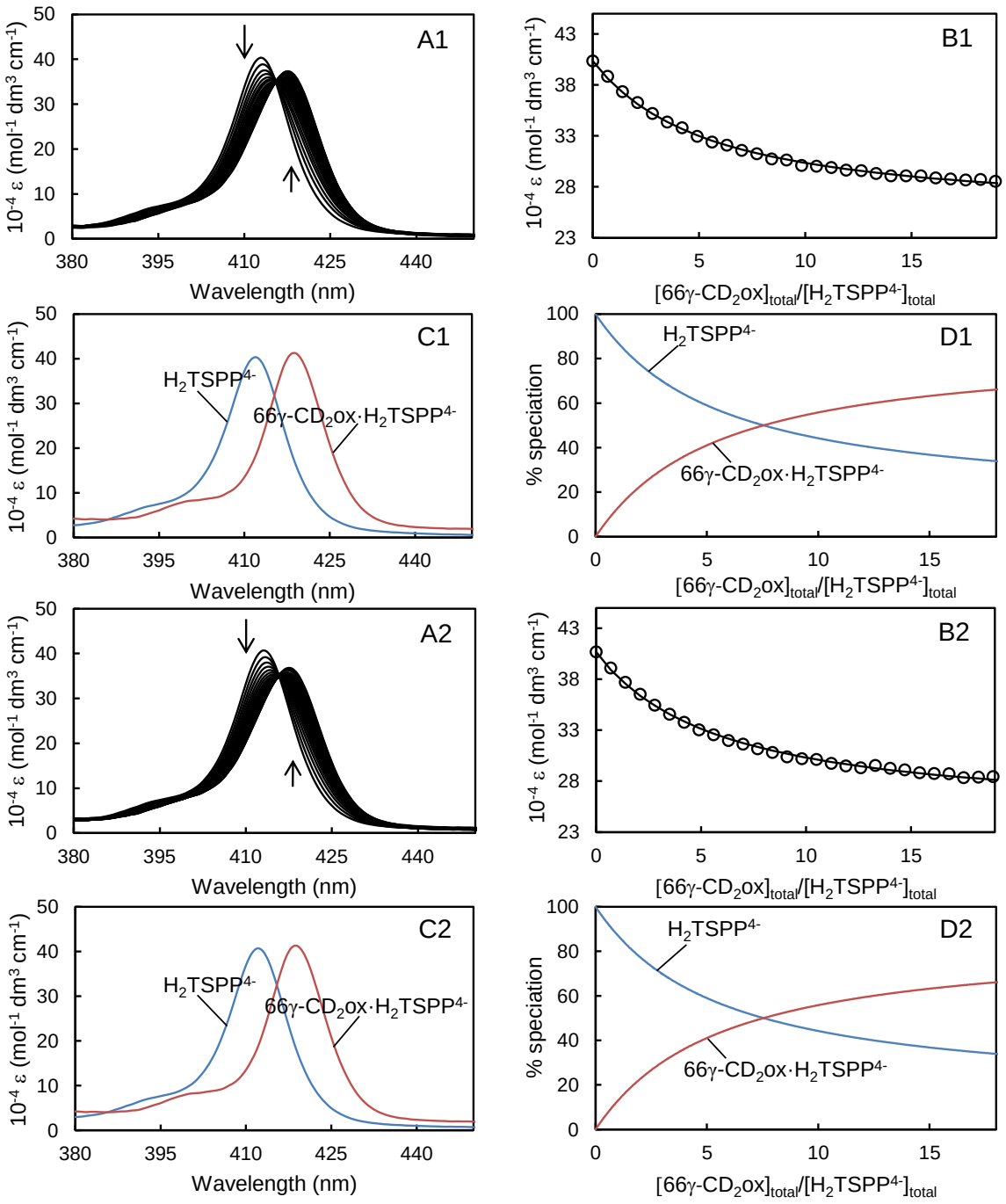

Figure A13: (A1, A2) Molar absorbance change of H_2TSPP^{4-} (1.05×10^{-6} mol dm^{-3}) in phosphate buffer, pH 7.0, I = 0.10 mol dm^{-3} with sequential injections (10 mm^3 each) of 66γ-CD_2ox (1.89×10^{-4} mol dm^{-3}) into both sample and reference cells. The arrows indicate the direction of molar absorbance change as the molar ratio of [66γ-CD_2ox]/[H_2TSPP^{4-}] increases. (B1, B2) Molar absorbance variation at 413 nm and the line of best fit of an algorithm for 1:1 host-guest complexation over the wavelength range 400-430 nm. (C1, C2) Calculated molar absorbance of free and complexed H_2TSPP^{4-}. (D1, D2) Speciation with [H_2TSPP^{4-}]$_{total}$ = 100%. Note: A1-D1: data at 278.2 K. A2-D2: data at 288.2 K.

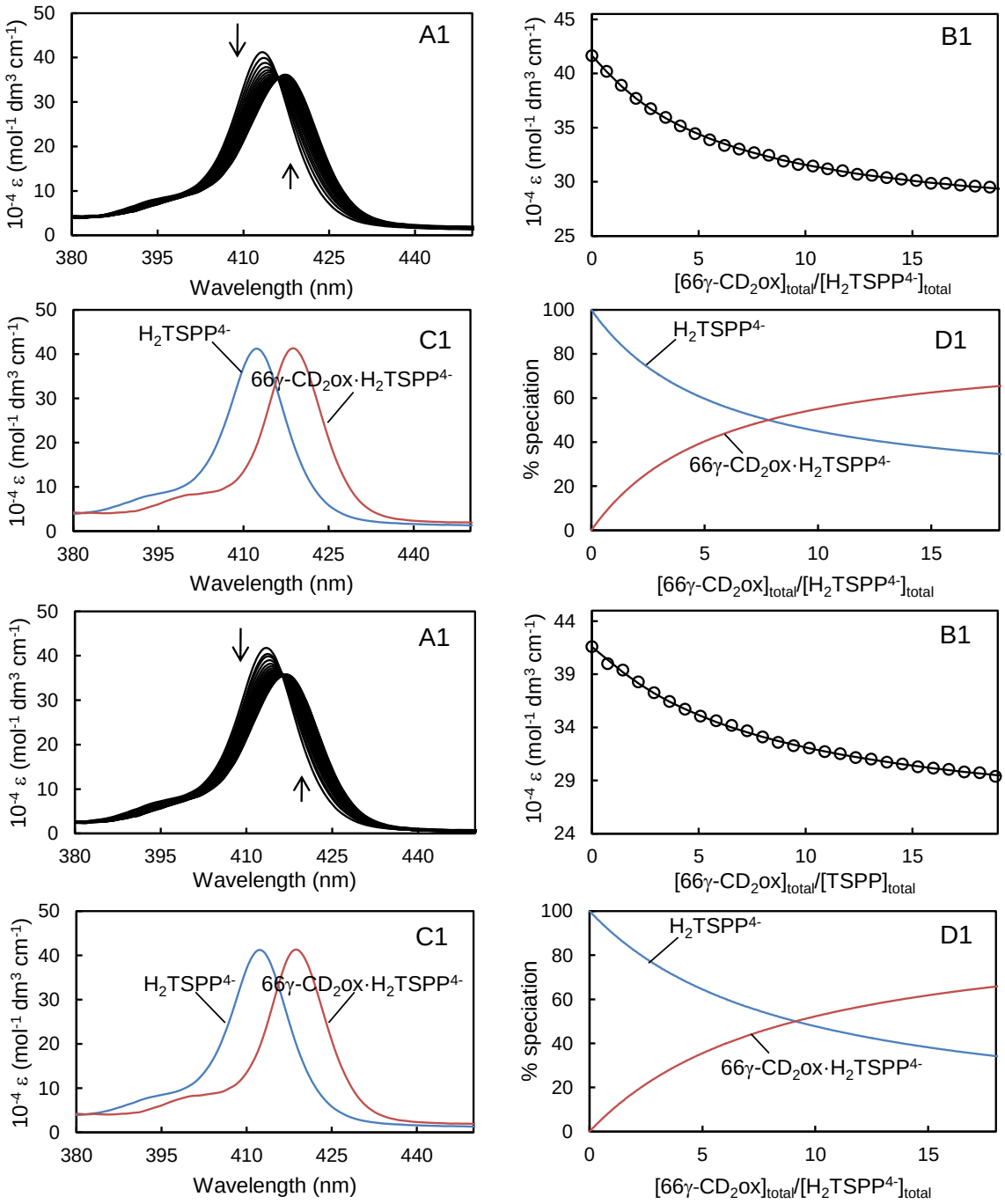

Figure A14: (A1, A2) Molar absorbance change of H_2TSPP^{4-} (1.05×10^{-6} mol dm^{-3}) in phosphate buffer, pH 7.0, I = 0.10 mol dm^{-3} with sequential injections (10 mm^3 each) of 66γ-CD_2ox (1.89×10^{-4} mol dm^{-3}) into both sample and reference cells. The arrows indicate the direction of molar absorbance change as the molar ratio of [66γ-CD_2ox]/[H_2TSPP^{4-}] increases. (B1, B2) Molar absorbance variation at 413 nm and the line of best fit of an algorithm for 1:1 host-guest complexation over the wavelength range 400-430 nm. (C1, C2) Calculated molar absorbance of free and complexed H_2TSPP^{4-}. (D1, D2) Speciation with $[H_2TSPP^{4-}]_{total}$ = 100%. Note: A1-D1: data at 298.2 K. A2-D2: data at 308.2 K.

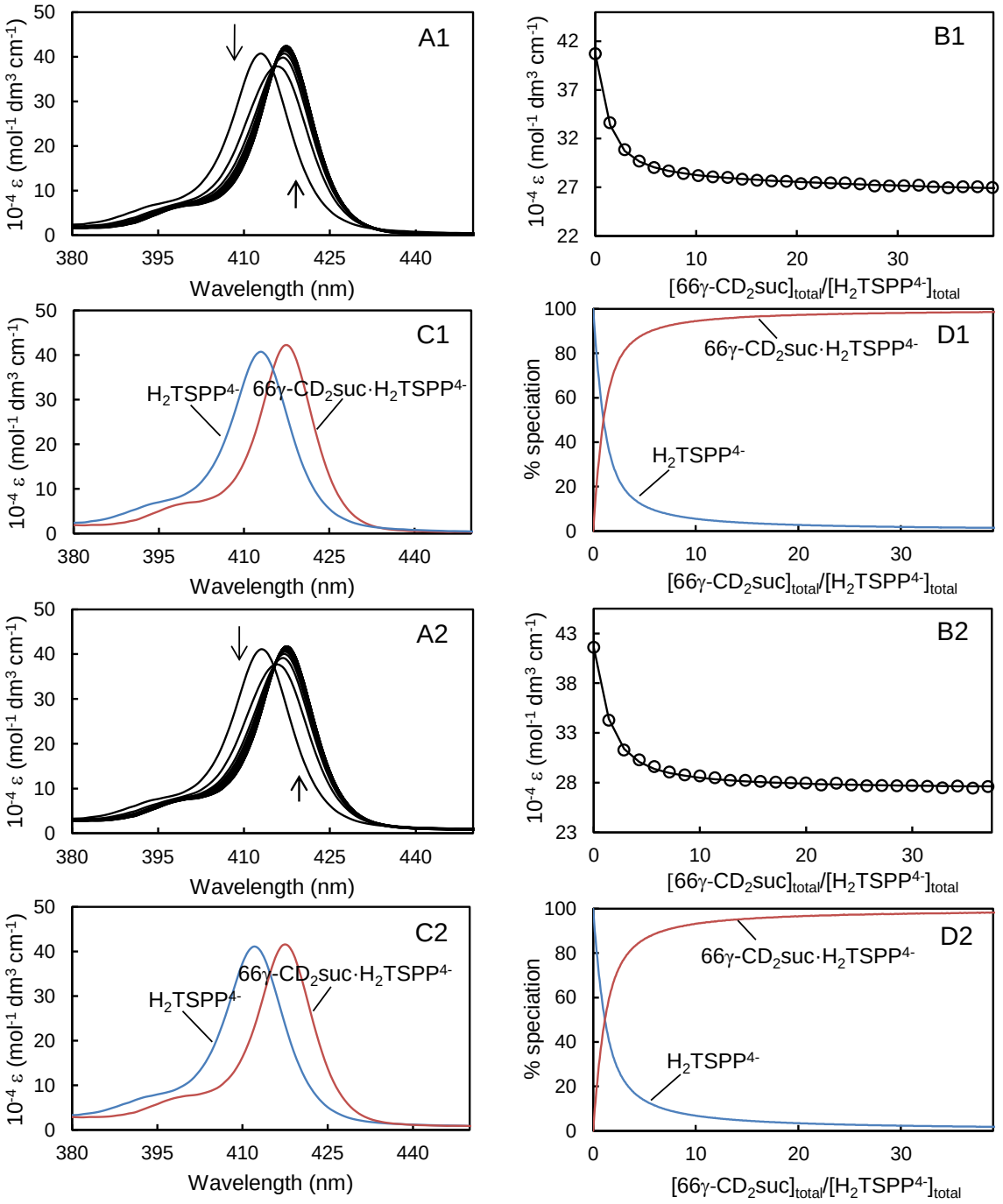

Figure A15: (A1, A2) Molar absorbance change of H_2TSPP^{4-} (1.05×10^{-6} mol dm^{-3}) in phosphate buffer, pH 7.0, I = 0.10 mol dm^{-3} with sequential injections (6 mm^3 each) of 66γ-CD_2suc (5.11×10^{-4} mol dm^{-3}) into both sample and reference cells. The arrows indicate the direction of molar absorbance change as the molar ratio of [66γ-CD_2suc]/[H_2TSPP^{4-}] increases. (B1, B2) Molar absorbance variation at 413 nm and the line of best fit of an algorithm for 1:1 host-guest complexation over the wavelength range 400-430 nm. (C1, C2) Calculated molar absorbance of free and complexed H_2TSPP^{4-}. (D1, D2) Speciation with $[H_2TSPP^{4-}]_{total}$ = 100%. Note: A1-D1: data at 278.2 K. D2-D2: data at 288.2 K.

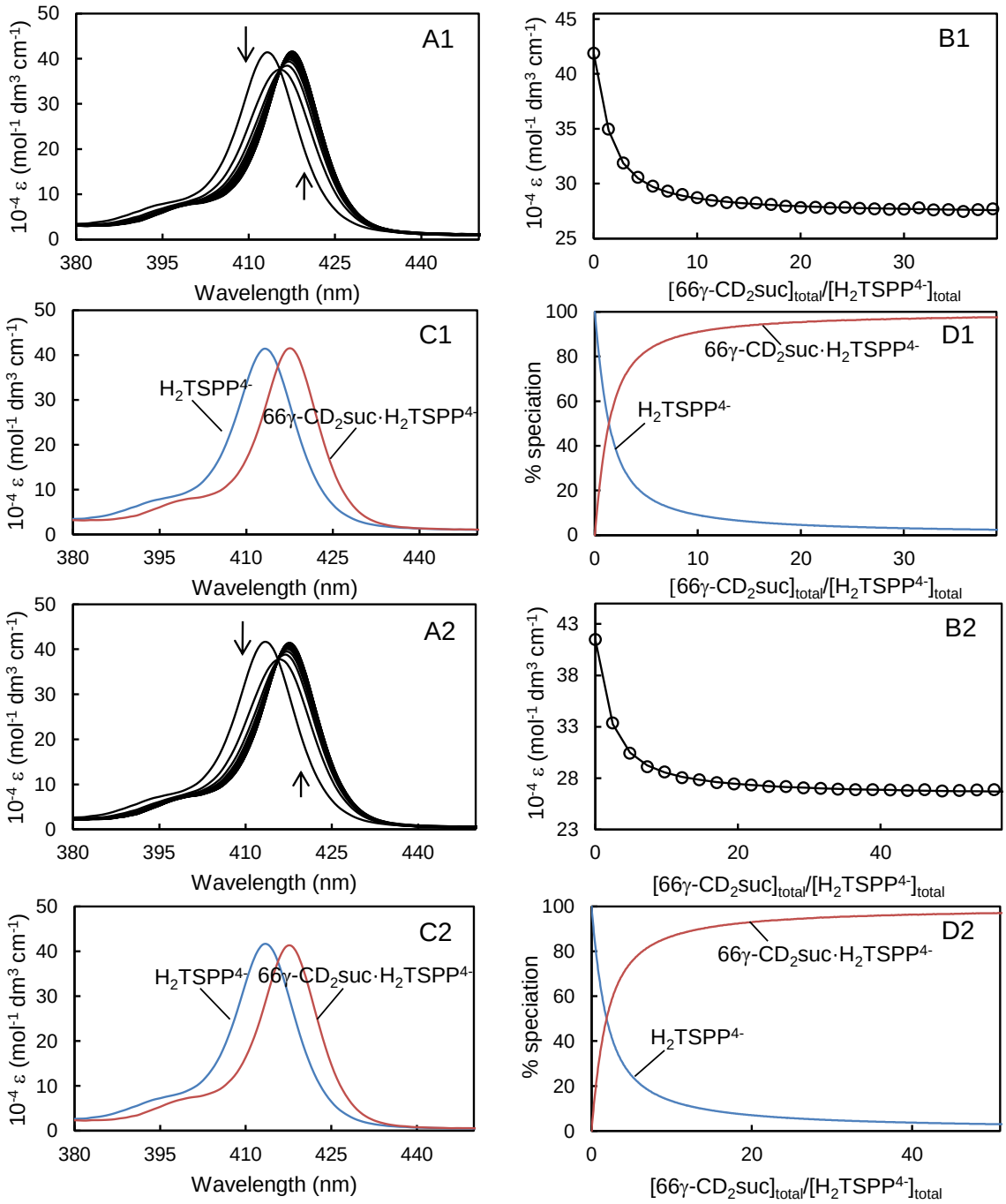

Figure A16: (A1, A2) Molar absorbance change of H_2TSPP^{4-} (1.05×10^{-6} mol dm^{-3}) in phosphate buffer, pH 7.0, I = 0.10 mol dm^{-3} with sequential injections (6 mm^3 and 10 mm^3 each for 298.2 and 308.2 K, respectively) of 66γ-CD_2suc (5.11×10^{-4} mol dm^{-3}) into both sample and reference cells. The arrows indicate the direction of molar absorbance change as the molar ratio of [66γ-CD_2suc]/[H_2TSPP^{4-}] increases. (B1, B2) Molar absorbance variation at 413 nm and the line of best fit of an algorithm for 1:1 host-guest complexation over the wavelength range 400-430 nm. (C1, C2) Calculated molar absorbance of free and complexed H_2TSPP^{4-}. (D1, D2) Speciation with $[H_2TSPP^{4-}]_{total}$ = 100%. Note: A1-D1: data at 298.2 K. A2-D2: data at 308.2 K.

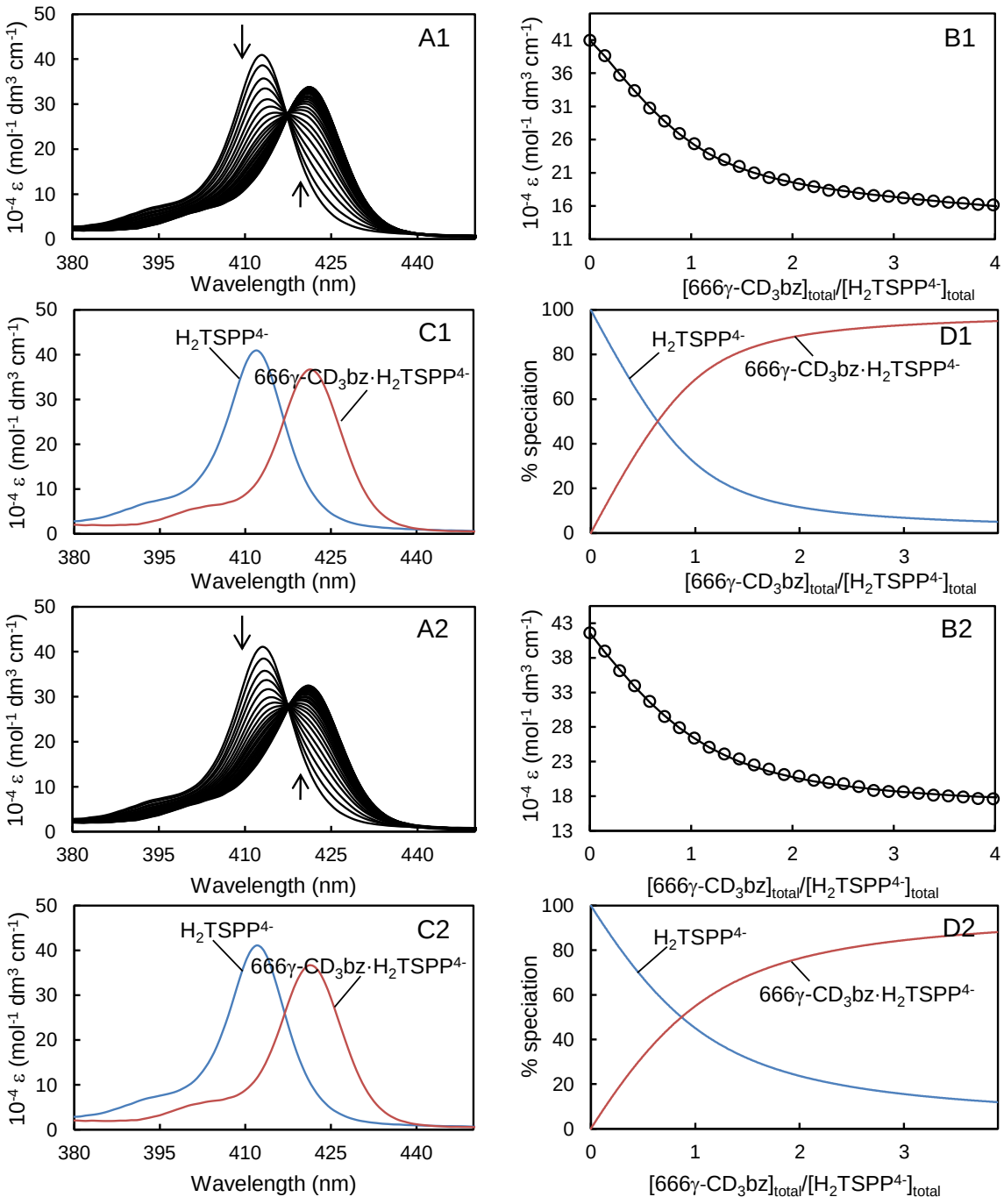

Figure A17: (A1, A2) Molar absorbance change of H_2TSPP^{4-} (1.05×10^{-6} mol dm^{-3}) in phosphate buffer, pH 7.0, I = 0.10 mol dm^{-3} with sequential injections (10 mm^3 each) of 666γ-CD_3bz (3.16×10^{-5} mol dm^{-3}) into both sample and reference cells. The arrows indicate the direction of molar absorbance change as the molar ratio of [666γ-CD_3bz]/[H_2TSPP^{4-}] increases. (B1, B2) Molar absorbance variation at 413 nm and the line of best fit of an algorithm for 1:1 host-guest complexation over the wavelength range 400-430 nm. (C1, C2) Calculated molar absorbance of free and complexed H_2TSPP^{4-}. (D1, D2) Speciation with $[H_2TSPP^{4-}]_{total}$ = 100%. Note: A1-D1: data at 278.2 K. A2-D2: data at 288.2 K.

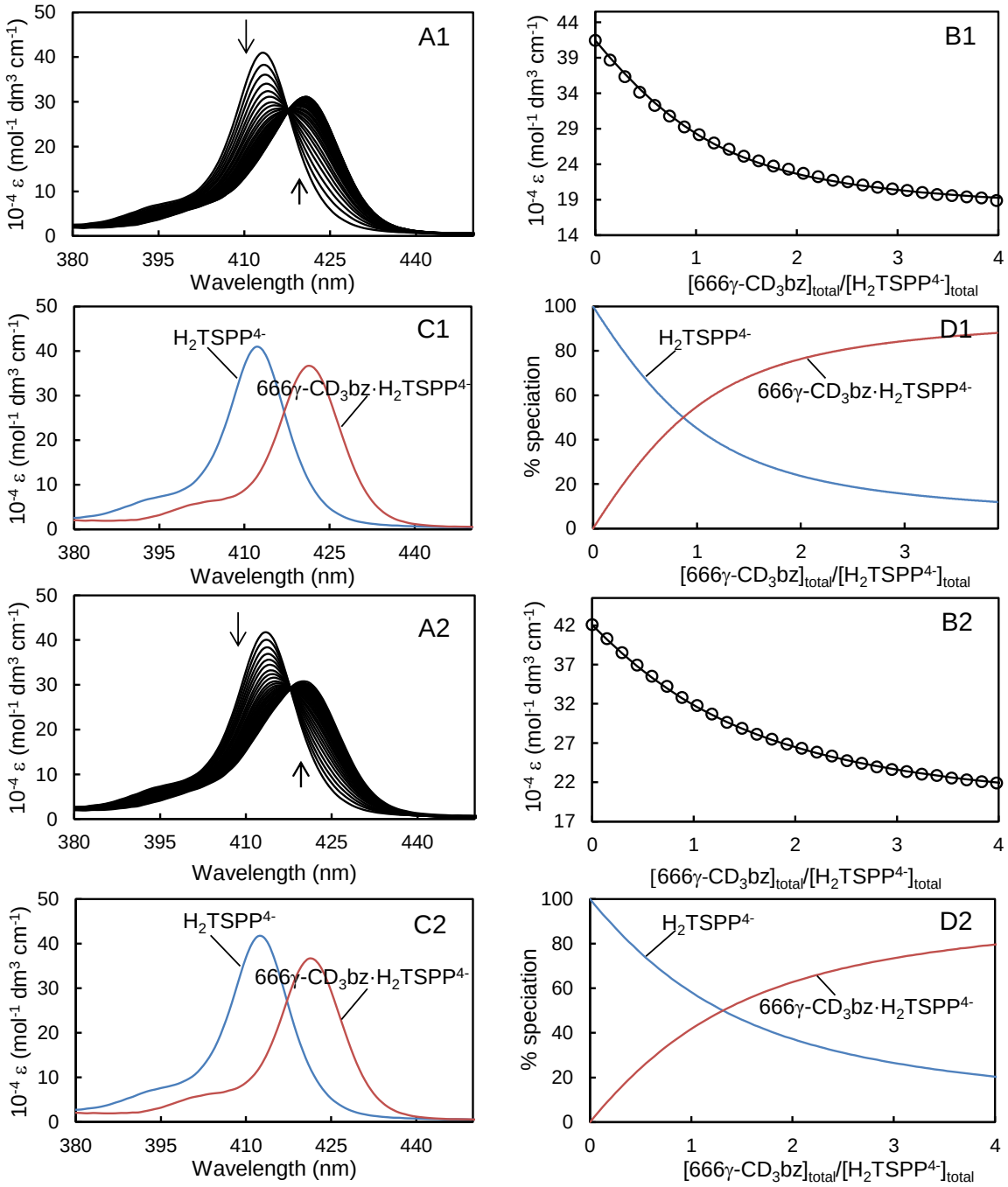

Figure A18: (A1, A2) Molar absorbance change of H_2TSPP^{4-} (1.05×10^{-6} mol dm^{-3}) in phosphate buffer, pH 7.0, I = 0.10 mol dm^{-3} with sequential injections (10 mm^3 each) of 666γ-CD_3bz (3.16×10^{-5} mol dm^{-3}) into both sample and reference cells. The arrows indicate the direction of molar absorbance change as the molar ratio of [666γ-CD_3bz]/[H_2TSPP^{4-}] increases. (B1, B2) Molar absorbance variation at 413 nm and the line of best fit of an algorithm for 1:1 host-guest complexation over the wavelength range 400-430 nm. (C1, C2) Calculated molar absorbance of free and complexed H_2TSPP^{4-}. (D1, D2) Speciation with [H_2TSPP^{4-}]$_{total}$ = 100%. Note: A1-D1: data at 298.2 K. A2-D2: data at 308.2 K.

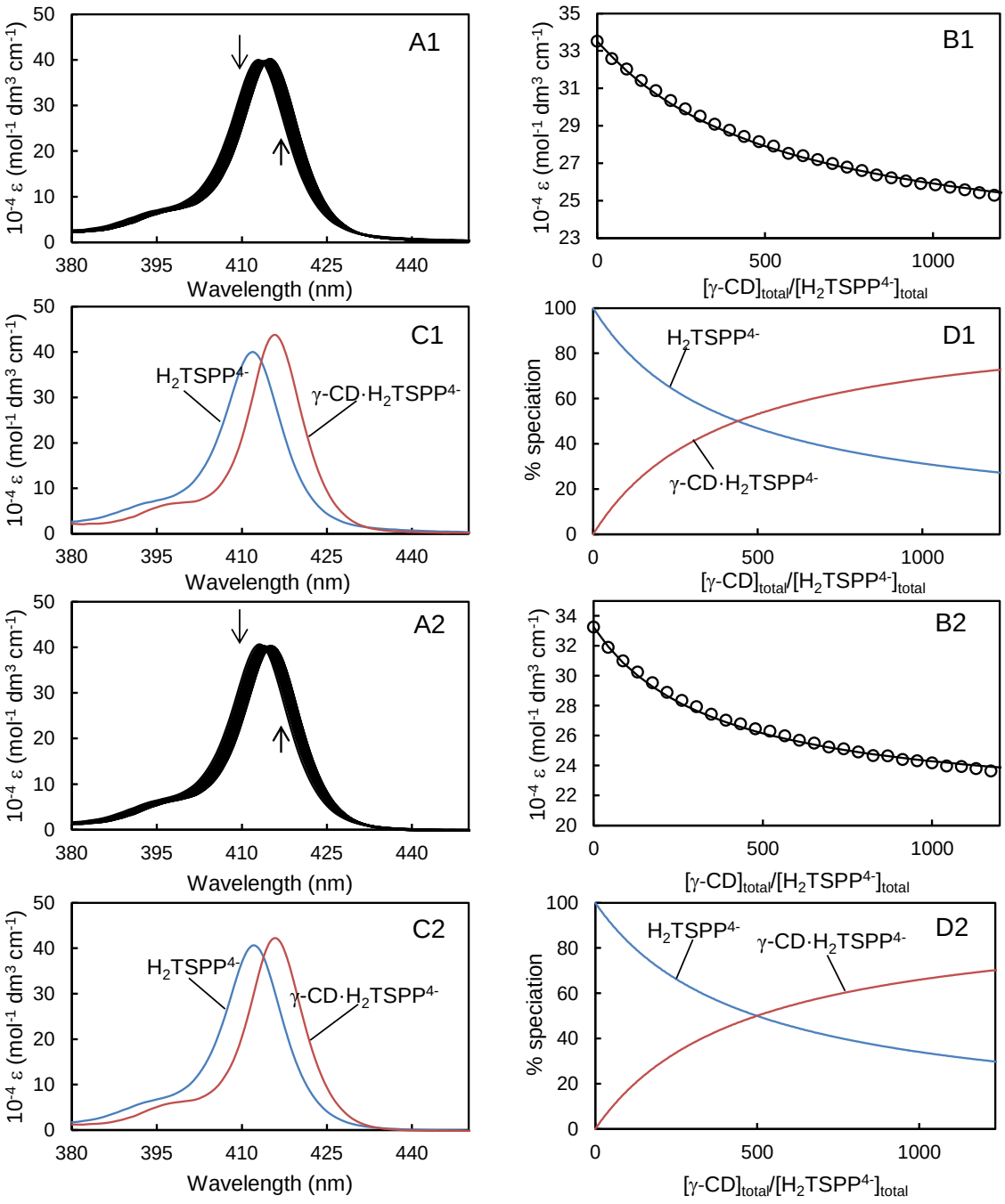

Figure A19: (A1, A2) Molar absorbance change of H_2TSPP^{4-} (1.05×10^{-6} mol dm^{-3}) in phosphate buffer, pH 7.0, I = 0.10 mol dm^{-3} with sequential injections (10 mm^3 each) of γ-CD (9.14×10^{-3} mol dm^{-3}) into both sample and reference cells. The arrows indicate the direction of molar absorbance change as the molar ratio of [γ-CD]/[H_2TSPP^{4-}] increases. (B1, B2) Molar absorbance variation at 410 nm and the tentative line of best fit of an algorithm for 1:1 host-guest complexation over the wavelength range 400-430 nm. (C1, C2) Calculated molar absorbance of free and complexed H_2TSPP^{4-}. (D1, D2) Speciation with [H_2TSPP^{4-}]total = 100%. Note: A1-D1: data at 278.2 K. A2-D2: data at 288.2 K.

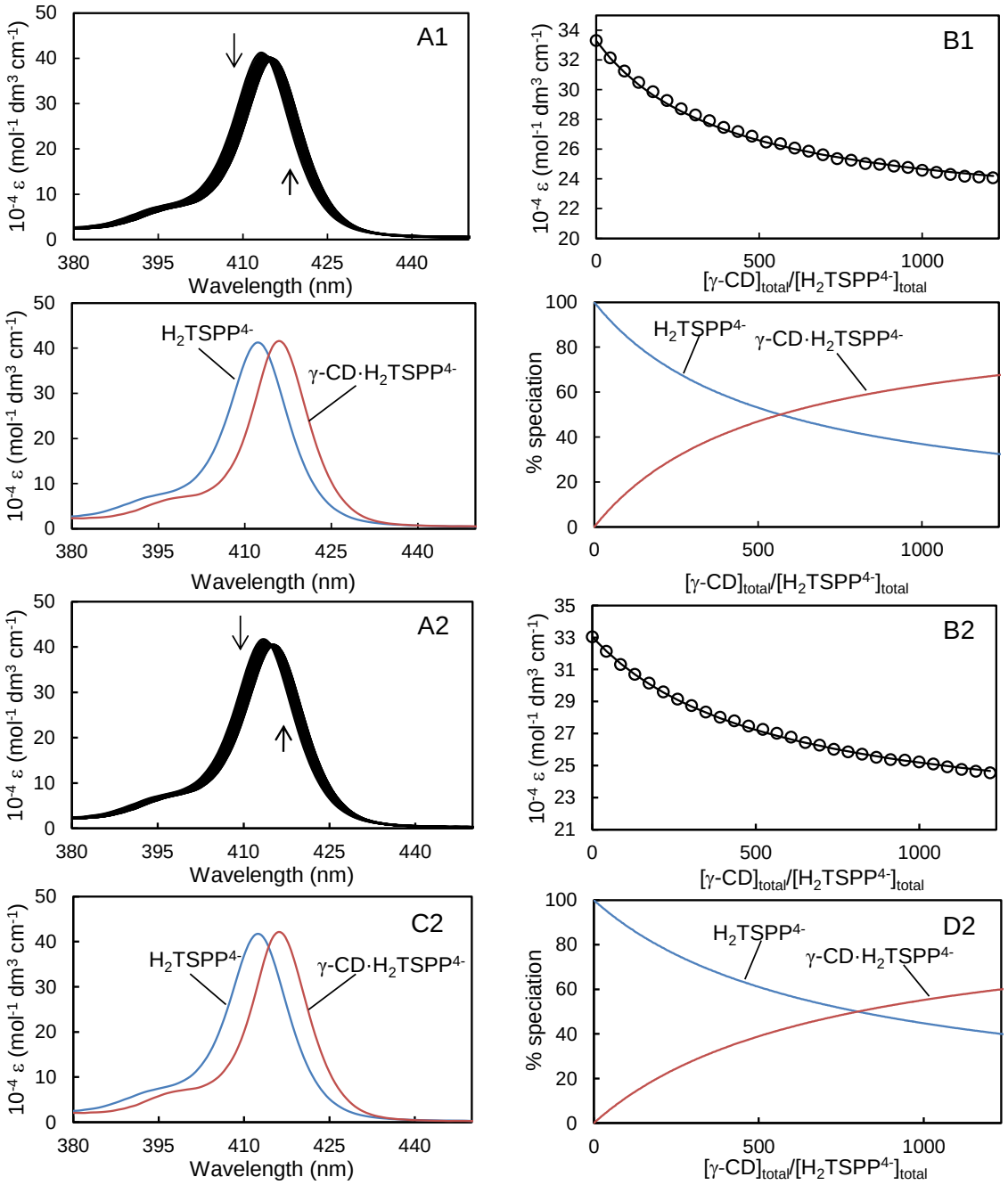

Figure A20: (A1, A2) Molar absorbance change of H_2TSPP^{4-} (1.05×10^{-6} mol dm^{-3}) in phosphate buffer, pH 7.0, I = 0.10 mol dm^{-3} with sequential injections (10 mm^3 each) of γ-CD (9.14×10^{-3} mol dm^{-3}) into both sample and reference cells. The arrows indicate the direction of molar absorbance change as the molar ratio of [γ-CD]/[H_2TSPP^{4-}] increases. (B1, B2) Molar absorbance variation at 410 nm and the tentative line of best fit of an algorithm for 1:1 host-guest complexation over the wavelength range 400-430 nm. (C1, C2) Calculated molar absorbance of free and complexed H_2TSPP^{4-}. (D1, D2) Speciation with $[H_2TSPP^{4-}]_{total}$ = 100%. Note: A1-D1: data at 298.2 K. A2-D2: data at 308.2 K.

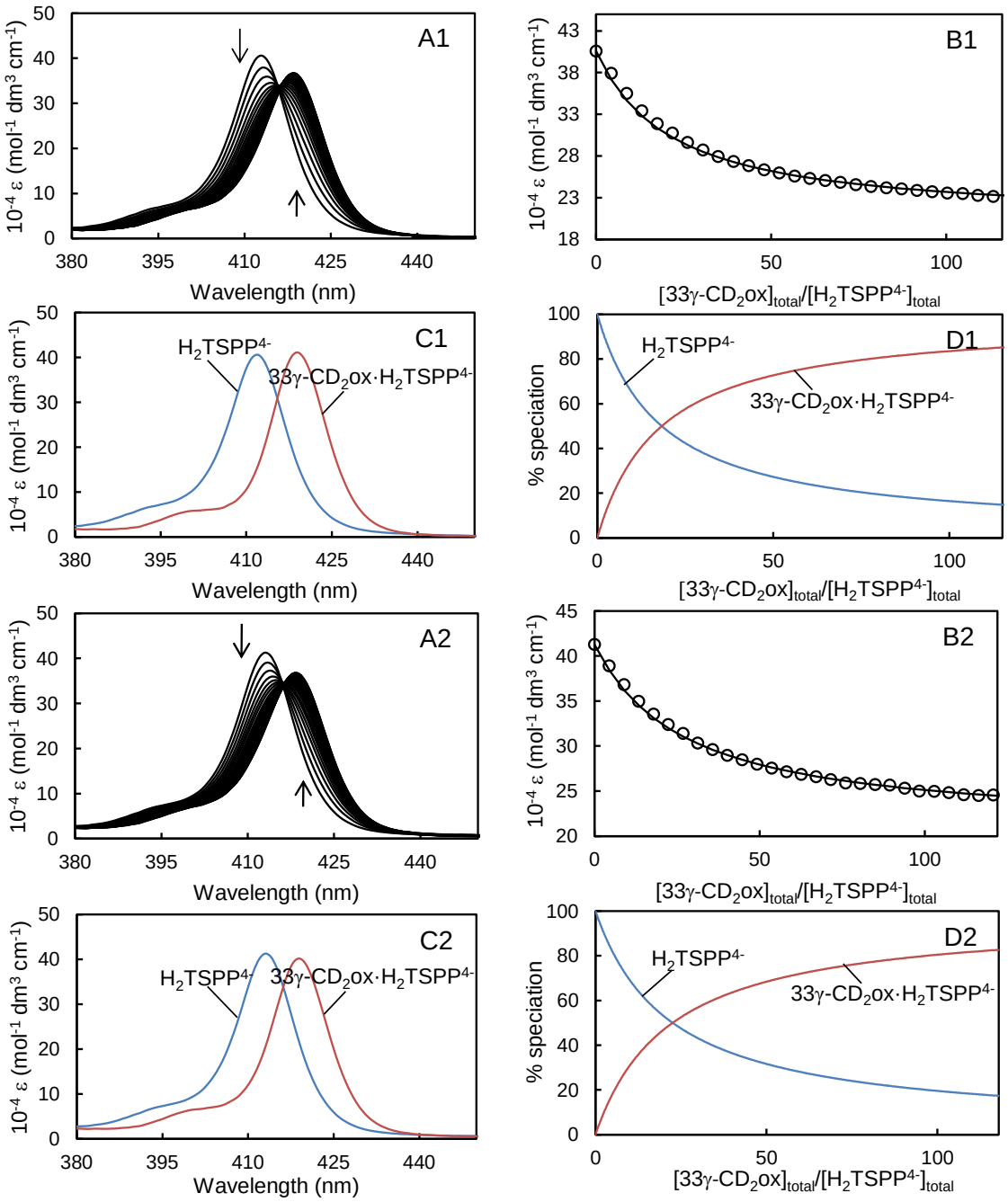

Figure A21: (A1, A2) Molar absorbance change of H_2TSPP^{4-} (1.05×10^{-6} mol dm^{-3}) in phosphate buffer, pH 7.0, I = 0.10 mol dm^{-3} with sequential injections (10 mm^3 each) of 33γ-CD_2ox (9.72×10^{-4} mol dm^{-3}) into both sample and reference cells. The arrows indicate the direction of molar absorbance change as the molar ratio of [33γ-CD_2ox]/[H_2TSPP^{4-}] increases. (B1, B2) Molar absorbance variation at 413 nm and the tentative line of best fit of an algorithm for 1:1 host-guest complexation over the wavelength range 400-430 nm. (C1, C2) Calculated molar absorbance of free and complexed H_2TSPP^{4-}. (D1, D2) Speciation with [H_2TSPP^{4-}]$_{total}$ = 100%. Note: A1-D1: data at 278.2 K. A2-D2: data at 288.2 K.

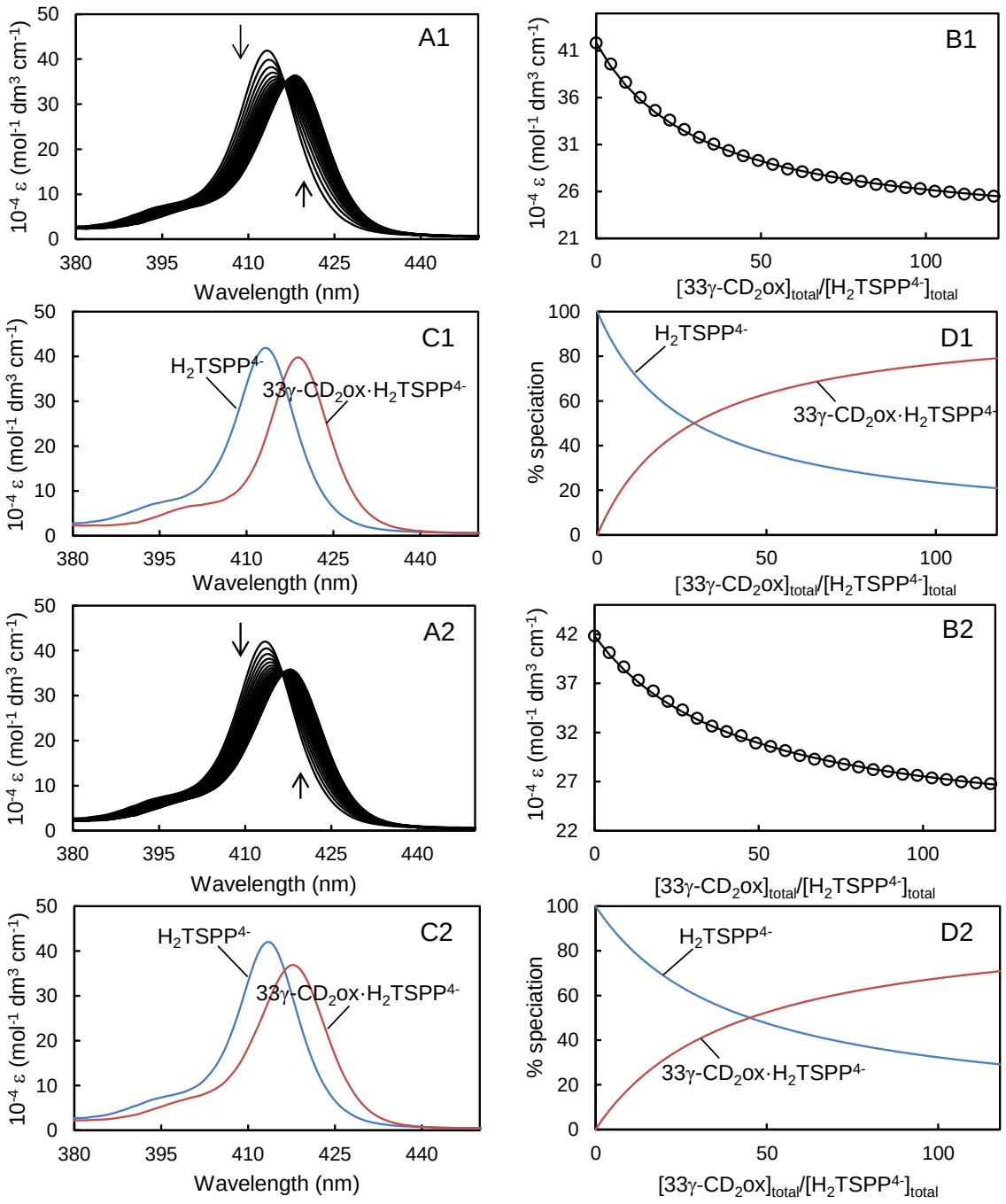

Figure A22: (A1, A2) Molar absorbance change of H_2TSPP^{4-} (1.05×10^{-6} mol dm^{-3}) in phosphate buffer, pH 7.0, I = 0.10 mol dm^{-3} with sequential injections (10 mm^3 each) of 33γ-CD_2ox (9.72×10^{-4} mol dm^{-3}) into both sample and reference cells. The arrows indicate the direction of molar absorbance change as the molar ratio of [33γ-CD_2ox]/[H_2TSPP^{4-}] increases. (B1, B2) Molar absorbance variation at 413 nm and the tentative line of best fit of an algorithm for 1:1 host-guest complexation over the wavelength range 400-430 nm. (C1, C2) Calculated molar absorbance of free and complexed H_2TSPP^{4-}. (D1, D2) Speciation with [H_2TSPP^{4-}]$_{total}$ = 100%. Note: A1-D1: data at 298.2 K. A2-D2: data at 308.2 K.

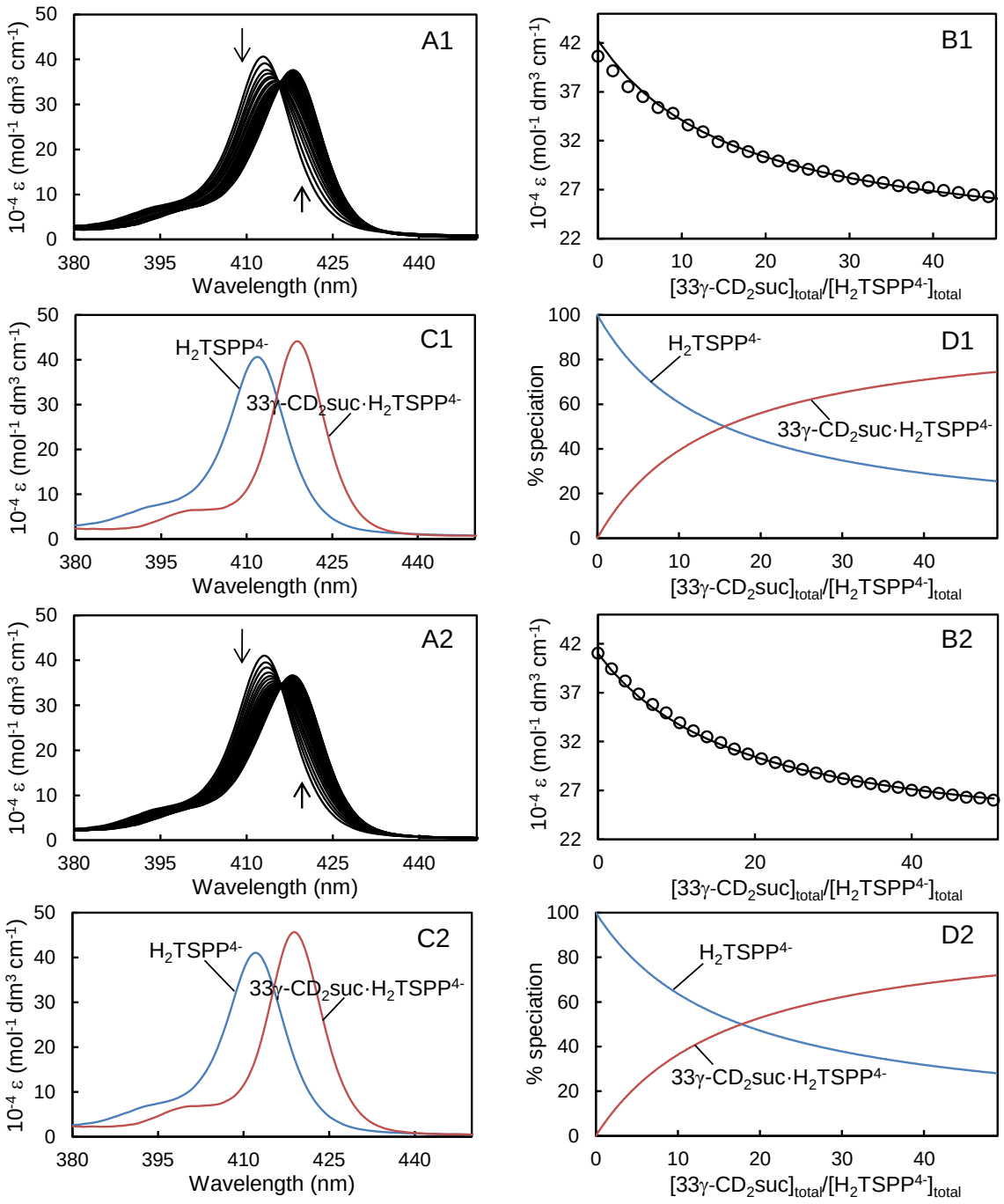

Figure A23: (A1, A2) Molar absorbance change of H_2TSPP^{4-} (1.05×10^{-6} mol dm^{-3}) in phosphate buffer, pH 7.0, I = 0.10 mol dm^{-3} with sequential injections (10 mm^3 each) of 33γ-CD_2suc (3.86×10^{-4} mol dm^{-3}) into both sample and reference cells. The arrows indicate the direction of molar absorbance change as the molar ratio of [33γ-CD_2suc]/[H_2TSPP^{4-}] increases. (B1, B2) Molar absorbance variation at 413 nm and the tentative line of best fit of an algorithm for 1:1 host-guest complexation over the wavelength range 400-430 nm. (C1, C2) Calculated molar absorbance of free and complexed H_2TSPP^{4-}. (D1, D2) Speciation with $[H_2TSPP^{4-}]_{total}$ = 100%. Note: A1-D1: data at 278.2 K. A2-D2: data at 288.2 K.

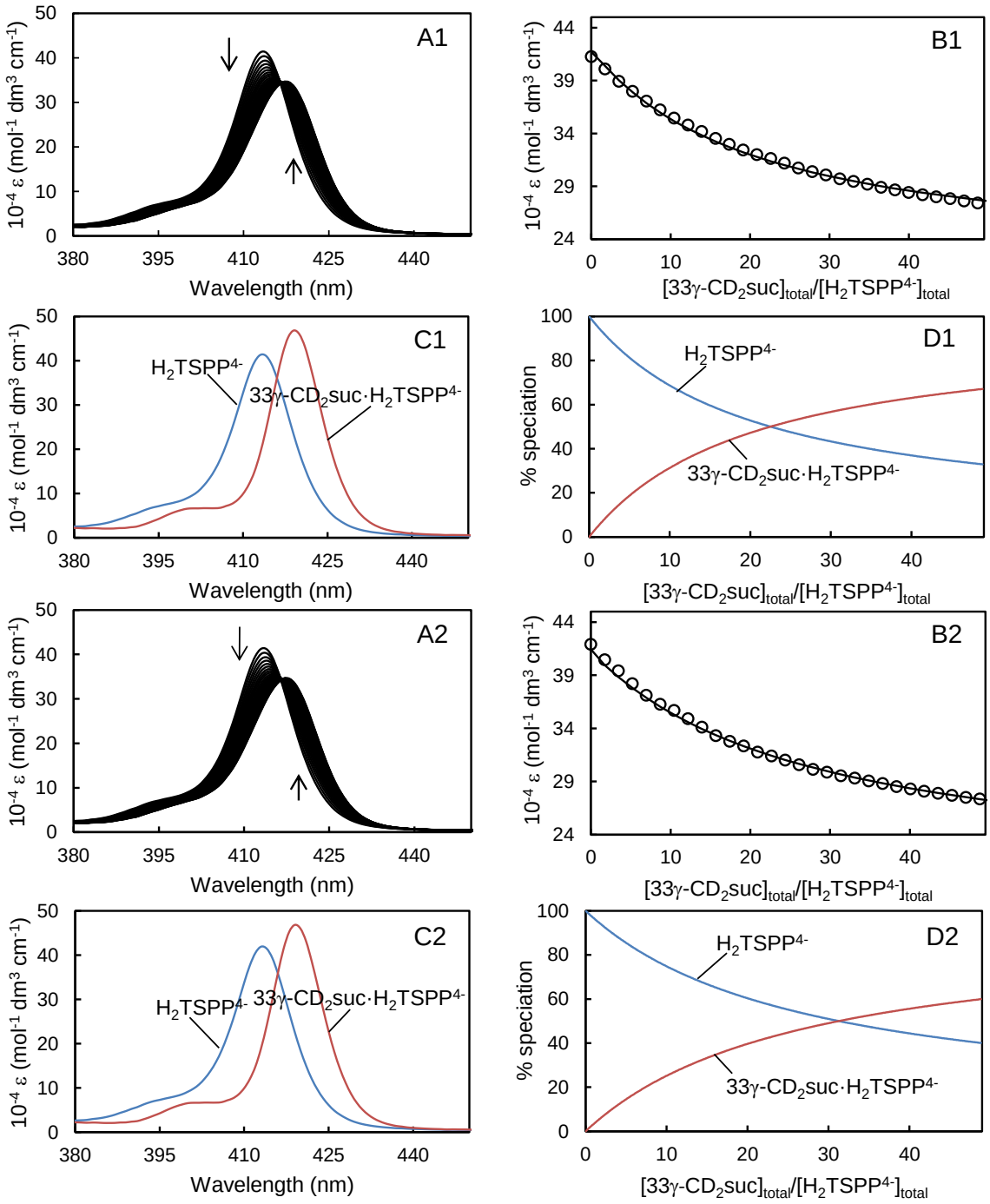

Figure A24: (A1, A2) Molar absorbance change of H_2TSPP^{4-} (1.05×10^{-6} mol dm^{-3}) in phosphate buffer, pH 7.0, I = 0.10 mol dm^{-3} with sequential injections (10 mm^3 each) of 33γ-CD_2suc (3.86×10^{-4} mol dm^{-3}) into both sample and reference cells. The arrows indicate the direction of molar absorbance change as the molar ratio of [33γ-CD_2suc]/[H_2TSPP^{4-}] increases. (B1, B2) Molar absorbance variation at 413 nm and the tentative line of best fit of an algorithm for 1:1 host-guest complexation over the wavelength range 400-430 nm. (C1, C2) Calculated molar absorbance of free and complexed H_2TSPP^{4-}. (D1, D2) Speciation with [H_2TSPP^{4-}]$_{total}$ = 100%. Note: A1-D1: data at 298.2 K. A2-D2: data at 308.2 K.

Molecular Modelling

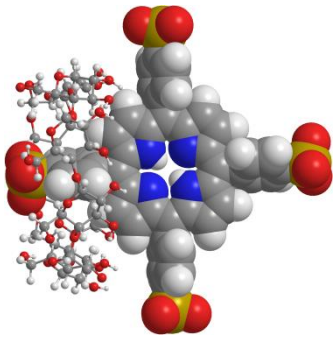

γ-CD.H_2TSPP^{4-} wide face

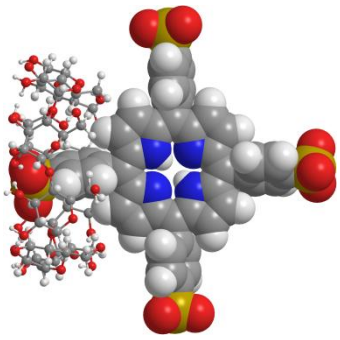

γ-CD.H_2TSPP^{4-} narrow face

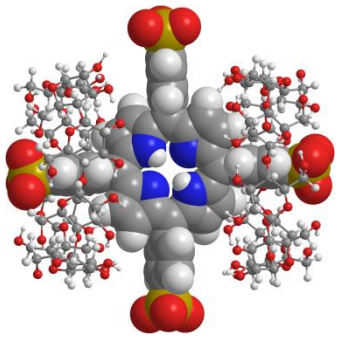

$(\gamma\text{-CD})_2.H_2TSPP^{4-}$ *anti*

two wide faces

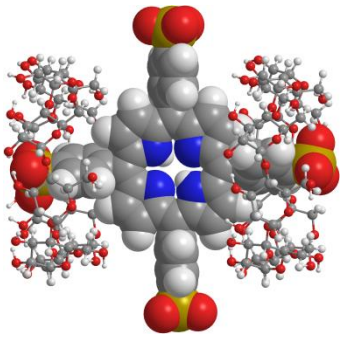

$(\gamma\text{-CD})_2.H_2TSPP^{4-}$ *anti*

one narrow and one wide face

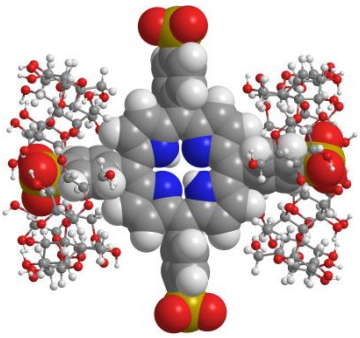

$(\gamma\text{-CD})_2.H_2TSPP^{4-}$ *anti*

two narrow faces

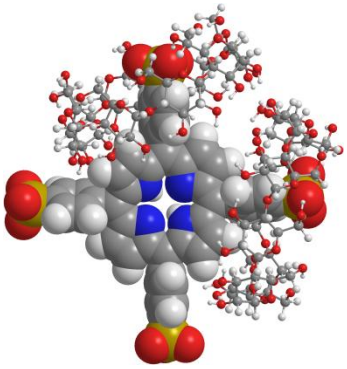

$(\gamma\text{-CD})_2.H_2TSPP^{4-}$ *syn*

two wide faces

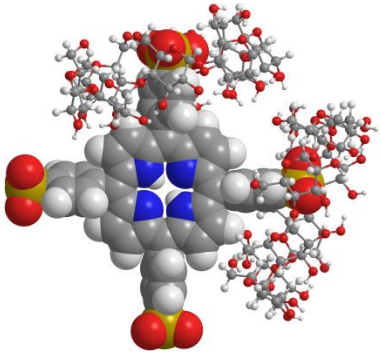

$(\gamma\text{-CD})_2.H_2TSPP^{4-}$ *syn*

one wide and one narrow face

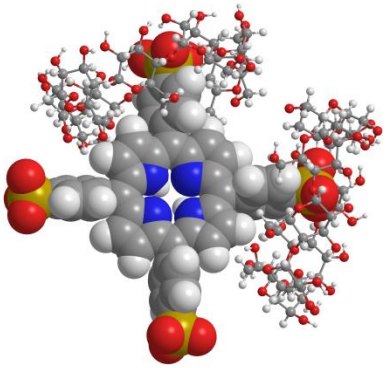

$(\gamma\text{-CD})_2.H_2TSPP^{4-}$ *syn*

two narrow faces

Figure A25: Energy minimised molecular models of the possible complexes involved in the γ-CD/H_2TSPP^{4-}/$(\gamma\text{-CD})_2.H_2TSPP^{4-}$ equilibrium using the PM7 method. Note: γ-CD = ball and stick, H_2TSPP^{4-} = space filling. Carbon = grey, hydrogen = white, oxygen = red, nitrogen = blue and sulphur = gold.

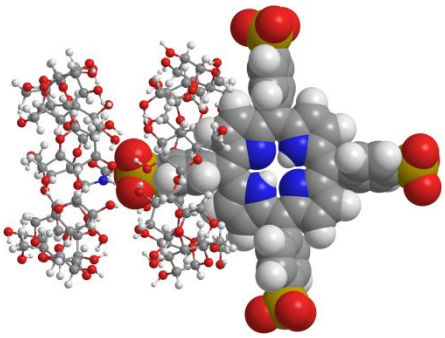

33γ-CD_2ox.H_2TSPP^{4-}non-cooperative
one narrow face

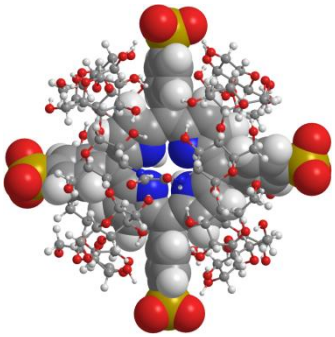

33γ-CD_2ox.H_2TSPP^{4-} *anti* cooperative
two wide faces

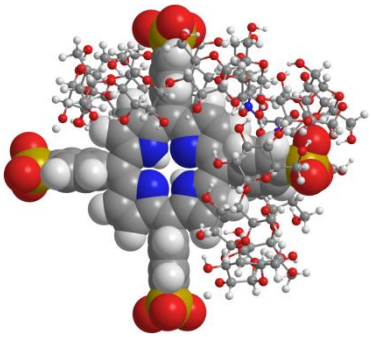

33γ-CD_2ox.H_2TSPP^{4-}*syn* cooperative
two wide faces

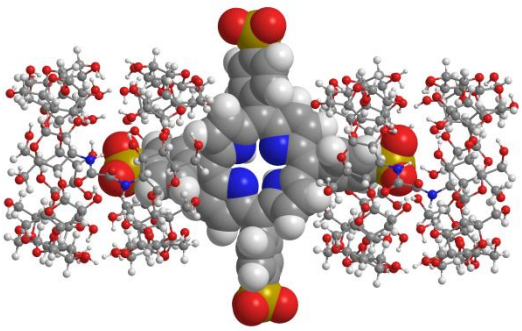

(33γ-CD_2ox)$_2$.H_2TSPP^{4-} non-cooperative
two narrow faces

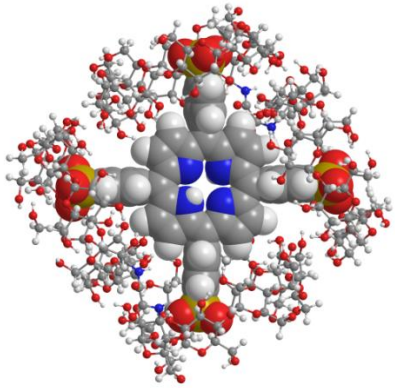

(33γ-CD_2ox)$_2$.H_2TSPP^{4-} cooperative
four wide faces

Figure A26: Energy minimised molecular models of the possible complexes involved in the 33γ-CD_2ox.H_2TSPP^{4-}/(33γ-CD_2ox)$_2$.H_2TSPP^{4-}equilibrium using the PM7 method. Note: 33γ-CD_2ox = ball and stick, H_2TSPP^{4-} = space filling. Carbon = grey, hydrogen = white, oxygen = red, nitrogen = blue and sulphur = gold.

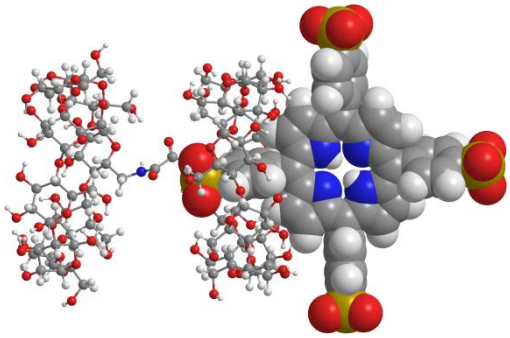

66γ-CD_2ox.H_2TSPP^{4-} non-cooperative

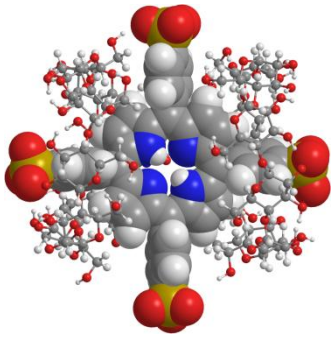

66γ-CD_2ox.H_2TSPP^{4-} *anti* cooperative

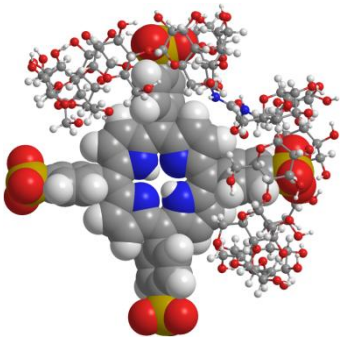

66γ-CD_2ox.H_2TSPP^{4-} *syn* cooperative

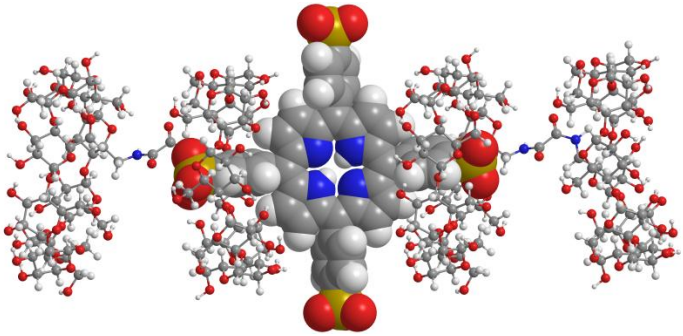

(66γ-CD_2ox)$_2$.H_2TSPP^{4-} non-cooperative
two wide faces

Figure A27: Energy minimised molecular models of the possible species involved in the 66γ-CD_2ox.H_2TSPP^{4-}/(66γ-CD_2ox)$_2$.H_2TSPP^{4-} equilibrium using the PM7 method. Note: 66γ-CD_2ox = ball and stick, H_2TSPP^{4-} = space filling. Carbon = grey, hydrogen = white, oxygen = red, nitrogen = blue and sulphur = gold.

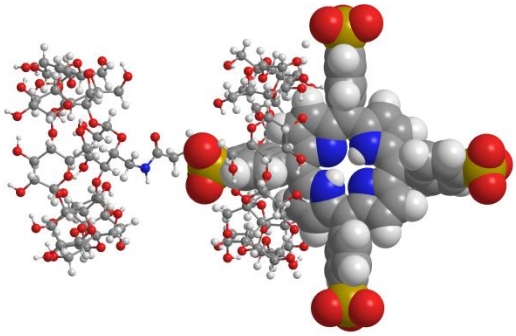

66γ-CD_2suc.H_2TSPP^{4-} non-cooperative complexation

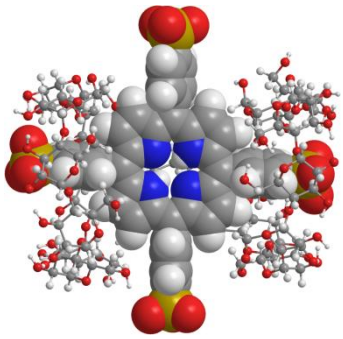

66γ-CD_2suc.H_2TSPP^{4-} *anti* cooperative

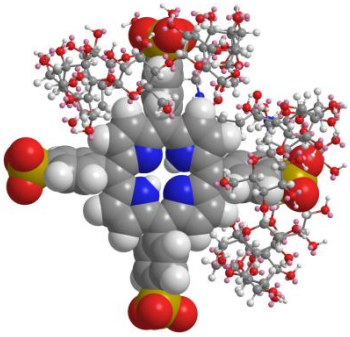

66γ-CD_2suc.H_2TSPP^{4-} *syn* cooperative

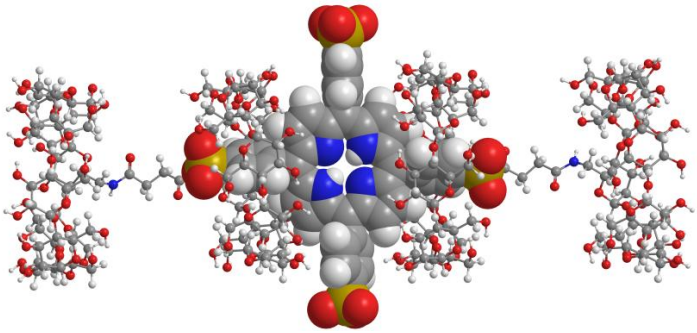

(66γ-CD_2suc)$_2$.H_2TSPP^{4-} non-cooperative
two wide faces

Figure A28: Energy minimised molecular models of the possible species involved in the 66γ-CD_2suc.H_2TSPP^{4-}/(66γ-CD_2suc)$_2$.H_2TSPP^{4-} equilibrium using the PM7 method. Note: 66γ-CD_2suc = ball and stick, H_2TSPP^{4-} = space filling. Carbon = grey, hydrogen = white, oxygen = red, nitrogen = blue and sulphur = gold.

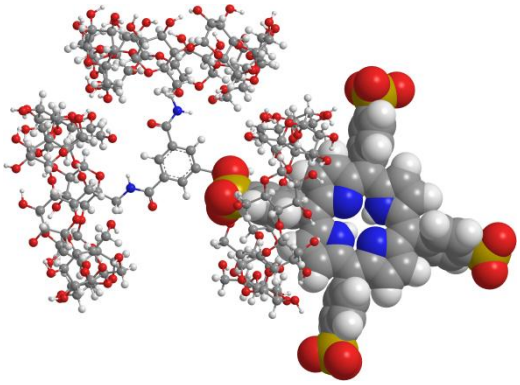

666γ-CD_3bz.H_2TSPP^{4-} non-cooperative

one narrow face

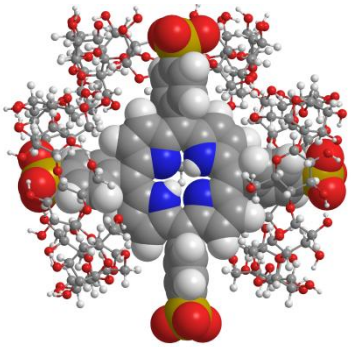

666γ-CD_3bz.H_2TSPP^{4-} cooperative
two narrow faces

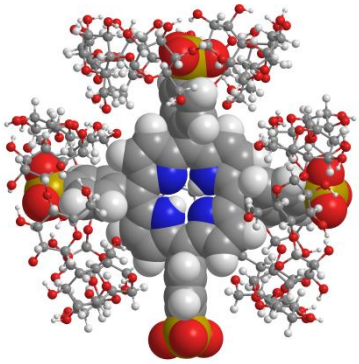

666γ-CD_3bz.H_2TSPP^{4-} cooperative
three narrow faces

Figure A29: Energy minimised molecular models of the possible species involved in the 666γ-CD_3bz.H_2TSPP^{4-} equilibrium using the PM7 method. Note: 666γ-CD_3bz = ball and stick, H_2TSPP^{4-} = space filling. Carbon = grey, hydrogen = white, oxygen = red, nitrogen = blue and sulphur = gold.

This page is intentionally left blank

Chapter 3

Complexation of 5,10,15,20-Tetra(*p*-carboxyphenyl)porphyrin by γ-Cyclodextrin, Linked γ-Cyclodextrin Dimers and a Linked γ-Cyclodextrin Trimer

3.1. INTRODUCTION

3.1.1. General

Porphyrins are sought after organic molecules for their applications in photodynamic therapy for the treatment of surface cancers.[1-5] However, the study of porphyrins in aqueous solution can be complicated by the presence of dimers and higher order aggregates.[6-11] Apart from the total concentration of porphyrin in solution, pH, temperature, ionic strength and electrolyte concentration substantially influence the formation of porphyrin aggregates.[12,13] This aggregation phenomenon has been widely studied with common water soluble porphyrins such as 5,10,15,20-tetra(*p*-sulfonatophenyl)porphyrin, H_2TSPP,[11,14,15] and 5,10,15,20-tetra(*p*-carboxyphenyl)porphyrin, H_2TCPP[6,16] which are particularly pertinent to this study. In acidic solutions (pH < 5) both of these porphyrins form J-aggregates (edge-by-edge or side-to-side assemblies).[12,14,16-19] However, these aggregates are of less concern under biological conditions as they occur at pH levels significantly lower than that of the bloodstream (pH = 7.4). At higher pH values H-aggregates (face-to-face assemblies) of the tetraanionic porphyrins H_2TSPP^{4-} and H_2TCPP^{4-} can form under biological conditions. This is most likely due to cations dissolved in the bloodstream partially screening the *p*-sulfonatophenyl or *p*-carboxyphenyl group negative charges.[20] This enables the hydrophobic planar porphyrin cores of two H_2TSPP^{4-} or H_2TCPP^{4-} to associate as a dimer with one porphyrin plane rotated 45° with respect to the other to minimise sulfonate or carboxylate charge repulsion.[17] Such H-aggregates may be detrimental to photodynamic therapy treatments as they cause changes in the physicochemical properties of porphyrins. These include changes in their UV-visible spectra, quantum yield, singlet and triplet state lifetimes and their production of singlet molecular oxygen, which is essential for photodynamic therapy.[21]

Complexation by cyclodextrins has been shown to improve the resistance of organic compounds to thermal and oxidative degradation, reduce side effects, increase bioavailability

and biological activity.[5,22-24] Furthermore, encapsulation of porphyrins by cyclodextrins has also been shown to significantly reduce porphyrin aggregation in aqueous solutions.[21,25-27] In Chapter 2 we observed that γ-cyclodextrin (γ-CD) and five of its modified forms could form strong host-guest complexes with H_2TSPP^{4-} in aqueous solutions. Slight changes in the absorption spectrum of an aqueous solution of H_2TSPP^{4-} (1.05×10^{-6} mol dm^{-3} at pH 7.0 in phosphate buffer) between 278.2-308.2 K were attributed to changes in a small percentage of the porphyrin being dimerised in solution. However, it is found that this small percentage of dimerised porphyrin had little effect on the host-guest equilibria between H_2TSPP^{4-} and γ-CD and its oligomers.

Conversely, H_2TCPP^{4-} has been shown to exhibit significantly more dimerisation than H_2TSPP^{4-} in neutral aqueous solutions.[11,13] Therefore, it is expected that increased dimerisation in aqueous solutions of H_2TCPP^{4-} may have a significant impact on the host-guest equilibrium between H_2TCPP^{4-} and γ-CD and its oligomers as illustrated in Figure 3.1. This dimerisation competes with the complexation of H_2TCPP^{4-} by γ-CD and its oligomers as supramolecular hosts for H_2TCPP^{4-} guests. Conversely, strong host-guest interactions between the γ-CD species and H_2TCPP^{4-} could lead to an effective way of decreasing H_2TCPP^{4-} aggregation and possibly improving is application as a photodynamic therapy agent.

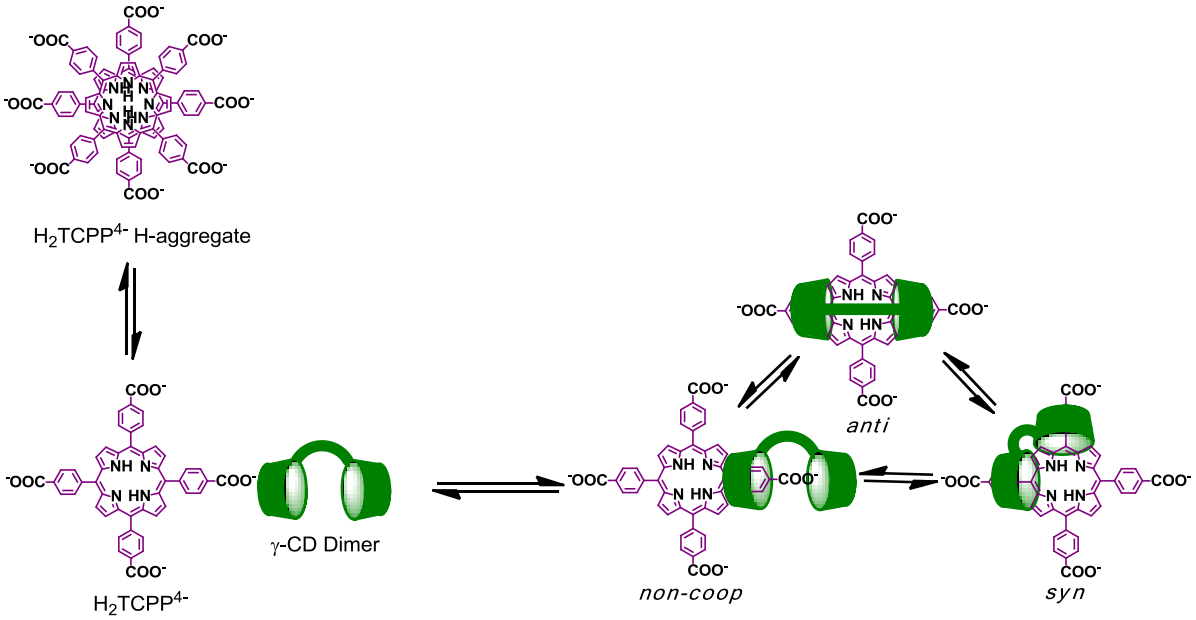

Figure 3.1: Potential equilibria between monomeric and dimeric tetraanionic H_2TCPP^{4-} and its cooperative and non-cooperative complexation by linked γ-CD dimers. (Note: in pH 7.0 aqueous solutions, the porphyrin is expected to exist primarily as tetraanionic H_2TCPP^{4-}, together with lesser amounts of monoprotonated H_3TCPP^{3-} and diprotonated H_4TCPP^{2-} forms as is discussed below).

3.1.2. Aims of this study

In this study the effect of porphyrin aggregation on the complexation of 5,10,15,20-tetra(*p*-carboxyphenyl)porphyrin, H_2TCPP (in neutral aqueous solutions H_2TCPP can exist in several ionised forms as is discussed later), by γ-CD and five of its modified forms (Figure 3.2). The oligomer hosts previously reported in Chapter 2, *N*,*N*′-bis((2^{A}S,3^{A}S)-3^A-deoxy-γ-cyclodextrin-3^A-yl) oxalamide (33γ-CD_2ox), *N*,*N*′-bis(3^A-deoxy-γ-cyclodextrin-3^A-yl) succinamide (33γ-CD_2suc), *N*,*N*′-bis(6^A-deoxy-γ-cyclodextrin-6^A-yl) oxalamide (66γ-CD_2ox), *N*,*N*′-bis(6^A-deoxy-γ-cyclodextrin-6^A-yl) succinamide (66γ-CD_2suc), and 1,3,5-*N*,*N*,*N*-tris(6^A-deoxy-6^A-γ-cyclodextrin)-benzene (666γ-CD_3bz) are also employed in the studies reported in this chapter.

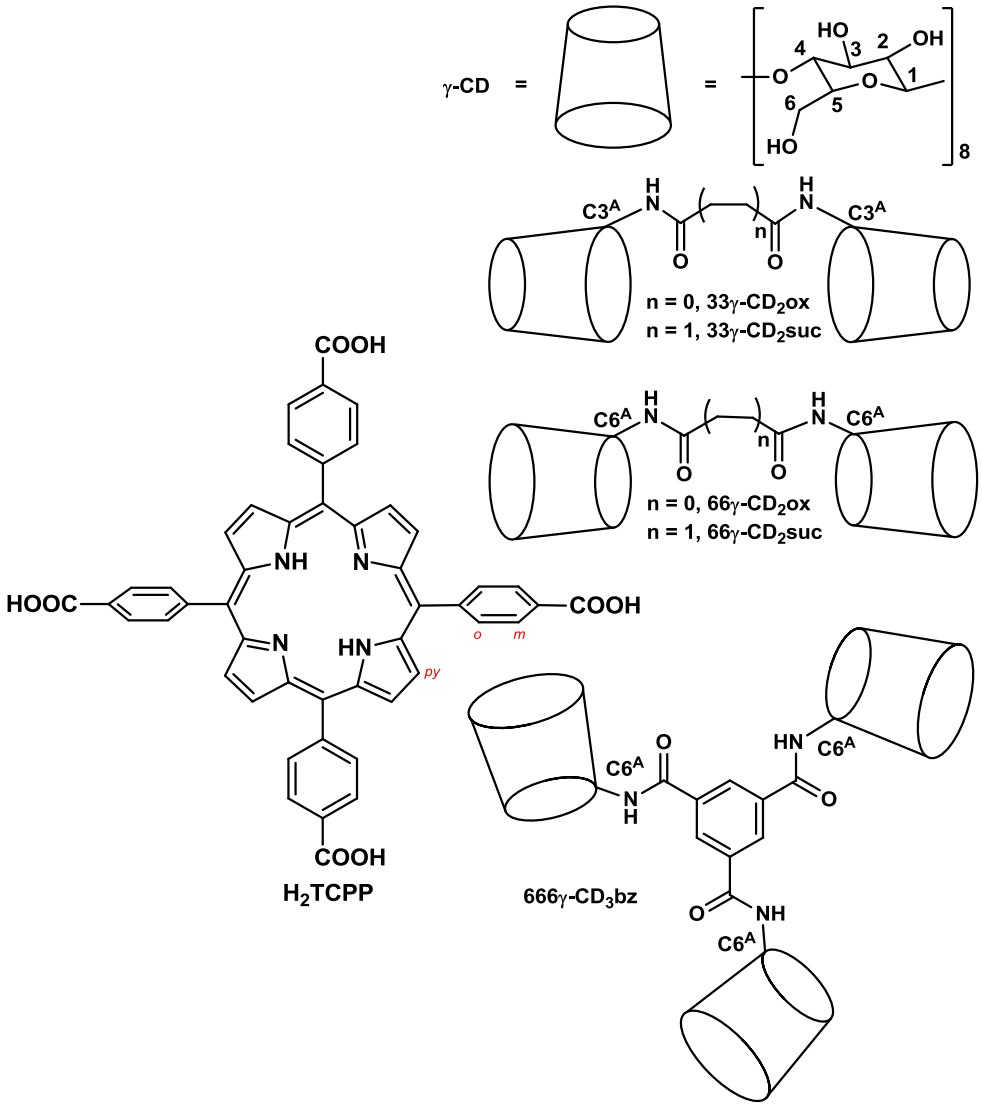

Figure 3.2: γ-Cyclodextrin, γ-CD, and its linked oligomers 33γ-CD_2ox, 33γ-CD_2suc, 66γ-CD_2ox, 66γ-CD_2suc, 666γ-CD_3bz and neutral 5,10,15,20-tetra(*p*-carboxyphenyl)porphyrin, H_2TCPP.

The aggregation of H_2TCPP (in its several ionised forms) in aqueous solutions and its complexation by the hosts, γ-CD and its linked oligomers, 33γ-CD_2ox, 66γ-CD_2ox, 33γ-CD_2suc, 66γ-CD_2suc and 666γ-CD_3bz are investigated through 2D ^{1}H NOESY NMR, UV-vis spectroscopy and molecular modelling. These studies are designed to provide insight into the effect of porphyrin aggregation on the host-guest complexation of H_2TCPP with γ-CD and its oligomers. Furthermore, the γ-CD annular orientation (3,3, 6,6 and 6,6,6) and variation in length of the covalent linker between the γ-CD annuli on the nature of the host-guest complexes formed in the γ-CD oligomer/H_2TCPP equilibria is also investigated.

3.2. SYNTHESIS

3.2.1. 5,10,15,20-tetra(*p*-carboxyphenyl)porphyrin, H_2TCPP

5,10,15,20-tetra(*p*-carboxyphenyl)porphyrin (H_2TCPP) was purchased from Sigma-Aldrich (approx. 75%) and was further purified by recrystallisation from a EtOH/DCM solution. The resulting crystals were left under high vacuum for three days until no solvent peaks were observed in the ^{1}H NMR spectrum.

3.2.2. Preparation of Cyclodextrin Oligomers

The cyclodextrin oligomers outlined in this chapter were prepared as described in Section 2.2 of Chapter 2 and in the literature.[28,29] The structures of the compounds were characterised by TLC, ^{1}H NMR, ^{13}C NMR, MS and elemental analysis (See Chapter 6).

3.3. IONISATION OF H_2TCPP IN AQUEOUS SOLUTIONS

The very low solubility of H_2TCPP in its un-ionised form in aqueous solution makes the determination of the individual pK_a values for the imine nitrogen atoms of the porphyrin core and the *p*-carboxyphenyl substituents difficult.[12] However, a recent spectrophotometric study showed that the pK_a values for the protonation of the imine nitrogens of H_2TCPP are pK_{a1} = 6.0 and pK_{a2} = 6.6 in aqueous NaCl (I = 0.10 mol dm^{-3}) at 298.2 K as shown in Equation 3.1.[30] The protonation of the *p*-carboxyphenyl groups are expected to occur at approximately pH 4.2 in accordance with the pK_a value for benzoic acid.[30] A speciation plot showing the ionisation of H_2TCPP in aqueous solution is shown in Figure 3.3 using the pK_a values for the protonation of the imine nitrogens from the literature[32] (As the precise pK_a values for the protonation of the *p*-carboxyphenyl groups are speculative they are not used in the derivation of the speciation plot.) Using the buffer solutions previously employed in the ^{1}H NMR and

UV-vis studies in Chapter 2 (phosphate buffer, pH 7.0, I = 0.10 mol dm^{-3}) the major proportion of the porphyrin (~70 %, Figure 3.3) is expected to exist as the tetraanion, H_2TCPP^{4-}, at 298.2 K in aqueous solution. However, some of the porphyrin is expected to be present as the monoprotonated form, H_3TCPP^{3-} (~27 %, Figure 3.3), together with a smaller amount as the diprotonated form, H_4TCPP^{2-} (~3 %, Figure 3.3), under these conditions. (These proportions are expected to change with temperature as is discussed later.).

$$H_4TCPP^{2-} \underset{+\,H^+}{\overset{pK_{a1} = 6.0}{\rightleftharpoons}} H_3TCPP^{3-} \underset{+\,H^+}{\overset{pK_{a2} = 6.6}{\rightleftharpoons}} H_2TCPP^{4-} \qquad \textbf{3.1}$$

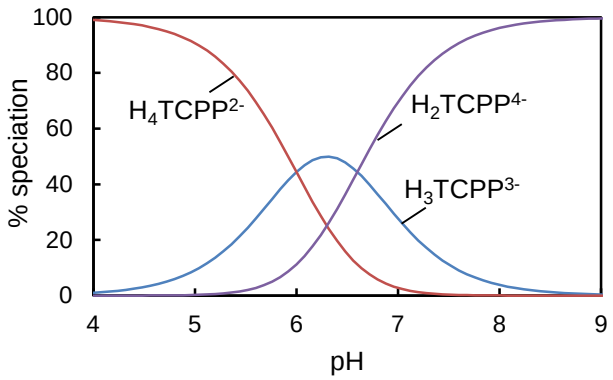

Figure 3.3: Speciation of the ionised forms of H_2TCPP relative to $[H_2TCPP]_{total}$ (2.0 × 10^{-6} mol dm^{-3}) as a function of pH in aqueous solution.

Whilst conducting these experiments at a higher pH (> pH 8) would assure the exclusive formation of H_2TCPP^{4-}, this would require the use of a different aqueous buffer solution than that employed in Chapter 2. As the nature of the supporting electrolyte can substantially affect the physiochemical properties of porphyrins,[12] the use of an aqueous buffer other than phosphate could complicate a direct comparison with the H_2TSPP^{4-} systems in Chapter 2. Accordingly the UV-vis and ^{1}H NMR determinations in this study are conducted in pH 7.0 phosphate buffer (I = 0.10 mol dm^{-3}) with the porphyrin being referred to as H_3TCPP^{3-}/H_2TCPP^{4-} representing the majority of the ionic porphyrin species present in solution (whilst

a very small amount of the porphyrin is expected to be present as H_4TCPP^{2-} it is omitted to simplify the nomenclature).

3.4. 2D ^{1}H NOESY NMR STUDIES

The $H_3TCPP^{3-}/H_2TCPP^{4-}$ monomers exist in dynamic equilibrium with their dimers in aqueous solution (as is discussed in detail in Section 3.5 below) and is characterised by a reported dimerisation constant, $K_D = 4.55 \times 10^4$ dm^3 mol^{-1} in pH 7.5 0.1 mol dm^{-3} aqueous KNO_3 at 298.2 K.[6] ($K_D = 3.59 \times 10^4 \pm 0.18$ dm^3 mol^{-1} in phosphate buffer, pH 7.0, $I = 0.10$ mol dm^{-3} as derived from dimerisation experiments in the next section) Thus, it is anticipated that in the present studies where the total $H_3TCPP^{3-}/H_2TCPP^{4-}$ concentration is 3.0×10^{-3} mol dm^{-3} in D_2O solution a substantial amount of dimerisation occurs (~93 % assuming $K_D = 3.59 \times 10^4 \pm 0.18$ dm^3 mol^{-1}). The ^{1}H NMR spectrum of this solution appears in Figure 3.4 from which it is seen that slightly broadened twin doublets arise from AB coupling between the *meta* and *ortho p*-carboxyphenyl protons, H_m (8.27 ppm, $J = 6$ Hz) and H_o (7.55 ppm, $J = 6$ Hz), while two broadened pyrrolic proton resonances, H_{py} (8.81 and 6.68 ppm), of equal area arise. As observed for H_2TSPP^{4-} in Section 2.3 of Chapter 2, the splitting and broadening of the H_{py} resonance is attributed to the effect of slow to intermediate (NMR timescale) tautomerism rates for the imine protons of $H_3TCPP^{3-}/H_2TCPP^{4-}$.[31] As discussed above, it is probable that the Na^+ and K^+ of the phosphate buffer partially screen the *p*-carboxyphenyl group negative charges and enable the hydrophobic planar porphyrin cores of two $H_3TCPP^{3-}/H_2TCPP^{4-}$ to associate as a dimer (H-aggregate) to a substantial extent.

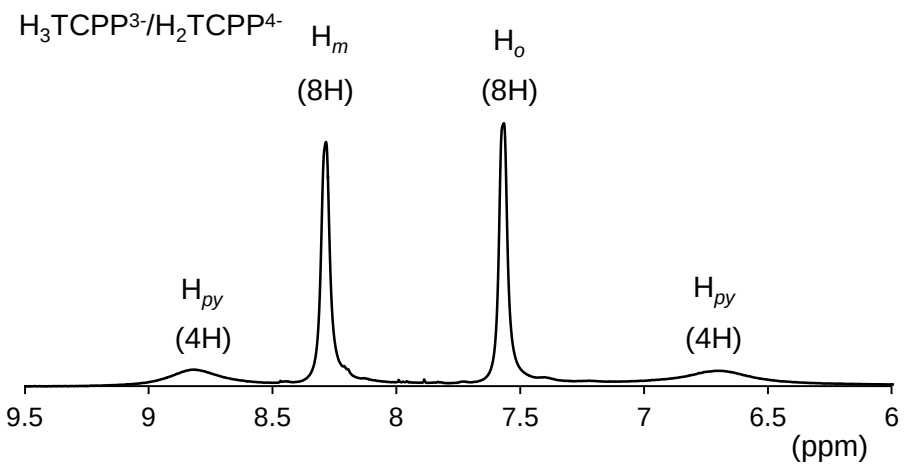

Figure 3.4: ^{1}H NMR (600 MHz) spectrum of a $H_3TCPP^{3-}/H_2TCPP^{4-}$ 3.0×10^{-3} mol dm^{-3} solution in D_2O (pD 7.0 phosphate buffer, I = 0.10 mol dm^{-3}) at 298.2 K.

The host–guest complexation of $H_3TCPP^{3-}/H_2TCPP^{4-}$ by γ-CD is first examined through the ^{1}H 1D NMR spectra of a 3.0×10^{-3} mol dm^{-3} γ-CD D_2O solution and of a 3.0×10^{-3} mol dm^{-3} γ-CD and 3.0×10^{-3} mol dm^{-3} $H_3TCPP^{3-}/H_2TCPP^{4-}$ D_2O solution, which appear in Figure 3.5. (Eighty percent of the $H_3TCPP^{3-}/H_2TCPP^{4-}$ is complexed by γ-CD in this solution, as calculated from the host-guest complexation constants K_{11} and K_{21} for the complexes γ-CD.$H_3TCPP^{3-}/H_2TCPP^{4-}$ and γ-CD_2.$H_3TCPP^{3-}/H_2TCPP^{4-}$ discussed in Section 3.5 below, and some of the free $H_3TCPP^{3-}/H_2TCPP^{4-}$ is likely to exist as a dimer as discussed above.) Upon complexation with $H_3TCPP^{3-}/H_2TCPP^{4-}$, an upfield shift is observed for the $H_{2\text{-}6}$ resonances of the γ-CD as a consequence of the *p*-carboxyphenyl groups of $H_3TCPP^{3-}/H_2TCPP^{4-}$ complexing within the γ-CD annulus. The resonances for γ-CD H_5, H_{6A} and H_{6B} overlap with that of H_2 and H_4 and are greatly broadened by comparison with the analogous resonances for γ-CD in the presence of H_2TSPP^{4-} in Figure 2.6 of Chapter 2 (the origin of this broadening is discussed below). The resonances for γ-CD H_5, H_{6A} and H_{6B} separate and show both greater changes in chemical shift consistent with their greater changes in magnetic environment and therefore chemical shift (H_5 3.90 → ~ 3.50 ppm, H_{6A} δ 3.88 → ~3.57 ppm, H_{6B} δ 3.88 → ~3.32 ppm) and broadening by comparison with the $H_{2,3,4}$ γ-CD resonances. The multiplets of the γ-CD $H_{2,4}$ resonances superimpose in the presence of H_3TCPP^{3-}

/H_2TCPP^{4-} and in turn superimpose on a broadened H_5 resonance. The greater chemical shift changes of the γ-CD H_5, H_{6A} and H_{6B} resonances are consistent with γ-CD complexing H_3TCPP^{3-}/H_2TCPP^{4-} though the narrow face of the annulus defined by the primary hydroxyl groups such that H_5, H_{6A} and H_{6B} are closer to the H_3TCPP^{3-}/H_2TCPP^{4-} core and experience a greater change in magnetic environment and chemical shift than do the γ-CD H_2, H_3 and H_4 protons as shown in Figure 3.6. (The γ-CD H_1 resonance shows little change in width or shift indicative of minimal interaction of the H_1 with H_3TCPP^{3-}/H_2TCPP^{4-} and is not further discussed.)

Given the well-defined γ-CD H_3 multiplet observed in the presence of H_3TCPP^{3-} /H_2TCPP^{4-} it appears that exchange between the free γ-CD and the complexed γ-CD.H_3TCPP^{3-}/H_2TCPP^{4-} and (γ-CD)$_2$.H_3TCPP^{3-}/H_2TCPP^{4-} is fast on the NMR timescale for these protons as a consequence of the small chemical shift changes induced by complexation: H_3 δ 3.96 → 3.88 ppm. In contrast, the broadening of the H_5, H_{6A} and H_{6B} resonances indicate that these protons are experiencing exchange between the free γ-CD and the complexed γ-CD.H_3TCPP^{3-}/H_2TCPP^{4-} and (γ-CD)$_2$.H_3TCPP^{3-}/H_2TCPP^{4-} at an intermediate rate on the NMR timescale which is consistent with their greater changes in magnetic environment and therefore chemical shift. (Of necessity all protons experience the same chemical exchange rate). As a consequence of their location on the outside of the γ-CD torus, the H_2 and H_4 resonances show lesser upfield shifts (H_2 δ 3.68 → ~3.54, H_4 δ 3.62 → ~3.49) due to changes in magnetic environment which occur as a consequence of the complexation of H_3TCPP^{3-}/H_2TCPP^{4-}.

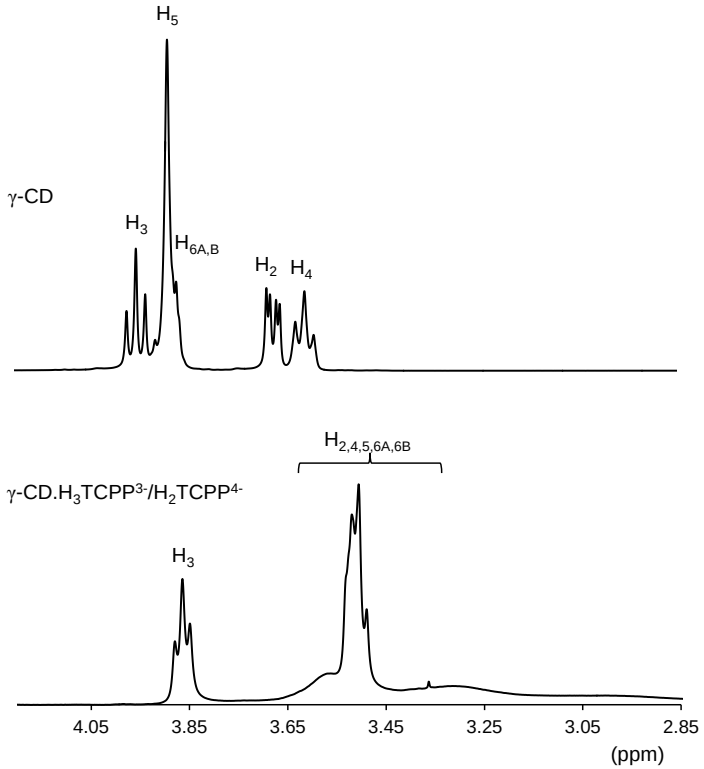

Figure 3.5: Top**,** the $H_{2\text{-}6}$ region of a ^{1}H NMR (600 MHz) spectrum of a γ-CD (3.0×10^{-3} mol dm^{-3}) solution in D_2O (pD 7.0 phosphate buffer, I = 0.10 mol dm^{-3}) at 298.2 K. Bottom, the spectrum of an equimolar solution of $H_3TCPP^{3-}/H_2TCPP^{4-}$ (3.0×10^{-3} mol dm^{-3}) and γ-CD (3.0×10^{-3} mol dm^{-3}) under the same experimental conditions.

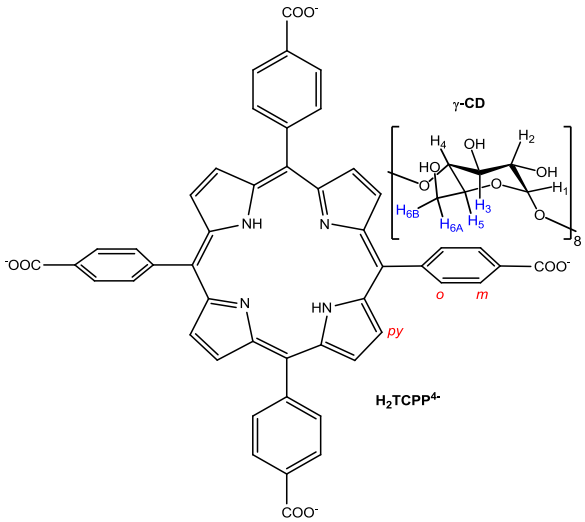

Figure 3.6: The deduced orientation of a single γ-CD complexing H_2TCPP^{4-} and the labelling of the annular γ-CD annular (H_3, H_5, H_{6A}, H_{6B}, blue) and external protons (H_1, H_2, H_4 black) and the H_2TCPP^{4-} pyrrolic and phenyl protons (H_{py}, H_o and H_m, red). Note: Whilst the porphyrin is shown in its tetraanionic form, H_2TCPP^{4-}, the mono- and diprotonated species are expected to complex in a similar orientation.

The 2D ^{1}H NOESY NMR spectrum of the 3.0×10^{-3} mol dm^{-3} γ-CD and 3.0×10^{-3} mol dm^{-3} $H_3TCPP^{3-}/H_2TCPP^{4-}$ D_2O solution is shown in Figure 3.7 (and Figure A1 in the Appendix), and serves as a comparison for similar spectra of the γ-CD oligomer.$H_3TCPP^{3-}/H_2TCPP^{4-}$ solutions. For γ-CD, the H_3 resonance can be separately identified as are the $H_3TCPP^{3-}/H_2TCPP^{4-}$ *p*-carboxyphenyl *meta* and *ortho* hydrogen, H_m and H_o, and pyrrolic hydrogen, H_{py}, resonances. As discussed earlier, an upfield shift in the resonances of H_5, H_{6A}, and H_{6B} annular protons of γ-CD creates overlapping signals with that of the H_2 and H_4 resonances, thus making the individual assignment of each resonance difficult. Nevertheless, cross-peaks between the overlapping γ-CD resonances and the $H_3TCPP^{3-}/H_2TCPP^{4-}$ resonances can be assigned to the H_5, H_{6A} and H_{6B} annular protons of γ-CD as previously observed for H_2TSPP^{4-} in Chapter 2.

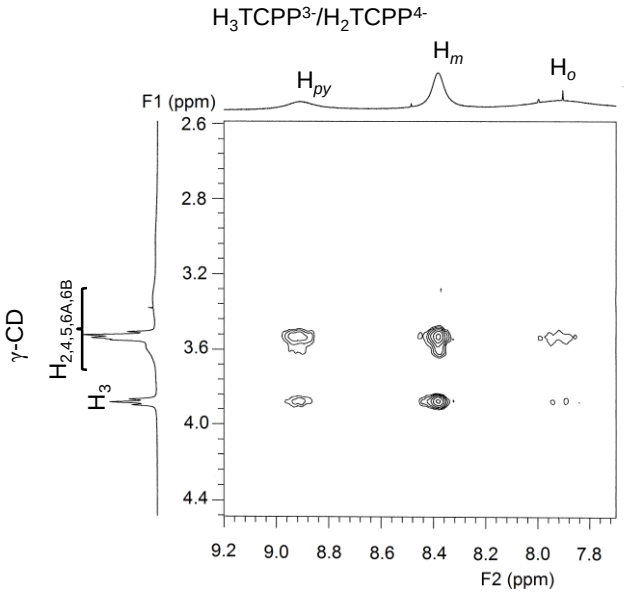

Figure 3.7: 2D ^{1}H NOESY NMR (600 MHz) spectrum of $H_3TCPP^{3-}/H_2TCPP^{4-}$ 3.0×10^{-3} mol dm^{-3} and equimolar γ-CD in D_2O (pD 7.0 phosphate buffer, I = 0.10 mol dm^{-3}) at 298.2 K with a mixing time of 300 ms. Cross–peaks arise from NOE interactions between the annular γ-CD protons (H_3, H_5, H_{6A} and H_{6B}) and the pyrrolic and phenyl protons, H_{py}, H_o and H_m of $H_3TCPP^{3-}/H_2TCPP^{4-}$. The amount of $H_3TCPP^{3-}/H_2TCPP^{4-}$ in the free state is ~ 20% of the total.

By comparison with the spectrum of $H_3TCPP^{3-}/H_2TCPP^{4-}$ alone (Figure 3.4) it is seen that several changes occur in the spectrum of the solution of equimolar $H_3TCPP^{3-}/H_2TCPP^{4-}$

and γ-CD in Figure 3.7: i) only the broad resonance assigned to the downfield H_{py} in the $H_3TCPP^{3-}/H_2TCPP^{4-}$ is observed while that of the upfield H_{py} has evidently broadened into the baseline, and ii) the resonance assigned to H_o is now substantially broadened while that assigned to H_m is broadened to a lesser extent. The origin of the selective broadening of the γ-CD $H_{5,6A,6B}$ resonances has been discussed above in terms of chemical exchange between free γ-CD and the complexed γ-CD.$H_3TCPP^{3-}/H_2TCPP^{4-}$ and $(\gamma\text{-CD})_2.H_3TCPP^{3-}/H_2TCPP^{4-}$. This necessarily involves $H_3TCPP^{3-}/H_2TCPP^{4-}$, its dimer and complexed forms also. Complexation of $H_3TCPP^{3-}/H_2TCPP^{4-}$ by γ-CD might increase the rate of tautomerism of the $H_3TCPP^{3-}/H_2TCPP^{4-}$ imine protons and broaden the H_{py} resonances, while complexation through the narrow face of γ-CD is likely to cause a greater magnetic environmental change for H_o than for H_m and thereby causes H_o to experience a larger change in chemical shift (δ 7.55 → 7.92 ppm) than does H_m (δ 8.27 → 8.38 ppm) and a consequently greater likelihood of entering the intermediate exchange regime of the NMR timescale. These observations are also consistent with the changes in spectra observed for H_2TSPP^{4-} in Chapter 2, however, the $H_3TCPP^{3-}/H_2TCPP^{4-}$ *p*-carboxyphenyl H_m resonance is significantly broadened by comparison with the analogous resonance for H_2TSPP^{4-}. The increased broadening of the $H_3TCPP^{3-}/H_2TCPP^{4-}$ *p*-carboxyphenyl H_m and H_o and γ-CD proton resonances in the γ-CD.$H_3TCPP^{3-}/H_2TCPP^{4-}$ spectrum by comparison with the analogous signals for γ-CD.H_2TSPP^{4-} could be a consequence of the greater K_{11} and K_{21} complexation constants characterising γ-CD.H_2TSPP^{4-} by comparison with those characterising γ-CD.$H_3TCPP^{3-}/H_2TCPP^{4-}$ (as discussed in the following section). The increase complexation K_{11} and K_{21} constants in the γ-CD.$H_3TCPP^{3-}/H_2TCPP^{4-}$ and $(\gamma\text{-CD})_2.H_3TCPP^{3-}/H_2TCPP^{4-}$ than γ-CD.H_2TSPP^{4-} and $(\gamma\text{-CD})_2.H_2TSPP^{4-}$ could lead to a slower exchange between the chemical environments (and magnetic environments also) of free and complexed species leading to increased broadening in the former than the latter.

Two particularly strong cross-peaks arising from the nuclear Overhauser effect, NOE, between the H_3, H_5, H_{6A} and H_{6B} annular protons of γ-CD and the H_m *p*-carboxyphenyl protons of $H_3TCPP^{3-}/H_2TCPP^{4-}$ appear in the 2D H^1 NOESY NMR spectrum as a consequence of their close proximities in the host-guest complex and the narrowness of the H_m resonance by comparison with those of H_{py} and H_o. Additional weaker cross-peaks arise from the NOE between the γ-CD H_3, H_5, H_{6A}, H_{6B} and the $H_3TCPP^{3-}/H_2TCPP^{4-}$ H_o proton. The intensity of these cross-peaks is significantly lower than that of those arising from H_m and H_{py} as a consequence of the greater broadening of the H_o resonance. In all cases the cross-peaks arising from NOE interactions between the H_3 protons of γ-CD and the H_m, H_o and H_{py} resonances of $H_3TCPP^{3-}/H_2TCPP^{4-}$ are of a lower intensity than the analogous signals for H_5, H_{6A} and, H_{6B}. These observations are consistent with the γ-CD H_3 proton being most distant from the $H_3TCPP^{3-}/H_2TCPP^{4-}$ protons and for complexation occurring through the narrow primary hydroxyl face of the annulus, consistent with earlier deductions[21] and that observed for H_2TSPP^{4-} in Chapter 2. (No cross-peaks arising from the γ-CD H_1 proton are observed for this system nor for the γ-CD oligomer systems.)

The host–guest complexation of $H_3TCPP^{3-}/H_2TCPP^{4-}$ by the oxalate and succinamide-linked dimers and benzene linked trimer, 33γ-CD_2ox, 33γ-CD_2suc, 66γ-CD_2ox, 66γ-CD_2suc and 666γ-CD_3bz are also studied by 2D ^{1}H NOESY NMR spectroscopy. In all five systems cross-peaks arising from nuclear Overhauser effects (NOE) between the *p*-carboxyphenyl H_o and H_m protons and the pyrrolic H_{py} protons of $H_3TCPP^{3-}/H_2TCPP^{4-}$ with the γ-CD annular H_3, H_5, H_{6A} and H_{6B} protons are observed. This is consistent with complexation of the *p*-carboxyphenyl groups as guests close in to the porphyrin core by the γ-CD annular host. A previous NMR study of α-CD, β-CD and γ-CD interactions with $H_3TCPP^{3-}/H_2TCPP^{4-}$ detected no complexation by α-CD, *p*-carboxyphenyl group complexation by β-CD through the wider annular face delineated by the C2 and C3 secondary hydroxyl groups and

p-carboxyphenyl group complexation by γ-CD through the narrow annular face delineated by the C6 primary hydroxyl groups.[21] The β-CD annulus has narrow and wide face diameters of 600 and 650 pm and a depth of 790 pm, and the corresponding dimensions for γ-CD are 750, 830 and 790 pm.[32] These compare with a phenyl ring width of ~470 pm, and indicate that the tightness of fit of the *p*-carboxyphenyl groups of $H_3TCPP^{3-}/H_2TCPP^{4-}$ in the β-CD and γ-CD annuli is likely to be a major factor in determining host-guest complex stereochemistry.

When $H_3TCPP^{3-}/H_2TCPP^{4-}$ is complexed by the γ-CD oligomers the pattern of cross-peaks change significantly as illustrated by Figure 3.8 (and Figure 3.9 and A1-A6 of the Appendix). As observed in Chapter 2, mono-substitution of the γ-CD in the oligomers causes their D-glucopyranose subunits to become chemically inequivalent and usually magnetically inequivalent also. Accordingly, the γ-CD $H_{2\text{-}6}$ proton resonances of the oligomers increase in number and are significantly broadened in most cases such that it is difficult to assign the individual resonances. The $H_3TCPP^{3-}/H_2TCPP^{4-}$ H_{py}, H_o and H_m resonances are also substantially broadened in the five oligomer systems studied compared with those of $H_3TCPP^{3-}/H_2TCPP^{4-}$ alone, and the chemical shift between the resonances of H_o and H_m are substantially decreased. Regardless of these chemical shift changes, the observed cross-peaks may be assigned to interactions between the H_3, H_5, H_{6A} and H_{6B} annular γ-CD protons of the γ-CD oligomers and the $H_3TCPP^{3-}/H_2TCPP^{4-}$ H_{py}, H_o and H_m protons.

Changes in the oligomer.$H_3TCPP^{3-}/H_2TCPP^{4-}$ 2D ^1H NOESY NMR spectra compared with that of γ-CD.$H_3TCPP^{3-}/H_2TCPP^{4-}$ are exemplified in Figure 3.8 for the 66γ-CD_2ox.$H_3TCPP^{3-}/H_2TCPP^{4-}$ system where strong cross-peaks are formed by the H_m protons because of the lesser broadened H_m resonance (a characteristic of the spectra of all five γ-CD oligomer systems). Cross-peaks of intermediate and weak intensities are formed by the H_{py} and H_o protons, respectively, which is consistent with the relative intensities for the γ-CD/H_2TSPP^{4-} system discussed above. This may be understood on the basis that

66γ-CD_2ox complexes two $H_3TCPP^{3-}/H_2TCPP^{4-}$ *p*-carboxyphenyl groups simultaneously (or ditopically) through the narrow face of each of its two γ-CD substituents in the *anti* configuration shown in Figure 3.1. The cooperative effect of such ditopic complexation is likely to cause a tight complexation which holds the H_{6A} and H_{6B} protons closer to the H_{py} protons than the H_o protons such that the cross-peaks arising from the former are stronger than those arising from the latter. (The cross-peaks arising from the H_m are the strongest for the same reasons as for those of the γ-CD.$H_3TCPP^{3-}/H_2TCPP^{4-}$ system.) Similar variations are seen in the spectrum of the 66γ-CD_2suc.$H_3TCPP^{3-}/H_2TCPP^{4-}$ system in which the H_m and H_o resonances have similar chemical shifts (Figure A5).

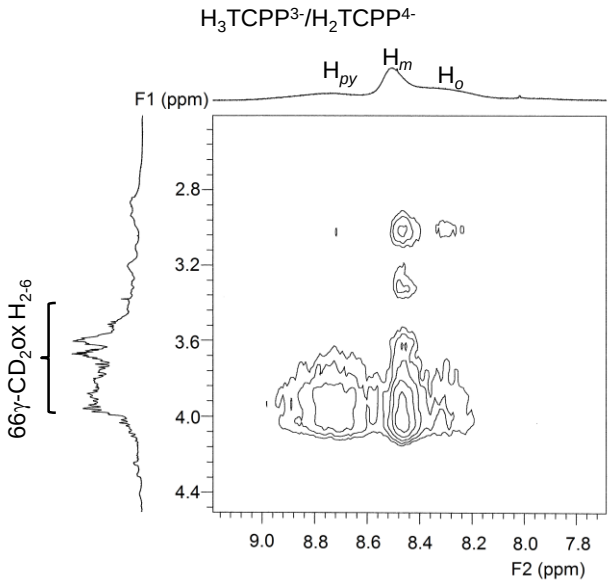

Figure 3.8: 2D ^{1}H NOESY NMR (600 MHz) spectrum of $H_3TCPP^{3-}/H_2TCPP^{4-}$ 3.0×10^{-3} mol dm^{-3} and equimolar 66γ-CD_2ox in D_2O (pD 7.0 phosphate buffer, I = 0.10 mol dm^{-3}) at 298.2 K with a mixing time of 300 ms. The amount of $H_3TCPP^{3-}/H_2TCPP^{4-}$ in the free state is < 1% of the total.

The spectrum of the 33γ-CD_2ox.$H_3TCPP^{3-}/H_2TCPP^{4-}$ system is shown in Figures 3.9 and A2 of the Appendix. The cooperative effect of the ditopic complexation is likely to cause a tight complexation which holds the H_3 protons closer to the H_{py} protons and the H_5, H_{6A} and H_{6B} protons closer to H_o and H_m such that the cross-peaks arising from the former are stronger than those arising from the latter. Once again the cross-peak arising from the H_m proton is the

strongest because of the sharper resonance arising from it and overlaps with that of H_o making it hard to distinguish between the two signals. Beyond these observations there is little more that can be deduced concerning host-guest complex structure for the 33γ-CD_2ox.H_3TCPP^{3-}/H_2TCPP^{4-} system or that of the 33γ-CD_2suc.H_3TCPP^{3-}/H_2TCPP^{4-} system (Figure A3 of the Appendix).

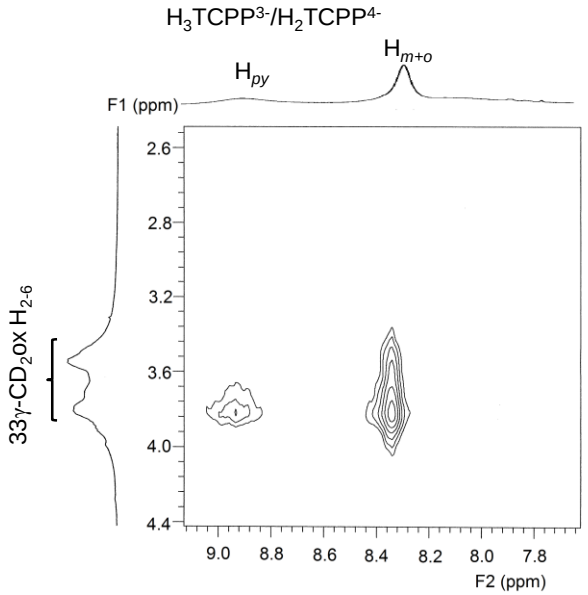

Figure 3.9: 2D ^{1}H NOESY NMR (600 MHz) spectrum of H_3TCPP^{3-}/H_2TCPP^{4-} 3.0×10^{-3} mol dm^{-3} and equimolar 33γ-CD_2ox in D_2O (pD 7.0 phosphate buffer, I = 0.10 mol dm^{-3}) at 298.2 K with a mixing time of 300 ms. The amount of H_3TCPP^{3-}/H_2TCPP^{4-} in the free state is ~ 8% of the total.

The 2D ^{1}H NOESY NMR spectrum of the 666γ-CD_3bz.H_3TCPP^{3-}/H_2TCPP^{4-} system (Figure A6) also shows significant cross-peaks arising from the H_3TCPP^{3-}/H_2TCPP^{4-} H_{py}, H_m and H_o proton resonances consistent with host-guest complexation which is expected to be tritopic in nature although this cannot be directly deduced from the spectrum.

The cross-peak patterns observed for the complexation of H_3TCPP^{3-}/H_2TCPP^{4-} by 33γ-CD_2ox and 33γ-CD_2suc (Figure 3.9 and Figures A2 and A3 of the Appendix) are similar to those of the analogous systems with H_2TSPP^{4-} in Chapter 2. However, the cross-peak patterns observed for the 66γ-CD_2ox, 66γ-CD_2suc, 666γ-CD_3bz systems (Figure 3.8 and Figures A4, A5 and A6 of the Appendix) are slightly different. For H_3TCPP^{3-}/H_2TCPP^{4-}, greater pyrrolic

cross-peaks are observed with 66γ-CD_2ox than 66γ-CD_2suc. This is the opposite of that observed for H_2TSPP^{4-} with the same dimer systems. Whilst the exact origin of these changes is unclear, it does suggest that a change in the shape of the ionic functional groups from planar *p*-carboxyphenyl to tetrahedral *p*-sulfonatophenyl effects the complexation of these groups by the narrow 6-hydroxyl faces of two γ-CD dimer annuli. The planar *p*-carboxyphenyl groups of H_3TCPP^{3-}/H_2TCPP^{4-} may allow 'tighter' complexation (with γ-CD protons H_{6A} and H_{6B}) in the 66γ-CD_2ox system than the 66γ-CD_2suc system. Conversely, the larger size of the tetrahedral *p*-sulfonatophenyl groups of H_2TSPP^{4-} may require a more flexible linker for 'tighter' complexation. Thus, it appears that the complexation through the narrower γ-CD faces of the 66γ-CD_2ox and 66γ-CD_2suc oligomers accentuates the effect of changing the porphyrin functional group from sulfonate to carboxylate on complexation by comparison with complexation through the wider faces of the 33γ-CD_2ox and 33γ-CD_2suc oligomers (This is further supported by the similar trends observed in the UV-vis and molecular modelling studies discussed below).

The cross-peak patterns observed for 666γ-CD_3bz.H_3TCPP^{3-}/H_2TCPP^{4-} and 666γ-CD_3bz.H_2TSPP^{4-} also differ. The cross-peaks between H_o and H_{py} with the annular protons of the γ-CD D-glucopyranose subunits of 666γ-CD_3bz are significantly stronger for the H_3TCPP^{3-}/H_2TCPP^{4-} system than those for the H_2TSPP^{4-} system. This is consistent with the annular protons of the γ-CD subunits being closer to the porphyrin core in the former than the latter, which could also be a consequence of the change in ionic functional groups discussed above.

Although the 2D ^{1}H NOESY NMR data are consistent with host-guest complexation occurring between γ-CD and the γ-CD oligomers and H_3TCPP^{3-}/H_2TCPP^{4-} they do not identify their stoichiometry. The broadening of the H_3TCPP^{3-}/H_2TCPP^{4-} resonances is likely to render a more detailed study in which the concentrations of the host and guest are

systematically varied difficult to interpret quantitatively. Accordingly, UV-vis spectroscopic studies are undertaken to determine the stoichiometry of host-guest complexation.

3.5. UV-VIS SPECTROSCOPIC STUDIES

3.5.1. $H_3TCPP^{3-}/H_2TCPP^{4-}$ Dimerisation

The UV-visible absorption spectra of ionic porphyrins in aqueous solution can deviate from Beer's law behaviour, as indicated by a weakened Soret band at increasing concentration, as a consequence of a dimerisation or higher aggregation.[12] Whilst the H_2TCPP porphyrin species in neutral aqueous solutions are expected to exist dominantly as a mixture of the ionised states, H_3TCPP^{3-} and H_2TCPP^{4-}, both species are expected to dimerise under these conditions. Although variable pH studies of the dimerisation in principle allows the calculation of the individual dimerisation constants, $K_{D,}$ for H_3TCPP^{3-} and H_2TCPP^{4-} it is generally the case that K_D has been determined at a single pH. Thus, the dimerisation of $H_3TCPP^{3-}/H_2TCPP^{4-}$ has been previously characterised by a dimerisation constant $K_{D=}$ 4.55×10^4 dm^{-3} mol^{-1} in pH 7.5 0.1 mol dm^{-3} aqueous KNO_3 at 298.2 K.[6] Under the conditions used in the UV-vis studies of H_2TSPP^{4-} in Chapter 2 ([H_2TSPP^{4-}] 1.05×10^{-6} mol dm^{-3} in phosphate buffer, pH 7.0, I = 0.10 mol dm^{-3}) and assuming $K_{D=}$ 4.55×10^4 mol dm^{-3}, ~8 % of $H_3TCPP^{3-}/H_2TCPP^{4-}$ would be in the dimeric form. However, the monomer/dimer equilibrium is heavily reliant on experimental conditions including pH, temperature and porphyrin concentration as well as the ionic strength and concentration of electrolytes in the buffer solution. Therefore, an investigation into the dimerisation of $H_3TCPP^{3-}/H_2TCPP^{4-}$ under the experimental conditions employed in this study must be undertaken before studying the host-guest complexation of $H_3TCPP^{3-}/H_2TCPP^{4-}$ with γ-CD and the γ-CD oligomers. Furthermore, the UV-vis experiments in this study is conducted at a higher $H_3TCPP^{3-}/H_2TCPP^{4-}$ concentration than

that of H_2TSPP^{4-} in Section 2.4 of Chapter 2 to increase the likelihood of porphyrin dimerisation in solution and to gain a greater understanding of its influence on the complexation of $H_3TCPP^{3-}/H_2TCPP^{4-}$ by γ-CD and its oligomers.

An indication of the temperature effect on the $H_3TCPP^{3-}/H_2TCPP^{4-}$ monomer/dimer equilibrium in the temperature range 308.2 K to 278.2 K is indicated by the variation of the absorption spectrum of a 2.00×10^{-6} mol dm^{-3} solution at four temperatures as shown in Figure 3.10. It is seen that there is a decrease in molar absorbance at 415 nm from 4.78×10^5 to 3.65×10^5 mol^{-1} dm^{-3} cm^{-1} between the temperature extremes and a corresponding change in absorbance maximum, λ_{max}, of 415 nm to 414 nm. The pK_a values of the porphyrin are expected to vary with temperature, which should also change the proportions of the different multiply ionised states (this is discussed in detail in a later section). However the presence of a sharp isosbestic point at 409 nm suggests two differently absorbing species existing in a labile equilibrium consistent with the temperature dependence of a $H_3TCPP^{3-}/H_2TCPP^{4-}$ monomer/dimer equilibrium. (The same isosbestic point is also observed at a constant temperature as the porphyrin concentration is varied which further suggests a monomer/dimer equilibrium, as is discussed in the following section).

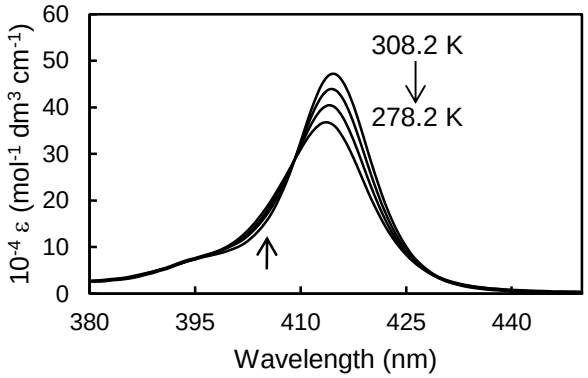

Figure 3.10: Temperature dependence of molar absorbance change of $H_3TCPP^{3-}/H_2TCPP^{4-}$ (2.00×10^{-6} mol dm^{-3}) in phosphate buffer, pH 7.0, I = 0.10 mol dm^{-3}.

These changes in the absorption spectrum of $H_3TCPP^{3-}/H_2TCPP^{4-}$ suggested significant dimerisation under these experimental conditions, which warranted a further quantitative investigation as is discussed below.

3.5.2. UV-Vis Studies of $H_3TCPP^{3-}/H_2TCPP^{4-}$ Dimerisation

The study of the $H_3TCPP^{3-}/H_2TCPP^{4-}$ dimerisation equilibria by UV-vis spectroscopy and the protocol for fitting the algorithms describing the equilibria to the changes in absorbance followed methods similar to those previously reported.[33] The model used to determine the dimerisation constants (K_D) assumes that labile equilibria exist such that the concentrations of free $H_3TCPP^{3-}/H_2TCPP^{4-}$ and that of the dimerised species, $(H_3TCPP^{3-}/H_2TCPP^{4-})_2$, very rapidly adjust as the UV-vis titrations proceed. Thus, the $H_3TCPP^{3-}/H_2TCPP^{4-}$ dimers form according to Equation 3.2:

$$H_3TCPP^{3-}/H_2TCPP^{4-} \overset{K_D}{\rightleftharpoons} (H_3TCPP^{3-}/H_2TCPP^{4-})_2 \qquad (\mathbf{3.2})$$

The dimerisation constant, $K_{D,}$ at equilibrium is given by:

$$K_D = [(H_3TCPP^{3-}/H_2TCPP^{4-})_2]/[\ H_3TCPP^{3-}/H_2TCPP^{4-}]^2 \qquad (\mathbf{3.3})$$

The absorbance at a particular wavelength is given by:

$$A(\lambda) = \varepsilon_{H_3TCPP^{3-}/H_2TCPP^{4-}}[H_3TCPP^{3-}/H_2TCPP^{4-}] + \varepsilon_{(H_3TCPP^{3-}/H_2TCPP^{4-})_2}[(H_3TCPP^{3-}/H_2TCPP^{4-})_2] \quad (\mathbf{3.4})$$

where $A(\lambda)$, $\varepsilon_{H_3TCPP^{3-}/H_2TCPP^{4-}}$ and $\varepsilon_{(H_3TCPP^{3-}/H_2TCPP^{4-})_2}$ represent the observed absorbance and apparent molar absorbances of $H_3TCPP^{3-}/H_2TCPP^{4-}$ and $(H_3TCPP^{3-}/H_2TCPP^{4-})_2$ respectively. The values of K_D were determined by best-fitting the dimerisation algorithm (Equations 3.3 and 3.4) to the $H_3TCPP^{3-}/H_2TCPP^{4-}$ absorbance data in the range 400-430 nm at 0.25 nm intervals as the $H_3TCPP^{3-}/H_2TCPP^{4-}$ concentration is increased using the HypSpec protocol.[34]

The dimerisation constant, $K_{D,}$ of $H_3TCPP^{3-}/H_2TCPP^{4-}$ was determined by monitoring the absorbance variation of $H_3TCPP^{3-}/H_2TCPP^{4-}$ solutions over concentrations in the range of

$1.95 \times 10^{-6} - 1.18 \times 10^{-5}$ mol dm^{-3} in in pH 7.0 phosphate buffer (I = 0.10 mol dm^{-3}). The UV-vis spectra of solutions were determined against reference solutions in matched 2 mm quartz cells and were recorded at 0.25 nm intervals using a Cary 5000 UV-vis spectrophotometer over the wavelength range 250-650 nm. Samples were 0.7 cm^3 in volume and were thermostated 298.2 K for 20 minutes before recording the spectra. The UV-vis titration, derived spectra and speciation plot for the $H_3TCPP^{3-}/H_2TCPP^{4-}$ monomer/dimer equilibrium are shown in Figure 3.11.

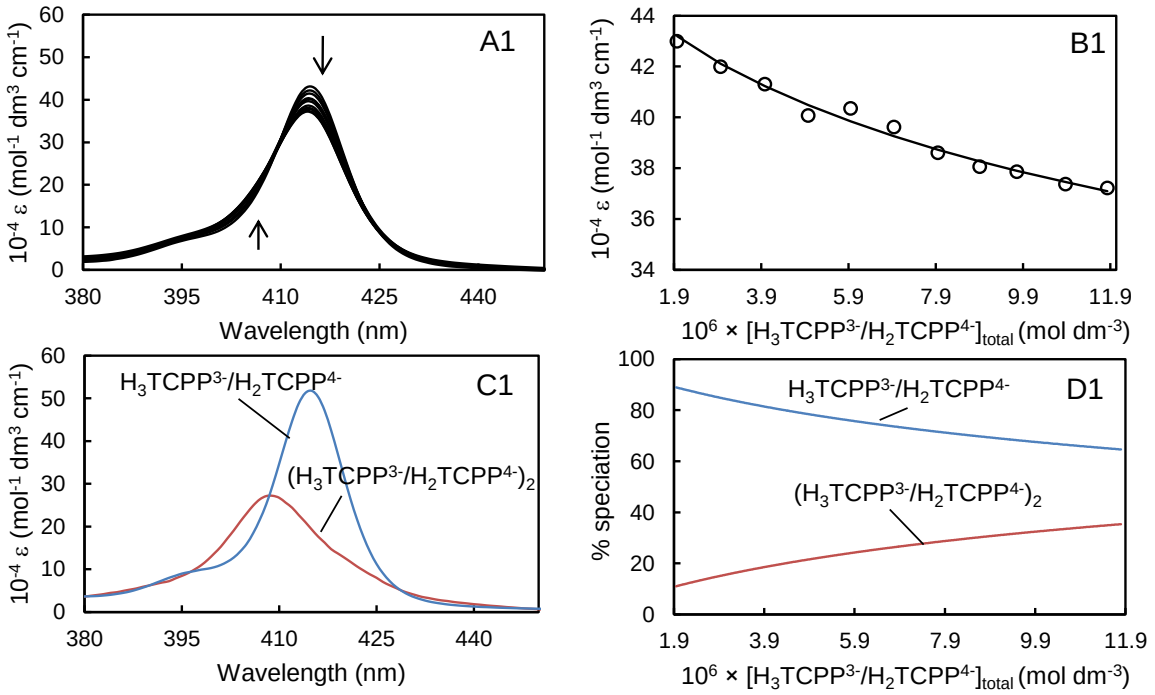

Figure 3.11: (A1) Molar absorbance change of $H_3TCPP^{3-}/H_2TCPP^{4-}$ (1.95×10^{-6} -1.18×10^{-5}) in phosphate buffer, pH 7.0, I = 0.10 mol dm^{-3} at 298.2 K. The arrows indicate the direction of molar absorbance change as the concentration of $H_3TCPP^{3-}/H_2TCPP^{4-}$ increases. (B1) Molar absorbance variation at 414 nm and the best fit of an algorithm for the dimerisation of $H_3TCPP^{3-}/H_2TCPP^{4-}$ over the wavelength range 400-430 nm. (C1) Calculated molar absorbance of monomer and dimer $H_3TCPP^{3-}/H_2TCPP^{4-}$. (D1) Speciation relative to [$H_3TCPP^{3-}/H_2TCPP^{4-}$]$_{total}$ = 100%.

A blue-shift and decrease in the intensity of the Soret band of the $H_3TCPP^{3-}/H_2TCPP^{4-}$ absorption spectrum is observed as the concentration of $H_3TCPP^{3-}/H_2TCPP^{4-}$ increases with an isosbestic point occurring at 409 nm. These observations are consistent with increased $H_3TCPP^{3-}/H_2TCPP^{4-}$ dimer formation at higher concentrations similar to that observed for

H_2TSPP^{4-} in previous studies.[11,13] The dimerisation constant, K_D, was determined to be (3.59 ± 0.18) × 10^4 dm^3 mol^{-1} in phosphate buffer, pH 7.0, I = 0.10 mol dm^{-3} at 298.2 K. (The error shown for K_D is derived from the best fit of Equation 3.4 to the absorbance data and the experimental error is estimated at < ± 5 %.). This is similar to the reported dimerisation constant reported in the literature (K_D = 4.55 × 10^4 mol dm^{-3} in pH 7.5 0.1 mol dm^{-3} aqueous KNO_3 at 298.2 K).[6] As previously mentioned, the monomer/dimer equilibrium is heavily reliant on the experimental conditions; therefore, the variation between the K_D values could arise from the difference in the pH and dissolved electrolytes of the two solutions in each experiment.

3.5.4. H_3TCPP^{3-}/H_2TCPP^{4-} Host-Guest Complexation

Different multiply ionised states of H_2TSPP (H_4TSPP^{2-} and H_2TSPP^{4-}) have been shown to complex within β-CD with the same orientation but with different K_{11} complexation constants.[35] Accordingly, H_3TCPP^{3-} and H_2TCPP^{4-} are expected to experience a similar change in host-guest complexation constants with γ-CD and its oligomers. As for the derivation of K_D in the previous section, the individual host-guest complexation constants, K_{11} and K_{21}, for the 1:1 and 2:1 host-guest complexes of H_3TCPP^{3-} and H_2TCPP^{4-} cannot be separately determined under the experimental conditions employed in this study. However, the overall host-guest complexation constants K_{11} and K_{21} of the mixture of multiply ionised porphyrins can be determined. The study of the host-guest equilibria by UV-vis spectroscopy and the protocol for fitting the algorithms describing the equilibria to the changes in absorbance followed methods similar to those employed in Chapter 2.[33] The model used to determine the host-guest complexation constants assumes that labile equilibria exist such that the concentrations of monomeric H_3TCPP^{3-}/H_2TCPP^{4-}, dimeric $(H_3TCPP^{3-}/H_2TCPP^{4-})_2$ and monomeric H_3TCPP^{3-}/H_2TCPP^{4-} complexed by either γ-CD or its linked oligomers 33γ-CD_2ox, 33γ-CD_2suc, 66γ-CD_2ox, 66γ-CD_2suc and 666γ-CD_3bz in the formation of 1:1, and

possibly 2:1, host-guest complexes very rapidly adjust as the UV-vis titrations proceed. Thus, the 1:1 and 2:1 host-guest γ-CD complexes with monomeric $H_3TCPP^{3-}/H_2TCPP^{4-}$ form according to Equations 3.8 and 3.9:

$$\gamma\text{-CD} + H_3TCPP^{3-}/H_2TCPP^{4-} \overset{K_{11}}{\rightleftharpoons} \gamma\text{-CD}.H_3TCPP^{3-}/H_2TCPP^{4-} \quad (\mathbf{3.8})$$

$$\gamma\text{-CD} + \gamma\text{-CD}.H_3TCPP^{3-}/H_2TCPP^{4-} \overset{K_{21}}{\rightleftharpoons} (\gamma\text{-CD})_2.H_3TCPP^{3-}/H_2TCPP^{4-} \quad (\mathbf{3.9})$$

The complexation constants K_{11} and K_{21}, at equilibrium are given by:

$$K_{11} = [\gamma\text{-CD}.H_3TCPP^{3-}/H_2TCPP^{4-}]/[\gamma\text{-CD}][H_3TCPP^{3-}/H_2TCPP^{4-}] \quad (\mathbf{3.10})$$

$$K_{21} = [(\gamma\text{-CD})_2.H_3TCPP^{3-}/H_2TCPP^{4-}]/([\gamma\text{-CD}.H_3TCPP^{3-}/H_2TCPP^{4-}][\gamma\text{-CD}]) \quad (\mathbf{3.11})$$

Given that $[H_3TCPP^{3-}/H_2TCPP^{4-}]_{total}$ and $[\gamma\text{-CD}]_{total}$ are the initial concentrations of the two complexation partners:

$$[H_3TCPP^{3-}/H_2TCPP^{4-}]_{total} = [H_3TCPP^{3-}/H_2TCPP^{4-}] + [(H_3TCPP^{3-}/H_2TCPP^{4-})_2] + [\gamma\text{-CD}.H_3TCPP^{3-}/H_2TCPP^{4-}] + [(\gamma\text{-CD})_2.H_3TCPP^{3-}/H_2TCPP^{4-}] \quad (\mathbf{3.12})$$

It follows that:

$$[\gamma\text{-CD}]_{total} = [\gamma\text{-CD}] + [\gamma\text{-CD}.H_3TCPP^{3-}/H_2TCPP^{4-}] + [(\gamma\text{-CD})_2.H_3TCPP^{3-}/H_2TCPP^{4-}] \quad (\mathbf{3.13})$$

The absorbance at a particular wavelength is given by Equation 3.14 when only a 1:1 complex forms, and by Equation 3.15 when both 1:1 and 2:1 complexes form.

$$A(\lambda) = \varepsilon_{H_3TCPP^{3-}/H_2TCPP^{4-}}[H_3TCPP^{3-}/H_2TCPP^{4-}] + \varepsilon_{(H_3TCPP^{3-}/H_2TCPP^{4-})_2}[(H_3TCPP^{3-}/H_2TCPP^{4-})_2] + \varepsilon_{(\gamma\text{-CD}.H_3TCPP^{3-}/H_2TCPP^{4-})}[\gamma\text{-CD}.H_3TCPP^{3-}/H_2TCPP^{4-}] \quad (\mathbf{3.14})$$

$$A(\lambda) = \varepsilon_{H_3TCPP^{3-}/H_2TCPP^{4-}}[H_3TCPP^{3-}/H_2TCPP^{4-}] + \varepsilon_{(H_3TCPP^{3-}/H_2TCPP^{4-})_2}[(H_3TCPP^{3-}/H_2TCPP^{4-})_2] + [\gamma\text{-CD}.H_3TCPP^{3-}/H_2TCPP^{4-}] + \varepsilon_{(\gamma\text{-CD}.\,H_3TCPP^{3-}/H_2TCPP^{4-})}[\gamma\text{-CD}.H_3TCPP^{3-}/H_2TCPP^{4-}] + \varepsilon_{((\gamma\text{-CD})_2.\,H_3TCPP^{3-}/H_2TCPP^{4-})}[(\gamma\text{-CD})_2.H_3TCPP^{3-}/H_2TCPP^{4-}] \quad (\mathbf{3.15})$$

In Equations 3.14 and 3.15 $A(\lambda)$, $\varepsilon_{H_3TCPP^{3-}/H_2TCPP^{4-}}$, $\varepsilon_{(H_3TCPP^{3-}/H_2TCPP^{4-})_2}$, $\varepsilon_{(\gamma\text{-CD}.H_3TCPP^{3-}/H_2TCPP^{4-})}$ and $\varepsilon_{((\gamma\text{-CD})_2.H_3TCPP^{3-}/H_2TCPP^{4-})}$ represent the observed absorbance and apparent molar absorbances of $H_3TCPP^{3-}/H_2TCPP^{4-}$, $(H_3TCPP^{3-}/H_2TCPP^{4-})_2$, $\gamma\text{-CD}.H_3TCPP^{3-}/H_2TCPP^{4-}$ and (γ-

CD)$_2$.H_3TCPP^{3-}/H_2TCPP^{4-} respectively. The values of K_{11} and K_{21} are determined by best-fitting the algorithm for either Equation 3.14 or 3.15 to the H_3TCPP^{3-}/H_2TCPP^{4-} absorbance data in the range 400-430 nm at 0.25 nm intervals as the γ-CD concentration is increased using the HypSpec protocol.[34] The same protocol is used for the other five systems.

3.5.5. UV-vis Titration studies

The experimental details of the UV-vis spectroscopic characterisation of the equilibria in which γ-CD and its oligomers complex H_3TCPP^{3-}/H_2TCPP^{4-} are now described. The UV-vis spectra of solutions were determined against reference solutions in matched 1 cm quartz cells and were recorded at 0.25 nm intervals using a Cary 5000 UV-vis spectrophotometer over the wavelength range 250-650 nm. The solutions were freshly prepared in aqueous phosphate buffer at pH 7.0 and I = 0.10 mol dm^{-3}. Samples were 2.0 cm^3 in volume and were thermostatted at 298.2 K for 30 minutes before starting the titration. The H_3TCPP^{3-}/H_2TCPP^{4-} solution concentrations were 2.00×10^{-6} mol dm^{-3} and were titrated with sequential injections (10 mm^3 each into both sample and reference cells unless stated otherwise) of either γ-CD (2.33×10^{-3} mol dm^{-3}), 33γ-CD$_2$ox (6.31×10^{-4} mol dm^{-3}), 33γ-CD$_2$suc (5.68×10^{-4} mol dm^{-3}), 66γ-CD$_2$ox (7.90×10^{-5} mol dm^{-3}), 66γ-CD$_2$suc (6.79×10^{-5} mol dm^{-3}) and 666γ-CD$_3$bz (8.46×10^{-5} mol dm^{-3}) also in aqueous phosphate buffer at pH 7.0 and I = 0.10 mol dm^{-3}.

The molar absorbance changes of H_3TCPP^{3-}/H_2TCPP^{4-} solutions with increasing concentrations of 33γ-CD$_2$ox, 66γ-CD$_2$ox and 666γ-CD$_3$bz and the best fits of algorithms describing the complexation processes at 298.2 K are shown in Figure 3.12. All of the UV-vis titration plots, derived spectra and speciation plots for the γ-CD and γ-CD oligomer host-guest systems are shown in Figures A7 – A15 of the Appendix.

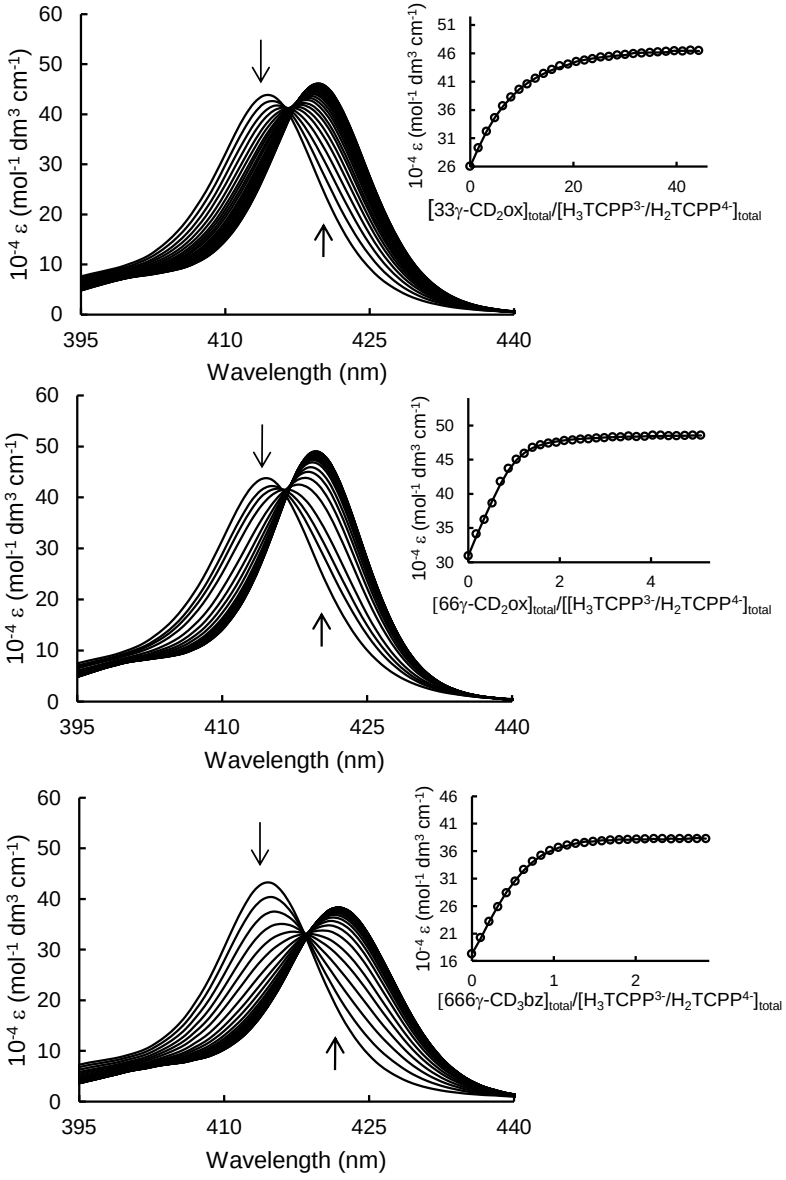

Figure 3.12: Molar absorbance change of $H_3TCPP^{3-}/H_2TCPP^{4-}$ (2.00×10^{-6} mol dm^{-3}) in phosphate buffer, pH 7.0, I = 0.10 mol dm^{-3} at 298.2 K with sequential injections (10 mm^3 each for 33γ-CD_2ox and 66γ-CD_2ox, 5 mm^3 each for 666γ-CD_3bz) of 33γ-CD_2ox (top, 6.31×10^{-4} mol dm^{-3}), 66γ-CD_2ox (middle, 7.90×10^{-5} mol dm^{-3}) 666γ-CD_3bz (bottom, 8.46×10^{-5} mol dm^{-3}) into both sample and reference cells. The arrows indicate the direction of molar absorbance change as the molar ratio of $[host]_{total}/[H_3TCPP^{3-}/H_2TCPP^{4-}]_{total}$ increases. Inset: Molar absorbance variation at 419 nm (for 33γ-CD_2ox and 66γ-CD_2ox) or 422 nm (for 666γ-CD_3bz) and the line of best fit of an algorithm for the monomer/dimer equilibrium and 1:1 and 2:1 host-guest complexation for the 33γ-CD_2ox.$H_3TCPP^{3-}/H_2TCPP^{4-}$ system and for the monomer/dimer equilibrium and 1:1 host-guest complexation for the 66γ-CD_2ox.$H_3TCPP^{3-}/H_2TCPP^{4-}$ and 666γ-CD_3bz.$H_3TCPP^{3-}/H_2TCPP^{4-}$ systems to the absorbance change over the wavelength range 400-430 nm.

A decrease in absorption at the λ_{max} of 414 nm of $H_3TCPP^{3-}/H_2TCPP^{4-}$ is observed for all six systems with the progressive increase of host-guest complex concentration with increase of the total host concentration. Simultaneously, the red-shifted spectra of the $H_3TCPP^{3-}/H_2TCPP^{4-}$ complexes of γ-CD, the four γ-CD dimers and the 666γ-CD_3bz trimer increased in intensity and their λ_{max} changed from 414 nm characterising a mixture of $H_3TCPP^{3-}/H_2TCPP^{4-}$ and $(H_3TCPP^{3-}/H_2TCPP^{4-})_2$ to 416 nm, 419 nm and 422 nm upon complexation in γ-CD, its four dimers and its trimer, respectively. These red shifts are consistent with $H_3TCPP^{3-}/H_2TCPP^{4-}$ experiencing a change in polarity of the local environment as it disaggregates and enters the hydrophobic γ-CD annulus upon formation of the host-guest complex.[36] The increase in the magnitude of this red-shift in the 33γ-CD_2ox.$H_3TCPP^{3-}/H_2TCPP^{4-}$, 33γ-$CD_2$suc.$H_3TCPP^{3-}/H_2TCPP^{4-}$, 66γ-$CD_2$ox.$H_3TCPP^{3-}/H_2TCPP^{4-}$ and 66γ-CD_2suc.$H_3TCPP^{3-}/H_2TCPP^{4-}$ systems by comparison with that of the γ-CD.$H_3TCPP^{3-}/H_2TCPP^{4-}$ system is consistent with a cooperative complexation effect where two γ-CD annuli complex $H_3TCPP^{3-}/H_2TCPP^{4-}$ simultaneously. This trend is also exemplified by a further increase in the red shift for the 666γ-CD_3bz.$H_3TCPP^{3-}/H_2TCPP^{4-}$ system, which is consistent with cooperative complexation of $H_3TCPP^{3-}/H_2TCPP^{4-}$ in three γ-CD annuli.

As previously discussed for H_2TSPP^{4-} in Section 2.4 of Chapter 2, UV-vis spectroscopic titrations may be used to determine the strength and cooperative nature of host-guest complexation and the number of species in the equilibria but cannot distinguish between the *syn* and *anti* modes of complexation of $H_3TCPP^{3-}/H_2TCPP^{4-}$ in the 1:1 host-guest complexes formed by the four γ-CD dimers (or through complexation by two γ-CD). If both complexing modes operate they are likely to be in a labile equilibrium as has been reported for the complexation of porphyrins by β-CD dimers.[37]

For the γ-CD, 33γ-CD_2ox and 33γ-CD_2suc systems, an algorithm for the monomer/dimer equilibrium and the formation of a 1:1 complex corresponding to Equation 3.8 can be fitted to

the UV-vis absorbance data (Figures A13 – A15 of the Appendix). However, these fits were moderate in quality. Furthermore, the isosbestic points for the γ-CD, 33γ-CD_2ox and 33γ-CD_2suc systems are slightly broadened by comparison with those of 66γ-CD_2ox, 66γ-CD_2suc, 666γ-CD_3bz (all of the isosbestic points are expected to be slightly broadened due to the presence of the monomer/dimer equilibrium, however, this should be consistent across all of the host systems). In the analogous systems for H_2TSPP^{4-} in Chapter 2, a similar broadening in isosbestic points was also observed in the γ-CD, 33γ-CD_2ox and 33γ-CD_2suc systems that increased with a decrease in temperature. This was also accompanied by poor fitting to the 1:1 host-guest algorithm and an unexpected temperature dependence in the derived molar absorbance of H_2TSPP^{4-}.γ-CD, H_2TSPP^{4-}.33γ-CD_2ox and H_2TSPP^{4-}.33γ-CD_2suc in which H_2TSPP^{4-} is expected to exist in monomeric form. The changes in molar absorbance were attributed to the presence of both 1:1 and 2:1 host-guest complexes in solution, of which an algorithm corresponding to the formation of these complexes was fitted to the absorbance data. Consequently, an algorithm corresponding to the monomer/dimer equilibrium and the formation of both 1:1 and 2:1 complexes according to Equations 3.14 and 3.15 was fitted to the absorbance data for the H_3TCPP^{3-}/H_2TCPP^{4-} host-guest systems described above (Figures A7 – A9). A better fit was obtained in each case and, while it is usually the case that the addition of an extra term to the algorithm yields a better fit, it was concluded that this was a more reliable representation of the complexation equilibria. The derived K_{11} and K_{21} appear in Table 3.1.

Table 3.1: Experimental complexation constants K_{11} and K_{21} for the complexation of $H_3TCPP^{3-}/H_2TCPP^{4-}$ by γ-CD, 33γ-CD_2ox and 33γ-CD_2suc determined from UV-vis titrations at 298.2 K in aqueous phosphate buffer at pH 7.0 and I = 0.10 mol dm^{-3}.

Host	K_{11} (10^{-3} × dm^3 mol^{-1})	K_{21} (10^{-3} × dm^3 mol^{-1})
γ-CD	4.76 ± 0.05	2.29 ± 0.11
33γ-CD_2ox	40.38 ± 0.40	18.70 ± 0.94
33γ-CD_2suc	81.04 ± 0.81	51.29 ± 2.46
66γ-CD_2ox	4751 ± 48	-
66γ-CD_2suc	6184 ± 62	-
666γ-CD_3bz	6557 ± 66	-

[a]The errors quoted for K_{11} and K_{21} are those derived from the best fits of either Equation 3.14 or 3.15 to the absorbance data. Experimental error is estimated at < ± 5 %.

It is apparent from Table 3.1 that the K_{11} characterising the γ-CD oligomer systems increase in the order γ-CD < 33γ-CD_2ox < 33γ-CD_2suc < 66γ-CD_2ox < 66γ-CD_2suc < 666γ-CD_3bz at 298.2 K and are between ~8 - 1400-fold larger than that of the native γ-CD system at 298.2 K. A similar order was observed for γ-CD oligomer complexes with H_2TSPP^{4-} in Section 2.4 of Chapter 2. This is consistent with a strong cooperative effect existing for complexation in the oligomer systems.

As with H_2TSPP^{4-} and the same oligomers in Table 2.1 of Chapter 2, the narrow primary-hydroxyl face is favoured for entrance of $H_3TCPP^{3-}/H_2TCPP^{4-}$ into the γ-CD annulus during host-guest complexation, as indicated by the larger K_{11} complexation constants for the 6,6- dimers and the 6,6,6- trimer by comparison with those for the 3,3- dimers. This is consistent with the $H_3TCPP^{3-}/H_2TCPP^{4-}$ phenyl rings being dominant factors in forming host-guest complexes as previously discussed for the 2D ^{1}H NOESY NMR data in Section 3.4. The phenyl rings have widths of ~470 pm which compare with primary- and secondary hydroxyl γ-CD face widths of 750 and 830 pm (and depth of 790 pm), respectively,[32] and as

consequence the smaller primary hydroxyl face more closely fits the phenyl rings to form more stable host-guest complexes.

For the 33γ-CD_2suc and 66γ-CD_2suc dimers, the longer succinamide linker coincides with larger K_{11} than is observed for the shorter oxalate-linked 33γ-CD_2ox and 66γ-CD_2ox dimers, respectively. As with H_2TSPP^{4-} with the same dimers in Chapter 2, this is consistent with the greater length and flexibility of the succinamide linker allowing easier formation of host-guest complexes than is the case for less flexible oxalate linker. The length and flexibility of the benzene linker of the 666γ-CD_3bz trimer may also aid host-guest complexation; however, it is difficult to quantify its contribution as tritopic complexation by three γ-CD annuli is also likely to contribute to the observed higher K_{11} complexation constant.

The K_{11} complexation constants for H_3TCPP^{3-}/H_2TCPP^{4-} with the γ-CD and the γ-CD oligomers are significantly larger than the analogous values for H_2TSPP^{4-} (Table 2.1 of Chapter 2) at 298.2 K, and there are two possible factors which impinge upon this. The extent of protonation of the porphyrin imine nitrogen groups may cause some variation in electrostatic interactions between the porphyrin and either γ-CD or its oligomers. If this effect is significant it may be that the lesser charge of H_3TCPP^{3-} may enhance complexation. However, the negatively charged *p*-carboxyphenyl and *p*-sulfonatophenyl groups of H_3TCPP^{3-}/H_2TCPP^{4-} and H_2TSPP^{4-} are at the periphery of the porphyrin core and are expected to exert the major influence on complexation. Thus, a major influence on complexation may be the stereochemical, charge distribution and consequent hydration differences between the smaller trigonal planar carboxylate group and the tetrahedral sulfonate group. It is notable that the increase in K_{11} for H_3TCPP^{3-}/H_2TCPP^{4-} by comparison with K_{11} for H_2TSPP^{4-} is greater for the 66γ-CD_2ox/66γ-CD_2suc/666γ-CD_3bz systems than for the 33γ-CD_2ox/33γ-CD_2suc systems. This suggests the shape of the anionic groups has a larger influence on the

complexation constants when complexation occurs through the narrow 6-hydroxyl face than when it occurs through the wider 3-hydroxyl face of the γ-CD annulus. This observation is further supported by greater changes in the 2D ^{1}H NOESY NMR spectra between H_2TSPP^{4-} and H_3TCPP^{3-}/H_2TCPP^{4-} in the 66γ-CD_2ox/66γ-CD_2suc/666γ-CD_3bz systems than in the 33γ-CD_2ox/33γ-CD_2suc systems as discussed in Section 3.4.

Gas phase models (Section 3.6) similar to those seen in Figure 2.16 of Chapter 2 can be constructed for the tetraanionic porphyrin, H_2TCPP^{4-} (the di- and triprotonated species are expected to complex with a similar orientation) with 33γ-CD_2ox (Figure 3.13) to give an initial idea of the conformational variations possible for the 2:1 host-guest complexes present in solution. In Figure 3.13a steric hindrance is minimised through monotopic *anti* complexation of H_2TCPP^{4-} (for which the gas phase heat of formation is -30937.86 kJ mol^{-1}). However, the equilibrium data in Table 3.1 show that K_{21} for (33γ-CD_2ox)$_2$.H_2TCPP^{4-} and (33γ-CD_2suc)$_2$.H_2TCPP^{4-} are 8-9- and 17-22-fold greater than K_{11} and K_{21} for the γ-CD.H_2TCPP^{4-} and (γ-CD)$_2$.H_2TCPP^{4-} complexes, respectively. This is consistent with cooperative ditopic complexation in both (33γ-CD_2ox)$_2$.H_2TCPP^{4-} and (33γ-CD_2suc)$_2$.H_2TCPP^{4-} in *syn* conformations similar to that shown in Figure 3.13b (*syn* (33γ-CD_2ox)$_2$.H_2TCPP^{4-} for which the gas phase heat of formation is -31377.68 kJ mol^{-1} as compared with -30937.86 kJ mol^{-1} for the *anti* (33γ-CD_2ox)$_2$.H_2TCPP^{4-}). Thus, both the solution phase experimental data and the gas phase data favour ditopic *syn* complexation in (33γ-CD_2ox)$_2$.H_2TCPP^{4-} and (33γ-CD_2suc)$_2$.H_2TCPP^{4-}.

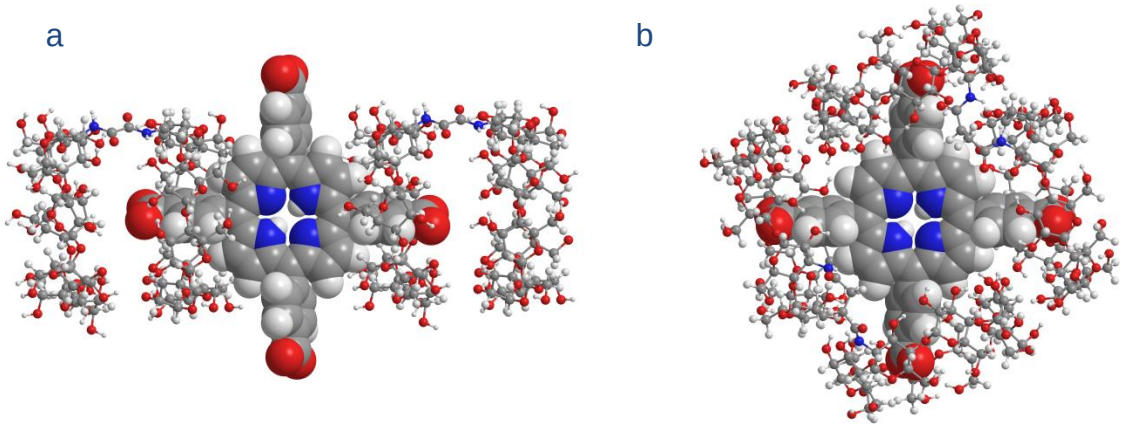

anti (33γ-CD_2ox)$_2$.H_2TCPP^{4-}
(non-cooperative)

syn (33γ-CD_2ox)$_2$.H_2TCPP^{4-}
(cooperative)

Figure 3.13: (a) Gas phase energy minimised molecular models for 2:1 non-cooperative *anti* (33γ-CD_2ox)$_2$.H_2TCPP^{4-} (heat of formation E = -30937.86 kJ mol^{-1}) and (b) cooperative *syn* (33γ-CD_2ox)$_2$.H_2TCPP^{4-} (E = -31377.68 kJ mol^{-1}) host-guest complexes show the latter to be more stable. (The steric crowding in cooperative *anti* (33γ-CD_2ox)$_2$.H_2TCPP^{4-} is too great for it to form.) Note: 33γ-CD_2ox is shown in ball and stick format, and H_2TCPP^{4-} in space filling format. Carbon = grey, hydrogen = white, oxygen = red and nitrogen = blue.

The up to 22-fold greater K_{21} at 298.2 K for the step-wise complexation of a second ditopic 33γ-CD_2ox and 33γ-CD_2suc with H_3TCPP^{3-}/H_2TCPP^{4-} by comparison with K_{21} for the complexation with a second γ-CD also indicates that a cooperative effect applies for the ditopic 33γ-CD_2ox and 33γ-CD_2suc dimers. As with H_2TSPP^{4-} in Section 2.4 of Chapter 2, this infers that in the (33γ-CD_2ox)$_2$.H_3TCPP^{3-}/H_2TCPP^{4-} and (33γ-CD_2suc)$_2$.H_3TCPP^{3-}/H_2TCPP^{4-} each of the four *p*-carboxyphenyl groups of H_3TCPP^{3-}/H_2TCPP^{4-} are complexed by either two 33γ-CD_2ox or two 33γ-CD_2suc probably in a *syn* conformation (further molecular modelling is in Section 3.6).

These considerations raise the question as to why the (66γ-CD_2ox)$_2$.H_3TCPP^{3-}/H_2TCPP^{4-} and (66γ-CD_2suc)$_2$.H_3TCPP^{3-}/H_2TCPP^{4-} complexes are not present to a detectable extent. An obvious difference is that the γ-CD annuli of 66γ-CD_2ox.H_3TCPP^{3-}/H_2TCPP^{4-} and 66γ-CD_2suc.H_3TCPP^{3-}/H_2TCPP^{4-} complex the H_3TCPP^{3-}/H_2TCPP^{4-} *p*-carboxyphenyl groups through the narrower primary hydroxyl faces of the γ-CD annuli which engenders a tighter complexation than does complexing through the wider secondary hydroxyl faces. This is

consistent with the substantially greater K_{11} characterising 66γ-CD_2ox.H_3TCPP^{3-}/H_2TCPP^{4-} and 66γ-CD_2suc.H_3TCPP^{3-}/H_2TCPP^{4-} by comparison with K_{11} for 33γ-CD_2ox.H_3TCPP^{3-}/H_2TCPP^{4-} and 33γ-CD_2suc.H_3TCPP^{3-}/H_2TCPP^{4-}, respectively. It appears from this that although 66γ-CD_2ox.H_3TCPP^{3-}/H_2TCPP^{4-} and 66γ-CD_2suc.H_3TCPP^{3-}/H_2TCPP^{4-} are the more stable complexes, their "tighter" stereochemistries allow less flexibility for the complexing of a second 66γ-CD_2ox or 66γ-CD_2suc (this was also observed for the same dimer systems and H_2TSPP^{4-} in Chapter 2).

The K_{21} for the γ-CD.H_3TCPP^{3-}/H_2TCPP^{4-}, 33γ-CD_2ox.H_3TCPP^{3-}/H_2TCPP^{4-} and 33γ-CD_2suc.H_3TCPP^{3-}/H_2TCPP^{4-} complexes are significantly larger than those observed for the analogous H_2TSPP^{4-} complexes at 298.2 K (Table 2.2 of Chapter 2). This also suggests that the planar shape of the *p*-carboxyphenyl groups of H_3TCPP^{3-}/H_2TCPP^{4-} enhances the formation of 2:1 host-guest complexes by comparison with the tetrahedral *p*-sulfonatophenyl groups of H_2TSPP^{4-}, consistent with what was observed for the 1:1 host-guest complexes as is discussed earlier.

A few earlier studies have characterised the complexation of H_3TCPP^{3-}/H_2TCPP^{4-} by cyclodextrin hosts. There is quite a large variation between the K_{11} complexation constants of H_3TCPP^{3-}/H_2TCPP^{4-} with γ-CD reported in the literature. An early study reported the K_{11} complexation constant of γ-CD.H_3TCPP^{3-}/H_2TCPP^{4-} to be 5.2×10^4 dm^3 mol^{-1} in pH 7.0. 0.1 mol dm^{-3} potassium phosphate solution.[38] Later studies reported significantly lower K_{11} values; 3.3×10^4 dm^3 mol^{-1} in pH 7.0 phosphate buffer at 295.2 K[21] and 1.0×10^4 dm^3 mol^{-1} (UV-vis)[39] or 5.6×10^3 dm^3 (fluorescence)[39] in pH 10.1 bicarbonate buffer at 298.2 K. The K_{11} (4.76×10^3 dm^3 mol^{-1} in pH 7.0 phosphate buffer at 298.2 K) for the complexation of γ-CD with H_3TCPP^{3-}/H_2TCPP^{4-} in this study is consistent with the more recent value 3.3×10^4 dm^3 mol^{-1} in pH 7.0 phosphate buffer at 295.2 K from the literature.[21] These differences in the derived K_{11} are not uncommon. As previously mentioned, the extent of H_3TCPP^{3-}

/H_2TCPP^{4-} dimerisation can be influenced by the porphyrin concentration, the pH, ionic strength, the presence of electrolytes and the temperature of the solution. Changes in pH could also lead to a change in the proportions of the multiply ionised porphyrins which could also affect the derived K_{11} complexation constants. The previous reports did not account for H_3TCPP^{3-}/H_2TCPP^{4-} dimerisation or for 2:1 host-guest complexes in their derivations of K_{11}. The presence of porphyrin dimers and 2:1 host-guest complexes affects the speciation of porphyrin monomers and 1:1 host-guest complexes in solution, and thus, can affect the derivation of K_{11}. The literature reports also used double reciprocal plots for the derivation of their K_{11} values, which are often unreliable for the determination complexation constants when more than one equilibrium is present in solution.[40] Therefore, the K_{11} derived from fitting the monomer/dimer equilibrium and the 1:1 and 2:1 host-guest complexation equilibria to UV-vis data in this study produce more reliable K_{11} values than those derived from exclusively fitting 1:1 host-guest complexation. This has been previously observed for fitting 1:1 and 2:1 or exclusively 1:1 host-guest complexation to UV-vis data of H_2TSPP^{4-} with β-CD.[41]

There are some reports of complexation of H_3TCPP^{3-}/H_2TCPP^{4-} by linked cyclodextrin oligomers.[37,42] One study reported the complexation of H_3TCPP^{3-}/H_2TCPP^{4-} by a 3,3-succinamide-linked β-CD dimer characterised by $K_{11} = 1.9 \times 10^6$ dm^3 mol^{-1} in pH 7.0 phosphate buffer at 298.2 K.[37] This is of a similar magnitude to 66γ-CD_2ox and 66γ-CD_2suc in this study, which are characterised by $K_{11} = 4.8 \times 10^6$ dm^3 mol^{-1} and $K_{11} = 6.2 \times 10^6$ dm^3 mol^{-1} respectively, under the same conditions. This could be expected, as the annular widths of their binding sites, the wider face of β-CD (650 pm)[32] and the narrow face of γ-CD (750 pm),[32] may both be of an appropriate size to accommodate the *p*-carboxyphenyl groups of H_3TCPP^{3-}/H_2TCPP^{4-}. It may also be noted that 2:1 host-guest complexes were not observed between the 3,3-succinamide-linked β-CD dimer and H_3TCPP^{3-}/H_2TCPP^{4-}.[37] This suggests

that the extra space associated with complexation of H_3TCPP^{3-}/H_2TCPP^{4-} via the wider secondary face of the γ-CD annulus (830 pm)[32] of the 3,3-linked γ-CD dimers is pivotal in the formation of 2:1 host-guest complexes. One study showed the complexation of H_3TCPP^{3-}/H_2TCPP^{4-} by a benzene-linked β-CD tetramer (the β-CD entities were linked through a C3 carbon of a D-glucopyranose unit on the wider secondary face) was characterised by a K_{11} complexation constant of 2.9×10^8 dm^3 mol^{-1} in pH 7.0 aqueous phosphate buffer at 298.2 K,[42] which was significantly larger than that of the benzene-linked γ-CD trimer in this study (6.6×10^6 dm^3 mol^{-1}) under the same conditions. The 44-fold increase in K_{11} could be a consequence of the extra cyclodextrin annulus in the tetramer than the trimer. However, the width of the cyclodextrin annuli and the length and flexibility of the oligomer tether are also expected to influence K_{11}. To the best of our knowledge there are no examples in the literature of the complexation of H_3TCPP^{3-}/H_2TCPP^{4-} by γ-CD dimers or trimers with which comparison may be made.

3.5.6. Thermodynamic Parameters

In Section 2.4 of Chapter 2 the Gibbs free energy, Δ*G*, enthalpy, Δ*H*, and entropy, Δ*S*, for host-guest complexation of H_2TSPP^{4-} by γ-CD and its linked oligomers are determined by variable temperature UV-vis titration studies. As the temperature of the solution changes, the pK_a values of the porphyrin are also expected to change (the pK_a values of common organic bases have been reported to increase between 0.05-0.3 pH units per 10 K increase in temperature).[43,44] Accordingly, the change in pK_a with temperature may lead to a change in the proportions of ionic porphyrin species in solution. As discussed earlier, the different porphyrin ionic species may have different K_{11} and K_{21} complexation constants with γ-CD and its oligomers in solution, which can complicate the determination of the thermodynamic parameters through variable temperature UV-vis titrations. The low pK_a values for the

protonation of H_2TSPP^{4-} (pK_{a1} = 4.85 and pK_{a2} = 4.91 at 298.2 K)[45] ensure that H_2TSPP^{4-} is almost exclusively in the tetraanionic form at pH 7.0 over the temperature range studied. Conversely, the highest pK_a values of H_2TCPP^{4-} are pK_{a1} = 6.0 and pK_{a2} = 6.6 at 298.2 K,[30] suggesting that a mixture of ionic states (primarily H_2TCPP^{4-}, with some H_3TCPP^{3-} and a small amount of H_4TCPP^{2-}) are present in aqueous solutions at pH 7.0. Assuming the largest temperature dependence discussed above (0.3 pH units per 10 K increase in temperature), the p*K*a values of H_2TCPP^{4-} could vary (pK_{a1} = 5.7-6.6 and pK_{a2} = 6.3-7.2) between the temperature extremes of the UV-vis titration studies of Chapter 2. This would significantly change the proportion of ionic porphyrin species to favour the formation of the mono- and diprotonated porphyrins H_3TCPP^{3-} and H_4TCPP^{2-} at lower temperatures. Thus, determination of the thermodynamic parameters for the host-guest complexation of H_3TCPP^{3-}/H_2TCPP^{4-} with γ-CD and its oligomers using UV-vis spectroscopy over a temperature range requires a determination of the individual K_{11} and K_{21} for the complexation of H_3TCPP^{3-} and H_2TCPP^{4-}, and the temperature dependences of the associated pK_a and K_D values in the phosphate buffer employed in this study. This is in principle achievable, but could lead to substantial error accumulation in the extraction of K_{11} and K_{21} and hence has not been attempted. An alternative approach would be to determine K_{11} and K_{21} at pH 9 in a different buffer, but this may incorporate a change in the effect of the supporting electrolyte on these parameters and also porphyrin decomposition at higher pH.

3.6. MOLECULAR MODELLING STUDIES

As with H_2TSPP^{4-} in in Section 2.5 of Chapter 2, molecular modelling studies are undertaken to gain greater insight into the possible different stereochemical modes of complexation in the host-guest systems of H_2TCPP^{4-}, with γ-CD and its linked γ-CD oligomers which neither

the 2D ^{1}H NOESY NMR or UV-vis studies reveal. (Molecular modelling of the analogous H_3TCPP^{3-} systems could also be undertaken but the difference in charge would complicate comparison with the H_2TSPP^{4-} systems and therefore is not undertaken.) Molecular models of the possible 1:1 and 2:1 host-guest complexes are constructed and their geometries optimised through the PM7 semi-empirical method using MOPAC2012.[46] For each 1:1 complex, a cooperative *syn* and cooperative *anti* complex as well as a non-cooperative complex are constructed. Cooperative and non-cooperative 2:1 host-guest complexes are also constructed. In this way the relative stabilities of the different complexation modes may be assessed in the gas phase.

These models are exemplified by non-cooperative *anti* $(33\gamma\text{-}CD_2ox)_2.H_2TCPP^{4-}$ and cooperative *syn* $(33\gamma\text{-}CD_2ox)_2.H_2TCPP^{4-}$ shown in Figure 3.13, and by the three possible $33\gamma\text{-}CD_2suc.H_2TCPP^{4-}$ host-guest complexes and the two possible $(33\gamma\text{-}CD_2suc)_2.H_2TCPP^{4-}$ host-guest complexes shown in Figure 3.14. (The other twenty four host-guest complexes modelled appear in Figures A16 – A20 in the Appendix). The gas phase heats of formation, *E*, for each complex are collected in Table 3.2.

Although the role of water is likely to be significant in determining the stereochemistries, stoichiometries and thermodynamics of the host-guest complexes formed through γ-CD and its oligomers complexing H_2TCPP^{4-}, the relative energies of these complexes in the gas phase provide insight into the observed aqueous phase stereochemistries and stoichiometries.

Table 3.2: Heats of formation, *E*, for the complexation of H_2TCPP^{4-} by γ-CD, 33γ-CD_2ox, 33γ-CD_2suc, 66γ-CD_2ox, 66γ-CD_2suc and 666γ-CD_3bz calculated through MOPAC2012.[46]

Host-Guest Complex	Heat of formation (*E*) kJ mol^{-1}
γ-CD.H_2TCPP^{4-} (wide face)	-8016.54
γ-CD.H_2TCPP^{4-} (narrow face)	-8019.33
anti (γ-CD)$_2$.H_2TCPP^{4-} (two narrow faces)	-15757.64
syn (γ-CD)$_2$.H_2TCPP^{4-} (two narrow faces)	-15635.65
anti (γ-CD)$_2$.H_2TCPP^{4-} (two wide faces)	-15739.59
syn (γ-CD)$_2$.H_2TCPP^{4-} (two wide faces)	-15653.22
anti (γ-CD)$_2$.H_2TCPP^{4-} (1 narrow and 1 wide face)	-15724.33
syn (γ-CD)$_2$.H_2TCPP^{4-} (1 narrow and 1 wide face)	-15702.97
33γ-CD_2ox.H_2TCPP^{4-} (non-coop) (one narrow face)	-15435.51
anti 33γ-CD_2ox.H_2TCPP^{4-} (coop) (two wide faces)	-15610.56
syn 33γ-CD_2ox.H_2TCPP^{4-}(coop) (two wide faces)	-15605.47
33γ-CD_2suc.H_2TCPP^{4-} (non-coop) (one narrow face)	-15497.66
anti 33γ-CD_2suc.H_2TCPP^{4-} (coop) (two wide faces)	-15769.62
syn 33γ-CD_2suc.H_2TCPP^{4-} (coop) (two wide faces)	-15650.81
66γ-CD_2ox.H_2TCPP^{4-} (non-coop) (one wide face)	-15397.16
anti 66γ-CD_2ox.H_2TCPP^{4-}(coop) (two narrow faces)	-15903.02
syn 66γ-CD_2ox.H_2TCPP^{4-} (coop) (two narrow faces)	-15621.15
66γ-CD_2suc.H_2TCPP^{4-} (non-coop) (one wide face)	-15480.11
anti 66γ-CD_2suc.H_2TCPP^{4-} (coop) (two narrow faces)	-15944.40
syn 66γ-CD_2suc.H_2TCPP^{4-} (coop) (two narrow faces)	-15782.92
666γ-CD_3bz.H_2TCPP^{4-} (1 narrow face annulus complexed)	-23278.89
666γ-CD_3bz.H_2TCPP^{4-} (2 narrow face annuli complexed)	-23393.05
666γ-CD_3bz.H_2TCPP^{4-} (3 narrow face annuli complexed)	-23794.46
(33γ-CD_2ox)$_2$.H_2TCPP^{4-} (non-coop) (two narrow faces)	-30937.86
syn (33γ-CD_2ox)$_2$.H_2TCPP^{4-} (coop) (four wide faces)	-31377.68
(33γ-CD_2suc)$_2$.H_2TCPP^{4-} (non.coop) (two narrow faces)	-30849.07
syn (33γ-CD_2suc)$_2$.H_2TCPP^{4-} (coop) (four wide faces)	-31793.34
(66γ-CD_2ox)$_2$.H_2TCPP^{4-} (non-coop) (two wide faces)	-31094.97
(66γ-CD_2suc)$_2$.H_2TCPP^{4-} (non-coop) (two wide faces)	-31147.11

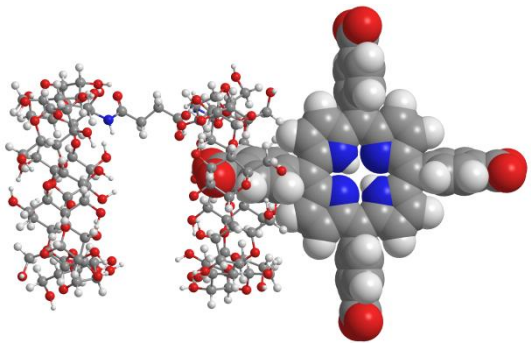

33γ-CD_2suc.H_2TCPP^{4-}
(non-cooperative) one narrow face

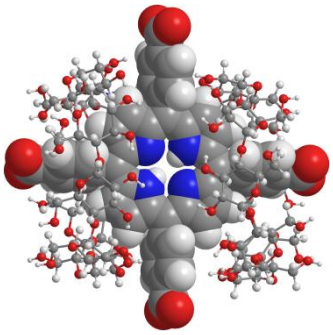

anti 33γ-CD_2suc.H_2TCPP^{4-}
(cooperative) two wide faces

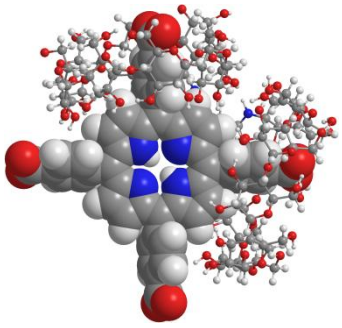

syn 33γ-CD_2suc.H_2TCPP^{4-}
(cooperative) two wide faces

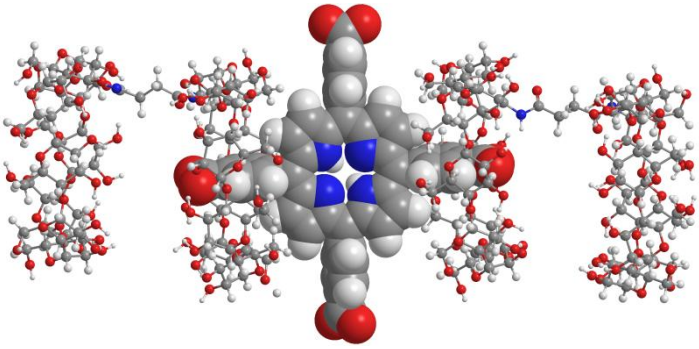

(33γ-CD_2suc)$_2$.H_2TCPP^{4-}
(non-cooperative) two narrow faces

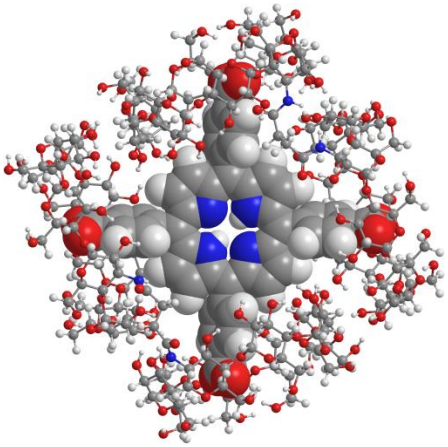

(33γ-CD_2suc)$_2$.H_2TCPP^{4-}
(cooperative) four wide faces

Figure 3.14: Energy minimised molecular models of the possible species involved in the 33γ-CD_2suc/H_2TCPP^{4-} equilibria derived using the PM7 method. For the potential 1:1 non-cooperative 33γ-CD_2suc.H_2TCPP^{4-} the heat of formation, E = -15497.66 kJ mol^{-1}, for *anti* 33γ-CD_2suc.H_2TCPP^{4-} E = -15769.62 kJ mol^{-1}, for *syn* 33γ-CD_2suc.H_2TCPP^{4-} E = -15650.81 kJ mol^{-1}, for 2:1 non-cooperative (33γ-CD_2suc)$_2$.H_2TCPP^{4-} E = -30849.07 kJ mol^{-1} and for cooperative *syn* (33γ-CD_2suc)$_2$.H_2TCPP^{4-} E = -31793.34 kJ mol^{-1}. Note: 33γ-CD_2suc = ball and stick, H_2TCPP^{4-} = space filling. Carbon = grey, hydrogen = white, oxygen = red and nitrogen = blue.

As for H_2TSPP^{4-} in Section 2.5 of Chapter 2, complexation of H_2TCPP^{4-} by a single γ-CD may occur by either the wide or narrow annular face. The *E* values for complexation by the narrow face are slightly lower than that of the wide face (2.79 kJ mol^{-1}, Table 3.2 and Figure A16 of the Appendix). This indicates that entry of the *p*-carboxyphenyl groups into the γ-CD annulus is probably the major contributing factor of H_2TCPP^{4-} to the energetics of host-guest complexation as partial complexation of the bulky pyrrolic core of H_2TCPP^{4-} would probably favour complexation through the wide face of γ-CD.

When H_2TCPP^{4-} is complexed by two γ-CD in a 2:1 host-guest complex, several different conformations may arise. The γ-CD annuli may complex through either the wide or narrow face in a *syn* or *anti* conformations in six possible 2:1 host-guest complexes: *anti* (two narrow faces), *syn* (two narrow faces), *syn* (two wide faces), *anti* (two wide faces), *anti* (one narrow and one wide face) and *syn* (one narrow and one wide face) as shown in Figure A16 of the Appendix. The *E* data for the complexes suggest that the *anti*-conformation is favoured over the *syn* conformation in all six systems, and is attributable to a lesser steric crowding in the *anti* complexes by comparison with that in the *syn* complexes. The *E* data also indicates that when 2:1 host-guest complexes are formed, the wide face is preferred over the narrow face for entrance into the γ-CD annulus in the *syn* conformation. This may be a consequence of the wide face allowing freedom of movement around H_2TCPP^{4-} such that steric hindrance is minimised in the *syn* 2:1 host-guest complexes.

These semi empirical calculations for the γ-CD dimer/H_2TCPP^{4-} systems give insight into the stability of the non-cooperative and cooperative *syn*- and *anti*-conformers of the host-guest complexes. In all cases the cooperative complexation modes showed larger *E*, and therefore a greater stability, than their non-cooperative counterparts. The *anti*-conformers are more stable than the *syn*-conformers in all of the systems.

For the 66γ-CD_2ox.H_2TCPP^{4-} complex (Figure A18 of the Appendix), the *anti* conformer is the most stable with an *E* 281.87 kJ mol^{-1} greater than that of the *syn* conformer. This may be attributed to the low flexibility of short oxalate linker hindering complexation on adjacent *p*-carboxyphenyl groups of H_2TCPP^{4-} in the *syn* conformation. This is in accord with the difference in *E* for the *anti* and *syn* 66γ-CD_2suc.H_2TCPP^{4-} decreasing to 161.48 kJ mol^{-1} (Figure A19 of the Appendix), which is attributable to the increased length and flexibility of the succinamide linker.

For 33γ-CD_2ox.H_2TCPP^{4-} (Figure A17 of the Appendix) and 33γ-CD_2suc.H_2TCPP^{4-} (Figure 3.14), the difference in *E* between the *syn* and *anti* conformers (5.09 and 118.37 kJ mol^{-1}, respectively) is less than in the analogous 6,6- dimer systems but the order of the differences in *E* is reversed. It appears that complexation through the wider γ-CD face may allow adjacent *p*-carboxyphenyl group complexation with less strain in 33γ-CD_2ox.H_2TCPP^{4-} and 33γ-CD_2suc.H_2TCPP^{4-}. However, the reversal in the *E* differences referred to above indicates that both the face through which H_2TCPP^{4-} enters the dimer γ-CD annuli and the linker contribute to the overall strain involved in the complexes and to *E*.

Models for the 666γ-CD_3bz.H_2TCPP^{4-} complex, complexing *p*-carboxyphenyl groups through one, two or three narrow annular faces (Figure A20 of the Appendix) show a progressive increase in *E* from -23278.89, to -23393.05 to -23794.46 kJ mol^{-1} with the respective step-wise differences being 114.16 and 401.41 kJ mol^{-1} consistent with increasing stability as the complex progresses from mono- to di- to tritopic. Evidently there is little hindrance to tritopic complexation which may be attributable to the substantially longer linkers between each pair of γ-CD annuli in 666γ-CD_3bz than in the four γ-CD dimers. This is in accord with 666γ-CD_3bz.H_2TCPP^{4-} exhibiting the largest K_{11} (Table 3.1) in the aqueous complexation studies discussed earlier. It is also in accord with 666γ-CD_3bz.H_2TCPP^{4-} exhibiting the largest UV-vis absorption red shift in aqueous solution (Figure 3.12).

The heats of formation, *E*, and the models for the non-cooperative and cooperative *syn* $(33\gamma\text{-}CD_2ox)_2.H_2TCPP^{4-}$ and $(33\gamma\text{-}CD_2suc)_2.H_2TCPP^{4-}$ 2:1 complexes appear in Table 3.2 and Figure 3.14 and Figure A17 of the Appendix. (The corresponding cooperative *anti* 2:1 complexes could not be energy minimised as a consequence of steric hindrance.) It is seen that *E* for the cooperative complexes are substantially more negative than those for the non-cooperative complexes with the differences being 439.82 kJ mol^{-1} $(33\gamma\text{-}CD_2ox)_2.H_2TCPP^{4-}$ and 944.27 kJ mol^{-1} $(33\gamma\text{-}CD_2suc)_2.H_2TCPP^{4-}$. This is consistent with ditopic complexation by $33\gamma\text{-}CD_2ox$ and $33\gamma\text{-}CD_2suc$ producing greater stability than monotopic complexation, and with the greater length and flexibility of the succinimide linker lessening steric hindrance and structural strain than does the oxalate linker. An overall scheme is shown in Figure 3.15 for the equilibria which are potentially possible for complexation of H_2TCPP^{4-} by $33\gamma\text{-}CD_2ox$ and $33\gamma\text{-}CD_2suc$ in the gas phase which may be compared with the complexes which energy minimised (Table 3.2 and Figures 3.13 and 3.14 and Figure A17 in the Appendix, respectively). The *E* values for the non-cooperative complexes of $(66\gamma\text{-}CD_2ox)_2.H_2TCPP^{4-}$ and $(66\gamma\text{-}CD_2suc)_2.H_2TCPP^{4-}$ (Table 3.2 and Figures A18 and A19 in the Appendix, respectively) are more negative than that for $(33\gamma\text{-}CD_2ox)_2.H_2TCPP^{4-}$ and $(33\gamma\text{-}CD_2suc)_2.H_2TCPP^{4-}$ (a difference of 157.11 and 298.25 kJ mol^{-1}, respectively). This data is in accordance with the trend observed with $(\gamma\text{-}CD_2)_2.H_2TCPP^{4-}$, where the wide face is preferred over the narrow face for the entrance of H_2TCPP^{4-} into the γ-CD annulus. The *E* values for the non-cooperative complexes of $(66\gamma\text{-}CD_2ox)_2.H_2TCPP^{4-}$ and $(66\gamma\text{-}CD_2suc)_2.H_2TCPP^{4-}$ are less negative than that of the cooperative complexes for $(33\gamma\text{-}CD_2ox)_2.H_2TCPP^{4-}$ and $(33\gamma\text{-}CD_2suc)_2.H_2TCPP^{4-}$ (a difference of 282.71 and 646.23 kJ mol^{-1}, respectively). This is indicative of the cooperative binding effect leading to increase of the inherent stability of the 2:1 host-guest complexes. Neither the cooperative *anti* nor the cooperative *syn* 2:1

(66γ-CD_2ox)$_2$.H_2TCPP^{4-} and (66γ-CD_2suc)$_2$.H_2TCPP^{4-} complexes could be energy minimised because of steric hindrance.

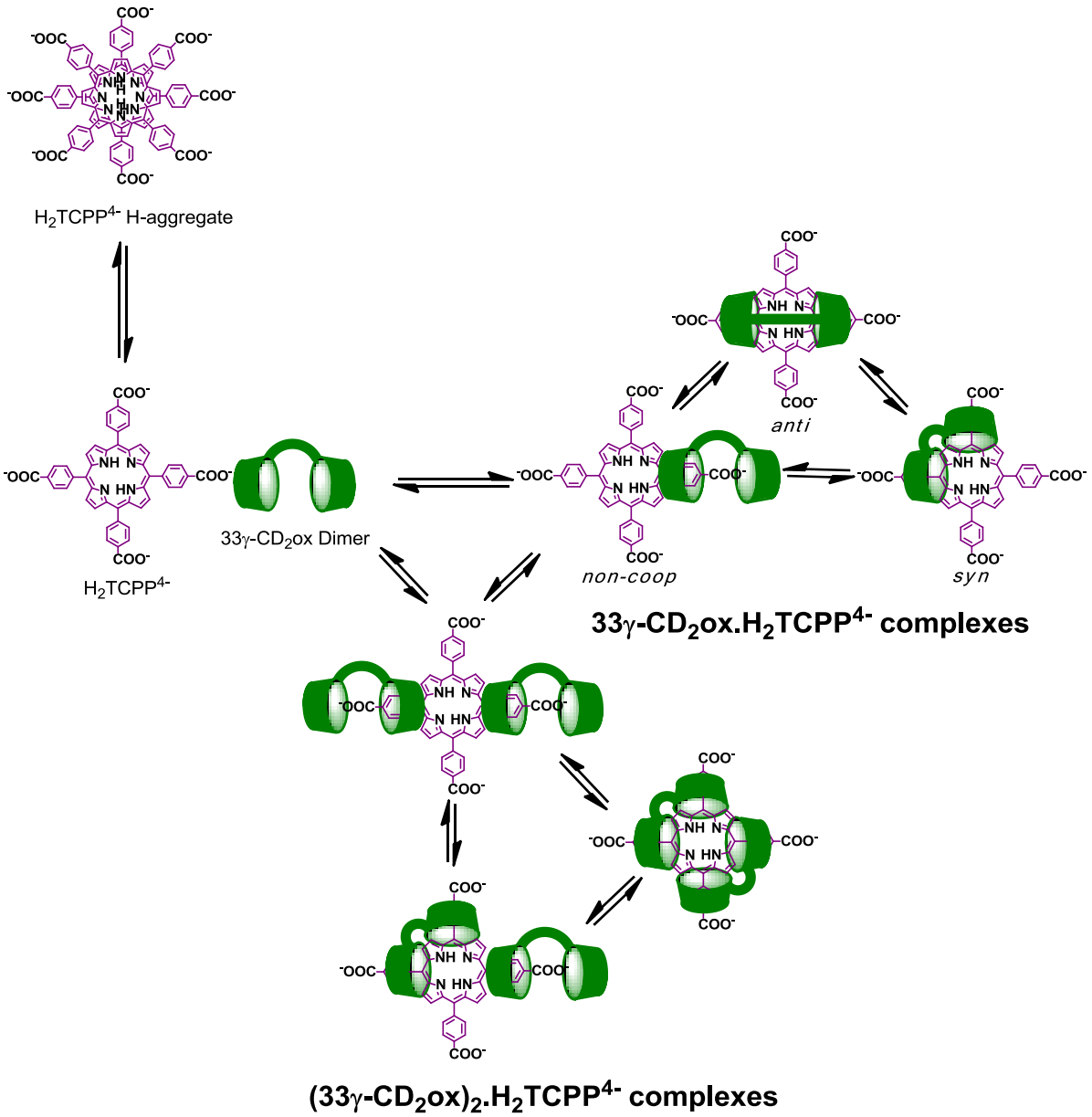

Figure 3.15: Scheme for the potential host-guest equilibria existing between tetraanionic H_2TCPP^{4-}, $(H_2TCPP^{4-})_2$ and the 33γ-CD_2ox dimer. A similar scheme applies for the 33γ-CD_2suc dimer and H_2TCPP^{4-}.

In general, the trends in the gas phase modelling experiments observed for H_2TCPP^{4-} and with γ-CD and its oligomers reflect the trends observed for the analogous H_2TSPP^{4-} complexes. However, some key differences in the gas phase complexation behaviour with the γ-CD hosts are apparent. The difference in energy of the *E* values between the *syn* and *anti*

conformers is less in the 66γ-CD_2ox and 66γ-CD_2suc dimer systems with H_2TCPP^{4-} (281.87 kJ mol^{-1} and 161.48 kJ mol^{-1}, respectively) than in H_2TSPP^{4-} (475.71 kJ mol^{-1} and 250.04 kJ mol^{-1}, respectively). This may suggest that the *syn* conformers of the 6,6- linked dimer complexes with H_2TCPP^{4-} experience less steric strain than that of H_2TSPP^{4-}, most likely as a consequence of the smaller planar carboxyl groups of H_2TCPP^{4-} allowing more freedom of movement than the tetrahedral sulfonyl groups of H_2TSPP^{4-}. The same relationships occurs to a lesser extent for the 33γ-CD_2ox and 33γ-CD_2suc dimer systems with H_2TCPP^{4-} (5.09 and 118.37 kJ mol^{-1}, respectively) and H_2TSPP^{4-} (7.17 and 162.37 kJ mol^{-1}, respectively) This suggests that the shape of the ionic functional group has less of an effect in stabilising *syn* complexation through the wider 3-hydroxyl face than that of the narrower 6-hydroxyl face of the γ-CD annuli.

Changes in the complexation behaviour of the 2:1 host-guest complexes of 33γ-CD_2ox and 33γ-CD_2suc dimer systems with H_2TCPP^{4-} compared to H_2TSPP^{4-} are also observed. The difference in the *E* values between the 2:1 non cooperative complexes and 2:1 *syn* cooperative complexes for $(33\gamma\text{-}CD_2ox)_2.H_2TCPP^{4-}$ and $(33\gamma\text{-}CD_2suc)_2.H_2TCPP^{4-}$ (439.82 kJ mol^{-1} and 944.27 kJ mol^{-1}, respectively) are greater than that observed for $(33\gamma\text{-}CD_2ox)_2.H_2TSPP^{4-}$ and $(33\gamma\text{-}CD_2suc)_2.H_2TSPP^{4-}$ (172.00 kJ mol^{-1} and 268.97 kJ mol^{-1}, respectively). This further suggests that the change in shape of the ionic functional groups from tetrahedral to planar helps to mediate steric strain and increase the stability of the 2:1 *syn* cooperative complexes.

The complexation behaviour of 666γ-CD_3bz.H_2TCPP^{4-} is also different than that of 666γ-CD_3bz.H_2TCPP^{4-}. The respective step-wise differences in *E* values between monotopic, ditopic and tritopic complexation in 666γ-CD_3bz.H_2TCPP^{4-} (114.16 and 401.41 kJ mol^{-1}) are larger than that of 666γ-CD_3bz.H_2TSPP^{4-} (62.92 and 249.12 kJ mol^{-1}). This is consistent with

the smaller planar *p*-carboxyphenyl groups of H_2TCPP^{4-} causing less steric hindrance than the tetrahedral *p*-sulfonatophenyl groups of H_2TSPP^{4-} in ditopic or tritopic trimer complexation.

3.7. SUMMARY AND CONCLUSIONS

The host-guest complexation of $H_3TCPP^{3-}/H_2TCPP^{4-}$ by γ-CD, 33γ-CD_2ox, 33γ-CD_2suc, 66γ-CD_2ox, 66γ-CD_2suc and 666γ-CD_3bz has been characterised in aqueous solutions by 2D ^{1}H NOSEY NMR and UV-vis spectroscopy. Furthermore, the host-guest complexation of H_2TCPP^{4-} with the same γ-CD species are investigated through molecular modelling in the gas phase by PM7 semi-empirical calculations. The 2D ^{1}H NOESY NMR spectra show that γ-CD and its oligomers complex $H_3TCPP^{3-}/H_2TCPP^{4-}$ as is evident from the cross-peaks arising from NOE interactions between the pyrrolic and *p*-carboxyphenyl protons of $H_3TCPP^{3-}/H_2TCPP^{4-}$ and the annular protons of γ-CD and its oligomers. The absorption spectrum of 2.00×10^{-6} mol dm^{-3} $H_3TCPP^{3-}/H_2TCPP^{4-}$ in aqueous phosphate buffer (pH 7.0 and I = 0.10 mol dm^{-3}) showed considerable variation between 278.2-308.2 K, suggesting $H_3TCPP^{3-}/H_2TCPP^{4-}$ aggregation at lower temperatures. Further UV-Vis titrations studies found that the monomer/dimer equilibrium is characterised by $K_D = 3.59 \times 10^4 \pm 0.18$ dm^3 mol^{-1} at 298.2 K. Additional UV-vis studies show that 1:1 host-guest complexes are predominant in the 66γ-CD_2ox, 66γ-CD_2suc and 666γ-CD_3bz systems, whilst γ-CD, 33γ-CD_2ox and 33γ-CD_2suc also form 2:1 host-guest complexes. The K_{11} values derived for 1:1 host-guest complexation are ~8 - 1400 fold larger for the γ-CD oligomers than for γ-CD at 298.2 K. Similar to H_2TSPP^{4-} in Chapter 2, this observation may suggest a strong cooperative effect when the γ-CD oligomers complex $H_3TCPP^{3-}/H_2TCPP^{4-}$. Despite increased porphyrin aggregation in $H_3TCPP^{3-}/H_2TCPP^{4-}$ compared to H_2TSPP^{4-}, the K_{11} complexation constants with γ-CD and its oligomers are greater with the former than the latter. This suggests that the difference in shape (from planar to tetrahedral) between the carboxyl and sulfonyl ionic

functional groups of the porphyrin phenyl rings significantly influences the host-guest complexation of the porphyrins by the γ-CD species. Furthermore, the studies show that increased porphyrin aggregation in the $H_3TCPP^{3-}/H_2TCPP^{4-}$ systems does not significantly impinge host-guest complexation by the γ-CD species. The K_{21} values derived for (33γ-CD_2ox)$_2$.$H_3TCPP^{3-}/H_2TCPP^{4-}$ and (33γ-CD_2suc)$_2$.$H_3TCPP^{3-}/H_2TCPP^{4-}$ are high by comparison with K_{21} (γ-CD)$_2$.$H_3TCPP^{3-}/H_2TCPP^{4-}$ consistent with both 33γ-CD_2ox and 33γ-CD_2suc complexing $H_3TCPP^{3-}/H_2TCPP^{4-}$ ditopically in their 2:1 complexes. Furthermore the K_{21} values derived for (33γ-CD_2ox)$_2$.$H_3TCPP^{3-}/H_2TCPP^{4-}$, (33γ-$CD_2$suc)$_2$.$H_3TCPP^{3-}$ /H_2TCPP^{4-} and (γ-CD)$_2$.$H_3TCPP^{3-}/H_2TCPP^{4-}$ at 298.2 K were significantly higher than those derived for the analogous systems with H_2TSPP^{4-} most likely as a consequence of the change in ionic functional groups discussed above.

Gas phase molecular modelling of H_2TCPP^{4-} with the γ-CD species shows that when two γ-CD annuli complex two adjacent *p*-carboxyphenyl groups of H_2TCPP^{4-} in the *syn* conformation the heat of formation, *E*, is less negative than when two distant *p*-carboxyphenyl groups are complexed in the *anti* configuration which is the most stable configuration. The difference in *E* between the *syn* and *anti* 33γ-CD_2ox.H_2TCPP^{4-} and 33γ-CD_2suc.H_2TCPP^{4-} complexes is smaller than for the *syn* and *anti* 66γ-CD_2ox.H_2TCPP^{4-} and 66γ-CD_2suc.H_2TCPP^{4-} complexes. This is attributed to the wide annular γ-CD faces of 33γ-CD_2ox and 33γ-CD_2suc allowing more flexibility in complexing H_2TCPP^{4-} than the narrow annular γ-CD faces of 66γ-CD_2ox and 66γ-CD_2suc. These gas phase models are expected to reflect the relative stabilities found for the complexes characterised in solution and indicate the importance of steric interactions in determining the relative magnitudes of these stabilities.

This study provides important information on the factors affecting the dimerisation and host-guest equilibria of a water soluble porphyrin, $H_3TCPP^{3-}/H_2TCPP^{4-}$ with γ-CD and γ-CD oligomers in aqueous solutions. The studies give insight into how complexation by γ-CD

and γ-CD oligomers reduces $H_3TCPP^{3-}/H_2TCPP^{4-}$ aggregation and may lead to better design of photodynamic therapy treatments in the treatment cancer.

3.8. REFERENCES

1. R. Bonnett, *Chem. Soc. Rev.*, 1995, **24**, 19-33.
2. J. Lai and M. Cooney, *Int. Ophthalmol. Clin.*, 1999, **39**, 163-174.
3. A. Juzeniene, Q. Peng and J. Moan, *Photochem. Photobiol. Sci.*, 2007, **6**, 1234-1245.
4. J. M. Dabrowski, M. M. Pereira, L. G. Arnaut, C. J. P. Monteiro, A. F. Peixoto, A. Karocki, K. Urbanska and G. Stochel, *Photochem. Photobiol.*, 2007, **83**, 897-903.
5. A. Mazzaglia, in *Cyclodextrins in Pharmaceutics, Cosmetics, and Biomedicine*, John Wiley & Sons, Inc., 2011, pp. 343-361.
6. R. F. Pasternack, P. R. Huber, P. Boyd, G. Engasser, L. Francesconi, E. Gibbs, P. Fasella, G. Cerio Venturo and L. d. Hinds, *J. Am. Chem. Soc.*, 1972, **94**, 4511-4517.
7. R. F. Pasternack, *Ann. N. Y. Acad. Sci.*, 1973, **206**, 614-630.
8. R. F. Pasternack, L. Francesconi, D. Raff and E. Spiro, *Inorg. Chem.*, 1973, **12**, 2606-2611.
9. K. Kano, T. Nakajima, M. Takei and S. Hashimoto, *Bull. Chem. Soc. Jpn.*, 1987, **60**, 1281-1287.
10. K. Kano, H. Minamizono, T. Kitae and S. Negi, *J. Phys. Chem. A*, 1997, **101**, 6118-6124.
11. A. Iosif and U. W. Grummt, *J. Prakt. Chem./Chem.- Ztg.*, 1997, **339**, 420-425.
12. S. E. Clarke, C. C. Wamser and H. E. Bell, *J. Phys. Chem. A*, 2002, **106**, 3235-3242.
13. A. Corsini and O. Herrmann, *Talanta*, 1986, **33**, 335-339.
14. J. M. Ribo, J. Crusats, J. A. Farrera and M. L. Valero, *J. Chem. Soc. Chem. Commun.*, 1994, 681-682.
15. K. M. Kadish, G. B. Maiya, C. Araullo and R. Guilard, *Inorg. Chem.*, 1989, **28**, 2725-2731.
16. N. C. Maiti, S. Mazumdar and N. Periasamy, *J. Phys. Chem. B*, 1998, **102**, 1528-1538.
17. A. D'Urso, M. E. Fragala and R. Purrello, *Chem. Commun.*, 2012, **48**, 8165-8176.

18. S. C. Doan, S. Shanmugham, D. E. Aston and J. L. McHale, *J. Am. Chem. Soc.*, 2005, **127**, 5885-5892.

19. M. Y. Choi, J. A. Pollard, M. A. Webb and J. L. McHale, *J. Am. Chem. Soc.*, 2003, **125**, 810-820.

20. N. C. Maiti, M. Ravikanth, S. Mazumdar and N. Periasamy, *J. Phys. Chem.*, 1995, **99**, 17192-17197.

21. J. Mosinger, V. Kliment, Jr., J. Sejbal, P. Kubat and K. Lang, *J. Porphyrins Phthalocyanines*, 2002, **6**, 514-526.

22. K. Watanabe, H. Kitagishi and K. Kano, *Angew. Chem., Int. Ed.*, 2013, **52**, 6894-6897.

23. K. Kano, H. Kitagishi, Y. Sone, N. Nakazawa and M. Kodera, *Eur. J. Inorg. Chem.*, 2006, 4043-4053.

24. T. Harada, H. L. McTernan, D.-T. Pham, S. F. Lincoln and T. W. Kee, *J. Phys. Chem. B*, 2015, **119**, 2425-2433.

25. Z. El-Hachemi, J.-A. Farrera, H. Garcia-Ortega, O. Ramirez-Gutierrez and J. M. Ribo, *J. Porphyrins Phthalocyanines*, 2001, **5**, 465-473.

26. J. M. Ribo, J.-A. Farrera, M. L. Valero and A. Virgili, *Tetrahedron*, 1995, **51**, 3705-3712.

27. J. Mosinger, M. Deumie, K. Lang, P. Kubat and D. M. Wagnerova, *J. Photochem. Photobiol., A*, 2000, **130**, 13-20.

28. H.-T. Nguyen, D.-T. Pham, S. F. Lincoln, J. Wang, X. Guo, C. J. Easton and R. K. Prud'homme, *Polym. Chem.*, 2013, **4**, 820-829.

29. D.-T. Pham, H. T. Ngo, S. F. Lincoln, B. L. May and C. J. Easton, *Tetrahedron*, 2010, **66**, 2895-2898.

30. J. Sobczynski, H. H. Toennesen and S. Kristensen, *Pharmazie*, 2013, **68**, 100-109.

31. R. B. M. Koehorst, U. Hofstra and T. J. Schaafsma, *Magn. Reson. Chem.*, 1988, **26**, 167-172.

32. W. Saenger, J. Jacob, K. Gessler, T. Steiner, D. Hoffmann, H. Sanbe, K. Koizumi, S. M. Smith and T. Takaha, *Chem. Rev.*, 1998, **98**, 1787-1802.

33. H. T. Ngo, Supramolecular Chemistry of β- and γ-Cyclodextrin Dimers. A PhD. Dissertaion, University of Adelaide, 2010.

34. HypSpec, Protonic Software, 2 Templegate Avenue, Leeds LS15 0HD, UK.

35. J. Mosinger, L. Slavetinska, K. Lang, P. Coufal and P. Kubat, *Org. Biomol. Chem.*, 2009, **7**, 3797-3804.

36. Y. Wang, B. Cohen, A. Aykac, A. Vargas-Berenguel and A. Douhal, *Photochem. Photobiol. Sci.*, 2013, **12**, 2119-2129.

37. F. Venema, H. F. M. Nelissen, P. Berthault, N. Birlirakis, A. E. Rowan, M. C. Feiters and R. J. M. Nolte, *Chem. Eur. J.*, 1998, **4**, 2237-2250.

38. S. Zhao and J. H. T. Luong, *J. Chem. Soc., Chem. Commun.*, 1994, 2307-2308.

39. S. Hamai and T. Ohshida, *J. Inclusion Phenom. Macrocyclic Chem.*, 2004, **50**, 209-217.

40. P. Thordarson, *Chem. Soc. Rev.*, 2011, **40**, 1305-1323.

41. K. Kano, R. Nishiyabu, T. Asada and Y. Kuroda, *J. Am. Chem. Soc.*, 2002, **124**, 9937-9944.

42. T. Jiang, M. Li and D. S. Lawrence, *J. Org. Chem.*, 1995, **60**, 7293-7297.

43. D. D. Perrin, *Aust. J. Chem.*, 1964, **17**, 484-488.

44. J. C. Reijenga, L. G. Gagliardi and E. Kenndler, *J. Chromatogr. A*, 2007, **1155**, 142-145.

45. A. Farajtabar, F. Gharib, P. Jamaat and N. Safari, *J. Chem. Eng. Data*, 2008, **53**, 350-354.

46. J. P. Stewart, Stewart Computational Chemistry, Colorado Springs, CO, 14.139W edn., 2012.

3.9. APPENDIX

2D ^{1}H NOESY NMR Spectra

a)

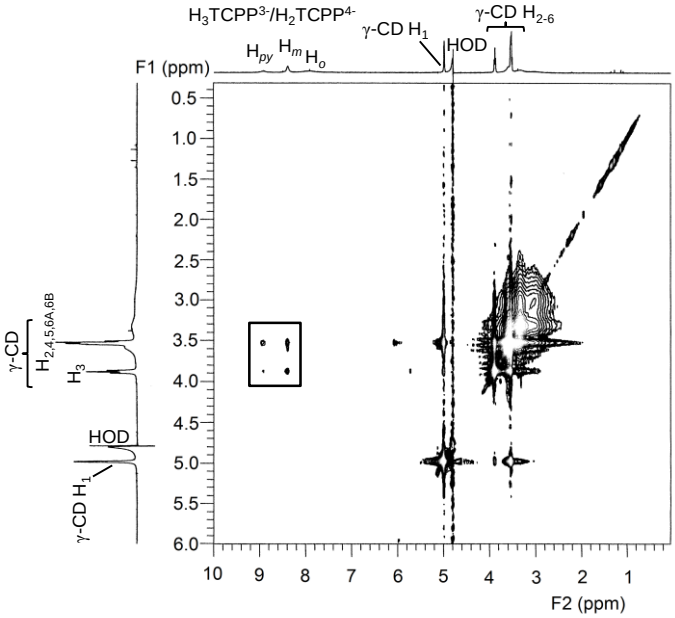

b)

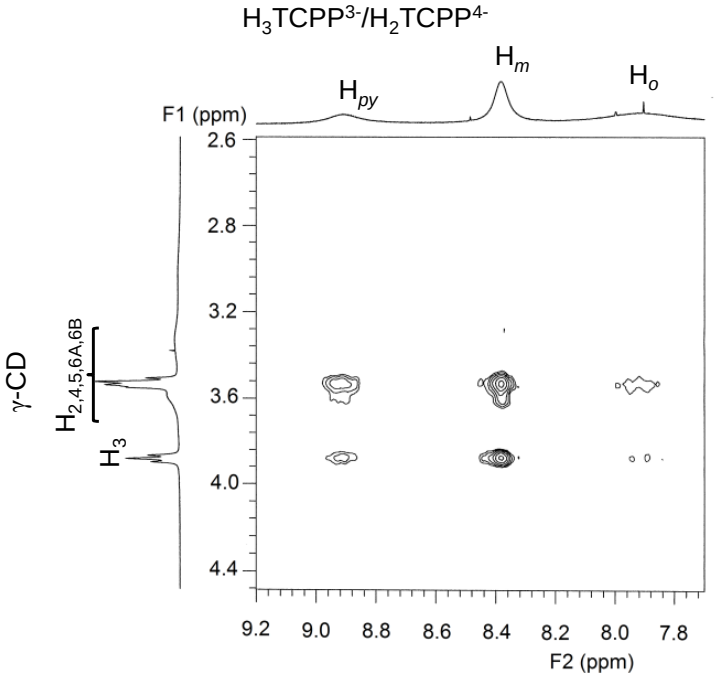

Figure A1: a) 2D ^{1}H NOESY NMR (600 MHz) spectrum of $H_3TCPP^{3-}/H_2TCPP^{4-}$ (3.0×10^{-3} mol dm^{-3}) and equimolar γ-CD in D_2O (pD 7.0 phosphate buffer, I = 0.10 mol dm^{-3}) at 298.2 K with a mixing time of 300 ms. b) Expanded aromatic resonance region. The amount of $H_3TCPP^{3-}/H_2TCPP^{4-}$ in the free state is ~ 20% of the total.

a)

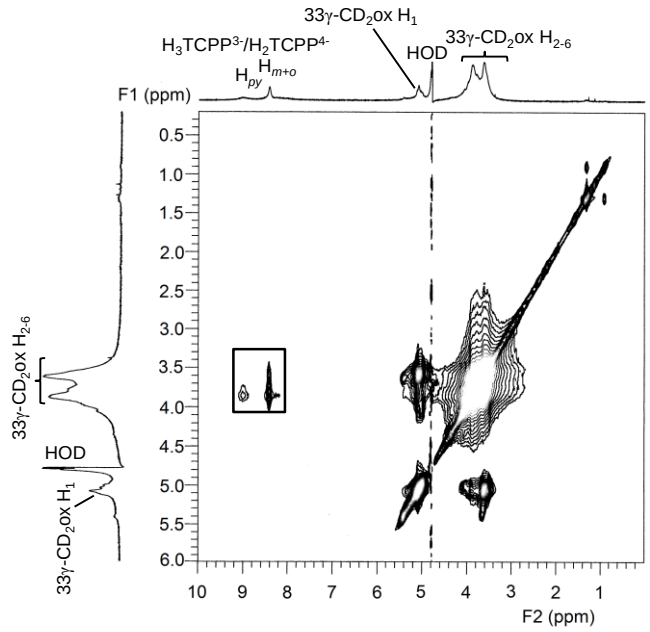

b)

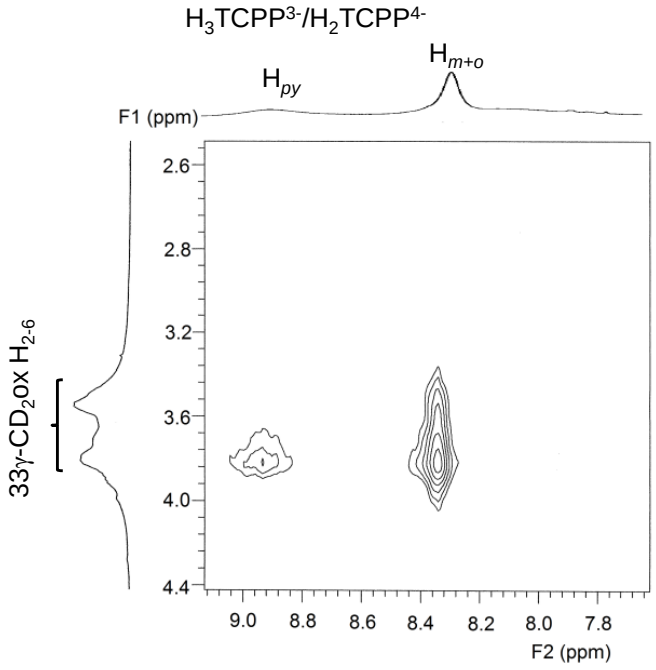

Figure A2: a) 2D ^{1}H NOESY NMR (600 MHz) spectrum of $H_3TCPP^{3-}/H_2TCPP^{4-}$ (3.0×10^{-3} mol dm^{-3}) and equimolar 33γ-CD_2ox in D_2O (pD 7.0 phosphate buffer, I = 0.10 mol dm^{-3}) at 298.2 K with a mixing time of 300 ms. Cross–peaks enclosed in the rectangle arise from interaction between the annular γ-CD protons $H_{3,5,6}$ of the CD annulus and the pyrrolic and phenyl protons of $H_3TCPP^{3-}/H_2TCPP^{4-}$. b) Expanded aromatic resonance region. The amount of $H_3TCPP^{3-}/H_2TCPP^{4-}$ in the free state is ~ 8% of the total.

a)

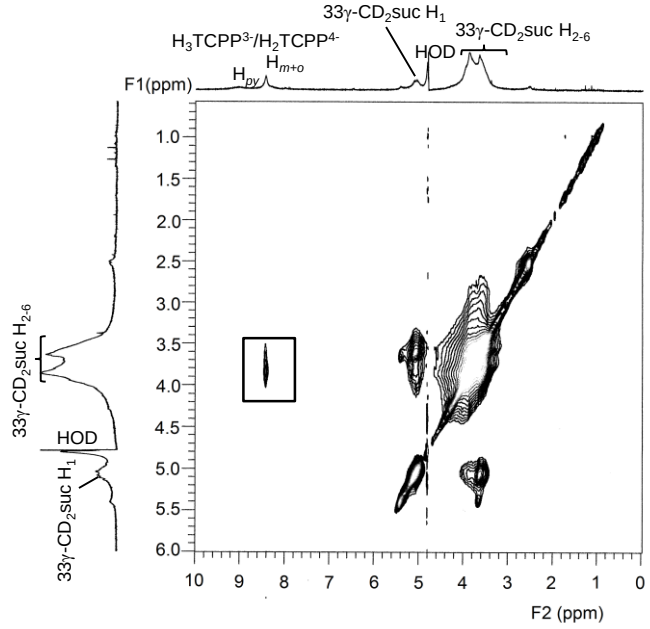

b)

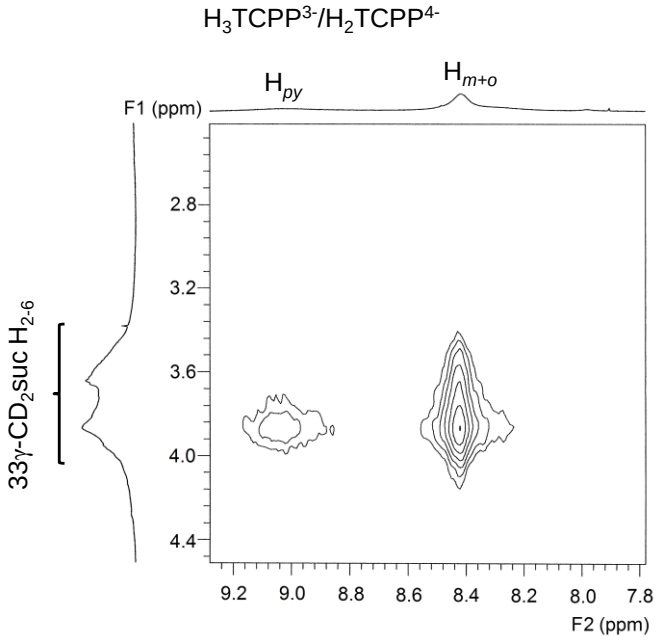

Figure A3: a) 2D ^{1}H NOESY NMR (600 MHz) spectrum of $H_3TCPP^{3-}/H_2TCPP^{4-}$ (3.0×10^{-3} mol dm^{-3}) and equimolar 33γ-CD_2suc in D_2O (pD 7.0 phosphate buffer, I = 0.10 mol dm^{-3}) at 298.2 K with a mixing time of 300 ms. Cross–peaks enclosed in the rectangle arise from interaction between the annular γ-CD protons $H_{3,5,6}$ of the CD annulus and the pyrrolic and phenyl protons of $H_3TCPP^{3-}/H_2TCPP^{4-}$. b) Expanded aromatic resonance region. The amount of $H_3TCPP^{3-}/H_2TCPP^{4-}$ in the free state is ~ 4% of the total.

a)

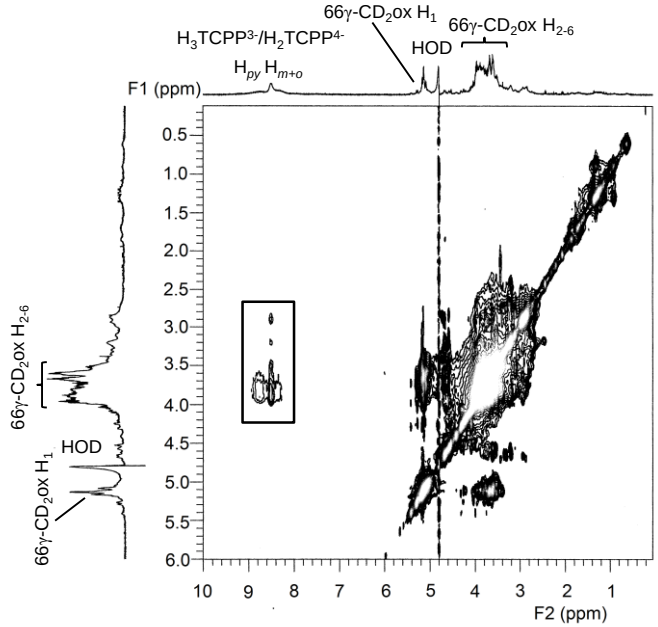

b)

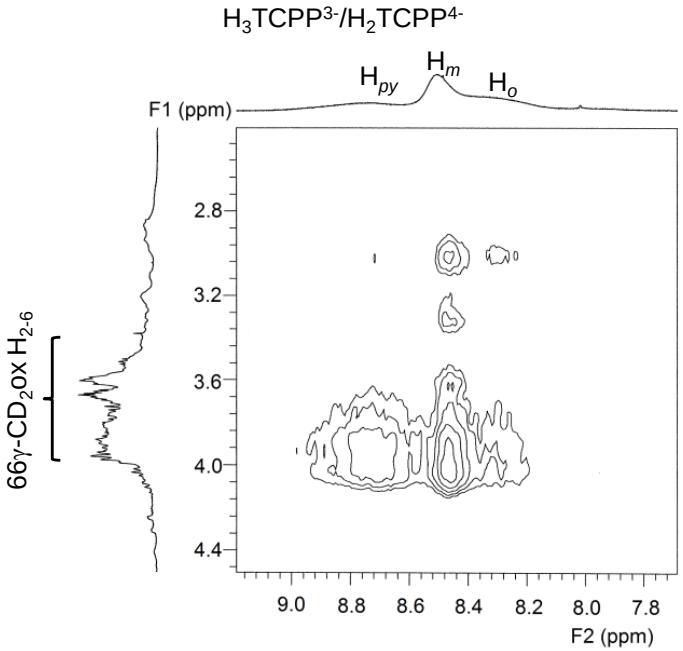

Figure A4: a) 2D ^{1}H NOESY NMR (600 MHz) spectrum of $H_3TCPP^{3-}/H_2TCPP^{4-}$ (3.0×10^{-3} mol dm^{-3}) and equimolar 66γ-CD_2ox in D_2O (pD 7.0 phosphate buffer, I = 0.10 mol dm^{-3}) at 298.2 K with a mixing time of 300 ms. Cross–peaks enclosed in the rectangle arise from interaction between the annular γ-CD protons $H_{3,5,6}$ of the CD annulus and the pyrrolic and phenyl protons of $H_3TCPP^{3-}/H_2TCPP^{4-}$. b) Expanded aromatic resonance region. The amount of $H_3TCPP^{3-}/H_2TCPP^{4-}$ in the free state is < 1 % of the total.

a)

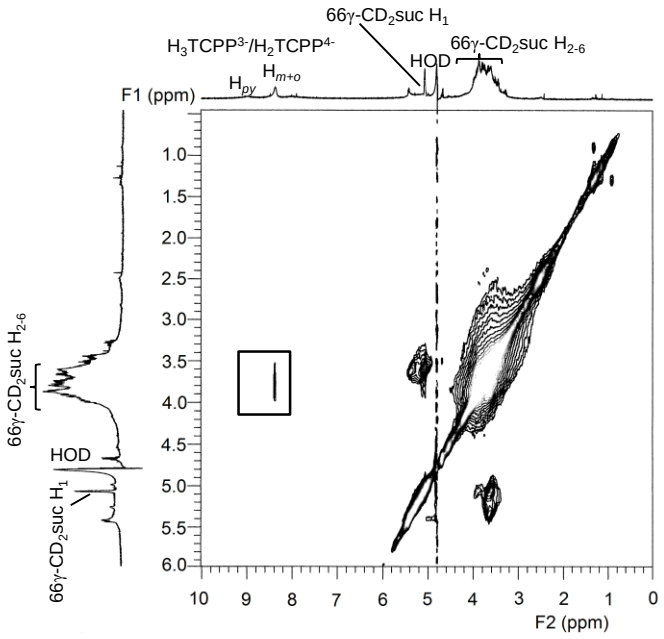

b)

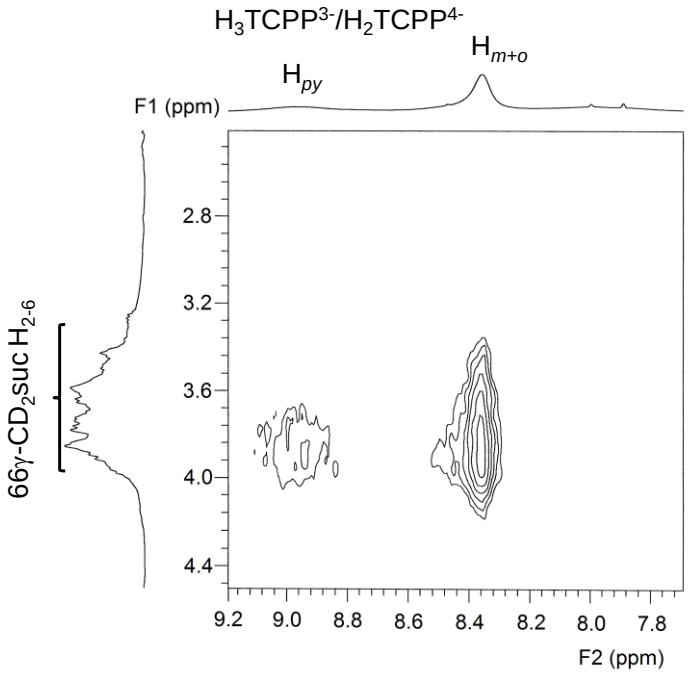

Figure A5: a) 2D ^{1}H NOESY NMR (600 MHz) spectrum of $H_3TCPP^{3-}/H_2TCPP^{4-}$ (3.0×10^{-3} mol dm^{-3}) and equimolar 66γ-CD_2suc in D_2O (pD 7.0 phosphate buffer, I = 0.10 mol dm^{-3}) at 298.2 K with a mixing time of 300 ms. Cross–peaks enclosed in the rectangle arise from interaction between the annular γ-CD protons $H_{3,5,6}$ of the CD annulus and the pyrrolic and phenyl protons of $H_3TCPP^{3-}/H_2TCPP^{4-}$. b) Expanded aromatic resonance region. The amount of $H_3TCPP^{3-}/H_2TCPP^{4-}$ in the free state is < 1% of the total.

a)

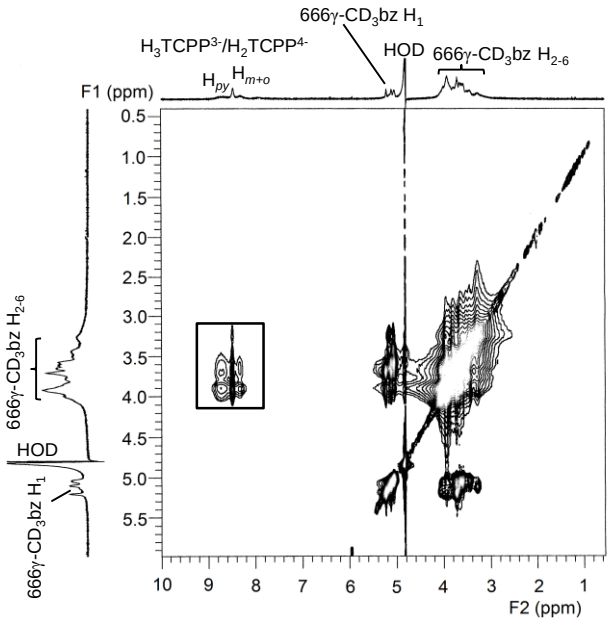

b)

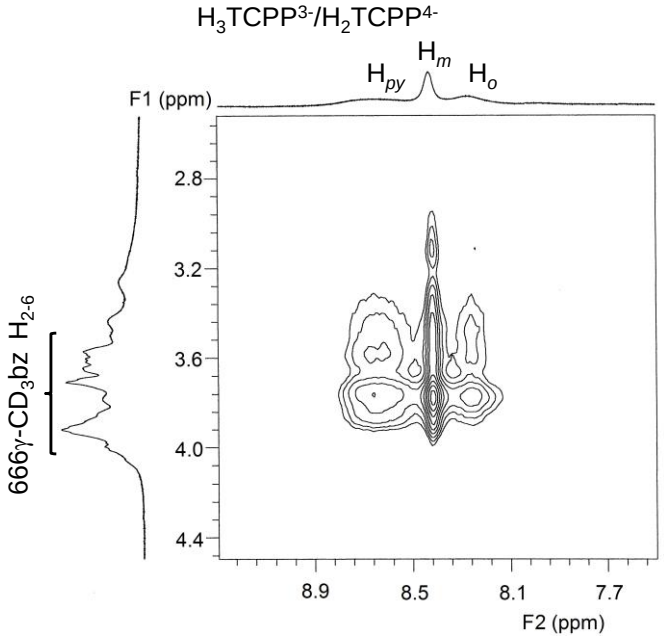

Figure A6: a) 2D ^{1}H NOESY NMR (600 MHz) spectrum of $H_3TCPP^{3-}/H_2TCPP^{4-}$ (3.0×10^{-3} mol dm^{-3}) and equimolar 666γ-CD_3bz in D_2O (pD 7.0 phosphate buffer, I = 0.10 mol dm^{-3}) at 298.2 K with a mixing time of 300 ms. Cross–peaks enclosed in the rectangle arise from interaction between the annular γ-CD protons $H_{3,5,6}$ of the γ-CD annulus and the pyrrolic and phenyl protons of $H_3TCPP^{3-}/H_2TCPP^{4-}$. b) Expanded aromatic resonance region. The amount of $H_3TCPP^{3-}/H_2TCPP^{4-}$ in the free state is < 1% of the total. Note: The phenyl proton resonances of 666γ-CD_3bz overlap with the H_m proton resonances of $H_3TCPP^{3-}/H_2TCPP^{4-}$ and subsequently could not be labelled on the 1D ^{1}H NMR spectrum.

UV-vis spectroscopy

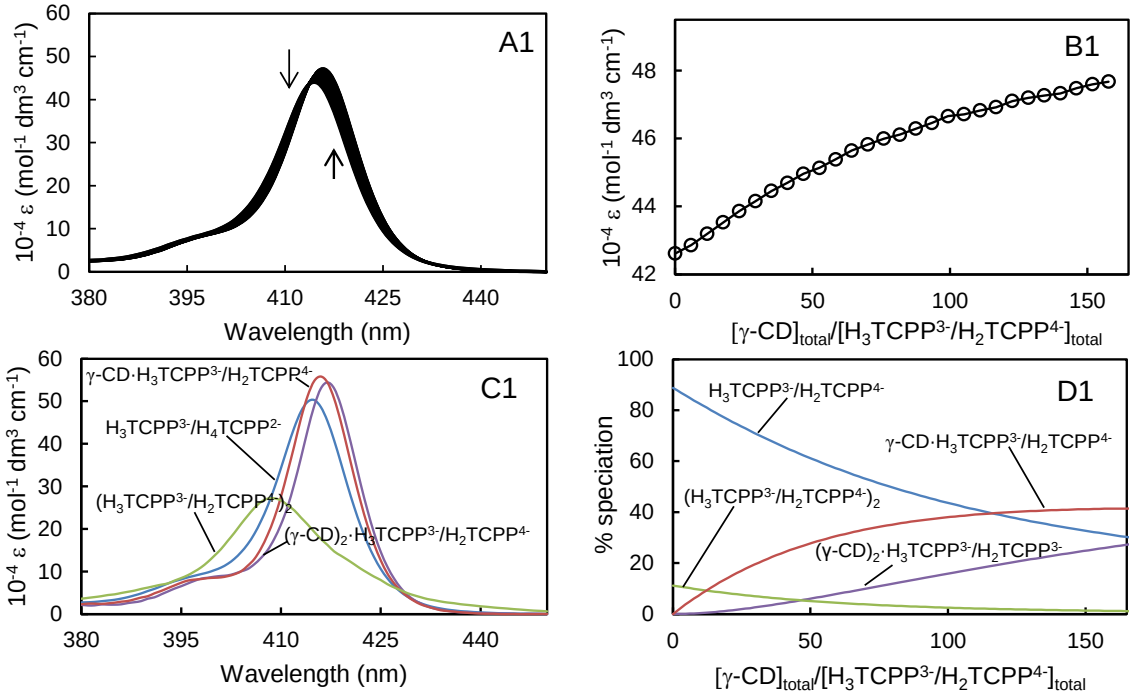

Figure A7: (A1) Molar absorbance change of $H_3TCPP^{3-}/H_2TCPP^{4-}$ (2.00×10^{-6} mol dm^{-3}) in phosphate buffer, pH 7.0, I = 0.10 mol dm^{-3} at 298.2 K with sequential injections (10 mm^3 each) of γ-CD (2.33×10^{-3} mol dm^{-3}) into both sample and reference cells. The arrows indicate the direction of molar absorbance change as the molar ratio of [γ-CD]/[$H_3TCPP^{3-}/H_2TCPP^{4-}$] increases. (B1) Molar absorbance variation at 416 nm and the line of best fit of an algorithm for the monomer/dimer equilibrium and 1:1 and 2:1 host-guest complexation over the wavelength range 400-430 nm. (C1) Calculated molar absorbance of monomer, dimer and complexed $H_3TCPP^{3-}/H_2TCPP^{4-}$. (D1) Speciation with [$H_3TCPP^{3-}/H_2TCPP^{4-}$]$_{total}$ = 100%. Note: A1-D1: data at 298.2 K.

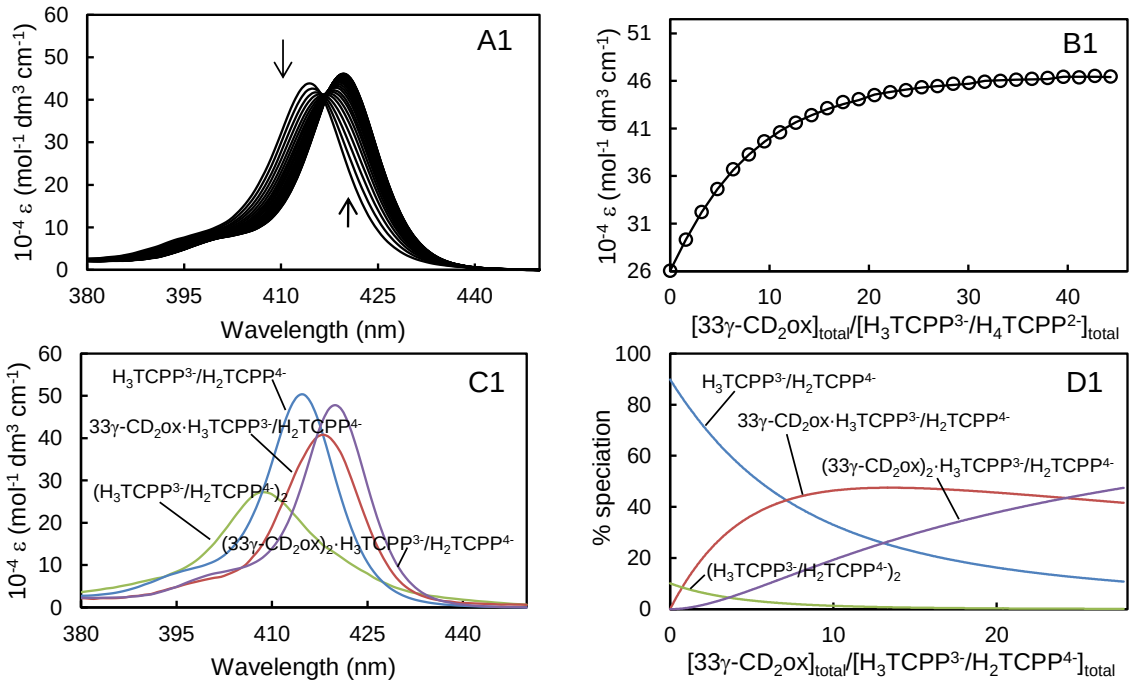

Figure A8: (A1) Molar absorbance change of $H_3TCPP^{3-}/H_2TCPP^{4-}$ (2.00×10^{-6} mol dm^{-3}) in phosphate buffer, pH 7.0, I = 0.10 mol dm^{-3} at 298.2 K with sequential injections (10 mm^3 each) of 33γ-CD_2ox (6.31×10^{-4} mol dm^{-3}) into both sample and reference cells. The arrows indicate the direction of molar absorbance change as the molar ratio of [33γ-CD_2ox]/[$H_3TCPP^{3-}/H_2TCPP^{4-}$] increases. (B1) Molar absorbance variation at 419 nm and the line of best fit of an algorithm for the monomer/dimer equilibrium and 1:1 and 2:1 host-guest complexation over the wavelength range 400-430 nm. (C1) Calculated molar absorbance of monomer, dimer and complexed $H_3TCPP^{3-}/H_2TCPP^{4-}$. (D1) Speciation with $[H_3TCPP^{3-}/H_2TCPP^{4-}]_{total}$ = 100%.

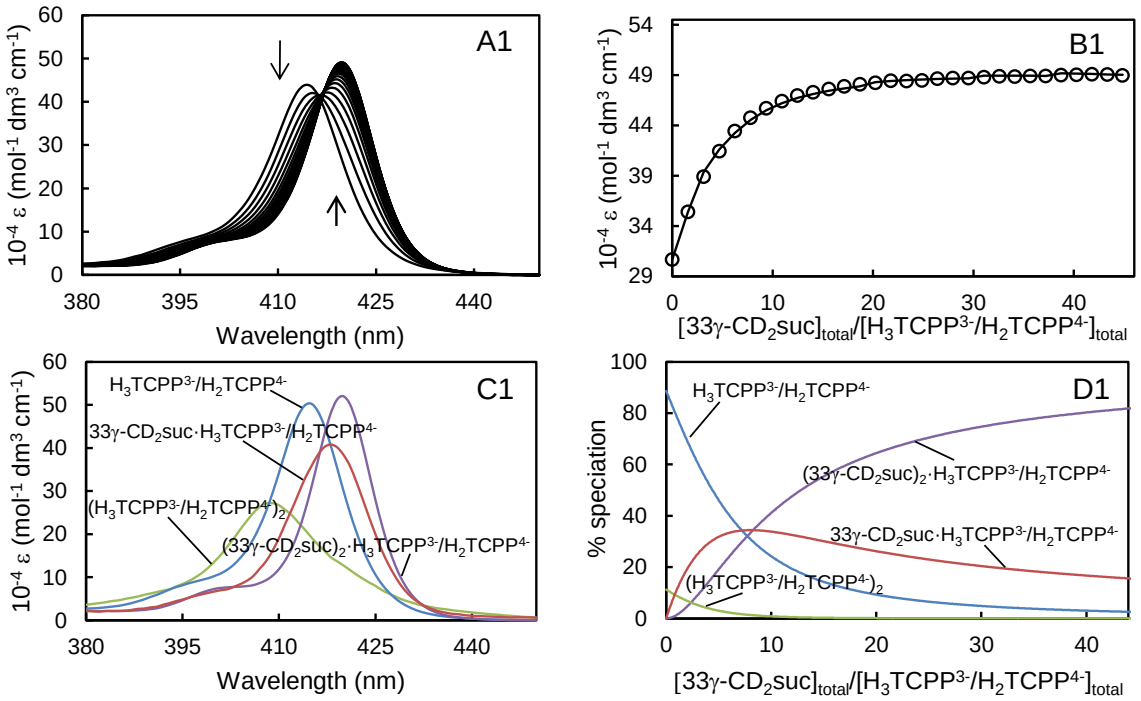

Figure A9: (A1) Molar absorbance change of $H_3TCPP^{3-}/H_2TCPP^{4-}$ (2.00×10^{-6} mol dm^{-3}) in phosphate buffer, pH 7.0, I = 0.10 mol dm^{-3} at 298.2 K with sequential injections (10 mm^3 each for 298.2 K, 15 mm^3 each for 308.2 K) of 33γ-CD_2suc (5.68×10^{-4} mol dm^{-3}) into both sample and reference cells. The arrows indicate the direction of molar absorbance change as the molar ratio of [33γ-CD_2suc]/[$H_3TCPP^{3-}/H_2TCPP^{4-}$] increases. (B1) Molar absorbance variation at 419 nm and the line of best fit of an algorithm for the monomer/dimer equilibrium and 1:1 and 2:1 host-guest complexation over the wavelength range 400-430 nm. (C1) Calculated molar absorbance of monomer, dimer and complexed $H_3TCPP^{3-}/H_2TCPP^{4-}$. (D1) Speciation with $[H_3TCPP^{3-}/H_2TCPP^{4-}]_{total}$ = 100%.

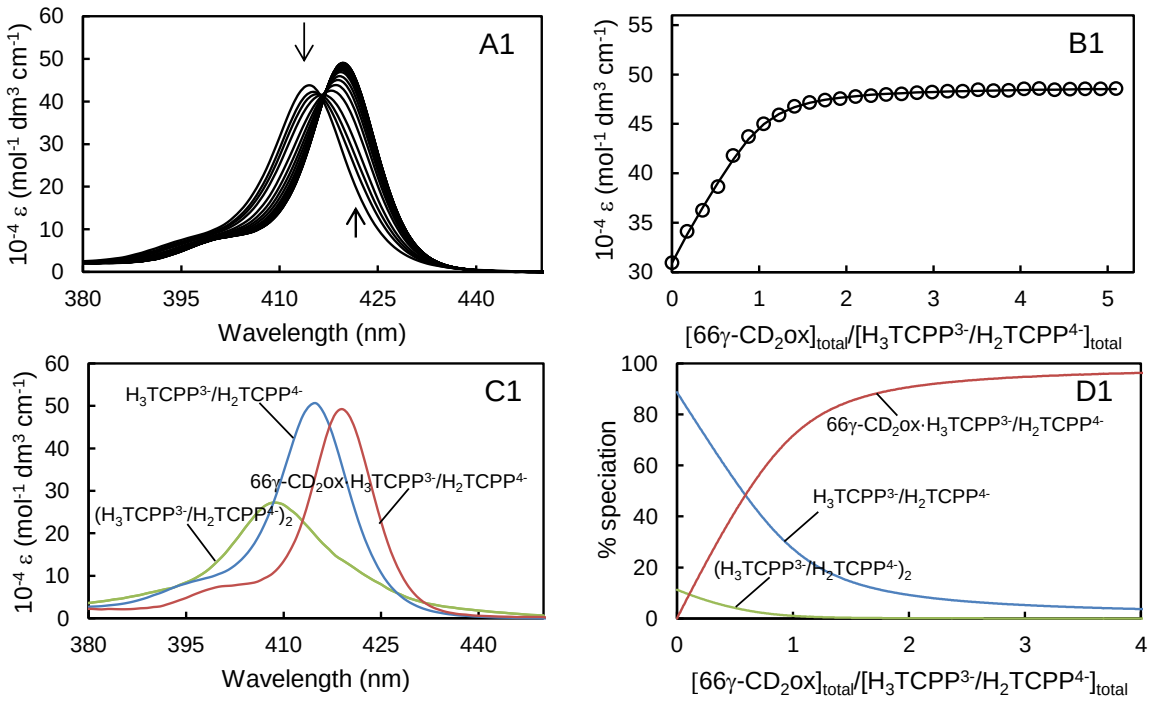

Figure A10: (A1) Molar absorbance change of $H_3TCPP^{3-}/H_2TCPP^{4-}$ (2.00×10^{-6} mol dm^{-3}) in phosphate buffer, pH 7.0, I = 0.10 mol dm^{-3} at 298.2 K with sequential injections (10 mm^3 each) of 66γ-CD_2ox (7.90×10^{-5} mol dm^{-3}) into both sample and reference cells. The arrows indicate the direction of molar absorbance change as the molar ratio of [66γ-CD_2ox]/[$H_3TCPP^{3-}/H_2TCPP^{4-}$] increases. (B1) Molar absorbance variation at 419 nm and the line of best fit of an algorithm for the monomer/dimer equilibrium and 1:1 host-guest complexation over the wavelength range 400-430 nm. (C1) Calculated molar absorbance of monomer, dimer and complexed $H_3TCPP^{3-}/H_2TCPP^{4-}$. (D1) Speciation with $[H_3TCPP^{3-}/H_2TCPP^{4-}]_{total}$ = 100%.

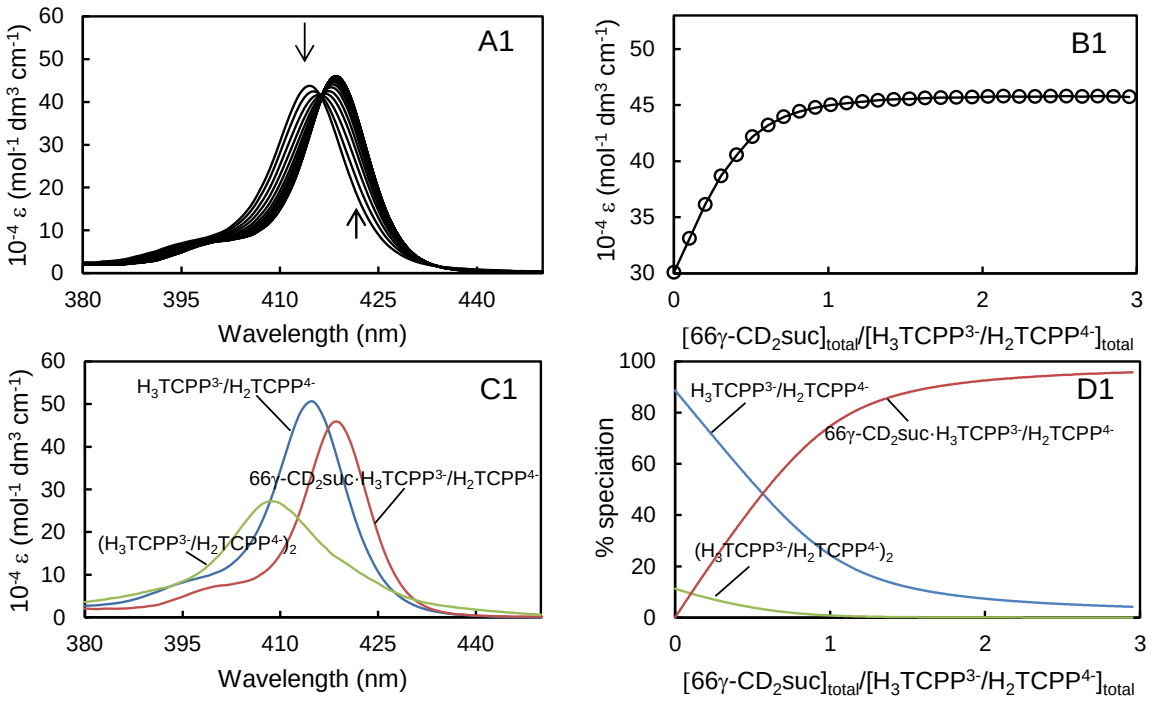

Figure A11: (A1) Molar absorbance change of $H_3TCPP^{3-}/H_2TCPP^{4-}$ (2.00×10^{-6} mol dm^{-3}) in phosphate buffer, pH 7.0, I = 0.10 mol dm^{-3} at 298.2 K with sequential injections (6 mm^3 each) of 66γ-CD_2suc (6.79×10^{-5} mol dm^{-3}) into both sample and reference cells. The arrows indicate the direction of molar absorbance change as the molar ratio of [66γ-CD_2suc]/[$H_3TCPP^{3-}/H_2TCPP^{4-}$] increases. (B1) Molar absorbance variation at 419 nm and the line of best fit of an algorithm for the monomer/dimer equilibrium and 1:1 host-guest complexation over the wavelength range 400-430 nm. (C1) Calculated molar absorbance of monomer, dimer and complexed $H_3TCPP^{3-}/H_2TCPP^{4-}$. (D1) Speciation with [$H_3TCPP^{3-}/H_2TCPP^{4-}$]$_{total}$ = 100%.

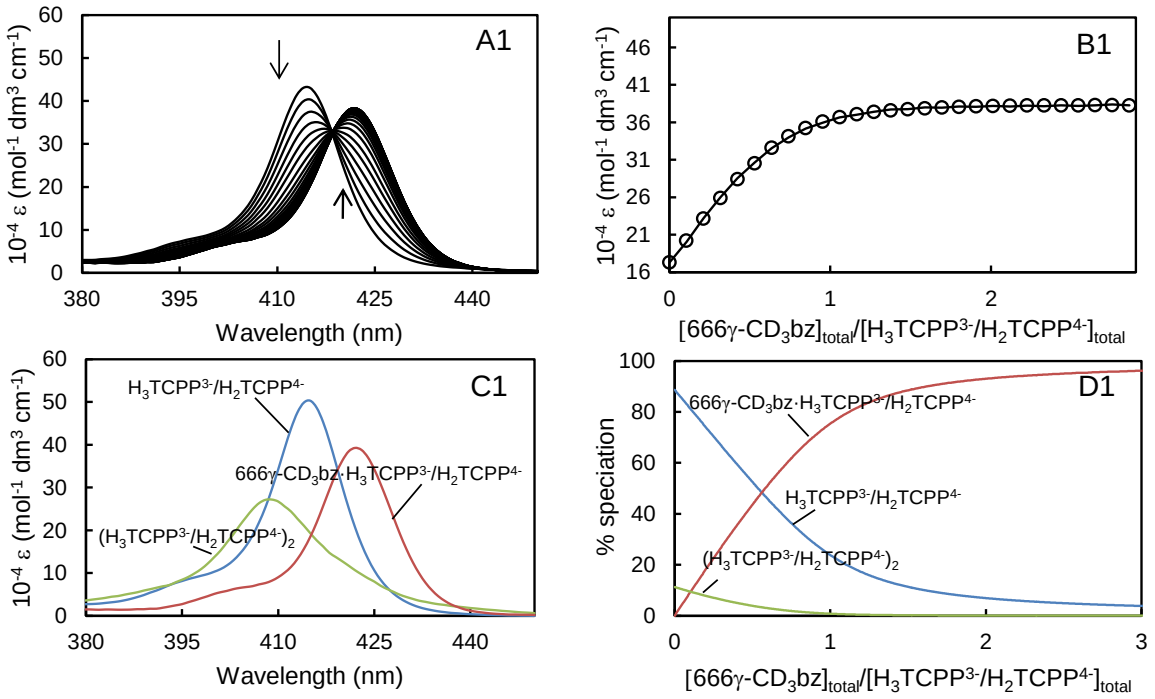

Figure A12: (A1) Molar absorbance change of $H_3TCPP^{3-}/H_2TCPP^{4-}$ (2.00×10^{-6} mol dm^{-3}) in phosphate buffer, pH 7.0, I = 0.10 mol dm^{-3} with sequential injections (5 mm^3 each) of 666γ-CD_3bz (8.46×10^{-5} mol dm^{-3}) into both sample and reference cells. The arrows indicate the direction of molar absorbance change as the molar ratio of [666γ-CD_3bz]/[$H_3TCPP^{3-}/H_2TCPP^{4-}$] increases. (B1) Molar absorbance variation at 422 nm and the line of best fit of an algorithm for the monomer/dimer equilibrium and 1:1 host-guest complexation over the wavelength range 400-430 nm. (C1) Calculated molar absorbance of monomer, dimer and complexed $H_3TCPP^{3-}/H_2TCPP^{4-}$. (D1) Speciation with $[H_3TCPP^{3-}/H_2TCPP^{4-}]_{total}$ = 100%. Note: A1-D1: data at 298.2 K

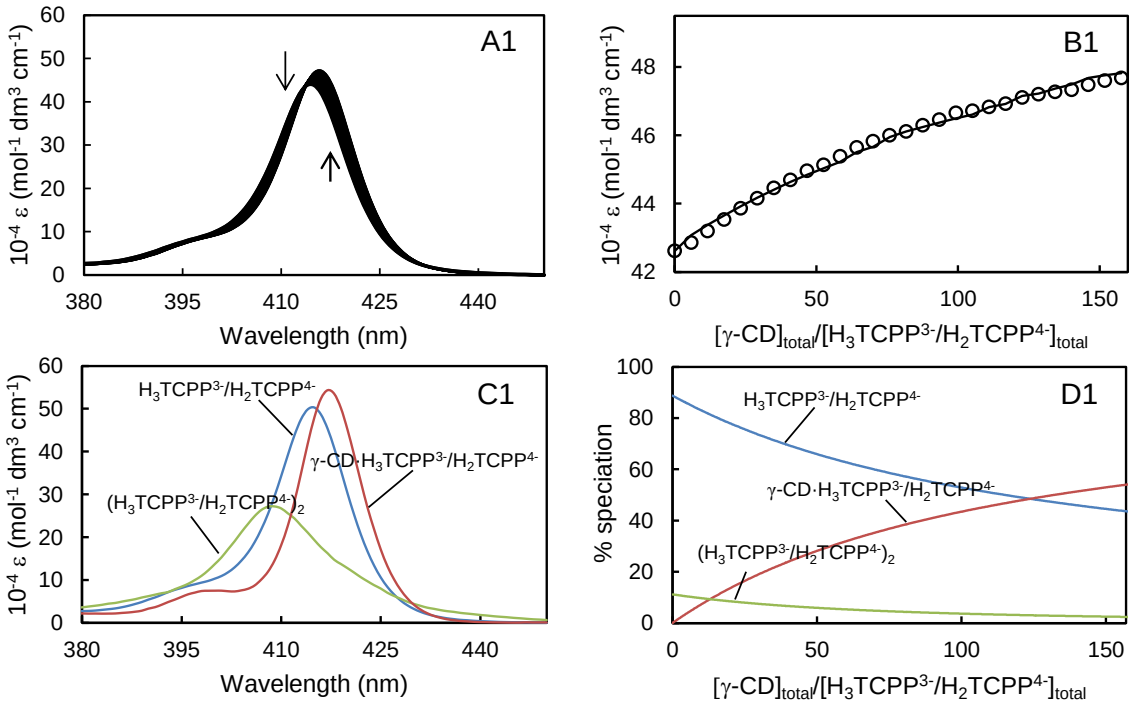

Figure A13: (A1) Molar absorbance change of $H_3TCPP^{3-}/H_2TCPP^{4-}$ (2.00×10^{-6} mol dm^{-3}) in phosphate buffer, pH 7.0, I = 0.10 mol dm^{-3} with sequential injections (10 mm^3 each) of γ-CD (2.33×10^{-3} mol dm^{-3}) into both sample and reference cells. The arrows indicate the direction of molar absorbance change as the molar ratio of $[\gamma\text{-CD}]/[H_3TCPP^{3-}/H_2TCPP^{4-}]$ increases. (B1) Molar absorbance variation at 416 nm and the line of best fit of an algorithm for the monomer/dimer equilibrium and 1:1 host-guest complexation over the wavelength range 400-430 nm. (C1) Calculated molar absorbance of monomer, dimer and complexed $H_3TCPP^{3-}/H_2TCPP^{4-}$. (D1) Speciation with $[H_3TCPP^{3-}/H_2TCPP^{4-}]_{total}$ = 100%.

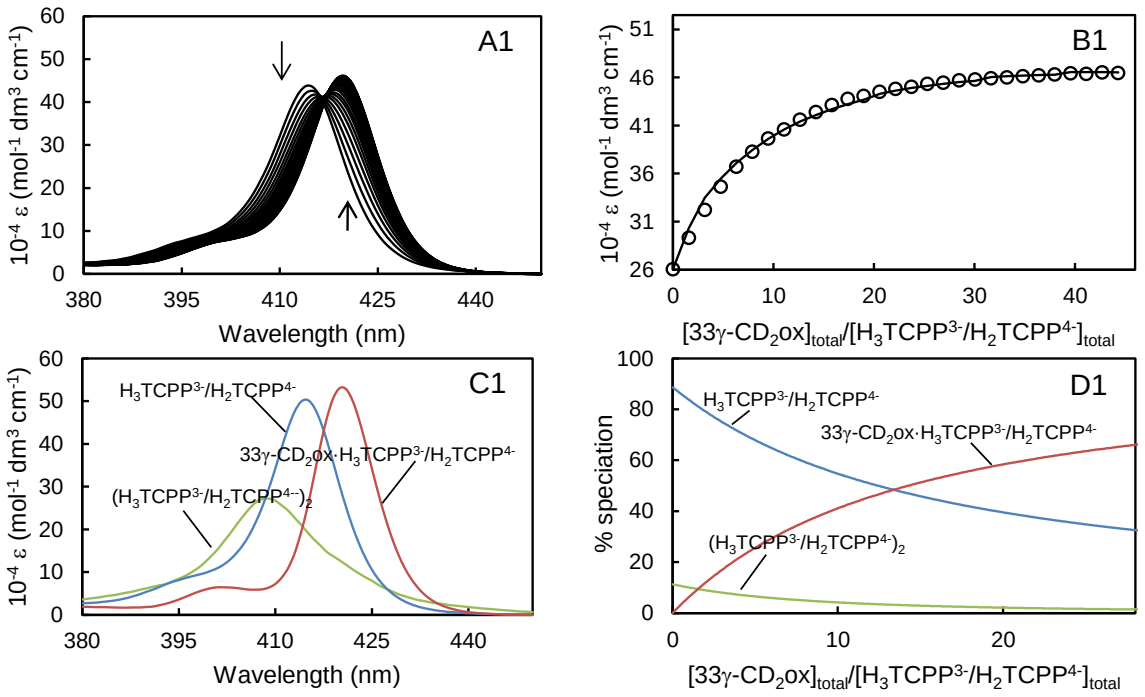

Figure A14: (A1) Molar absorbance change of $H_3TCPP^{3-}/H_2TCPP^{4-}$ (2.00×10^{-6} mol dm^{-3}) in phosphate buffer, pH 7.0, I = 0.10 mol dm^{-3} at 298.2 K with sequential injections (10 mm^3 each) of 33γ-CD_2ox (6.31×10^{-4} mol dm^{-3}) into both sample and reference cells. The arrows indicate the direction of molar absorbance change as the molar ratio of [33γ-CD_2ox]/[$H_3TCPP^{3-}/H_2TCPP^{4-}$] increases. (B1) Molar absorbance variation at 419 nm and the line of best fit of an algorithm for the monomer/dimer equilibrium and 1:1 host-guest complexation over the wavelength range 400-430 nm. (C1) Calculated molar absorbance of monomer, dimer and complexed $H_3TCPP^{3-}/H_2TCPP^{4-}$. (D1) Speciation with [$H_3TCPP^{3-}/H_2TCPP^{4-}$]$_{total}$ = 100%.

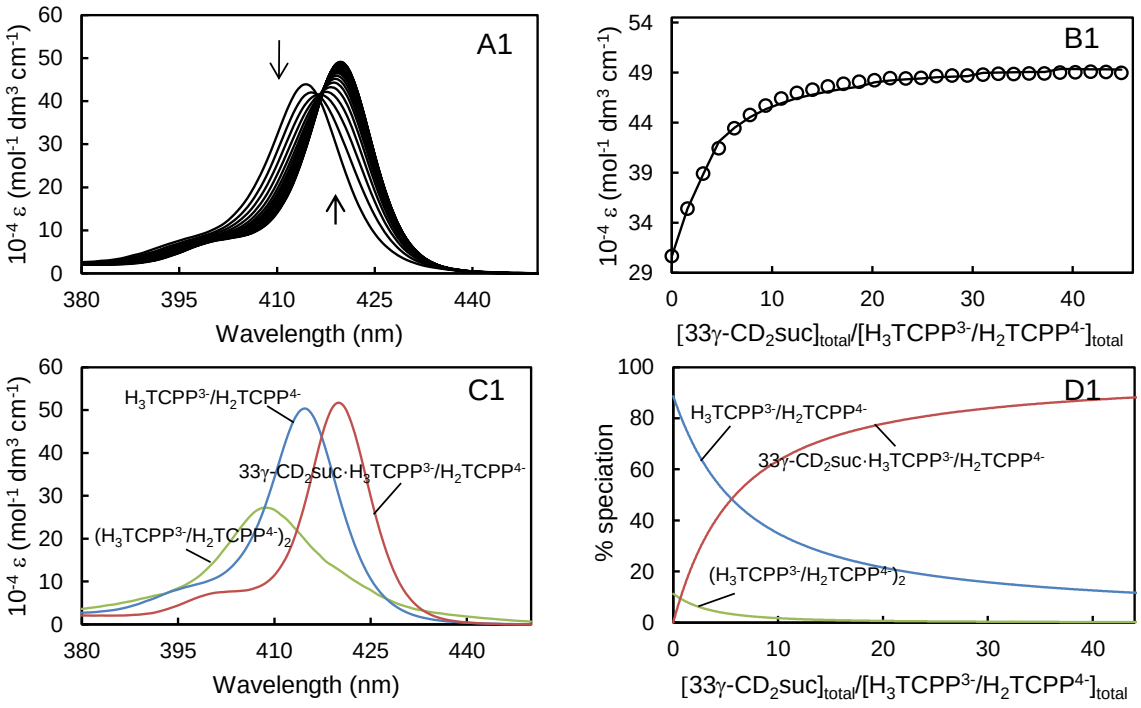

Figure A15: (A1) Molar absorbance change of $H_3TCPP^{3-}/H_2TCPP^{4-}$ (2.00×10^{-6} mol dm^{-3}) in phosphate buffer, pH 7.0, I = 0.10 mol dm^{-3} at 298.2 K with sequential injections (10 mm^3 each) of 33γ-CD_2suc (5.68×10^{-4} mol dm^{-3}) into both sample and reference cells. The arrows indicate the direction of molar absorbance change as the molar ratio of [33γ-CD_2suc]/[$H_3TCPP^{3-}/H_2TCPP^{4-}$] increases. (B1) Molar absorbance variation at 419 nm and the line of best fit of an algorithm for the monomer/dimer equilibrium and 1:1 host-guest complexation over the wavelength range 400-430 nm. (C1) Calculated molar absorbance of monomer, dimer and complexed $H_3TCPP^{3-}/H_2TCPP^{4-}$. (D1) Speciation with [$H_3TCPP^{3-}/H_2TCPP^{4-}$]$_{total}$ = 100%.

Molecular Modelling

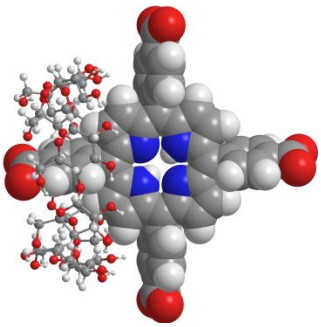

γ-CD.H_2TCPP^{4-} wide face

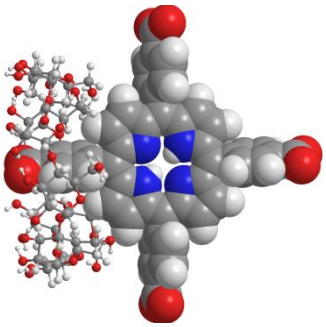

γ-CD.H_2TCPP^{4-} narrow face

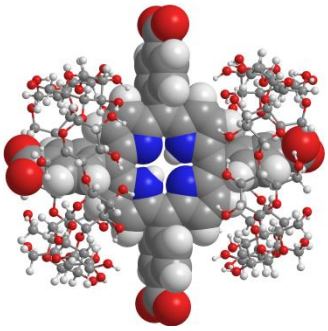

$(\gamma\text{-CD})_2.H_2TCPP^{4-}$ *anti*

two wide faces

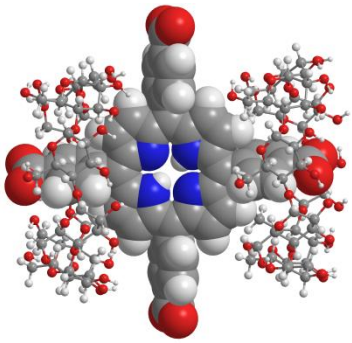

$(\gamma\text{-CD})_2.H_2TCPP^{4-}$ *anti*

one narrow and one wide face

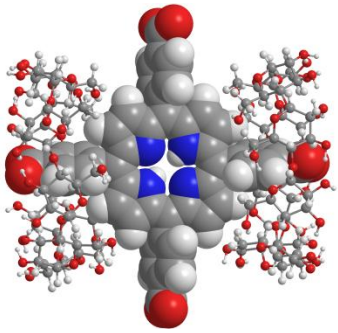

$(\gamma\text{-CD})_2.H_2TCPP^{4-}$ *anti*

two narrow faces

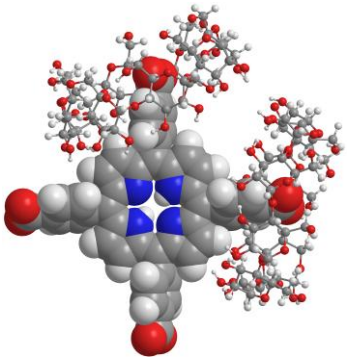

$(\gamma\text{-CD})_2.H_2TCPP^{4-}$ *syn*

two wide faces

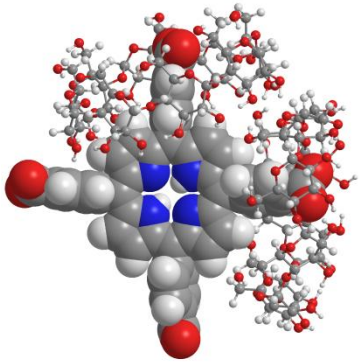

$(\gamma\text{-CD})_2.H_2TCPP^{4-}$ *syn*

one wide and one narrow face

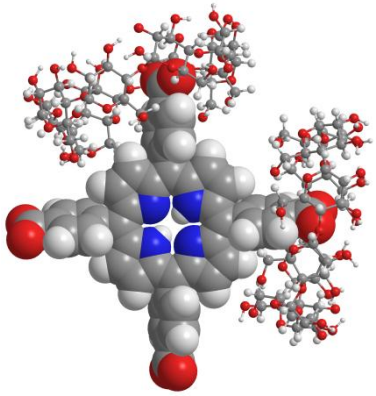

$(\gamma\text{-CD})_2.H_2TCPP^{4-}$ *syn*

two narrow faces

Figure A16: Energy minimised molecular models of the possible complexes involved in the γ-CD/H_2TCPP^{4-} equilibrium using the PM7 method. Note: γ-CD = ball and stick, H_2TCPP^{4-} = space filling. Carbon = grey, hydrogen = white, oxygen = red and nitrogen = blue.

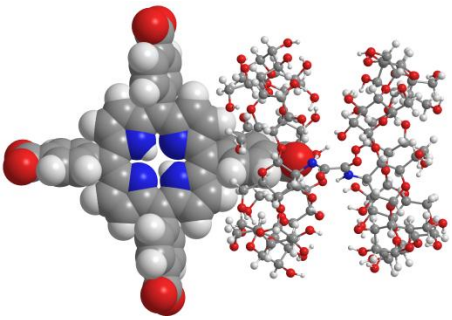

33γ-CD_2ox.H_2TCPP^{4-} non-cooperative
one narrow face

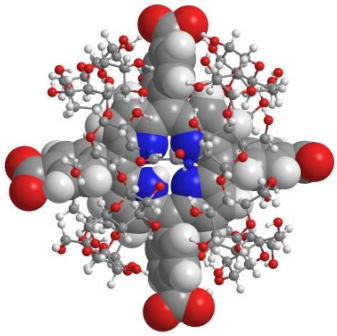

33γ-CD_2ox.H_2TCPP^{4-} *anti* cooperative
two wide faces

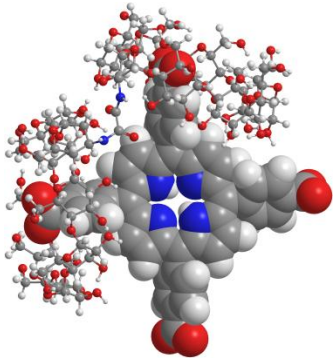

33γ-CD_2ox.H_2TCPP^{4-} *syn* cooperative
two wide faces

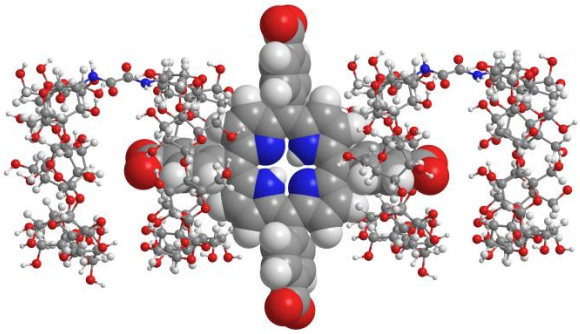

(33γ-CD_2ox)$_2$.H_2TCPP^{4-} non-cooperative
two narrow faces

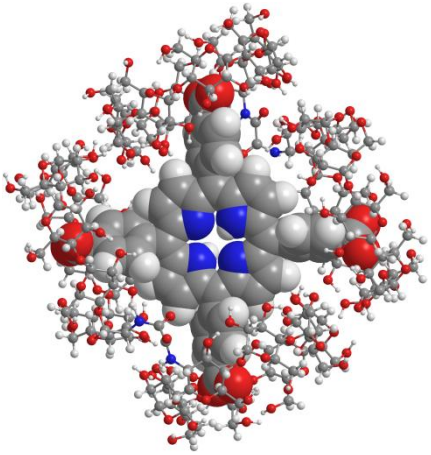

(33γ-CD_2ox)$_2$.H_2TCPP^{4-} cooperative
four wide faces

Figure A17: Energy minimised molecular models of the possible complexes involved in the (33γ-CD_2ox)$_2$.H_2TCPP^{4-}/(33γ-CD_2ox)$_2$.H_2TCPP^{4-}equilibrium using the PM7 method. Note: 33γ-CD_2ox = ball and stick, H_2TCPP^{4-} = space filling. Carbon = grey, hydrogen = white, oxygen = red and nitrogen = blue.

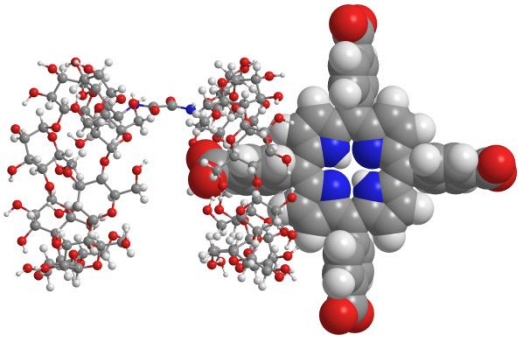

66γ-CD_2ox.H_2TCPP^{4-} non-cooperative

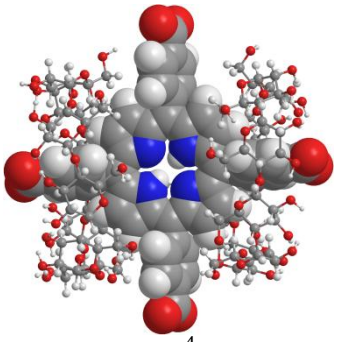

66γ-CD_2ox.H_2TCPP^{4-} *anti* cooperative

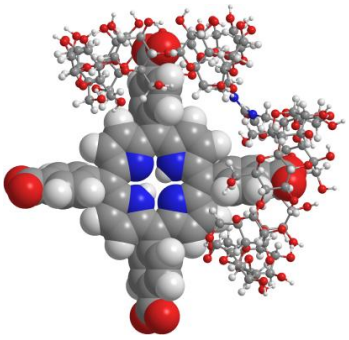

66γ-CD_2ox.H_2TCPP^{4-} *syn* cooperative

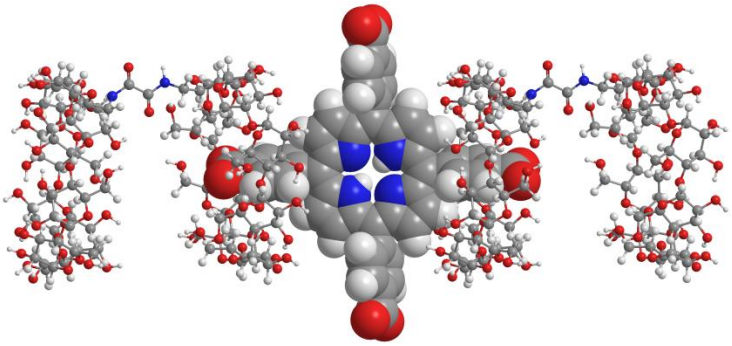

(66γ-CD_2ox)$_2$.H_2TCPP^{4-} non-cooperative
two wide faces

Figure A18: Energy minimised molecular models of the possible species involved in the 66γ-CD_2ox.H_2TCPP^{4-} equilibrium using the PM7 method. Note: 66γ-CD_2ox = ball and stick, H_2TCPP^{4-} = space filling. Carbon = grey, hydrogen = white, oxygen = red and nitrogen = blue.

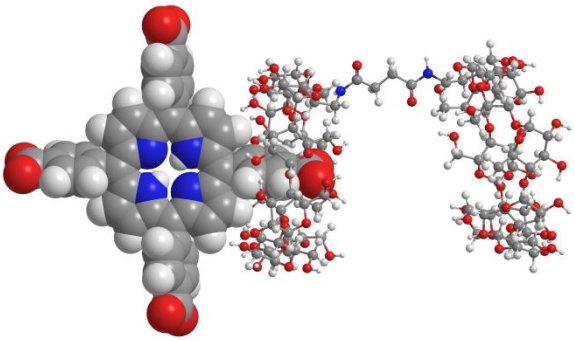

66γ-CD_2suc.H_2TCPP^{4-} non-cooperative complexation

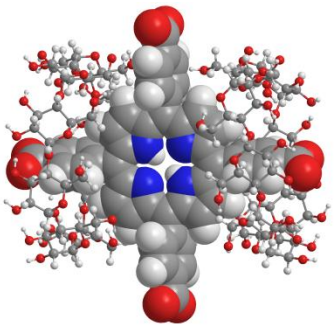

66γ-CD_2suc.H_2TCPP^{4-} *anti* cooperative

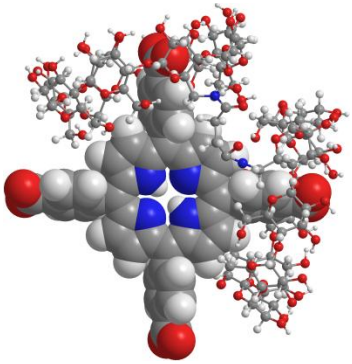

66γ-CD_2suc.H_2TCPP^{4-} *syn* cooperative

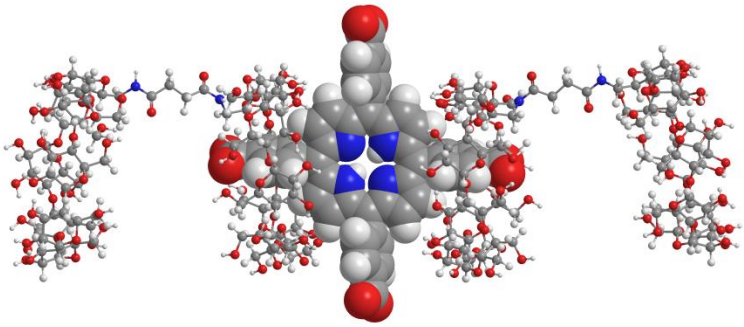

(66γ-CD_2suc)$_2$.H_2TCPP^{4-} non-cooperative
two wide faces

Figure A19: Energy minimised molecular models of the possible species involved in the 66γ-CD_2suc.H_2TCPP^{4-} equilibrium using the PM7 method. Note: 66γ-CD_2suc = ball and stick, H_2TCPP^{4-} = space filling. Carbon = grey, hydrogen = white, oxygen = red and nitrogen = blue.

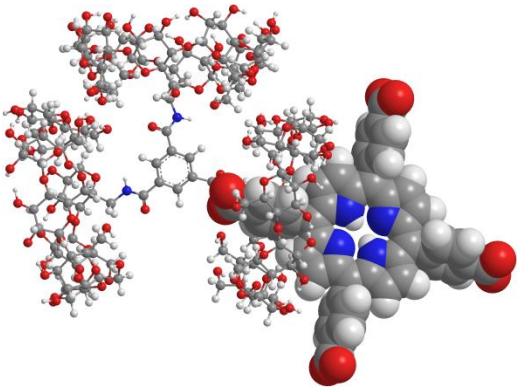

H_2TCPP^{4-}.666γ-CD_3bz non-cooperative

one narrow face

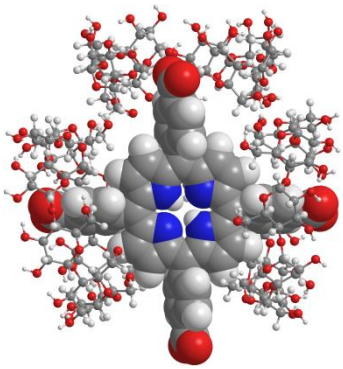

H_2TCPP^{4-}.666γ-CD_3bz cooperative
two narrow faces

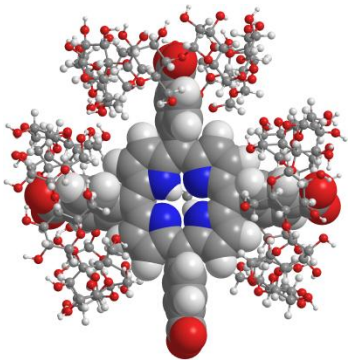

H_2TCPP^{4-}.666γ-CD_3bz cooperative 3 annuli
three narrow faces

Figure A20: Energy minimised molecular models of the possible species involved in the H_2TCPP^{4-}.666γ-CD_3bz equilibrium using the PM7 method. Note: 666γ-CD_3bz = ball and stick, H_2TCPP^{4-} = space filling. Carbon = grey, hydrogen = white, oxygen = red and nitrogen = blue.

Chapter 4

Host-Guest Networks of Linked γ-Cyclodextrin Oligomers and Porphyrin Substituted Poly(acrylate)

4.1 INTRODUCTION

4.1.1. General

Porphyrins are central to many biological processes and as a consequence of their aromatic character they absorb strongly in the UV-visible radiation range, have intense fluorescence emissions, coordinate a wide range of metal ions and are amenable to chemical modification. As a consequence they have been subject to considerable research, and a number of practical applications exemplified by DNA binding,[1] oxygen carrying,[2-4] light harvesting[5-9] and photodynamic therapy[10-14] have been studied. However, while porphyrins display many interesting characteristics, their low water solubility and bioavailability[15] places limits on their study. Although this problem may be addressed through the incorporation of polar substituents, porphyrins are excreted by the body relatively quickly as a consequence of their low molecular weight when judged on a biological scale.[16] This increases the effective dose needed in therapeutic porphyrin treatments, which may lead to undesirable side effects.

One possible solution to address this low porphyrin bioavailability is the use of native and modified cyclodextrins, sometimes referred to as "nanocarriers".[17-20] Porphyrins are solubilised through complexation in cyclodextrin hydrophobic annuli such that their bloodstream concentration and bioavailability is usually increased. In Chapter 2 it was determined that γ-cyclodextrin, γ-CD, and linked γ-CD oligomers were suitable hosts for 5,10,15,20-tetra(*p*-sulfonatophenyl)porphyrinate, H_2TSPP^{4-}, guests with the complexation constants of the di- and tritopic complexes formed by γ-CD oligomers being greater than the monotopic complexes formed by γ-CD. This coincides with the observations by others that cyclodextrin dimers complex porphyrins more strongly than cyclodextrin monomers.[21,22] Another method of increasing porphyrin bioavailability is their incorporation into water soluble polymers. This allows porphyrins to circulate longer *in vivo* and facilitates novel

medical treatments.[16,23,24] Furthermore, some water-soluble polymers, such as poly(acrylate) (PAA) are known to form hydrogels, and this process has previously been controlled with the addition of cyclodextrin oligomers,[25-27] and in principle they may be adapted as porphyrin delivery systems. The complexation of 5-(4-β-alanylaminophenyl)-10,15,20-tris(4-sulfonatophenyl) porphinatoiron(III) substituted poly(acrylate)s by a per-*O*-methylated β-CD dimer with a pyridine linker have been reported previously as artificial substitutes for haemoglobin.[16] The authors suggested the possibility of the formation of intra-strand or inter-strand polymer crosslinks by the complexation of two porphyrin substituents of the substituted poly(acrylate) by the β-CD dimer; however, this concept was not further explored. To the best of our knowledge, the thermodynamic parameters of host-guest complexation of porphyrin substituted poly(acrylate)s by cyclodextrin dimers and the effect of host-guest complexation at the macroscopic level are unknown. Investigating these systems in detail could potentially lead to the development of materials that combine the therapeutic properties porphyrins with the hydrogelation properties of water-soluble polymers.

4.1.2. Aims of this study

The aims of this study are to extend understanding of the factors controlling the formation of supramolecular assemblies in aqueous solutions through the interactions of a porphyrin substituted PAA and γ-CD or linked γ-CD oligomers. Accordingly, this study involves the preparation of 3% randomly substituted sodium 5-(*p*-β-alanylaminophenyl)-10,15,20-tris(*p*-sulfonatophenyl)-porphyrin poly(acrylate) (PAATSPPala*, Figure 4.1) as well as five linked γ-CD oligomers (33γ-CD_2ox, 33γ-CD_2suc, 66γ-CD_2ox, 66γ-CD_2suc and 666γ-CD_3bz, Figure 3.1). (*The two NH hydrogens and the 3- charge of the porphyrin have been omitted to simplify the condensed name.)

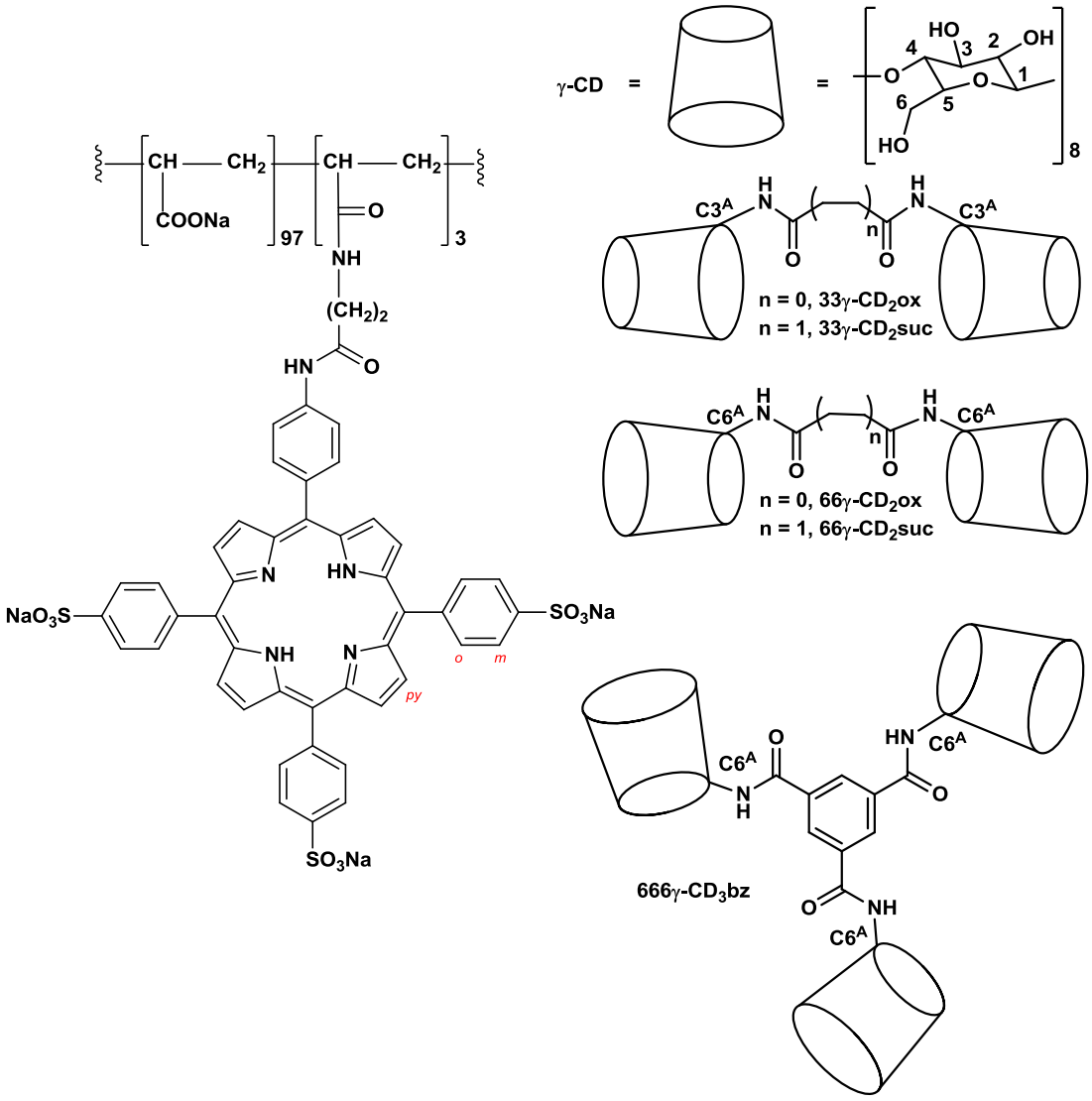

Figure 4.1: γ-Cyclodextrin, γ-CD, and its linked oligomers 33γ-CD_2ox, 33γ-CD_2suc, 66γ-CD_2ox, 66γ-CD_2suc and 666γ-CD_3bz and the sodium salt of 3% randomly substituted 5-(*p*-β-alanylaminophenyl)-10,15,20-tris(*p*-sulfonatophenyl)-porphyrin substituted poly(acrylate), PAATSPPala.

The host-guest complexation of the porphyrin substituents, TSPPala, of PAATSPPala by the cyclodextrin hosts, γ-CD and its linked oligomers, 33γ-CD_2ox, 33γ-CD_2suc, 66γ-CD_2ox, 66γ-CD_2suc and 666γ-CD_3bz is investigated at the molecular level by 2D ^{1}H NOESY NMR and UV-vis spectroscopy and at the macroscopic level by rheology. These experiments are designed to provide insight into the formation of cyclodextrin oligomer-porphyrin substituted poly(acrylate) host-guest complexes at the molecular and macroscopic levels (Figure 4.2).

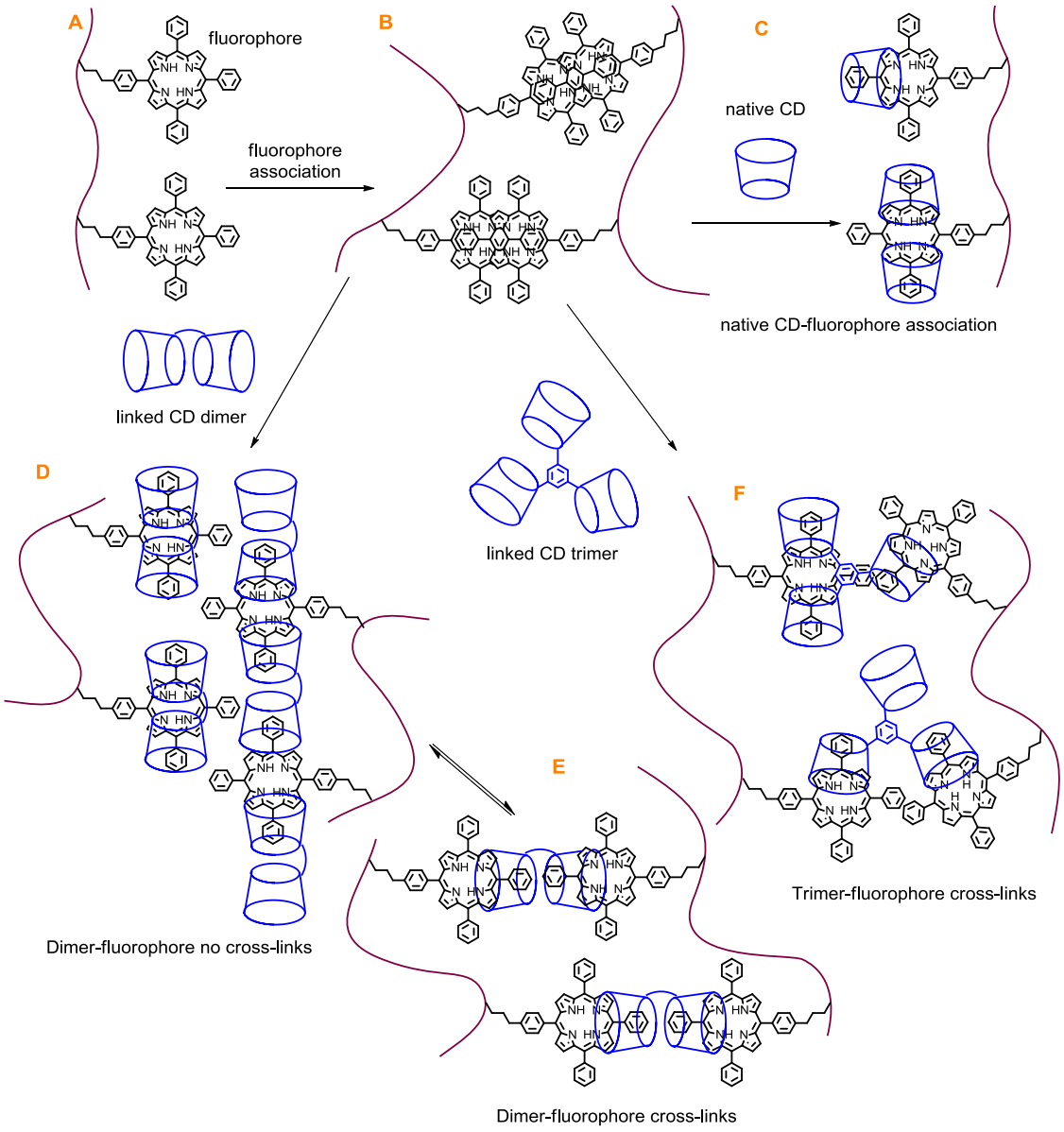

Figure 4.2: Schematic of potential aggregation interactions of PAATSPPala alone (A and B) and host-guest complexation with γ-CD (C) and linked γ-CD dimers (D and E) and a linked γ-CD trimer (F) (The SO_3^- groups have been omitted for clarity.).

4.2 SYNTHESIS

4.2.1. Preparation of 3% 5-(*p*-β-alanylaminophenyl)-10,15,20-tris(*p*-sulfonatophenyl)-porphyrin randomly substituted poly(acrylate)

5-(*p*-Aminophenyl)-10,15,20-tris(*p*-sulfonatophenyl)-porphyrin[29] (Figure 4.3 A) was substituted with boc-β-alanine using 1-ethyl-3-(3-dimethylaminopropyl)carbodiimide (EDC) and 4-dimethylaminopyridine (DMAP) to give 5-(*p*-boc-β-alanylaminophenyl)-10,15,20-tris(*p*-sulfonatophenyl)-porphyrin (Figure 4.3 B) with a 69 % yield.[16] This compound was then deprotected using trifluoroacetic acid (TFA) to afford 5-(*p*-β-alanylaminophenyl)-10,15,20-tris(*p*-sulfonatophenyl)-porphyrin (Figure 4.3 C) with a 95 % yield.[16] The final porphyrin was then randomly substituted onto PAA through amide coupling using EDC and DMAP. The reaction mixture was diluted with 40 wt% aqueous sodium hydroxide and was then reprecipitated in methanol (multiple times). The solid product was purified by dialysis and the final dry product, 3% randomly substituted 5-(*p*-β-alanylaminophenyl)-10,15,20-tris(*p*-sulfonatophenyl)-porphyrin substituted poly(acrylate) (PAATSPPala, Figure 4.3 D), was obtained as the sodium salt in a 90 % yield. The degree of substitution was determined to be 3.0 ± 0.3 % by ^{1}H NMR spectroscopy according to the literature method.[30]

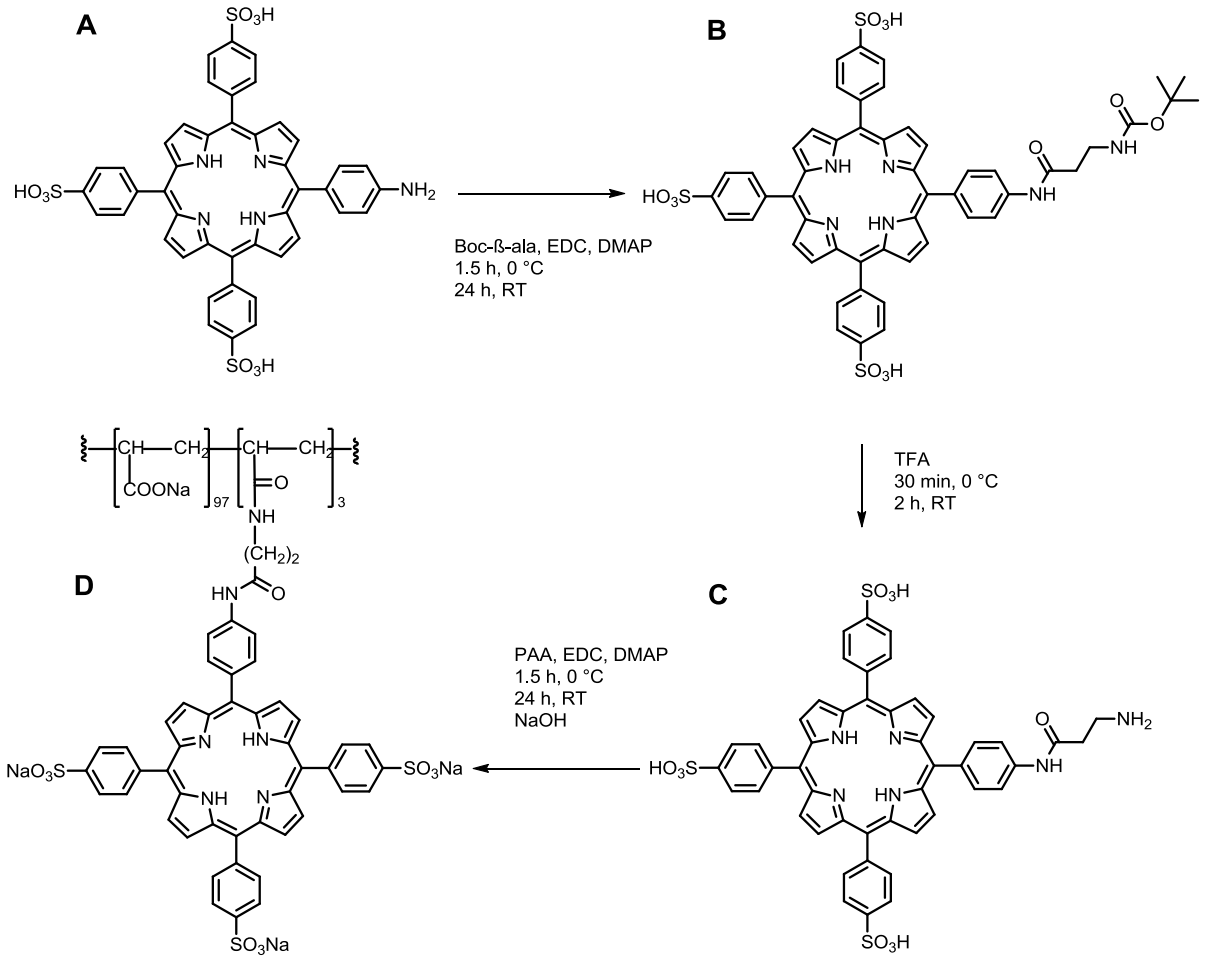

Figure 4.3: Synthetic scheme for the preparation of 3 % randomly substituted PAATSPPala.

4.2.2. Preparation of Cyclodextrin Oligomers

The cyclodextrins oligomers discussed in this chapter were prepared as described in Section 2.2 of Chapter 2 and in the literature.[25,31] The oligomers were characterised by TLC, ^{1}H NMR, ^{13}C NMR, MS and elemental analysis (See Chapter 6).

4.3. 2D NOESY ^{1}H NMR STUDIES

The porphyrin ^{1}H NMR resonances of TSPPala in D_2O at 298.2 K (Figure 4.4) are significantly broadened when compared with those of free H_2TSPP^{4-} (Figure 2.5 of Chapter 2). This is a consequence of exchange at the intermediate rates on the NMR timescale between magnetic environments within the porphyrin as it moves with respect to the attached

PAA backbone. This has been previously observed for similarly porphyrin substituted poly(acrylate)s,[16] where the two broad resonances of the aromatic region and were assigned to the pyrrolic and phenyl hydrogens of the porphyrin substituent, respectively. Accordingly, the porphyrin proton resonances in this study were assigned to the pyrrolic (H_{py}) and *meta* and *ortho* phenyl (H_{m+o}) hydrogens, respectively (Figure 4.4).

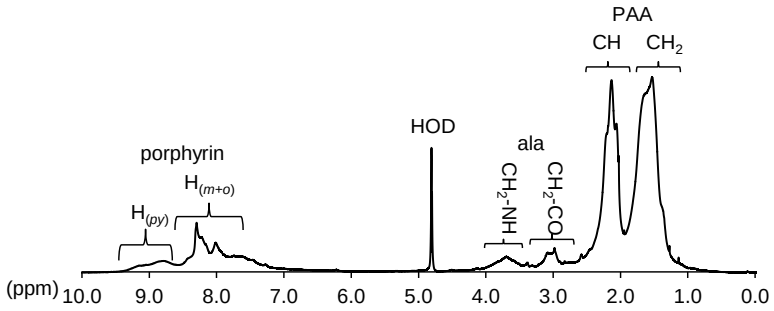

Figure 4.4: ^{1}H NMR (500 MHz) spectrum of a PAATSPPala ([TSPPala] = 3.0×10^{-3} mol dm^{-3}) in D_2O (pD 7.0 phosphate buffer, I = 0.10 mol dm^{-3}) at 298.2 K.

At the PAATSPPala concentrations used in the present ^{1}H NMR studies ([porphyrin substituent] = 3.0×10^{-3} mol dm^{-3} in D_2O) collisions between PAATSPPala strands are likely to be frequent enough such that the porphyrin substituents of PAATSPPala aggregate as seen with H_2TSPP^{4-} in Figure 2.5 of Chapter 2 and in the literature.[32,33] However, this aggregation is expected to be hindered by the attachment of the porphyrin substituents to the poly(acrylate) backbone and is difficult to observe through ^{1}H NMR spectroscopy due to the broadening of the porphyrin proton resonances. (The possibility of porphyrin substituent aggregation is explored further in the following sections.)

The host–guest interactions between TSPPala with γ-CD and its oxalate or succinamide-linked dimers and benzene-linked trimer, 33γ-CD_2ox, 33γ-CD_2suc, 66γ-CD_2ox, 66γ-CD_2suc and 666γ-CD_3bz, respectively, were studied using 2D ^{1}H NOESY NMR

spectroscopy. The 2D ^{1}H NOESY NMR spectra for PAATSPPala D_2O solutions with γ-CD and 666γ-CD_3bz are shown in Figure 4.5, and the analogous spectra for the γ-CD dimer systems are shown in Figures A1-A4 of the Appendix.

Complexation with the TSPPala porphyrin substituents of PAATSPPala causes a shift and broadening in the proton resonances of γ-CD which makes the assignment of the individual protons (H_{2-6}) uncertain. For the oligomer systems, monosubstitution of the γ-CD subunits in the oligomers causes their glucopyranose subunits to be both chemically and magnetically inequivalent also. Accordingly, the γ-CD H_{2-6} proton resonances of the oligomers increase in number and are significantly broadened compared with those of γ-CD alone in D_2O,[34] such that it is difficult to assign the individual resonances.

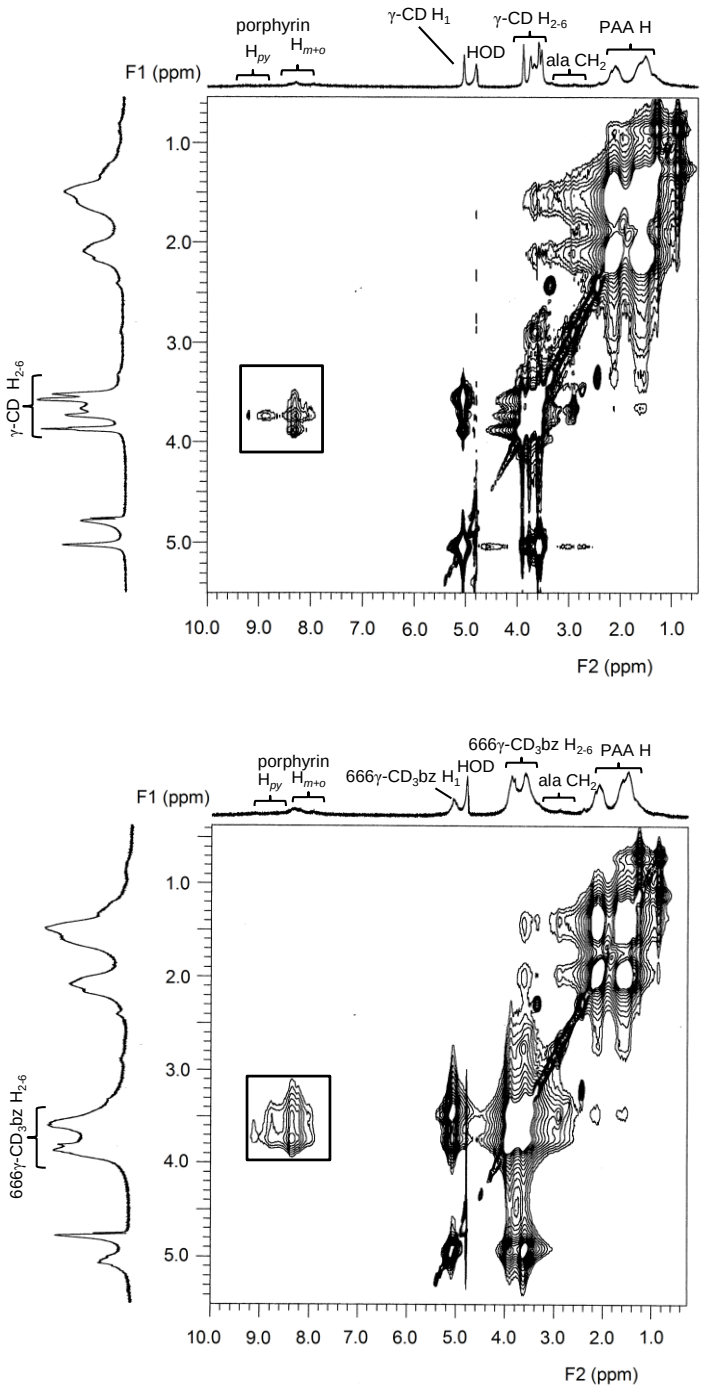

Figure 4.5: 2D ^{1}H NOESY NMR (600 MHz) spectrum of 3% randomly substituted PAATSPPala ([TSPPala] = 3.0×10^{-3} mol dm^{-3}) and equimolar γ-CD (top) and 666γ-CD_3bz (bottom) in D_2O (pD 7.0 phosphate buffer, I = 0.10 mol dm^{-3}) at 298.2 K with a mixing time of 300 ms. Cross–peaks enclosed in the rectangle arise from interaction between the annular γ-CD protons $H_{3,5,6}$ of the cyclodextrin annulus and the pyrrolic (H_{py}) and phenyl protons (H_{m+o}) of the porphyrin substituent. Note: The broadened phenyl proton resonances of 666γ-CD_3bz (8.4 ppm) overlap with the broadened phenyl proton resonances of PAATSPPala and consequently could not be labelled on the 1D ^{1}H NMR spectrum.

Previous studies have shown that porphyrin-cyclodextrin interactions occur with the internal protons ($H_{3,5,6}$) of the γ-CD annulus as seen in Section 2.3 of Chapter 2 and in literature studies.[32,35] Accordingly, strong cross-peaks arising from nuclear Overhauser effects (NOE) between H_{m+o} of the porphyrin substituents of PAATSPPala and the $H_{3,5,6}$ annular protons of γ-CD and its linked oligomers occur in the spectra of all of the systems (Figure 4.5 and Figures A1-A4 of the Appendix). This observation is consistent with the *p*-sulfonatophenyl groups of the porphyrin substituents, TSPPala, complexing as guests within the annuli of γ-CD and linked γ-CD oligomer hosts. As for H_2TSPP^{4-}, the width of the *p*-sulfonatophenyl groups (~470 pm) of PAATSPPala are of a suitable size to complex within the narrow (750 pm in diameter)[36] and wide (830 pm in diameter)[36] face of the annuli of γ-CD and the linked γ-CD oligomer hosts (with a depth of 790 pm).[36] In addition, less prominent cross–peaks arise from interactions between H_{py} of the porphyrin substituents and the $H_{3,5,6}$ annular protons of γ-CD and its linked CD oligomers. These cross-peaks were more evident in the γ-CD oligomer systems (as exemplified by 666γ-CD_3bz, Figure 4.5 bottom), suggesting that the cyclodextrin annuli are closer to the pyrrolic hydrogens in these systems compared with native γ-CD. Furthermore, cross-peaks between porphyrin substituents and the $H_{3,5,6}$ annular protons of the γ-CD subunits were more prominent in the 6,6- linked dimer and 6,6,6- linked trimer systems than the 3,3- linked dimer systems. This suggests "tighter" complexation in these systems which is further supported by the larger K_{11} complexation constants obtained for the 6,6- linked dimer and 6,6,6- linked trimer systems than the 3,3-linked dimer systems (discussed in detail in the next section). Although the 2D ^{1}H NOESY NMR data are consistent with host-guest complexation occurring between γ-CD and the γ-CD oligomers and the porphyrin substituents (TSPPala) of PAATSPPala, they do not identify their stoichiometry. Spectral broadening of the TSPPala, γ-CD and linked γ-CD oligomer resonances makes any further deductions about the orientation of host-guest

complexation difficult. Studies in which the concentrations of the host and guest are systematically varied would be difficult to interpret quantitatively. Therefore, UV-vis spectroscopic studies were undertaken to determine the stoichiometry of host-guest complexation and the stability of the host-guest complexes formed, as is considered in detail below.

4.4. UV-VIS SPECTROSCOPIC STUDIES

4.4.1. Porphyrin Substituent Dimerisation

It has been previously determined that native H_2TSPP^{4-} can dimerise at high concentrations in aqueous solutions.[33] In Chapter 2 (Figure 2.9) it was observed that a slight change in the intensity of the absorbance maxima of a 1.05×10^{-6} mol^{-1} dm^{-3} solution of H_2TSPP^{4-} in aqueous phosphate buffer at pH 7.0 and I = 0.10 mol dm^{-3} at 413 nm from 4.15×10^5 to 4.02×10^5 mol^{-1} dm^{-3} occurred between the temperature extremes and this was attributed to a small amount of dimerisation (< 4 % of the of the total H_2TSPP^{4-} concentration). Steric hindrance associated with attachment to the poly(acrylate) backbone is expected to decrease the extent of porphyrin aggregation. However, it has been previously reported that aromatic chromophores attached to the poly(acrylate) backbone can interact with each other at high concentrations in aqueous solutions.[16,27]

An indication of the effect of temperature on the monomer/dimer equilibrium of the porphyrin substituents attached to the PAA backbone in the temperature range 308.2 K to 278.2 K was gained by determining the UV-vis absorption spectrum of an aqueous solution of PAATSPPala 3.10×10^{-6} mol dm^{-3} in porphyrin substituents, TSPPala, at four temperatures as shown in Figure 4.6. It is seen that there is a slight decrease in molar absorbance at 412 nm from 2.01×10^5 to 1.94×10^5 mol^{-1} dm^{-3} between the temperature extremes and a corresponding change in absorbance maximum, λ_{max}, of 412 nm to 411 nm.

This small change is consistent with a temperature dependence of a porphyrin substituent monomer/dimer equilibrium. Therefore, at a ~3-fold higher concentration than the H_2TSPP^{4-} dimerisation experiments in Chapter 2, a similar change in the absorbance maxima (< 4 %) is observed for the porphyrin substituents of PAATSPPala. However, porphyrin substituent, TSPPala, dimerisation, or possibly higher aggregation, in PAATSPPala involves porphyrin *substituents* attached to the poly(acrylate) backbone most probably on a single strand at the PAATSPPala concentration of the UV-Vis studies. As with H_2TSPP^{4-}, this small amount of dimerisation is unlikely to significantly impinge on the determination of thermodynamic data for the host-guest complexation of TSPPala by γ-CD and its oligomers. However, this evidence for TSPPala aggregation in PAATSPPala assumes greater importance at the greater concentrations of the rheological studies discussed in Section 4. 5.

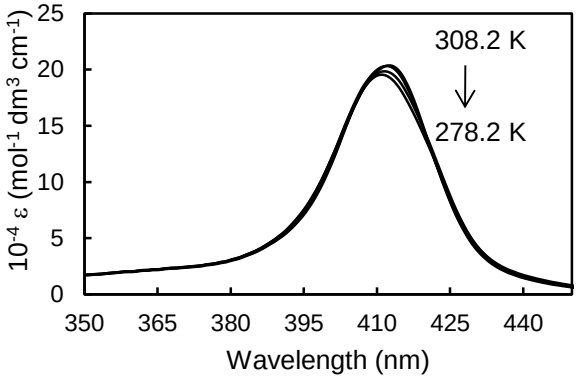

Figure 4.6: Temperature dependence of the molar absorbance of PAATSPPala (3.10×10^{-6} mol dm^{-3} in TSPPala) in phosphate buffer, pH 7.0, I = 0.10 mol dm^{-3}.

4.4.2. Equilibria

The study of the host-guest equilibria by UV-vis spectroscopy and the protocol for fitting the algorithms describing the equilibria to the changes in absorbance followed methods similar to those previously reported.[37] The model used to determine the host-guest complexation constants assumes that labile equilibria exist such that the concentrations of free porphyrin

substituents in PAATSPPala (TSPPala) and that complexed by either γ-CD or its linked oligomers 33γ-CD_2ox, 33γ-CD_2suc, 66γ-CD_2ox, 66γ-CD_2suc and 666γ-CD_3bz in the formation of 1:1, and possibly 2:1, host-guest complexes very rapidly adjust as the UV-vis titrations proceed. Thus, the 1:1 and 2:1 host-guest γ-CD complexes with the porphyrin substituents (TSPPala) form according to Equations 4.1 and 4.2:

$$\gamma\text{-CD} + \text{TSPPala} \overset{K_{11}}{\rightleftharpoons} \gamma\text{-CD.TSPPala} \quad (\mathbf{4.1})$$

$$\gamma\text{-CD} + \gamma\text{-CD.TSPPala} \overset{K_{21}}{\rightleftharpoons} (\gamma\text{-CD})_2\text{.TSPPala} \quad (\mathbf{4.2})$$

The complexation constants K_{11} and K_{21}, at equilibrium are given by

$$K_{11} = [\gamma\text{-CD.TSPPala}]/ [\gamma\text{-CD}][\text{TSPPala}] \quad (\mathbf{4.3})$$

$$K_{21} = [(\gamma\text{-CD})_2\text{.TSPPala}]/ ([\gamma\text{-CD.TSPPala}][\gamma\text{-CD}]) \quad (\mathbf{4.4})$$

Given that $[\text{TSPPala}]_{total}$ and $[\gamma\text{-CD}]_{total}$ are the initial concentrations of the two complexation partners:

$$[\text{TSPPala}]_{total} = [\text{TSPPala}] + [\gamma\text{-CD.TSPPala}] + [(\gamma\text{-CD})_2\text{.TSPPala}] \quad (\mathbf{4.5})$$

It follows that:

$$[\gamma\text{-CD}]_{total} = [\gamma\text{-CD}] + [\ \gamma\text{-CD.TSPPala}] + [(\gamma\text{-CD})_2\text{.TSPPala}] \quad (\mathbf{4.6})$$

The absorbance at a particular wavelength is given by Equation 4.7 when only a 1:1 complex forms, and by Equation 4.8 when both 1:1 and 2:1 complexes form. In Equations 4.7 and 4.8 $A(\lambda)$, ε_1, ε_{11} and ε_{21} represent the observed absorbance and apparent molar absorbances of TSPPala, γ-CD.TSPPala and $(\gamma\text{-CD})_2$.TSPPala respectively. The values of K_{11} and K_{21} are determined by best-fitting the algorithm for either Equation 4.7 or 4.8 to the PAATSPPala absorbance data in the range 380-430 nm at 0.25 nm intervals as the γ-CD concentration is increased using the HypSpec protocol. [38] The same protocol is used for the other five systems.

$$A(\lambda) = \varepsilon_1[\text{TSPPala}] + \varepsilon_{11}[\gamma\text{-CD.TSPPala}] \quad (\mathbf{4.7})$$

$$A(\lambda) = \varepsilon_1[\text{TSPPala}] + \varepsilon_{11}[\gamma\text{-CD.TSPPala}] + \varepsilon_{21}[(\gamma\text{-CD})_2.\ \text{TSPPala}] \quad \textbf{(4.8)}$$

4.4.3. UV-Vis Titration Studies

The experimental details of the UV-vis spectroscopic characterisation of the equilibria in which γ-CD and its oligomers complex TSPPala are now described. The UV-vis spectra of solutions were determined against reference solutions in matched 1 cm quartz cells and were recorded at 0.25 nm intervals using a Cary 5000 UV-Vis spectrophotometer over the range of 250-650 nm. The solutions were freshly prepared in aqueous phosphate buffer at pH 7.0 and I = 0.10 mol dm^{-3}. Samples were 2.0 cm^3 in volume and were thermostatted at 278.2, 288.2, 298.2 and 308.2 K for 30 min before starting the titration. The PAATSPPala solutions were 3.10×10^{-6} mol dm^{-3} in [TSPPala] and were titrated using sequential injections (10 mm^3 each into both sample and reference cells unless stated otherwise) of either γ-CD (1.01×10^{-2} mol dm^{-3}), 33γ-CD_2ox (2.65×10^{-3} mol dm^{-3}), 33γ-CD_2suc (1.24×10^{-3} mol dm^{-3}), 66γ-CD_2ox (2.52×10^{-4} mol dm^{-3}), 66γ-CD_2suc (1.21×10^{-4} mol dm^{-3}) and 666γ-CD_3bz (6.57×10^{-5} mol dm^{-3}) also in aqueous phosphate buffer at pH 7.0 and I = 0.10 mol dm^{-3}.

The molar absorbance changes of PAATSPPala solutions with increasing concentrations of 33γ-CD_2ox, 66γ-CD_2ox and 666γ-CD_3bz and the best fits of algorithms describing the complexation processes at 298.2 K are shown in Figure 4.7. All of the variable temperature UV-vis titrations, derived spectra and speciation plots for all γ-CD and γ-CD oligomer host-guest systems are shown in Figures A5–A26 of the Appendix.

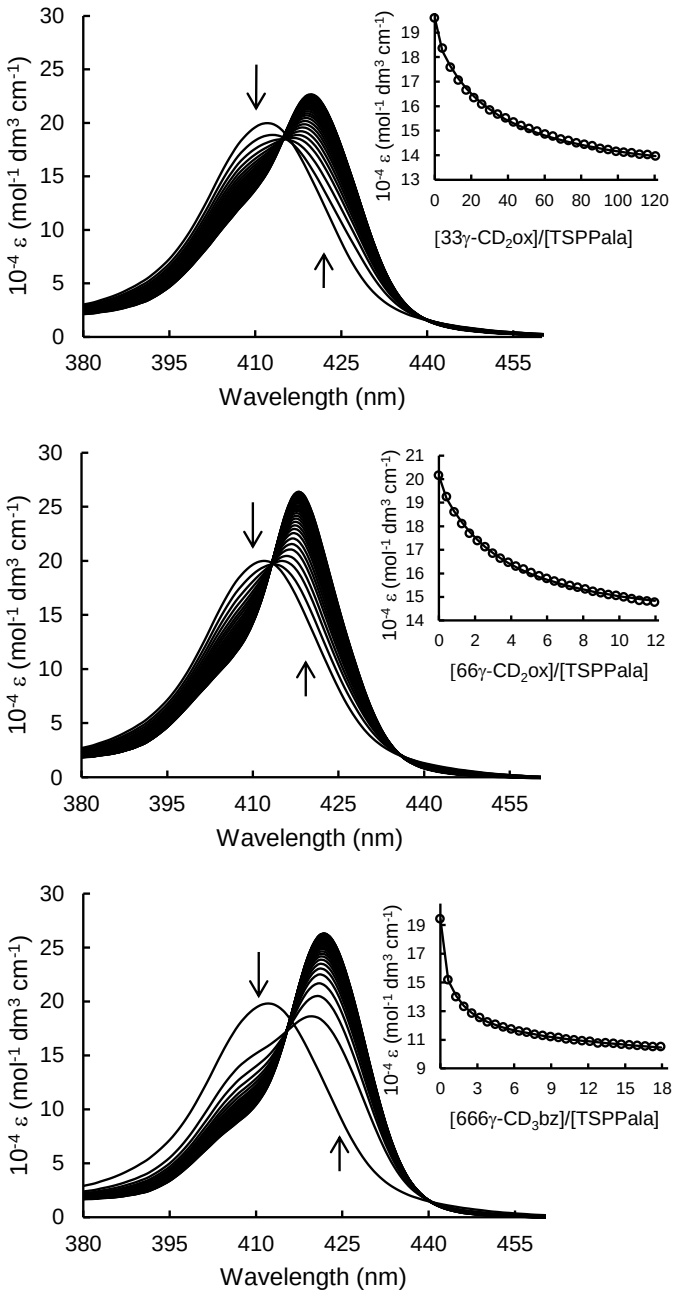

Figure 4.7: Molar absorbance change of the porphyrin substituents of PAATSPPala ([TSPPala] = 3.10×10^{-6} mol dm^{-3}) in phosphate buffer, pH 7.0, I = 0.10 mol dm^{-3} at 298.2 K with sequential injections (10 mm^3 each for 33γ-CD_2ox and 66γ-CD_2ox and 6 mm^3 for 666γ-CD_3bz) of 33γ-CD_2ox (top, 2.65×10^{-3} mol dm^{-3}), 66γ-CD_2ox (middle, 2.52×10^{-4} mol dm^{-3}) 666γ-CD_3bz (bottom, 6.57×10^{-4} mol dm^{-3}) into both sample and reference cells. The arrows indicate the direction of molar absorbance change as the molar ratio of $[host]_{total}/[TSPPala]_{total}$ increases. Inset: Molar absorbance variation at 410 nm and the line of best fit of an algorithm for 1:1 or 1:1 and 2:1 host-guest complexation over the wavelength range 380-430 nm.

A decrease in absorption at the λ_{max} of 412 nm of PAATSPPala is observed for all six systems with the progressive increase of host-guest complex concentration with increase of the total host concentration. Simultaneously, the red-shifted spectra of the TSPPala complexes of γ-CD, the four γ-CD dimers and the 666γ-CD_3bz trimer increase and their λ_{max} changed from 412 nm characterising free TSPPala to 416 nm with native γ-CD, 418 nm with 66γ-CD_2ox, 419 nm with 66γ-CD_2suc, 420 nm with both 33γ-CD_2ox and 33γ-CD_2ox and 422 nm with 666γ-CD_3bz. These red shifts are consistent with TSPPala experiencing a change in polarity of the local environment as it enters the hydrophobic γ-CD annulus upon formation of host-guest (similar to free H_2TSPP^{4-} in Figure 2.10 of Chapter 2 and previous studies).[15] The increase in the magnitude of this red-shift in the 33γ-CD_2ox/PAATSPPala, 66γ-CD_2ox/PAATSPPala, 33γ-CD_2suc/PAATSPPala and 66γ-CD_2suc/PAATSPPala systems by comparison with that of the γ-CD/PAATSPPala system is consistent with a cooperative complexation effect where two γ-CD annuli complex TSPPala simultaneously. This trend is also exemplified by a further increase in the red shift for the 666γ-CD_3bz/PAATSPPala system, which could be an indication of tritopic cooperative complexation of the TSPPala substituents of PAATSPPala by three γ-CD annuli.

The K_{11} complexation constants of all the oligomer systems are given in Table 4.1 and are plotted in Figure 4.8 from which it is seen that those characterising the γ-CD oligomer systems were between 19 - 307-fold larger than that of the native γ-CD system at 298.2 K. This consistent with a strong cooperative effect existing for complexation in the oligomer systems. The complexation constants, K_{11}, increase in the order γ-CD < 33γ-CD_2ox < 33γ-CD_2suc < 66γ-CD_2suc < 66γ-CD_2ox < 666γ-CD_3bz at 298.2 K. Similar to H_2TSPP^{4-} (Table 2.1 of Chapter 2), the narrow primary-hydroxyl face is favoured for entrance of the porphyrin substituents into the γ-CD annulus, as indicated by the larger K_{11} complexation constants for the 6,6- dimers and 6,6,6- trimer by comparison with those of the 3,3- dimers. This is

consistent with the porphyrin *p*-sulfonatophenyl rings being dominant factors in forming host-guest complexes. The *p*-sulfonatophenyl rings have widths of ~470 pm which compare with primary- and secondary hydroxyl γ-CD face widths of 750 and 830 pm (and depth of 790 pm), respectively,[36] and as consequence the smaller primary hydroxyl face more closely fits the *p*-sulfonatophenyl rings to form more stable host-guest complexes. This is in accord with the appearance of cross-peaks between the *p*-sulfonatophenyl protons and the γ-CD annular protons in the 2D NOESY ^{1}H NMR spectra (Figure 4.5 and Figures A1 – A4 of the Appendix).

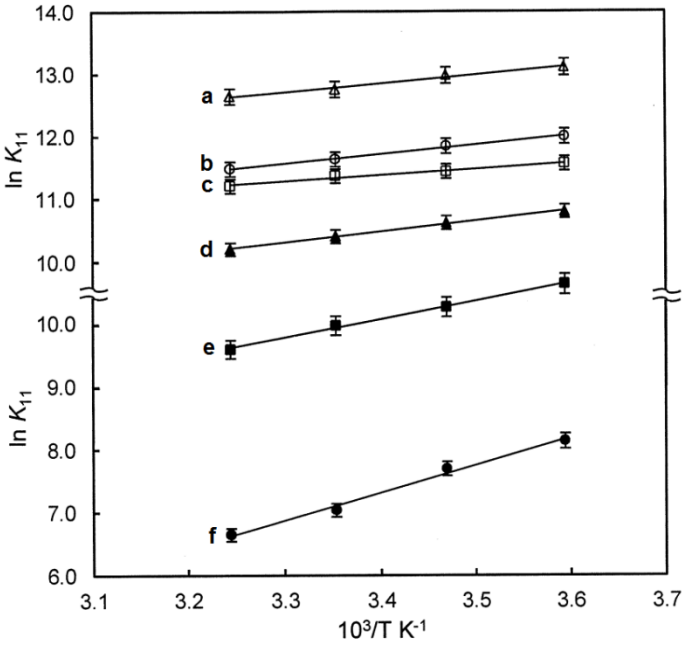

Figure 4.8: Plot of lnK_{11} determined by UV-Vis absorption spectroscopy at various temperatures against $10^3/T$ for the complexation of TSPPala by 666γ-CD_3bz (**a**, R^2 = 0.9826), 66γ-CD_2ox (**b**, R^2 = 0.9947), 66γ-CD_2suc (**c**, R^2 = 0.9875), 33γ-CD_2suc (**d**, R^2 = 0.9961), 33γ-CD_2ox (**e**, R^2 = 0.9965) and γ-CD (**f**, R^2 = 0.9907). Solid lines represent best fit of the van't Hoff equation to the K_{11} data. Note: y-axis is split to avoid overlapping data sets.

Table 4.1: Complexation constants K_{11} and thermodynamic parameters for the complexation of TSPPala by γ-CD, 33γ-CD_2ox, 33γ-CD_2suc, 66γ-CD_2ox, 66γ-CD_2suc and 666γ-CD_3bz at different temperatures by UV-Vis titrations in aqueous phosphate buffer at pH 7.0 and I = 0.10 mol dm^{-3}.[a]

Host	T (K)	K_{11} (10^{-3} × dm^3 mol^{-1})	ΔH_{11} (kJ mol^{-1})	ΔG_{11} (kJ mol^{-1})	$T\Delta S_{11}$ (kJ mol^{-1})
γ-CD	308.2	0.770 ± 0.02	-36.58 ± 1.83	-16.97 ± 0.77	-19.61 ± 0.98
	298.2	1.134 ± 0.02	-36.58 ± 1.83	-17.61 ± 0.77	-18.97 ± 0.95
	288.2	2.197 ± 0.04	-36.58 ± 1.83	-18.25 ± 0.77	-18.25 ± 0.92
	278.2	3.420 ± 0.07	-36.58 ± 1.83	-18.88 ± 0.77	-17.70 ± 0.89
33γ-CD_2ox	308.2	14.81 ± 0.15	-24.27 ± 1.21	-24.67 ± 1.23	0.40 ± 0.02
	298.2	21.63 ± 0.22	-24.27 ± 1.21	-24.66 ± 1.23	0.38 ± 0.02
	288.2	29.01 ± 0.29	-24.27 ± 1.21	-24.64 ± 1.23	0.37 ± 0.02
	278.2	41.81 ± 0.42	-24.27 ± 1.21	-24.63 ± 1.23	0.36 ± 0.02
33γ-CD_2suc	308.2	27.02 ± 0.27	-14.27 ± 0.72	-26.17 ± 1.31	11.90 ± 0.59
	298.2	33.01 ± 0.33	-14.27 ± 0.72	-25.79 ± 1.29	11.51 ± 0.58
	288.2	41.30 ± 0.41	-14.27 ± 0.72	-25.40 ± 1.27	11.13 ± 0.56
	278.2	49.02 ± 0.49	-14.27 ± 0.72	-25.01 ± 1.25	10.74 ± 0.54
66γ-CD_2ox	308.2	96.76 ± 0.97	-12.65 ± 0.63	-29.42 ± 1.47	16.77 ± 0.84
	298.2	113.2 ± 1.13	-12.65 ± 0.63	-28.88 ± 1.44	16.23 ± 0.81
	288.2	139.8 ± 1.40	-12.65 ± 0.63	-28.33 ± 1.42	15.68 ± 0.78
	278.2	163.0 ± 1.63	-12.65 ± 0.63	-27.79 ± 1.39	15.14 ± 0.76
66γ-CD_2suc	308.2	73.76 ± 0.74	-8.26 ± 0.41	-28.76 ± 1.44	20.50 ± 1.02
	298.2	85.59 ± 0.86	-8.26 ± 0.41	-28.10 ± 1.40	19.83 ± 0.99
	288.2	93.28 ± 0.93	-8.26 ± 0.41	-27.43 ± 1.37	19.17 ± 0.96
	278.2	105.6 ± 1.06	-8.26 ± 0.41	-26.77 ± 1.34	18.50 ± 0.93
666γ-CD_3bz	308.2	309.0 ± 3.00	-11.55 ± 0.58	-32.37 ± 1.62-	20.82 ± 1.04
	298.2	346.5 ± 3.50	-11.55 ± 0.58	-31.70 ± 1.58	20.15 ± 1.01
	288.2	434.3 ± 4.30	-11.55 ± 0.58	-31.02 ± 1.55	19.47 ± 0.97
	278.2	491.9 ± 4.90	-11.55 ± 0.58	-30.35± 1.52	18.80 ± 0.94

[a]The errors quoted for K_{11} are those derived from the best fits of either Equation 4.7 or 4.8 to the absorbance data. The errors quoted for ΔH_{11}, ΔG_{11} and $T\Delta S_{11}$ are those derived from the fit of Equation 4.11 to the K_{11} data. Experimental error in in all four parameters is estimated at < ± 5 %.

It has been established that cooperative 1:1 host-guest complexes of γ-CD dimers (or 2:1 complexes of γ-CD) and porphyrins can exist in either the *syn* or *anti* conformation

(Figure 2.12 of Chapter 2 and in the literature[39]). It is likely that both conformations exist in a labile equilibrium for the complexation of TSPPala by 33γ-CD_2ox, 33γ-CD_2suc, 66γ-CD_2ox and 66γ-CD_2suc (Figure 4.9). In Section 2.5 of Chapter 2, gas phase molecular modelling studies of the linked γ-CD dimers and H_2TSPP^{4-} showed that the less sterically strained *anti* conformation was more stable than the more sterically strained *syn* conformation in all systems. (When interconversion between *anti* and *syn* conformations occurs it is likely that it proceeds through a transient monotopic 1:1 complex, but this is not shown in Figure 4.9.) However, in the case of PAATSPPala, the 5-(*p*-β-alanylaminophenyl)-group linking the porphyrin to the poly(acrylate) backbone is unavailable for complexation such that only three *p*-sulfonatophenyl groups, TSPPala, may be complexed. In this case, the dimer/TSPPala substituent equilibrium may favour the formation of *syn* 1:1 cooperative complexes to minimise interactions with the poly(acrylate) backbone.

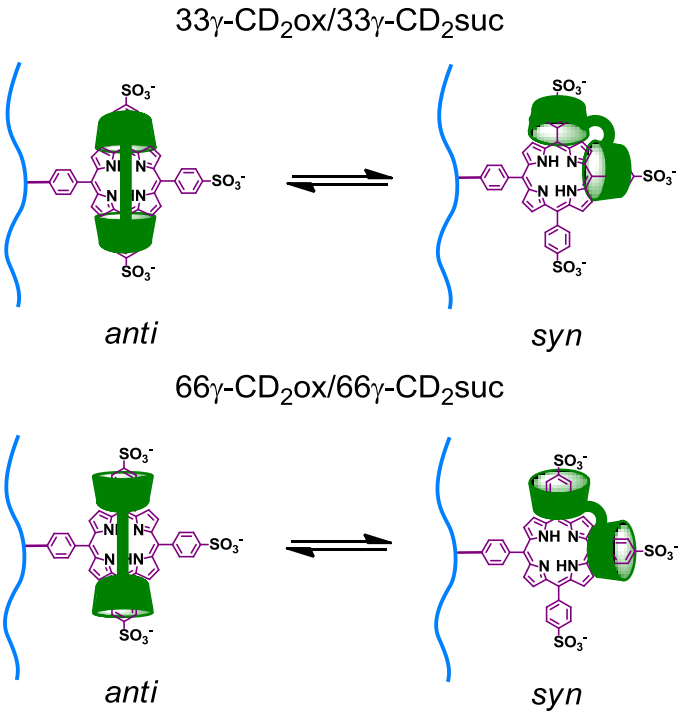

Figure 4.9: Potential 1:1 *anti* or 1:1 *syn* cooperative host-guest complexes between TSPPala and the 3,3- or 6,6-linked γ-CD dimers.

For the 33γ-CD_2ox and 33γ-CD_2suc dimers, the longer succinamide linker coincides with a larger K_{11} than the shorter oxalate linker. This is consistent with the greater length and flexibility of the succinamide linker allowing easier formation of host-guest complexes than is the case for less flexible oxalate linker and is consistent with the trend observed for the K_{11} complexation constants of H_2TSPP^{4-} with 33γ-CD_2ox and 33γ-CD_2suc (Table 2.1 of Chapter 2). An opposite trend is observed for the 66γ-CD_2ox/66γ-CD_2suc dimer pair where the longer more flexible dimer appears to form less stable 1:1 host-guest complexes as evidenced by a smaller K_{11} than that of the shorter less flexible dimer. This observation may be explained if the *syn* conformation of 1:1 host-guest complexation is preferred over the *anti* conformation in the 66γ-CD_2ox/66γ-CD_2suc dimer pair with TSPPala. The shorter oxalate linker may restrict the freedom of movement of the second γ-CD annulus more significantly than the longer succinate linker, and thus, aid the complexation of an adjacent *p*-sulfonatophenyl group through the narrow 6-hydroxyl face. In contrast, the less constrained fitting of TSPPala entering through the wider secondary hydroxyl faces of 33γ-CD_2ox renders the effect of the decreased flexibility of the oxalate linker less effective in increasing K_{11} so that the complexation constant for TSPPala.33γ-CD_2suc is still larger than TSPPala.33γ-CD_2ox.

Whilst the length and flexibility of the benzene linker of the 666γ-CD_3bz trimer may also aid host-guest complexation, it is difficult to quantify its contribution as the tritopic complexation by three γ-CD annuli should also contribute to the observed higher K_{11} complexation constants. It may also be noted that the steric hindrance associated with the attachment of the porphyrin substituent to the poly(acrylate) backbone is expected to decrease the likelihood of the formation of tritopic complexes compared to H_2TSPP^{4-} (as is discussed below).

As one would expect, the K_{11} complexation constants of 33γ-CD_2ox, 33γ-CD_2suc, 66γ-CD_2ox, 66γ-CD_2suc and 666γ-CD_3bz with TSPPala are less than those observed for

H_2TSPP^{4-} at 298.2 K (Table 2.1 of Chapter 2). This is consistent with the blocking of one *p*-sulfonatophenyl complexation site by the large poly(acrylate) backbone significantly hindering host-guest interactions between these γ-CD species and the TSPPala substituents of PAATSPPala compared with those of H_2TSPP^{4-}. The decrease in the K_{11} values at 298.2 K from H_2TSPP^{4-} to TSPPala is more apparent in the 66γ-CD_2suc (941.5×10^3 to 85.59×10^3 dm^3 mol^{-1}) and 666γ-CD_3bz (2210×10^3 to 346.50×10^3 dm^3 mol^{-1}) systems compared with 33γ-CD_2ox (32.64×10^3 to 21.63×10^3 dm^3 mol^{-1}), 33γ-CD_2suc (36.67×10^3 to 33.01×10^3 dm^3 mol^{-1}) and 66γ-CD_2ox (132.6×10^3 to 113.1×10^3 dm^3 mol^{-1}). In the case of 66γ-CD_2suc, steric hindrance from the poly(acrylate) backbone of PAATSPPala may decrease the stability of *anti* 1:1 host-guest complexes, and substantially decrease their K_{11} values compared with those for free H_2TSPP^{4-}. For 666γ-CD_3bz, the decrease in K_{11} values of TSPPala compared with those for H_2TSPP^{4-} may arise from there being one less *p*-sulfonatophenyl group available for tritopic complexation complexation to occur, or from the third γ-CD subunit increasing the likelihood of steric hindrance from the poly(acrylate) backbone, or a combination of both.

For the γ-CD, 33γ-CD_2ox, 33γ-CD_2suc, 66γ-CD_2suc and 666γ-CD_3bz systems, an algorithm for formation of a 1:1 complex corresponding to Equation 4.1 can in some cases be fitted to the UV-vis absorbance data (Figures A17 - A26 of the Appendix). However, a broadening of the apparent isosbestic point increases with decreasing temperature is consistent with the formation of a second host-guest complex; the 2:1 complex. The spectrum of PAATSPPala alone shows a small decrease in molar absorbance and a small blue shift in λ_{max} with a decreasing temperature probably due to a change of position in the monomer/dimer equilibrium as discussed earlier and shown in Figure 4.6. The fitting of an algorithm for 1:1 complexation gives poor fits to the data at lower temperatures and the spectrum derived for the 1:1 complex shows a systematic change in molar absorbance with

change in temperature (Figures A17 – A26). This is not expected for the γ-CD.TSPPala, 33γ-CD_2ox.TSPPala, 33γ-CD_2suc.TSPPala, 66γ-CD_2ox.TSPPala, 66γ-CD_2suc.TSPPala and 666γ-CD_3bz.TSPPala complexes in which TSPPala is expected to exist in the monomeric form. An algorithm corresponding to the formation of both a 1:1 and a 2:1 complex according to Equations 4.1 and 4.2 is readily fitted to the absorbance data and the derived 1:1 and 2:1 complex spectra show no significant variation with temperature for five of the systems with the exception being the 66γ-CD_2ox.TSPPala system as may be seen from Figures A6 – A10 and A13- A16 of the Appendix.

Table 4.2: Complexation constants K_{21} for the complexation of TSPPala by γ-CD, 33γ-CD_2ox, 33γ-CD_2suc, 66γ-CD_2suc and 666γ-CD_3bz at different temperatures by UV-Vis titrations in aqueous phosphate buffer at pH 7.0 and I = 0.10 mol dm^{-3}.[b]

Host	T (K)	K_{21} (dm^3 mol^{-1})
γ-CD	308.2	250 ± 15
	298.2	340 ± 30
	288.2	455 ± 40
	278.2	810 ± 75
33γ-CD_2ox	308.2	390 ± 35
	298.2	650 ± 60
	288.2	750 ± 70
	278.2	1510 ± 140
33γ-CD_2suc	308.2	400 ± 35
	298.2	680 ± 65
	288.2	825 ± 80
	278.2	1560 ± 140
66γ-CD_2suc	308.2	385 ± 30
	298.2	630 ± 50
	288.2	720 ± 60
	278.2	1450 ± 130
666γ-CD_3bz	308.2	705 ± 65
	298.2	900 ± 85
	288.2	1210 ± 110
	278.2	2390 ± 220

[b]The errors quoted for K_{21} are those derived from the best fit of Equation 4.8 to the absorbance data. Experimental error is estimated at < ± 5 %.

It is concluded that this explains the apparent isosbestic point broadening and is a more reliable representation of the complexation equilibria. The derived K_{11} and K_{21} appear in Tables 4.1 and 4.2, respectively.

The data in Tables 4.1 and 4.2 show that the K_{21} (at 298.2 K) for characterising the complexation of a second host to form (γ-CD)$_2$.TSPPala, (33γ-CD$_2$ox)$_2$.TSPPala, (33γ-CD$_2$suc)$_2$.TSPPala, (66γ-CD$_2$suc)$_2$.TSPPala and (666γ-CD$_3$bz)$_2$.TSPPala are much lower than their analogous K_{11}. This decreased stability is expected due to steric hindrance associated from complexing two hosts onto the porphyrin substituent guest. The K_{21} values of the γ-CD oligomers are only ~2-3-fold greater than that of the γ-CD, suggesting only a statistical increase in K_{21} associated with an increase in the number of γ-CD annuli of the host. This suggests monotopic complexation of the second γ-CD oligomer either through one γ-CD annulus of each oligomer or a combination of monotopic and ditopic complexation (Figure 4.10). (It is also possible that simultaneous monotopic complexation of TSPPala substituents on the same strand may occur as shown in Figure 4.10.) Whilst 2:1 3,3-linked γ-CD dimer.H_2TSPP^{4-} complexes can be formed by two γ-CD dimers binding ditopically (as seen in Figure 2.14 of Chapter 2), the blocking of one complexation site by attachment of the poly(acrylate) backbone removes the possibility of these complexes forming with PAATSPPala. Accurate gas phase molecular modelling studies of the complexation of TSPPala by γ-CD and the linked γ-CD oligomers (similar to those observed in Section 2.5 of Chapter 2 for H_2TSPP^{4-}) could not be undertaken because of the large size of the poly(acrylate) backbone of PAATSPPala. However it is likely that the *syn* and *anti* conformations of the montopic noncooperative 2:1 host-guest complexes exist in the (γ-CD)$_2$.TSPPala, (33γ-CD$_2$ox)$_2$.TSPPala, (33γ-CD$_2$suc)$_2$.TSPPala, (66γ-CD$_2$suc)$_2$.TSPPala and (666γ-CD$_3$bz)$_2$.TSPPala equilibria as well as a combination of monotopic and ditopic complexation as exemplified by a 3,3-linked dimer in Figure 4.10.

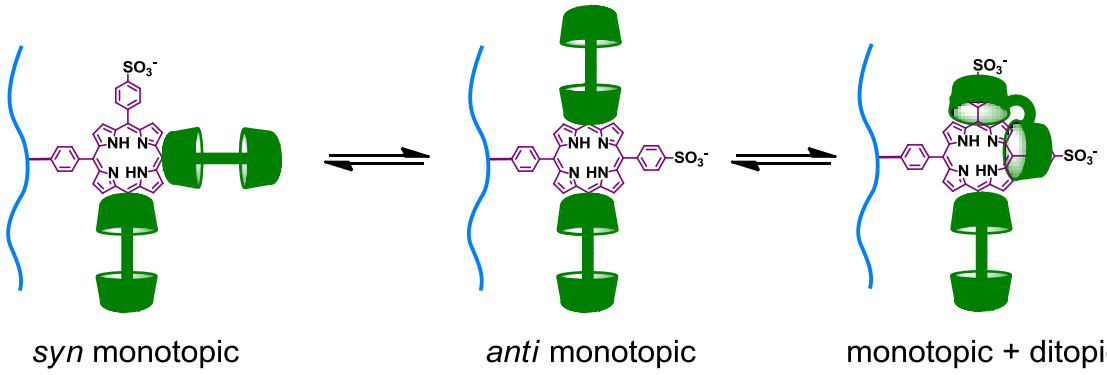

Figure 4.10: Potential 2:1 non-cooperative host-guest complexes between PAATSPPala and a 3,3-linked γ-CD dimer.

The isosbestic points for the 66γ-CD_2ox systems (Figure 4.7 and A11-12 of the Appendix) are sharp compared with the those of the other host.PAATSPPala systems and the data obtained for this system fit well to Equation 4.1 with minimal variation in the derived molar absorbance spectrum for the 1:1 complex with a change in temperature. In this system the predominant species are the free porphyrin substituent and 1:1 host-guest complex. These considerations raise the question as to why the (66γ-CD_2ox)$_2$.TSPPala complex is not present to a detectable extent. The 66γ-CD_2ox.TSPPala system shows the highest K_{11} complexation constants of the four dimer systems (most likely as a result of its restricted stereochemistry of ditopic complexation as discussed earlier). This 'tight' cooperative 1:1 host-guest complex may decrease the flexibility required to accommodate complexation by a second 66γ-CD_2ox in the formation of a 2:1 host-guest complex such that it does not form to a detectable extent.

To the best of our knowledge, only one other study has reported the K_{11} stability constant characterising the complexation of a porphyrin substituted poly(acrylate) by a linked CD dimer.[16] The study showed that $K_{11} = 1.7 \times 10^6$ dm^3 mol^{-1} characterised the complexation of a 2.6% 5-(4-β-alanylaminophenyl)-10,15,20-tris(4-sulfonatophenyl)porphinatoiron(III) randomly substituted poly(acrylate) by a per-*O*-methylated β-CD dimer with a pyridine linker in aqueous phosphate buffer at pH 7.0 and 298.2 K. The K_{11} for the literature complex is 17-

to 80-fold higher than that of TSPPala with the γ-CD dimers in this study under similar conditions. This probably a consequence of the coordinate bond formed between Fe(III) of the porphinatoiron(III) subunit and the pyridine substituent of the β-CD dimer linker. No 2:1 host-guest complexes were observed in the literature study.

4.4.4. Determination of Thermodynamic Parameters

The relationship between the Gibbs free energy change (ΔG), enthalpy change (ΔH) and entropy change (ΔS) are given by the van't Hoff equation:

$$\Delta G = -RT\ln K \qquad (\mathbf{4.9})$$

Where R is the ideal gas constant and T is the absolute temperature and

$$\Delta G = \Delta H - T\Delta S \qquad (\mathbf{4.10})$$

and from Equation 4.9 and 4.10

$$\ln K_{11} = -\Delta H/RT + \Delta S/R \qquad (\mathbf{4.11})$$

The plot of $\ln K_{11}$ versus $1/T$ according to Equation 4.11 is a van't Hoff plot, of which the slope and the intercept represent $-\Delta H°/R$ and $\Delta S°/R$, respectively.

Using the van't Hoff plots (Figure 4.8), ΔH_{11} and $T\Delta S_{11}$ were calculated from the slopes and the intercepts for the complexation of TSPPala by γ-CD or its oxalate or succinamide-linked dimers and benzene linked trimer, 33γ-CD_2ox, 33γ-CD_2suc, 66γ-CD_2ox, 66γ-CD_2suc and 666γ-CD_3bz. The complexation constants K_{11} or K_{21} derived at 278.2, 288.2, 298.2 and 308.2 K as well as thermodynamic parameters ΔG_{11}, ΔH_{11} and $T\Delta S_{11}$ are summarised in Table 4.1. (Because of the higher error estimates for K_{21} characterising the 2:1 host-guest complexes between the γ-CD species and TSPPala, a similar analysis was not undertaken.) The errors shown for K_{11} and K_{21} are data fitting errors, the maximum experimental errors for K_{11} and K_{21} are estimated to be ± 5%. The errors shown for ΔG_{11}, ΔH_{11} and $T\Delta S_{11}$ are those from fitting the van't Hoff equation to the UV-vis data.

The smaller K_{11} for the γ-CD.TSPPala complex is a consequence of a high ΔH_{11} (compared with the other systems in Table 4.1) and a large negative $T\Delta S_{11}$. This is attributable to the entropy decrease arising from γ-CD and TSPPala forming a single complex offsetting the entropy increase arising from the displacement of water molecules from the γ-CD annulus by TSPPala on formation of the γ-CD.TSPPala complex. (The complexation of H_2TSPP^{4-} by γ-CD is characterised by small positive $T\Delta S_{11}$ and less negative ΔH_{11} (Table 2.1, Chapter 2)). The negative entropy contribution of the γ-CD.TSPPala complex may be explained by the decrease in rotational freedom of the porphyrin substituents of PAATSPPala compared to free H_2TSPP^{4-} leading to increase order in the former relative to the latter.

A decrease in $T\Delta S_{11}$ characterising the 33γ-CD_2ox.TSPPala and 66γ-CD_2ox.TSPPala complexes compared with their analogous complexes with H_2TSPP^{4-} is also observed. However, the 33γ-CD_2ox.TSPPala and 66γ-CD_2ox.TSPPala complexes $T\Delta S_{11}$ are positive which infers that the entropy decrease on forming 33γ-CD_2ox.PAATSPPala and 66γ-CD_2ox.TSPPala from 33γ-CD_2ox or 66γ-CD_2ox with TSPPala is now offset by the increase in entropy arising from expulsion of water from the two γ-CD annuli of the dimers.

An increase in $T\Delta S_{11}$ characterising the 33γ-CD_2suc.TSPPala, 66γ-CD_2suc.TSPPala complexes compared with their analogous complexes with H_2TSPP^{4-} is observed. In these cases, the increase in flexibility of their linkers as well as unfavourable steric interactions may lead to an increase in the disorder of these systems and an increase in $T\Delta S_{11}$ compared to H_2TSPP^{4-}. Thus, for both 3,3- and 6,6-linked dimers, the shorter oxalate linker favours a greater enthalpic and entropic stabilisation of host-guest complexation by comparison with the longer succinate linker as evidenced by larger ΔH_{11} and smaller positive $T\Delta S_{11}$ for the formation of the 33γ-CD_2ox.TSPPala and 66γ-CD_2ox.TSPPala complexes, respectively, by comparison with the 33γ-CD_2suc.TSPPala and 66γ-CD_2suc.TSPPala complexes. (While the

ΔH_{11} for the oligomer complexes are smaller than that for the γ-CD.PAATSPPala complex, their much larger positive $T\Delta S_{11}$ yield substantially greater K_{11} values.)

The 666γ-CD_3bz.PAATSPPala complex is characterised by the largest positive $T\Delta S_{11}$ and a ΔH_{11} in the midrange of those in this study which combine to give the largest K_{11} magnitudes over the studied temperature range. This is attributable to the three γ-CD subunits of 666γ-CD_3bz contributing to increased steric hindrance as well as an increased water expulsion from the three γ-CD annuli upon complexation which offsets the entropy decrease arising from 666γ-CD_3bz and PAATSPPala forming a single complex.

4.4.5. Entropy-Enthalpy Compensation

It has been observed in a wide range of cyclodextrin studies that a linear relationship exists between $T\Delta S_{11}$ and ΔH_{11} for the complexation by α-CD, β-CD and γ-CD hosts of a large variety of guest species in host-guest 1:1 complexes.[40] This relationship is represented by Equation 4.12 in which $T\Delta S_{11}$ and ΔH_{11} are experimental data, α is the slope of a plot of $T\Delta S_{11}$ against ΔH_{11} and $T\Delta S_{11,0}$ is observed when $\Delta H_{11} = 0$ ($\Delta H_{11,0}$) at the zero intercept.

$$T\Delta S_{11} = \alpha\Delta H_{11} + T\Delta S_{11,0} \qquad (\mathbf{4.12})$$

A plot of $T\Delta S_{11}$ and ΔH_{11} data from the literature[40] for a the formation of a wide range of 1:1 γ-CD.guest host-guest complexes is shown in Figure 4.11 and is characterised by $\alpha = 0.97$ and $T\Delta S_{11,0} = 15$ kJ mol^{-1}. Thus, α indicates the extent to which changes in complex stability (proportional to ΔG_{11}) occur as a consequence of enthalpic stabilisation, $\Delta\Delta H$, induced by variation of the identity of the host is cancelled by entropic loss, $\Delta\Delta S$, through Equation 4.13:

$$\Delta G_{11} = (1 - \alpha)\Delta\Delta H_{11} \qquad (\mathbf{4.13})$$

such that only (1 - α) of the enthalpic increase can add to the host-guest complex stabilisation. Thus, $T\Delta S_{11,0}$ is the inherent host-guest complex stability, $\Delta G_{11,0}$, when $\Delta H_{11} = 0$ ($\Delta H_{11,0}$). (It should be noted that Equation 4.12 does not represent a necessary relationship, but is one also observed for a variety equilibria not involving cyclodextrins.)

The $T\Delta S_{11}$ and ΔH_{11} data for the complexation of TSPPala with γ-CD, 33γ-CD_2ox, 33γ-CD_2suc, 66γ-CD_2ox, 66γ-CD_2suc and 666γ-CD_3bz at 298.2 K are plotted in Figure 4.11 together with the analogous data for H_2TSPP^{4-} from Figure 2.15 of Chapter 2 and known data for γ-CD host-guest complexes.[40] When the data for all of the γ-CD and γ-CD host-guest complexes from Chapter 2 and 4 are plotted together a tentative linear relationship is observed (R^2 = 0.827, best-fit line not shown). However, the entropy-enthalpy compensatory effect is often governed by the complexation sites of the host rather than the stereochemistry of the guest; therefore this low R^2 might be expected.[40] The sets of oligomers complex TSPPala or H_2TSPP^{4-} through either the narrow 6-hydroxyl face (750 pm in diameter)[36] or the wide 3-hydroxyl face (830 pm in diameter)[36]. Accordingly, the host data sets are separated by the γ-CD annular face in which the host complexes the guest i.e. narrow 6-hyrdoxyl face (66γ-CD_2ox, 66γ-CD_2suc and 666γ-CD_3bz), wide 3-hydroxyl face (33γ-CD_2ox, 33γ-CD_2suc) or both (native γ-CD).

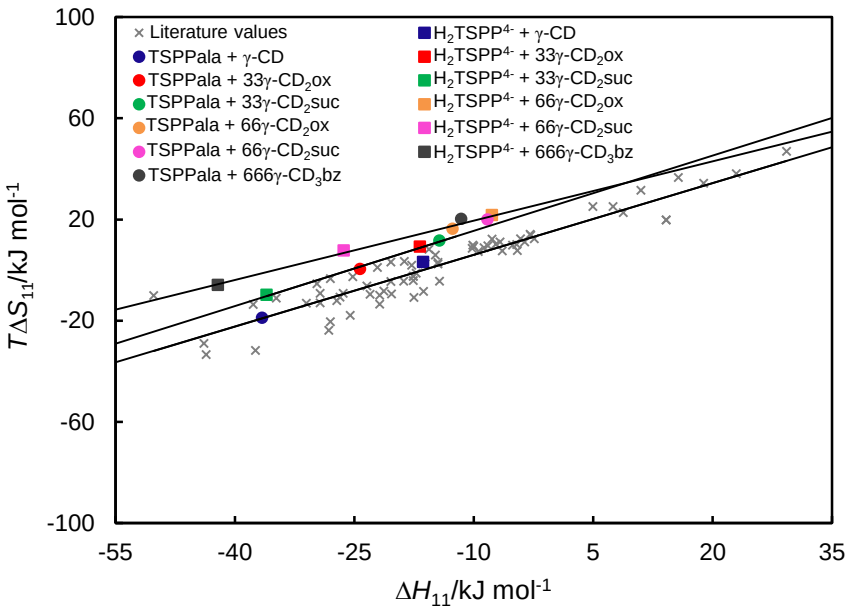

Figure 4.11: Plot of $T\Delta S_{11}$ against ΔH_{11} for the 1:1 complexes formed by the hosts γ-CD, 33γ-CD_2ox, 33γ-CD_2suc, 66γ-CD_2ox, 66γ-CD_2suc and 666γ-CD_3bz with the guests H_2TSPP^{4-} (From Figure 2.15 of Chapter 2) and the TSPPala substituents of PAATSPPala from this study as well as analogous data from the literature for γ-CD with various hosts.[40]

A plot of $T\Delta S_{11}$ vs ΔH_{11} for 66γ-CD_2ox, 66γ-CD_2suc and 666γ-CD_3bz with H_2TSPP^{4-} and TSPPala yields a linear least squares fit of Equation 4.12 (R^2 = 0.99) with α = 0.78 and $T\Delta S_{11,0}$ = 27 kJ mol^{-1}. Similarly, a plot of the $T\Delta S_{11}$ vs ΔH_{11} for 33γ-CD_2ox, 33γ-CD_2suc with H_2TSPP^{4-} and TSPPala yields a linear least squares fit of Equation 4.12 (R^2 = 0.99) with α = 0.99 and $T\Delta S_{11,0}$ = 25 kJ mol^{-1}. The data for the complexes of H_2TSPP^{4-} and TSPPala with γ-CD fall within the range of the literature data where α = 0.97 and $T\Delta S_{11,0}$ = 15 kJ mol^{-1}.[40] The data shows that at $T\Delta S_{11,0}$, the host-guest complexes of H_2TSPP^{4-} and TSPPala with the 3,3-linked and 6,6-linked oligomer species are, respectively, 12 kJ mol^{-1} and 10 kJ mol^{-1} more stable than that of γ-CD. This may be explained by the cooperative complexation effect discussed earlier leading to much more stable host-guest complexes. Furthermore, the 6,6-linked oligomer host-guest complexes are 2 kJ mol^{-1} more stable than the analogous 3,3-linked oligomer host-guest complexes. This observation suggests that the narrower 6-

hydroxyl face of the γ-CD annulus is a more suitable fit for the *p*-sulfonatophenyl groups of H_2TSPP^{4-} and TSPPala than is the wider 3-hydroxyl face. The slope for the 3,3-linked linked oligomer systems yield α = 0.99. This suggests that in host-guest complexation of H_2TSPP^{4-} and TSPPala by the 3,3- linked oligomer systems, only 1 % of the enthalpic gain ($\Delta\Delta H_{11}$) induced by system alterations is reflected in the net increase of the complex stability ($\Delta\Delta G_{11}$), whereas 99 % of the enthalpic gain ($\Delta\Delta H_{11}$) is cancelled out by the entropic loss ($\Delta\Delta S_{11}$). The slope for the 6,6-linked linked oligomer systems yield α = 0.78. This suggests that in host-guest complexation of H_2TSPP^{4-} and TSPPala by the 6,6-linked oligomer systems, 22 % of the enthalpic gain ($\Delta\Delta H_{11}$) induced by system alterations is reflected in the net increase of the complex stability ($\Delta\Delta G_{11}$), whereas 78 % of the enthalpic gain ($\Delta\Delta H_{11}$) is cancelled out by the entropic loss ($\Delta\Delta S_{11}$). This observation may be attributable to the wider 3-hydroxyl face of the γ-CD annulus experiencing increased conformational changes through greater ring flexibility or greater desolvation as compared with the 6-hydroxyl face of the γ-CD annulus.

4.5. RHEOLOGY

Host-guest interactions between the CD oligomers and the TSPPala substituents of PAATSPPala on the molecular level are expected to affect the viscosities of their solutions on the macroscopic level. Rheological measurements were carried out using a Physica MCR 501 (Anton Parr GmbH) stress–controlled rheometer with a 25 mm cone and plate geometry. The temperature was controlled at 298.2 ± 0.1 K by a Peltier plate. Rheological samples were prepared by dissolution of PAATSPPala alone and with γ-CD, 33γ-CD_2ox, 33γ-CD_2suc, 66γ-CD_2ox, 66γ-CD_2suc and 666γ-CD_3bz in 0.10 mol dm^{-3} aqueous sodium chloride to ensure screening of the electrostatic interactions between the carboxylate groups. The solution pH was adjusted to 7.0 with 0.10 mol dm^{-3} aqueous sodium hydroxide solution. The rheologically determined viscosity provides an indication of the extent to which cross-linking

between PAATSPPala strands occurs in the presence of the linked γ-CD oligomers. The variations in viscosities of the six PAATSPPala solutions with equimolar concentrations of TSPPala substituents and γ-CD or the γ-CD oligomers with shear rate are shown in Figure 4.11. The zero–shear viscosity variations, corresponding to the viscosities extrapolated from those observed at the lowest shear rates, are shown in Figure 4.12.

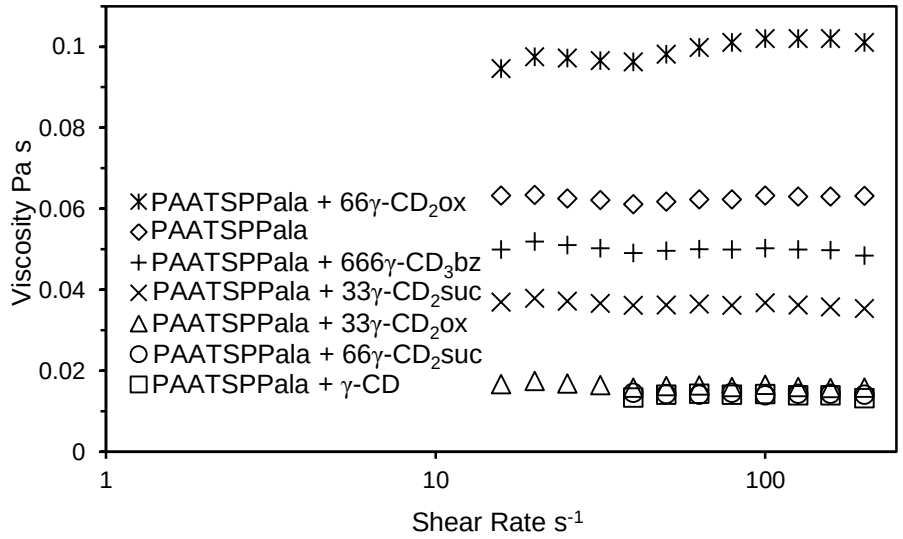

Figure 4.11: Viscosity variations with shear rate of a 5 wt% aqueous solutions of PAATSPPala alone in which the TSPPala substituent concentration is 1.22×10^{-2} mol dm^{-3} and in solutions containing either equimolar γ-CD, 33γ-CD_2ox, 33γ-CD_2suc, 66γ-CD_2ox, 66γ-CD_2suc or 666γ-CD_3bz at pH = 7.0 and [NaCl] = 0.10 mol dm^{-3} at 298.2 K.

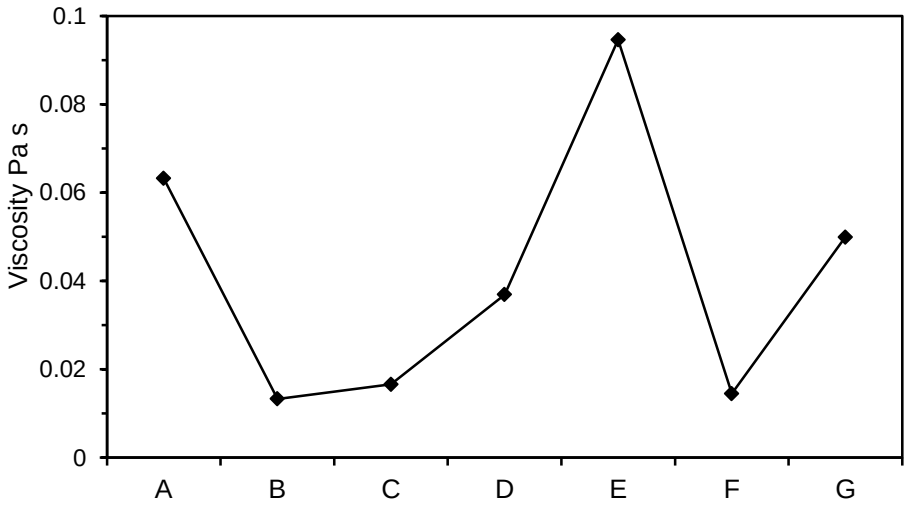

Figure 4.12: Zero-shear viscosities of 5 wt% aqueous solutions of PAATSPPala alone in which the TSPPala substituent concentration is 1.22×10^{-2} mol dm^{-3} (A, 0.0632 Pa s) and with the addition of either equimolar γ-CD (B, 0.0133 Pa s), 33γ-CD_2ox (C, 0.0166 Pa s), 33γ-CD_2suc (D, 0.0369 Pa s), 66γ-CD_2ox (E, 0.0946 Pa s), 66γ-CD_2suc (F, 0.0145 Pa s) or 666γ-CD_3bz (G, 0.0499 Pa s) at pH = 7.0 and [NaCl] = 0.10 mol dm^{-3} at 298.2 K. (The quantities in brackets are the zero shear viscosities.)

The PAATSPPala solutions show little variation in viscosity with shear rate (Figure 4.11) and the zero shear viscosities range from 0.0133 Pa s for a solution of 5.0 wt% PAATSPPala with γ-CD to 0.0946 Pa s for a solution of PAATSPPala with 66γ-CD_2ox (Figure 4.12). The variation of viscosity magnitude within the seven solutions A-G reflects the balance between TSPPala substituent intra- and inter-strand aggregation, TSPPala substituent complexation within strands and between adjacent strands by γ-CD and its oligomers. Thus, for the solutions of PAATSPPala containing either 33γ-CD_2ox (C, 0.0166 Pa s), 33γ-CD_2suc (D, 0.0369 Pa s), 66γ-CD_2suc (F, 0.0145 Pa s) or 666γ-CD_3bz (G, 0.0499 Pa s) viscosity is less than that for that containing PAATSPPala alone (A, 0.0632 Pa s) consistent with the dominant effect being the intra-strand complexation of porphyrin substituents decreasing inter-strand porphyrin substituent aggregation and lowering solution viscosity by ~20 - 80 %. The exception to this is the PAATSPPala solution containing 66γ-

CD_2ox (E, 0.0946 Pa s) in which viscosity increases by ~50% consistent with the formation of inter-strand cross-links forming between adjacent strands through simultaneous complexation by 66γ-CD_2ox of two porphyrin substituents on adjacent strands.

The trend in the PAATSPPala solution viscosities shows little correlation between the variations in zero-shear viscosities and the magnitude of the complexation constants, K_{11} and K_{21} determined from the UV-vis titration data. This observation can be attributed to two factors. First, the rheological experiments were conducted at a much higher (~4000-fold) concentrations than the UV-vis titration experiments. At these higher concentrations, collisions between strands are much more probable, which could lead to π-π stacking between porphyrin substituents forming cross-links between strands. Secondly, the rheological experiments were performed at an equimolar host-guest concentration, whereas in the UV-vis titration experiments the host concentration was progressively increased. At the rheological host/guest concentrations the stoichiometric ratio favours the formation of 1:1 porphyrin substituent.γ-CD-oligomer complexes. If these complexes are ditopically or tritopically cooperative (as seen in the UV-vis titration experiments), they will disfavour the formation of inter-strand cross-links due to all γ-CD annuli being occupied by a single porphyrin substituent.

The zero-shear viscosity values for the PAATSPPala solutions increase in the order of γ-CD/PAATSPPala < 66γ-CD_2suc/PAATSPPala < 33γ-CD_2ox/PAATSPPala < 33γ-CD_2suc/PAATSPPala < 666γ-CD_3bz/PAATSPPala < PAATSPPala alone < 66γ-CD_2ox/PAATSPPala (Figure 4.12). As expected, native γ-CD decreases the viscosity of the PAATSPPala solutions by complexing the porphyrin substituents and largely precluding their inter-strand π-π stacking interactions and decreasing solution viscosity. (A similar trend has been observed for octadecyl[41] and dansyl[27] substituted poly(acrylate)s where the viscosities of their aqueous solutions arising from substituent aggregation were greatly diminished by

the addition of β-CD as a consequence of the octadecyl or dansyl substituents being complexed by β-CD.) Inter-strand cross-links could arise when two or more γ-CD annuli are linked, potentially simultaneously complexing porphyrin substituents on adjacent strands to increasing the solutions viscosity. However, in the case of 33γ-CD_2ox, 33γ-CD_2suc, 66γ-CD_2suc and 666γ-CD_3bz, a ~20–80 % decrease in the solutions viscosity was observed. This may suggest that cooperative complexation may encapsulate two *p*-sulfonatophenyl groups on one porphyrin substituent, and compete with the formation of inter-strand cross-links. This process will also hinder the formation of porphyrin-porphyrin π-π stacking interactions and the net effect is a decrease in the viscosity of the PAATSPPala solutions.

The observation that the 66γ-CD_2ox dimer increases PAATSPPala solution viscosity by approximately 50 % coincides with this dimer being distinguished as the only γ-CD species to form a 1:1 host-guest complex in the UV-vis studies. The complexation of porphyrin substituents is labile and for a γ-CD dimer there must be an initial formation of a montopic γ-CD dimer.porphyrin substituent host-guest complex as the ditopic complex forms with a single porphyrin substituent. Such a monotopic complex in the more concentrated rheology solutions is a potential precursor to the ditopic complexation by the γ-CD dimer of two porphyrin substituents on adjacent PAATSPPala strands which is a significant occurence with the 66γ-CD_2ox dimer (Figure 4.13). While the reason that this only occurs to a significant extent for 66γ-CD_2ox is not readily identified, it seems likely that its preference for the formation of a 1:1 66γ-CD_2ox.porphyrin substituent complex, as opposed to the formation of both 1:1 and 2:1 complexes by γ-CD and the other γ-CD oligomers, may be relevant to this.

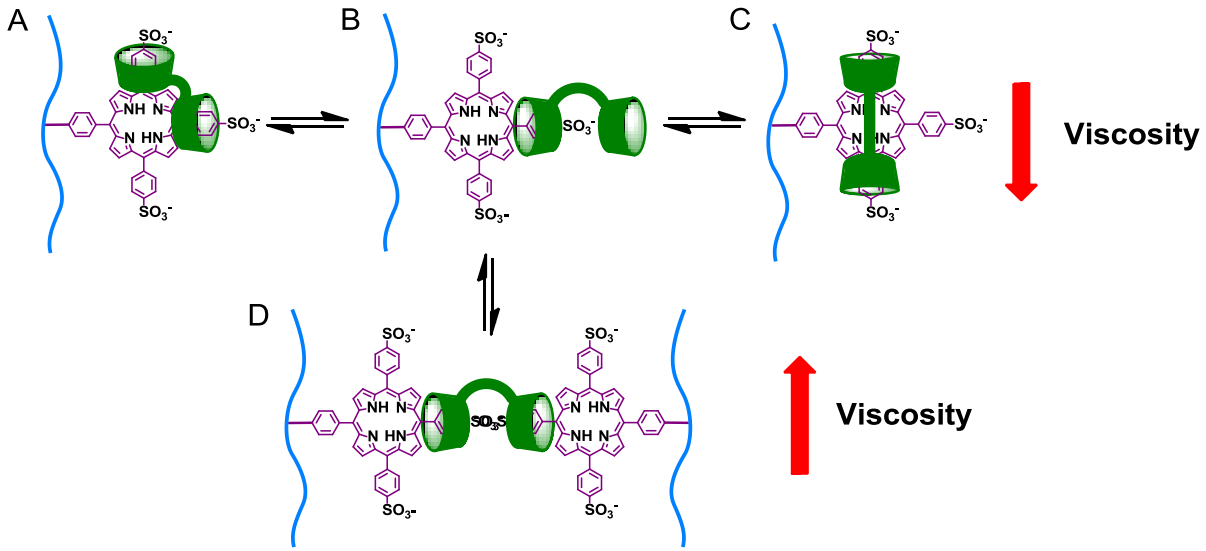

Figure 4.13: Potential host-guest complexes between TSPPala and 66γ-CD_2ox. A) ditopic 1:1 *anti* complex, B) monotopic 1:1 complex C) ditopic 1:1 *syn* complex. D) ditopic 1:2 cross-linked complex.

Although the rheological experiments did not yield viscosities high enough to form a hydrogel, they do suggest that changes on the molecular scale alter the properties of the bulk material. In this study, the space between the linked γ-CD units ultimately lead to cooperatively bound complexes that disfavour the formation of inter-strand cross-links. By reducing the length and flexibility of the γ-CD oligomer linkers or increasing their steric bulk, cooperative complexation of the porphyrin substituents may be reduced making inter-strand crosslinks more prevalent. This could be key to controlling the formation of a porphyrin substituted poly(acrylate) hydrogel with γ-CD oligomers.

4.6. SUMMARY AND CONCLUSIONS

The host-guest complexation of the TSPPala substituents of PAATSPPala by γ-CD, 33γ-CD_2ox, 33γ-CD_2suc, 66γ-CD_2ox, 66γ-CD_2suc or 666γ-CD_3bz has been characterised in aqueous solution by 2D ^{1}H NOESY NMR and UV-vis spectroscopy and rheology. The 2D ^{1}H

NOESY NMR spectra show that γ-CD and its oligomers complex the TSPPala substituents of the substituted poly(acrylate), PAATSPPala, as is evident from cross-peaks arising from NOE interactions between the pyrrolic and *p*-sulfonatophenyl protons of the porphyrin substituents and the annular protons of γ-CD and its oligomers. The UV-vis studies show that 1:1 host-guest complexes are dominant in the 66γ-CD_2ox system whilst the other host systems formed both 1:1 and 2:1 host-guest complexes. The K_{11} values derived for 1:1 host guest complexation are 19-307-fold larger for the γ-CD oligomers than for γ-CD at 298.2 K. This observation is consistent with a strong cooperative effect when the γ-CD oligomers complex the TSPPala substituents of PAATSPPala. The K_{21} values derived for (33γ-CD_2ox)$_2$.TSPPala, (33γ-CD_2suc)$_2$.TSPPala, (66γ-CD_2suc)$_2$.TSPPala and (666γ-CD_3bz)$_2$.TSPPala are ~2-3-fold higher than the K_{21} of (γ-CD)$_2$.TSPPala. This is consistent with the statistical advantage of complexation associated with the extra γ-CD annuli of the oligomers, suggesting 2:1 monotopic host-guest complexation in these systems.

The ΔH and $T\Delta S$ data characterising 33γ-CD_2ox.TSPPala, 33γ-CD_2ox.TSPPala, 66γ-CD_2ox.TSPPala, 66γ-CD_2suc.TSPPala and 666γ-CD_3bz.TSPPala shows their formation to be exothermic and entropy-driven where the entropy increase probably arises dominantly through expulsion of water from their γ-CD annuli upon complexation of the TSPPala substituents of PAATSPPala. The formation of the γ-CD.TSPPala complex is exothermic and enthalpically stabilised apparently as a consequence of the entropic increase arising from expulsion of water from their γ-CD annuli being offset by the decrease in entropy resulting from the host and guest forming a single host-guest complex. This observation is not seen in the γ-CD oligomer systems, probably due to steric effects between the poly(acrylate) backbone and extra γ-CD subunits.

The $T\Delta S_{11}$ and ΔH_{11} data for the complexation of TSPPala with γ-CD, 33γ-CD_2ox, 33γ-CD_2suc, 66γ-CD_2ox, 66γ-CD_2suc and 666γ-CD_3bz at 298.2 K were plotted with the

analogous data for H_2TSPP^{4-} from Figure 2.15 of Chapter 2 and literature data of γ-CD host-guest complexes. It is found that the 6,6- linked γ-CD oligomer host-guest complexes show greater stability and greater enthalpic stabilisation than do their 3,3- linked counterparts. This observation may be attributable to either the greater width of the 3-hydroxyl face of the γ-CD annulus experiencing increased conformational changes through greater ring flexibility or greater desolvation as compared with the narrower 6-hydroxyl face of the γ-CD annulus.

In concentrated 5.0 wt % solutions of PAATSPPala and γ-CD and the γ-CD oligomers, rheological determinations show that in most cases host-guest complexation decreases solution viscosity. This is consistent with intra-strand complexation occurring to a greater extent than inter-strand complexation. In contrast, it was found that 66γ-CD_2ox significantly increased the formation of inter-strand cross-links. The reason for this is not obvious, but is coincident with 66γ-CD_2ox being the sole γ-CD oligomer forming only 1:1 host-guest complexes with the TSPPala substituents of PAATSPPala in a single strand in contrast to the other γ-CD oligomers which also form 2:1 host-guest complexes. This may indicate that the constraints imposed by its stereochemistry on host-guest complexation are responsible for both its propensity of 66γ-CD_2ox to dominantly form 1:1 host-guest complexes in dilute PAATSPPala and to form inter-strand cross-links in more concentrated PAATSPPala solution.

This study provides interesting insights into the factors affecting the host-guest complexation of the TSPPala substituents of PAATSPPala by γ-CD and γ-CD oligomers in aqueous solution and may lead to better design of therapeutic hydrogels. Further studies with either different porphyrin substituents, or different γ-CD oligomers, or both will provide greater insight into the host-guest complexation of porphyrin substituted poly(acrylate)s by γ-CD oligomers.

4.7. REFERENCES

1. L. Wang, H. Li, G. Fang, J. Zhou and D. Cao, *Sens. Actuators, B*, 2014, **196**, 653-662.
2. K. Kano, H. Kitagishi, S. Tamura and A. Yamada, *J. Am. Chem. Soc.*, 2004, **126**, 15202-15210.
3. T. Ueda, H. Kitagishi and K. Kano, *Inorg. Chem.*, 2014, **53**, 543-551.
4. K. Kano, H. Kitagishi, T. Mabuchi, M. Kodera and S. Hirota, *Chem. Asian J.*, 2006, **1**, 358-366.
5. J. H. Kim, M. Lee, J. S. Lee and C. B. Park, *Angew. Chem., Int. Ed.*, 2012, **51**, 517-520, S517/511-S517/511.
6. H.-J. Son, S. Jin, S. Patwardhan, S. J. Wezenberg, N. C. Jeong, M. So, C. E. Wilmer, A. A. Sarjeant, G. C. Schatz, R. Q. Snurr, O. K. Farha, G. P. Wiederrecht and J. T. Hupp, *J. Am. Chem. Soc.*, 2013, **135**, 862-869.
7. J. G. Woller, J. K. Hannestad and B. Albinsson, *J. Am. Chem. Soc.*, 2013, **135**, 2759-2768.
8. Y.-H. Jeong, M. Son, H. Yoon, P. Kim, D.-H. Lee, D. Kim and W.-D. Jang, *Angew. Chem., Int. Ed.*, 2014, **53**, 6925-6928.
9. J. Luo, M. Xu, R. Li, K.-W. Huang, C. Jiang, Q. Qi, W. Zeng, J. Zhang, C. Chi, P. Wang and J. Wu, *J. Am. Chem. Soc.*, 2014, **136**, 265-272.
10. A. Juzeniene, Q. Peng and J. Moan, *Photochem. Photobiol. Sci.*, 2007, **6**, 1234-1245.
11. V. V. Serra, A. Zamarron, M. A. F. Faustino, M. C. Iglesias-de la Cruz, A. Blazquez, J. M. M. Rodrigues, M. G. P. M. S. Neves, J. A. S. Cavaleiro, A. Juarranz and F. Sanz-Rodriguez, *Bioorg. Med. Chem.*, 2010, **18**, 6170-6178.
12. X. Zhu, W. Lu, Y. Zhang, A. Reed, B. Newton, Z. Fan, H. Yu, P. C. Ray and R. Gao, *Chem. Commun.*, 2011, **47**, 10311-10313.

13. Z. Kejik, R. Kaplanek, T. Briza, J. Kralova, P. Martasek and V. Kral, *Supramol. Chem.*, 2012, **24**, 106-116.

14. A. P. Thomas, P. S. Saneesh Babu, S. Asha Nair, S. Ramakrishnan, D. Ramaiah, T. K. Chandrashekar, A. Srinivasan and M. Radhakrishna-Pillai, *J. Med. Chem.*, 2012, **55**, 5110-5120.

15. Y. Wang, B. Cohen, L. Jicsinszky and A. Douhal, *Langmuir*, 2012, **28**, 4363-4372.

16. K. Kano, T. Ochi, S. Okunaka, Y. Ota, K. Karasugi, T. Ueda and H. Kitagishi, *Chem. - Asian J.*, 2011, **6**, 2946-2955.

17. K. Sasaki, H. Nakagawa, X. Zhang, S. Sakurai, K. Kano and Y. Kuroda, *Chem. Commun.*, 2004, 408-409.

18. R. Nishiyabu and K. Kano, *Eur. J. Org. Chem.*, 2004, 4985-4988.

19. M. Vinodh, F. H. Alipour, A. A. Mohamod and T. F. Al-Azemi, *Molecules*, 2012, **17**, 11763-11799.

20. H. Kitagishi, S. Hatada, T. Itakura, Y. Maki, Y. Maeda and K. Kano, *Org. Biomol. Chem.*, 2013, **11**, 3203-3211.

21. F. Venema, A. E. Rowan and R. J. M. Nolte, *J. Am. Chem. Soc.*, 1996, **118**, 257-258.

22. K. Kano, H. Kitagishi, M. Kodera and S. Hirota, *Angew. Chem., Int. Ed.*, 2005, **44**, 435-438.

23. Y. Kobayashi, Y. Takashima, A. Hashidzume, H. Yamaguchi and A. Harada, *Sci. Rep.*, 2013, **3**, 1243, 1244 pp.

24. J. F. Lovell, A. Roxin, K. K. Ng, Q. Qi, J. D. McMullen, R. S. Da Costa and G. Zheng, *Biomacromolecules*, 2011, **12**, 3115-3118.

25. H.-T. Nguyen, D.-T. Pham, S. F. Lincoln, J. Wang, X. Guo, C. J. Easton and R. K. Prud'homme, *Polym. Chem.*, 2013, **4**, 820-829.

26. J. Wang, L. Li, X. Guo, L. Zheng, D.-T. Pham, S. F. Lincoln, H. T. Ngo, P. Clements, B. L. May, R. K. Prud'homme and C. J. Easton, *Ind. Eng. Chem. Res.*, 2011, **50**, 7566-7571.

27. J. Wang, D.-T. Pham, T. W. Kee, S. N. Clafton, X. Guo, P. Clements, S. F. Lincoln, R. K. Prud'homme and C. J. Easton, *Macromolecules*, 2011, **44**, 9782-9791.

28. R. Luguya, L. Jaquinod, F. R. Fronczek, M. G. H. Vicente and K. M. Smith, *Tetrahedron*, 2004, **60**, 2757-2763.

29. W. J. Kruper, Jr., T. A. Chamberlin and M. Kochanny, *J. Org. Chem.*, 1989, **54**, 2753-2756.

30. X. Guo, A. A. Abdala, B. L. May, S. F. Lincoln, S. A. Khan and R. K. Prud'homme, *Macromolecules*, 2005, **38**, 3037-3040.

31. D.-T. Pham, H. T. Ngo, S. F. Lincoln, B. L. May and C. J. Easton, *Tetrahedron*, 2010, **66**, 2895-2898.

32. J. M. Ribo, J.-A. Farrera, M. L. Valero and A. Virgili, *Tetrahedron*, 1995, **51**, 3705-3712.

33. A. Iosif and U. W. Grummt, *J. Prakt. Chem./Chem.- Ztg.*, 1997, **339**, 420-425.

34. H.-J. Schneider, F. Hacket, V. Ruediger and H. Ikeda, *Chem. Rev.*, 1998, **98**, 1755-1785.

35. Z. El-Hachemi, J.-A. Farrera, H. Garcia-Ortega, O. Ramirez-Gutierrez and J. M. Ribo, *J. Porphyrins Phthalocyanines*, 2001, **5**, 465-473.

36. W. Saenger, J. Jacob, K. Gessler, T. Steiner, D. Hoffmann, H. Sanbe, K. Koizumi, S. M. Smith and T. Takaha, *Chem. Rev.*, 1998, **98**, 1787-1802.

37. H.-T. Nguyen, D.-T. Pham, C. J. Easton and S. F. Lincoln, *Aust. J. Chem.*, 2013, **66**, 1057-1064.

38. HypSpec, Protonic Software, 2 Templegate Avenue, Leeds LS15 0HD, UK.

39. F. Venema, H. F. M. Nelissen, P. Berthault, N. Birlirakis, A. E. Rowan, M. C. Feiters and R. J. M. Nolte, *Chem. Eur. J.*, 1998, **4**, 2237-2250.

40. M. V. Rekharsky and Y. Inoue, *Chem. Rev.*, 1998, **98**, 1875-1917.

41. L. Li, X. Guo, L. Fu, R. K. Prud'homme and S. F. Lincoln, *Langmuir*, 2008, **24**, 8290-8296.

4.8. APPENDIX

2D NOESY ^{1}H NMR Spectra

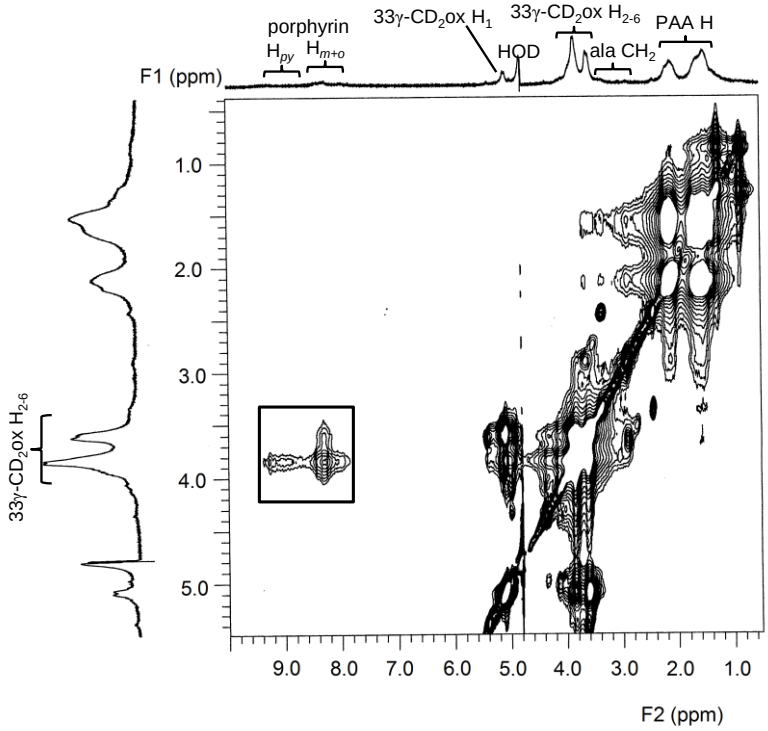

Figure A1: 2D ^{1}H NOESY NMR (600 MHz) spectrum of 3% substituted PAATSPPala ([TSPPala] = 3.0×10^{-3} mol dm^{-3}) and equimolar 33γ-CD_2ox in D_2O (pD 7.0 phosphate buffer, I = 0.10 mol dm^{-3}) at 298.2 K with a mixing time of 300 ms. Cross–peaks enclosed in the rectangle arise from interaction between the annular γ-CD protons $H_{3,5,6}$ of the cyclodextrin annulus and the pyrrolic (H_{py}) and phenyl (H_{m+o}) protons of the TSPPala substituent.

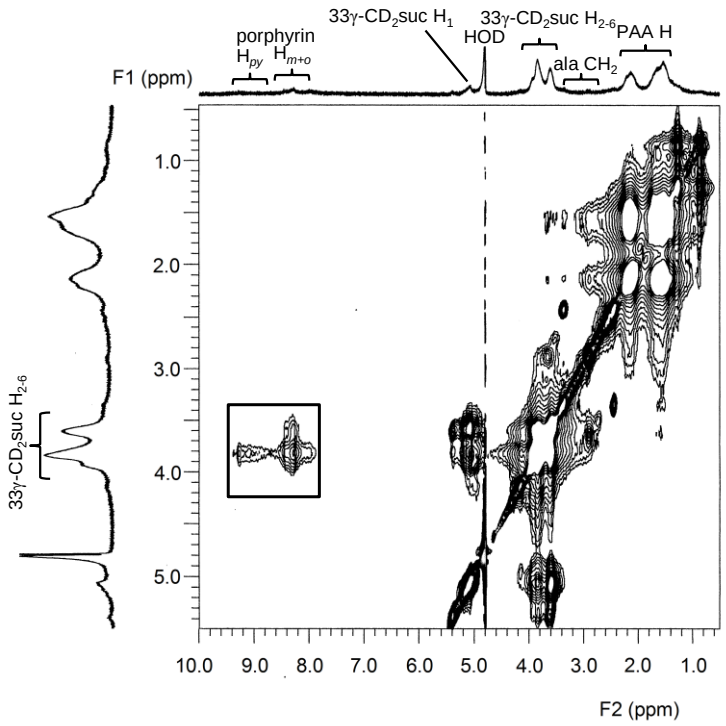

Figure A2: 2D ^{1}H NOESY NMR (600 MHz) spectrum of 3% substituted PAATSPPala ([TSPPala] = 3.0×10^{-3} mol dm^{-3}) and equimolar 33γ-CD_2suc in D_2O (pD 7.0 phosphate buffer, I = 0.10 mol dm^{-3}) at 298.2 K with a mixing time of 300 ms. Cross–peaks enclosed in the rectangle arise from interaction between the annular γ-CD protons $H_{3,5,6}$ of the cyclodextrin annulus and the pyrrolic (H_{py}) and phenyl protons (H_{m+o}) of the TSPPala substituent.

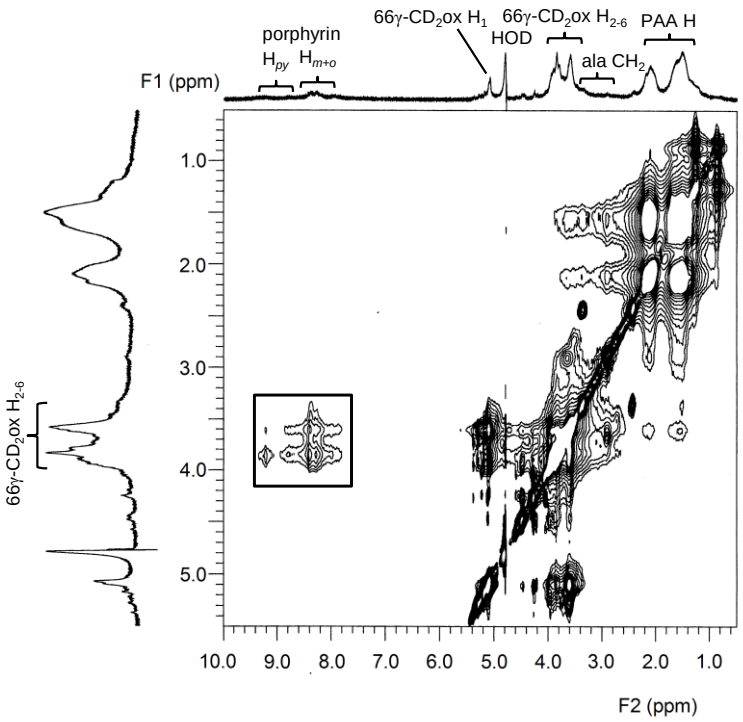

Figure A3: 2D ^{1}H NOESY NMR (600 MHz) spectrum of 3% substituted PAATSPPala ([TSPPala] = 3.0×10^{-3} mol dm^{-3}) and equimolar 66γ-CD_2ox in D_2O (pD 7.0 phosphate buffer, I = 0.10 mol dm^{-3}) at 298.2 K with a mixing time of 300 ms. Cross–peaks enclosed in the rectangle arise from interaction between the annular γ-CD protons $H_{3,5,6}$ of the cyclodextrin annulus and the pyrrolic (H_{py}) and phenyl protons (H_{m+o}) of the TSPPala substituent.

.

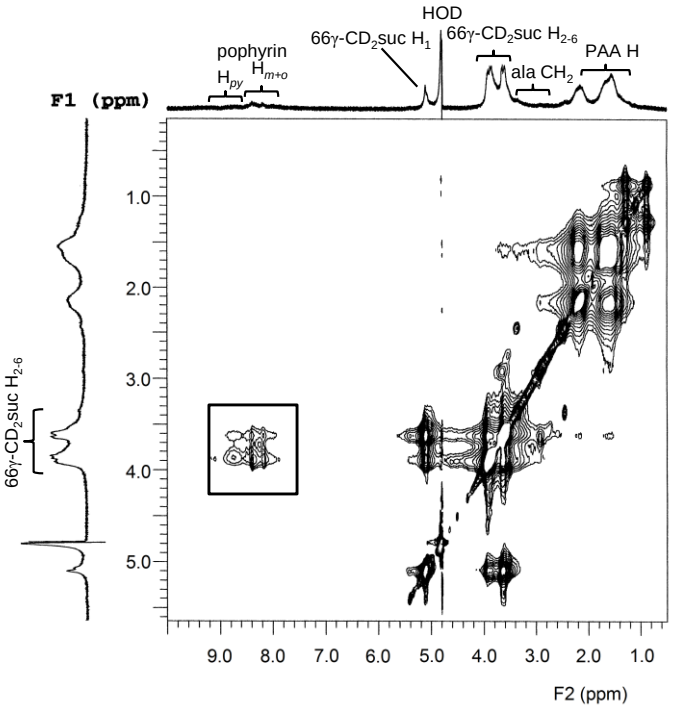

Figure A4: 2D ^{1}H NOESY NMR (600 MHz) spectrum of 3% substituted PAATSPPala ([TSPPala] = 3.0×10^{-3} mol dm^{-3}) and equimolar 66γ-CD_2suc in D_2O (pD 7.0 phosphate buffer, I = 0.10 mol dm^{-3}) at 298.2 K with a mixing time of 300 ms. Cross–peaks enclosed in the rectangle arise from interaction between the annular γ-CD protons $H_{3,5,6}$ of the cyclodextrin annulus and the pyrrolic (H_{py}) and phenyl protons (H_{m+o}) of the TSPPala substituent.

Variable Temperature UV-Vis Spectra

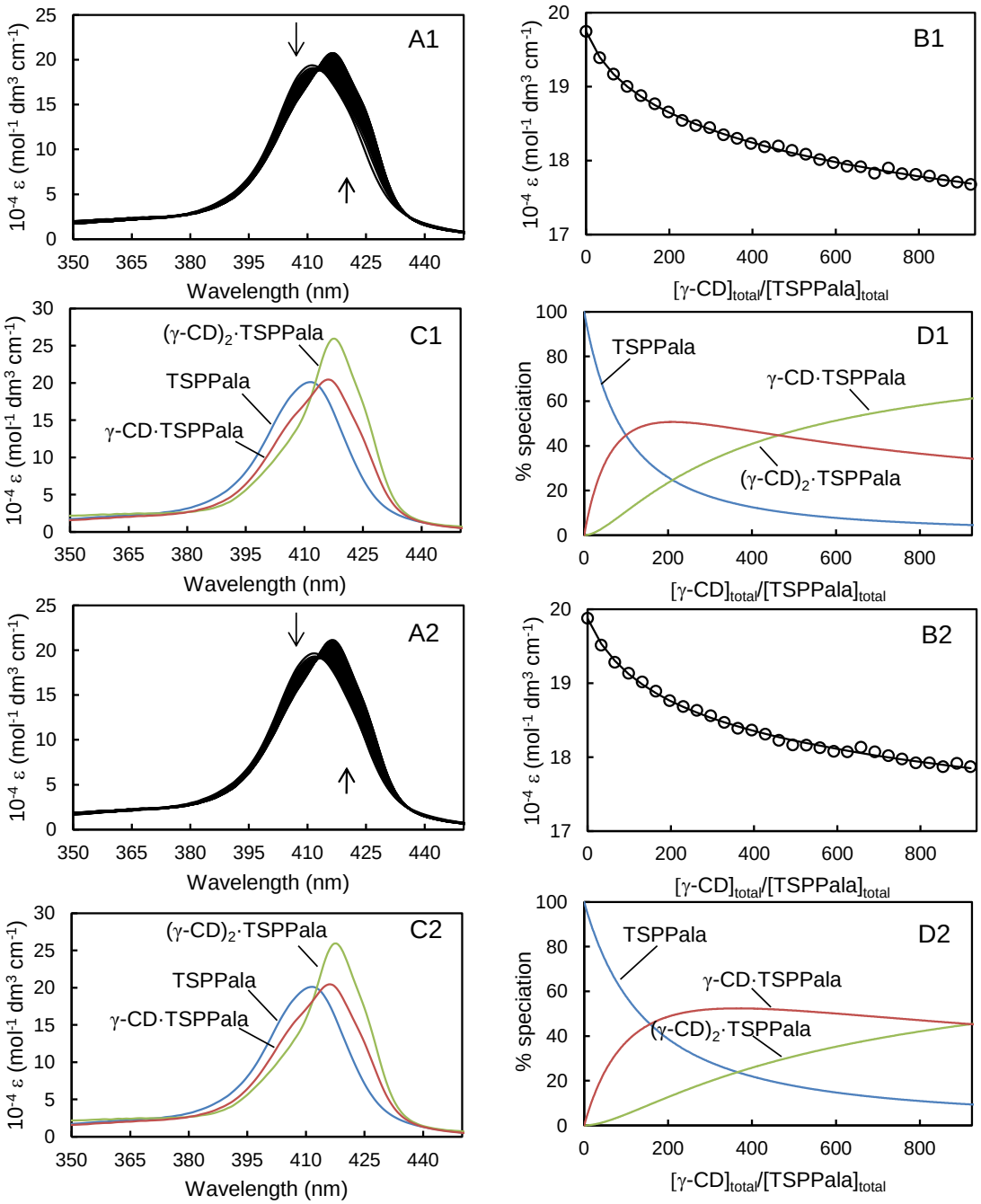

Figure A5: (A1, A2) Molar absorbance change of the porphyrin substituents of PAATSPPala ([TSPPala] = 3.10 × 10^{-6} mol dm^{-3}) in phosphate buffer, pH 7.0, I = 0.10 mol dm^{-3} with sequential injections (10 mm^3 each) of γ-CD (1.01 × 10^{-2} mol dm^{-3}) into both sample and reference cells. The arrows indicate the direction of molar absorbance change as the molar ratio of [γ-CD]/[TSPPala] increases. (B1, B2) Molar absorbance variation at 410 nm and the line of best fit of an algorithm for 1:1 and 2:1 host-guest complexation over the wavelength range 380-430 nm. (C1, C2) Calculated molar absorbance of free and complexed TSPPala. (D1, D2) Speciation with $[TSPPala]_{total}$ = 100%. Note: A1-D1: data at 278.2 K. A2-D2: data at 288.2 K.

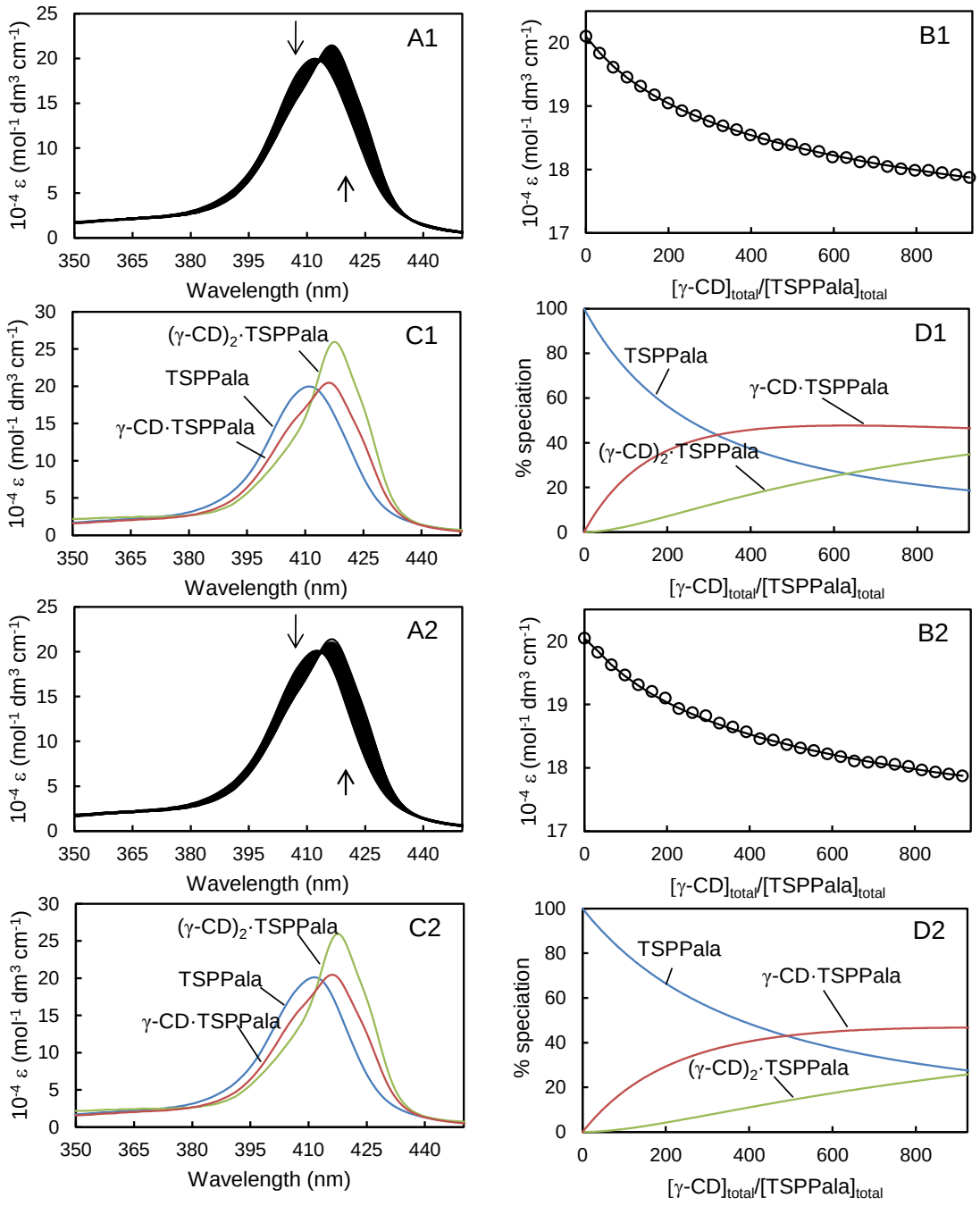

Figure A6: (A1, A2) Molar absorbance change of the porphyrin substituents of PAATSPPala ([TSPPala] = 3.10×10^{-6} mol dm^{-3}) in phosphate buffer, pH 7.0, I = 0.10 mol dm^{-3} with sequential injections (10 mm^3 each) of γ-CD (1.01×10^{-2} mol dm^{-3}) into both sample and reference cells. The arrows indicate the direction of molar absorbance change as the molar ratio of [γ-CD]/[TSPPala] increases. (B1, B2) Molar absorbance variation at 410 nm and the line of best fit of an algorithm for 1:1 and 2:1 host-guest complexation over the wavelength range 380-430 nm. (C1, C2) Calculated molar absorbance of free and complexed TSPPala. (D1, D2) Speciation with $[TSPPala]_{total}$ = 100%. Note: A1-D1: data at 298.2 K. A2-D2: data at 308.2 K.

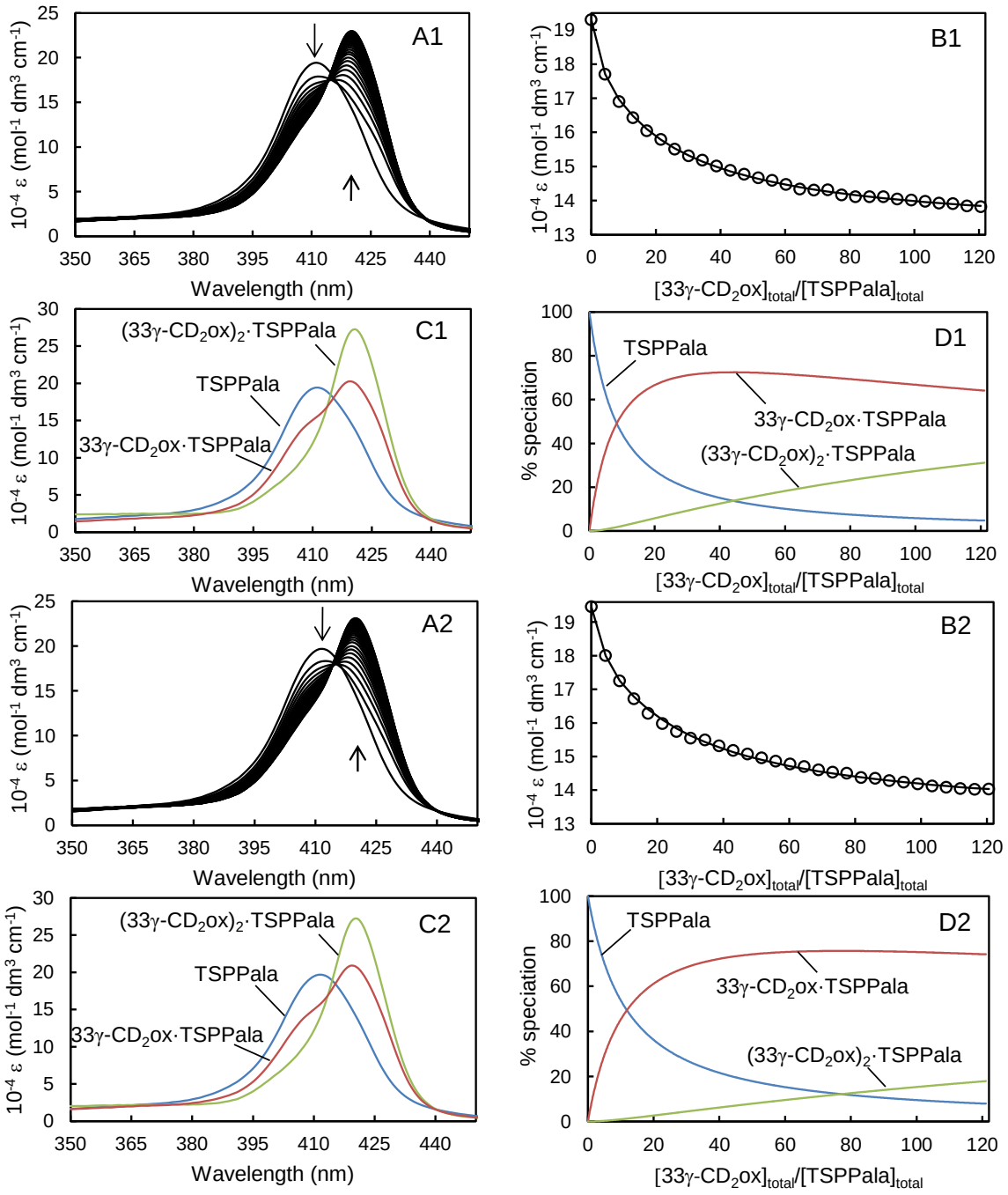

Figure A7: (A1, A2) Molar absorbance change of the porphyrin substituents of PAATSPPala ([TSPPala] = 3.10 × 10^{-6} mol dm^{-3}) in phosphate buffer, pH 7.0, I = 0.10 mol dm^{-3} with sequential injections (10 mm^3 each) of 33γ-CD$_2$ox (2.65 × 10^{-3} mol dm^{-3}) into both sample and reference cells. The arrows indicate the direction of molar absorbance change as the molar ratio of [33γ-CD$_2$ox]/[TSPPala] increases. (B1, B2) Molar absorbance variation at 410 nm and the line of best fit of an algorithm for 1:1 and 2:1 host-guest complexation over the wavelength range 380-430 nm. (C1, C2) Calculated molar absorbance of free and complexed TSPPala. (D1, D2) Speciation with [TSPPala]$_{total}$ = 100%. Note: A1-D1: data at 278.2 K. A2-D2: data at 288.2 K.

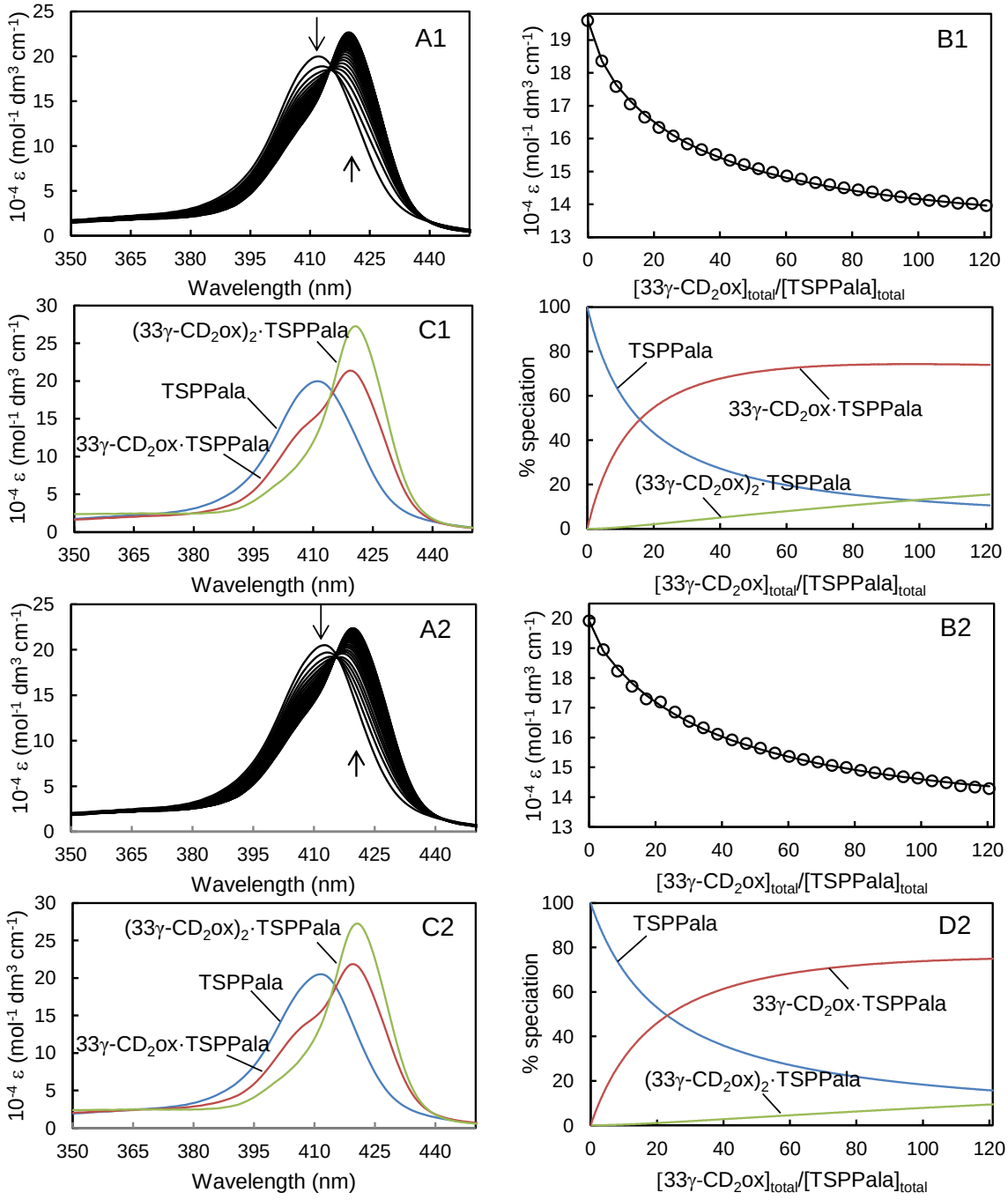

Figure A8: (A1, A2) Molar absorbance change of the porphyrin substituents of PAATSPPala ([TSPPala] = 3.10×10^{-6} mol dm^{-3}) in phosphate buffer, pH 7.0, I = 0.10 mol dm^{-3} with sequential injections (10 mm^3 each) of 33γ-CD_2ox (2.65×10^{-3} mol dm^{-3}) into both sample and reference cells. The arrows indicate the direction of molar absorbance change as the molar ratio of [33γ-CD_2ox]/[TSPPala] increases. (B1, B2) Molar absorbance variation at 410 nm and the line of best fit of an algorithm for 1:1 and 2:1 host-guest complexation over the wavelength range 380-430 nm. (C1, C2) Calculated molar absorbance of free and complexed TSPPala. (D1, D2) Speciation with $[\text{TSPPala}]_{\text{total}}$ = 100%. Note: A1-D1: data at 298.2 K. A2-D2: data at 308.2 K.

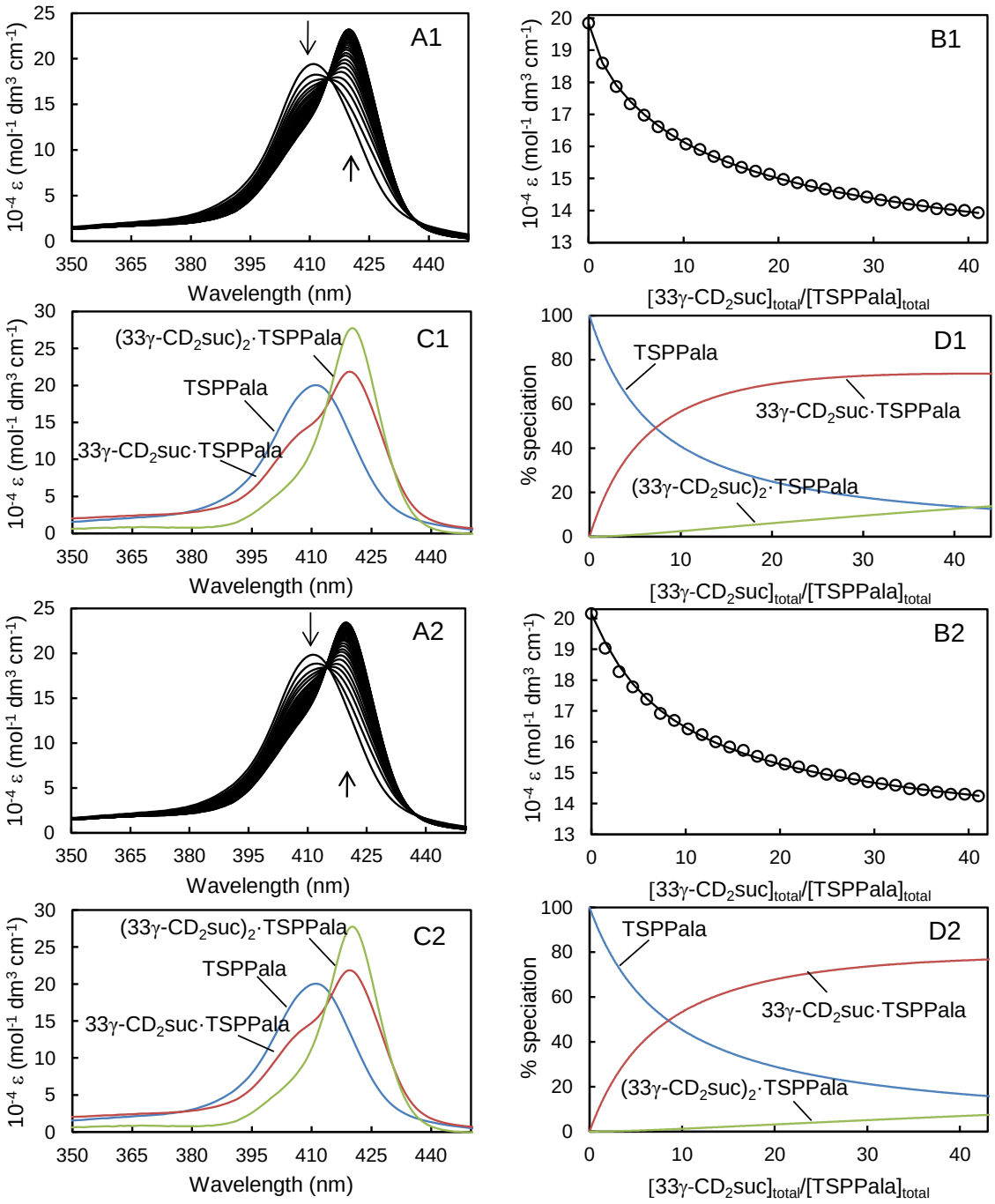

Figure A9: (A1, A2) Molar absorbance change of the porphyrin substituents of PAATSPPala ([TSPPala] = 3.10 × 10^{-6} mol dm^{-3}) in phosphate buffer, pH 7.0, I = 0.10 mol dm^{-3} with sequential injections (8 mm^3 each) of 33γ-CD_2suc (1.24 × 10^{-3} mol dm^{-3}) into both sample and reference cells. The arrows indicate the direction of molar absorbance change as the molar ratio of [33γ-CD_2suc]/[TSPPala] increases. (B1, B2) Molar absorbance variation at 410 nm and the line of best fit of an algorithm for 1:1 and 2:1 host-guest complexation over the wavelength range 380-430 nm. (C1, C2) Calculated molar absorbance of free and complexed TSPPala. (D1, D2) Speciation with [TSPPala]total = 100%. Note: A1-D1: data at 278.2 K. A2-D2: data at 288.2 K.

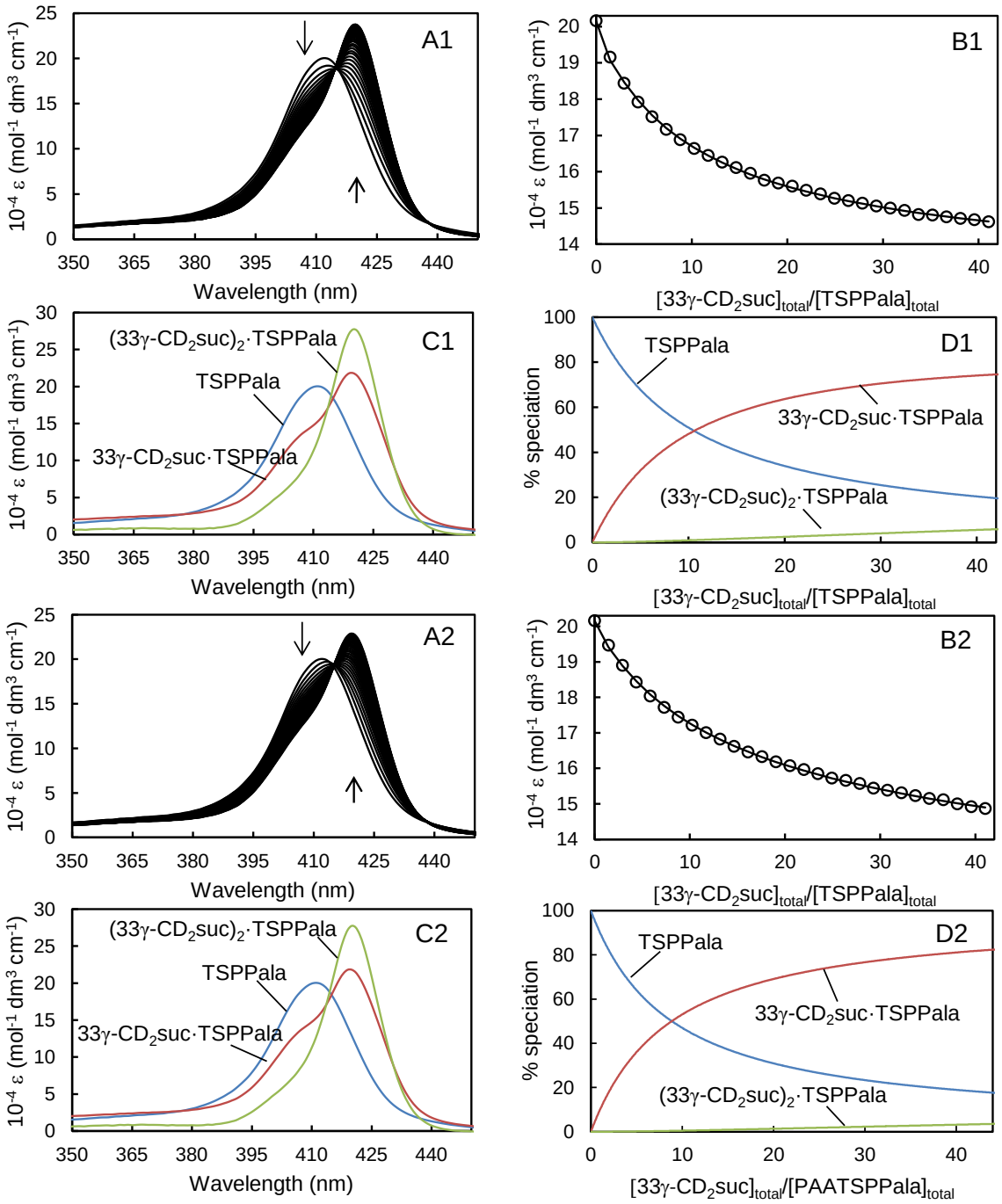

Figure A10: (A1, A2) Molar absorbance change of the porphyrin substituents of PAATSPPala ([TSPPala] = 3.10 × 10^{-6} mol dm^{-3}) in phosphate buffer, pH 7.0, I = 0.10 mol dm^{-3} with sequential injections (8 mm^3 each) of 33γ-CD$_2$suc (1.24 × 10^{-3} mol dm^{-3}) into both sample and reference cells. The arrows indicate the direction of molar absorbance change as the molar ratio of [33γ-CD$_2$suc]/[TSPPala] increases. (B1, B2) Molar absorbance variation at 410 nm and the line of best fit of an algorithm for 1:1 and 2:1 host-guest complexation over the wavelength range 380-430 nm. (C1, C2) Calculated molar absorbance of free and complexed TSPPala. (D1, D2) Speciation with [TSPPala]$_{total}$ = 100%. Note: A1-D1: data at 298.2 K. A2-D2: data at 308.2 K.

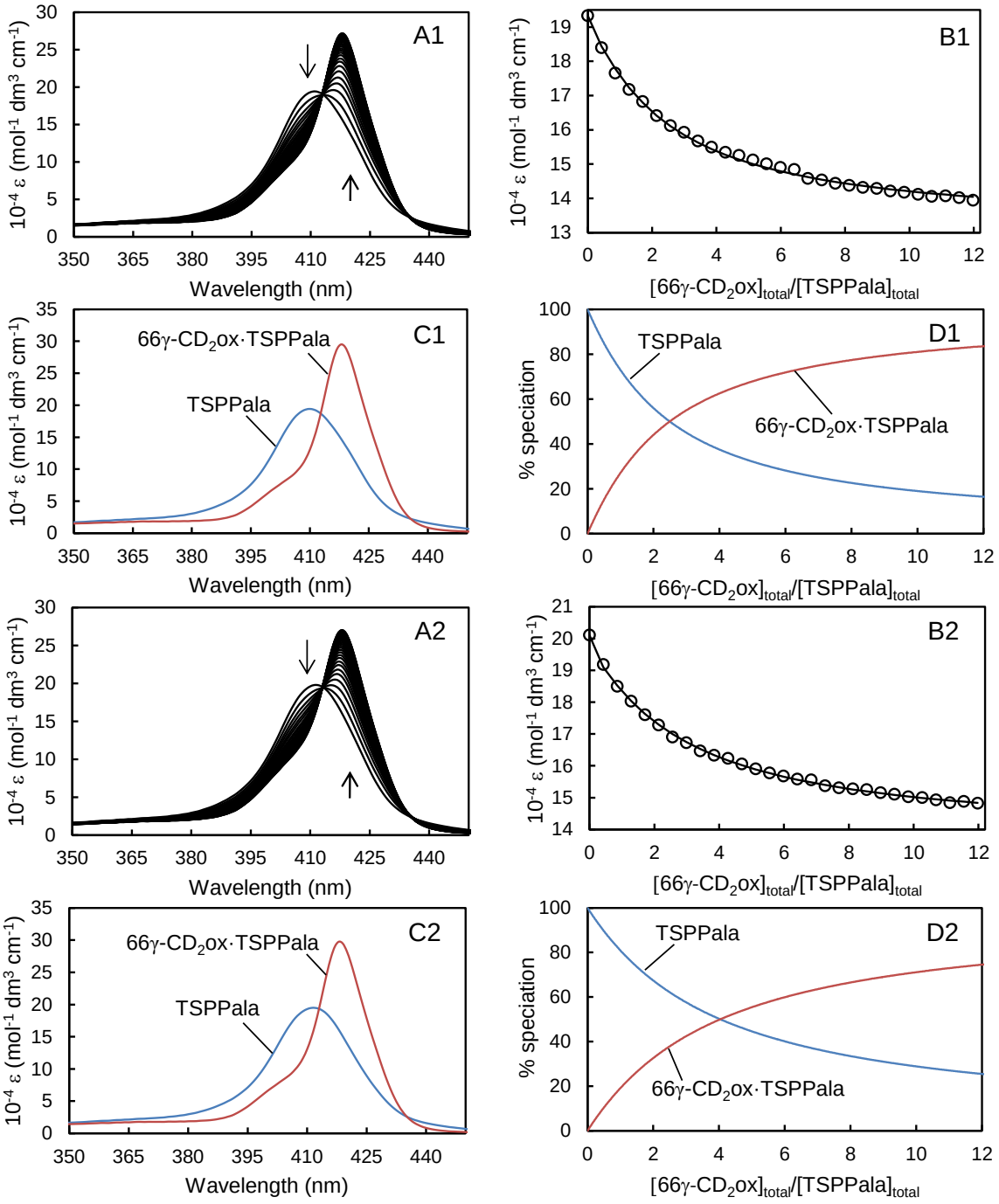

Figure A11: (A1, A2) Molar absorbance change of the porphyrin substituents of PAATSPPala ([TSPPala] = 3.10×10^{-6} mol dm^{-3}) in phosphate buffer, pH 7.0, I = 0.10 mol dm^{-3} with sequential injections (10 mm^3 each) of 66γ-CD$_2$ox (2.52×10^{-4} mol dm^{-3}) into both sample and reference cells. The arrows indicate the direction of molar absorbance change as the molar ratio of [66γ-CD$_2$ox]/[TSPPala] increases. (B1, B2) Molar absorbance variation at 410 nm and the line of best fit of an algorithm for 1:1 host-guest complexation over the wavelength range 380-430 nm. (C1, C2) Calculated molar absorbance of free and complexed TSPPala. (D1, D2) Speciation with [TSPPala]$_{total}$ = 100%. Note: A1-D1: data at 278.2 K. A2-D2: data at 288.2 K.

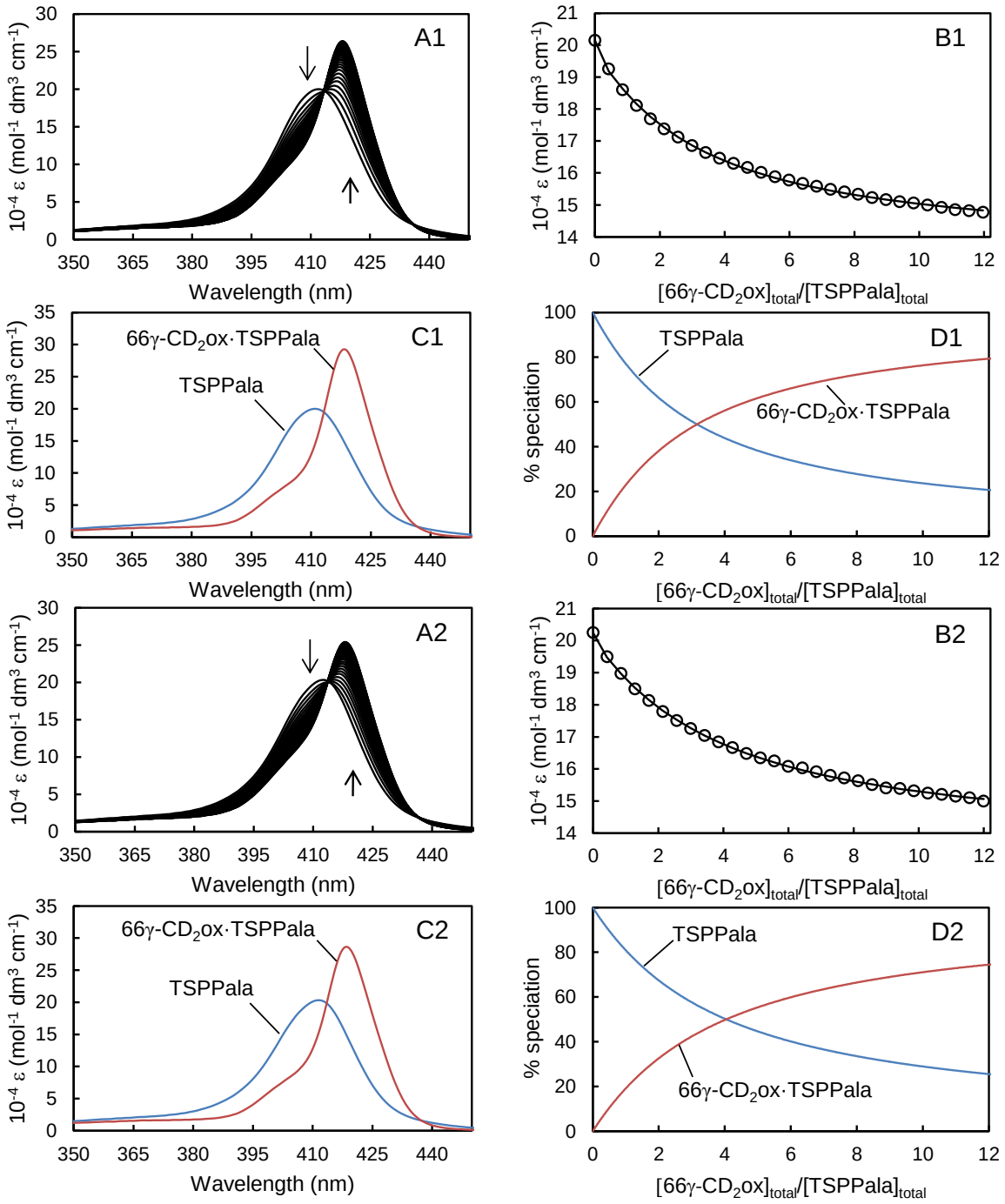

Figure A12: (A1, A2) Molar absorbance change of the porphyrin substituents of PAATSPPala ([TSPPala] = 3.10×10^{-6} mol dm^{-3}) in phosphate buffer, pH 7.0, I = 0.10 mol dm^{-3} with sequential injections (10 mm^3 each) of 66γ-CD$_2$ox (2.52×10^{-4} mol dm^{-3}) into both sample and reference cells. The arrows indicate the direction of molar absorbance change as the molar ratio of [66γ-CD$_2$ox]/[TSPPala] increases. (B1, B2) Molar absorbance variation at 410 nm and the line of best fit of an algorithm for 1:1 host-guest complexation over the wavelength range 380-430 nm. (C1, C2) Calculated molar absorbance of free and complexed TSPPala. (D1, D2) Speciation with [TSPPala]$_{total}$ = 100%. Note: A1-D1: data at 298.2 K. A2-D2: data at 308.2 K.

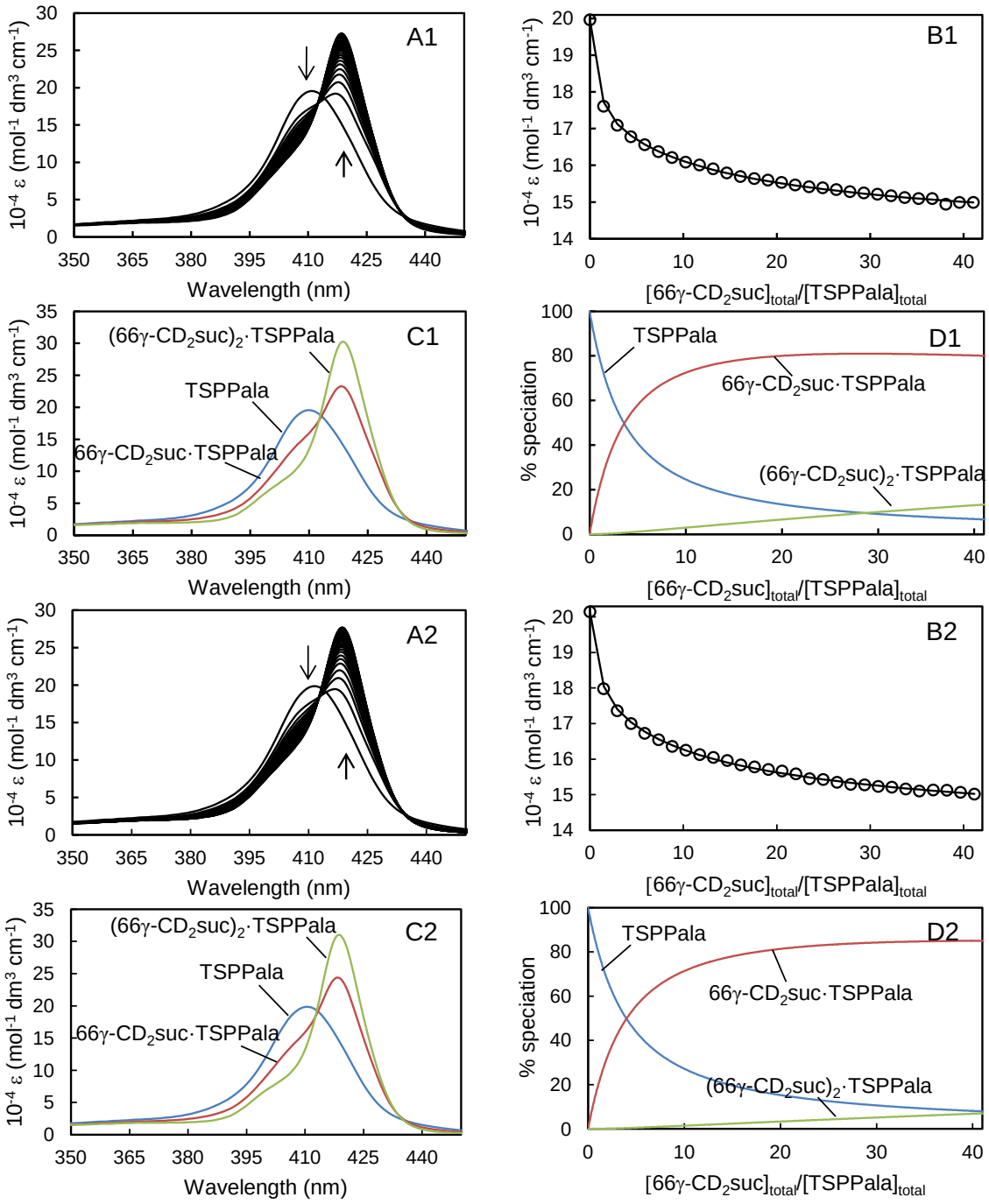

Figure A13: (A1, A2) Molar absorbance change of the porphyrin substituents of PAATSPPala ([TSPPala] = 3.10 × 10^{-6} mol dm^{-3}) in phosphate buffer, pH 7.0, I = 0.10 mol dm^{-3} with sequential injections (8 mm^3 each) of 66γ-CD$_2$suc (1.21 × 10^{-3} mol dm^{-3}) into both sample and reference cells. The arrows indicate the direction of molar absorbance change as the molar ratio of [66γ-CD$_2$suc]/[TSPPala] increases. (B1, B2) Molar absorbance variation at 410 nm and the line of best fit of an algorithm for 1:1 and 2:1 host-guest complexation over the wavelength range 380-430 nm. (C1, C2) Calculated molar absorbance of free and complexed TSPPala. (D1, D2) Speciation with [TSPPala]$_{total}$ = 100%. Note: A1-D1: data at 278.2 K. A2-D2: data at 288.2 K.

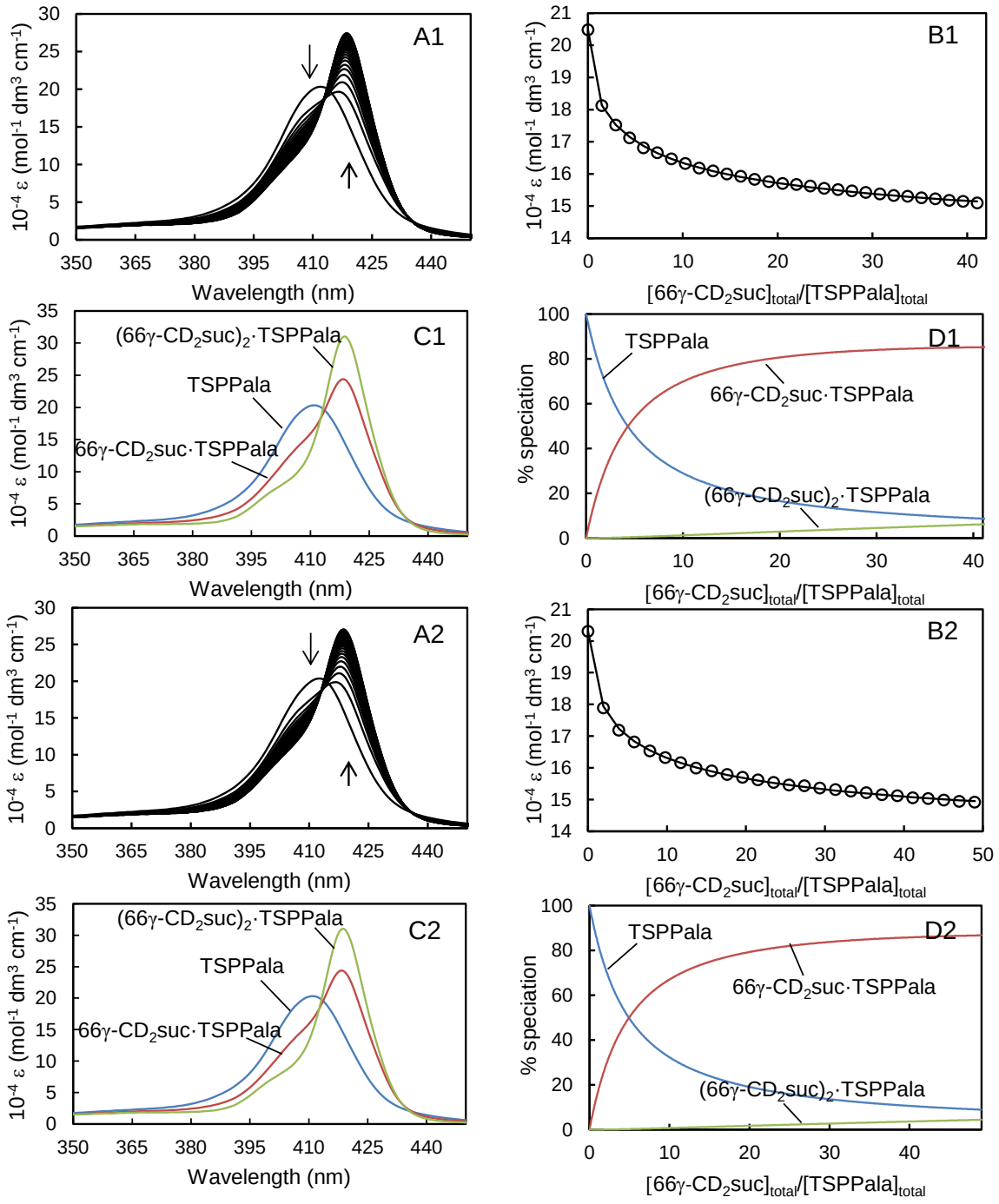

Figure A14: (A1, A2) Molar absorbance change of the porphyrin substituents of PAATSPPala ([TSPPala] = 3.10 × 10^{-6} mol dm^{-3}) in phosphate buffer, pH 7.0, I = 0.10 mol dm^{-3} with sequential injections (8 or 10 mm^3 each for 298.2 and 308.2 K, respectively) of 66γ-CD$_2$suc (1.21 × 10^{-3} mol dm^{-3}) into both sample and reference cells. The arrows indicate the direction of molar absorbance change as the molar ratio of [66γ-CD$_2$suc]/[TSPPala] increases. (B1, B2) Molar absorbance variation at 410 nm and the line of best fit of an algorithm for 1:1 and 2:1 host-guest complexation over the wavelength range 380-430 nm. (C1, C2) Calculated molar absorbance of free and complexed TSPPala. (D1, D2) Speciation with [TSPPala]$_{total}$ = 100%. Note: A1-D1: data at 298.2 K. A2-D2: data at 308.2 K.

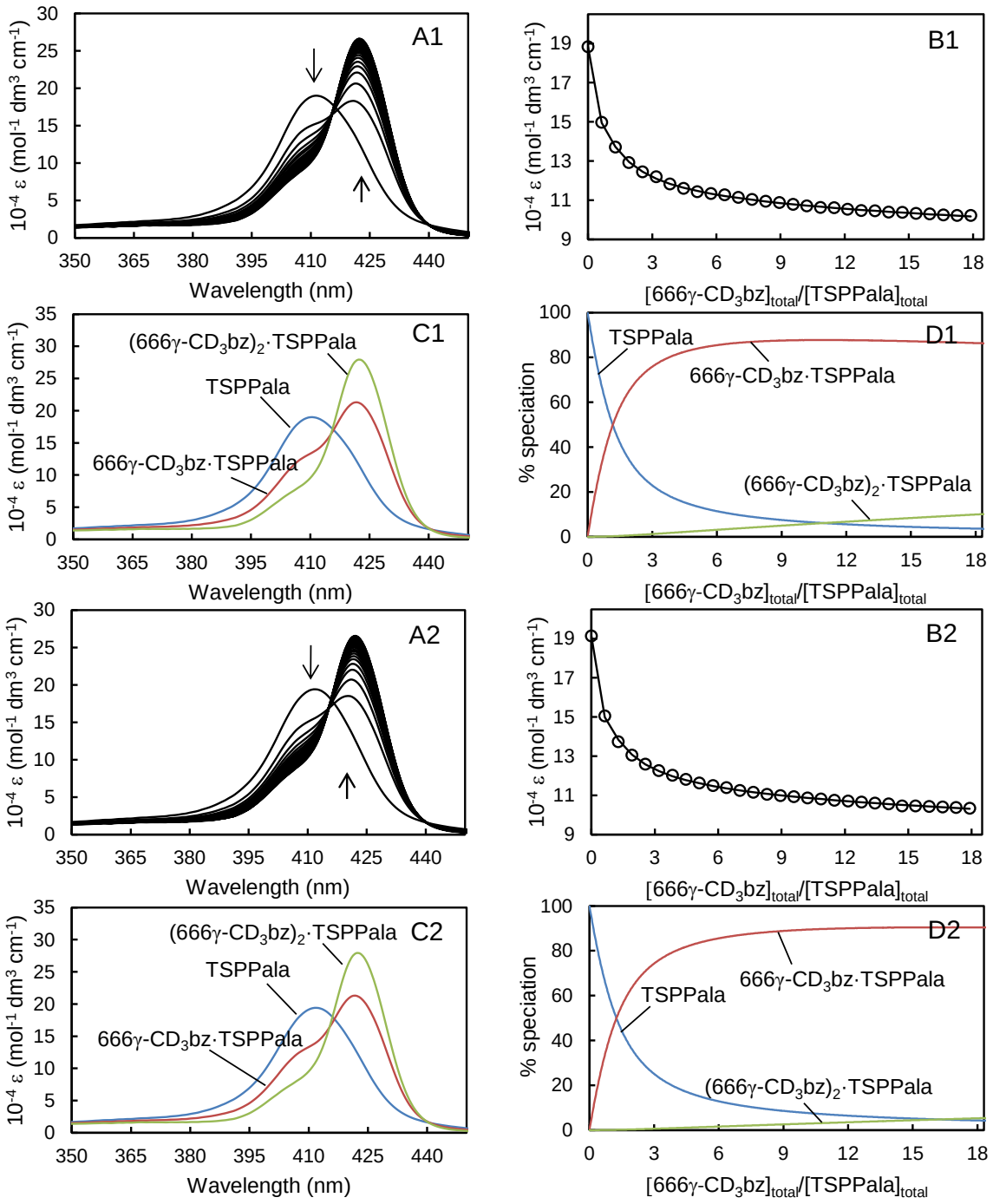

Figure A15: (A1, A2) Molar absorbance change of the porphyrin substituents of PAATSPPala ([TSPPala] = 3.10×10^{-6} mol dm^{-3}) in phosphate buffer, pH 7.0, I = 0.10 mol dm^{-3} with sequential injections (6 mm^3 each) of 666γ-CD$_3$bz (6.57×10^{-4} mol dm^{-3}) into both sample and reference cells. The arrows indicate the direction of molar absorbance change as the molar ratio of [666γ-CD$_3$bz]/[TSPPala] increases. (B1, B2) Molar absorbance variation at 410 nm and the line of best fit of an algorithm for 1:1 and 2:1 host-guest complexation over the wavelength range 380-430 nm. (C1, C2) Calculated molar absorbance of free and complexed TSPPala. (D1, D2) Speciation with [TSPPala]$_{total}$ = 100%. Note: A1-D1: data at 278.2 K. A2-D2: data at 288.2 K.

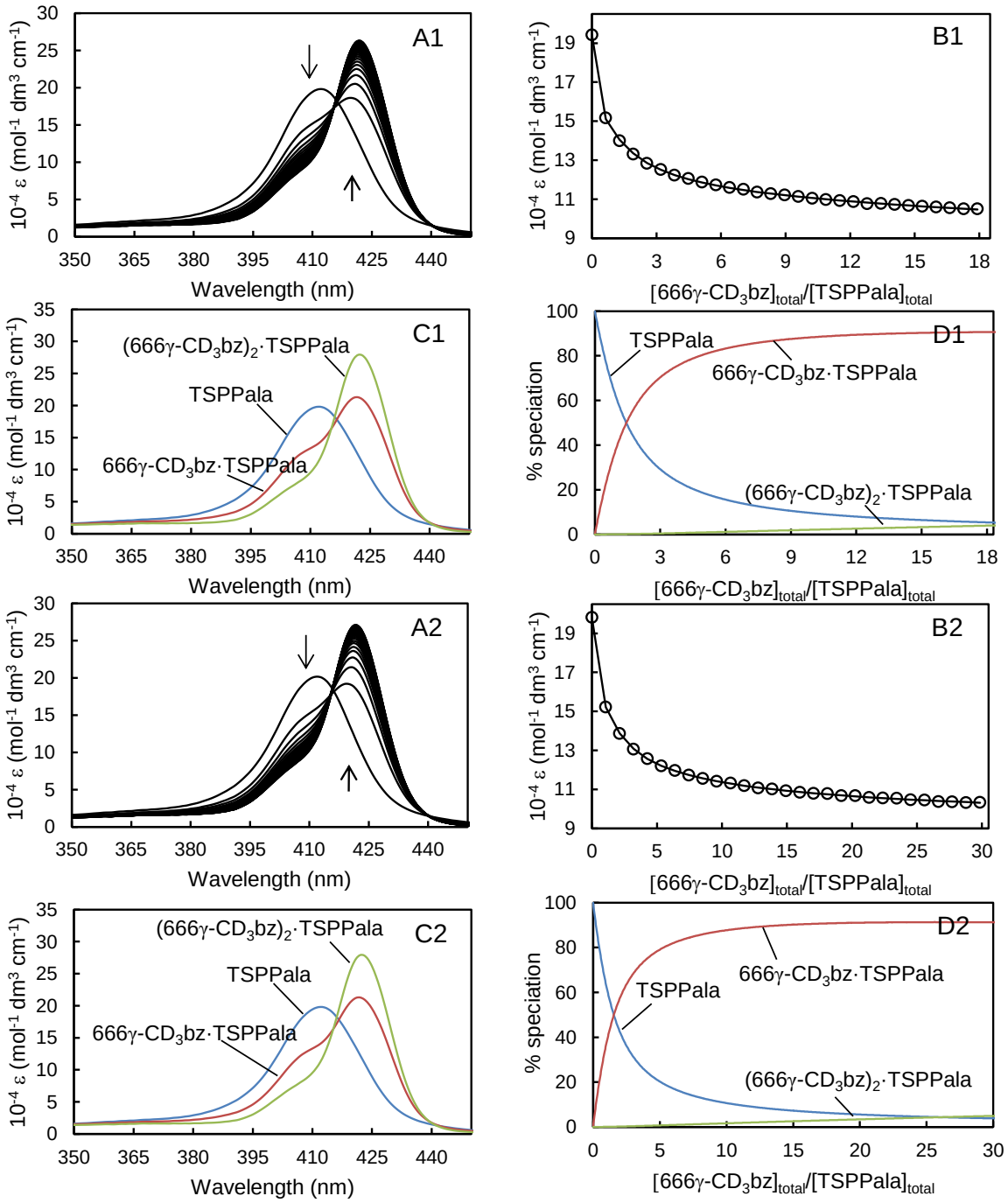

Figure A16: (A1, A2) Molar absorbance change of the porphyrin substituents of PAATSPPala ([TSPPala] = 3.10 × 10^{-6} mol dm^{-3}) in phosphate buffer, pH 7.0, I = 0.10 mol dm^{-3} with sequential injections (6 or 10 mm^3 each for 298.2 and 308.2 K, respectively) of 666γ-CD$_3$bz (6.57 × 10^{-4} mol dm^{-3}) into both sample and reference cells. The arrows indicate the direction of molar absorbance change as the molar ratio of [666γ-CD$_3$bz]/[TSPPala] increases. (B1, B2) Molar absorbance variation at 410 nm and the line of best fit of an algorithm for 1:1 and 2:1 host-guest complexation over the wavelength range 380-430 nm. (C1, C2) Calculated molar absorbance of free and complexed TSPPala. (D1, D2) Speciation with [TSPPala]$_{total}$ = 100%. Note: A1-D1: data at 298.2 K. A2-D2: data at 308.2 K.

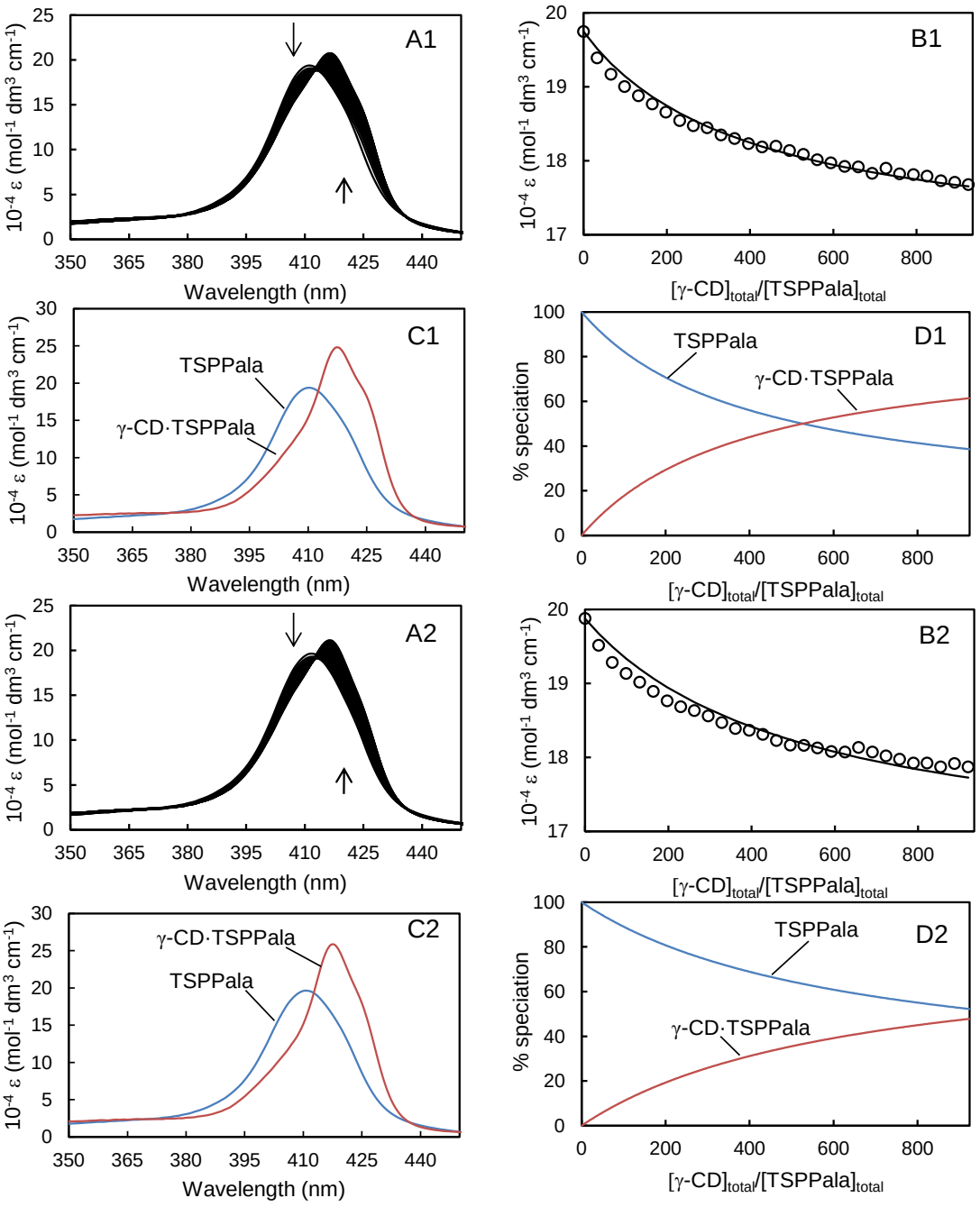

Figure A17: (A1, A2) Molar absorbance change of the porphyrin substituents of PAATSPPala ([TSPPala] = 3.10 × 10^{-6} mol dm^{-3}) in phosphate buffer, pH 7.0, I = 0.10 mol dm^{-3} with sequential injections (10 mm^3 each) of γ-CD (1.01 × 10^{-2} mol dm^{-3}) into both sample and reference cells. The arrows indicate the direction of molar absorbance change as the molar ratio of [γ-CD]/[TSPPala] increases. (B1, B2) Molar absorbance variation at 410 nm and the line of best fit of an algorithm for 1:1 host-guest complexation over the wavelength range 380-430 nm. (C1, C2) Calculated molar absorbance of free and complexed TSPPala. (D1, D2) Speciation with $[TSPPala]_{total}$ = 100%. Note: A1-D1: data at 278.2 K. A2-D2: data at 288.2 K.

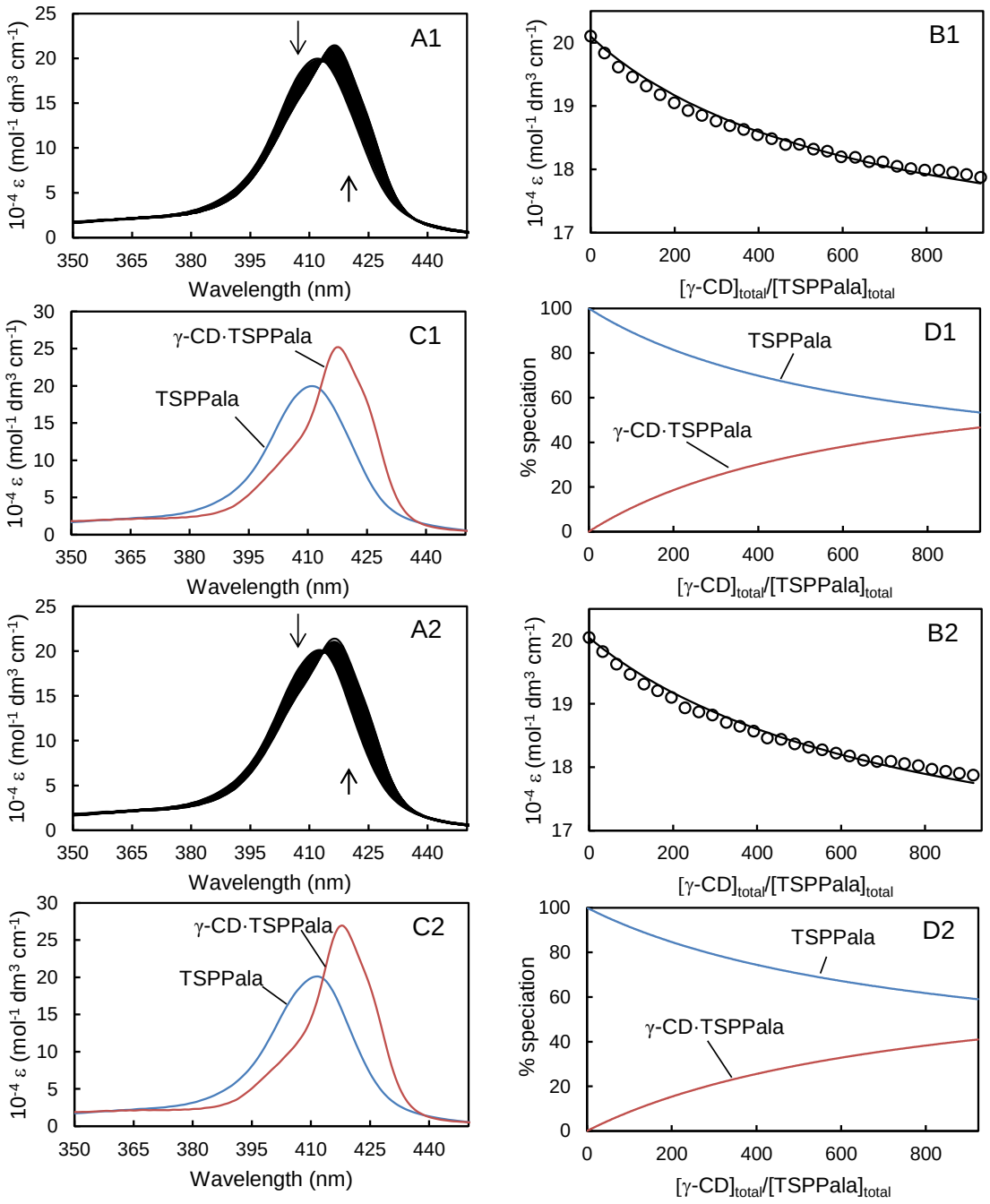

Figure A18: (A1, A2) Molar absorbance change of the porphyrin substituents of PAATSPPala ([TSPPala] = 3.10×10^{-6} mol dm^{-3}) in phosphate buffer, pH 7.0, I = 0.10 mol dm^{-3} with sequential injections (10 mm^3 each) of γ-CD (1.01×10^{-2} mol dm^{-3}) into both sample and reference cells. The arrows indicate the direction of molar absorbance change as the molar ratio of [γ-CD]/[TSPPala] increases. (B1, B2) Molar absorbance variation at 410 nm and the line of best fit of an algorithm for 1:1 host-guest complexation over the wavelength range 380-430 nm. (C1, C2) Calculated molar absorbance of free and complexed TSPPala. (D1, D2) Speciation with $[TSPPala]_{total}$ = 100%. Note: A1-D1: data at 298.2 K. A2-D2: data at 308.2 K.

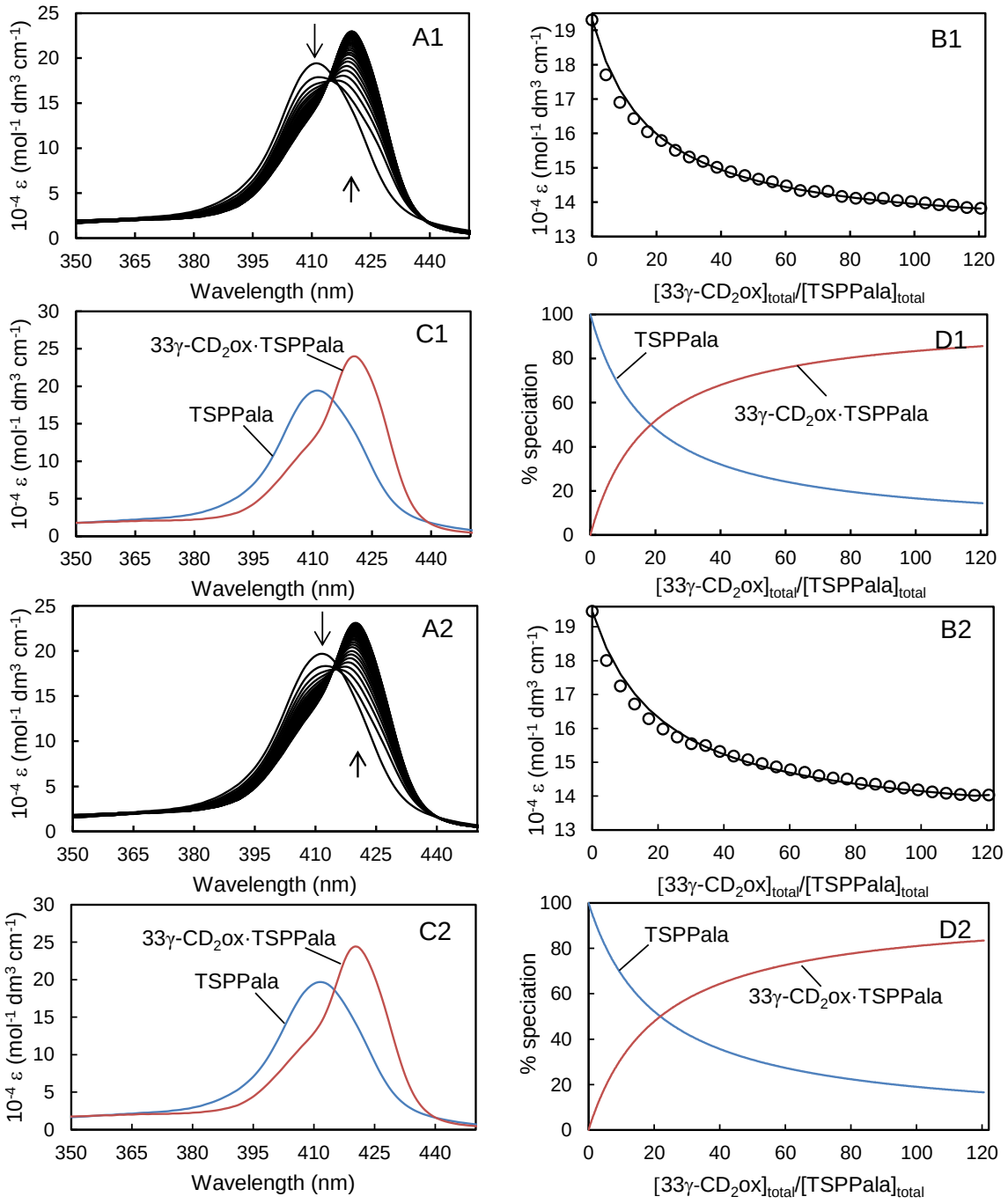

Figure A19: (A1, A2) Molar absorbance change of the porphyrin substituents of PAATSPPala ([TSPPala] = 3.10×10^{-6} mol dm^{-3}) in phosphate buffer, pH 7.0, I = 0.10 mol dm^{-3} with sequential injections (10 mm^3 each) of 33γ-CD$_2$ox (2.65×10^{-3} mol dm^{-3}) into both sample and reference cells. The arrows indicate the direction of molar absorbance change as the molar ratio of [33γ-CD$_2$ox]/[TSPPala] increases. (B1, B2) Molar absorbance variation at 410 nm and the tentative line of best fit of an algorithm for 1:1 host-guest complexation over the wavelength range 380-430 nm. (C1, C2) Calculated molar absorbance of free and complexed TSPPala. (D1, D2) Speciation with [TSPPala]$_{total}$ = 100%. Note: A1-D1: data at 278.2 K. A2-D2: data at 288.2 K.

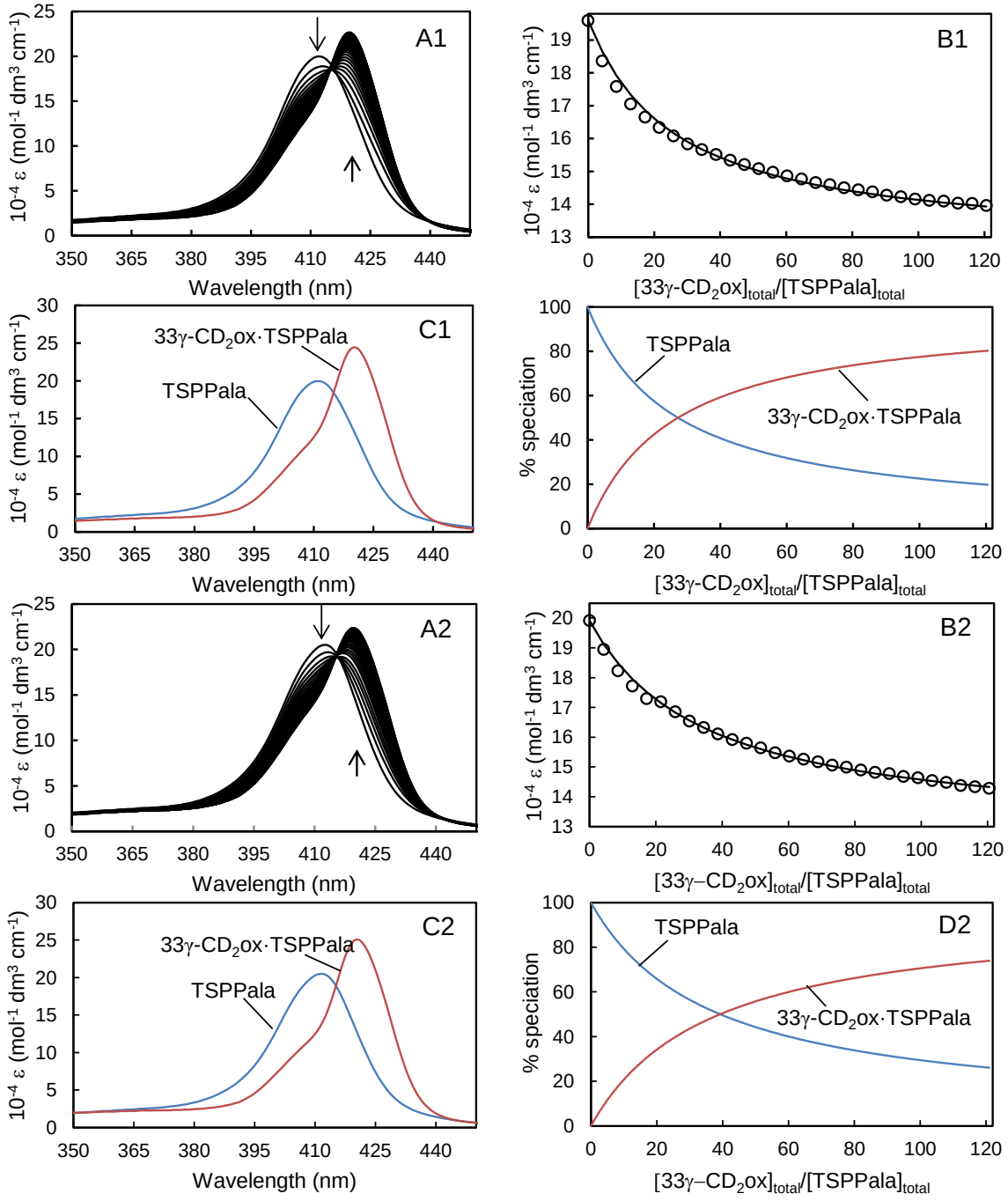

Figure A20: (A1, A2) Molar absorbance change of the porphyrin substituents of PAATSPPala ([TSPPala] = 3.10×10^{-6} mol dm^{-3}) in phosphate buffer, pH 7.0, I = 0.10 mol dm^{-3} with sequential injections (10 mm^3 each) of 33γ-CD$_2$ox (2.65×10^{-3} mol dm^{-3}) into both sample and reference cells. The arrows indicate the direction of molar absorbance change as the molar ratio of [33γ-CD$_2$ox]/[TSPPala] increases. (B1, B2) Molar absorbance variation at 410 nm and the tentative line of best fit of an algorithm for 1:1 host-guest complexation over the wavelength range 380-430 nm. (C1, C2) Calculated molar absorbance of free and complexed TSPPala. (D1, D2) Speciation with [TSPPala]$_{total}$ = 100%. Note: A1-D1: data at 298.2 K. A2-D2: data at 308.2 K.

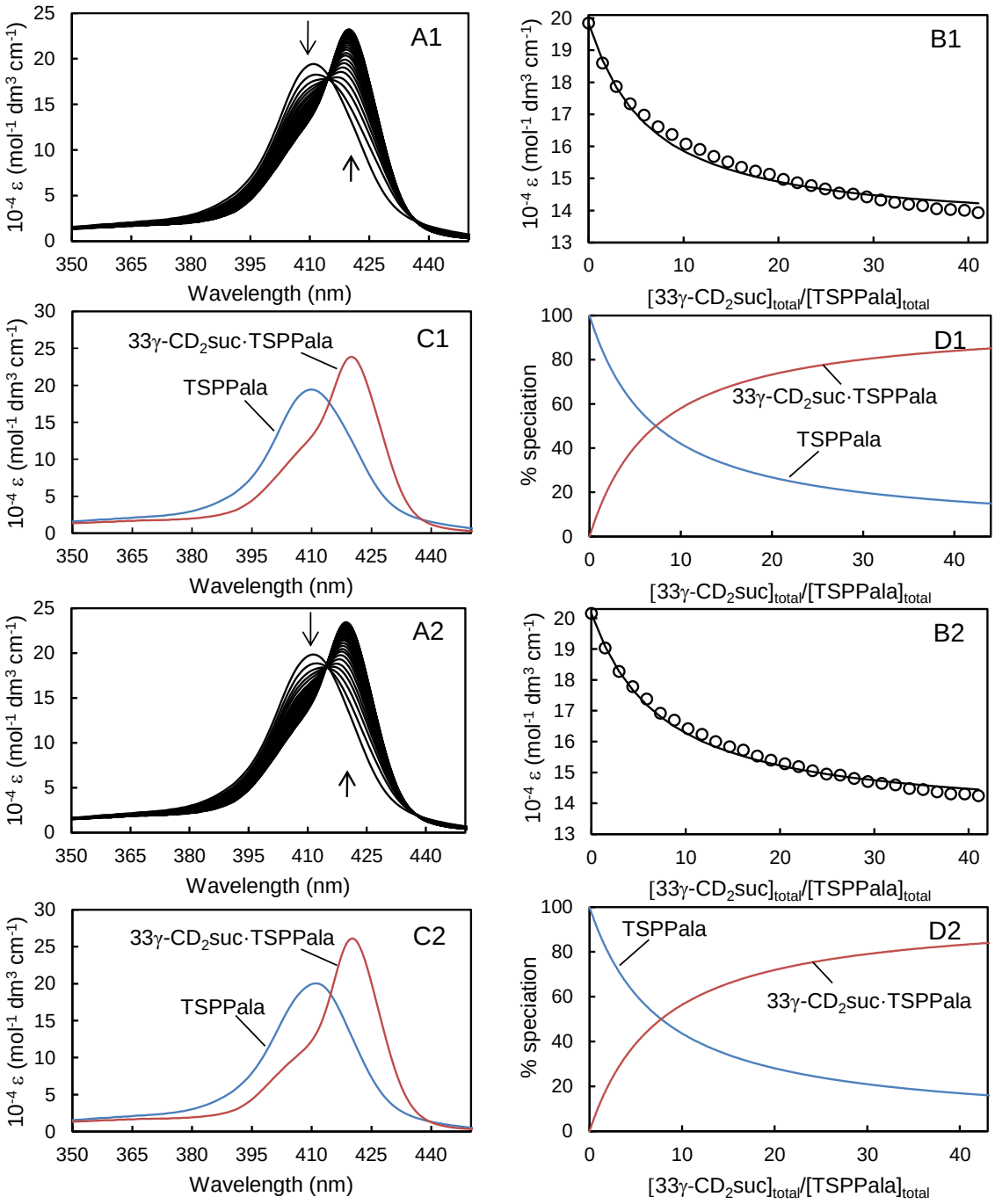

Figure A21: (A1, A2) Molar absorbance change of the porphyrin substituents of PAATSPPala ([TSPPala] = 3.10×10^{-6} mol dm^{-3}) in phosphate buffer, pH 7.0, I = 0.10 mol dm^{-3} with sequential injections (8 mm^3 each) of 33γ-CD_2suc (1.24×10^{-3} mol dm^{-3}) into both sample and reference cells. The arrows indicate the direction of molar absorbance change as the molar ratio of [33γ-CD_2suc]/[TSPPala] increases. (B1, B2) Molar absorbance variation at 410 nm and the line of best fit of an algorithm for 1:1 host-guest complexation over the wavelength range 380-430 nm. (C1, C2) Calculated molar absorbance of free and complexed TSPPala. (D1, D2) Speciation with [TSPPala]total = 100%. Note: A1-D1: data at 278.2 K. A2-D2: data at 288.2 K.

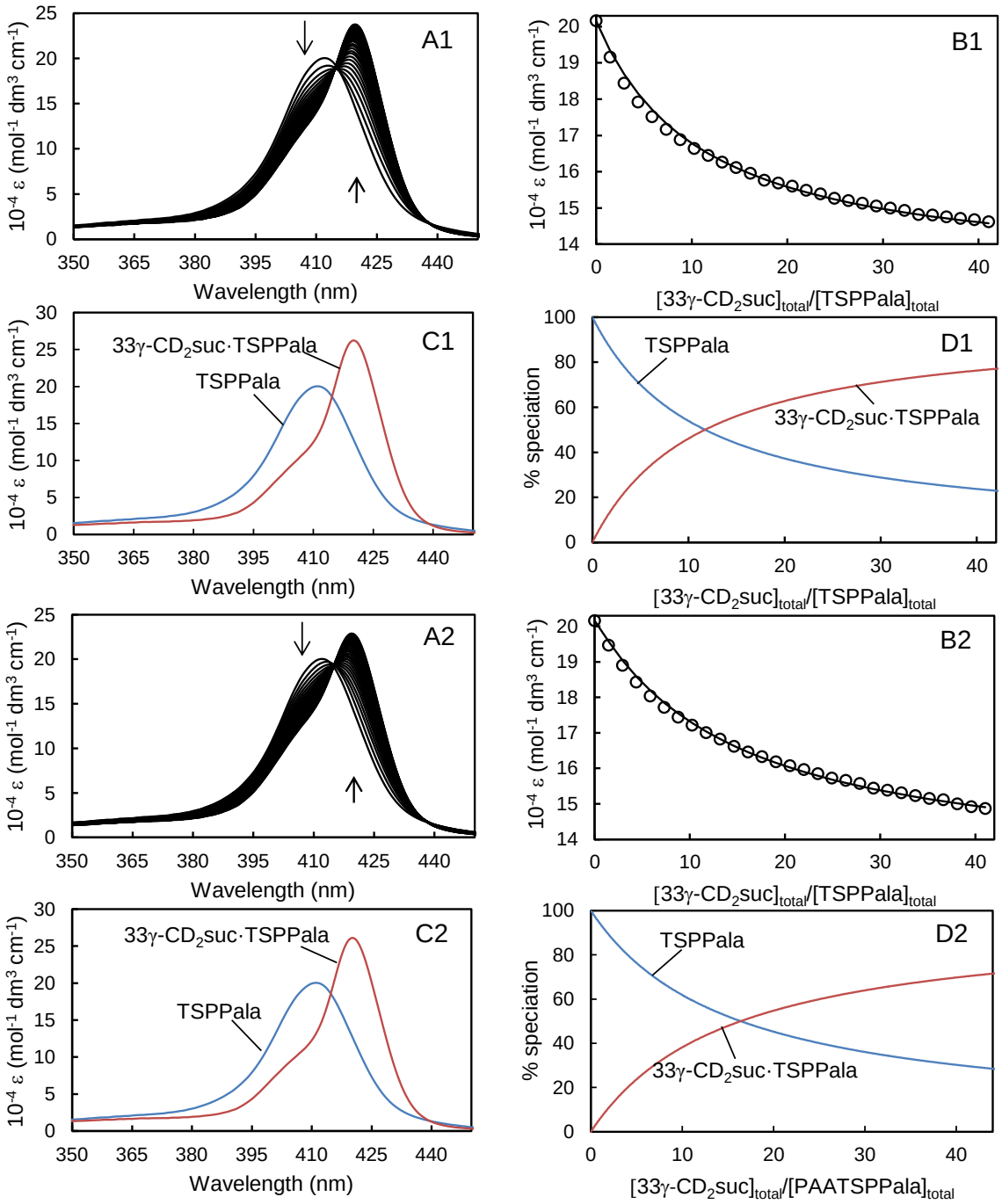

Figure A22: (A1, A2) Molar absorbance change of the porphyrin substituents of PAATSPPala ([TSPPala] = 3.10×10^{-6} mol dm^{-3}) in phosphate buffer, pH 7.0, I = 0.10 mol dm^{-3} with sequential injections (8 mm^3 each) of 33γ-CD_2suc (1.24×10^{-3} mol dm^{-3}) into both sample and reference cells. The arrows indicate the direction of molar absorbance change as the molar ratio of [33γ-CD_2suc]/[TSPPala] increases. (B1, B2) Molar absorbance variation at 410 nm and the line of best fit of an algorithm for 1:1 host-guest complexation over the wavelength range 380-430 nm. (C1, C2) Calculated molar absorbance of free and complexed TSPPala. (D1, D2) Speciation with $[TSPPala]_{total}$ = 100%. Note: A1-D1: data at 298.2 K. A2-D2: data at 308.2 K.

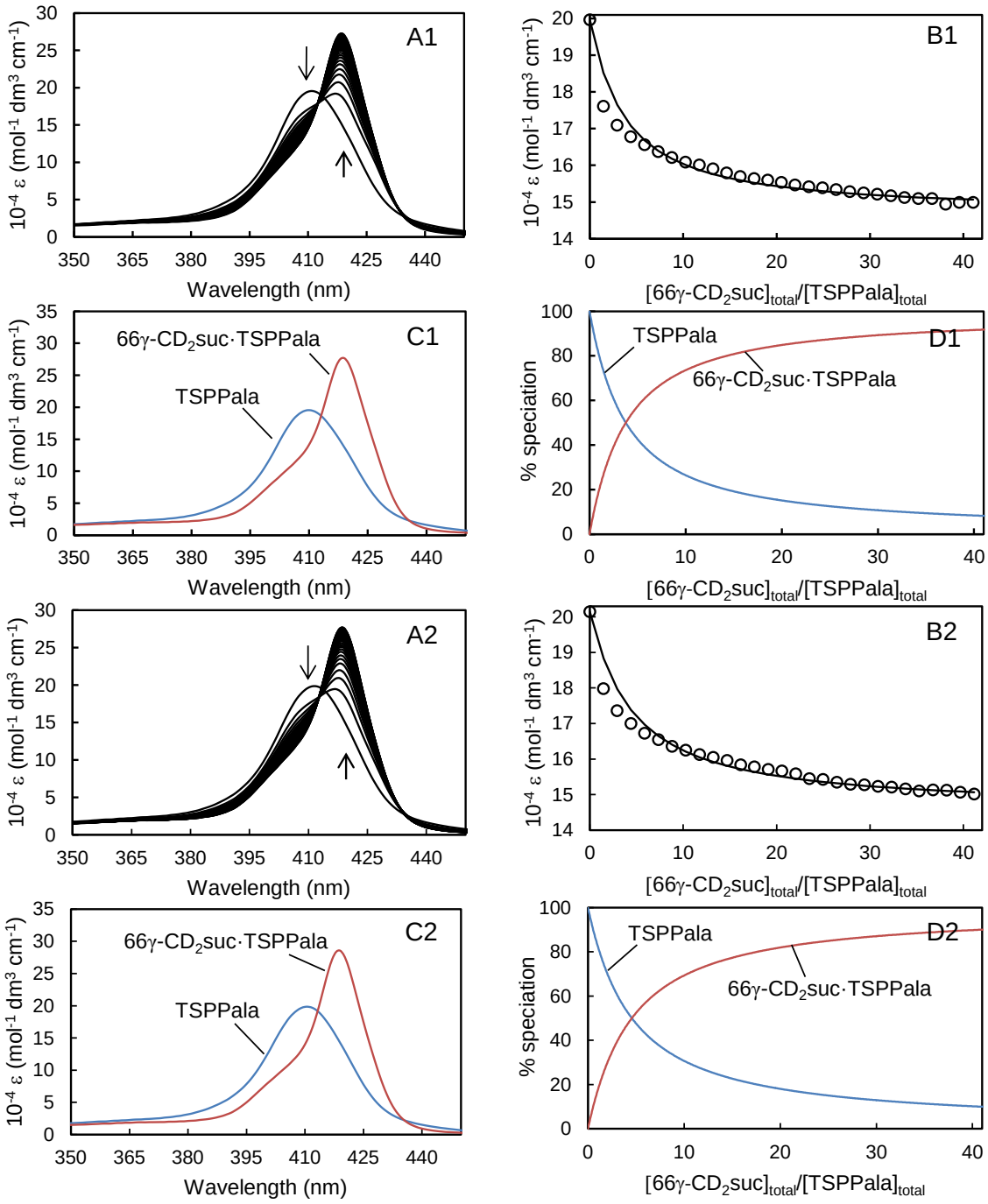

Figure A23: (A1, A2) Molar absorbance change of the porphyrin substituents of PAATSPPala ([TSPPala] = 3.10 × 10^{-6} mol dm^{-3}) in phosphate buffer, pH 7.0, I = 0.10 mol dm^{-3} with sequential injections (8 mm^3 each) of 66γ-CD$_2$suc (1.21 × 10^{-3} mol dm^{-3}) into both sample and reference cells. The arrows indicate the direction of molar absorbance change as the molar ratio of [66γ-CD$_2$suc]/[TSPPala] increases. (B1, B2) Molar absorbance variation at 410 nm and the line of best fit of an algorithm for 1:1 host-guest complexation over the wavelength range 380-430 nm. (C1, C2) Calculated molar absorbance of free and complexed TSPPala. (D1, D2) Speciation with [TSPPala]$_{total}$ = 100%. Note: A1-D1: data at 278.2 K. A2-D2: data at 288.2 K.

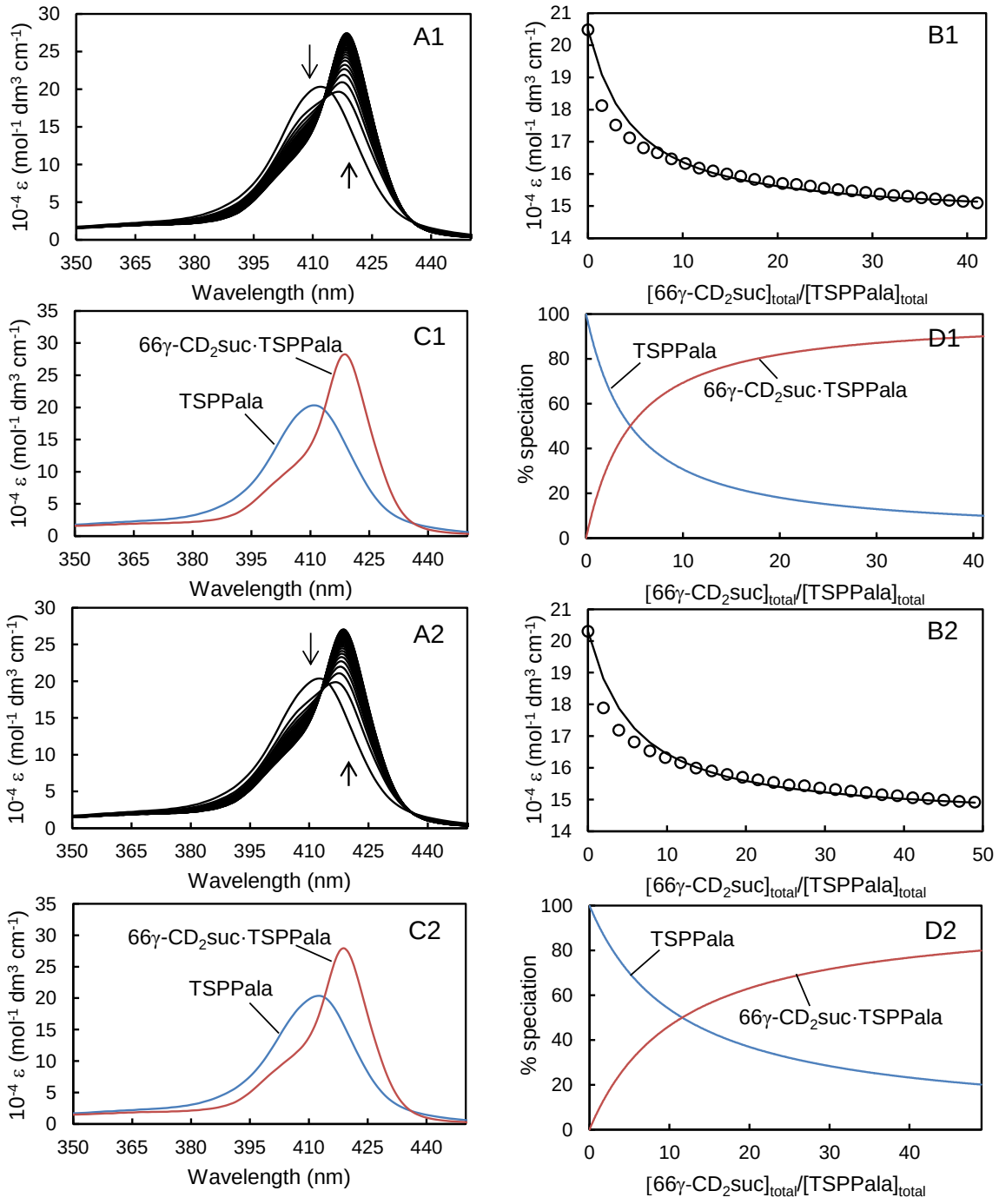

Figure A24: (A1, A2) Molar absorbance change of the porphyrin substituents of PAATSPPala ([TSPPala] = 3.10×10^{-6} mol dm^{-3}) in phosphate buffer, pH 7.0, I = 0.10 mol dm^{-3} with sequential injections (8 or 10 mm^3 each for 298.2 and 308.2 K, respectively) of 66γ-CD$_2$suc (1.21×10^{-3} mol dm^{-3}) into both sample and reference cells. The arrows indicate the direction of molar absorbance change as the molar ratio of [66γ-CD$_2$suc]/[TSPPala] increases. (B1, B2) Molar absorbance variation at 410 nm and the line of best fit of an algorithm for 1:1 host-guest complexation over the wavelength range 380-430 nm. (C1, C2) Calculated molar absorbance of free and complexed TSPPala. (D1, D2) Speciation with $[TSPPala]_{total}$ = 100%. Note: A1-D1: data at 298.2 K. A2-D2: data at 308.2 K.

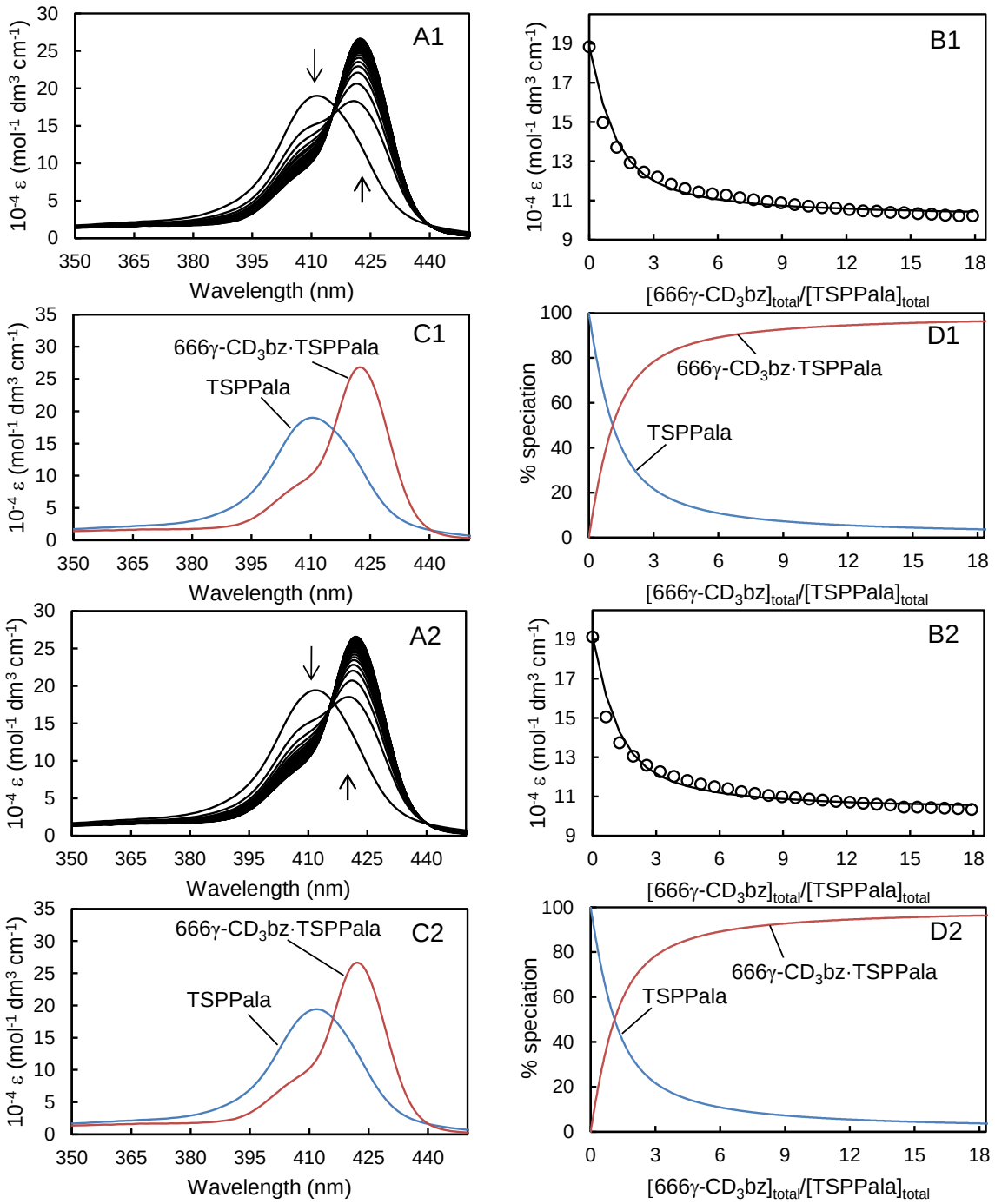

Figure A25: (A1, A2) Molar absorbance change of the porphyrin substituents of PAATSPPala ([TSPPala] = 3.10×10^{-6} mol dm^{-3}) in phosphate buffer, pH 7.0, I = 0.10 mol dm^{-3} with sequential injections (6 mm^3 each) of 666γ-CD$_3$bz (6.57×10^{-4} mol dm^{-3}) into both sample and reference cells. The arrows indicate the direction of molar absorbance change as the molar ratio of [666γ-CD$_3$bz]/[TSPPala] increases. (B1, B2) Molar absorbance variation at 410 nm and the line of best fit of an algorithm for 1:1 host-guest complexation over the wavelength range 380-430 nm. (C1, C2) Calculated molar absorbance of free and complexed TSPPala. (D1, D2) Speciation with [TSPPala]$_{total}$ = 100%. Note: A1-D1: data at 278.2 K. A2-D2: data at 288.2 K.

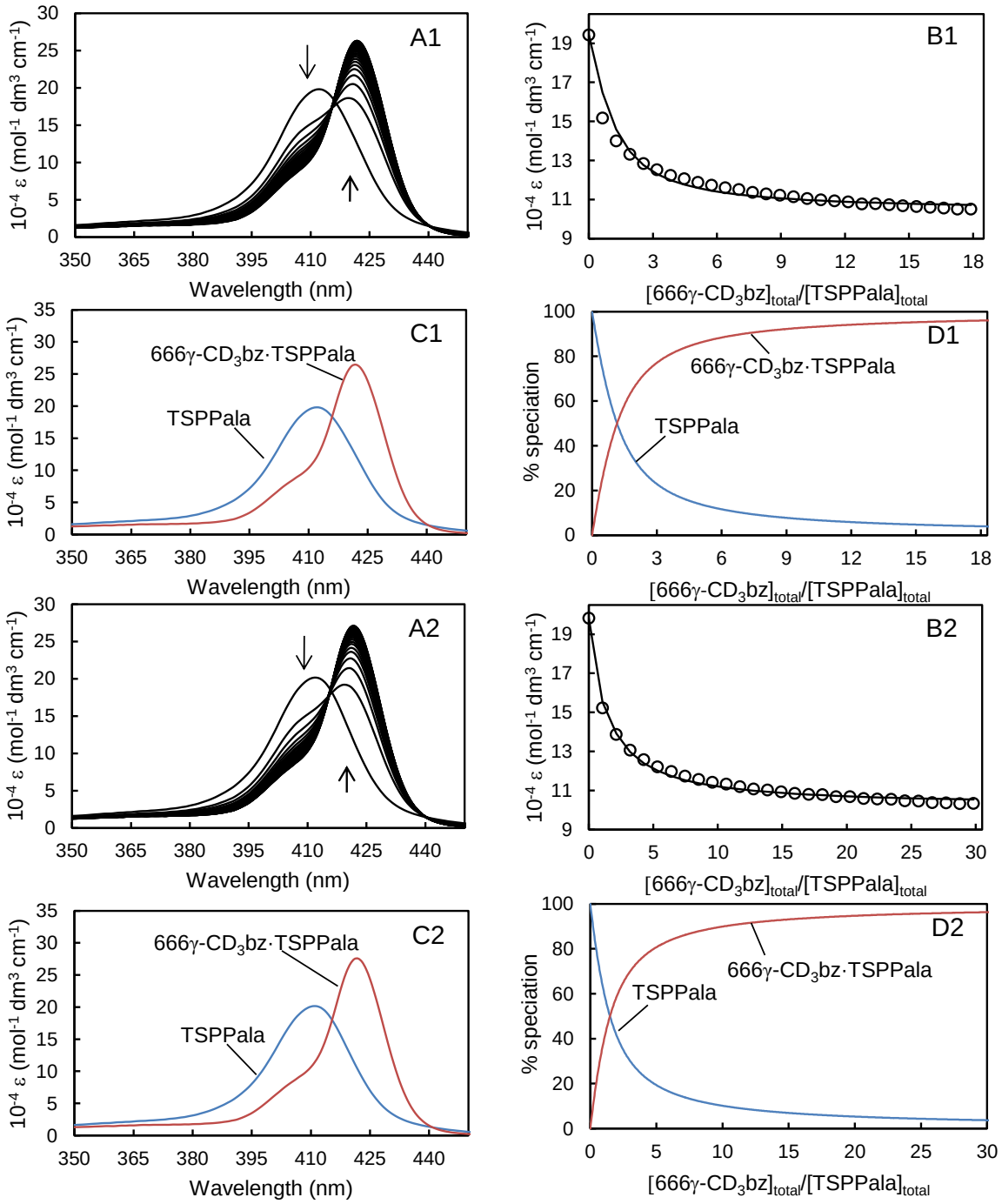

Figure A26: (A1, A2) Molar absorbance change of the porphyrin substituents of PAATSPPala ([TSPPala] = 3.10 × 10^{-6} mol dm^{-3}) in phosphate buffer, pH 7.0, I = 0.10 mol dm^{-3} with sequential injections (6 or 10 mm^3 each for 298.2 and 308.2 K, respectively) of 666γ-CD$_3$bz (6.57 × 10^{-4} mol dm^{-3}) into both sample and reference cells. The arrows indicate the direction of molar absorbance change as the molar ratio of [666γ-CD$_3$bz]/[TSPPala] increases. (B1, B2) Molar absorbance variation at 410 nm and the line of best fit of an algorithm for 1:1 host-guest complexation over the wavelength range 380-430 nm. (C1, C2) Calculated molar absorbance of free and complexed TSPPala. (D1, D2) Speciation with [TSPPala]$_{total}$ = 100%. Note: A1-D1: data at 298.2 K. A2-D2: data at 308.2 K.

Chapter 5

Host-Guest Chemistry of Isomeric Linked β- and γ-Cyclodextrin Dimers and Naphthyl Substituted Poly(acrylate)s in Aqueous Solution

5.1. INTRODUCTION

5.1.1 General

The ability of naturally occurring α-, β-, and γ-cyclodextrins, α-CD, β-CD, and γ-CD, and their modified forms to act as hosts through the complexation of a wide range of guest species in their annuli to form host-guest complexes is well established.[1-16] We are particularly interested in host-guest complexation of cyclodextrin substituents on polymers with hydrophobic guest species and similar interactions of hydrophobic guest substituents on polymers with cyclodextrins both within single polymer strands and between polymer strands.[17-28] The aggregation of polymer strands through host-guest complexation of substituents in aqueous solution can produce polymeric networks which potentially have applications in drug delivery, biosensing, biological coating, tissue engineering and nanodevices.[29-34] Thus, an understanding of the molecular and macroscopic factors controlling this host-guest chemistry is of considerable interest.

5.1.2 Aims of this study

In this study, we seek to extend such understanding through a study of poly(acrylate) (PAA) 3% randomly substituted with isomeric 1- or 2-naphthyl-sulfonamide through either a aminoethyl tether, PAA1NSen and PAA2NSen, or a aminohexyl tether, PAA1NShn and PAA2NShn, and their host-guest complexes formed with β-CD, γ-CD and their isomeric succinamide–linked dimers, 33β-CD_2suc, 66β-CD_2suc, 33γ-CD_2suc and 66γ-CD_2suc shown in Figure 5.1. (No such complexes are observed to form with α-CD.) Insight into host-guest complexation in solution is gained through 2D ^{1}H NMR and fluorescence spectroscopy and rheology.

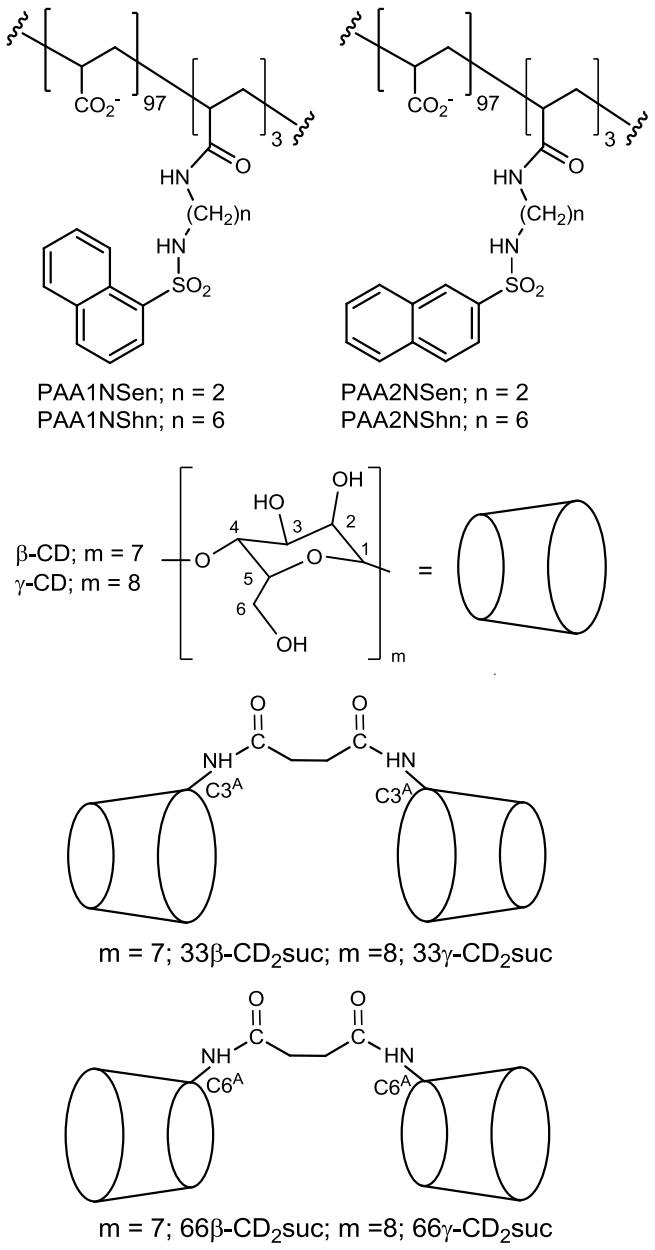

Figure 5.1. Structures of PAA1NSen, PAA2NSen, PAA1NShn, PAA2NShn, β-CD, γ-CD, 33β-CD_2suc, 33γ-CD_2suc, 66β-CD_2suc and 66γ-CD_2suc.

5.2. SYNTHESIS

The preparation of the 3% randomly substituted 1-naphthyl modified poly(acrylate)s (PAA1NSen and PAA1NShn) were prepared as outlined in a previous study.[35] The 2-naphthyl modified poly(acrylate)s were prepared in a similar manner without the use of a 4-nitrophenol substituted intermediate. 2-Naphthalene sulfonyl chloride was treated with either

1,2-diaminoethane or 1,6-diaminohexane to yield *N*-(2-aminoethyl)-2-naphthyl-sulfonamide (2NSen) or *N*-(6-aminohexyl)-2-naphthyl-sulfonamide (2NShn) with reasonable yields. The 3% randomly substituted 2-naphthyl modified poly(acrylate)s were then prepared by modifying the literature method.[17,18] The preparation and characterisation of these compounds are outlined in Chapter 6.

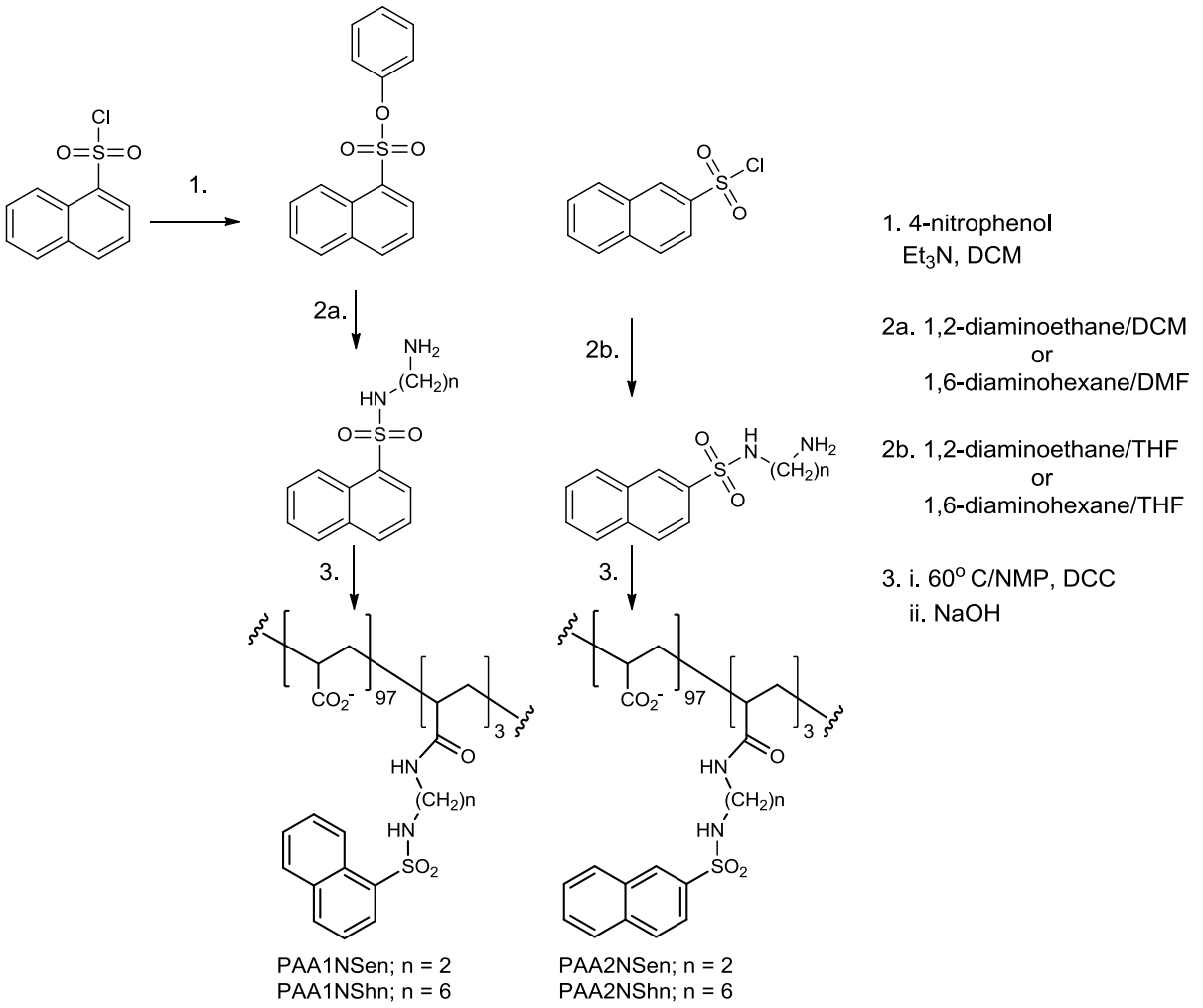

Figure 5.2. Synthesis of PAA1NSen, PAA2NSen, PAA1NShn, PAA2NShn.

The succinamide-linked β-CD and γ-CD dimers, 33β-CD_2suc 66β-CD_2suc 33γ-CD_2suc and 66γ-CD_2suc were synthesised as reported previously.[36-39] It should be noted that 2D ^{1}H NOESY NMR, fluorescence spectroscopy and rheological studies of the host-guest complexation of PAA1NSen and PAA1NShn by β-CD, γ-CD, 33β-CD_2suc, 66β-CD_2suc,

33γ-CD_2suc and 66γ-CD_2suc have been previously reported elsewhere.[35] However, a significant portion of this work needed to be repeated experimentally or the data fitting was revised. Accordingly, the repeated experiments (and some of the originals) will be presented in this work along with new data for PAA1NSen and PAA1NShn with α-CD and PAA2NSen and PAA2NShn with α-CD, β-CD, γ-CD, 33β-CD_2suc, 66β-CD_2suc, 33γ-CD_2suc and 66γ-CD_2suc

5.3. 2D ^{1}H NOESY NMR STUDIES

None of the 2D ^{1}H NOESY NMR spectra of the α-CD D_2O solutions show cross-peaks arising from host-guest interactions of α-CD with either PAA1NSen, PAA1NShn, PAA2NSen or PAA2NShn (Figures A1, A7, A14 and A20 of the Appendix) whereas those of the β-CD, γ-CD, 33β-CD_2suc, 66β-CD_2suc, 33γ-CD_2suc and 66γ-CD_2suc solutions all show cross-peaks arising from NOE interactions between the either the host β-CD or γ-CD H_3, H_5 and H_6 annular protons and the 1- and 2-naphthyl guest protons of either PAA1NSen, PAA1NShn, PAA2NSen or PAA2NShn (Figures 5.3-5.5 and Figures A2-A6, A8-A13, A15-A19 and A21-A24 of the Appendix). Evidently, the α-CD annulus, which has diameters of 470 and 530 pm, at the wide and narrow faces, respectively, and a depth of 790 pm[5] is too small to readily accommodate the naphthyl substituents, which have an estimated length of ~650 pm and width of ~470 pm, to a sufficient extent for host-guest complexation to occur. In contrast, the β-CD annulus has narrow and wide face diameters of 600 and 650 pm and a depth of 790 pm, and the corresponding dimensions for γ-CD are 750, 830 and 790 pm,[5] which allow both to form host-guest complexes with the 1- and 2-naphthyl substituents.

The cross-peaks seen in the 2D ^{1}H NOESY NMR spectra of D_2O solutions of β-CD, γ-CD and their succinate-linked dimers and the naphthyl-substituted poly(acrylate)s show substantial variations which provide stereochemical insight into the host-guest complexes

formed. (The data for all twenty-four systems are collected in Table 5.1.) Thus, the spectrum of a solution equimolar in β-CD and PAA1NSen shows cross-peaks arising from NOE interactions of the annular β-CD H_3, H_5 and H_6 protons with the 1-naphthyl protons of PAA1NSen as a result of host-guest complexation, but none for the β-CD H_2 and H_4 protons on the exterior surface of β-CD and more distant from the 1-naphthyl guest residing in the β-CD annulus (Figure 5.3).

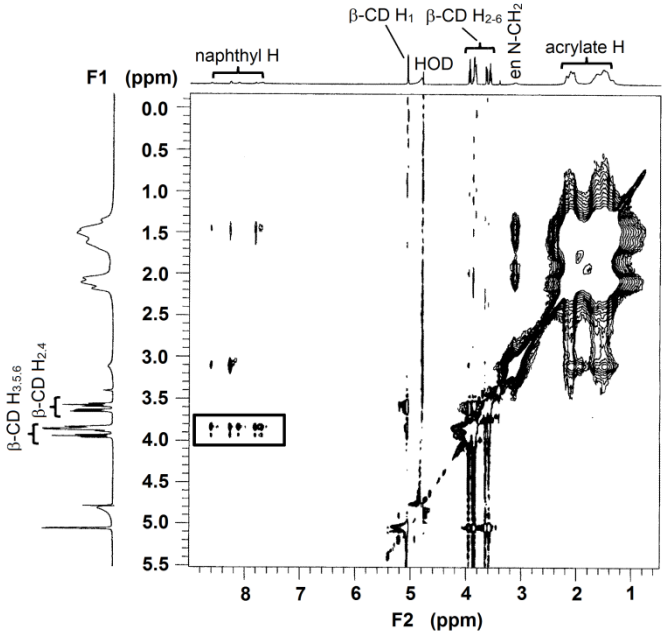

Figure 5.3. 2D ^{1}H NOESY NMR (600 MHz) spectrum of 3% substituted PAA1NSen (1.43 wt%, [1NSen] = 3.0×10^{-3} mol dm^{-3}) and equimolar β-CD in D_2O at pD 7.0 (0.10 mol dm^{-3} in NaCl) at 298.2 K. Cross–peaks enclosed in the rectangle arise from NOE interactions between the annular β-CD $H_{3,5,6}$ protons and the naphthyl protons of the 1NSen substituent.

No cross-peaks are seen for a NOE interaction between the β-CD H_3, H_5 and H_6 protons with those of the aminoethyl tether attaching the 1-naphthyl substituent to the poly(acrylate) backbone. Their absence indicates that the average distance between these protons is too great for NOE interactions to produce significant cross-peaks as is also the case for the complexes formed by 33β-CD_2suc and 33γ-CD_2suc (Figures A3 and A5 of the Appendix). For the 66β-CD_2suc and 66γ-CD_2suc complexes cross-peaks arising from the analogous

protons are indistinguishable from the background. (Figures A4 and A6 of the Appendix). However, such cross-peaks do appear in the spectrum of the analogous γ-CD solution (Figure A2 of the Appendix).

Cross-peaks consistent with the complexation of the 2-naphthyl substituents of PAA2NSen in the β-CD annuli of 66β-CD_2suc are seen in Figure 5.4. However, the β-CD proton resonances are now broadened as is sometimes observed for mono-substituted cyclodextrins as a result of all seven glucopyranose components becoming molecularly inequivalent and sometimes magnetically inequivalent also.

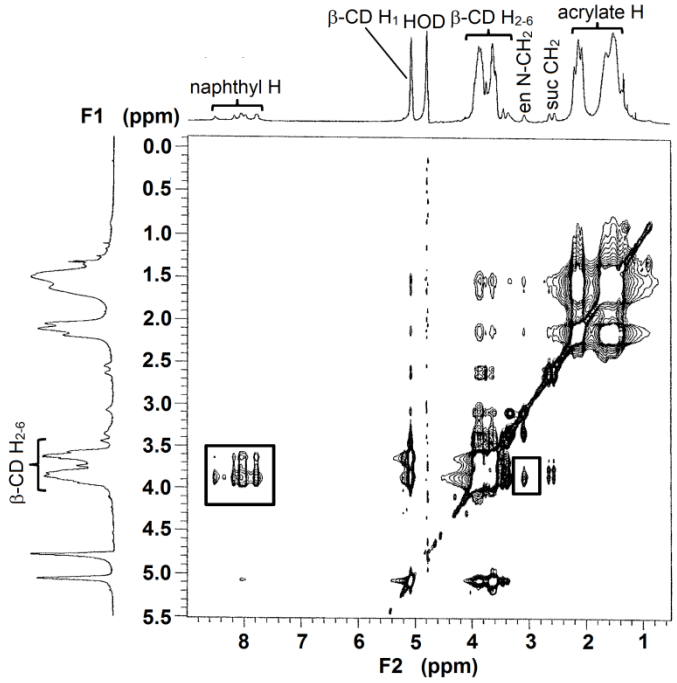

Figure 5.4. 2D ^{1}H NOESY NMR (600 MHz) spectrum of 3% substituted PAA2NSen (1.43 wt%, [2NSen] = 3.0×10^{-3} mol dm^{-3}) and equimolar 66β-CD_2suc in D_2O at pD 7.0 (0.10 mol dm^{-3} in NaCl) at 298.2. Cross-peaks enclosed in the rectangles arise from NOE interactions between the annular β-CD $H_{3,5,6}$ protons of 66β-CD_2suc with the naphthyl (left) and N-CH_2 (right) protons of the 2NSen substituent.

This results in a variation in chemical shifts and sometimes a broadened β-CD multiplet which is reflected in the cross-peaks arising from the host-guest complex. (Intermediate exchange rates between the free and complexed states can also cause resonance broadening.)

While these data do not reveal the stereochemistry of the complexation by 66β-CD_2suc, an enhanced complex stability discussed below is consistent with ditopic complexation of two 2-naphthyl substituents of PAA2NSen. (Resonance broadening is seen in most of the linked β-CD and γ-CD dimer systems to some extent.) A cross-peak arising from interaction between the β-CD annuli of 66β-CD_2suc and the aminoethyl protons of PAA2NSen is observed, as is also the case for the analogous β-CD and 33β-CD_2suc system (Figures A15 and A17 of the Appendix) but not for the γ-CD and the two γ-CD linked-dimer systems (Figures A16, A18 and A19 of the Appendix).

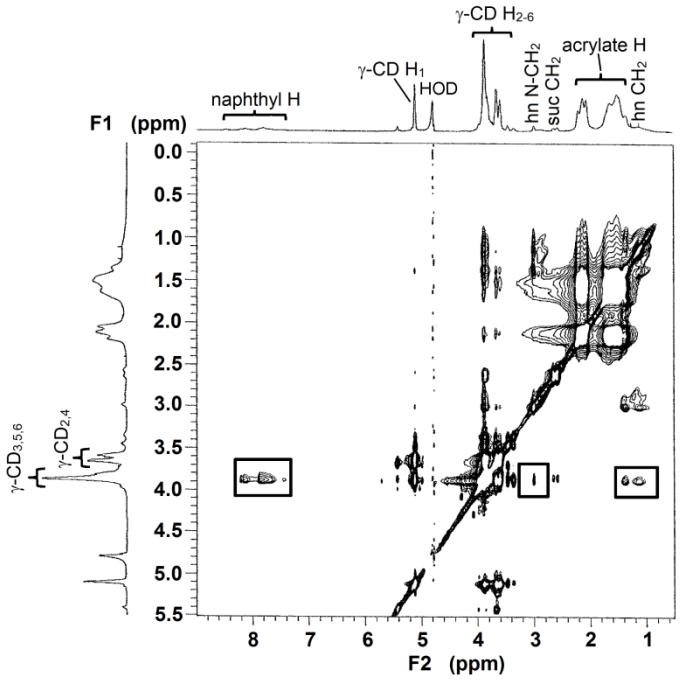

Figure 5.5. 2D ^{1}H NOESY NMR (600 MHz) spectrum of 3% substituted PAA2NShn (1.43 wt%, [2NShn] = 3.0×10^{-3} mol dm^{-3}) and equimolar 66γ-CD_2suc in D_2O at pD 7.0 (0.10 mol dm^{-3} in NaCl) at 298.2 K. Cross-peaks enclosed in the rectangle arise from NOE interactions between the annular γ-CD $H_{3,5,6}$ protons of 66γ-CD_2suc with the naphthyl (left), N-CH_2 (middle) and other hexyl CH_2 (right) protons of the 2NShn substituent.

The 2D ^{1}H NOESY NMR spectrum of a D_2O solution of 66γ-CD_2suc and PAA2NShn (Figure 5.5) shows cross-peaks arising from the NOE interactions between the γ-CD H_3, H_5

and H_6 protons and the 2-naphthyl *N*-CH_2- and the other four –$(CH_2)_4$- protons of the aminohexyl tether. (The γ-CD H_3, H_5 and H_6 resonances are broadened but are still distinguishable from the H_2 and H_4 resonances.) The analogous spectra of the corresponding β–CD, γ-CD, 33β-CD_2suc, 66β-CD_2suc and 33γ-CD_2suc solutions also show these three sets of cross-peaks (Figures A21-25 of the Appendix).

Table 5.1. Cross-peaks arising from NOE interactions between the cyclodextrin H_3, H_5 and H_6 protons and the 3% randomly naphthyl-substituted poly(acrylate) naphthyl, N-CH_2 and -$(CH_2)_4$- protons in D_2O at pD 7.0 (0.10 mol dm^{-3} in NaCl) at 298.2 K.

Guest / Host	PAA1NSen[a] cross-peaks	PAA2NSen[a] cross-peaks	PAA1NShn[b] cross-peaks	PAA2NShn[b] cross-peaks
β-CD	naphthyl N-CH_2-	naphthyl N-CH_2-	naphthyl N-CH_2-, -$(CH_2)_4$-[c]	naphthyl N-CH_2-, -$(CH_2)_4$-
33β-CD_2suc	naphthyl[c]	naphthyl N-CH_2-	naphthyl N-CH_2-, -$(CH_2)_4$-[c]	naphthyl N-CH_2-, -$(CH_2)_4$-
66β-CD_2suc	naphthyl[c]	naphthyl N-CH_2-	naphthyl, N-CH_2-, -$(CH_2)_4$-[c]	naphthyl N-CH_2-, -$(CH_2)_4$-
γ-CD	naphthyl N-CH_2-	naphthyl	naphthyl -$(CH_2)_4$-[c]	naphthyl N-CH_2-, -$(CH_2)_4$-
33γ-CD_2suc	naphthyl[c]	naphthyl	naphthyl N-CH_2-, -$(CH_2)_4$-[c]	naphthyl N-CH_2-, -$(CH_2)_4$-
66γ-CD_2suc	naphthyl[c]	naphthyl	naphthyl -$(CH_2)_4$-[c]	naphthyl N-CH_2-, -$(CH_2)_4$-

[a] Cross peaks with naphthyl and N-CH_2 protons possible.
[b] Cross peaks with naphthyl, N-CH_2 and -$(CH_2)_4$-.protons possible.
[c] Data from previous study.[35]

For all systems, cross-peaks arising from the naphthyl proton resonances are observed (Table 5.1) consistent with the 1- and 2-naphthyl substituents dominating the formation of the host-guest complexes. Of the PAA1NSen systems, a cross-peak arising from the N-CH_2- protons is clearly observed in the presence of γ-CD with weak indications of analogous cross-peaks obscured by noise in the presence of 66β-CD_2suc and 66γ-CD_2suc, but no such cross-peaks in the presence of 33β-CD_2suc and 33γ-CD_2suc. Cross-peaks arising from N-CH_2-

proton interactions are observed for PAA2NSen in the presence of β-CD, 33β-CD_2suc and 66β-CD_2suc. Individually, the origins of differences cannot be identified, but collectively they reflect subtle combinations of the effect of changes in naphthyl substituent and cyclodextrin stereochemistry on host-guest complex configurations.

The lengthening of the tether in PAA1NShn and PAA2NShn results in the -$(CH_2)_4$- protons generating cross-peaks for all six PAA1NShn and PAA2NShn systems. This is consistent with complexation of both the naphthyl substituent and its tether for all twelve systems, possibly in two or more conformations in dynamic equilibria. While the observed cross-peaks reflect the proximity of interacting host and guest protons they do not necessarily reflect the relative stabilities of the host-guest complexes formed which is considered in detail below.

5.4. FLUORIMETRIC STUDIES

All four naphthyl-substituted poly(acrylate)s show fluorescence arising from their naphthyl substituents in aqueous solution at pH 7.0. Titration of their solutions with α-CD solution causes small changes in fluorescence consistent with negligible host–guest complexation occurring (Figures A25, A30, A38 and A45 of the Appendix) and in accord with the 2D H^1 NOESY NMR data previously discussed. This is in marked contrast to titrations of their solutions with β-CD and γ-CD solutions and those of the corresponding linked dimers which generate either increases or decreases in fluorescence depending upon the identity of the titrant (Figures 5.6 and 5.7 and Table 5.2) consistent with the formation of 1:1 host-guest complexes according to Equations 5.1 and 5.2. Thus, fluorescence increases with titration of 33β-CD_2suc solution into PAA1NSen and PAA2NShn solution as complexation of the naphthyl fluorophores in the β-CD annuli of 33β-CD_2suc occurs (Figures 5.6a and 5.7a). In contrast, fluorescence decreases with titration

of 33γ-CD_2suc solution into PAA1NSen and PAA2NShn solutions (Figures 5.6b and 5.7b). These pairs of data sets exemplify the twenty-four β-CD- and γ-CD-based systems studied for which the derived K_{11} and the direction of fluorescence change are collected in Table 5.2. While complexation by β-CD and its linked dimers simply increase the naphthyl substituent fluorescence, the γ-CD and its dimers decrease the uncomplexed naphthyl substituent fluorescence and generate a new red-shifted fluorescence peak attributable to the complexed fluorophore. The implications of this are discussed later. (All of the fluorimetric titration data are collected in Figures 5.6, 5.7 and A25-A49)

5.4.1. Fluorimetric Stability Constant Determination

The complexaton constant, K_{11}, was derived through Equations 5.1–5.5 from the variation of flourescence observed for each titration following a scheme similar to that previously reported.[25] Thus, the naphthyl substituents in PAA1NSen, PAA1NShn, PAA2NSen and PAA2NShn are complexed by either β-CD, γ-CD, 33β-CD_2suc, 66β-CD_2suc, 33γ-CD_2suc or 66γ-CD_2suc to form the 1:1 host-guest complexes exemplified by β-CD.PAA2NSen as shown in Equation 5.1 where K_{11} is the host-guest complexation constant expressed as in Equation 5.2.

$$\beta\text{-CD} + \text{PAA2NSen} \underset{}{\overset{K_{11}}{\rightleftharpoons}} \beta\text{-CD.PAA2NSen} \qquad (\mathbf{5.1})$$

$$K_{11} = [\beta\text{-CD.PAA2NSen}]/[\beta\text{-CD}]\,[\text{PAA2NSen}] \qquad (\mathbf{5.2})$$

Given that $[\beta\text{-CD}]_{total}$ and $[\text{PAA2NSen}]_{total}$ and are the initial concentrations at the commencement of the titration, which are related to the concentrations [β-CD], [β-CD.PAA2NSen] and [PAA2NSen] through Equations 5.3 and 5.4 as the titration proceeds,

it follows that the observed fluorescence, *F*, at a particular wavelength is given by Equation 5.5 where

$$[\beta\text{-CD}]_{total} = [\beta\text{-CD.PAA2NSen}] + [\beta\text{-CD}] \quad (\mathbf{5.3})$$

$$[\text{PAA2NSen}]_{total} = [\beta\text{-CD.PAA2NSen}] + [\text{PAA2NSen}] \quad (\mathbf{5.4})$$

$$F = I_{\text{PAA2NSen}}[\text{PAA2NSen}] + I_{\beta\text{-CD.PAA2NSen}}[\beta\text{-CD.PAA2NSen}] \quad (\mathbf{5.5})$$

I_{PAA2NSen}, and $I_{\beta\text{-CD.PAA2NSen}}$ represent the observed fluorescences of PAA2NSen and β-CD.PAA2NSen respectively. The value of K_{11} was determined by best fitting an algorithm based on Equations 5.2-5.5 to the variation of the fluorescence spectra in the range 320-420 nm at 0.5 nm intervals as the β-CD concentration was varied using the HypSpec protocol.[40] The same protocol was used for the other PAA1NSen and PAA1NShn systems in the range 320-420 nm and for the PAA2NSen and PAA2NShn systems in the range 330-380 nm. Algorithms for complexations involving 1:2 and 2:1 host/guest stoichiometries in addition to, or separate from the 1:1 stoichiometry could not be fitted to the data.

Irrespective of the identity of the naphthyl substituted poly(acrylate), K_{11} increases with the nature of the host in the sequence β-CD < 33β-CD_2suc < 66β-CD_2suc (Table 5.2). This is consistent with ditopic complexation of two naphthyl substituents by 33β-CD_2suc and 66β-CD_2suc increasing the stability of their 1:1 host-guest complexes over those formed by β-CD, and with the orientation of the β-CD annuli of 66β-CD_2suc favouring complexation to a greater extent than the orientation of the β-CD annuli of 33β-CD_2suc. The K_{11} characterising the 1:1 complexes formed by β-CD refer to the complexation of a single naphthyl substituent while the substantially greater K_{11} characterising the 1:1 complexes formed by 33β-CD_2suc and 66β-CD_2suc infer some ditopic complexation of two naphthyl substituents to form a chelate-like structure in a single naphthyl-substituted poly(acrylate) strand in equilibrium with monotopic complexation of a single naphthyl substituent as shown in Figure 5.8.

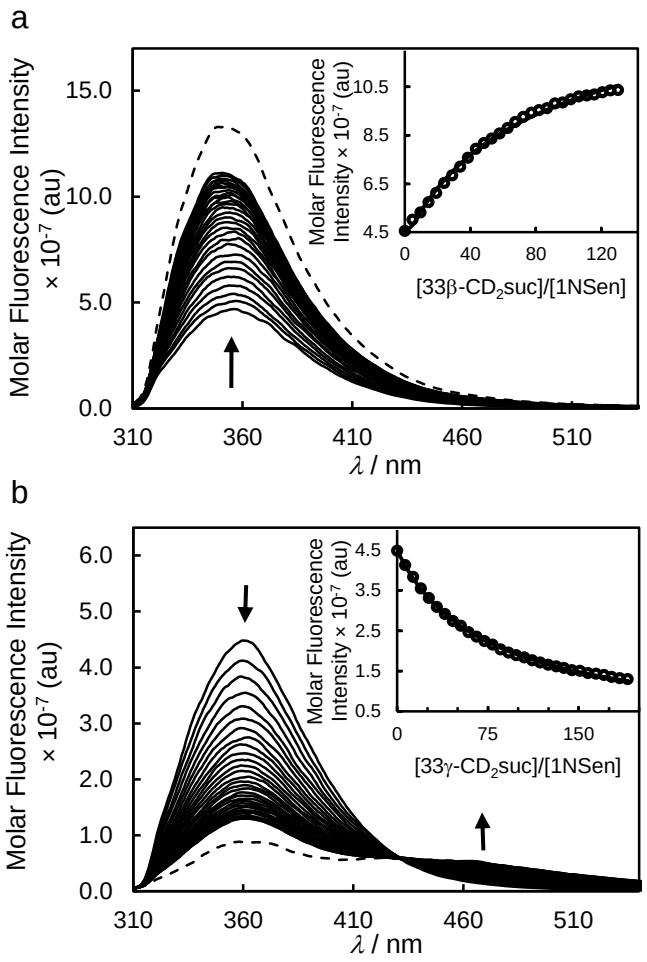

Figure 5.6. a) Variation in the emission spectra of 0.0033 wt% PAA1NSen solution ([1NSen] = 1.0×10^{-5} mol dm^{-3}) in pH 7.0 phosphate buffer (I = 0.10 mol dm^{-3}) at 298.2 K upon sequential injection (0.010 cm^3 each) of 33β-CD_2suc titrant solution (1.02×10^{-2} mol dm^{-3}). Excitation wavelength λ_{ex} = 290 nm with both excitation and emission slits of 5 nm. The arrow indicates the direction of fluorescence changes as the ratio of [33β-CD_2suc]$_{total}$/[1NSen]$_{total}$ increases. The dashed spectrum is that derived for the fully complexed 1NSen: λ_{max} = 360 nm and 350 nm for the free and complexed naphthyl substituent, respectively. Inset: Variation in the molar fluorescence (circles) at 360 nm. The solid curve represents the best fit of the algorithm for 1:1 complexation in the range 330–420 to give K_{11} = 1160 ± 30 dm^3 mol^{-1}. b) As for a) except that the titrant solution was 2.63×10^{-3} mol dm^{-3} of 33γ-CD_2suc in 0.050 cm^3 aliquots and K_{11} = 2150 ± 110 dm^3 mol^{-1}. The λ_{max} = 360 nm and 364 nm for the free and complexed 1NSen, respectively, and the isosbestic point occurs at 430 nm. Note: The data for figure b is from a previous study with revised fitting.[35]

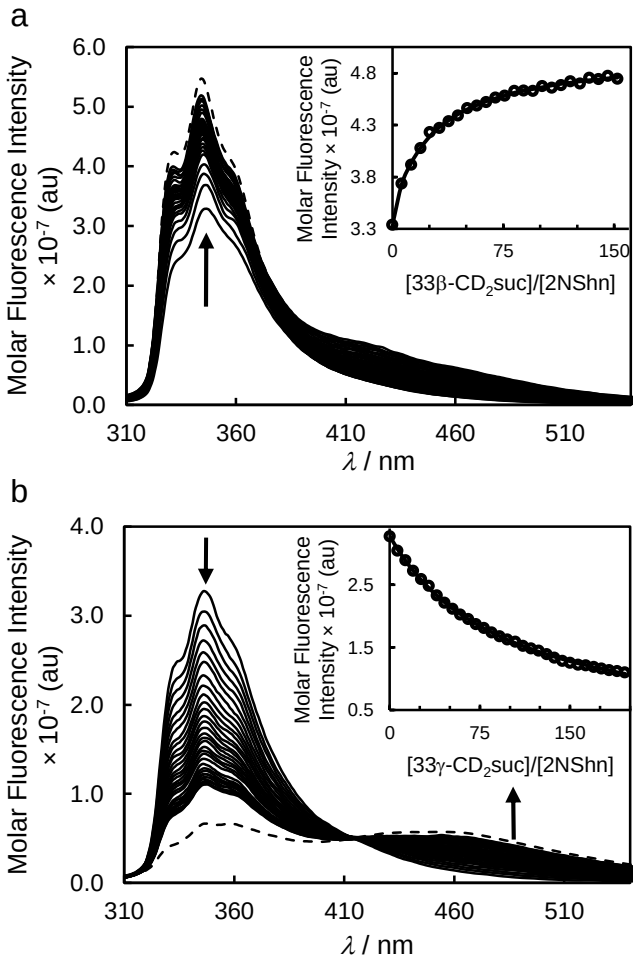

Figure 5.7. a) Variation in the emission spectra of 0.0034 wt% PAA2NShn solution ([2NShn] = 1.0×10^{-5} mol dm^{-3}) in pH 7.0 phosphate buffer (I = 0.10 mol dm^{-3}) at 298.2 K upon sequential injection (0.050 cm^3 each) of 33β-CD_2suc titrant solution (2.54×10^{-3} mol dm^{-3}). Excitation wavelength λ_{ex} = 290 nm with both excitation and emission slits of 5 nm. The arrow indicates the direction of fluorescence changes as the ratio of [33β-CD_2suc]$_{total}$/[2NShn]$_{total}$ increases. The dashed spectrum is that derived for the fully complexed 2NShn: λ_{max} = 347 nm and 344 nm for the free and complexed naphthyl substituent, respectively. Inset: Variation in the molar fluorescence (circles) at 346 nm. The solid curve represents the best fit of the algorithm for 1:1 complexation in the range 330–380 to give K_{11} = 3800 ± 30 dm^3 mol^{-1}. b) As for a) except that the titrant solution was 2.49×10^{-3} mol dm^{-3} in 33γ-CD_2suc and K_{11} = 1790 ± 90 dm^3 mol^{-1}. The λ_{max} = 347 nm and 345 nm for the free and complexed 2NShn, respectively, and the isosbestic point occurs at 413 nm.

Table 5.2. Stability constants for host-guest complexation of 3% randomly substituted PAA1NSen, PAA2NSen, PAA1NShn and PAA2NShn by β-CD, γ-CD and their succinamide-linked dimers determined by fluorimetric titrations in aqueous pH 7.0 phosphate buffer (I = 0.10 mol dm^{-3}) at 298.2 K.

Guest / Host	PAA1NSen K_{11} dm^3 mol^{-1}	PAA2NSen K_{11} dm^3 mol^{-1}	PAA1NShn K_{11} dm^3 mol^{-1}	PAA2NShn K_{11} dm^3 mol^{-1}
β-CD	440 ± 20[a,c]	450 ± 10[b]	140 ± 7[b]	2370 ± 15[b]
33β-CD$_2$suc	1160 ± 40[b]	1450 ± 20[b]	1990 ± 60[b]	3800 ± 30[b]
66β-CD$_2$suc	2220 ± 60[b]	2900 ± 30[b]	8020 ± 400[b]	10000 ± 500[b]
γ-CD	100 ± 5[a,d]	290 ± 10[a]	330 ± 15[a,c]	140 ± 5[b]
33γ-CD$_2$suc	2150 ± 110[a,d]	2130 ± 100[a]	2920 ± 120[a.d]	1790 ± 90[a]
66γ-CD$_2$suc	590 ± 30[a]	600 ± 30[a]	620 ± 30[a]	595 ± 30[a]

[a]Fluorescence of naphthyl fluorophore at 360 nm decreases with addition of cyclodextrin titrant.
[b]Fluorescence of naphthyl fluorophore at 360 nm increases with addition of cyclodextrin titrant.
[c] Data from previous study. [35]

[d] Data from previous study with revised fitting. [35]

The conformation shown for 66β-CD$_2$suc in Figure 5.8 is but one which may be assumed as rotation about the succinate tether occurs such that the complexing naphthyl substituent has access to either end of the β-CD annuli. However, while a naphthyl substituent may have access to the narrow face of a β-CD annulus in some conformations of 66β-CD$_2$suc, ditopic complexation through both narrow faces induces substantially steric crowding and is disfavoured by comparison with the ditopic complexation through the wider face of the β-CD annuli shown in Figure 5.8. (The deduction that ditopic complexation occurs on a single naphthyl-substituted poly(acrylate) strand arises from the increase in K_{11} by comparison with K_{11} for monotopic complexation by β-CD; an increase which is unlikely to occur for ditopic complexation of two naphthyl substituents on

separate substituted poly(acrylate) strands.) The greater K_{11} characterising the 66β-CD_2suc complexes by comparison with those for the 33β-CD_2suc complexes is attributable to the outward sterically less hindered orientation of the wide faces of the two β-CD annuli from the dimer most effectively acommodating the naphthyl substituents. The opposite orientation of the β-CD annuli in 33β-CD_2suc presents the narrow β-CD faces which are evidently more sterically hindered to complexation. These orientations cause the ditopic 66β-CD_2suc complex to be more stable than the ditopic 33β-CD_2suc complex and for equilibrium between the mono- and ditopic complexes to favour the latter more strongly for 66β-CD_2suc than for 33β-CD_2suc. The ditopic complexes are likely to be dominant in both systems given their increased K_{11} by comparison with those of the analogous β-CD systems.

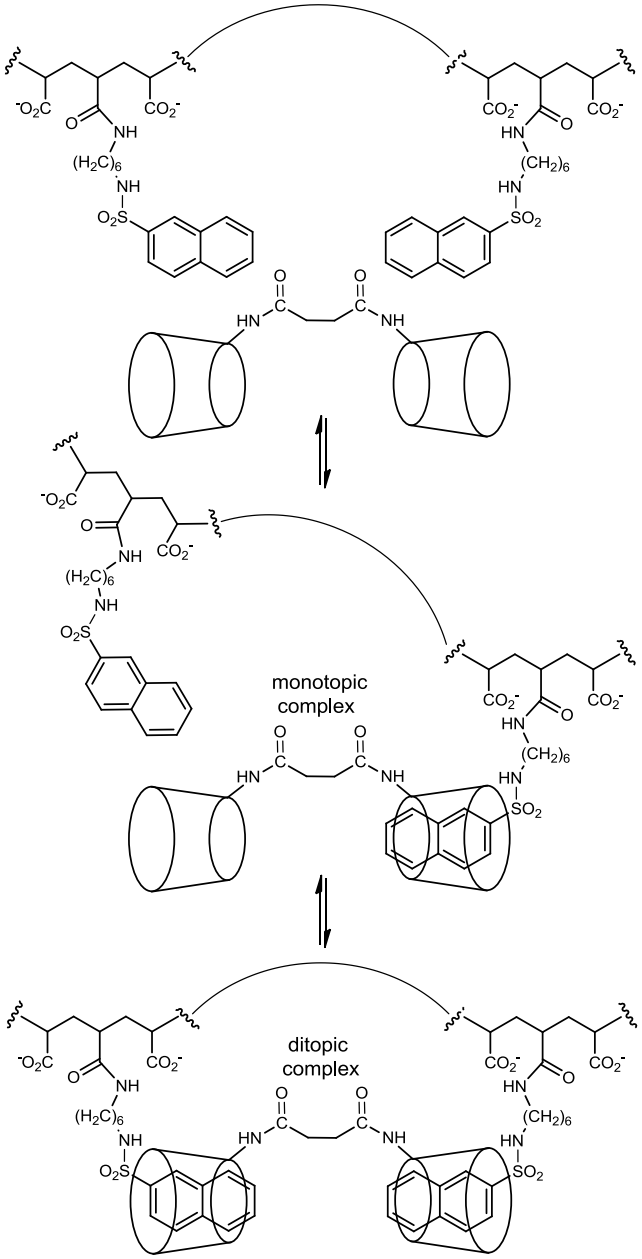

Figure 5.8. Sequential mono- and ditopic host-guest complexation by 66β-CD_2suc of the 2-naphthyl substituents of PAA2NShn. The aminohexyl tether component also enters the 66β-CD_2suc annuli and probably facilitates π-π interactions between the naphthyl substituents in the ditopic complex.

The previously discussed 2D ^{1}H NOESY NMR spectra show the complexation of the naphthyl substituent and the N-CH_2- and–$(CH_2)_6$- linker units for the 33β-CD_2suc.PAA1NShn, 66β-CD_2suc.PAA1NShn, 33β-CD_2suc.PAA1NShn and 66β-

CD_2suc.PAA1NShn complexes which infers that two naphthyl substituents are able to pass through both β-cyclodextrin annuli and form π-π interactions which molecular modelling using the MM2 protocol in Chem3D Ultra[41] shows to be feasible (Figure 5.9). Such π-π interactions should further increase the strength of ditopic complexation of PAA1NShn and PAA2NShn by 33β-CD_2suc and 66β-CD_2suc. This is probably reflected in the greater K_{11} for these four systems by comparision with the K_{11} for the analogous PAA1NSen and PAA2NSen systems in which the shorter aminoethyl tether is likely to restrict π-π interactions.

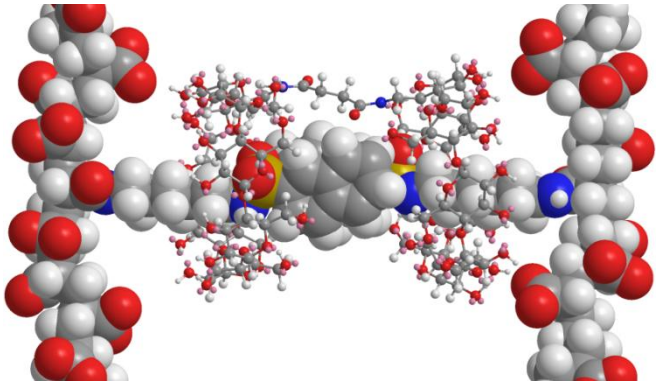

Figure 5.9. Energy minimised model of proposed intra-strand ditopic complexation of two naphthyl substituents of PAA2NShn (space filling) by 66β-CD_2suc (ball and stick) derived using the MM2 protocol of Chem3D Ultra.

The K_{11} characterising the β-CD complexes with all four naphthyl substituted poly(acrylate)s are significantly smaller than those for the complexes of the two linked β-CD dimers consistent with the ditopic nature of the latter complexes increasing their stability. However, the K_{11} = 140 and 2370 dm^3 mol^{-1} characterising the β-CD.PAA1NShn and β-CD.PAA2NShn complexes, respectively, indicate major differences their nature. In both cases 2D ^{1}H NOESY NMR spectra (Figures A8 and A21 of the Appendix) show the complexation of the naphthyl substituent and the -$(CH_2)_4$-

aminohexyl linker units. This is explicable through an equilibrium in which the naphthyl substituent is either complexed in the β-CD annulus or passes through it such that the aminohexyl linker units enter the annulus. Alternatively, the naphthyl substituent and the linker units may complex simultaneously in the β-CD annulus, which appears possible for the less sterically hindered. β-CD.PAA2NShn, but the available data neither allows a choice between these possibilities nor a definitive explanation of their greatly different K_{11}. (A comparison may be made with randomly 1.6 and 2.3% 1-naphthyl and 1.3 and 1.9 % 2- naphthyl substituted poly(acrylamide) for which K_{11} = 70, 140, 160 and 230 dm^3 mol^{-1}, respectively, in aqueous solution are reported.[42])

Annuli orientation also affects 33γ-CD_2suc and 66γ-CD_2suc complexations with the four naphthyl substituted poly(acrylate)s for each of which the variation of the magnitudes of K_{11} for the 1:1 host-guest complexes is: γ-CD < 66γ-CD_2suc < 33γ-CD_2suc (Table 5.2). The narrow faces of the γ-CD annuli of 33γ-CD_2suc appear to better match the size of the naphthyl substituents to give more stable complexes. However, K_{11} shows only minor variations with the identity of the naphthyl substituent and tether for complexation by either γ-CD, 33γ-CD_2suc or 66γ-CD_2suc evidently as a consequence of a less constraining fit within the γ-CD annuli corresponding host-guest complexes (by comparison with that of the β-CD annuli in their analogous complexes). Comparison of these K_{11} with those for the analogous γ-CD complexes (Table 5.2) show a a six-fold decrease on going from the 66γ-CD_2suc/PAA1NSen to the γ-CD/PAA1NSen system, a four-fold decrease on going from the 66γ-CD_2suc/PAA2NShn to the γ-CD/PAA2NShn system and only two-fold differences between K_{11} for the other two systems. However, the changes in naphthyl substituent absorbance induced by linked γ-CD dimer complexation is

much greater than that induced by γ-CD complexation which infers a smaller environmental change being experienced by the naphthyl substituents in the latter case.

5.4.2. Fluorescence Variation

The host-guest complexation of the 1- and 2-naphthyl substituents of the substituted poly(acrylate)s by cyclodextrins transfers them from an aqueous environment to a complexed environment which either enhances or quenches their fluorescence as seen from Figures 5.6 and 5.7. In more general terms, it is observed that the fluorescence of a range of organic fluorophores is enhanced upon complexation by cyclodextrins[42-46] while that of others is quenched.[47-49] Broadly, fluorescence enhancement is attributed to a lengthening of the excited state lifetime through a decrease in the singlet-excited state fluorophore interaction with water molecules, thereby decreasing inter-system crossing and increasing fluorescence quantum yield.[42,43] Conversely, quenching by cyclodextrin complexation indicates a decrease in the fluorophore excited state lifetime and has been attributed to specific interactions between the cyclodextrin and the fluorophore, such as hydrogen bonding.[47-49]

With two exceptions, complexation by β-CD and its linked dimers enhance the fluorescence of the 1- and 2-naphthyl substituents of the substituted poly(acrylate)s whereas complexation by γ-CD and its linked dimers quench their fluorescence as seen from Figures 5.6, 5.7, A27-A29, A31-A37, A39-A44, A46, A47, A49 and Table 5.2. (The exceptions are the β-CD/PAA1NSen system in which fluorescence is quenched and the γ-CD/PAA2NShn system in which fluorescence is enhanced as seen in Figures A26 and A48 of the Appendix, respectively.) The smaller β-CD annulus is expected to more closely fit the naphthyl substituents in a lengthwise orientation with the expulsion of most water from the annulus whereas the γ-CD annulus is expected to fit the naphthyl substituents less closely with the expulsion of less water from the annulus. On this basis, the naphthyl substituents complexed in the β-CD annulus experience a substantial decrease in interaction with water with an

enhancement of fluorescence occurring, whereas those complexed in the γ-CD annulus probably experience interactions with water in the annulus of longer duration than collisional times and experience quenching.

Some indication of stereochemical differences arising from complexation in the β-CD and γ-CD annuli is gained from energy minimised molecular modelling using the MM2 protocol in Chem3D Ultra (Figure 5.10).[41] This indicates that the 2-naphthyl substituents of PAA2NSen are likely to be complexed lengthwise through the wide end of the β-CD annulus such that the fluorophore is less exposed to water and fluorescence increases. Similar complexation by γ-CD may also occur, but the increased annular width may also allow the 2-naphthyl substituents to complex perpendicularly to the γ-CD annular axis such that there is a more extensive interaction with the γ-CD hydroxyl groups of longer duration than the time of collisional interaction with water in the uncomplexed state such that fluorescence is quenched. It is also likely that variations in the extent of hydrogen bonding between the naphthyl substituent sulfonamide group and the β-CD and γ-CD hydroxyl groups vary significantly between systems. Thus, there may be several interactions producing quenching of the naphthyl substituents complexed in γ-CD annuli.

The complexation of the 1- and 2- naphthyl substituents by β-CD and γ-CD cause much smaller fluorescence changes than do the corresponding linked dimers consistent with the latter inducing a greater environmental change for the naphthyl fluorophores. Complexation by β-CD and its dimers increase the naphthyl substituent fluorescence, sometimes with a proportionately greater increase at longer wavelengths, consistent with the complexed naphthyl substituent fluorescence range extending to longer wavelengths. In contrast, the γ-CD and its dimers decrease the uncomplexed naphthyl substituent fluorescence and generate an isosbestic point and a new red-shifted fluorescence peak attributable to the complexed fluorophore.

Similar fluorescence titrations could not be performed for the complexation of the free naphthyl substituents 1NSen, 2NSen, 1NShn and 2NShn due to poor aqueous solubility. However, similar observations of contrasting fluorescence behaviour has been previously reported for 2-methylnaphthanoate (2-MN) for 1:1 complexation with β-[45] and γ-CD.[46]

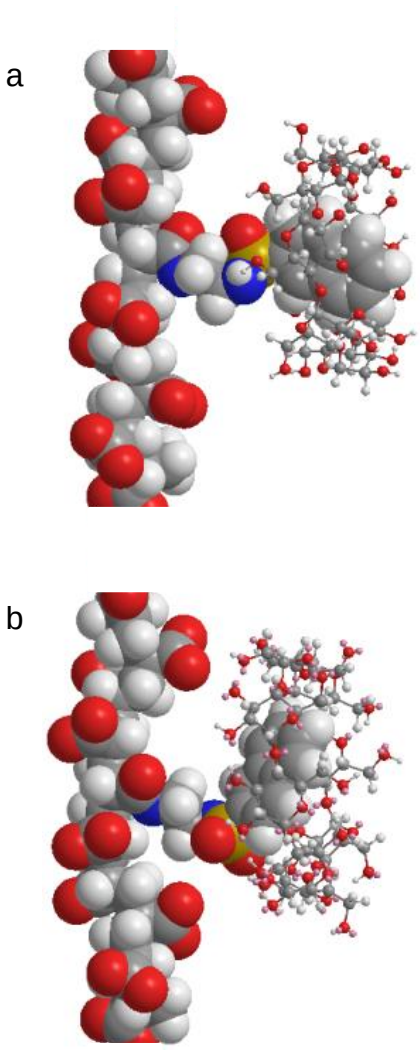

Figure 5.10. Chem3D MM2 energy minimised models of 1:1 host-guest complexes of a) β-CD (ball and stick) and b) γ-CD (ball and stick) with PAA2NSen (space filling).

The seemingly anomalous fluorescence quenching observed in the β-CD/PAA1NSen system is in contrast to the fluorescence enhancement seen in the other β-CD and β-CD dimer systems which enhance fluorescence. This may be a result of the naphthyl substituents of PAA1NSen being the most sterically hindered such that the β-CD/PAA1NSen complex is

constrained to a complexation stereochemistry producing fluorescence quenching which is not required by the less sterically hindered PAA2NSen and more flexible PAA1NShn and PAA2NShn, and which results in these systems assuming stereochemistries producing fluorescence enhancement. As discussed above, the ditopic 33β-CD_2suc and 66β-CD_2suc complex PAA1NSen more strongly than does β-CD and apparently impose complexation stereochemistries resulting in fluorescence enhancement.

In contrast, the enhancement of fluorescence in the γ-CD/PAA2NShn system appears anomalous by comparison with the fluorescence quenching seen in the other eleven γ-CD and γ-CD-dimer systems (Table 5.2). However, the γ-CD/PAA2NShn system is probably the most flexible of all of these systems and this evidently allows it to attain a complexation stereochemistry in which fluorescence enhancement dominates. Thus, the long hexyl tether of PAA2NShn may both compete with the 2-naphthyl substituent in complexing within the γ-CD annulus, and also complex simultaneously with the 2-naphthyl substituent in the γ-CD annulus and thereby exclude water and greatly decrease its quenching effect to give an overall fluorescence enhancement.

5.5. RHEOLOGICAL STUDIES

Rheological measurements were carried out using a Physica MCR 501 (Anton Parr GmbH) stress–controlled rheometer with a 25 mm cone and plate geometry. Temperature was controlled at 298.2 ± 0.1 K by a Peltier plate. Rheological samples were prepared by dissolution of PAA1NSen, PAA1NShn, PAA2NSen and PAA2NShn alone and with 33β-CD_2suc, 66β-CD_2suc, 33γ-CD_2suc or 66γ-CD_2suc in 0.10 mol dm^{-3} aqueous sodium chloride. The solution pH was adjusted to 7.0 with 0.10 mol dm^{-3} aqueous sodium hydroxide solution.

The rheologically determined viscosity provides an indication of the extent to which inter-strand cross-linking between naphthyl substituted poly(acrylate) strands occurs in the presence of the linked β-CD and γ-CD dimers. Thus, the viscosities of 5.0 wt % PAA1NSen, PAA2NSen, PAA1NShn and PAA2NShn solutions either alone or containing either 33β-CD_2suc, 66β-CD_2suc, 33β-CD_2suc or 66β-CD_2suc, where the concentrations of either the β-CD or γ-CD annuli were equal to that of the naphthyl substituents, are determined over a shear rate range to give extrapolated zero shear viscosities. The variations in viscosities of the five PAA2NSen and the five PAA2NShn solutions with shear rate are shown in Figure 5.11 and those of the five PAA1NSen and the five PAA1NShn solutions are shown in Figure A50 of the Appendix. It is seen that viscosity variation with shear rate is small. All of the zero shear rate data are collected in Table 5.3 and are displayed in Figure 5.12. The zero shear viscosities range from 0.0147 Pa s for a solution of 5.0 wt % solution of PAA1NSen alone to 29.200 Pa s for a 5.0 wt % solution of PAA2NShn in the presence of equimolar 2-naphthyl substituents and β-CD annuli of 66β-CD_2suc; a two thousand-fold range. (The zero shear viscosities of all four naphthyl-substituted poly(acrylate)s solutions containing either β-CD or γ-CD solutions are very similar to those of the naphthyl poly(acrylate) solutions alone and are not further discussed.)

The formation of inter-strand cross-links between polymer components in aqueous solution competes with the formation of intra-strand cross-links within individual polymer strands. Such competition is likely to occur more in the 5.0 wt % in solutions of the four naphthyl-substituted poly(acrylate)s of this study where collision between strands is much more probable than is the case in the much less concentrated 0.034 wt % solutions of the fluorimetric studies.

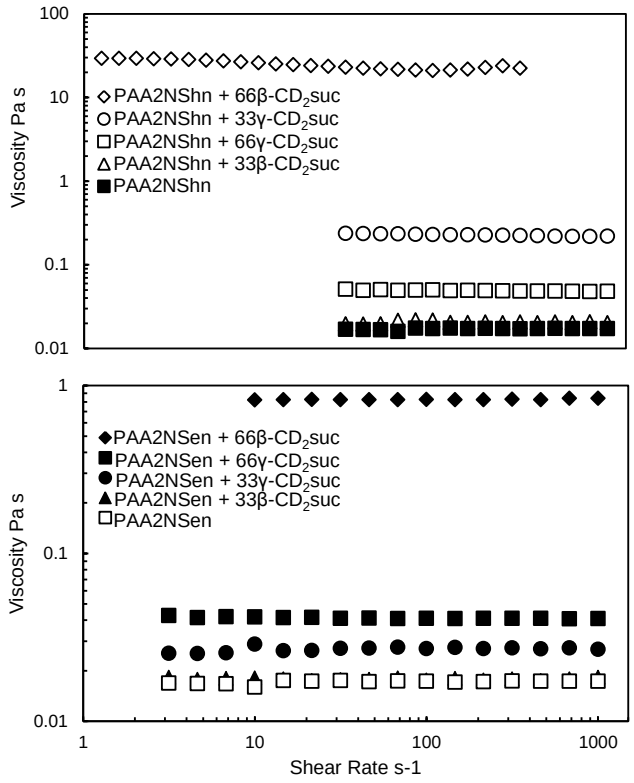

Figure 5.11. Viscosity variations with shear rate of 5 wt % aqueous solutions of PAA2NSen and PAA2NShn alone and in the presence of 33β-CD_2suc, 66β-CD_2suc, 33-γCD_2suc and 66γ-CD_2suc at pH 7.0 and [NaCl] = 0.10 mol dm^{-3} at 298.2 K. The concentrations of the β-CD and γ-CD substituents in the linked dimers are equal to those of the 2NSen or 2NShn poly(acrylate) substituents.

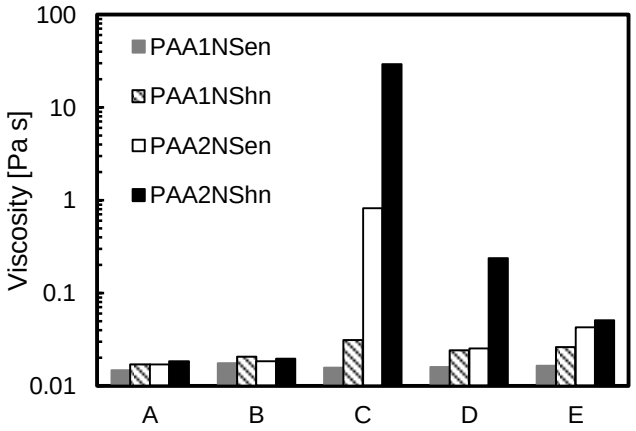

Figure 5.12. Zero-shear viscosities of 5 wt % aqueous PAA1NSen (grey column), PAA1NShn (hatched column), PAA2NSen (white column) and PAA2NShn (black column) alone and in the presence of 33β-CD_2suc, 33γ-CD_2suc, 66β-CD_2suc and 66γ-CD_2suc at pH 7.0 and [NaCl] = 0.1 M at 298.2 K. The concentrations of the β-CD and γ-CD substituents in the linked dimers are equal to those of either the 2NSen or 2NShn poly(acrylate) substituents. A) no CD, B) 33β-CD_2suc, C) 66β-CD_2suc, D) 33γ-CD_2suc and E) 66γ-CD_2suc.

Table 5.3. Zero-shear viscosities[a] (Pa s) of 5 wt % aqueous PAA1NSen, PAA1NShn, PAA2NSen and PAA2NShn alone and in the presence of 33β-CD_2suc, 33γ-CD_2suc, 66β-CD_2suc and 66γ-CD_2suc at pH 7.0 and [NaCl] = 0.10 mol dm^{-3} at 298.2 K.

Guest / Host	PAA1NSen Pa s	PAA2NSen Pa s	PAA1NShn Pa s	PAA2NShn Pa s
No Host	0.0147[b]	0.0172	0.0169[b]	0.0185
33β-CD_2suc	0.0175[b]	0.0206	0.0183[b]	0.0195
66β-CD_2suc	0.0156[b]	0.0315	0.8210[b]	29.200
33γ-CD_2suc	0.0159[b]	0.0242	0.0254[b]	0.2380
66γ-CD_2suc	0.0164[b]	0.0263	0.0427[b]	0.0510

[a]Experimental error ≤ ± 5%.
[b] Data from previous study. [35]

Such competition is likely to occur to a greater extent in the presence of the β-CD and γ-CD linked cyclodextrin dimers as is reflected in the zero-shear viscosity data shown in Figure 5.12 and Table 5.3. The zero shear viscosities of 5.0 wt % solutions of PAA1NSen and PAA2NSen (0.0147 and 0.0169 Pa s) are slightly smaller than that of PAA1NShn and PAA2NShn solutions (0.0172 and 0.0185 Pa s), consistent with the shorter aminoethyl tether of PAA1NSen and PAA2NSen restricting any association between naphthyl substituents to a greater extent than the longer aminohexyl tether of PAA1NShn and PAA2NShn largely because of steric hindrance from the poly(acrylate) backbone. These values are similar to the zero shear viscosity of a 5.0 wt % solution of 3% dodecyl-substituted poly(acrylate) (PAAC12), but about four orders of magnitude smaller than that of a 5.0 wt % solution of 3% octadecyl-substituted poly(acrylate) (PAAC18).[26] This suggests that the intermolecular π–π interaction between either the 1- or 2-naphthyl substituents is of similar strength to hydrophobic association between the dodecyl substituents but much weaker than that between the octadecyl substituents of the corresponding substituted poly(acrylate)s.

The zero-shear viscosities of all four naphthyl-substituted poly(acrylate)s increase slightly in the presence of 33β-CD_2suc and show a pattern whereby the longer aminohexyl linker increase viscosity to a greater extent through forming an inter-strand cross-link through

ditopic complexation of the 1- and 2-naphthyl substituents by 33β-CD_2suc. This is in marked contrast to the viscosity pattern shown by in the presence of 66β-CD_2suc where a combination of the presentation of the wide face of the β-CD annuli for complexation and the less sterically hindered 2-naphthyl substituents produce by far the greatest zero-shear viscosities for the 66β-CD_2suc/PAA2NSen and 66β-CD_2suc/PAA2NShn with the latter showing the greatest viscosity as a result of the greater flexibility afforded by the aminohexyl linker. (The structure of an inter-strand cross-link in the 66β-CD_2suc/PAA2NShn system is probably similar to that shown in Figure 5.9.) The increase in viscosity shown by the 66β-CD_2suc/PAA1NShn system is much less because of the steric hindrance to complexation of the 1-naphthyl substituent, and the increase for the 66β-CD_2suc/PAA1NSen is even less because of the additional restriction imposed by the short aminoethyl linker. It is notable that the K_{11} variation (Table 5.2) observed for complexation dominantly on single strands in dilute solution for these systems reflects the relative order of their viscosity variations although the range of the latter was much greater. Just as the K_{11} magnitudes are the largest observed so are the three larger viscosities the largest observed in this study. This suggests that the same stereochemical factors control the magnitudes of both parameters to a similar extent. Thus, it appears that the reason for PAA1NSen solutions with all four naphthyl-substituted poly(acrylate)s showing the lowest viscosities and smallest range thereof is dominantly controlled by the steric hindrance against complexation by the stereochemistry of the 1-naphthyl substituent and the shortness of the aminoethyl tether. The viscosity magnitudes and their variations are significantly greater for the other three naphthyl-substituted poly(acrylate)s as is now discussed.

The increase in γ-CD annular size in 33γ-CD_2suc causes significant increases in viscosity through inter-strand cross-linking with PAA1NShn, PAA2NSen and PAA2NShn by comparison with that of the analogous 33β-CD_2suc solutions to the extent that the viscosity

of the 33γ-CD_2suc/PAA2NShn system is the third highest determined. (This is opposite to the trend in K_{11} (Table 5.2) where those characterising 33β-CD_2suc are larger than those for 33γ-CD_2suc, and indicates that the relative importance of the factors controlling intra- and inter-strand complexation differs.) The high viscosity of the 33γ-CD_2suc/PAA2NShn system is attributable to 33γ-CD_2suc presenting the narrow face of the γ-CD annulus for complexation of the 2-naphthyl substituent, which it fits more closely than the wide face, combined with the length of the aminohexyl tether of PAA2NShn which decreases steric hindrance. In contrast the viscosity of the 66γ-CD_2suc/PAA2NShn system decreases substantially by comparison and this is attributable to the less closely fitting wide face of the γ-CD annulus being presented for complexation of the 2-naphthyl substituent.

5.6. SUMMARY AND CONCLUSIONS

Two existing and two new isomeric 3% 1- and 2-naphthyl randomly substituted poly(acrylate)s, PAA1NSen, PAA2NSen, PAA1NShn and PAA2NShn are synthesised and their complexation by β-CD, γ-CD and their corresponding isomeric succinamide-linked cyclodextrin dimers, 33β-CD_2suc, 33γ-CD_2suc, 66γ-CD_2suc and 66γ-CD_2suc were studied in both dilute and concentrated aqueous solutions. In dilute solutions 2D ^{1}H NOESY NMR studies show the naphthyl substituents of the substituted poly(acrylate)s to complex in the annuli of all six cyclodextrin species studied, as do the aminohexyl tethers of both PAA1NShn and PAA2NShn. There is a marked difference between the effect on the fluorescence of the naphthyl substituted poly(acrylate)s by β-CD and its linked dimers which enhance fluorescence in eleven of the twelve systems studied and that of γ-CD and its linked dimers which quench fluorescence in eleven of the additional twelve systems studied. (The two exceptions quench and enhance fluorescence, respectively.) These differences arise from

the differing dimensions of the β-CD and γ-CD annuli and the stereochemistry of host-guest complexation.

Fluorimetric studies yielded twenty-four 1:1 formation constants, K_{11}, dominantly for host-guest complexation of the naphthyl substituents of single strands of the four naphthyl-substituted poly(acrylate)s by β-CD and γ-CD and their linked dimers which show a seventy-fold variation in magnitude. The most stable complexes of each of the naphthyl-substituted poly(acrylate)s were formed by 66β-CD_2suc for which K_{11} = 2220 – 10000 dm^3 mol^{-1} at 298.2 K. Other substantial variations occur according to the variations between β-CD and γ-CD annuli being the principle complexing agent, and the stereochemistry of the 1- or 2-naphthyl substituent and the different lengths of the aminoethyl and aminohexyl tethers securing them to the poly(acrylate) backbone. In concentrated 5.0 wt % solutions of the four naphthyl-substituted poly(acrylate)s and the β-CD and γ-CD linked dimers rheological determinations show the same factors to play similar but proportionately different roles in forming inter-strand cross-links to generate a two thousand-fold range of zero-shear viscosities. The highest viscosity is 29.200 Pa s for the 66β-CD_2suc/PAA2NShn system with the lowest being 0.0147 Pa s for PAA1NSen alone.

5.7. REFERENCES

1. C. J. Easton and S. F. Lincoln, *Chem. Soc. Rev.*, 1996, **25**, 163-170.
2. K.A. Connors, *Chem. Rev*. 1997, **97**, 1325–1357.
3. J. Szejtli, *Chem. Rev.*, 1998, **98**, 1743-1754.
4. H.-J. Schneider, F. Hacket, V. Rüdiger and H. Ikeda, *Chem. Rev.*, 1998, **98**, 1755-1786.
5. W. Saenger, J. Jacob, K. Gessler, T. Steiner, D. Hoffmann, H. Sanbe, K. Koizumi, S. M. Smith and T. Takaha, *Chem. Rev.*, 1998, **98**, 1787-1802.
6. M.V. Rekharsky and Y. Inoue, *Chem. Rev*. 1998, **98** 1875–1917.
7. A. R. Khan, P. Forgo, K. J. Stine and V. T. D'Souza, *Chem. Rev.*, 1998, **98**, 1977-1996.
8. S. A. Nepogodiev and J. F. Stoddart, *Chem. Rev.* 1998, **98**, 1959-1976.
9. C. J. Easton and S. F. Lincoln, *Modified Cyclodextrins: Scaffolds and Templates for Supramolecular Chemistry*, Imperial College Press, London, 1999.
10. J. M. Haider and Z. Pikramenou, *Chem. Soc. Rev.*, 2005, **34**,120-132.
11. G. Wenz, B.-H. Han, and A. Müller, *Chem. Rev.*, 2006, **106**, 782-817.
12. Y. Liu and Y. Chen, *Acc. Chem. Res.*, 2006, **39**, 681-691
13. R. Villalonga, R. Cao and A. Fragoso, *Chem. Rev.* 2007 **107** 3088–3116.
14. F. Bellia, D. La Mendola, C. Pedone, E. Rizzarelli, M. Saviano G. Vecchio, *Chem. Soc. Rev.*, 2009, **38**, 2756-2781.
15. A. Harada, A. Hashidzume, H. Yamaguchi and Y. Takashima, *Chem. Rev.*, 2009, **109**, 5974–6023.
16. S. F. Lincoln and D.-T. Pham, *Cyclodextrins: From Nature to Nanotechnology, Chapter 10 in Supramolecular Chemistry: From Molecules to Nanomaterials,* 2012. P. A. Gale and J. W. Steed (eds), John Wiley & Sons Ltd., Chichester, UK, pp. 955-982.

17. X. Guo, A. A. Abdala, B. L. May, S. F. Lincoln, S. A. Khan and R. K. Prud'homme, *Macromolecules*, 2005, **38**, 3037-3040.

18. X. Guo, A. A. Abdala, B. L. May, S. F. Lincoln, S. A. Khan and R. K. Prud'homme, *Polymer*, 2006, **47**, 2976-2983.

19. X. Guo, J. Wang, L. Li, C. R. Pacheco, L. Fu, R. K. Prud'homme and S. F. Lincoln, *Polym. Mat. Sci. Eng.* 2007, **97**, 543-544.

20. L. Li, X. Guo, L. Fu, R. K. Prud'homme and S. F. Lincoln, *Langmuir*, 2008, **24**, 8290-8296.

21. L. Li, X. Guo, J. Wang, P. Liu, R. K. Prud'homme, B. L. May and S. F. Lincoln, *Macromolecules*, 2008, **41**, 8677-8681.

22. J. Wang, L. Li, H. Ke, P. Liu, L. Zheng, X. Guo and S. F. Lincoln, *Asia-Pac. J. Chem. Eng.*, 2009, **4**, 537-543.

23. J. Wang, D.-T. Pham, X. Guo, L. Li, S. F. Lincoln, Z. Luo, H. Ke, L. Zheng and R. K. Prud'homme, *Ind. Eng. Chem. Res.*, 2010, **49**, 609-612.

24. X. Guo, J. Wang, L. Li, D.-T. Pham, P. Clements, S. F. Lincoln, B. L. May, Q. Chen, L. Zheng and R. K. Prud'homme, *Macromol. Rapid Commun.*, 2010, **31**, 300-304.

25. J. Wang, D.-T. Pham, T. W. Kee, S. N. Clafton, X. Guo, P. Clements, S. F. Lincoln and R. K. Prud'homme, *Macromolecules*, 2011, **44**, 9782-9791.

26. J. Wang, L. Li, X. Guo, L. Zheng, D.-T. Pham, S. F. Lincoln, H. T. Ngo, P. Clements, B. L. May, R. K. Prud'homme and C. J. Easton, *Ind. Eng. Chem. Res.* 2011, **50**, 7566-7571.

27. H.-T. Nguyen, D.-T. Pham, S. F. Lincoln, J. Wang, X. Guo, C. J. Easton and R. K. Prud'homme, *Polym. Chem.* 2013, **3**, 820-829.

28. D.-T. Pham, H.-T. Nguyen, S. F. Lincoln, J. Wang, X. Guo, C. J. Easton and R. K Prud'homme, *J. Polym. Sci., A, Polym. Chem*. 2015, **53**, 1278-1286.

29. N. A. Peppas, Y. Huang, M. Torres-Lugo, J. H. Ward and J. Zhang, *Annu. Rev. Biomed. Eng.*, 2000, **2**, 9-29.

30. K. Y. Lee and D. J. Mooney, *Chem. Rev.*, 2001, **101**, 1869-1879.

31. A. P. Nowak, V. Breedveld, L. Pakstis, B. Ozbas, D. J. Pine, D. Pochan and T. J. Deming, *Nature*, 2002, **417**, 424-428.

32. N. M. Sangeetha and U. Maitra, *Chem. Soc. Rev.*, 2005, **34**, 821-836.

33. G. R. Hendrickson and L. A. Lyon, *Soft Matter*, 2009, **5**, 29-35.

34. N. Huebsch and D. J. Mooney, *Nature*, 2009, **462**, 426-432.

35. H. T. Ngo, Supramolecular Chemistry of β- and γ-Cyclodextrin Dimers. A PhD. Dissertaion, University of Adelaide, 2010.

36. S. E. Brown, J. H. Coates, D. R. Coghlan, C. J. Easton, S. J. Vaneyk, W. Janowski, A. Lepore, S. F. Lincoln, Y. Luo, B. L. May, D. S. Schiesser, P. Wang and M. L. Williams, *Aust. J. Chem.*, 1993, **46**, 953-958.

37. C. J. Easton, S. J. van Eyk, S. F. Lincoln, B. L. May, J. Papageorgiou and M. L. Williams, *Aust. J. Chem.*, 1997, **50**, 9-12.

38. D.-T. Pham, H. T. Ngo, S. F. Lincoln, B. L. May and C. J. Easton, *Tetrahedron*, 2010, **66**, 2895-2898.

39. B. L. May, P. Clements, J. Tsanaktsidis, C. J. Easton and S. F. Lincoln, *J. Chem. Soc, Perkin Trans. 1*, 2000, 463-469.

40. HypSpec, Protonic Software, 2 Templegate Avenue, Leeds LS15 0HD, UK.

41. Chem3D Ultra, CambridgeSoft Co., 100 Cambridge Park Drive, MA 02140, USA.

42. A. Harada, F. Ito, I. Tomatsu, K. Shimoda, A. Hashidzume, Y. Takashima, H. Yamaguchi and S. Kamitori, *J. Photochem. Photobiol. A: Chem.* 2006, **179**, 13-19.

43. G. Grabner, K. Rechthaler, B. Mayer and G. Köhler, *J. Phys. Chem. A*, 2000, **104**, 1365-1376.

44. M. Cervero and F. Mendicuti, *J. Phys. Chem. B*, 2000, **104**, 1572-1580.

45. J. M. Madrid, F. Mendicuti and W. L. Mattice, *J. Phys. Chem. B*, 1998, **102**, 2037-2044.

46. J. M. Madrid and F. Mendicuti, *Appl. Spectrosc.*, 1997, **51**, 1621-1627.

47. M. Seel and T. C. Werner, *Appl Spectrosc*, 2005, **59**, 691-695.

48. M. Shaikh, Y. M. Swamy and H. Pal, *J. Photochem. Photobiol. A: Chem.*, 2013, **258**, 41-50.

49. M. Shaikh, J. Mohanty, M. Sundararajan, A. C. Bhasikuttan and H. Pal, *J. Phys. Chem. B*, 2012, **116**, 12450-12459.

2D ^{1}H NOESY NMR Spectra

PAA1NSen

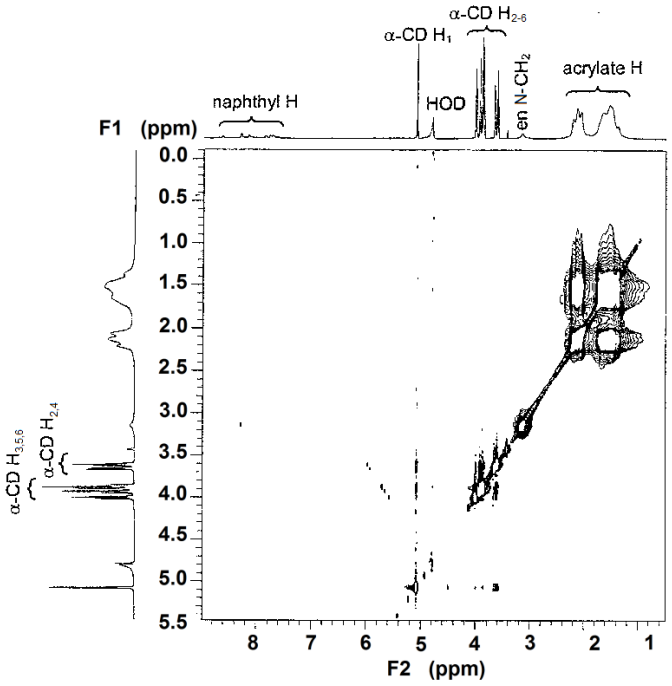

Figure A1. 2D ^{1}H NOESY NMR (600 MHz) spectrum of 3% substituted PAA1NSen (1.43 wt%, [1NSen] = 3.0×10^{-3} mol dm^{-3}) and equimolar α-CD in D_2O at pD 7.0 (0.10 mol dm^{-3} in NaCl) at 298.2 K with a mixing time of 300 ms. No significant cross-peaks were observed.

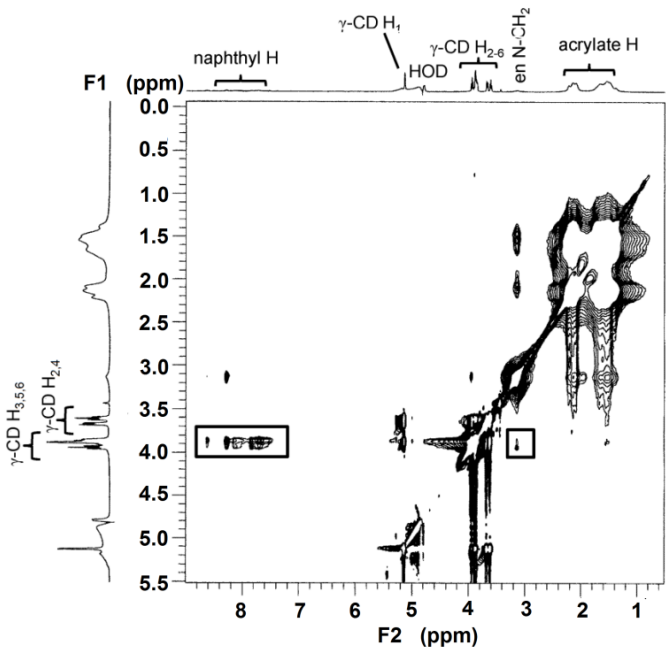

Figure A2. 2D ^{1}H NOESY NMR (600 MHz) spectrum of 3% substituted PAA1NSen (1.43 wt%, [1NSen] = 3.0×10^{-3} mol dm^{-3}) and equimolar γ-CD in D_2O at pD 7.0 (0.10 mol dm^{-3} in NaCl) at 298.2 K with a mixing time of 300 ms. Cross–peaks enclosed in the rectangles arise from interactions between the annular γ-CD $H_{3,5,6}$ protons with the naphthyl (left) and the N-CH_2 (right) protons of the 1NSen substituent.

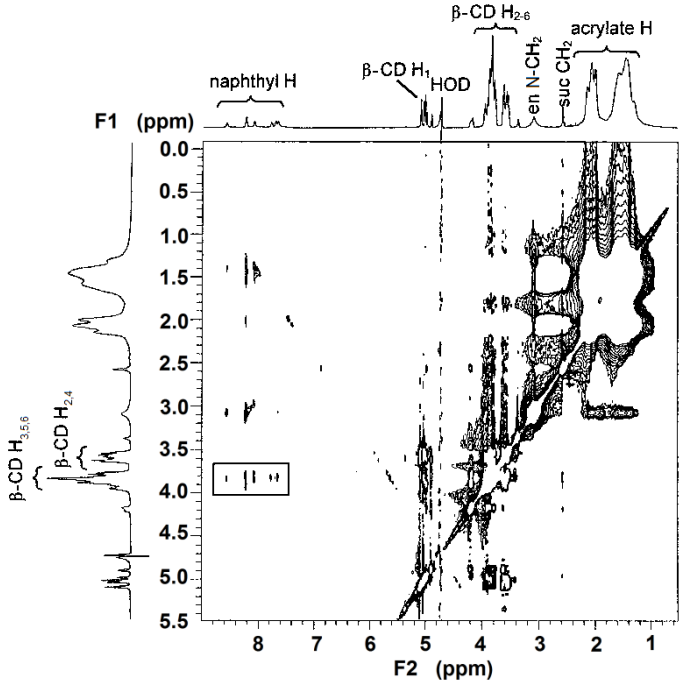

Figure A3. 2D ^{1}H NOESY NMR (600 MHz) spectrum of 3% substituted PAA1NSen (1.43 wt%, [1NSen] = 3.0×10^{-3} mol dm^{-3}) and equimolar 33β-CD_2suc in D_2O at pD 7.0 (0.10 mol dm^{-3} in NaCl) at 298.2 K with a mixing time of 300 ms. Cross–peaks enclosed in the rectangle arise from interactions between the annular β-CD $H_{3,5,6}$ protons of 33β-CD_2suc and the naphthyl protons of the 1NSen substituent. Note: This spectrum is from a previous study.[35]

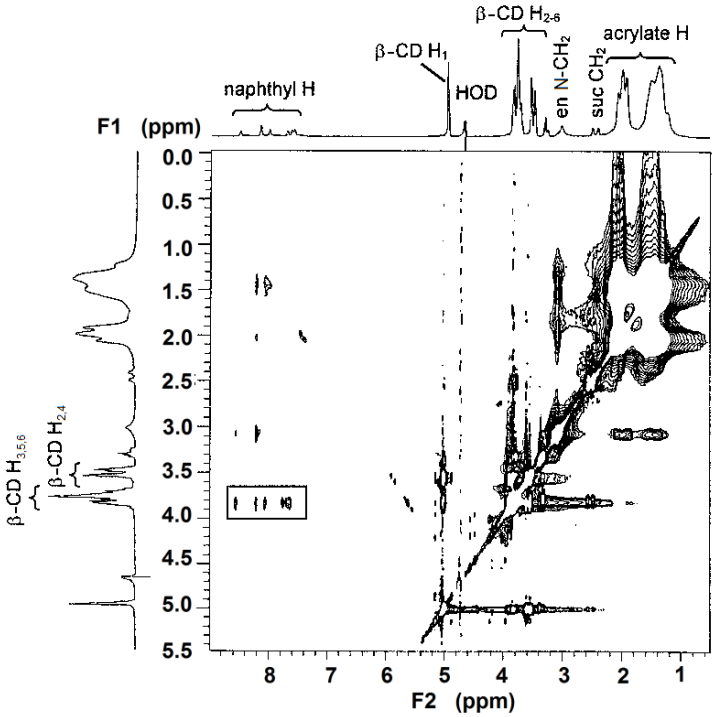

Figure A4. 2D ^{1}H NOESY NMR (600 MHz) spectrum of 3% substituted PAA1NSen (1.43 wt %, [1NSen] = 3.0×10^{-3} mol dm^{-3}) and equimolar 66β-CD_2suc in D_2O at pD 7.0 (0.10 mol dm^{-3} in NaCl) at 298.2 K with a mixing time of 300 ms. Cross-peaks enclosed in the rectangle arise from interactions between the annular β-CD $H_{3,5,6}$ protons and naphthyl protons of the 1NSen substituent. Note: This spectrum is from a previous study.[35]

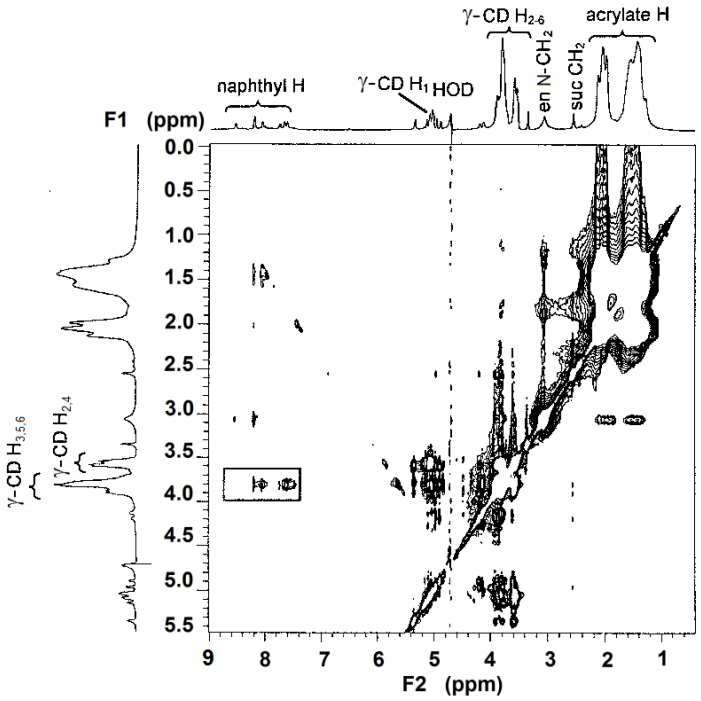

Figure A5. 2D ^{1}H NOESY NMR (600 MHz) spectrum of 3% substituted PAA1NSen (1.43 wt%, [1NSen] = 3.0×10^{-3} mol dm^{-3}) and equimolar 33γ-CD_2suc in D_2O at pD 7.0 (0.10 mol dm^{-3} in NaCl) at 298.2 K with a mixing time of 300 ms. Cross-peaks enclosed in the rectangle arise from interactions between the annular γ-CD $H_{3,5,6}$ protons of 33γ-CD_2suc and the naphthyl protons of the 1NSen substituent. Note: This spectrum is from a previous study.[35]

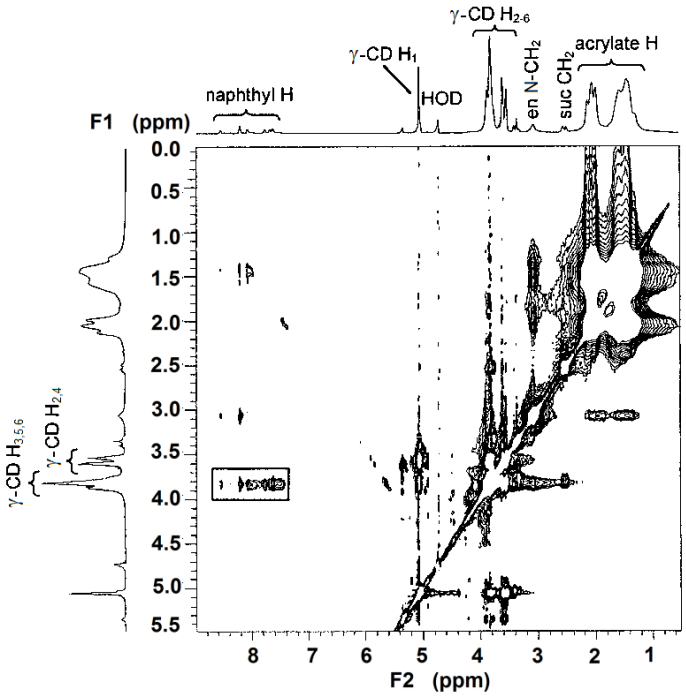

Figure A6. 2D ^{1}H NOESY NMR (600 MHz) spectrum of 3% substituted PAA1NSen (1.43 wt%, [1NSen] = 3.0×10^{-3} mol dm^{-3}) and equimolar 66γ-CD_2suc in D_2O at pD 7.0 (0.10 mol dm^{-3} in NaCl) at 298.2 K with a mixing time of 300 ms. Cross-peaks enclosed in the rectangle arise from interactions between the annular γ-CD $H_{3,5,6}$ protons of 66γ-CD_2suc and the naphthyl protons of the 1NSen substituent. Note: This spectrum is from a previous study.[35]

PAA1NShn

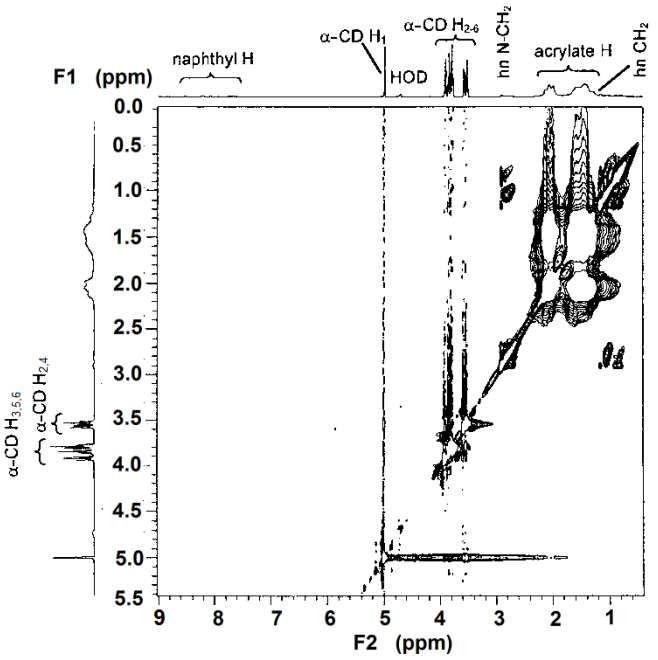

Figure A7. 2D ^{1}H NOESY NMR (600 MHz) spectrum of 3% substituted PAA1NShn (1.43 wt%, [1NShn] = 3.0×10^{-3} mol dm^{-3}) and equimolar α-CD in D_2O at pD 7.0 (0.10 mol dm^{-3} in NaCl) at 298.2 K with a mixing time of 300 ms. No significant cross-peaks were observed.

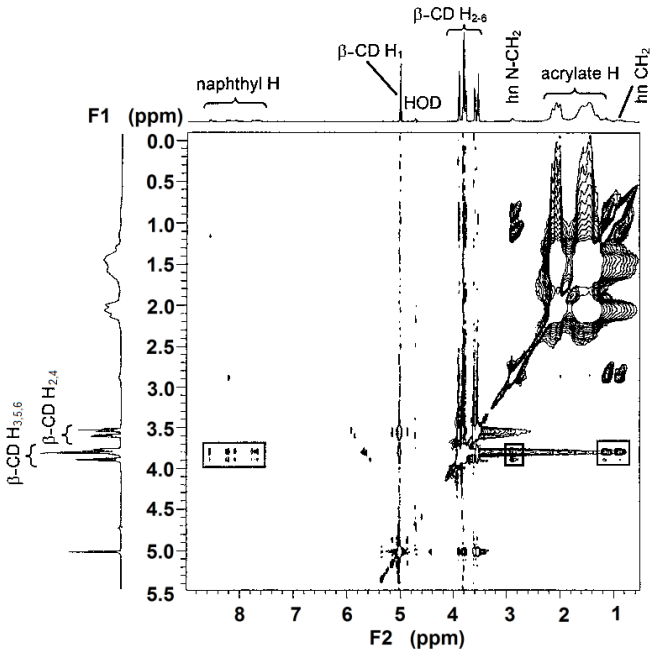

Figure A8. 2D ^{1}H NOESY NMR (600 MHz) spectrum of 3% substituted PAA1NShn (1.43 wt%, [1NShn] = 3.0×10^{-3} mol dm^{-3}) and equimolar β-CD in D_2O at pD 7.0 (0.10 mol dm^{-3} in NaCl) at 298.2 K with a mixing time of 300 ms. Cross-peaks enclosed in the rectangles arise from interactions between the annular β-CD $H_{3,5,6}$ protons with the naphthyl (left), N-CH_2 (middle) and other hexyl CH_2 (right) protons of the 1NShn substituent. Note: This spectrum is from a previous study.[35]

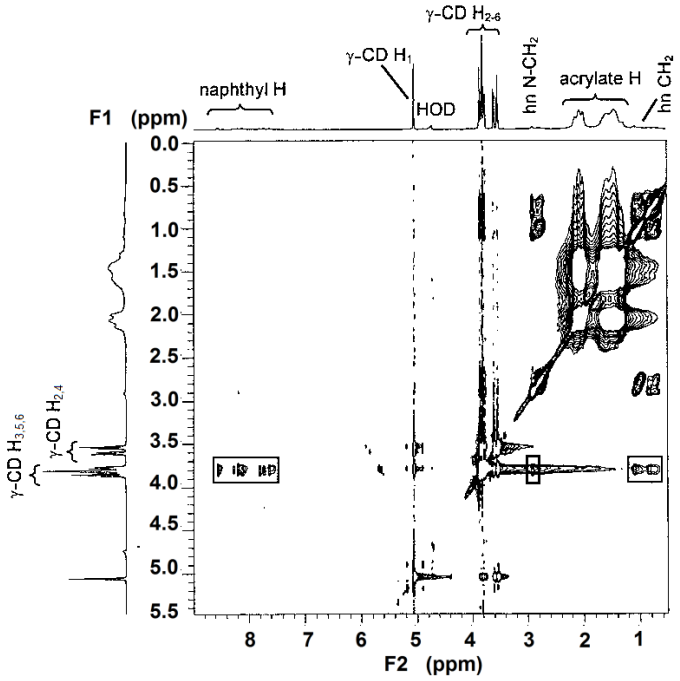

Figure A9. 2D ^{1}H NOESY NMR (600 MHz) spectrum of 3% substituted PAA1NShn (1.43 wt%, [1NShn] = 3.0×10^{-3} mol dm^{-3}) and equimolar γ-CD in D_2O at pD 7.0 (0.10 mol dm^{-3} in NaCl) at 298.2 K with a mixing time of 300 ms. Cross-peaks enclosed in the rectangles arise from interactions between the annular γ-CD $H_{3,5,6}$ protons with the naphthyl (left), N-CH_2 (middle) and other hexyl CH_2 (right) protons of the 1NShn substituent. Note: This spectrum is from a previous study.[35]

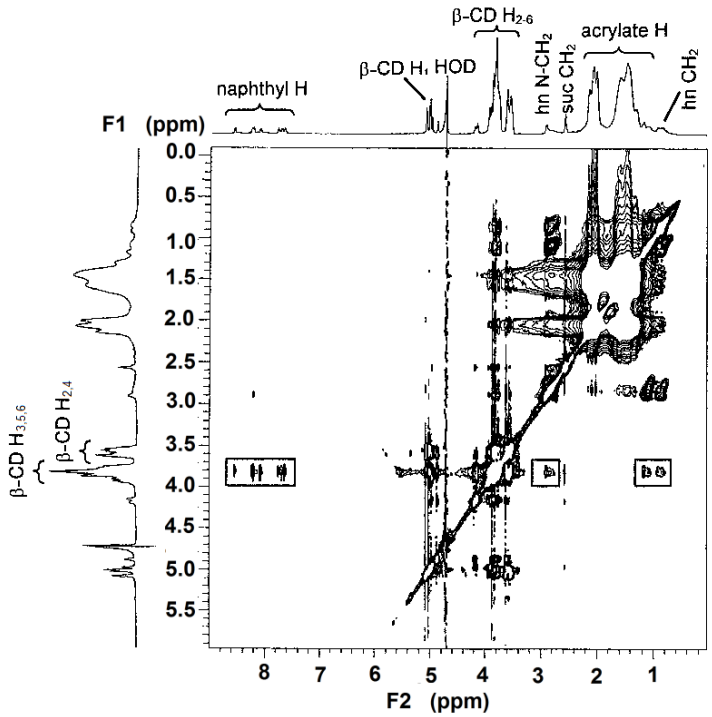

Figure A10. 2D ^{1}H NOESY NMR (600 MHz) spectrum of 3% substituted PAA1NShn (1.43 wt%, [1NShn] = 3.0×10^{-3} mol dm^{-3}) and equimolar 33β-CD_2suc in D_2O at pD 7.0 (0.10 mol dm^{-3} in NaCl) at 298.2 K with a mixing time of 300 ms. Cross-peaks enclosed in the rectangle arise from interactions between the annular β-CD $H_{3,5,6}$ protons of 33β-CD_2suc with the naphthyl (left) and N-CH_2 (middle) and other hexyl CH_2 (right) protons of the 1NShn substituent. Note: This spectrum is from a previous study.[35]

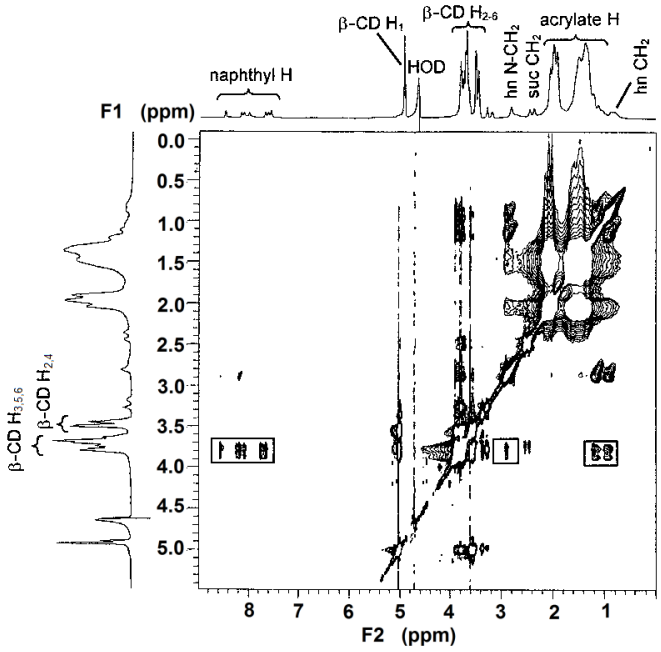

Figure A11. 2D ^{1}H NOESY NMR (600 MHz) spectrum of 3% substituted PAA1NShn (1.43 wt%, [1NShn] = 3.0×10^{-3} mol dm^{-3}) and equimolar 66β-CD_2suc in D_2O at pD 7.0 (0.10 mol dm^{-3} in NaCl) at 298.2 K with a mixing time of 300 ms. Cross-peaks enclosed in the rectangle arise from interactions between the annular β-CD $H_{3,5,6}$ protons of 66β-CD_2suc with the naphthyl (left), N-CH_2 (middle) and other hexyl CH_2 (right) protons of the 1NShn substituent. Note: This spectrum is from a previous study.[35]

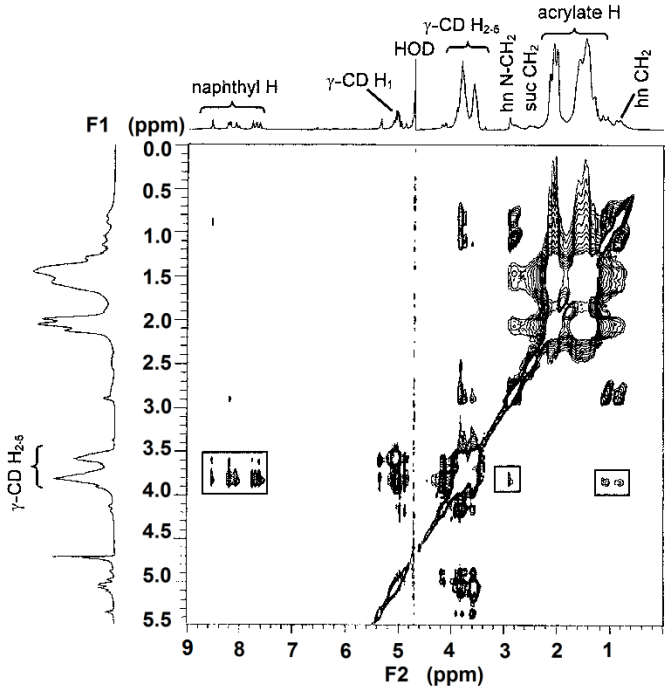

Figure A12. 2D ^{1}H NOESY NMR (600 MHz) spectrum of 3% substituted PAA1NShn (1.43 wt%, [1NShn] = 3.0×10^{-3} mol dm^{-3}) and equimolar 33γ-CD_2suc in D_2O at pD 7.0 (0.10 mol dm^{-3} in NaCl) at 298.2 K with a mixing time of 300 ms. Cross-peaks enclosed in the rectangles arise from interactions between the annular γ-CD $H_{3,5,6}$ protons of 33γ-CD_2suc with the naphthyl (left), N-CH_2 (middle) and other hexyl CH_2 (right) protons of the 1NShn substituent. Note: This spectrum is from a previous study.[35]

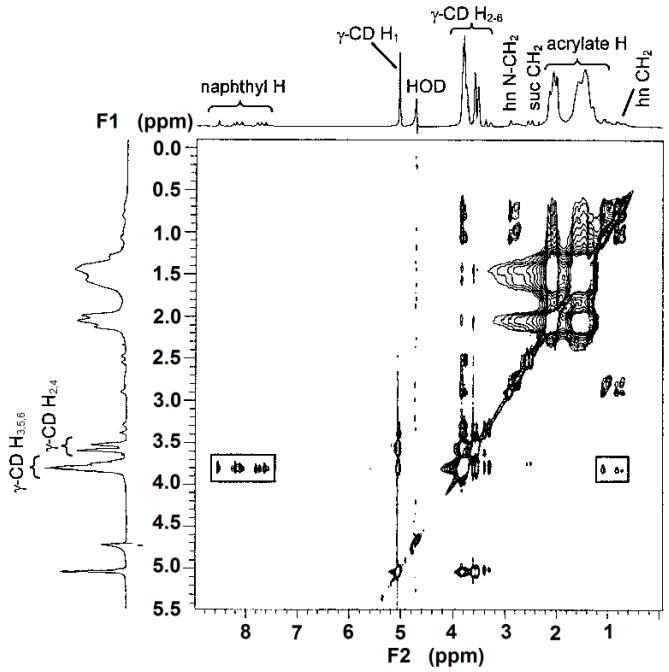

Figure A13. 2D ^{1}H NOESY NMR (600 MHz) spectrum of 3% substituted PAA1NShn (1.43 wt%, [1NShn] = 3.0×10^{-3} mol dm^{-3}) and equimolar 66γ-CD_2suc in D_2O at pD 7.0 (0.10 mol dm^{-3} in NaCl) at 298.2 K with a mixing time of 300 ms. Cross-peaks enclosed in the rectangles arise from interactions between the annular γ-CD $H_{3,5,6}$ protons of 66γ-CD_2suc with the naphthyl (left) and hexyl CH_2 (right) protons of the 1NShn substituent. Note: This spectrum is from a previous study.[35]

PAA2NSen

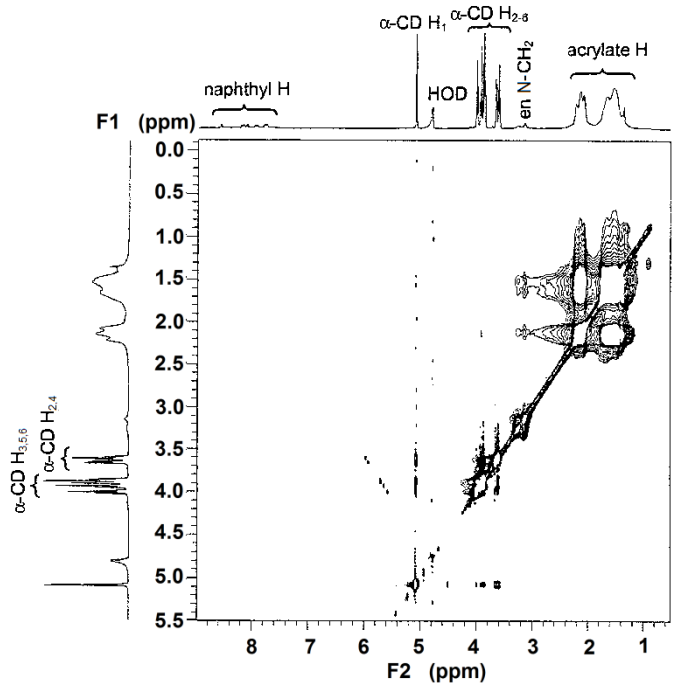

Figure A14. 2D ^{1}H NOESY NMR (600 MHz) spectrum of 3% substituted PAA2NSen (1.43 wt%, [2NSen] = 3.0×10^{-3} mol dm^{-3}) and equimolar α-CD in D_2O at pD 7.0 (0.10 mol dm^{-3} in NaCl) at 298.2 K with a mixing time of 300 ms. No significant cross-peaks were observed.

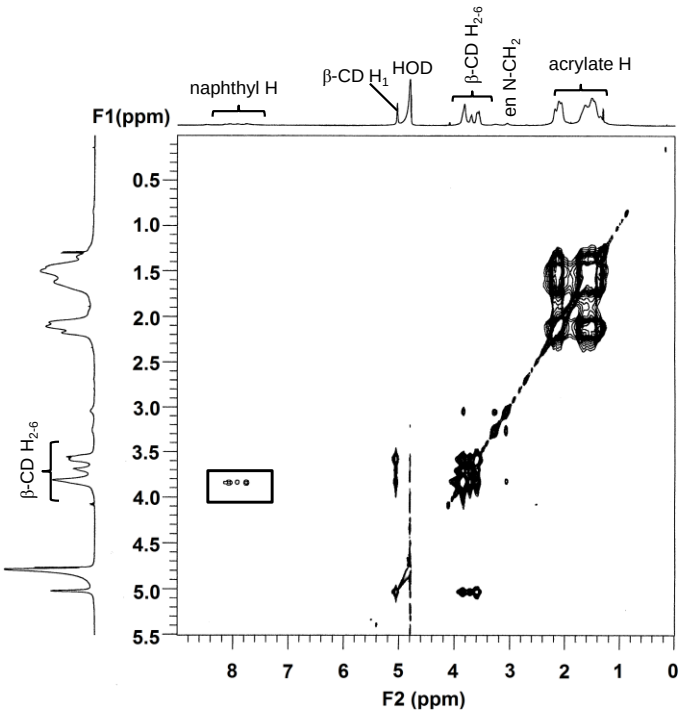

Figure A15. 2D ^{1}H NOESY NMR (600MHz) spectrum of 3% substituted PAA2NSen (1.43 wt%, [2NSen] = 3.0×10^{-3} mol dm^{-3}) and equimolar β-CD in D_2O at pD 7.0 (0.10 mol dm^{-3} in NaCl) at 298.2 K with a mixing time of 300 ms. Cross–peaks enclosed in the rectangles arise from interaction between the annular β-CD $H_{3,5,6}$ protons and the naphthyl protons (left) and N-CH_2 (right) of the 2NSen substituent.

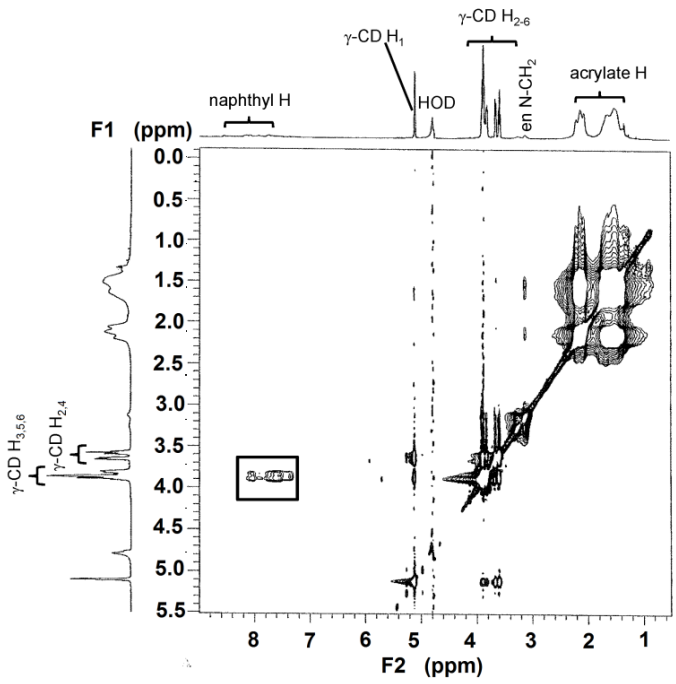

Figure A16. 2D ^{1}H NOESY NMR (600 MHz) spectrum of 3% substituted PAA2NSen (1.43 wt%, [2NSen] = 3.0×10^{-3} mol dm^{-3}) and equimolar γ-CD in D_2O at pD 7.0 (0.10 mol dm^{-3} in NaCl) at 298.2 K with a mixing time of 300 ms. Cross–peaks enclosed in the rectangle arise from interactions between the annular γ-CD $H_{3,5,6}$ protons and the naphthyl protons of the 2NSen substituent.

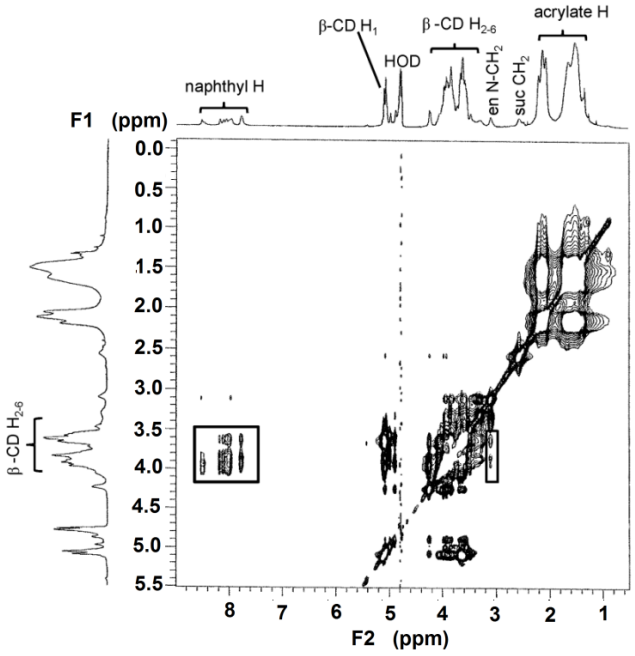

Figure A17. 2D ^{1}H NOESY NMR (600 MHz) spectrum of 3% substituted PAA2NSen (1.43 wt%, [2NSen] = 3.0×10^{-3} mol dm^{-3}) and equimolar 33β-CD_2suc in D_2O at pD 7.0 (0.10 mol dm^{-3} in NaCl) at 298.2 K with a mixing time of 300 ms. Cross–peaks enclosed in the rectangle arise from interactions dominantly between the annular β-CD $H_{3,5,6}$ protons of 33β-CD_2suc and the naphthyl protons of the 2NSen substituent. It appears that combination of inequivalence in the glucopyranose units of 33β-CD_2suc arising from substitution at C^{3A} and complexation appears to have increased the δ range for the $H_{3,5,6}$ protons which in turn increased the δ range for the cross-peaks.

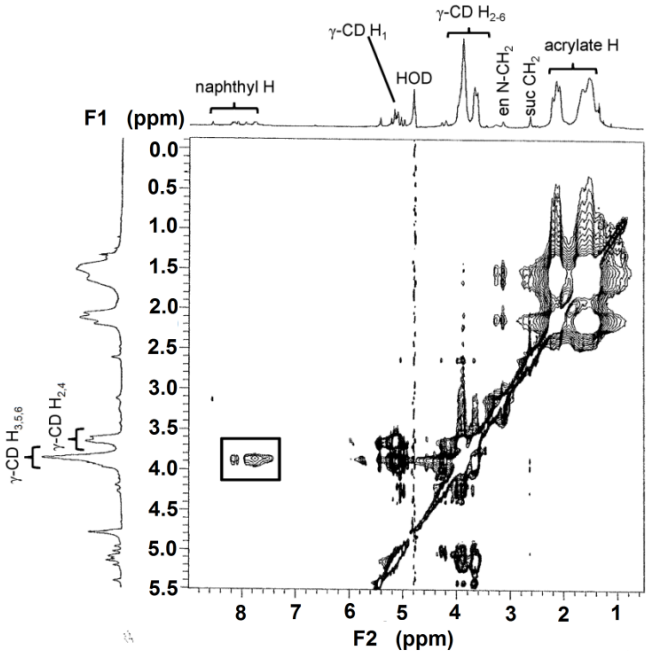

Figure A18. 2D ^{1}H NOESY NMR (600 MHz) spectrum of 3% substituted PAA2NSen (1.43 wt%, [2NSen] = 3.0×10^{-3} mol dm^{-3}) and equimolar 33γ-CD_2suc in D_2O at pD 7.0 (0.10 mol dm^{-3} in NaCl) at 298.2 K with a mixing time of 300 ms. Cross-peaks enclosed in the rectangle arise from interactions between the annular γ-CD $H_{3,5,6}$ protons of 33γ-CD_2suc and the naphthyl protons of the 2NSen substituent.

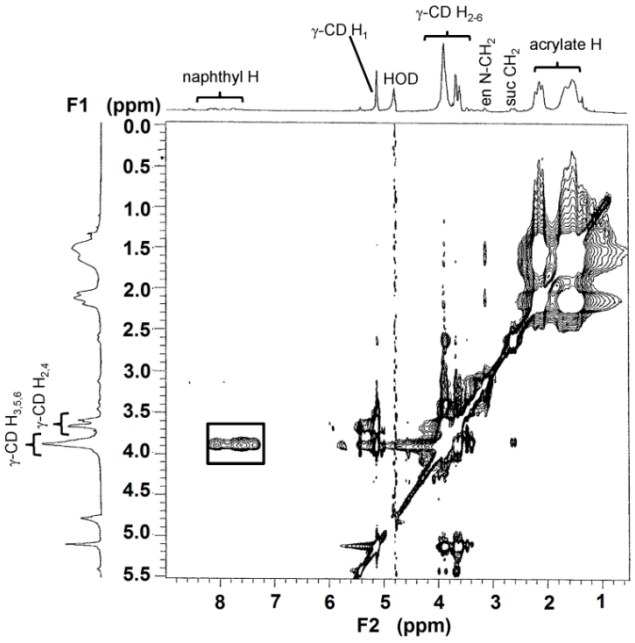

Figure A19. 2D ^{1}H NOESY NMR (600 MHz) spectrum of 3% substituted PAA2NSen (1.43 wt%, [2NSen] = 3.0×10^{-3} mol dm^{-3}) and equimolar 66γ-CD_2suc in D_2O at pD 7.0 (0.10 mol dm^{-3} in NaCl) at 298.2 K with a mixing time of 300 ms. Cross-peaks enclosed in the rectangle arise from interactions between the annular γ-CD $H_{3,5,6}$ protons of 66γ-CD_2suc and the naphthyl protons of the 2NSen substituent.

PAA2NShn

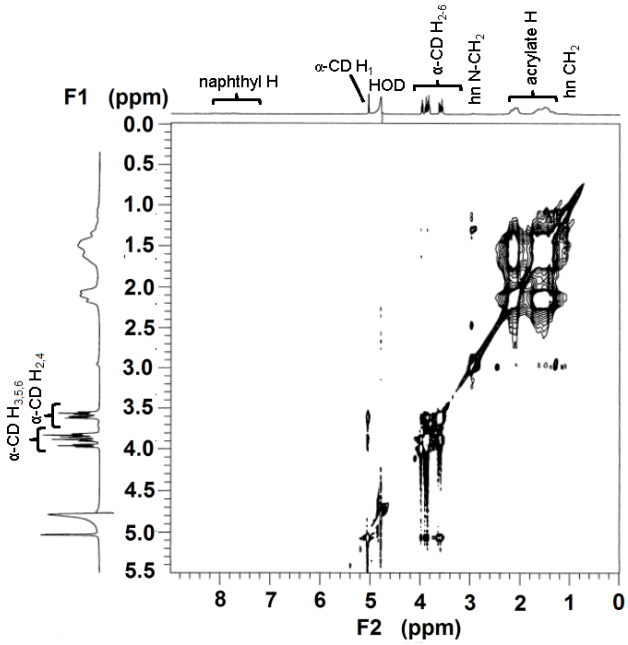

Figure A20. 2D ^{1}H NOESY NMR (600 MHz) spectrum of 3% substituted PAA2NShn (1.43 wt%, [2NShn] = 3.0×10^{-3} mol dm^{-3}) and equimolar α-CD in D_2O at pD 7.0 (0.10 mol dm^{-3} in NaCl) at 298.2 K with a mixing time of 300 ms. No significant cross-peaks appear.

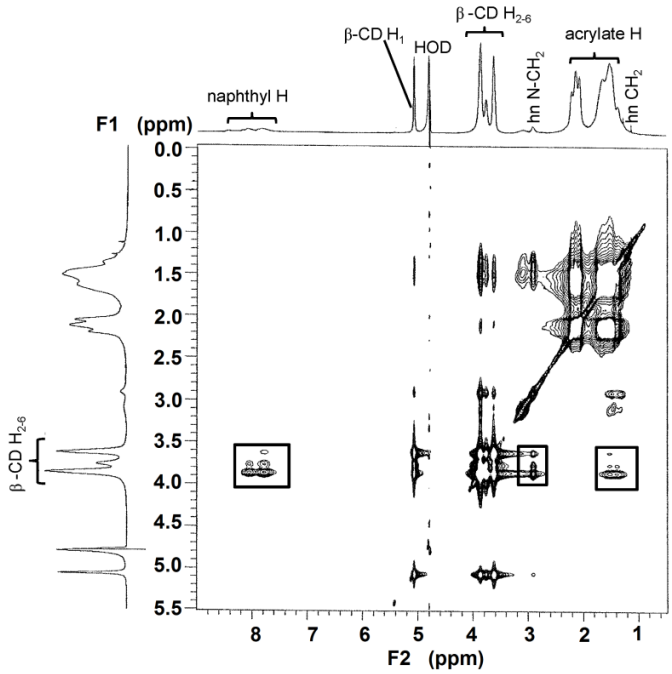

Figure A21. 2D ^{1}H NOESY NMR (600 MHz) spectrum of 3% substituted PAA2NShn (1.43 wt%, [2NShn] = 3.0×10^{-3} mol dm^{-3}) and equimolar β-CD in D_2O at pD 7.0 (0.10 mol dm^{-3} in NaCl) at 298.2 K with a mixing time of 300 ms. Cross-peaks enclosed in the rectangles arise from interactions between the annular β-CD $H_{3,5,6}$ protons with the naphthyl (left), N-CH_2 (middle) and other hexyl CH_2 (right) protons of the 2NShn substituent.

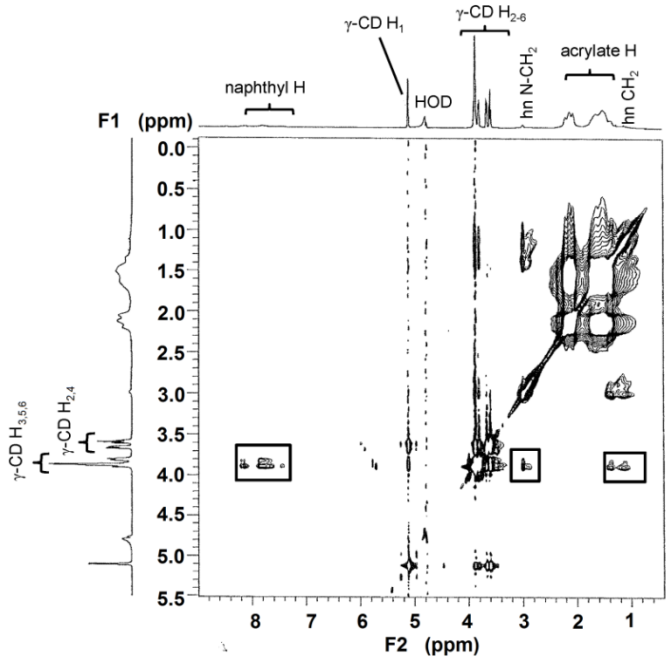

Figure A22. 2D ^{1}H NOESY NMR (600 MHz) spectrum of 3% substituted PAA2NShn (1.43 wt%, [2NShn] = 3.0×10^{-3} mol dm^{-3}) and equimolar γ-CD in D_2O at pD 7.0 (0.10 mol dm^{-3} in NaCl) at 298.2 K with a mixing time of 300 ms. Cross-peaks enclosed in the rectangles arise from interactions between the annular γ-CD protons $H_{3,5,6}$ with the naphthyl (left), N-CH_2 (middle) and other hexyl CH_2 (right) protons of the 2NShn substituent.

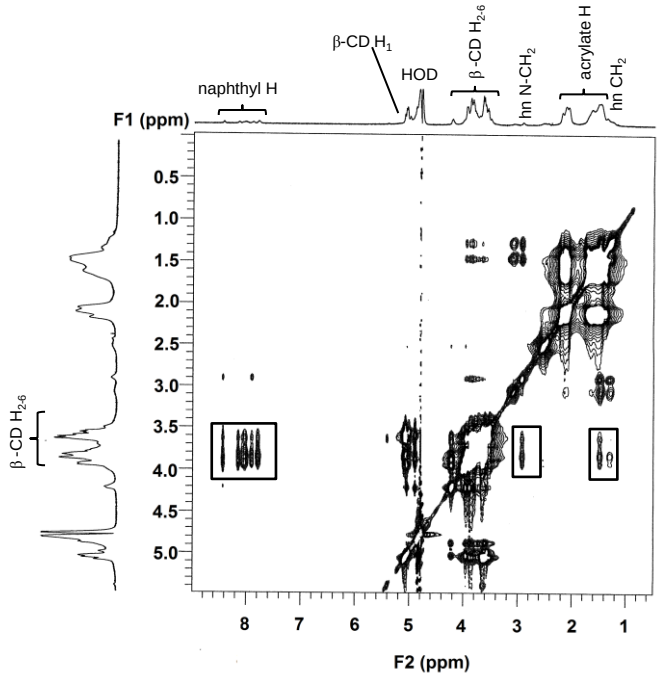

Figure A23. 2D ^{1}H NOESY NMR (600 MHz) spectrum of 3% substituted PAA2NShn (1.43 wt%, [2NShn] = 3.0×10^{-3} mol dm^{-3}) and equimolar 33β-CD_2suc in D_2O at pD 7.0 (0.10 mol dm^{-3} in NaCl) at 298.2 K with a mixing time of 300 ms. Cross-peaks enclosed in the rectangles arise from interactions between the annular β-CD $H_{3,5,6}$ protons of 33β-CD_2suc with the naphthyl (left), N-CH_2 (middle) and other hexyl CH_2 (right) protons of the 2NShn substituent (right). It appears that combination of inequivalence in the glucopyranose units of 33β-CD_2suc arising from substitution at C^{3A} and complexation has increased the δ range for the $H_{3,5,6}$ protons which in turn increased the δ range for the cross-peaks.

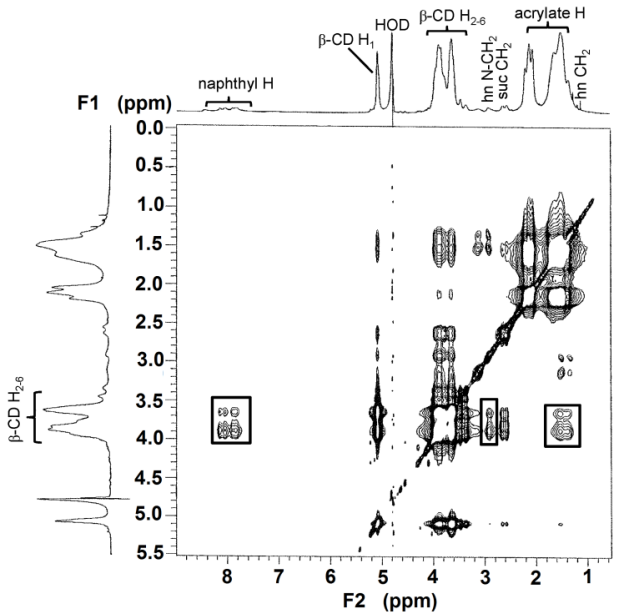

Figure A24. 2D ^{1}H NOESY NMR (600MHz) spectrum of 3% substituted PAA2NShn (1.43 wt%, [2NShn] = 3.0×10^{-3} mol dm^{-3}) and equimolar 66β-CD_2suc in D_2O (pD 7.0 phosphate buffer, I = 0.10 mol dm^{-3}) at 298.2 K with a mixing time of 300 ms. Cross-peaks enclosed in the rectangle arise from interactions between the annular β-CD $H_{3,5,6}$ protons of 66β-CD_2suc with the naphthyl (left), N-CH_2 (middle) and other hexyl CH_2 (right) protons of the 2NShn substituent (right). It appears that combination of inequivalence in the glucopyranose units of 66β-CD_2suc arising from substitution at C^{6A} and complexation has increased the δ range for the $H_{3,5,6}$ protons which in turn increased the δ range for the cross-peaks.

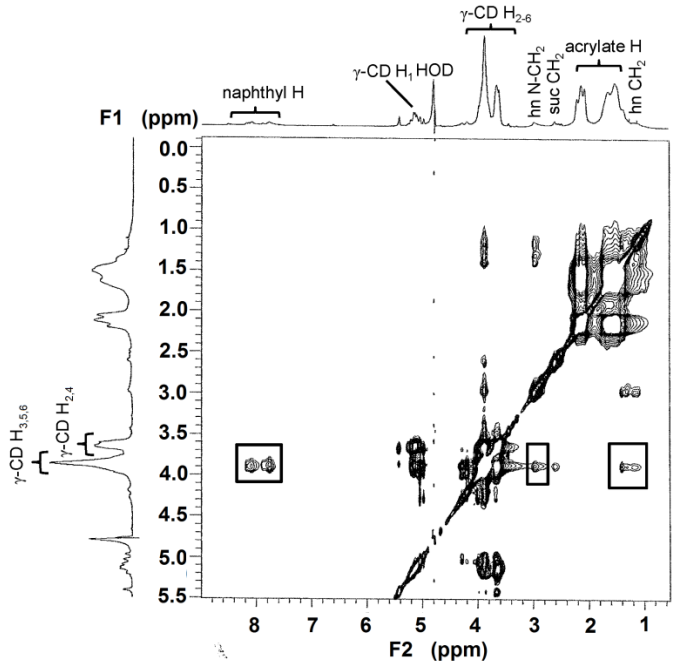

Figure A24. 2D ^{1}H NOESY NMR (600MHz) spectrum of 3% substituted PAA2NShn (1.43 wt%, [2NShn] = 3.0×10^{-3} mol dm^{-3}) and equimolar 33γ-CD_2suc in D_2O at pD 7.0 (0.10 mol dm^{-3} in NaCl) at 298.2 K with a mixing time of 300 ms. Cross-peaks enclosed in the rectangles arise from interactions between the annular γ-CD $H_{3,5,6}$ protons with the naphthyl protons (left), N-CH_2 (middle) and other hexyl CH_2 (right) protons of the 2NShn substituent.

Fluorimetric Titrations

Fluorimetric Titrations of PAA1NSen Complexation

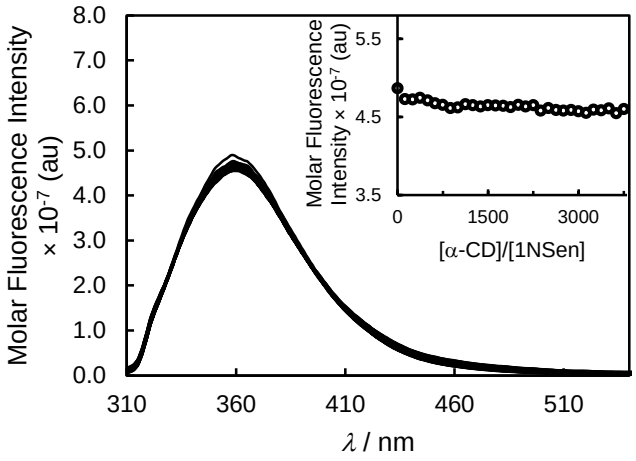

Figure A25. Variation in the emission spectra of 0.0033 wt% PAA1NSen solution ([1NSen] = 1.0×10^{-5} mol dm^{-3}) in pH 7.0 phosphate buffer (I = 0.10 mol dm^{-3}) at 298.2 K upon sequential injection (0.050 cm^3 each) of α-CD titrant solution (1.06×10^{-2} mol dm^{-3}). Excitation wavelength λ_{ex} = 290 nm with both excitation and emission slits of 5 nm. The fluorescence change was insufficient to attempt fitting a complexation algorithm to it.

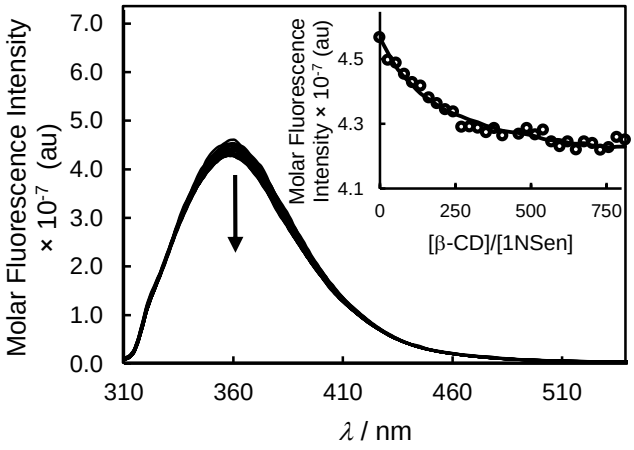

Figure A26. Variation in the emission spectra of 0.0033 wt% PAA1NSen solution ([1NSen] = 1.0×10^{-5} mol dm^{-3}) in pH 7.0 phosphate buffer (I = 0.10 mol dm^{-3}) at 298.2 K upon sequential injection (0.050 cm^3 each) of β–CD titrant solution (1.06×10^{-2} mol dm^{-3}). Excitation wavelength λ_{ex} = 290 nm with both excitation and emission slits of 5 nm. The arrow indicates the direction of fluorescence changes as the ratio of $[\beta\text{–CD}]_{total}/[1NSen]_{total}$ increases. λ_{max} = 360 nm and 359 nm for the free and complexed 1NSen, respectively. Inset: variation in the relative fluorescence (circles) at 360 nm. The solid curve represents the best fit of the algorithm for a 1:1 complexation model in the range 330–420 nm. Note: The data for this figure is from a previous study.[35]

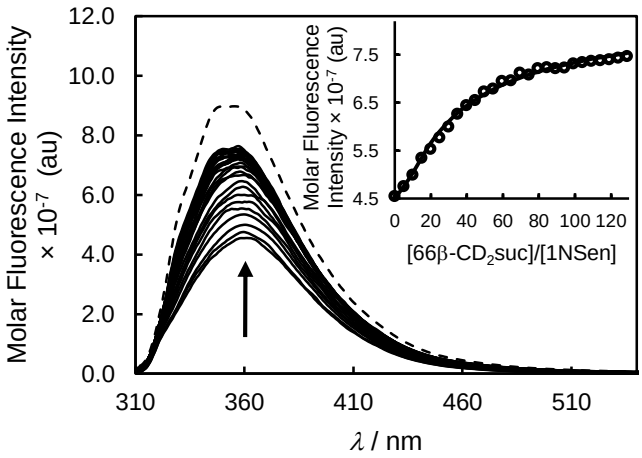

Figure A27. Variation in the emission spectra of 0.0033 wt% PAA1NSen solution ([1NSen] = 1.0×10^{-5} mol dm^{-3}) in pH 7.0 phosphate buffer (I = 0.10 mol dm^{-3}) at 298.2 K upon sequential injection (0.020 cm^3 each) of 66β-CD_2suc titrant solution (4.95×10^{-3} mol dm^{-3}). Excitation wavelength λ_{ex} = 290 nm with both excitation and emission slits of 5 nm. The arrow indicates the direction of fluorescence changes as the ratio of [66β-CD_2suc]$_{total}$/[1NSen]$_{total}$ increases. The dashed spectrum is that derived for the fully complexed 1NSen: λ_{max} = 360 nm and 350 nm for the free and complexed 1NSen, respectively. Inset: Variation in the relative fluorescence (circles) at 360 nm. The solid curve represents the best fit of the algorithm for a 1:1 complexation model in the range 330–420 nm.

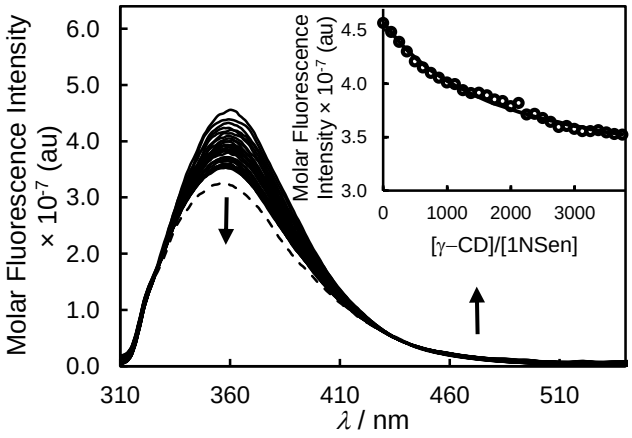

Figure A28. Variation in the emission spectra of 0.0033 wt% PAA1NSen solution ([1NSen] = 1.0×10^{-5} mol dm^{-3}) in pH 7.0 phosphate buffer (I = 0.10 mol dm^{-3}) at 298.2 K upon sequential injection (0.050 cm^3 each) of γ-CD titrant solution (4.96×10^{-2} mol dm^{-3}). Excitation wavelength λ_{ex} = 290 nm with both excitation and emission slits of 5 nm. The arrow indicates the direction of fluorescence changes as the ratio of $[\gamma\text{-CD}]_{total}/[1NSen]_{total}$ increases. The dashed spectrum is that derived for the fully complexed 1NSen: λ_{max} = 360 nm and 355 nm for the free and complexed 1NSen, respectively. Inset: Variation in the relative fluorescence (circles) at 360 nm, isosbestic point at 430 nm. The solid curve represents the best fit of the algorithm for a 1:1 complexation model in the range 330–420 nm. Note: The data for this figure is from a previous study with revised fitting.[35]

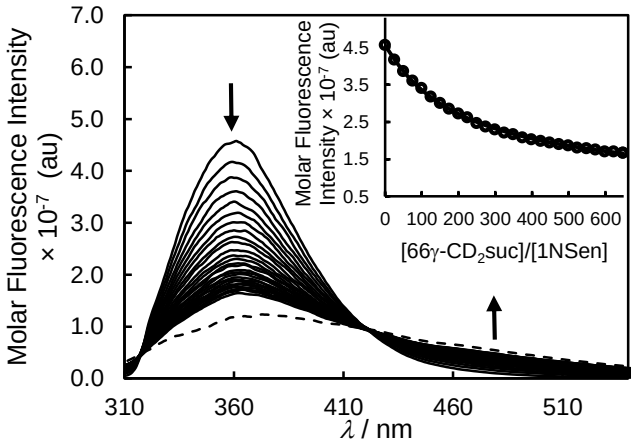

Figure A29. Variation in the emission spectra of 0.0033 wt% PAA1NSen solution ([1NSen] = 1.0×10^{-5} mol dm^{-3}) in pH 7.0 phosphate buffer (I = 0.10 mol dm^{-3}) at 298.2 K upon sequential injection (0.050 cm^3 each) of 66γ-CD_2suc titrant solution (1.00×10^{-2} mol dm^{-3}). Excitation wavelength λ_{ex} = 290 nm with both excitation and emission slits of 5 nm. The arrow indicates the direction of fluorescence changes as the ratio of [66γ-CD_2suc]$_{total}$/[1NSen]$_{total}$ increases. The dashed spectrum is that derived for the fully complexed 1NSen: λ_{max} = 360 nm and 364 nm for the free and complexed 1NSen, respectively, isosbestic points at 320 and 420 nm. Inset: Variation in the relative fluorescence (circles) at 360 nm. The solid curve represents the best fit of the algorithm incorporating 1:1 host–guest complexation models in the range 330–420 nm.

Fluorimetric Titrations of PAA1NShn Complexation

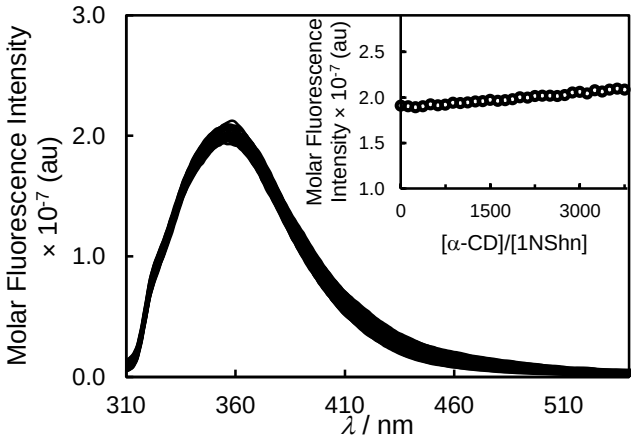

Figure A30. Variation in the emission spectra of 0.0034 wt% PAA1NShn solution ([1NShn] = 1.0×10^{-5} mol dm^{-3}) in pH 7.0 phosphate buffer (I = 0.10 mol dm^{-3}) at 298.2 K upon sequential injection (0.050 cm^3 each) of α-CD titrant solution (1.06×10^{-2} mol dm^{-3}). Excitation wavelength λ_{ex} = 290 nm with both excitation and emission slits of 5 nm. The fluorescence change was insufficient to attempt fitting a complexation algorithm to it.

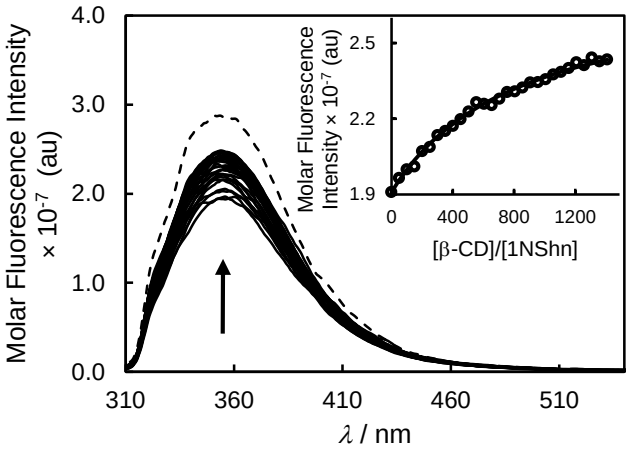

Figure A31. Variation in the emission spectra of 0.0034 wt% PAA1NShn solution ([1NShn] = 1.0×10^{-5} mol dm^{-3}) in pH 7.0 phosphate buffer (I = 0.10 mol dm^{-3}) at 298.2 K upon sequential injection (0.065 cm^3 each) of β-CD titrant solution (1.55×10^{-2} mol dm^{-3}). Excitation wavelength λ_{ex}= 290 nm with both excitation and emission slits of 5 nm. The arrow indicates the direction of fluorescence changes as the ratio of $[\beta\text{-CD}]_{total}/[1\text{NShn}]_{total}$ increases. The dashed spectrum is that derived for the fully complexed 1NShn: λ_{max}= 360 nm and 350 nm for the free and complexed 1NShn, respectively. Inset: Variation in the relative fluorescence (circles) at 360 nm. The solid curve represents the best fit of the algorithm for a 1:1 complexation model in the range 330–420 nm.

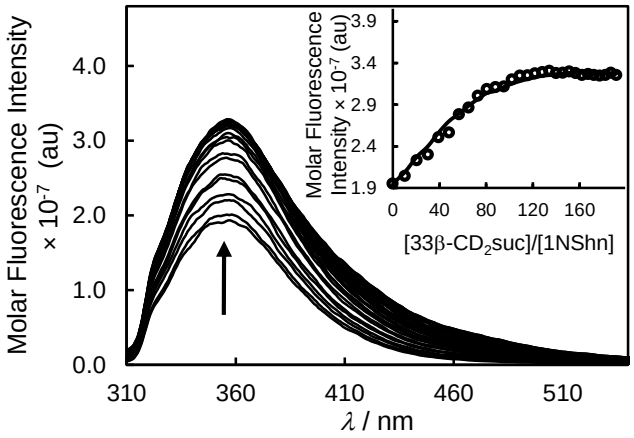

Figure A32. Variation in the emission spectra of 0.0034 wt% PAA1NShn solution ([1NShn] = 1.0×10^{-5} mol dm^{-3}) in pH 7.0 phosphate buffer (I = 0.10 mol dm^{-3}) at 298.2 K upon sequential injection (0.050 cm^3 each) of 33β-CD_2suc titrant solution (4.26×10^{-3} mol dm^{-3}). Excitation wavelength λ_{ex} = 290 nm with both excitation and emission slits of 5 nm. The arrow indicates the direction of fluorescence changes as the ratio of [33β-CD_2suc]$_{total}$/[1NShn]$_{total}$ increases. λ_{max}= 360 nm and 355 nm for the free and complexed 1NShn, respectively. Inset: Variation in the relative fluorescence (circles) at 360 nm. The solid curve represents the best fit of the algorithm for a 1:1 complexation model in the range 330–420 nm.

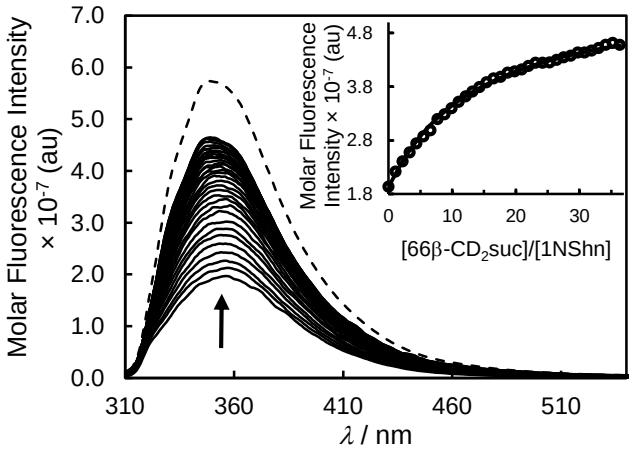

Figure A34. Variation in the emission spectra of 0.0034 wt% PAA1NShn solution ([1NShn] = 1.0×10^{-5} mol dm^{-3}) in pH 7.0 phosphate buffer (I = 0.10 mol dm^{-3}) at 298.2 K upon sequential injection (0.010 cm^3 each) of 66β-CD_2suc titrant solution (2.17×10^{-3} mol dm^{-3}). Excitation wavelength λ_{ex} = 290 nm with both excitation and emission slits of 5 nm. The arrow indicates the direction of fluorescence changes as the ratio of [66β-CD_2suc]$_{total}$/[1NShn]$_{total}$ increases. The dashed spectrum is that derived for the fully complexed 1NShn: λ_{max}= 360 nm and 350 nm for the free and complexed 1NShn, respectively. Inset: Variation in the relative fluorescence (circles) at 360 nm. The solid curve represents the best fit of the algorithm incorporating 1:1 host–guest complexation models in the range 330–420 nm

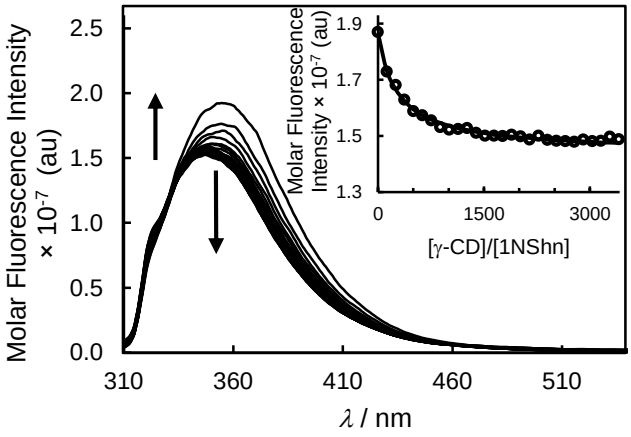

Figure A35. Variation in the emission spectra of 0.0034 wt% PAA1NShn solution ([1NShn] = 1.0×10^{-5} mol dm^{-3}) in pH 7.0 phosphate buffer (I = 0.10 mol dm^{-3}) at 298.2 K upon sequential injection (0.050 cm^3 each) of γ-CD titrant solution (4.96×10^{-2} mol dm^{-3}). Excitation wavelength λ_{ex} = 290 nm with both excitation and emission slits of 5 nm. The arrows indicate the direction of fluorescence changes as the ratio of $[\gamma\text{-CD}]_{total}/[1NShn]_{total}$ increases. λ_{max} = 360 nm and 346 nm for the free and complexed 1NShn, respectively, isosbestic point at 330 nm. Inset: Variation in the relative fluorescence (circles) at 360 nm. The solid curve represents the best fit of the algorithm for a 1:1 complexation model in the range 330–420 nm. Note: The data for this figure is from a previous study .[35]

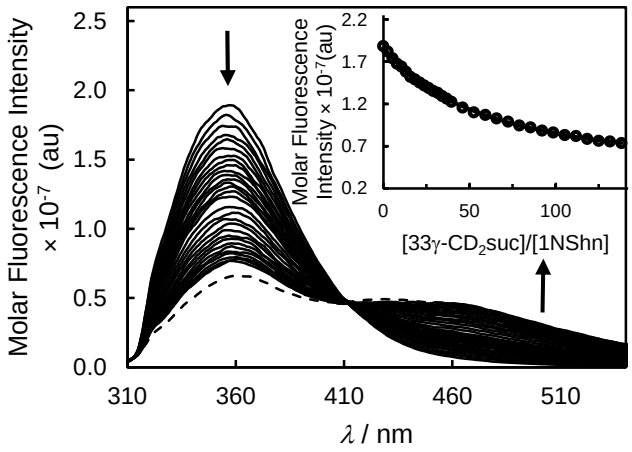

Figure A36. Variation in the emission spectra of 0.0034 wt% PAA1NShn solution ([1NShn] = 1.0×10^{-5} mol dm^{-3}) in pH 7.0 phosphate buffer (I = 0.10 mol dm^{-3}) at 298.2 K upon sequential injection (0.020 cm^3 for the first 15 aliquots, then 0.050 cm^3 thereafter) of 33γ-CD_2suc titrant solution (2.63×10^{-3} mol dm^{-3}). Excitation wavelength λ_{ex} = 290 nm with both excitation and emission slits of 5 nm. The arrows indicate the direction of fluorescence changes as the ratio of $[33\gamma\text{-}CD_2suc]_{total}/[1NShn]_{total}$ increases. The dashed spectrum is that derived for the fully complexed 1NShn: λ_{max} = 360 nm and 354 nm for the free and complexed 1NShn, respectively, isosbestic point at 412 nm. Inset: Variation in the relative fluorescence (circles) at 360 nm. The solid curve represents the best fit of the algorithm for a 1:1 complexation model in the range 320–420 nm. Note: The data for this figure is from a previous study with revised fitting.[35]

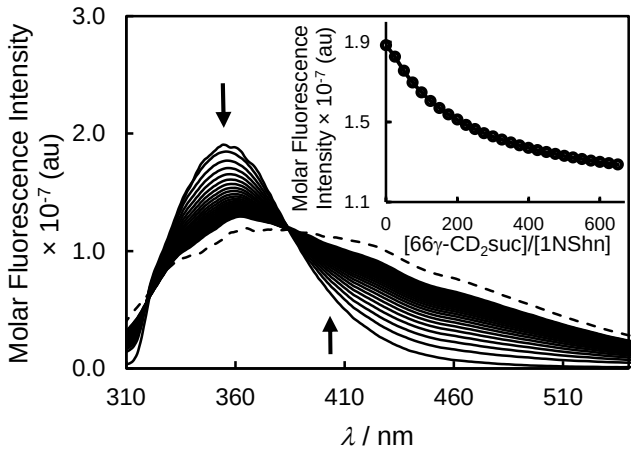

Figure A37: Top: Variation in the emission spectra of 0.0034 wt% PAA1NShn solution ([1NShn] = 1.0×10^{-5} mol dm^{-3}) in pH 7.0 phosphate buffer (I = 0.10 mol dm^{-3}) at 298.2 K upon sequential injection (0.050 cm^3 each) of 66γ-CD_2suc titrant solution (1.00×10^{-2} mol dm^{-3}). Excitation wavelength λ_{ex}= 290 nm with both excitation and emission slits of 5 nm. The arrows indicate the direction of fluorescence changes as the ratio of [66γ-CD_2suc]$_{total}$/[1NShn]$_{total}$ increases. The dashed spectrum is that derived for the fully complexed 1NShn: λ_{max}= 360 nm and 365 nm for the free and complexed 1NShn, isosbestic points at 320 and 380 nm. Inset: Variation in relative fluorescence (circles) at 360 nm. The solid curve represents the best fit of the algorithm incorporating 1:1 host–guest complexation models in the range 330–420 nm.

Fluorimetric Titrations of PAA2NSen Complexation

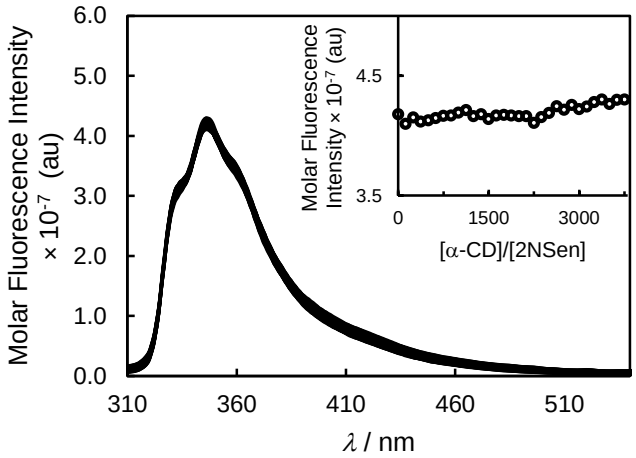

Figure A38. Variation in the emission spectra of 0.0033 wt% PAA2NSen solution ([2NSen] = 1.0×10^{-5} mol dm^{-3}) in pH 7.0 phosphate buffer (I = 0.10 mol dm^{-3}) at 298.2 K upon sequential injection (0.050 cm^3 each) of α-CD titrant solution (1.06×10^{-2} mol dm^{-3}). Excitation wavelength λ_{ex} = 290 nm with both excitation and emission slits of 5 nm. The fluorescence change was insufficient to attempt fitting a complexation algorithm to it.

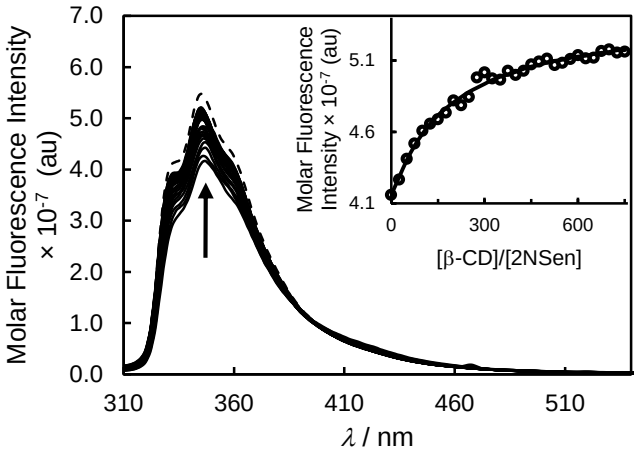

Figure A39. Variation in the emission spectra of 0.0033 wt% PAA2NSen solution ([2NSen] = 1.0×10^{-5} mol dm^{-3}) in pH 7.0 phosphate buffer (I = 0.10 mol dm^{-3}) at 298.2 K upon sequential injection (0.050 cm^3 each) of β-CD titrant solution (1.00×10^{-2} mol dm^{-3}). Excitation wavelength λ_{ex} = 290 nm with both excitation and emission slits of 5 nm. The arrow indicates the direction of fluorescence changes as the ratio of $[\beta\text{-CD}]_{total}/[2NSen]_{total}$ increases. The dashed spectrum is that derived for the fully complexed 2NSen: λ_{max} = 347 nm and 344 nm for the free and complexed 2NSen, respectively. Inset: Variation in the relative fluorescence (circles) at 346 nm. The solid curve represents the best fit of the algorithm for a 1:1 complexation model in the range 330–380 nm.

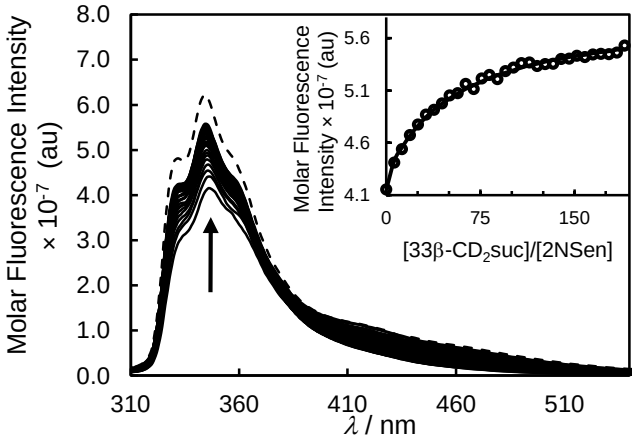

Figure A40. Variation in the emission spectra of 0.0033 wt% PAA2NSen solution ([2NSen] = 1.0×10^{-5} mol dm^{-3}) in pH 7.0 phosphate buffer (I = 0.10 mol dm^{-3}) at 298.2 K upon sequential injection (0.050 cm^3 each) of 33β-CD_2suc titrant solution (2.54×10^{-3} mol dm^{-3}). Excitation wavelength λ_{ex} = 290 nm with both excitation and emission slits of 5 nm. The arrow indicates the direction of fluorescence changes as the ratio of $[33\beta\text{-}CD_2suc]_{total}/[2NSen]_{total}$ increases. The dashed spectrum is that derived for the fully complexed 2NSen λ_{max} = 347 nm and 344 nm for the free and complexed 2NSen, respectively. Inset: Variation in the relative fluorescence (circles) at 346 nm. The solid curve represents the best fit of the algorithm for a 1:1 complexation model in the range 330–380 nm.

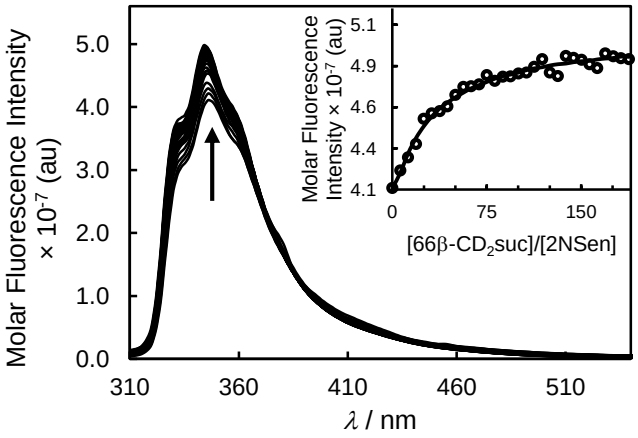

Figure A41. Variation in the emission spectra of 0.0033 wt% PAA2NSen solution ([2NSen] = 1.0×10^{-5} mol dm^{-3}) in pH 7.0 phosphate buffer (I = 0.10 mol dm^{-3}) at 298.2 K upon sequential injection (0.050 cm^3 each) of 66β-CD_2suc titrant solution (2.51×10^{-3} mol dm^{-3}). Excitation wavelength λ_{ex} = 290 nm with both excitation and emission slits of 5 nm. The arrow indicates the direction of fluorescence changes as the ratio of [66β-CD_2suc]$_{total}$/[2NSen]$_{total}$ increases. λ_{max}= 347 nm and 344 nm for the free and complexed 2NSen, respectively. Inset: Variation in the relative fluorescence (circles) at 346 nm. The solid curve represents the best fit of the algorithm for a 1:1 complexation model in the range 330–380.

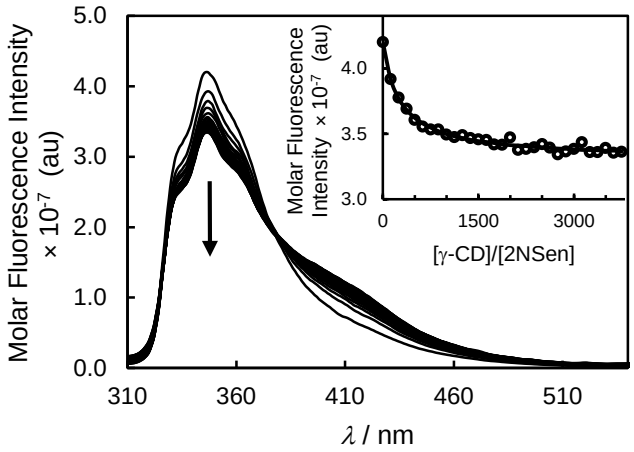

Figure A42. Variation in the emission spectra of 0.0033 wt% PAA2NSen solution ([2NSen] = 1.0×10^{-5} mol dm^{-3}) in pH 7.0 phosphate buffer (I = 0.10 mol dm^{-3}) at 298.2 K upon sequential injection (0.050 cm^3 each) of γ-CD titrant solution (5.00×10^{-2} mol dm^{-3}). Excitation wavelength λ_{ex} = 290 nm with both excitation and emission slits of 5 nm. The arrows indicate the direction of fluorescence changes as the ratio of $[\gamma\text{-CD}]_{total}/[2NSen]_{total}$ increases. λ_{max} = 347 nm and 345 nm for the free and complexed 2NSen, respectively, isosbestic point at 380 nm. Inset: Variation in relative fluorescence (circles) at 346 nm. The solid curve represents the best fit of the algorithm for a 1:1 complexation model in the range 330–380 nm.

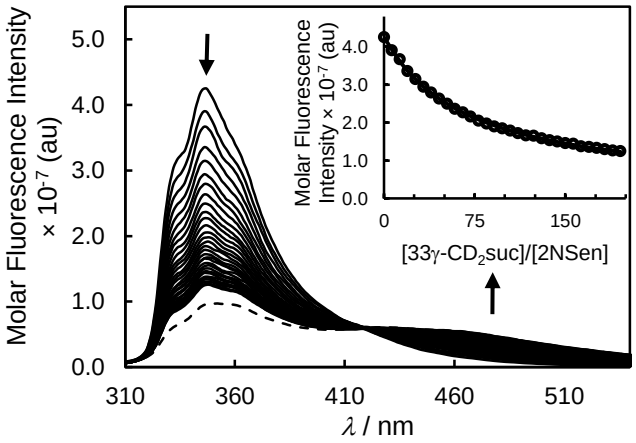

Figure A43. Variation in the emission spectra of 0.0033 wt% PAA2NSen solution ([2NSen] = 1.0×10^{-5} mol dm^{-3}) in pH 7.0 phosphate buffer (I = 0.10 mol dm^{-3}) at 298.2 K upon sequential injection (0.050 cm^3 each) of 33γ-CD_2suc titrant solution (2.61×10^{-3} mol dm^{-3}). Excitation wavelength λ_{ex} = 290 nm with both excitation and emission slits of 5 nm. The arrows indicate the direction of fluorescence changes as the ratio of $[33\gamma\text{-}CD_2suc]_{total}/[2NSen]_{total}$ increases. The dashed spectrum is that derived for the fully complexed 2NSen: λ_{max}= 347 nm and 345 nm for the free and complexed 2NSen, respectively, isosbestic point at 413 nm. Inset: Variation in the relative fluorescence (circles) at 346 nm. The solid curve represents the best fit of the algorithm for a 1:1 complexation model in the range 330–380 nm.

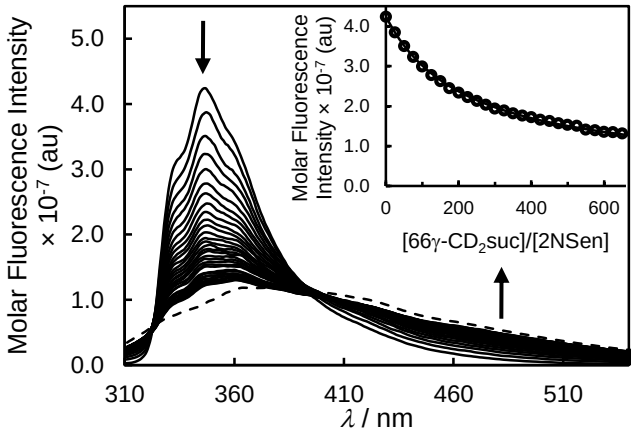

Figure A44. Variation in the emission spectra of 0.0033 wt% PAA2NSen solution ([2NSen] = 1.0×10^{-5} mol dm^{-3}) in pH 7.0 phosphate buffer (I = 0.10 mol dm^{-3}) at 298.2 K upon sequential injection (0.050 cm^3 each) of 66γ-CD_2suc titrant solution (1.00×10^{-2} mol dm^{-3}). Excitation wavelength λ_{ex} = 290 nm with both excitation and emission slits of 5 nm. The arrows indicate the direction of fluorescence changes as the ratio of [66γ-CD_2suc]$_{total}$/[2NSen]$_{total}$ increases. The dashed spectrum is that derived for the fully complexed 2NSen: λ_{max}= 347 nm and 362 nm for the free and complexed 2NSen, respectively, isosbestic points at 322 and 395 nm. Inset: Variation in the relative fluorescence (circles) at 346 nm. The solid curve represents the best fit of the algorithm for a 1:1 complexation model in the range 330–380 nm.

Fluorimetric Titrations of PAA2NShn Complexation

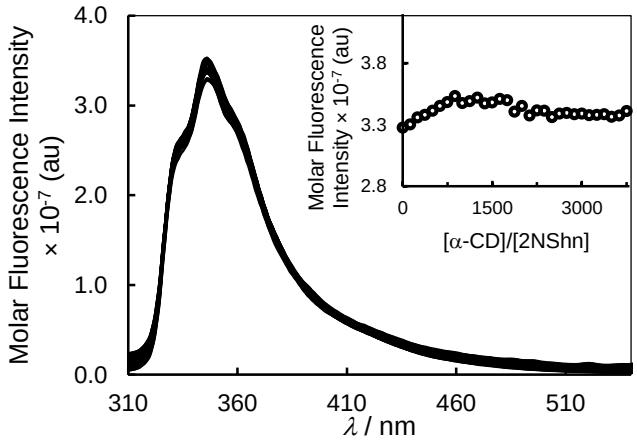

Figure A45. Variation in the emission spectra of 0.0034 wt% PAA2NShn solution ([2NShn] = 1.0×10^{-5} mol dm^{-3}) in pH 7.0 phosphate buffer (I = 0.10 mol dm^{-3}) at 298.2 K upon sequential injection (0.050 cm^3 each) of α-CD titrant solution (1.06×10^{-2} mol dm^{-3}). Excitation wavelength λ_{ex} = 290 nm with both excitation and emission slits of 5 nm. The fluorescence change was insufficient to attempt fitting a complexation algorithm to it.

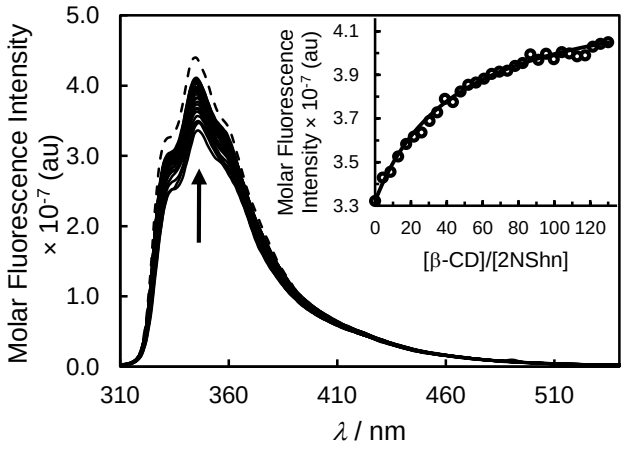

Figure A46. Variation in the emission spectra of 0.0034 wt% PAA2NShn solution ([2NShn] = 1.0×10^{-5} mol dm^{-3}) in pH 7.0 phosphate buffer (I = 0.10 mol dm^{-3}) at 298.2 K upon sequential injection (0.010 cm^3 each) of β-CD titrant solution (8.68×10^{-3} mol dm^{-3}). Excitation wavelength λ_{ex} = 290 nm with both excitation and emission slits of 5 nm. The arrow indicates the direction of fluorescence changes as the ratio of $[\beta\text{-CD}]_{total}/[2NShn]_{total}$ increases. The dashed spectrum is that derived for the fully complexed 2NShn: λ_{max} = 347 nm and 345 nm for the free and complexed 2NShn, respectively. Inset: Variation in the relative fluorescence (circles) at 346 nm. The solid curve represents the best fit of the algorithm for a 1:1 complexation model in the range 330–380 nm.

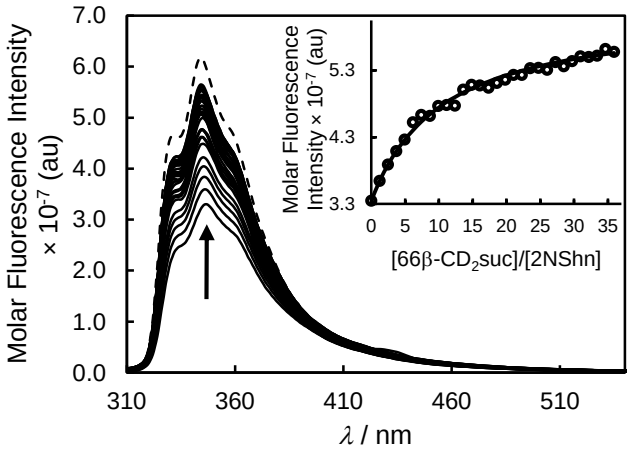

Figure A47. Variation in the emission spectra of 0.0034 wt% PAA2NShn solution ([2NShn] = 1.0×10^{-5} mol dm^{-3}) in pH 7.0 phosphate buffer (I = 0.10 mol dm^{-3}) at 298.2 K upon sequential injection (0.010 cm^3 each) of 66β-CD_2suc titrant solution (2.48×10^{-3} mol dm^{-3}). Excitation wavelength λ_{ex} = 290 nm with both excitation and emission slits of 5 nm. The arrow indicates the direction of fluorescence changes as the ratio of [66β-CD_2suc]$_{total}$/[2NShn]$_{total}$ increases. λ_{max}= 347 nm and 345 nm for the free and complexed 2NShn, respectively. Inset: Variation in the relative fluorescence (circles) at 346 nm. The solid curve represents the best fit of the algorithm for a 1:1 complexation model in the range 330–380 nm.

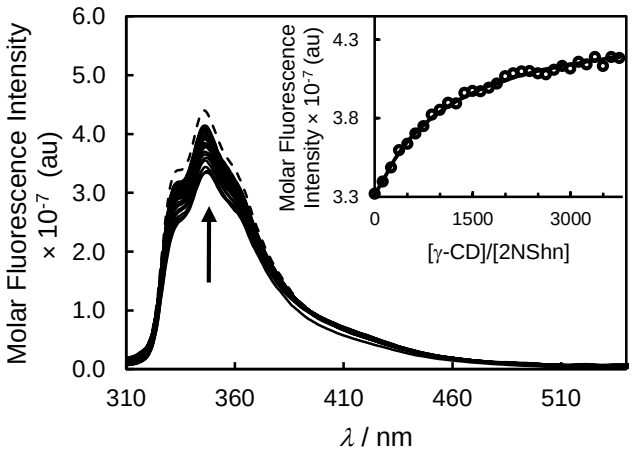

Figure A48. Variation in the emission spectra of 0.0034 wt% PAA2NShn solution ([2NShn] = 1.0×10^{-5} mol dm^{-3}) in pH 7.0 phosphate buffer (I = 0.10 mol dm^{-3}) at 298.2 K upon sequential injection (0.050 cm^3 each) of γ-CD titrant solution (5.00×10^{-2} mol dm^{-3}). Excitation wavelength λ_{ex} = 290 nm with both excitation and emission slits of 5 nm. The arrow indicates the direction of fluorescence changes as the ratio of $[\gamma\text{-CD}]_{total}/[2NShn]_{total}$ increases. The dashed spectrum is that derived for the fully complexed 2NShn: λ_{max} = 347 nm and 346 nm for the free and complexed 2NShn, respectively. Inset: Variation in the relative fluorescence (circles) at 346 nm. The solid curve represents the best fit of the algorithm for a 1:1 complexation model in the range 330–380 nm.

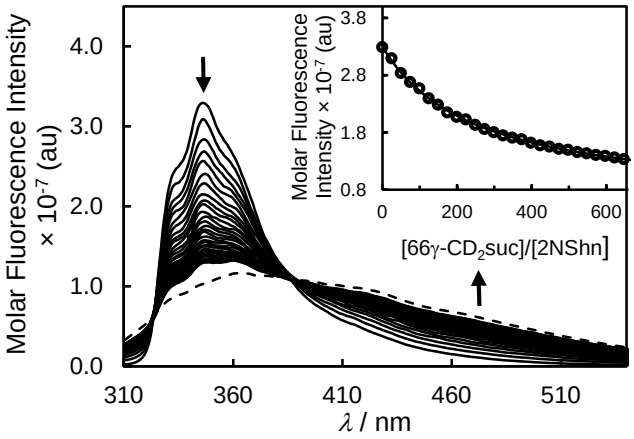

Figure A49. Variation in the emission spectra of 0.0034 wt% PAA2NShn solution ([2NSen] = 1.0×10^{-5} mol dm^{-3}) in pH 7.0 phosphate buffer (I = 0.10 mol dm^{-3}) at 298.2 K upon sequential injection (0.050 cm^3 each) of 66γ-CD_2suc titrant solution (1.00×10^{-2} mol dm^{-3}). Excitation wavelength λ_{ex} = 290 nm with both excitation and emission slits of 5 nm. The arrows indicate the direction of fluorescence changes as the ratio of [66γ-CD_2suc]$_{total}$/[2NShn]$_{total}$ increases. The dashed spectrum is that derived for the fully complexed 2NShn: λ_{max}= 347 nm and 362 nm for the free and complexed 2NShn, respectively. Isosbestic points occur at 320 nm and 390 nm Inset: Variation in the relative fluorescence (circles) at 346 nm. The solid curve represents the best fit of the algorithm for a 1:1 complexation model in the range 330–380 nm.

Rheology

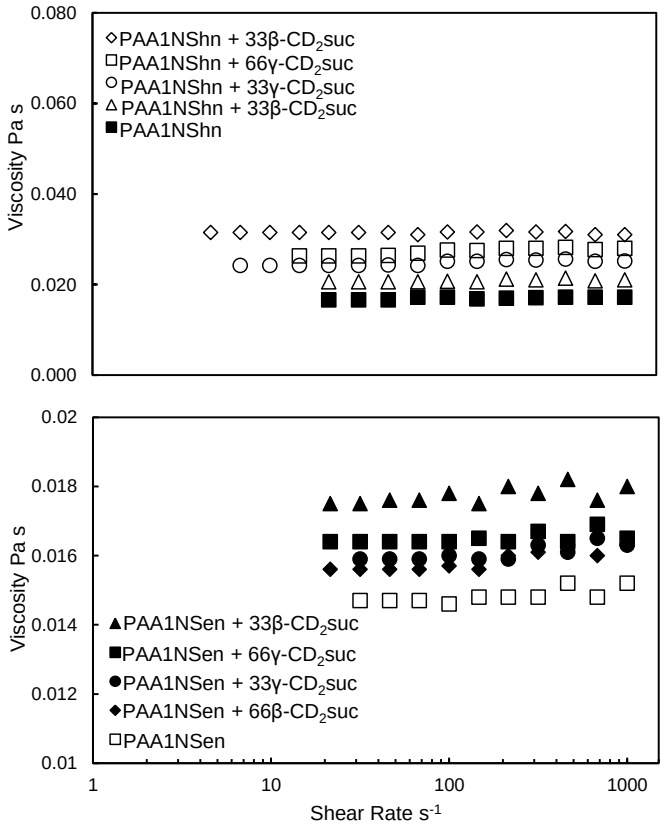

Figure A50. Viscosity variations with shear rate of 5 wt % aqueous solutions of PAA1NSen and PAA1NShn alone and in the presence of 33β-CD_2suc, 66β-CD_2suc, 33-γCD_2suc and 66-γCD_2suc at pH 7.0 and [NaCl] = 0.10 mol dm^{-3} at 298.2 K. The concentrations of the β-CD and γ-CD substituents in the linked dimers are equal to those of the 1NSen or 1NShn poly(acrylate) substituents. Note: The data for this figure is from a previous study.[35]

This page is intentionally left blank

Chapter 6

Experimental Section

6.1. GENERAL

6.1.1. Instrumental

Routine 1D ^{1}H and ^{13}C NMR spectra were recorded on a Varian Gemini ACP-300 (300.145 MHz and 75.4 MHz, respectively) spectrometer, unless otherwise stated. Spectra of samples were obtained in either $CDCl_3$, DMSO-d_6, D_2O solutions with either tetramethylsilane (δ_H 0.0 for $SiMe_4$) or $CDCl_3$ (δ_C 77.0) providing reference resonances in $CDCl_3$ solutions, the residual proton solvent resonance (δ_H 2.49) or the solvent carbon resonance (δ_C 39.5) providing reference resonances in DMSO-d_6, or external aqueous trimethylsilylpropiosulfonic acid (δ_{HOD} 4.79), providing the reference resonance D_2O. Chemical shifts are cited on the δ scale in parts per million, ppm, followed by multiplicity and assignment. The following abbreviations are used to report multiplicity: s, singlet; d, doublet; t, triplet; q, quartet; m, multiplet; br, broad. The δ value at the centre of the multiplet resonance is recorded excepted for signals where a multiplet is well resolved in which case the δ values for all individual multiplet components are given. The 2D ^{1}H NOESY NMR spectra were recorded on a Varian Inova 600 (599.957 MHz) spectrometer, using a standard pulse sequence with a mixing time of 300 ms.

Electrospray ionisation mass spectra, ESI-MS, were recorded on a Finnigan MAT ion trap LC-Q octapole mass spectrometer. Gas chromatography - mass spectrometry, GC-MS, data was obtained using a Shimadzu GC-MS spectrometer. Samples were dissolved in either Milli-Q water, HPLC grade methanol or a mixture of both at a concentration of 0.5 mg cm^{-3}. MALDI TOF mass spectra were acquired using a Bruker Ultrafle Xtreme MALDI/TOF mass spectrometer (Bruker Daltonik GmbH) operating in linear mode under the control of Flex Control software (Version 3.3, Bruker Daltonik GmbH). External calibration was carried out using peptide standards (Bruker Daltonik GmbH), over a range of 800 to 4500 D, which was

analysed under the same conditions as that of the sample. Spectra were obtained at various locations over the surface of the matrix spot at an intensity determined by the operator. The sample was dissolved in 1 cm^3 water and diluted to 100 $\mu g/cm^3$ with an aqueous 0.1 % trifluoroacetic acid (TFA) solution. A 1 mm^3 portion was mixed with 1 mm^3 sinapinic acid in water/acetonitrile/TFA (V/V/V) (10/90/0.1) solution and 1 mm^3 of this mixture was applied to an 800 µm Anchor Chip target plate (Bruker Daltonik GmbH, Bremen, Germany) and air dried. Analysis was performed in both positive and negative mode. The MS spectra obtained were analysed using Flex Analysis software (Version 3.3, Bruker Daltonik GmbH) employing smoothing, background subtractions and peak detection algorithms. Elemental analyses were performed by the Microanalytical Service of the Chemistry Department, University of Otago, New Zealand. Since cyclodextrin derivatives contain associated water molecules, fractional numbers of water molecules were added to the molecular formula to give the best fit to the microanalytical data.

Thin-layer chromatography, TLC, was carried out on Merck Kieselgel 60 F_{254} on aluminium-backed sheets. For analysis of β- and γ-cyclodextrin derivatives, plates were developed with 7:7:5:4 v/v ethylacetate/propan-2-ol/ammonium hydroxide/water. The compounds were visualised by drying the plate, dipping it into a 1% sulphuric acid in ethanol solution and followed by heating with a heat-gun. To visualise amino bearing cyclodextrins, plates were dried prior to dipping into 0.5% ninhydrin in ethanol and heated with a heat-gun before dipping in 1% sulphuric acid in ethanol. For the preparations of modified cyclodextrins described in the following sections, R_c represents the R_f of a substituted cyclodextrin relative to the R_f of the parent cyclodextrin.

UV-visible absorbance spectra were recorded using a Varian CARY 5000 UV-VIS-NIR spectrophotometer equipped with matched 1.0 cm path length quartz cells (unless stated otherwise) over a range of required wavelengths at 0.25 nm intervals. Each solution was run

against a reference solution containing all components of the solution of interest except the absorbing compound. Solutions were pre-equilibrated at 298.2 ± 0.2 K, unless stated otherwise and maintained at this temperature during measurement by means of a thermostatted cell block. All solutions were freshly prepared prior to measurement.

Fluorescence measurements were recorded using a Varian CARY Eclipse spectrofluorimeter equipped with a 1.0 cm path length quartz cell. Spectra were obtained over a range of desired wavelengths at 0.5 nm intervals, with both excitation and emission slit widths of 5 nm (unless stated otherwise), using a 1% transmittance emission filter. The emission spectra obtained were not corrected for instrumental factors. Solutions were pre-equilibrated at 298.2 ± 0.2 K and maintained at this temperature during measurement by means of a thermostatted cell block. All solutions were freshly prepared prior to measurement.

Rheological measurements were carried out at the State Key Laboratory of Chemical Engineering, East China University of Science and Technology, Shanghai 200237, China using a Physica MCR 501 (Anton Parr GmbH) stress–controlled rheometer with a 25 mm cone and plate geometry. Temperature was controlled at 298.2 ± 0.1 K by a Peltier plate. Rheological samples were prepared by dissolution of the poly(acrylates) in 0.10 mol dm^{-3} aqueous sodium chloride to ensure screening of the electrostatic interactions between the carboxylate groups. The solution pH was adjusted to 7.0 with 0.10 mol dm^{-3} aqueous sodium hydroxide solution.

6.1.2. Materials

Water was purified with a Milli-Q system to give a resistivity of > 15 MΩ cm. Triethylamine (Ajax) was dried by distillation. All organic solvents, *N*,*N*-dimethylformamide (APS), pyridine (Ajax), diethyl ether (Chem Supply), acetone (Chem Supply), ethanol (Ajax),

methanol (Ajax), *N*-methylpyrrolidin-2-one (Fluka), tetrahydrofuran (Chem Supply), dichloromethane (Chem Supply), chloroform (Chem Supply) and ethyl acetate (Chem Supply) were of HPLC grade and were used without further purification.

Column chromatography was carried out using Davisil 43-60 micron chromatography silica. Aluminium oxide column chromatography was carried out using Acros Organics basic activated aluminium oxide, 50-200 micron, Brockman activity I with appropriate amount of water added to give Brockman activity III. Bio-Rex 70 resin was purchased from Bio-Rad Laboratories Inc., CA and was converted to the acid form using 3.0 mol dm^{-3} hydrochloric acid.

β-Cyclodextrin and γ-CD were obtained from Nihon Shokuhin Kako Co. The cyclodextrins were dried to a constant weight over P_2O_5 containing an indicator (Sicapent) under vacuum and stored in the dark under refrigeration. 2-Naphthalenesulfonyl chloride (Sigma-Aldrich, 97%), 4-nitrophenol (Sigma-Aldrich, 98%), 1,2-diaminoethane (Ajax), ammonium hydroxide solution (Sigma-Aldrich, 28%), 1,6-diaminohexane (Sigma-Aldrich), *N*,*N*'-dicyclohexylcarbodiimide (DCC, Merck, 98%), 1-ethyl-3-(3-dimethylaminopropyl)carbodiimide (EDC, Sigma-Aldrich), 2,4,6-triisopropylbenzenesulfonyl chloride (Sigma-Aldrich, 98%), oxalyl chloride (Sigma-Aldrich), trifluoroacetic acid (TFA, Sigma-Aldrich) and 4-(dimethylamino)pyridine (DMAP, Sigma-Aldrich, 99%) were used as supplied without further purification. Poly(acrylic) acid (PAA), (M_w = 250,000, $M_w/M_n \approx 2$) 35 wt% aqueous solution (Sigma-Aldrich) was diluted to approximately 10 wt% and freeze-dried to give a white solid.

5,10,15,20-Tetra(*p*-carboxyphenyl)porphyrin (H_2TCPP) was purchased from Sigma-Aldrich (approx. 75%) and was further purified by recrystallisation from EtOH/DCM. The resulting crystals were left under high vacuum for three days until no solvent peaks were observed in

the ^{1}H NMR spectrum. Tetrasodium 5,10,15,20-tetra(*p*-sulfonatophenyl)porphyrin (Na_4H_2TSPP),[1] 3^A-amino-3^A-deoxy-(2^AS,3^AS)-γ-cyclodextrin (3γ-$CDNH_2$),[2] *N*,*N*′-Bis((2^AS,3^AS)-3^A-deoxy-γ-cyclodextrin-3^A-yl) succinamide (33γ-CD_2suc),[2] *N*,*N*′-bis(6^A-deoxy-γ-cyclodextrin-6^A-yl) succinamide (66γ-CD_2suc),[2] 1,3,5-trinitrophenyl benzene,[3] boc-β-alanine,[4] 5-(*p*-aminophenyl) -10, 15, 20-triphenylporphyrin,[5] *N*,*N*′-Bis((2^AS,3^AS)-3^A-deoxy-β-cyclodextrin-3^A-yl) succinamide (33β-CD_2suc),[6] *N*,*N*′-bis(6^A-deoxy-β-cyclodextrin-6^A-yl) succinamide (66β-CD_2suc),[6] PAA1NSen[7] and PAA1NShn[7] were prepared according to the literature methods.

6.2. EXPERIMENTAL FOR CHAPTER 2

6.2.1. Syntheses

6.2.1.1. Bis(4-nitrophenyl) oxalate[8]

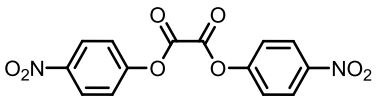

A method similar the one reported in the literature was used to prepare the title compound.[8] To a stirred solution of oxalyl chloride (2.0 g, 15.9 mmol) in dichloromethane (100 cm^3), was added 4-nitrophenol (5.0 g, 36.2 mmol) in one portion, followed by triethylamine (3.66 g, 36.2 mmol) dropwise over 15 min. The mixture was stirred over night at room temperature, the crude product precipitate was filtered off, washed with dichloromethane (40 cm^3) and chloroform (20 cm^3) and dried under vacuum to give the crude product as a cream powder. The crude product was recrystallised from ethyl acetate to give the title compound as a cream powder (4.00 g, 80 %). ^{1}H NMR: δ_H (DMSO-d_6) 8.43 (d, *J* = 9.0 Hz, 4 H, ArH), 7.6 (d, *J* = 9.0 Hz, 4 H, ArH). ^{13}C NMR: δ_C (DMSO-d_6) 163.9 (ester C=O), 154.7, 145.6, 125.71, 122.82 (ArC).

6.2.1.2. *N*,*N′*-Bis((2^{A}S,3^{A}S)-3^{A}-deoxy-γ-cyclodextrin-3^{A}-yl) oxalamide, 33γ-CD$_2$ox^2

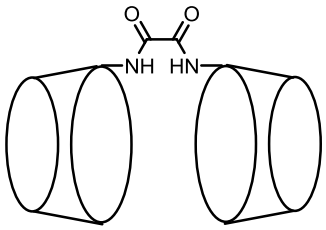

The title compound was prepared by modifying a method from the literature.[2] (2^{A}S,3^{A}S)-3^{A}-amino-3^{A}-deoxy-γ-cyclodextrin (0.62 g, 0.463 mmol) was dissolved in pyridine (20 cm^3) and stirred at room temperature for 15 min. Bis(4-nitrophenyl) oxalate (55.6 mg, 0.185 mmol) was added to this solution in two portions over a period of 1 h. The reaction mixture was then stirred for 48 h at room temperature before being added dropwise to diethyl ether (200 cm^3) with vigorous stirring. The resultant precipitate was collected by centrifugation, washed with acetone and diethyl ether and dried under vacuum. The product was dissolved in H_2O and run down a BioRex 70 (H^+) column then freeze dried to give the title compound as a golden powder. Yield: 0.35 g, (72 %) TLC: Rc = 0.42. ^{1}H NMR: δ_H (D_2O) 5.33-5.00 (m, 16 H, H1), 4.20-3.55 (m, 96 H, H2-6). ^{13}C NMR, δ_C (D_2O): 161.0 (C=O), 102.3 (C1), 80.7, (C4), 73.6, 71.0, 69.4 (C2,3,5), 60.9 (C6), 60.8 (C6^{A}), 51.7 (C3^{A}). MALDI mass spectrum *m*/*z*: 2667 [M + Na]$^+$. Elemental Analysis: $C_{98}H_{160}N_2O_{80}.18H_2O$: C, 39.62; H, 6.65; N 0.95. Found: C, 39.60, H, 6.70, N, 0.98.

6.2.1.3. *N,N′*-Bis(6^{A}-deoxy-γ-cyclodextrin-6^{A}-yl) oxalamide, 66γ-CD$_2$ox^{2}

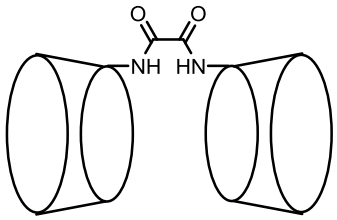

The title compound was prepared by modifying a method from the literature.[2] 6^{A}-Amino-6^{A}-deoxy-γ-cyclodextrin (1.3 g, 1.0 mmol) was dissolved in pyridine (20 cm^3) and stirred at room temperature for 15 min. Bis(4-nitrophenyl) oxalate (120.0 mg, 0.4 mmol) was added to this solution in two portions over a period of 1 h. The reaction mixture was then stirred for 48 h at room temperature before being added dropwise to diethyl ether (200 cm^3) with vigorous stirring. The resultant precipitate was collected by centrifugation, washed with acetone and diethyl ether and dried under vacuum. The product was dissolved in H_2O and run down a BioRex 70 (H^+) column then freeze dried to give the title compound as a white powder. Yield: 0.61 g, (60 %) TLC: Rc = 0.56. ^{1}H NMR: δ_H (D_2O) 5.11 (s, 16 H, H1), 4.08-3.46 (m, 96 H, H2-6). ^{13}C NMR, δ_C (D_2O): 153.0 (C=O), 100.9 (C1), 79.8 (C4), 72.6, 71.0, 70.4 (C2,3,5), 59.6 (C6^{B-H}), 41.0 (C6^{A}), 51.7 (C3^{A}). MALDI mass spectrum *m*/*z*: 2667 $[M + Na]^+$. Elemental Analysis: $C_{98}H_{160}N_2O_{80}.18H_2O$: C, 39.62; H, 6.65; N 0.95. Found: C, 39.64, H, 6.68, N, 0.99.

6.2.1.4. 1,3,5-*N,N,N*-tris(6^{A}-deoxy-6^{A}-γ-cyclodextrin)-benzene, 666γ-CD$_3$bz^3

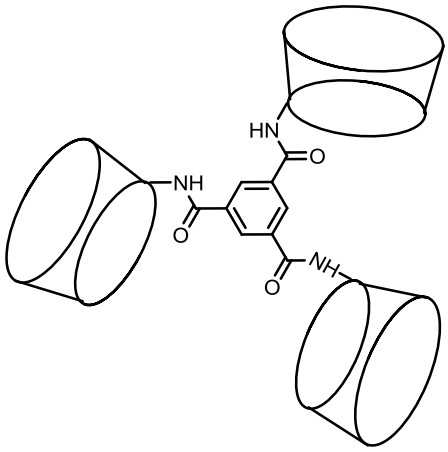

The title compound was prepared by modifying the literature method.[3] 6^{A}-Amino-6^{A}-deoxy-γ-cyclodextrin (0.75 g, 0.57 mmol) was dissolved in pyridine (30 cm^3) and stirred at room temperature for 15 min. 1,3,5-Trinitrophenyl-benzene (96 mg, 0.167 mmol) was added to this solution with stirring over 1 h. The reaction mixture was stirred for a further 48 h at room temperature before being added dropwise to acetone (600 cm^3) with vigorous stirring. The resultant precipitate was collected by centrifugation, washed with acetone and diethyl ether and dried under vacuum. The product was dissolved in water and run down a BioRex 70 (H^+) column. The collected aqueous fractions containing the product were freeze dried to obtain the title compound as a white powder. Yield: 490 mg (72%). TLC: Rc = 0.35. ^{1}H NMR δ_H (D_2O): 8.33 (s, 3H, ArH); 5.30-5.00 (m, 24H, γ-CD H1); 4.20–3.05 (m, 144 H, γ-CD H2–H6). ^{13}C NMR: δ_C (D_2O): 171.60 (amide C=O), 137.47 (Ar C-C=O), 131.92 (Ar C-H), 104.17 (C1), 85.94 (C4^{A}), 83.35-82.24 (C2-4), 75.72-74.29 (C2, C3, C5), 62.99-62.69 (C6), 43.39 (C6^{A}). MALDI Mass spectrum m/z: 4064.5 $[M + Na]^+$ Elemental analysis: $C_{153}H_{243}N_3O_{120}.30H_2O$: C, 40.07; H, 6.66; N, 0.92. Found: C, 40.17; H, 6.63; N, 0.94.

6.2.2. Sample Preparation

6.2.2.1. Sample Preparation for ^{1}H NMR Studies

Solutions for NOESY ^{1}H NMR were prepared in D_2O (pD 7.0, I = 0.10 mol dm^{-3}) at 298.2 K and contained H_2TSPP^{4-} and the cyclodextrin hosts (3.0×10^{-3} mol dm^{-3}, each) in 1 cm^3. The samples were made up so that the concentration of H_2TSPP^{4-} was equimolar with that of the complete hosts γ-CD, 33γ-CD_2ox, 33γ-CD_2suc, 66γ-CD_2ox, 66γ-CD_2suc and 666γ-CD_3bz. When the solids were dissolved a portion of the solution was transferred to the NMR tube.

6.2.2.2. Sample Preparation for UV–vis Studies

All stock solutions were freshly prepared in aqueous phosphate buffer at (pH 7.0, I = 0.10 mol dm^{-3}). A solution of H_2TSPP^{4-} (1.24×10^{-4} mol dm^{-3}) was prepared and then diluted to 1.05×10^{-6} mol dm^{-3}. The H_2TSPP^{4-} solution (2 cm^3) was then injected with 10 mm^3 sequential injections of the host solutions γ-CD (9.14×10^{-3} mol dm^{-3}), 33γ-CD_2ox (9.72×10^{-4} mol dm^{-3}), 33γ-CD_2suc (3.86×10^{-4} mol dm^{-3}), 66γ-CD_2ox (1.89×10^{-4} mol dm^{-3}), 66γ-CD_2suc (5.11×10^{-4} mol dm^{-3}) and 666γ-CD_3bz (3.16×10^{-5} mol dm^{-3}) unless stated otherwise. A typical experiment was injected with 30 aliquots of the host solution with 3 min of stirring between injections.

6.2.3. Molecular Modelling

Molecular modelling and MM2 energy minimisations were performed in the gas-phase with ChemBio3D® Ultra 12.0 software and geometry optimisations were performed using the PM7 semi-empirical method in MOPAC2012.[9] The Broyden-Fletcher-Goldfarb-Shanno (BFGS) optimisation procedure was employed for all PM7 optimisation, and additional keywords, XYZ (for geometry optimisation using Cartesian coordinates) and CHARGE = n were used as appropriate.

6.3. EXPERIMENTAL FOR CHAPTER 3

6.3.1. Sample Preparation

6.3.1.1. Sample Preparation for ^{1}H NMR Studies

Solutions for NOESY ^{1}H NMR were prepared in D_2O (pD 7.0, I = 0.10 mol dm^{-3}) at 298.2 K and contained H_2TCPP and the cyclodextrin hosts (3.0×10^{-3} mol dm^{-3}, each) in 1 cm^3. The samples were made up so that the concentration of $H_3TCPP^{3-}/H_2TCPP^{4-}$ was equimolar with that of the complete hosts γ-CD, 33γ-CD_2ox, 33γ-CD_2suc, 66γ-CD_2ox, 66γ-CD_2suc and 666γ-CD_3bz. When the solids were dissolved a portion of the solution was transferred to the NMR tube.

6.3.1.2. Sample Preparation for Dimerisation UV–vis Studies

All stock solutions were freshly prepared in aqueous phosphate buffer at (pH 7.0, I = 0.10 mol dm^{-3}). A solution of $H_3TCPP^{3-}/H_2TCPP^{4-}$ (9.99×10^{-5} mol dm^{-3}) was prepared and then diluted to 1.18×10^{-5} mol dm^{-3} – 1.95×10^{-6} mol dm^{-6} with a spectrum recorded at each dilution.

6.3.1.3. Sample Preparation for Host-Guest Complexation UV–vis Studies

All stock solutions were freshly prepared in aqueous phosphate buffer at (pH 7.0, I = 0.10 mol dm^{-3}). A solution of $H_3TCPP^{3-}/H_2TCPP^{4-}$ (9.99×10^{-5} mol dm^{-3}) was prepared and then diluted to 2.00×10^{-6} mol dm^{-3}. The $H_3TCPP^{3-}/H_2TCPP^{4-4-}$ solution (2 cm^3) was then injected with 10 mm^3 sequential injections of the host solutions γ-CD (2.33×10^{-3} mol dm^{-3}), 33γ-CD_2ox (6.31×10^{-4} mol dm^{-3}), 33γ-CD_2suc (5.68×10^{-4} mol dm^{-3}), 66γ-CD_2ox (7.90×10^{-5}

mol dm^{-3}), 66γ-CD_2suc (6.79×10^{-5} mol dm^{-3}) and 666γ-CD_3bz (8.46×10^{-5} mol dm^{-3}) unless stated otherwise. A typical experiment was injected with 30 aliquots of the host solution with 3 min of stirring between injections.

6.3.2. Molecular Modelling

Molecular modelling and MM2 energy minimisations were performed in the gas-phase with ChemBio3D® Ultra 12.0 software and geometry optimisations were performed using the PM7 semi-empirical method in MOPAC2012.[9] The Broyden-Fletcher-Goldfarb-Shanno (BFGS) optimisation procedure was employed for all PM7 optimisation, and additional keywords, XYZ (for geometry optimisation using Cartesian coordinates) and CHARGE = n were used as appropriate.

6.4. EXPERIMENTAL FOR CHAPTER 4

6.4.1. Syntheses

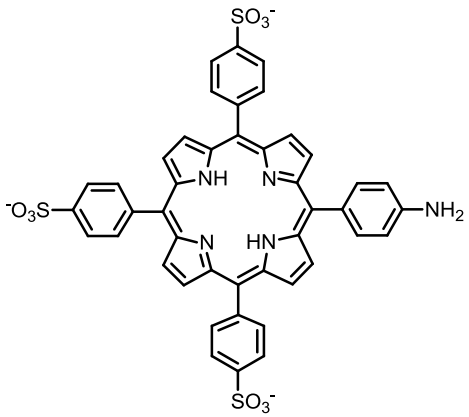

6.4.1.1. 5-(*p*-Aminophenyl)-10,15,20-tris(*p*-sulfonatophenyl)-porphyrin[5]

The title compound was prepared by modifying a literature procedure.[5] 5-(*p*-Aminophenyl)-10,15,20-triphenyl porphyrin (0.60 g, 0.95 mmol) was dissolved in 98% sulphuric acid (30 cm^3) and heated with stirring at 70 °C for 2 days. The solution was then stirred under

nitrogen at room temperature for a further 3 days then poured on to cold water (200 cm^3) with stirring. The green precipitate was collected by centrifugation and repeatedly washed with cold water until the eluent was pH 7. The precipitates were collected and freeze dried to give the title compound as a green/brown powder (0.77 g, 93 %). This material was only slightly soluble in water or DMSO, and satisfactory NMR spectra could not be obtained. ^{1}H NMR δ_H (DMSO-d_6 as the trisodium salt of the title compound): 8.95 (d, *J* = 5.1 Hz, 2 H, β-pyrrole) 8.80 (s, 4 H, β-pyrrole), 8.79 (d, 2 H, *J* = 5.1 Hz, β-pyrrole), 8.17 (d, 6 H, *J* = 8.1 Hz, *meta p*-sulfonatophenyl), 8.05 (d, 6 H, *J* = 8.1 Hz, *ortho p*-sulfonatophenyl), 7.84 (d, 2 H, *J* = 8.4 Hz, *meta p*-aminophenyl), 7.00 (d, 2 H, *J* = 8.4 Hz, *ortho p*-aminophenyl) 5.53 (s, 2 H, amino NH_2), -2.73 (s, 2 H, pyrrole NH). Mass spectrum m/z: 870 $[M + 3H]^+$.

6.4.1.2. 5-(*p*-boc-β-alanylaminophenyl)-10,15,20-tris(*p*-sulfonatophenyl)-porphyrin[10]

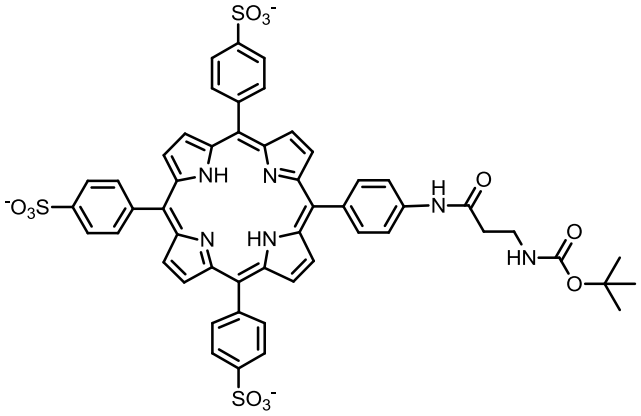

The title compound was prepared by modifying a literature procedure.[10] A solution of boc-β-alanine (0.33 g, 1.74 mmol), EDC (0.40 g, 2.61 mmol) and DMAP in DMF was stirred at 0 °C under nitrogen for 1 h. 5-(*p*-Aminophenyl)-10,15,20-tris(*p*-sulfonatophenyl)-porphyrin (0.77 g, 0.87 mmol), was added and left to stir at 0 °C for 30 min then at room temperature for 24 h. The solvent was removed under reduced pressure and the product was purified by

silica-gel column chromatography using 7:3 DCM/MeOH as the solvent to give the title compound as a purple solid (0.60 g, 69 %). ^{1}H NMR δ_H (DMSO-d_6): 10.60 (s, 1 H, amide NH), 8.87 (s, 8 H, β-pyrrole), 8.18, 8.05 (dd, 12 H, *p*-sulfonatophenyl), 8.16, 8.08 (dd, 4 H, *p*-aminophenyl), 3.35 (t, 2 H), 2.68 (t, 2 H), 1.55 (s, 9 H, tert-butyl), -2.93 ppm (s, 2 H). Mass spectrum m/z: 1040 $[M + 3H]^+$.

6.4.1.3. 5-(*p*-β-alanylaminophenyl)-10,15,20-tris(*p*-sulfonatophenyl)-porphyrin[10]

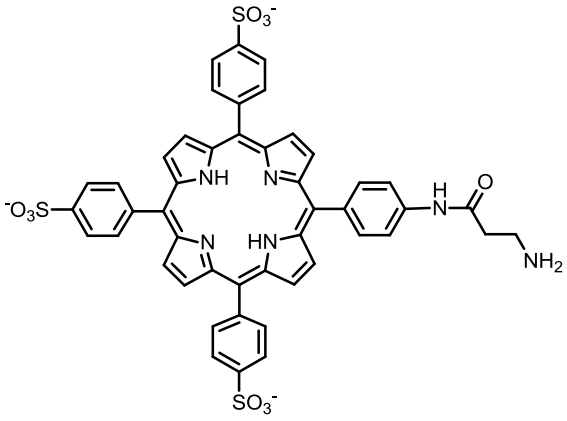

The title compound was prepared by modifying a literature procedure.[10] 5-(4-Boc-β-alanine)-10,15,20-tris(4-sulfonatophenyl)-porphyrin (0.6 g, 0.56 mmol) was added to trifluoroacetic acid (0.5 cm^3) in dichloromethane (10 cm^3) and stirred for 30 min at 0°C under an N_2. After further stirring for 2 h at room temperature, the solvent was evaporated and the residue was reprecipitated using methanol/diethyl ether to give the title compound as a dark red powder (0.50 g, 95%). ^{1}H NMR δ_H (DMSO-d_6): 10.60 (s, 1 H, amide NH), 8.86 (s, 2 H, β-pyrrole), 8.84 (s, 6 H, β-pyrrole), 8.19, 8.03 (dd, 12 H, *p*-sulfonatophenyl), 8.16, 8.05 (dd, 4 H, *p*-aminophenyl), 8.08 (s, 2 H, amino NH_2), 3.23 (t, 2 H, H_2N-CH_2), 2.88 (t, 2 H, O=C-CH_2), -2.93 ppm (s, 2 H). Mass spectrum m/z: 941 $[M + 3H]^+$.

6.4.1.4. Preparation of 3.0 % randomly substituted sodium 5-(*p*-β-alanylaminophenyl)-10,15,20-tris(*p*-sulfonatophenyl)-porphyrin poly(acrylate), PAATSPPala[10]

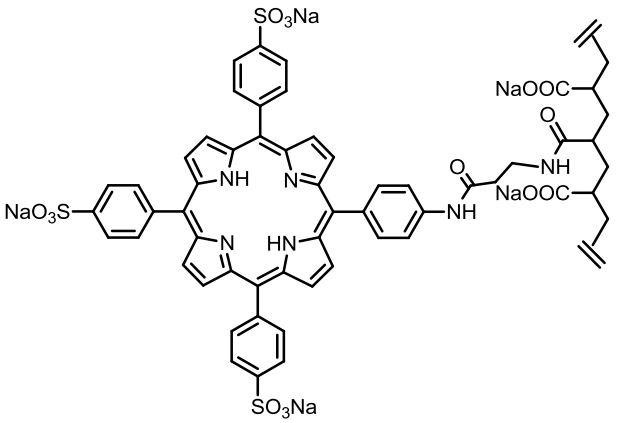

The title compound was prepared by modifying a literature procedure.[10] A mixture of PAA (0.45 g, 5.56 mmol) and DMAP (208 mg, 1.68 mmol) in DMF (10 cm^3) was stirred for 15 min at 0 °C. EDC (130 mg, 0.84 mmol) was then added to the solution and stirred for 1 h at 0 °C. TSPPala (0.27 g, 0.29 mmol) was then added into the activated PAA solution and stirred for 0.5 h at 0 °C. After further stirring at room temperature for 24 h, 40 wt % aqueous sodium hydroxide (60 cm^3) was added. The resulting precipitate was filtered and washed with methanol (2 × 40 cm^3). The crude product was dissolved in water (12.5 cm^3) and added dropwise to methanol (100 cm^3) and the precipitate formed was collected (this step was repeated). The solid was dissolved in water (30 cm^3) and dialysed (Spectra/Por 3 tubing, molecular weight cut-off 3,500 g mol^{-1}) against deionised water until the conductivity of the water outside the tube remained constant. The final dry product was obtained as the sodium poly(acrylate) salt by freeze-drying after concentrating the solution to 10 cm^3 by evaporation in a 90 % yield. The degree of substitution was determined to be 3.0 ± 0.3 % by ^{1}H NMR spectroscopy according to the literature method.[11,12]

6.4.2. Sample Preparation

6.4.2.1. Sample Preparation for ^{1}H NMR Studies

Solutions for 2D NOESY ^{1}H NMR were prepared in D_2O (pD 7.0, I = 0.10 mol dm^{-3}) at 298.2 K and contained 3.0×10^{-3} mol dm^{-3} each of the TSPPala substituents of PAATSPPala and the cyclodextrin hosts in 1 cm^3. The samples were made up so that the concentration of porphyrin substituents was equimolar with that of the hosts γ-CD, 33γ-CD_2ox, 33γ-CD_2suc, 66γ-CD_2ox, 66γ-CD_2suc and 666γ-CD_3bz. When the solids were dissolved a portion of the solution was transferred to the NMR tube.

6.4.2.2. Sample Preparation for UV–vis Studies

All stock solutions were freshly prepared in aqueous phosphate buffer at (pH 7.0, I = 0.10 mol dm^{-3}). A solution of PAATSPPala (6.17×10^{-5} mol dm^{-3}) was prepared and then diluted to 3.10×10^{-6} mol dm^{-3} using the molecular weight determined below. Determination of the molecular weight of porphyrin substituents in 3% randomly substituted PAA:

$$M_{w(PAATSPPala)} = [(M_{w(CH_2CHCOONa)} \times 97) + (M_{w(CH_2CHCOTSPPala)} \times 3)]/3$$

$$= 4100.3 \text{ g mol}^{-1}$$

The initial solutions of PAATSPPala (2 cm^3) were sequentially diluted with 10 mm^3 aliquots of stock solutions of each CD host: γ-CD (1.01×10^{-2} mol dm^{-3}), 33γ-CD_2ox (2.65×10^{-3} mol dm^{-3}), 33γ-CD_2suc (1.24×10^{-3} mol dm^{-3}), 66γ-CD_2ox (2.52×10^{-4} mol dm^{-3}), 66γ-CD_2suc (1.21×10^{-3} mol dm^{-3}) and 666γ-CD_3bz (6.57×10^{-5} mol dm^{-3}) unless stated otherwise. A typical experiment was injected with 30 aliquots of the host solution with 3 min of stirring between injections.

6.5. EXPERIMENTAL FOR CHAPTER 5

6.5.1. Syntheses

6.5.1.1. Preparation of *N*-(2-aminoethyl)-2-naphthyl-sulfonamide, 2NSen

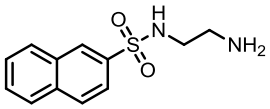

A solution of 2-naphtahlene sulfonyl chloride (227 mg, 1 mmol) in tetrahydrofuran (10 cm^3) was added dropwise over 4 h to a solution of 1,2-diaminoethane (900 mg, 15 mmol) in tetrahydrofuran (10 cm^3). The solvent was removed under reduced pressure and the precipitate was dissolved in dichloromethane (50 cm^3). The resulting mixture was acidified to pH < 2 with 10 wt % hydrochloric acid solution (20 cm^3) and the solution was washed with dichloromethane (3 × 20 cm^3). The aqueous solution was made basic to pH > 10 by 10 wt % with aqueous sodium hydroxide solution (30 cm^3) and extracted with dichloromethane (5 × 20 cm^3). The combined dichloromethane solution was washed with water (4 × 100 cm^3), then brine (50 cm^3) and dried over magnesium sulfate. The solution was filtered and the solvent was removed under reduced pressure to afford *N*-(2-aminoethyl)-2-napthalene sulfonamide as a cream powder. Yield: 110 mg (47 %); δ_H (DMSO-d_6) 8.43 (s, 1H, ArH1), 8.16 (m, 2H, ArH3,4), 8.12 (d, *J* = 8.5 Hz, 1H, ArH8), 7.71 (d, *J* = 8.5 Hz, 1H, ArH5), 7.69 (m, 2H, ArH6,7) , 2.72 (t, *J* = 6.5 Hz, 2H, $SO_2NHC\underline{H}_2$), 2.49 (t, *J* = 6.5 Hz, 2H, $C\underline{H}_2NH_2$). Mass spectrum m/z: 250.12.

6.5.1.2. Preparation of *N*-(6-aminohexyl)-2-naphthyl-sulfonamide, 2NShn

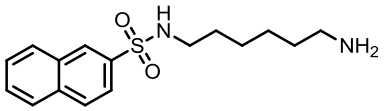

A solution of 2-naphtahlene sulfonyl chloride (227 mg, 1 mmol) in tetrahydrofuran (10 cm^3) was added dropwise over 4 h to a solution of 1,6-diaminohexane (2.0 g, 17 mmol) in tetrahydrofuran (10 cm^3) and stirred for 48 h. The mixture was then filtered, the solvent was removed under reduced pressure and the precipitate was dissolved in dichloromethane (50 cm^3). The resulting mixture was acidified to pH < 2 with 10 wt % hydrochloric acid solution (20 cm^3) and the solution was washed with dichloromethane (3 × 20 cm^3). The aqueous solution was made basic with 10 wt % aqueous sodium hydroxide solution (30 cm^3) and extracted by dichloromethane (5 × 20 cm^3). The combine dichloromethane solution was then washed by water (4 × 100 cm^3), then brine (50 cm^3) and dried over magnesium sulfate. The solvent was removed to give a yellow oil that was run down a basic alumina column (Brockman Activity III) and eluted with dichloromethane (300 cm^3), 1% aqueous methanol (300 cm^3), 2% aqueous methanol (300 cm^3) and then 5% aqueous methanol (300 cm^3). The fractions containing product were combined and the solvent was removed under reduced pressure to give the title compound as a yellow/green oil. Yield: 80 mg (22 %); δ_H (DMSO-d_6) 8.45 (s, 1H, ArH1), 8.14 (m, 2H, ArH3,4), 8.10 (d, *J* = 8.5 Hz, 1H, ArH8), 7.73 (d, *J* = 8.5 Hz, 1H, ArH5), 7.70 (m, 2H, ArH6,7) 2.77 (t, *J* = 7.0 Hz, 2H, SO_2NHCH_2), 2.35 (t, *J* = 7.0 Hz, 2H, $C\underline{H}_2NH_2$), 1.24-1.00 (m, 8H, $(CH_2)_4$). Mass spectrum m/z: 306.25.

6.5.1.3. General procedure for the preparation of the 3% randomly substituted naphthyl-sulfonamide poly(acrylate)s

The 3% randomly 2-naphthyl substituted poly(acrylate)s were prepared according to a general procedure reported in the literature.[11,12] The solid poly(acrylic acid), PAA (1.9 g, 26.4 mmol of -COOH groups) was dissolved in *N*-methylpyrrolidin-2-one (60 cm^3) at 60 ^oC and stirred for 24 h. Either 2NSen or 2NShn (0.79 mmol) in *N*-methylpyrrolidin-2-one (7.5 cm^3) was added followed by dicyclohexylcarbodiimide (0.79 mmol) in *N*-methylpyrrolidin-2-one (7.5 cm^3) and the reaction mixture was stirred at 60 ^oC for 48 h. After cooling to room temperature, 40 wt % aqueous sodium hydroxide (60 cm^3) was added. The resulting precipitate was filtered and washed with *N*-methylpyrrolidin-2-one (2 × 30 cm^3) and methanol (2 × 40 cm^3) at 60 ^oC. The crude product was dissolved in water (12.5 cm^3) and added dropwise to methanol (100 cm^3) and the precipitate formed was collected (this step was repeated). The solid was dissolved in water (30 cm^3) and dialysed (Spectra/Por 3 tubing, molecular weight cut-off 3,500 g mol^{-1}) against deionised water until the conductivity of the water outside the tube remained constant. The final dry product was obtained as the sodium poly(acrylate) salt by freeze-drying after concentrating the solution to 10 cm^3 by evaporation. Typical yields were 80–90 %. The degree of substitution was determined to be 3.0 ± 0.3 % by ^1H NMR spectroscopy according to the literature method.[11,12]

6.5.2. Sample Preparation

6.5.2.1. Sample Preparation for ^1H NMR Studies

Solutions for 1D and 2D ^1H–NOESY NMR experiments were prepared in D_2O in 0.10 mol cm^{-3} sodium chloride. The solution pH was adjusted to 7.0 with 0.10 mol dm^{-3} aqueous

sodium hydroxide solution. Each sample contained 1.43 wt% in either PAA1NSen, PAA2NSen, PAA1NShn or PAA2NShn (3.0×10^{-3} mol dm^{-3} of 1NSen or 2NSen groups and 2.94×10^{-3} mol dm^{-3} of 1NShn or 2NShn groups) and an equimolar concentration of β-CD, γ-CD or their linked CD dimers.

6.5.2.2. Sample Preparation for Fluorescence Studies

Stock solutions of 5.0 wt% in either PAA1NSen, PAA1NShn, PAA2NSen or PAA2NShn were prepared in pH 7.0 phosphate buffer (KH_2PO_4 0.0195 mol dm^{-3}, Na_2HPO_4 0.0268 mol dm^{-3}) at constant ionic strength I = 0.10 mol dm^{-3}. For fluorescence studies, the stock solutions were diluted to make 0.0330 wt% and 0.0033 wt% in either PAA1NSen, PAA2NSen, PAA1NShn and PAA2NShn which correspond to 1.0×10^{-5} mol dm^{-3} of either 1NSen, 2NSen, 1NShn or 2NShn groups, respectively, based on their calculated molecular weights determined below.

Determination of the molecular weights of 1NSen, 2NSen, 1NShn and 2NShn in 3% randomly substituted PAAs:

$$M_{w(1NSen)} = [(M_{w(CH_2CHCOONa)} \times 97) + (M_{w(CH_2CHCO1NSen)} \times 3)]/3$$

$$= 3343 \text{ g mol}^{-1}$$

$$M_{w(1NShn)} = [(M_{w(CH_2CHCOONa)} \times 97) + (M_{w(CH_2CHCO1NShn)} \times 3)]/3$$

$$= 3399 \text{ g mol}^{-1}$$

The initial solutions for fluorescence studies of 1.0×10^{-5} mol dm^{-3} of either [1NSen], [2NSen], [1NShn] or [2NShn] (2.00 cm^3) were sequentially diluted with 0.050 cm^3 aliquots of stock solutions of each CD host: β-CD (1.06×10^{-2} mol dm^{-3}), γ-CD (4.96×10^{-2} mol dm^{-3}), 33β-CD$_2$suc (2.49×10^{-3} mol dm^{-3}), 66β-CD$_2$suc (2.31×10^{-3} mol dm^{-3}), 33γ-CD$_2$suc (2.63×10^{-3} mol dm^{-3}) or 66γ-CD$_2$suc (1.00×10^{-3} mol dm^{-3}) unless stated otherwise. In a typical titration experiment, 30 aliquots of either host were added.

6.6. REFERENCES

1. Z. Dong and P. J. Scammells, *J. Org. Chem.*, 2007, **72**, 9881-9885.
2. D.-T. Pham, H. T. Ngo, S. F. Lincoln, B. L. May and C. J. Easton, *Tetrahedron*, 2010, **66**, 2895-2898.
3. H.-T. Nguyen, D.-T. Pham, S. F. Lincoln, J. Wang, X. Guo, C. J. Easton and R. K. Prud'homme, *Polym. Chem.*, 2013, **4**, 820-829.
4. S. Guha, M. G. B. Drew and A. Banerjee, *Chem. Mater.*, 2008, **20**, 2282-2290.
5. W. J. Kruper, Jr., T. A. Chamberlin and M. Kochanny, *J. Org. Chem.*, 1989, **54**, 2753-2756.
6. H. T. Ngo, P. Clements, C. J. Easton, D.-T. Pham and S. F. Lincoln, *Aust. J. Chem.*, 2010, **63**, 687-692.
7. H. T. Ngo, Supramolecular Chemistry of β- and γ-Cyclodextrin Dimers. A PhD. Dissertaion, University of Adelaide, 2010.
8. M. M. Rauhut, L. J. Bollyky, B. G. Roberts, M. Loy, R. H. Whitman, A. V. Iannotta, A. M. Semsel and R. A. Clarke, *J. Amer. Chem. Soc.*, 1967, **89**, 6515-6522.
9. J. P. Stewart, Stewart Computational Chemistry, Colorado Springs, CO, 14.139W edn., 2012.
10. K. Kano, T. Ochi, S. Okunaka, Y. Ota, K. Karasugi, T. Ueda and H. Kitagishi, *Chem. - Asian J.*, 2011, **6**, 2946-2955.
11. X. Guo, A. A. Abdala, B. L. May, S. F. Lincoln, S. A. Khan and R. K. Prud'homme, *Macromolecules*, 2005, **38**, 3037-3040.
12. X. Guo, A. A. Abdala, B. L. May, S. F. Lincoln, S. A. Khan and R. K. Prud'homme, *Polymer*, 2006, **47**, 2976-2983.